



A University of Sussex DPhil thesis

Available online via Sussex Research Online:

<http://sro.sussex.ac.uk/>

This thesis is protected by copyright which belongs to the author.

This thesis cannot be reproduced or quoted extensively from without first obtaining permission in writing from the Author

The content must not be changed in any way or sold commercially in any format or medium without the formal permission of the Author

When referring to this work, full bibliographic details including the author, title, awarding institution and date of the thesis must be given

Please visit Sussex Research Online for more information and further details

SIALIC ACID DERIVATIVES AND MIMETICS:
TOOLS FOR THE INVESTIGATION OF SIALIC ACID
PROCESSING ENZYMES

Mathew Stanley

August 2011

Submitted in partial fulfilment towards the requirements for the degree of
Doctor of Philosophy (DPhil)

I hereby declare that this thesis has not been and will not be, submitted in whole or in part to another university for the award of any other degree.

Signature

UNIVERSITY OF SUSSEX

MATHEW STANLEY

SUBMITTED FOR THE DEGREE OF DOCTOR OF PHILOSOPHY (DPHIL)

**SIALIC ACID DERIVATIVES AND MIMETICS: TOOLS FOR THE INVESTIGATION OF
SIALIC ACID PROCESSING ENZYMES**

SUMMARY

I. Synthesis and inhibitory activity of sialic acid derivatives targeting viral sialate-*O*-acetyltransferases and sialate-*O*-acetyltransferases

Sialate-*O*-acetylation is a common structural modification of sialic acid, which has been associated with many human disease states (including cancer and autoimmune disease). This highly regulated and tissue-specific modification is carried out by sialate-*O*-acetyltransferase (SOAE) and sialate-*O*-acetyltransferase (SOAT) enzymes.

The availability of these enzymes make inhibition studies a viable endeavour, considering that SOAT/SOAE inhibitors may provide interesting tools/drug leads for the development of antiviral compounds or treatments for various disease states. A synthesis of suitable 4-*O*- and 9-*O*-functionalised sialic acid derivatives has been established which enabled the investigation of 4- and 9-sialate-*O*-acetyltransferase enzymes. Sialic acid derivatives were screened for the inhibition of a set of viral SOAEs and while no inhibition of 4-SOAE could be detected, a 9-*O*-methyl derivative showed inhibition of the recombinant influenza C virus SOAE. The functionalised sialic acid motif thus serves as an initial template for the design and synthesis of future sialic acid derivatives towards SOAT/SOAT inhibition.

II. New tools for the characterization and investigation of influenza virus neuraminidases: towards novel influenza virus sensors

Tamiflu™ (Oseltamivir), has been employed as a mimetic of the sialic acid “oxocarbenium” intermediate formed during enzymatic hydrolysis, leading to inhibition of virus-bound neuraminidase (NA) enzyme. Phospha-isosteres of oseltamivir provide access to monoesters which retain the efficacy of the pharmacophore and allow the synthesis of novel influenza neuraminidase-specific materials.

Phospha-oseltamivir-stabilised gold nanoparticles (“TamiGold”) have been synthesised and NA inhibition studies with “small TamiGold” show activity against influenza virus strains investigated compared to control gold nanoparticles. The binding interactions displayed by “large TamiGold” may provide the basis for a colorimetric method of influenza detection and as such a novel prototype influenza sensor. To the best of our knowledge this is the first example of a multivalent approach to influenza virus binding utilising sialylmimetic scaffolds immobilised on a nanoparticle platform which specifically target the NA (instead of the hemagglutinin, HA). The synthesis of phospha-oseltamivir conjugates and their ligation to biological reporter groups afford small molecule tools with high affinity and selectivity towards influenza NA. These derivatives can be applied towards novel multivalent phospha-oseltamivir materials and used as novel diagnostics, independent of existing methods.

Sialic Acid Derivatives and Mimetics: Tools for the Investigation of Sialic Acid Processing Enzymes

Contents

Acknowledgements.....	7
Abbreviations.....	8
Abstract.....	13
I. Synthesis and inhibitory activity of sialic acid derivatives for targeting viral sialate-<i>O</i>-acetyltransferases and sialate-<i>O</i>-esterases	
I.1. Introduction.....	15
I.1.1. Sialic acids: nature's promiscuous carbohydrates.....	15
I.1.1.1. Biosynthesis of sialic acids.....	18
I.1.1.2. Chemical syntheses of sialic acid.....	20
I.1.2. <i>O</i> -Glycosylation of sialic acids: a specific problem.....	20
I.1.3. Biological <i>O</i> -Acetylation of sialic acids.....	22
I.1.3.1. The processing enzymes of <i>O</i> -acetylated sialic acids.....	25
I.1.4. Sialate- <i>O</i> -acetyltransferases (SOATs).....	25
I.1.4.1. Proposed mechanism of <i>O</i> -acetylation: post-sialylation.....	26
I.1.4.2. Proposed mechanism of <i>O</i> -acetylation: pre-sialylation.....	28
I.1.4.3. Speculation upon the catalytic nature of SOAT enzymes.....	30
I.1.5. Sialate- <i>O</i> -acetyltransferases (SOAETs).....	33
I.1.5.1. Viral and bacterial sialate- <i>O</i> -acetyltransferases.....	35
I.1.5.1. The HEF of influenza C: the archetypal SOAET.....	37
I.1.6. Synthetic sialic acid derivatives towards SOATs.....	43
I.2. Results and discussion.....	44
I.2.1. Project rationalisation.....	44
I.2.1.1. Inhibitor design.....	44

I.2.2.	Synthesis of the α -sialoside precursor.....	45
I.2.3.	Potential inhibitors.....	46
I.2.4.	Syntheses of 4- <i>O</i> -modified sialoside derivatives	49
	I.2.4.1. Methylation of the 4-hydroxy group.....	49
	I.2.4.1. Phosphonylation of the 4-hydroxy group.....	50
I.2.5.	Syntheses of 9- <i>O</i> -modified sialoside derivatives	52
	I.2.5.1. Methylation of the 9-hydroxy group.....	52
	I.2.5.2. Phosphonylation of the 9-hydroxy group.....	57
I.2.6.	Towards non-competitive (irreversible) inhibitors.....	59
I.2.7.	Investigation of the inhibitory activity against viral SOAEs.....	60
	I.2.7.1. Results and discussion of inhibition studies	61
I.2.8.	Conclusion	62
I.2.9.	Future scope.....	63
II.	New tools for the characterization and investigation of influenza virus neuraminidases: towards novel influenza virus sensors	
II.1.	Introduction.....	65
II.1.1.	Introduction to the influenza virus.....	65
	II.1.1.1. Influenza A virus	65
	II.1.1.2. Pandemic influenza (H1N1, H5N1)	66
II.1.2.	The role of neuraminidase and hemagglutinin in influenza virus replication.....	67
	II.1.2.1. Hemagglutinin.....	68
	II.1.2.2. Neuraminidase.....	71
II.1.3.	Influenza therapeutics	73
	II.1.3.1. Neuraminidase inhibitors.....	74
	II.1.3.2. M2 protein blockers.....	75
	II.1.3.3. IMP dehydrogenase inhibitors.....	76
	II.1.3.4. RNA polymerase inhibitors.....	76
II.1.4.	Oseltamivir: a neuraminidase inhibitor.....	77

II.1.4.1. Oseltamivir vs. influenza virus: emerging resistance	80
II.1.4.2. Syntheses of oseltamivir	81
II.1.4.3. A synthetic strategy towards phospho-isosteres of oseltamivir.....	82
II.1.5. The concept of multivalency to achieve stronger binding.....	85
II.1.5.1. Mechanisms of binding enhancement.....	86
II.1.5.2. Chelation effects	86
II.1.5.3. Statistical rebinding.....	86
II.1.6. Multivalency with regards to influenza	87
II.1.6.1. Synthetic platforms towards multivalent inhibitors of influenza virus HA and NA	87
II.1.6.2. Multivalent sialic acid derivatives: low molecular weight scaffolds	88
II.1.6.3. Multivalent sialic acid derivatives: polymeric scaffolds	90
II.1.6.4. Multivalent sialic acid derivatives: other scaffolds.....	93
II.1.6.5. Multivalency and influenza therapeutics: targeting the NA	94
II.1.6.6. Multivalent Sialylmimetics: low molecular weight scaffolds.....	94
II.1.6.7. Multivalent sialylmimetics: polymeric scaffolds.....	96
II.1.6.8. Multivalent sialylmimetics: other scaffolds.....	97
II.1.7. Nanoparticles	99
II.1.7.1. Gold nanoparticles: quantum size effect	100
II.1.7.2. Gold nanoparticles: bonding	100
II.1.8. Gold nanoparticle synthesis and characterisation.....	101
II.1.8.1. Brust-Shiffrin method	102
II.1.8.2. Turkevitch method with ligand-exchange	105
II.1.8.3. Place exchange reactions: further functionalisation.....	106
II.1.9. Characterisation of gold nanoparticles	107
II.1.9.1. Gold nanoparticles: size and shape	107

II.1.9.2. Stability of gold nanoparticles.....	107
II.1.9.3. Analysis of gold nanoparticles.....	109
II.1.9.4. Surface plasmon resonance (SPR) band	110
II.1.10. Influenza and gold nanoparticles.....	112
II.1.11. Influenza and other nanoparticles.....	115
II.1.12. Novel colorimetric methods of influenza detection.....	115
II.2. Results and discussion	118
II.2.1. Project rationalisation.....	118
II.2.2. Strategies towards gold nanoparticles derivatised with phospho-oseltamivir ...	119
II.2.2.1. Synthesis of dimeric phospho-oseltamivir	120
II.2.2.2. Neuraminidase (NA) inhibition studies with dimeric phospho-oseltamivir.....	124
II.2.3. Synthesis of functionalised gold nanoparticles	124
II.2.3.1. Brust-Shiffrin method	125
II.2.3.2. "Small" methylphosphonate-stabilised gold nanoparticles as a control sample	125
II.2.3.3. Phospho-oseltamivir-stabilised gold nanoparticles: "small TamiGold".....	127
II.2.3.4. Turkevitch method and ligand exchange.....	130
II.2.3.5. "Large" methylphosphonate-stabilised gold nanoparticles as a control sample	130
II.2.3.6. Phospho-oseltamivir-stabilised gold nanoparticles: "large TamiGold".....	131
II.2.4. Gold nanoparticle characterisation: "small TamiGold" and control sample.....	133
II.2.4.1. UV-Vis spectroscopy.....	133
II.2.4.2. High resolution transmission electron microscopy (HRTEM)... ..	134
II.2.4.3. Diffusion ordered spectroscopy (DOSY) NMR	137
II.2.4.4. ¹ H NMR.....	139
II.2.4.5. Dynamic light scattering (DLS).....	141

II.2.4.6. Mass spectrometry.....	141
II.2.4.7. Energy dispersive X-ray (EDX) analysis.....	142
II.2.5. Gold nanoparticle characterisation: "large TamiGold" and control sample.....	144
II.2.5.1. UV-Vis spectroscopy.....	144
II.2.5.2. Transmission electron microscopy (TEM)	150
II.2.5.3. Dynamic light scattering (DLS).....	152
II.2.5.4. ¹ H NMR.....	156
II.2.5.5. Physical observations	156
II.2.5.6. Gold nanoparticle stability with respect to influenza sensor application	157
II.2.6. Investigation into NA inhibition by functionalised gold nanoparticles: "small TamiGold"	157
II.2.7. Investigation into NA inhibition by functionalised gold nanoparticles: "large TamiGold"	161
II.2.7.1. TEM study with influenza A virus (H1N1)	161
II.2.7.2. Preliminary UV-Vis study with influenza A virus (H1N1)	165
II.2.8. Conclusions	167
II.2.9. Towards phospho-oseltamivir based tools for the investigation of neuraminidase.....	169
II.2.10. Syntheses of "clickable" phospho-oseltamivir derivatives	169
II.2.10.1 Neuraminidase (NA) inhibition studies	171
II.2.11. Conjugation to reporter groups.....	171
II.2.11.1. Neuraminidase (NA) inhibition studies	175
II.2.11.2. Fluorescence titrations with NA.....	175
II.2.12. Conclusions	177
II.2.13. Future scope.....	178
III. Experimental section	181
III.1. General procedures	181
III.2. Synthetic procedures towards α-O-sialoside derivatives	182

III.3. SOAE inhibition assays	210
III.3.1. Viruses and recombinant viral sialate- <i>O</i> -acetylsterases	210
III.3.2. Enzyme and inhibitors	210
III.3.3. <i>p</i> -Nitrophenylacetate (pNPA) inhibition assay	210
III.4. Synthetic procedures towards phospho-oseltamivir derivatives	211
III.5. Nanoparticle syntheses	239
III.6. Nanoparticle characterisation	241
III.7. Inhibition of neuraminidase (NA) activity	243
III.8. Fluorescence experiments	244
III.8.1. Fluorescence titration	244
IV. References	245
V. Appendices	261
V.1. Appendix 1: PLE experiments	261
V.2. Appendix 2: Dynamic light scattering (DLS)	265
V.3. Appendix 3: Gold nanoparticle inhibition assays: calculation of ligand surface coverage	268
V.4. NMR data	269
V.4.1. ¹ H NMR	269
V.4.2. ¹³ C NMR of target compounds	300
V.4.3. ³¹ P NMR of target compounds	305

Acknowledgements

First and foremost, I would like to thank Dr. Hansjörg Streicher for allowing me the opportunity and freedom to pursue my DPhil under his supervision. Thank you for your guidance, honesty, resolve and encouragement. It is very much appreciated.

Very special thanks goes to Dr. Benoit Carbain, my friend and predecessor in the Streicher group, for his development of the phospho-oseltamivir synthesis but more importantly his continued support and friendship throughout the time spent at Sussex and beyond.

A big thank you to all of my other friends and colleagues at Sussex, past and present, for making the time spent in and out of the lab very enjoyable.

Thank you to Dr. I. Day and Dr. A. Abdul-Sada for their assistance with NMR spectroscopy and mass spectrometry respectively.

I would like to sincerely thank Prof. R. Vlasak and group (University of Salzburg, Austria) for carrying out viral SOAE inhibition assays with the sialic acid derivatives synthesised herein, Prof. R. A. Field and Dr. A. Rashid (John Innes Centre, Norwich, UK) for the EDX and MALDI-MS analyses of “small TamiGold” and control gold nanoparticles and the NIMR, for carrying out inhibition assays using the phospho-oseltamivir derivatives synthesised herein.

Thank you to Hoffmann-La Roche Ltd. for the donation of valuable starting material and to the EPSRC for the funding of my DPhil studies.

Last but not least, I would like to thank Charlotte for somehow managing to put up with a chemist for far longer than he probably deserves.

Abbreviations

Ac	acetone
Ac ₂ O	acetic anhydride
AcCl	acetyl chloride
AcCoA	acetyl coenzyme A
AcOH	acetic acid
AFM	atomic force microscopy
Ala	alanine
Arg	arginine
Asn	asparagine
Asp	aspartic acid
AuNPs	gold nanoparticles
BCoV	bovine coronavirus
Bn	benzyl
BocON	2-(<i>tert</i> -Butoxycarbonyloxyimino)-2-phenylacetonitrile
BToV	bovine Torovirus
CMP	cytidine monophosphate
CNS	central nervous system
COSY	correlated spectroscopy
cryo-TEM	cryogenic transmission electron microscopy
DBU	1,8-diazabicyclo[5.4.0]undec-7-ene
DCM	dichloromethane
DE	diethyl ether
DFP	diisopropylfluoro-phosphate
DIPEA	<i>N,N</i> -diisopropylethylamine
DLS	dynamic light scattering
DMAP	dimethylaminopyridine

DMF	<i>N,N</i> -dimethylformamide
DMP	2,2-dimethoxypropane
DMSO	dimethylsulfoxide
DNA	deoxyribonucleic acid
DOSY	diffusion ordered spectroscopy
DVLO	Derjaguin-Landau-Verwey-Overbeek theory
EA	ethyl acetate
EDX	energy dispersive x-ray analysis
ELISA	enzyme-linked immunosorbent assay
ESI	electrospray ionisation
EtOH	ethanol
FRET	fluorescence resonance energy transfer
Glu	glutamic acid
Gly	glycine
HA	hemagglutinin
HE	hemagglutinin-esterase protein(s)
HE12-GFP	recombinant haemagglutinin esterase from influenza C/Cal/78 virus
HEF	hemagglutinin-esterase-fusion protein(s)
HI assay	hemagglutinin inhibition assay
His	histidine
HPAI	highly pathogenic avian influenza virus
HR-ESI-MS	high resolution ESI-MS
HR-MS	high resolution mass spectrometry
HRTEM	high resolution transmission electron microscopy
IMP	inosine 5'-monophosphate
ISAV	infectious salmon anaemia virus
J	coupling constant (Hz)
K_i	inhibition constant

KOH	potassium hydroxide
LPAI	low pathogenic avian influenza viruses
Lys	lysine
MALDI	matrix assisted laser desorption ionisation
MAS	mercaptosuccinic acid
Me	methyl
Mel	iodomethane
MeOH	methanol
MES	mercaptoethansulfonate
MHV	murine hepatitis virus
MMP-AuNPs	monomethylphosphonate stabilised gold nanoparticles
MPLC	medium performance liquid chromatography
MS	mass spectrometry
MUNANA	2-(4-Methylumbelliferyl)- α -D-N-acetylneuraminic acid
NA	neuraminidase
NaH	sodium hydride
NaOMe	sodium methoxide
Neu5,9Ac ₂	<i>N</i> -acetyl-9- <i>O</i> -acetylneuraminic acid
Neu5Ac	<i>N</i> -acetylneuraminic acid
Neu5Gc	<i>N</i> -glycolylneuraminic acid
NHS-Fluorescein	5/6-carboxyfluorescein succinimidyl ester
nI	absorption (refractive) index
NMR	nuclear magnetic resonance
nR	refractive index
OAc	<i>O</i> -acetyl
PCR	polymerase chain reaction
PE	petroleum ether

Phe	phenylalanine
PLE	porcine liver esterase
pNPA	<i>para</i> -nitrophenyl acetate
Pro	proline
p-TsOH.H ₂ O	<i>para</i> -toluenesulfonic acid monohydrate
PV	puffinosis coronavirus
Py	pyridine
PyBOP	benzotriazol-1-yl-oxypyrrolidinephosphonium hexafluorophosphate
RDE	receptor destroying enzyme
R _H	hydrodynamic radius
RIDTs	rapid influenza diagnostic tests
RNA	ribonucleic acid
S	spike protein(s)
SA	sialic acid(s)
SDAV	sialodacryoadenitis virus
SED	spin-echo difference spectroscopy
SEM	scanning electron microscopy
Ser	serine
Siglecs	sialic acid binding Ig-like lectins
SLS	static light scattering
SOAE	sialate- <i>O</i> -acetyl esterase(s)
SPR	surface plasmon resonance
TBAI	tetrabutylammonium iodide
TBDMS	<i>tert</i> -butyldimethylsilyl
TBDMSCl	<i>tert</i> -butyldimethylsilyl chloride
TEM	transmission electron microscopy
TGA	thermogravimetric analysis
THF	tetrahydrofuran

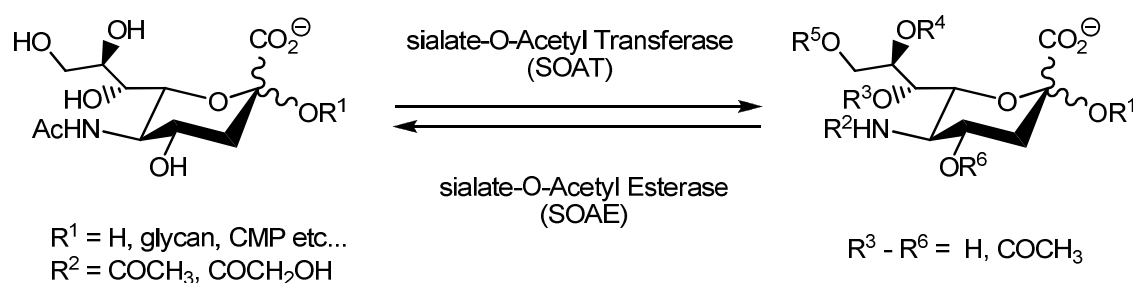
Thr	threonine
TLC	thin layer chromatography
TMSBr	bromotrimethylsilane
TOAB	tetraoctylammonium bromide
Tol	toluene
Tris	<i>tris</i> -(hydroxymethyl)aminomethane
TsCl	<i>para</i> -toluenesulfonyl chloride
Tyr	tyrosine
Val	valine
VDW	van der Waals
WHO	World Health Organization
XPS	x-ray photoelectron spectroscopy

Abstract

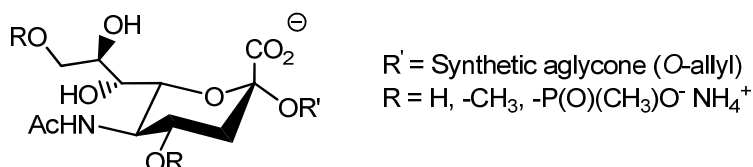
Sialic acids are a group of biologically important 9-carbon sugars which decorate cell surface glycoconjugates, the glycocalyx and thus the cells of higher organisms.

Sialate-*O*-acetylation is a common sialic acid structural modification which has been associated with human disease states (including tumour growth, leukaemia, microbial infection and autoimmune disease). This highly regulated and tissue-specific modification is carried out by sialate-*O*-acetyltransferase (SOAT) and sialate-*O*-acetyltransferase enzymes (SOAT).

Enzymatic processing of sialic acid *O*-acetylation



Sialic acid derivatives for the investigation of viral SOAEs

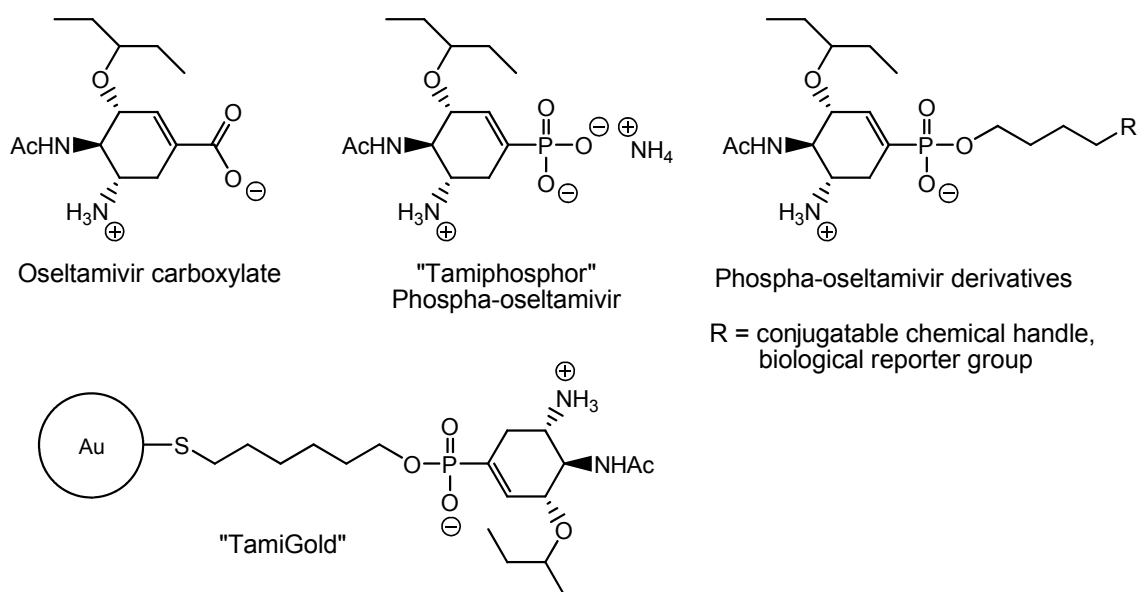


The burgeoning availability of these enzymes make enzyme inhibition studies a viable and worthwhile endeavour, considering that inhibitors of SOAT/SOAE activity may provide interesting tools and potential drug leads for the development of new antiviral compounds or treatments for various disease states.

The synthesis of suitable 4-*O*- and 9-*O*-functionalised sialic acid derivatives has enabled the investigation of 4- and 9-sialate-*O*-acetyltransferase enzymes. Sialic acid derivatives were screened for the inhibition of a set of viral SOAEs and while no inhibition of 4-SOAE could be detected, a 9-*O*-methyl derivative showed inhibition of the recombinant influenza C virus SOAE. The functionalised sialic acid motif thus serves as an initial template for the design and synthesis of future sialic acid derivatives which can be further developed towards SOAT/SOAT inhibition.

Influenza continues to be of major concern to health authorities globally. Tamiflu (oseltamivir), a leading anti-influenza prophylactic, has been employed as a mimetic of the sialic acid “oxocarbenium” intermediate formed during enzymatic α -sialoglycoconjugate hydrolysis, leading to inhibition of virus-bound neuraminidase (NA) enzyme. Phospha-isosteres of oseltamivir provide access to a variety of monoesters which retain the efficacy of the pharmacophore and thus allow the design and synthesis of novel influenza neuraminidase-specific materials, diagnostic tools and NA inhibitors. Phospha-oseltamivir-stabilised gold nanoparticles (“TamiGold”) have been synthesised and preliminary NA inhibition studies with “small TamiGold” show distinct inhibitory activity against influenza virus strains investigated compared to control gold nanoparticles. The binding interaction and optical properties displayed by “large TamiGold” may provide the basis for a colorimetric method of influenza detection and as such a novel prototype influenza sensor. To the best of our knowledge this is the first example of a multivalent approach to influenza virus binding utilising sialylmimetic scaffolds immobilised on a nanoparticle platform which specifically target the NA (instead of the hemagglutinin, HA). The synthesis of phospha-oseltamivir conjugates and their ligation to useful biological reporter groups afford small molecule tools with high affinity and selectivity towards influenza NA. These derivatives can now be applied towards novel multivalent phospha-oseltamivir materials and used as novel diagnostics, independent of existing methods.

Phospha-oseltamivir materials and derivatives as novel diagnostics/tools for influenza NA



Synthesis and inhibitory activity of sialic acid derivatives for targeting viral sialate-*O*-acetyltransferases and sialate-*O*-acetyltransferases

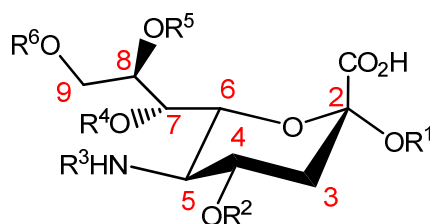
I.1. Introduction

I.1.1. Sialic acids: nature's promiscuous carbohydrates

Sialic acids are a family of approximately fifty derivatives (known currently) of the nine-carbon sugar, neuraminic acid.^{1,2} As part of the nonulosonic family of 9-carbons sugars, they are widely distributed in nature though sialic acids are mostly found in the animal kingdom, particularly amongst higher organisms (including humans).^{1,2}

The major structural feature of these polyhydroxy- α -keto acids is the amino group at the C5 position and the carboxyl group at the C1 position which gives the acid a negative charge in the physiological pH range (pKa 2.2, therefore classed as strong organic acid).³

Different types of sialic acids are common to different organisms in differing amounts⁴ (see figure 1) and since this particular carbohydrate is not stable in the free-amino form, it is often found as an *N*-acylated derivative, with *N*-acetylneuraminic acid (Neu5Ac) and *N*-glycolylneuraminic acid (Neu5Gc) being the most common compounds (see figure 2).⁴ Typically however, Neu5Ac and derivatives thereof tend to be the most common forms of sialic acid expressed in higher organisms.^{1,5,6}



- R¹ = aglycone
- R² = H, COCH₃
- R³ = COCH₃, COCH₂OH, COCH₂COCH₃
- R⁴ = H, COCH₃
- R⁵ = H, COCH₃, CH₃, SO₃H
- R⁶ = H, COCH₃, COCHOHCH₃, PO₃H₂

Figure 1. The substitution pattern of naturally occurring sialic acids. The numbering system of sialic acid derivatives is highlighted (red).

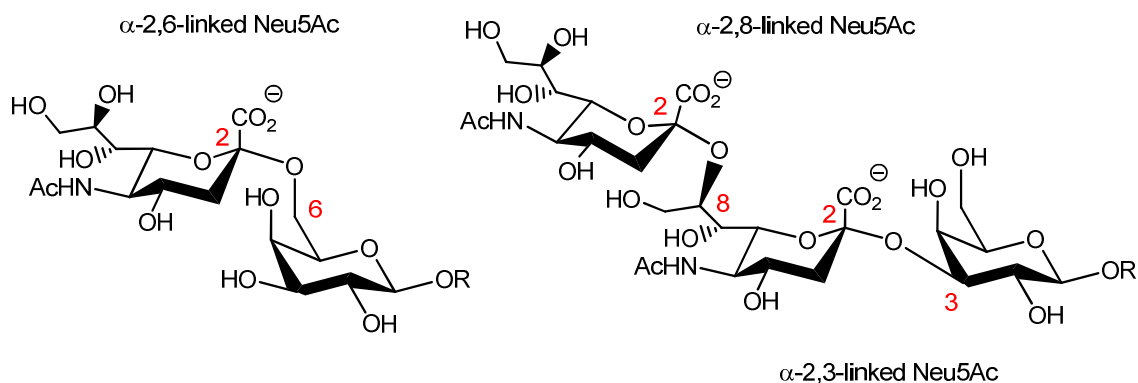


Figure 3. The natural linkages of sialic acid (R = glycoconjugate).

The structural diversity⁵ of sialic acids is reflected by the many biologically important processes in which they play a significant role, often related to cellular and molecular recognition events.^{1,6,13}

For example, the negatively charged nature of these carbohydrates lend themselves to the binding and transport of positively charged molecules and in the attraction/repulsion of cells (for example, erythrocytes in the bloodstream) and molecules (including pharmaceuticals).⁶

As commonly occurring constituents of glycoproteins, sialic acids lead to the high viscosity of mucins of endothelial linings and regulate the conformation of gangliosides (important sialic acid carrying glycoconjugates)¹¹ as well as being vital components of cell membrane supramolecular structures (thus influencing membrane components such as ion channels and hormone receptors).^{6,5} Another discovery is that sialic acid is an essential moiety of mucin as a hydroxyl radical scavenger.¹⁴

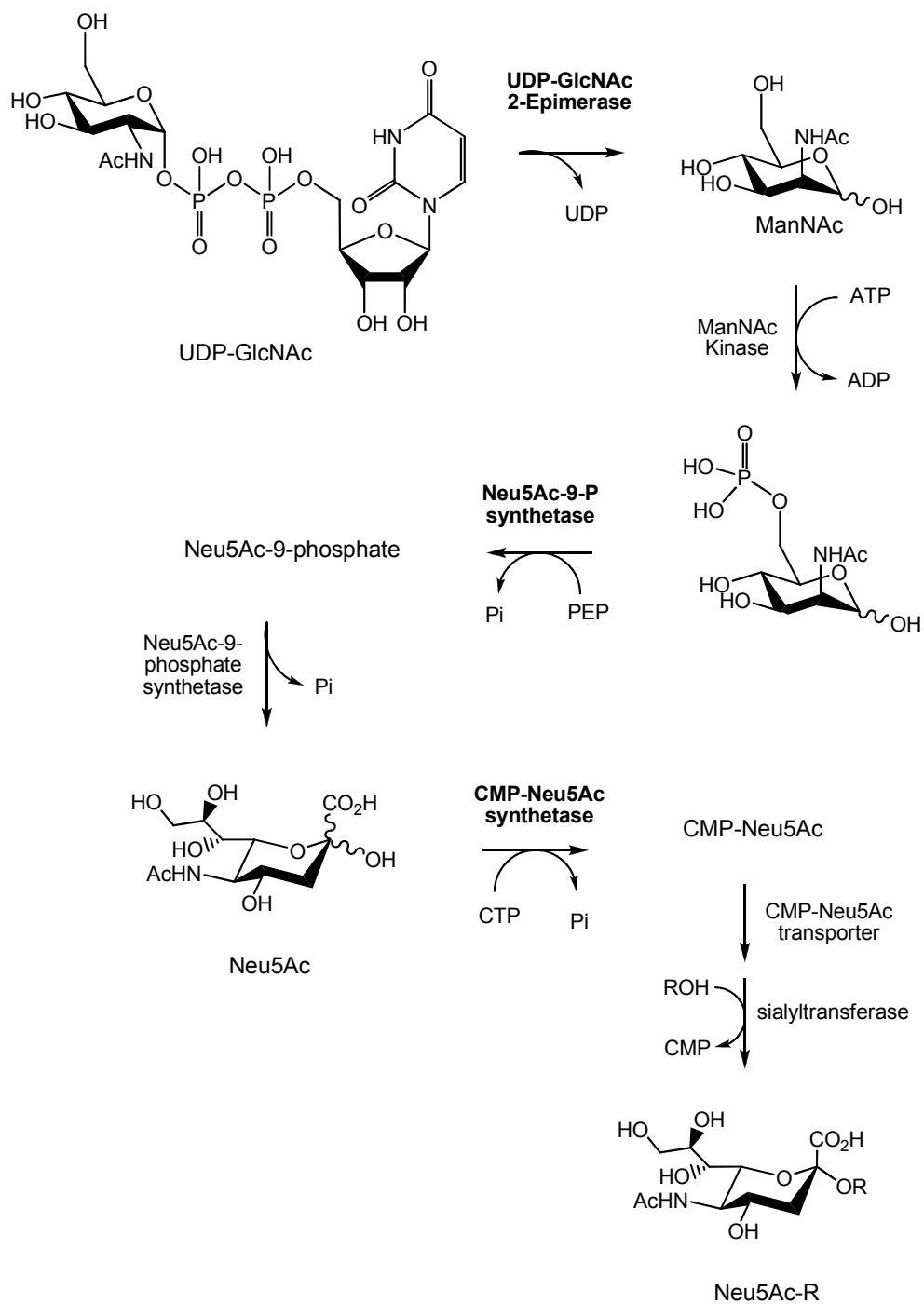
Their exposed position in carbohydrate chains enable sialic acid to act as a protective barrier against glycoprotein degradation by protease enzymes,^{1,13} provides the immune system with a method of distinguishing between self and non-self structures according to their sialic acid pattern,⁶ and in many infection processes, bacterial colonisation can be limited by the sialic acid coat covering the host cell surface.⁶

In contrast however, due to their accessibility and abundance,^{6,9} sialic acids are used by a variety of pathogenic agents such as viruses (for example, influenza), bacteria (for example, *Helicobacter pylori*) and protozoa (for example, *Trypanosoma cruzi*) to bind to host cells via sialic acid-containing receptors.^{6,13}

1.1.1.1. Biosynthesis of sialic acids

The biosynthesis of sialic acid varies slightly between different organisms. The abridged version of Neu5Ac biosynthesis (see scheme 1) begins in the cytosol (of the cell) with the condensation of phosphoenol-pyruvate with *N*-acetylmannosamine-6-phosphate (primarily by Neu5Ac-9-phosphate synthetase though also by sialic acid aldolase to a lesser extent) forming Neu5Ac-phosphate (Neu5AcP). A crucial enzyme in this long biosynthetic pathway is an epimerase, which converts UDP-*N*-acetylglucosamine into the *N*-acetylmannosamine-6-phosphate precursor.^{6,10}

Dephosphorylation of the Neu5AcP results in the free monosaccharide Neu5Ac, which is then activated to the important natural sialyl donor, CMP-Neu5Ac (in the nucleus), which can then be transferred by a range of sialyltransferase enzymes (in the Golgi apparatus) onto nascent glycolipids and glycoproteins.⁶



Scheme 1. The biosynthesis of Neu5Ac from UDP-GlcNAc.

Adapted from; *Chemical Reviews* **2002**, 102, 439-469.

1.1.1.2. Chemical syntheses of sialic acid

Sialic acid has generally been extracted from natural sources, these include the edible birds' nest of the *Collocalia* swift, colominic acid, milk and egg yolk. However, yields are low and the associated purification processes are non-trivial.^{15,16}

The chemical synthesis of sialic acid has been carried out using the traditional Cornforth method (the Aldol reaction of *N*-acetyl-glucosamine and oxaloacetate in basic conditions with subsequent decarboxylation)¹⁷ and other asymmetric synthetic approaches.¹⁸ However, these methodologies suffer from low yields (Cornforth method), material-consuming protecting group strategies and the synthesis of unwanted intermediates or isomers, making direct synthetic methods unattractive both in terms of cost and labour.^{18,15}

The application of enzymatic (incorporating Neu5Ac aldolase or Neu5Ac synthase) and whole-cell based approaches (for example, engineered *E. coli*) towards sialic acid synthesis have improved the availability of sialic acid somewhat, though commercially available sialic acid is still moderately expensive.¹⁵

1.1.2. O-Glycosylation of sialic acids: a specific problem

Sialic acid glycosylation with sialic acid donors is an important step towards the synthesis of naturally occurring sialic acid containing biomolecules and synthetic non-natural sialic acid derivatives for the investigation of sialic acid biology.

The simple appearance of the reaction masks the subtle synthetic difficulty often encountered.^{19,20} Indeed, the formation of sialic acid glycosides (sialosides) is one of the "biggest challenges" in sialic acid chemistry.² In biological systems, enzymatic reactions overcome many of the inherent problems of sialylation reactions which plague chemical synthetic approaches.

The majority of naturally occurring sialic acids are α -ketosidically linked (that is, in the case of sialic acids, the anomeric substituent occupies an equatorial position)²¹ and thus with regards to the particular chair conformation of sialic acids (5C_2), the anomeric substituent is occupying a position which is disfavoured by the stereoelectronic "anomeric effect".^{19,20}

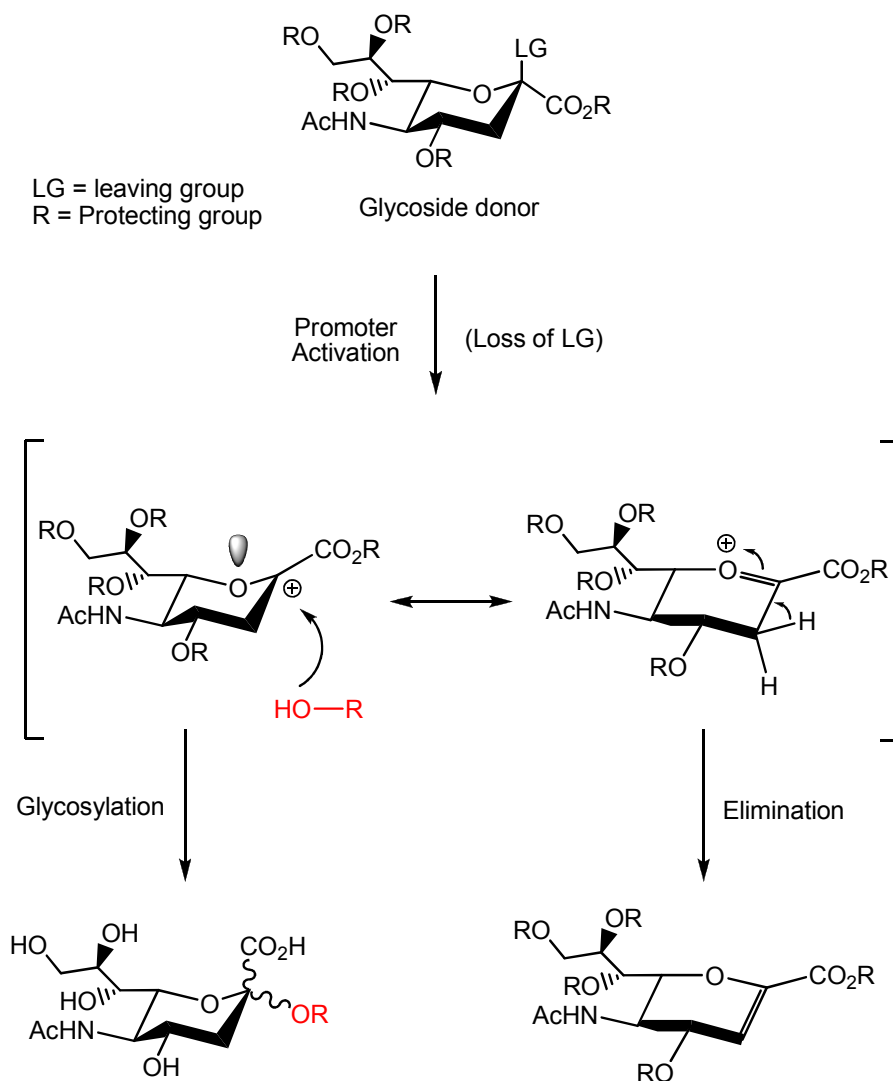
Typical *O*-glycosylation reactions proceed via nucleophilic substitution of a sialyl acceptor (R-OH) upon a suitable sialyl donor (for example, a β -2-chloro derivatives)²² often using some type of reaction promoter, such as a Ag(I) salt (as in standard Koenigs-Knorr glycosylation procedures).^{20,22} The stereoselectivity of such reactions is often problematic due to the difficulty in getting a clean S_N2 process at the anomeric centre, particularly since formation of the oxocarbenium intermediate gives an S_N1 component to the reaction and thus frequently both α and β anomers are formed (see scheme 2).²²

Solvent effects and the nature of the interaction between the metal-promoter and the oxocarbenium intermediate also strongly dictate the stereochemical outcome.²⁰

The selectivity issue of forming solely α -sialosides with sialic acids is even more complicated than in the case of simpler carbohydrates due to a number of structural features of sialic acid which make such selectivity difficult to achieve.^{20,19,21}

The presence of the carboxylate group (C1) at the anomeric carbon, for example, causes the oxocarbenium ion intermediate (formed during the glycosylation reaction) to be unstable due to its electron withdrawing effect and also interferes with the nucleophilic attack of the glycoside acceptor.^{19,21}

The lack of a substituent at the C3 position removes the possibility of neighbouring group participation (for example, ortho-ester formation) in directing the stereochemistry of the glycoside.^{19,20,21} Indeed, coupled with the effects of the carboxylate group, the lack of a C3 substituent also renders sialic acid derivatives susceptible to 2,3-elimination reactions (glycal formation), a prevalent side product.¹⁹ Even the polyhydroxy-glycerol moiety (C7-9) affects sialic acid glycosylation by reducing the reactivity of a sialyl donor through steric effects.²¹



Scheme 2. Heteroatom glycosylation with a sialic acid donor with competing elimination.

Many unusual methods (including exotic sialyl-donors and novel protecting group strategies) applied to the sialylation reaction have been developed in order to improve the synthetic outcome compared to traditional methods.² Very recent examples include the use of a novel *N,N*-diacetylsialyl chloride sialyl donor²³ and highly α -selective sialyl-phosphate donors.²⁴ Though recent trends in the synthesis of sialic acid derivatives tend towards chemoenzymatic and whole-cell approaches to overcome synthetic problems.²

1.1.3. Biological O-Acetylation of sialic acids

The structure and substituents of sialic acid are highly changeable^{1,2} and as such, one important modification of sialic acid is *O*-acetylation at the hydroxy functional groups (C4, C7, C8 and C9 positions) (see figure 4).^{4,11}

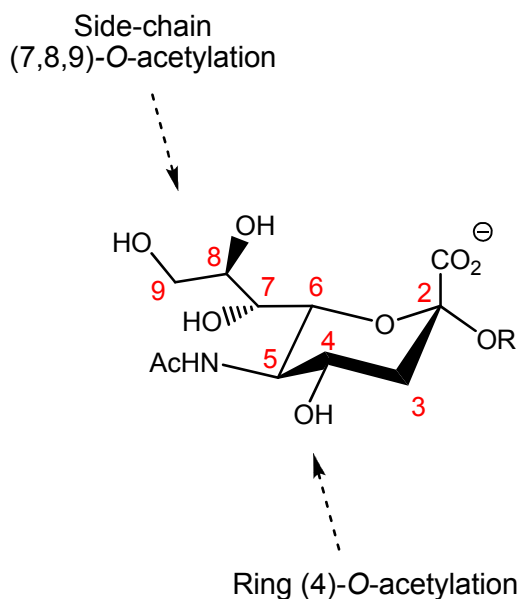


Figure 4. The sites of *O*-acetylation on Neu5Ac

O-Acetylation occurs principally on sialic acids α -2,6-linked to *N*-linked oligosaccharides on glycoproteins, as well as on α -2,3-linked sialic acids on *O*-glycans of certain glycoproteins,⁵ with *N*-acetyl-9-*O*-acetylneuraminic acid (Neu5,9Ac2) being the most common *O*-acetylated sialic acid.^{1,25} It is a highly regulated tissue-specific modification.¹² Chemically, *O*-acetylation introduces a hydrophobic element to the sialic acid moiety, therefore changing the chemical characteristics of the molecule by altering size, net charge, hydrogen bonding and glycoconjugate conformation.⁵

O-Acetylation of acetyl groups from the 7- and 8-OH to the 9-OH have been shown to migrate under physiological conditions. Because of this, it had been considered (until recently)^{26,27} that for *O*-acetylation of the sialic acid side-chain hydroxy functionality, a single enzyme was responsible (*vide infra*) for acetyl transfer to the 7-OH followed by migration to the 8- or 9-OH (enzymatically or non-enzymatically).¹⁰

O-acetylation of sialic acids is apparent in many higher animals and in certain bacteria,¹¹ and plays a key role in modulating various biological processes (see figure 5).^{3,6,11} In fact, *O*-acetylated sialic acids play crucial roles in immune system regulation, organism development, cancer processes and a plethora of other biological and pathophysiological events.^{6,13}

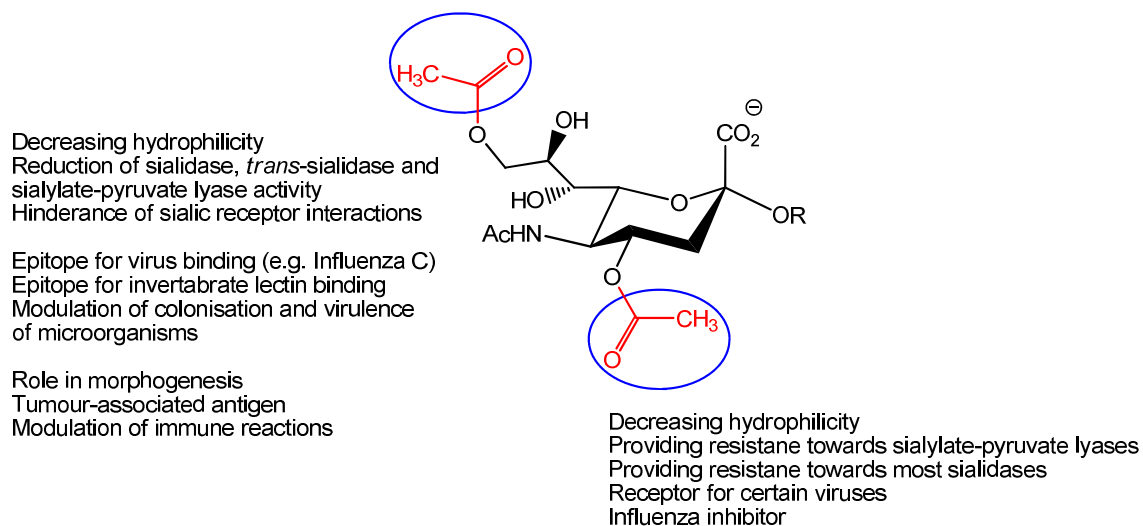


Figure 5. The biological significance of sialate-*O*-acetylation at the 4- and 9-positions. Adapted from; *Glycoconjugate Journal* **2000**, 17, 485-499.

The interest in sialate-*O*-acetylation in recent years has mainly focused upon *O*-acetylation of the sialic acid poly-hydroxy side chain, which seems to be the more widespread acetylation modification, particularly in humans.²⁸

However, *O*-acetylation of the pyranose ring (4-*O*-acetylation) is also common, with 4-*O*-sialic acids being discovered in horses, donkeys, echidnas, guinea pigs, rabbits, rats to name but a few species.²⁸

The effects of *O*-acetylation are wide ranging. For example, *O*-acetylation prevents the degradation of sialylated glycoconjugates by sialidase enzymes (which cleave the glycosidic bond) and other various sialic acid catabolic enzymes such as *trans*-sialidases and sialate-pyruvate-lyases.^{28,16}

Another example is the involvement of the *O*-acetylated GD3 ganglioside (a class of sialic acid-carrying glycoconjugate)¹¹ in cell death (apoptosis).³ Increased *O*-acetylation acts as a regulatory process by reducing the apoptotic effect by accumulating in cell mitochondria.¹¹ Indeed, *O*-acetylation of the GD3 ganglioside has also been implicated in cell growth and differentiation¹¹ and more generally sialic acid *O*-acetylation (specifically Neu5,Ac2 expression) has been implicated in certain types of cancer (human basalioma and melanoma)¹¹ where both under- and over-expression of *O*-acetylated sialic acids are involved in disease progression.^{1,11,25,29}

Neu5,9Ac2 is also aberrantly expressed in ovarian cancer, colorectal carcinoma and childhood acute lymphoblastic leukaemia (ALL).^{11,30}

The *O*-acetylation of sialic acid epitopes on cell surfaces also regulates the activity of specific types of sialic acid recognising proteins, the so-called, siglecs and selectins. The masking of sialic acid epitopes on siglecs such as sialoadhesin (Siglec-1), CD22 (Siglec-2) and Myelin Associated Glycoprotein (MAG) affect their biological roles in the immune

and hematopoietic (blood-cell forming) systems or in the central nervous system (CNS) as their main functions are related to cell signalling and cell-cell interactions.¹³

The same can be said for selectins (for example, L-selectin) where *O*-acetylation disrupts the interaction between the selectins and their recognition determinants (for example, the tetrasaccharides sialyl Lewis^x and sialyl Lewis^a) and thereby disrupting inflammation and immunological processes.¹³

In many cases, *O*-acetylation renders sialic acids useless as molecular targets for foreign pathogens, as the site of action becomes hindered by the acetylated group.⁵

This is particularly true for the binding of influenza A and B viruses, whereby 9-*O*-acetylation of sialic acid inhibits the binding process.¹¹ However, *O*-acetylation may also generate specific sialic acid receptors for certain pathogens, for example, influenza C virus and the mouse hepatitis-C virus (MHV).

1.1.3.1. The processing enzymes of O-acetylated sialic acids

The amount of *O*-acetylated sialic acid expressed in certain tissues appears to be dependent on the interplay between certain sialate-metabolising enzymes, in particular, sialate-*O*-acetyltransferases (SOATs) and sialate-*O*-acetylsterases (SOAEs) (*vide infra*),^{11,26} Along with sialidase enzymes (involved in glycosidic bond cleavage of glycans) SOATs and SOAEs play essential roles in sialic acid metabolism.¹⁶

There are also hypotheses for the involvement of other sialic acid processing enzymes (such as certain sialyltransferases) and other more intricate levels of regulation in *O*-acetylated sialic acid metabolism (discussed below).^{11,12,26,28}

1.1.4. Sialate-O-acetyltransferases (SOATs)

Sialate-*O*-acetyltransferases are the enzymes which transfer an acetyl moiety to one or more hydroxy groups on sialic acid molecules.⁵ There are two main mammalian SOAT systems known (as yet without complete isolation, purification and characterisation) which include guinea pig liver (4-SOAT) and rat liver, bovine submandibular glands and human colon 7(9)-SOAT (*vide infra*).²⁶

The sialate-7(9)- nomenclature stems from the fact that the *O*-Ac moiety can non-enzymatically migrate from the 7-OH to the 8-OH and/or 9-OH (as mentioned) under physiological conditions.¹⁰

SOAT activity is not limited to mammalian systems and is found wherever sialic acid *O*-acetylation metabolism is present.²⁷ Indeed, bacterial SOAT involvement in the *O*-acetylation of polysialic species and their subsequent relationship to pathogenicity is increasing in evidence and as such clinical relevance.²⁶ For example, *Neisseria meningitidis* group B and C cause meningitis and in the case of the mucosal pathogen

Campylobacter jejuni, cause gastroenteritis and in some strains, Guillain-Barre syndrome (GBS), a serious autoimmune degenerative disorder.^{10,27}

It is generally believed that more than one type of SOAT enzyme (predominantly associated with the Golgi membrane)^{10,26} are responsible for catalysing the *O*-acetylation of sialic acid hydroxy moieties with regards to mammalian systems.¹¹ Their classification is dependent on the type of hydroxy group/s being acetylated, that is, whether on the poly-hydroxy side chain or the pyranose ring. As such, these enzymes are referred to as sialate-7(9)- and sialate-4-*O*-acetyltransferases.⁵

Other research into SOAT activity^{26,27} suggests individual sialate-*O*-acetyltransferases for action upon the 7-OH and 9-OH in some cases, potentially leading to a more diverse *O*-acetyltransferase family than previously thought (*vide infra*).

Since *O*-acetylation of the polyhydroxy side chain appears to be the more prevalent Neu5Ac modification in man, 4-*O*-acetylation and interest in the 4-SOATs has been somewhat neglected in comparison to 7(9)-SOATs.²⁸

The identification of 4-OAc expression in man though in small amounts,³¹ and evidence of 4-*O*-acetylation of Neu4Ac5Gc (as part of the ganglioside GM3 implicated in human colon cancer),³¹ appear more widespread than currently presumed and have made 4-SOATs as attractive targets as 7(9)-SOATs.¹⁰

In terms of their substrate specificity, recent investigation of SOATs indicated that typically, larger disialylated substrates such as sialyl-oligosaccharides, sialyllactoses and even gangliosides (sialic acid containing glycosphingolipids, for example GD3) are better substrates than free Neu5Ac and (in turn) Neu5Gc with α -2,6 linkages being preferred to α -2,8 linkages (in the case of 4-SOAT from guinea pig liver).^{11,28}

In fact, there seems to be a remarkable variation of substrate and linkage specificity between SOATs of different origin, for example, between *O*-glycans and *N*-glycans and the type of sialic acid containing biomolecule, for example, gangliosides, glycoproteins, oligosaccharides and free sialic acids.^{10,28}

More generally, SOAT enzymes show mixed tolerances for substrate specificity. Some exhibit high specificity in their mode of action, with *O*-acetyl groups being found among glycolipids and glycoproteins in the same cell type and even between sialic acid residues on the same molecule³² whereas some SOATs (for example, the 4-SOAT from guinea pig liver which strictly esterifies only the 4-OH), have a wider substrate specificity (with various types of free and bound sialic acids) than many other SOATs identified.²⁶

1.1.4.1. Proposed mechanism of O-acetylation: post-sialylation

The mechanism of *O*-acetylation by SOATs has been postulated in the literature over the past decade. Previous studies have concluded that the donor compound for *O*-

acetylation is acetyl coenzyme A (AcCoA) from cytosolic sources³² and that in the majority of the early systems investigated, SOAT substrates have been shown to be glycosidically bound to sialyl-oligosaccharides.²⁷

One hypothesis corresponding to experimental SOAT data is based on a simplified mechanism where side chain *O*-acetylation occurs on a sialic acid residue post-enzymatic sialylation (see figure 6), that is, after the formation of a sialyl-containing glycoprotein in the Golgi apparatus of a cell (from the sialyltransferase substrate CMP-Neu5Ac).¹⁶

The AcCoA donor (transported separately into the Golgi apparatus) is then provided to the SOAT enzyme which then transfers the acetyl moiety to the sialic acid (glycosidically bound) at the 7-OH, after which migration to the 9-OH can occur (refer to figure 7).^{5,16} Supporting evidence from theoretical studies also suggests that the 7-OH is the most likely site of acetylation.³³ It is presumed that the 4-SOAT would follow a similar pattern^{6,16}

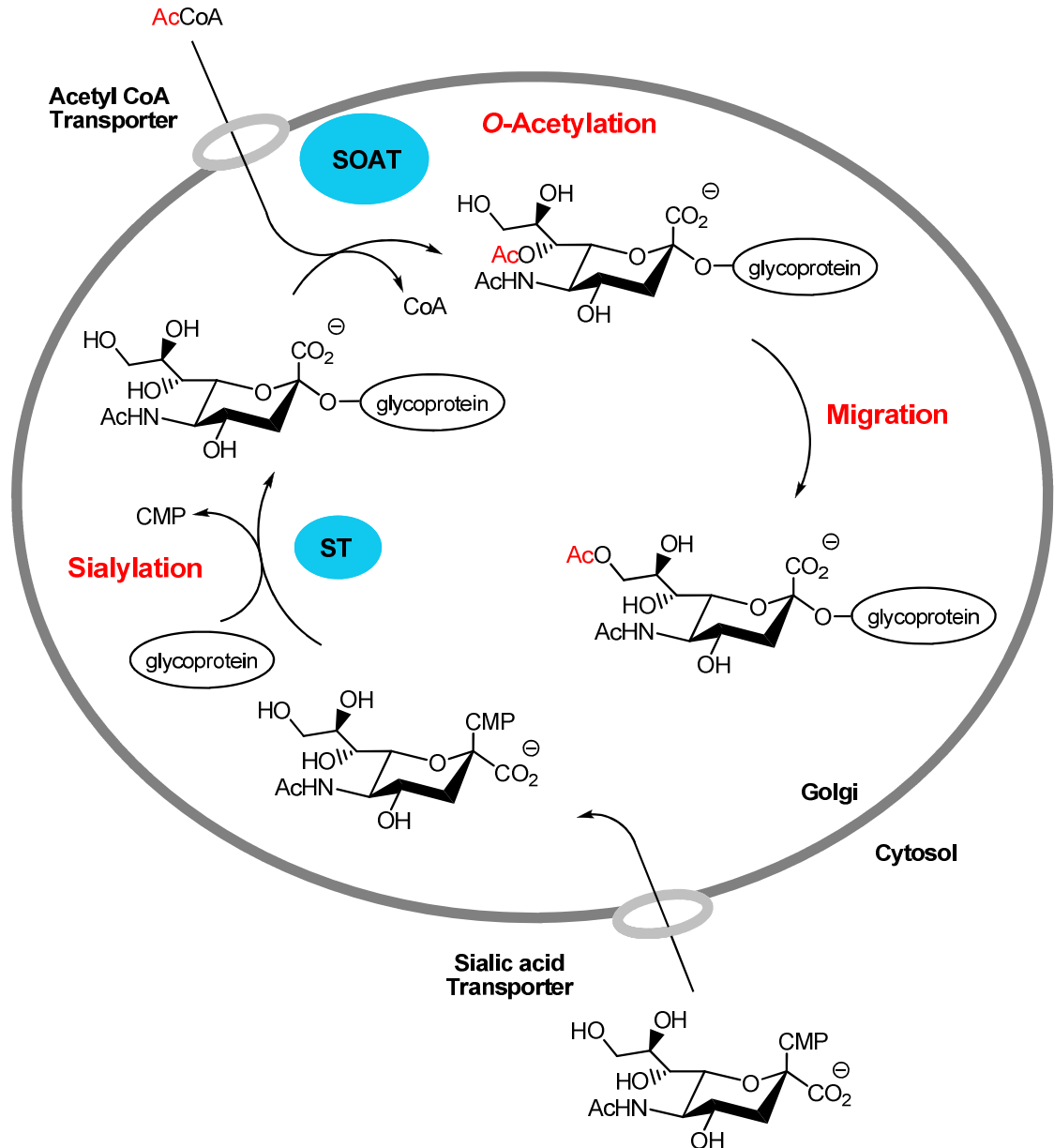


Figure 6. A schematic of the proposed mechanism (post-sialylation) for side-chain *O*-acetylation of sialic acids. ST (sialyltransferase). Adapted from; *Advances in Experimental Medicine and Biology: Metabolism and role of O-acetylated sialic acids*; Molecular Immunology of Complex Carbohydrates 2; Kluwer Academic/Plenum Publishers,; New York, **2001**; Vol. 491.

1.1.4.2. Proposed mechanism of *O*-acetylation: pre-sialylation

Another proposed mechanism is the possibility of *O*-acetylation of sialic acid whilst at the CMP-Neu5Ac (sialyl donor) stage, that is, before sialylation by a sialyltransferase enzyme (see figure 7).¹⁶

O-acetylated CMP-Neu5Ac (in contrast to conflicting studies)³² is considered the most suitable substrate for both 7(9)-SOATs and 4-SOATs (under the experimental conditions used).²⁸ This sheds doubt on the previous mechanism and instead tends to fit a

hypothesis where *O*-acetylation occurs pre-sialylation (at the sialyl donor stage) or as speculated in some scenarios³⁴ via the formation of a protein-complex between the Golgi-bound SOAT, the CMP-Neu5Ac (or Neu5Gc) transporter and the sialyltransferase (transferring the final acetylated product) in the Golgi apparatus, possibly including an interaction with an acetylated sialic acid intermediate. This proposed mechanism is also put forward to describe 4-*O*-acetylation.^{6,11,12,16,28}

This overall reaction pathway proposed is based on a *trans*-membrane reaction consisting of two stages. The first step involves formation of an acetyl intermediate utilising exogenous AcCoA, followed by transfer from the acetyl intermediate to the sialic acid, with the hypothesised intermediate believed to be CMP-Neu5Ac.¹²

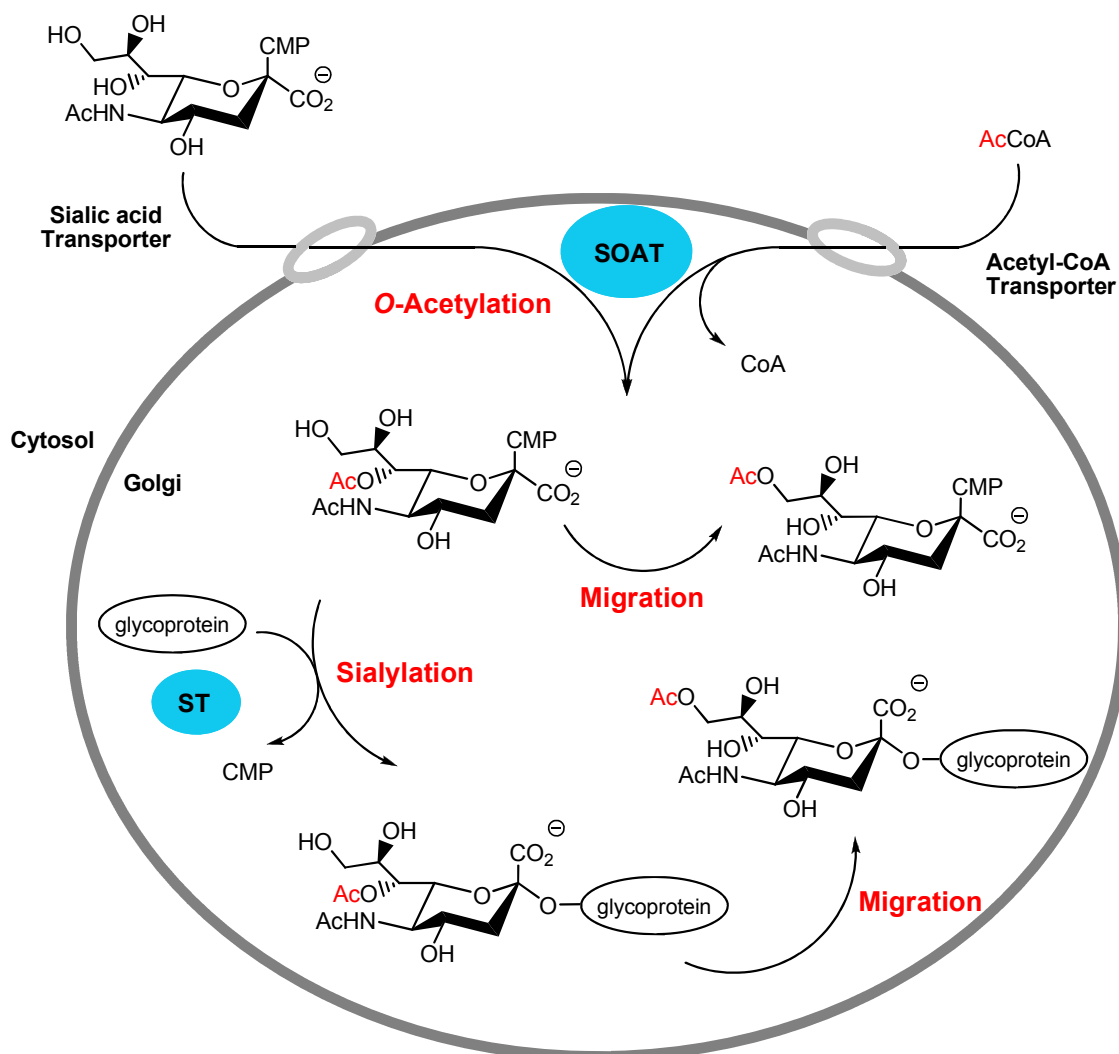


Figure 7. A schematic of the proposed mechanism (pre-sialylation) for side-chain *O*-acetylation of sialic acids via CMP-Neu5Ac precursor. ST (sialyltransferase). Adapted from; *Biological Chemistry* **2004**, 385, 145-152.

Research into the regulation of sialic acid in human colon mucosa indicates that CMP-Neu5Ac and AcCoA transporters are of vital importance for SOAT activity, going so far as to provide evidence for the existence of a sialyltransferase enzyme capable of mediating the transfer of Neu5,9Ac2 to CMP-Neu5,9Ac2 to glycoproteins.¹²

1.1.4.3. Speculation upon the catalytic nature of SOAT enzymes

There appears to be a high level of sequence divergence among enzymes exhibiting SOAT activity and (somewhat speculatively) in the structural characteristics that define SOAT enzymes from various organisms.³⁵ Without mechanistic knowledge of the SOAT reaction (particularly of mammalian systems), the elucidation of the SOAT reaction by various SOAT expressing organisms is difficult.

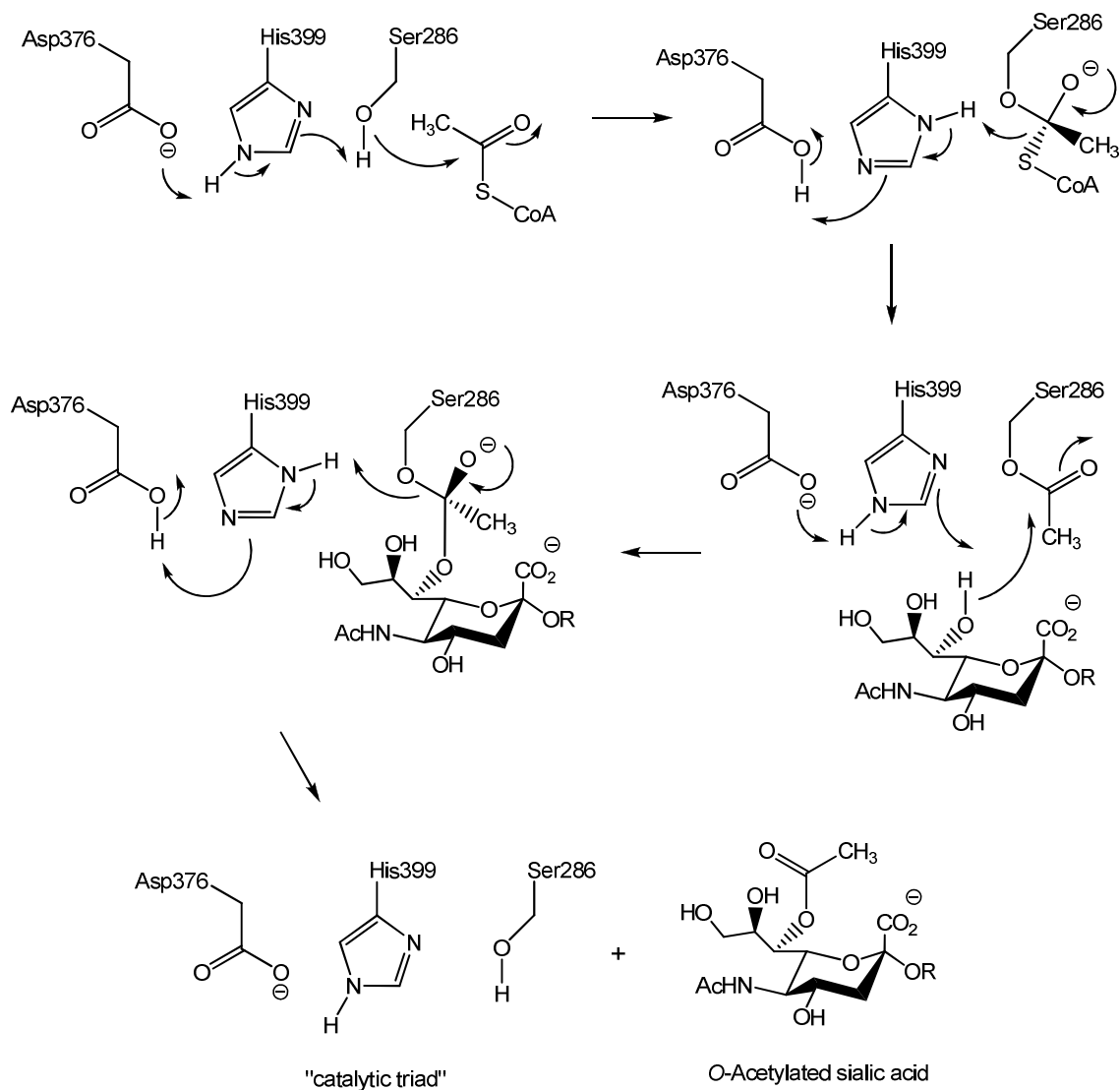
It has been speculated in accordance with the enzyme-complex mechanism that both a hydrolase activity and transferase activity are essential enzymatic steps in the mammalian *O*-acetylation procedure.^{11,34} However, without isolation and characterisation of a fully purified SOAT, this cannot be verified.

Studies on the solubilisation of a 4-SOAT from guinea pig liver uncovered another peculiar aspect of SOAT activity regarding speculation that an unknown co-factor is required for enzyme activity.²⁸

This unknown co-factor (lost during enzyme purification) resulted in loss of SOAT activity, hinting at the possibility of a previously unknown regulatory mechanism for *O*-acetylation.³⁶ The identity of this co-factor is not known, neither is it known if it is required for all SOATs or just certain subtypes.

With regards to bacterial SOATs some structural information can be inferred from studies which identified several bacteria with genes that express SOAT activity. These included; *Escherichia coli* K1 (NeuO),³⁷ *Camphylobacter jejuni* (NeuD),²⁷ group B *streptococci* (NeuD),³⁸ serogroup W-135 and Y *meningococci* (OatWY).³⁵ These SOATs have been shown to belong to the NodL-LacA-CysE family,²⁷ part of the hexapeptide repeat protein family (a large group consisting of general bacterial transferases which are restricted to microorganisms).³⁹

The recent discovery that the bacterial SOAT expressed by *Neisseria meningitidis* serogroup C (OatC) belongs to the same serine hydrolase family (α/β hydrolase enzymes) as viral SOAE enzymes and not the hexapeptide repeat protein family hints at the possibility that the structural characteristics and mechanisms of mammalian SOAT activity are likely to be similar to that of SOAE enzymes (*vide infra*).³⁹ Therefore if mammalian SOAT enzymes express serine hydrolase structural characteristics a characteristic double-displacement (“ping-pong”) mechanism may be expected, utilising a “catalytic triad” of Ser-His-Asp within the enzyme active site (see scheme 3).³⁹



Scheme 3. Proposed reaction mechanism of the OatC-catalyzed *O*-acetylation of the capsular polysaccharide of *Neisseria meningitidis* C (NmC-CPS). The OatC enzyme is a type of bacterial-SOAT and is believed to utilise a double-displacement mechanism for *O*-acetyl hydrolysis.

Studies carried out to date have shown that there are most likely many types of SOAT with specific *O*-acetylation activity independent of the type of organism.^{1,26,27}

For example, the determination of *O*-acetylation at the 7-OH of sialic acids by mammalian SOAT from bovine submandibular glands^{1,26} and the bacterial SOAT expressed by *Neisseria meningitidis* serogroup C (OatC).³⁹

In contrast however, the SOAT from the bacteria *Campylobacter jejuni* was conclusively determined from NMR studies (of the site of *O*-acetylation by the SOAT enzyme) that SOAT activity was specific in this case to the 9-OH and categorically did not involve migration of an acetyl moiety from the 7-OH as indicated by SOATs from other biological sources.^{26,27}

It has even been postulated that in events where the 7-OH is the target, the 7-*O*-acetylated product may have particular advantageous chemical and/or time-limited characteristics necessary for processing/transport of a particular glycoconjugate or for a time-limited biological response.²⁷

Examples of the variety of specificity (in terms of substrate and site of action) and even potential mechanistic discrepancies between SOATs from various organisms hint at the possibility of a wide ranging family of SOATs.^{12,26} Where *O*-acetylation appears to be highly regulated by many different pathways/mechanisms, specific to the organism, tissue type, growth regulation and even specific to sialyltransferase activity.^{28,11,10}

If you also include the example of bacterial group B Streptococcus, where sialic acids are *O*-acetylated before sialic acid activation, that is, pre-CMP-Neu5Ac formation (in contrast to the proposed mechanisms of SOAT activity)²⁷ points toward the conclusion that there are (conceivably) three parallel pathways which have developed for sialate-*O*-acetylation; from free Neu5Ac,⁴⁰ after conversion to the sialyl donor species CMP-Neu5Ac,^{12,36} or after sialyl transfer to glycan.²⁷

This diverse SOAT complexity may in some form may be a reason why SOATs, particularly of eukaryotic origin have evaded identification and purification for so long, with many obstacles preventing the cloning and purification of these SOATs. Particularly their membrane (Golgi) bound nature and the potential co-dependence of other proteins/co-factors for activity.²⁷ If one also adds regulation by substrate specificity and sialic acid linkage preference (that is, α -2,6- vs. α -2,8- vs. α -2,3-), the complexity of SOAT activity increases further.^{12,27,28,11}

1.1.5. Sialate-O-acetylsterases (SOAEs)

O-Acetyl groups are removed from sialic acids in biological processes during the life cycle of the compound. This process is carried out by sialate-*O*-acetylsterase enzymes (SOAE)^{1,25,41}

These SOAEs are found in a variety of organisms and pathogens.⁴² In mammals, there are two forms, one operating in the cytoplasm and the other in the lysosomal compartment of cells, being able to hydrolyse acetyl functionality on glycosidically linked or free sialic acid.^{29,32,41}

An example of the important role SOAE enzymes play in human biology is the regulation (negatively) of the activity of B-cell receptors by masking the CD22 (Siglec-2) binding sites (α -2,6 sialylated glycans) through 9-*O*-acetylation.^{43,44}

A recent study showed the expression of a defective SOAE in patients with auto-immune disease (including Crohn's disease, Sjogren's disease and lupus erythmatosus) led to

enhanced B-cell receptor mediated expression of 9-*O*-acetylated sialic acid. Therefore, since the SOAE function contributes to the maintenance and balance of B-cell activation, a causal link is suggested between loss of SOAE activity and autoimmune disease.⁴⁵

Various bacteria also produce this enzyme to help bacterial colonisation by making sialic acid more susceptible towards microbial sialidase action (enzymes which cleave the glycosidic bond) (refer to figure 8).⁵

Because *O*-acetylated sialic acids are typically considered to be poor substrates of certain sialyltransferases and CMP-sialic acid synthase enzymes, SOAE activity in the cytoplasm is thought to recycle *O*-acetylated sialic acids that have been transported to the cytoplasm (from lysosomes) whereas the other SOAE type, working in the lysosomal compartment of cells, can traverse the endoplasmic reticulum whilst sequestered in its compartments.³²

The main target of SOAE action is most commonly the removal of 9-*O*-acetylated groups from sialic acid, however, some organisms and pathogens make use of 4-*O*-acetylated groups as their specific receptor determinant.^{41,42,46}

However, sialate-*O*-acetylsterases corresponding to deacetylation at the C7 and C8 position have so far not been isolated from any organism or pathogen.²⁵

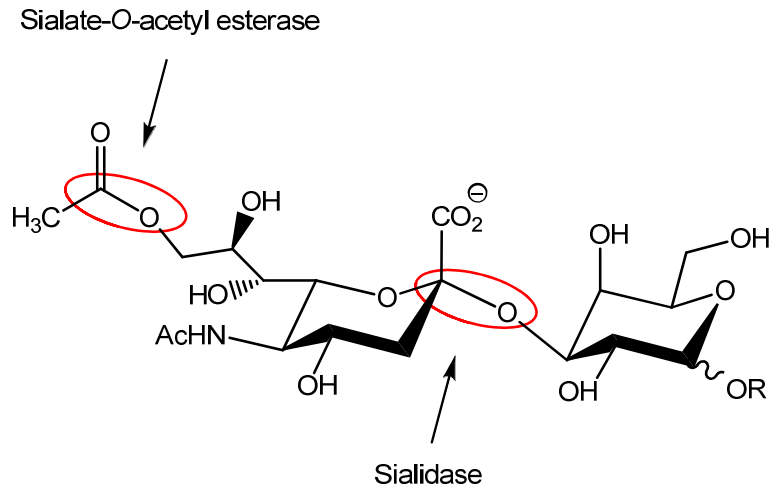


Figure 8. The site of action for sialate-*O*-acetyl esterase in comparison to sialidase “receptor destroying enzymes” using a 9-*O*-acetylated sialylated glycan as a substrate (R = glycoconjugate).

1.1.5.1. Viral and bacterial sialate-*O*-acetyl esterases

Evidence is accumulating that SOAEs are involved in host infection by certain bacterial and viral species.^{26,47} For example, recent studies suggest that bacterial SOAEs regulate *O*-acetyl expression in polysaccharide chains found on the bacterial surface.⁴¹

Several viruses make use of *O*-acetylated sialic acid to bind to target cells because of their accessibility and abundance on various cellular glycoconjugates.^{3,48}

Indeed, certain types of viruses,^{1,25,49} though originally associated with the influenza C virus,⁵⁰ not only bind to these modified *O*-acetylated sialic acids but also concurrently express acetyl esterase activity with the ability to de-*O*-acetylate the sialic acid receptors.^{3,4}

It is because of this that such viral *O*-acetyl esterases are termed “receptor destroying enzymes” (RDE’s) (likened to the sialidase enzymes of the influenza A and B viruses (refer to figure 9),^{3,4} the RDE of influenza C being the archetypal SOAE enzyme (*vide infra*).^{5,51} Influenza C itself is known to cause upper respiratory tract infections and has a risk of producing complications leading to lower-respiratory tract infections in young children.⁴⁹

Viral RDE’s with such *O*-acetyl esterase functionality are known as Hemagglutinin-Esterase (HE) proteins,⁵¹ or as in the case of influenza C, where the viral surface glycoprotein which exhibits this RDE functionality, also plays a part in viral membrane fusion (and subsequently infection),^{50,49} the term Hemagglutinin-Esterase-Fusion (HEF) protein is used.⁴⁸⁻⁵³

The abundance of sialic acid receptors from a viral perspective has a drawback, that is, the reduced infectivity of a viral species due to the high avidity (highly selective) binding nature of virions to non-target cell sialic acid receptors (resulting in non-reversible binding and loss of viral infectivity).^{48,54} Loss of infectivity may result also from newly formed viral progeny becoming bound to *O*-acetylated sialic acid receptors whilst exiting the cell membrane.¹

The RDE function of the viral *O*-acetyl esterases therefore provides an escape ticket for certain viruses, allowing high-affinity yet reversible binding to sialic acid receptor determinants,⁵⁴ whilst also preventing viral aggregate formation, allowing the progeny to maintain the infectivity of the virus.⁵⁵

Initially it seems counter-intuitive that a bifunctional protein carries two conflicting functions, however the balance between the functions appears essential for efficient viral replication.¹⁰

The main sialic acid receptor determinants that SOAEs of certain viruses show specificity for are 9-*O*-acetylated or 4-*O*-acetylated sialic acid substrates (see table 1).^{3,5} Interestingly, all sialic acid *O*-acetyl esterases so far identified cannot hydrolyse 7-*O*-acetylated groups (with the exception of the di-acetylated substrate preferred by bovine torovirus esterase).²⁶ For example, influenza C, BCoV (bovine coronavirus) and certain porcine viruses possess sialate-9-*O*-acetyl esterase (deacetylation at C9), whilst other viruses such as infectious salmon anaemia virus (ISAV), murine hepatitis virus (MHV), puffinosis coronavirus (PV)^{9,56} possess sialate-4-*O*-acetyl esterase (deacetylation at C4).^{42,50,51} BCoV (bovine coronavirus) in particular are of relevance to the livestock industry to the livestock industry through the infection of calves and adult cattle (causing a reduction in productivity).⁴⁹ The closely related human respiratory viruses HCoV-OC43 and HKU1 are also implicated in human illness and disease, for example, they are known to cause gastroenteritis and neurological disorders.^{57,58}

Family	Genus	Species	Substrate
<i>Orthomyxoviridae</i>	Influenza C virus	Influenza C virus	Neu5,9Ac2
	Isavirus	Infectious salmon anemia virus	Neu4,5Ac2
<i>Coronaviridae</i>	Coronavirus	Human coronavirus OC43	Neu5,9Ac2
		Bovine coronavirus	Neu5,9Ac2
		Hemagglutinating encephalomyelitis virus	Neu5,9Ac2
		Mouse hepatitis virus	Neu4,5Ac2
		Puffinosis coronavirus	Neu4,5Ac2
		Sialodacryoadenitis virus	Neu4,5Ac2
		Torovirus	Bovine torovirus
	Porcine torovirus	Neu5,9Ac2	

Table 1. Examples of viruses which utilise sialate-*O*-acetyltransferase enzymes and their respective *O*-acetylated sialic acid substrate. Adapted from; *Glycoconjugate Journal* **2004**, 20, 551-561 and *European Journal of Medicinal Chemistry* **2011**, 46, 2852-2860.

1.1.5.1. HEF of influenza C: the archetypal SOAE

Most data concerning the structural characterisation of viruses that exhibit sialate-*O*-acetyltransferase action relate to the influenza C virus, which shows specific activity for 9-*O*-acetylated substrates (see figure 9) with only a few primary structures of other viral HE proteins known.^{1,50}

The HEF of influenza C consists of three HEF subunits (making the HEF a trimeric protein) which can be further divided into the HEF1 and HEF2 regions. The HEF monomer is divided into three domains; an elongated protein stem involved in membrane fusion, an esterase domain (E) and a receptor binding domain (R) (the R and E domains are in close proximity to each other).⁵⁰

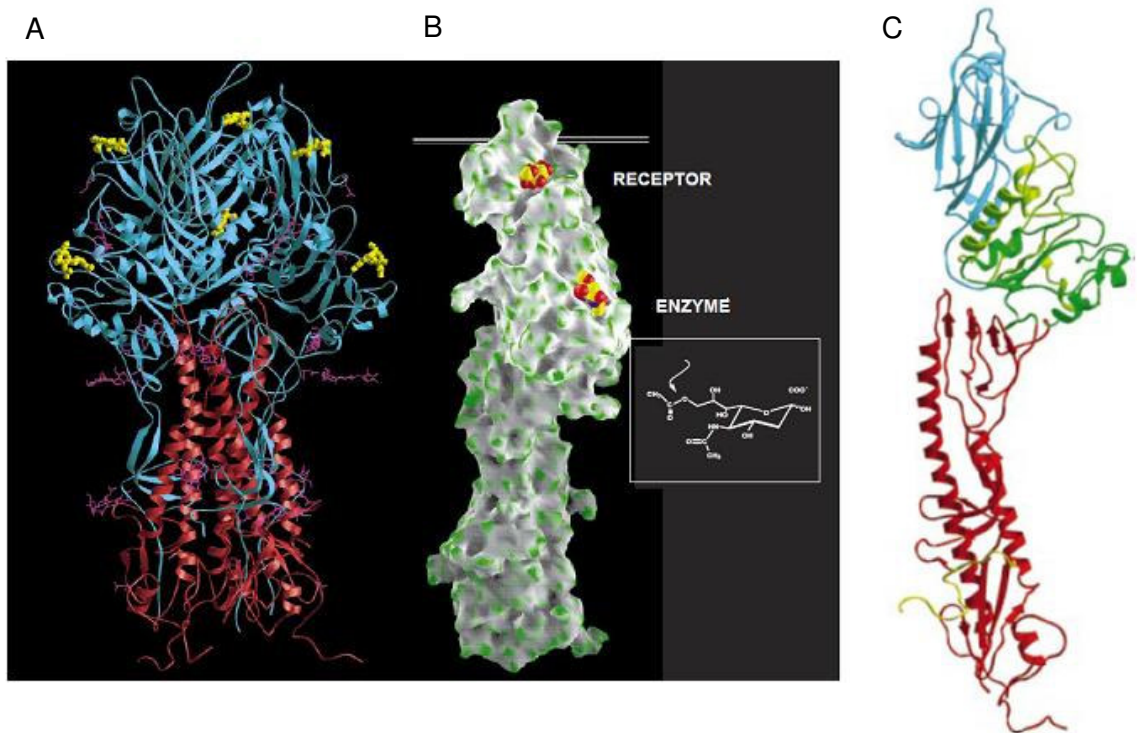


Figure 9. (A) The structure of the influenza C virus HEF trimer showing the HEF1 (blue) and HEF2 (red); (B) a surface representation of the HEF monomer showing the receptor and esterase binding site; (C) a ribbon diagram of the HEF monomer with protein sequence segments coloured by domain (fusion, red; esterase, green; receptor, blue); the fusion peptide is shown in yellow. (Reprinted with permission from Macmillan Publishers Ltd.; *Nature* **1998**, 396, 92-96.)

The elucidation of the Influenza C HEF X-ray crystal structure,^{50,54} revealed that the RDE contains a Ser-Asp-His catalytic triad, with Ser-57 being the main catalytic amino acid residue.⁵⁴ Also, as found in the active sites of more general serine-based esterase and protease enzymes such as chymotrypsin and trypsin,⁴⁶ the SOAE consists of a consensus amino acid motif of Phe-Gly-Asp-Ser.⁵⁴

The HEF1 protein subunit (see figure 9) consists of two distinct areas where the Neu5,9Ac2 substrate can be accommodated.^{48,54} The amino acid residues of Tyr-127, Thr-170 and Gly-172 are involved in binding to Neu5,9Ac2, with the critical interaction between the protein and the 9-*O*-acetyl group being mediated by the hydroxy group of Tyr-227 and Arg-236 (see figure 10).⁵⁰

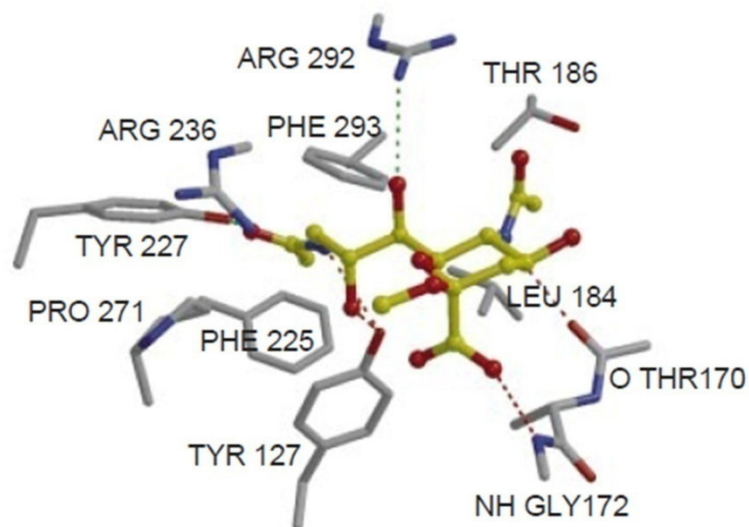


Figure 10. *O*-Acetylated sialic acid determinant bound to the receptor binding site of the influenza C HEF. (Reprinted with permission from Macmillan Publishers Ltd.; *Nature* **1998**, 396, 92-96.)

This essential interaction is also helped by the formation of a non-polar pocket in the binding site to accommodate the acetyl methyl group (formed by Phe-225, Phe-293 and Pro-271).⁵⁰

The esterase (SOAE) active site itself (see figure 11) consists of the residues Ser-57 along with His-355 and Asp-352 (the catalytic triad) which render the essential serine residue more nucleophilic, thus allowing the deacetylation reaction to occur (see scheme 4).

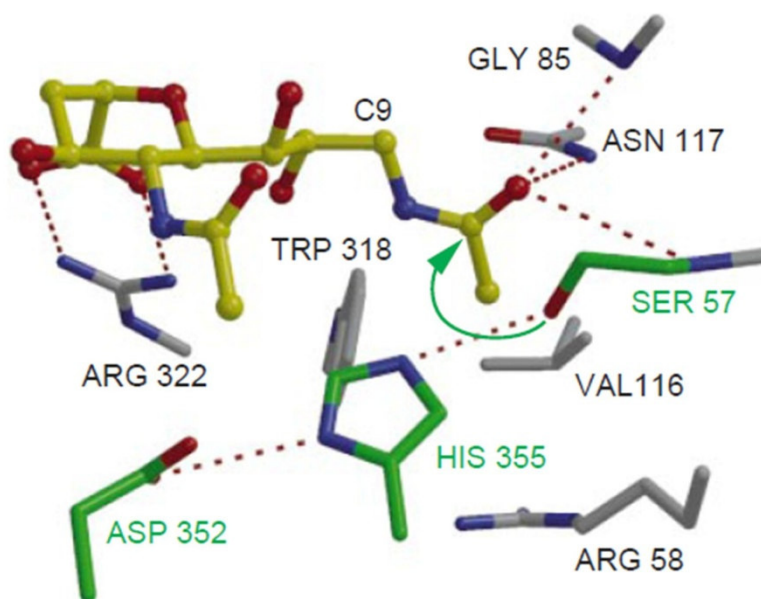
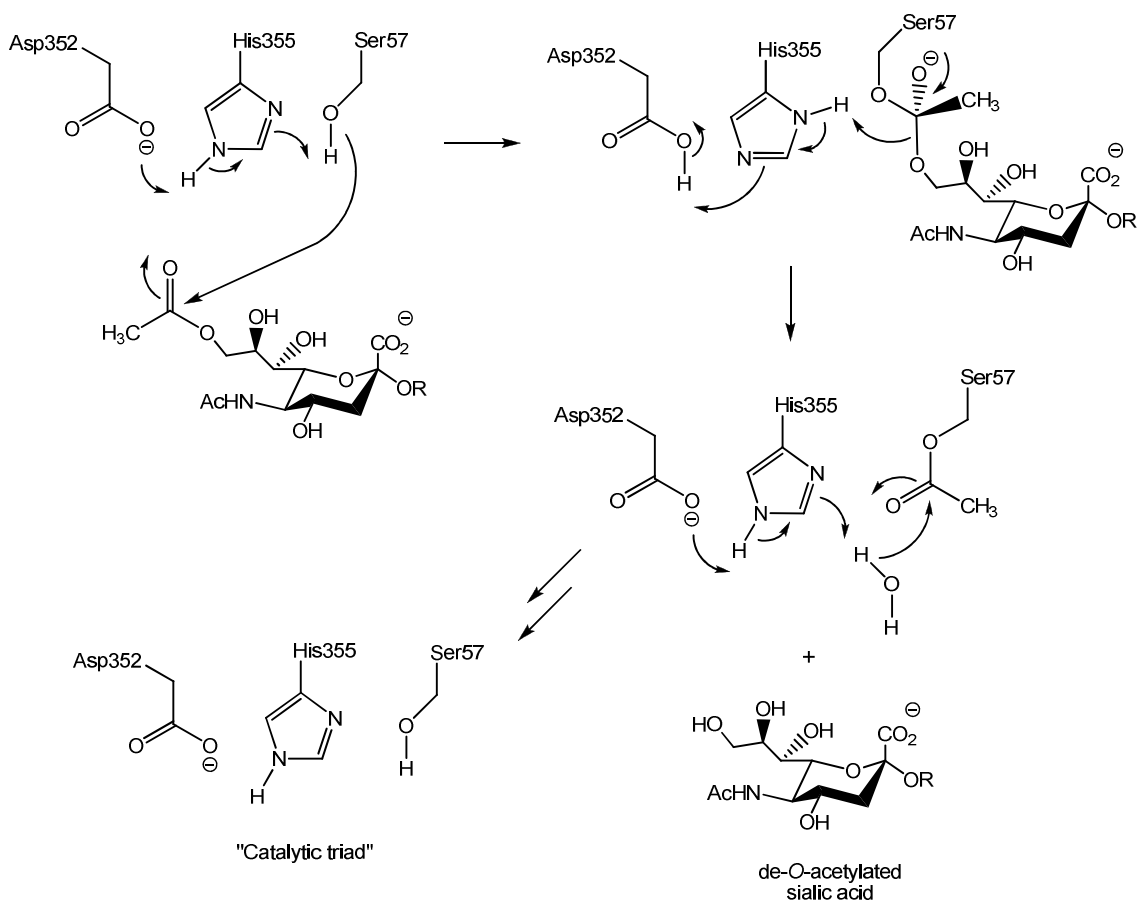


Figure 11. The HEF enzymatic active site, indicating the catalytic triad (green) and the sialic acid substrate (yellow). (Reprinted with permission from Macmillan Publishers Ltd.; *Nature* **1998**, 396, 92-96.)

Other amino acid residues, such as Gly-85 (the NH group), Asn-117 (the side chain) and Ser-57 (the NH group) form an “oxyanion” hole, used for the stabilization of tetrahedral transition state formed during deacetylation reaction,⁴⁶ whereas Arg-322 is thought to contribute to binding by contributing two hydrogen bonds to the sialoside carboxylate group.^{49,54} Substitution (by active mutagenesis) of Ser-57 and His-355 by Ala resulted in reduced esterase activity by approximately 90%, thus confirming the important catalytic role of the residues.⁵⁴



Scheme 4. The mechanism of deacetylation of Neu5,9Ac2 by the SOAE (a serine hydrolase) of the Influenza C HEF.

NMR and molecular modelling studies have elucidated the mechanism and mode of action of *O*-acylesterases (based upon the Influenza-C and BCoV esterase).⁴⁹ These studies concluded that two major pharmacophoric groups are absolutely essential for SOAE activity, the α -configuration of the substrate at the anomeric centre and the presence of the carboxylate group for binding to the Arg-322 residue in the enzyme active site (mentioned above).⁴⁹

Interestingly, molecular modelling results concluded that though a β -configured substrate could theoretically fit in to the enzyme active site, the important carboxylate-Arg-322 interaction is disrupted. As such, the loss of this interaction provides a rationalisation as to why β -configured substrates are not suitable substrates for Influenza-C and coronavirus SOAEs.⁴⁹

This study also highlighted a number of other interesting factors that contribute to a better understanding of viral SOAE activity. Firstly, that the release of the acetate moiety via enzymatic hydrolysis is independent of the nature of the alglycone (determined from NMR experiments with various sialylated species incubated with Influenza-C and BCoV esterase) which is essentially attributed to the low amount of interaction between the

protein surface and the aglycone (determined by modelling studies).⁴⁹ Secondly, the discovery that the Ser-57 catalytic residue is essential for binding and correct substrate orientation, as well as esterase activity. This stems from the fact that upon complexation of a suitable substrate to the enzyme active site, the carbonyl group of the Ser-57 moves from its original position (where it blocks the “oxyanion” hole) to facilitate an internal hydrogen bond with a His-355 ring nitrogen, thus opening up the “oxyanion” hole for substrate binding of the 9-OAc moiety.⁴⁹ Moreover, research has indicated a similar mode of action between both types of viral esterases investigated, supporting the notion of conservation of enzyme active site and mechanistic processes between different SOAE species.⁴⁹

Other studies have also highlighted the conservation of the esterase active sites of HE(F) proteins between viral species compared to the active site of influenza C SOAE.^{46,48,52,59}

Those residues that make up the important “oxyanion” hole are also often conserved in an equivalent manner, for example, in bovine torovirus (BToV) HEs, Gly85 is substituted by Ser.⁵⁴

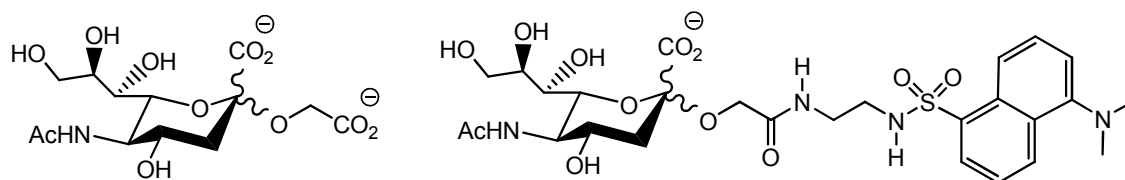
In other respects however, there are differences between HE(F) proteins of viral species. For example, differences in quaternary protein structure between influenza C virus (trimeric) and coronavirus HE proteins (di-sulphide bonded homodimers),^{50,52} differences in protein sequence identity (with the general exception of catalytic active site residues) between the influenza C HEF and other viral HEs (for example, ISAV-HE, TCoV, BCoV) and variation in the receptor binding domain of HEs between and among orthomyxo- and coronaviral HEs.^{50,52,59}

It is obvious that the SOAE family displays varied substrate specificity from exclusive hydrolysis of a single *O*-acetylated derivative to hydrolysing more than one type of *O*-acetylated substrate.⁴¹ For example, the SOAE enzymes of horse liver (which show both 4- and 9-SOAE activity) could potentially be isoenzymes of the same structure.⁴¹ Such structures may reveal similarities and difference between enzyme active sites for SOAEs of varied specificity.

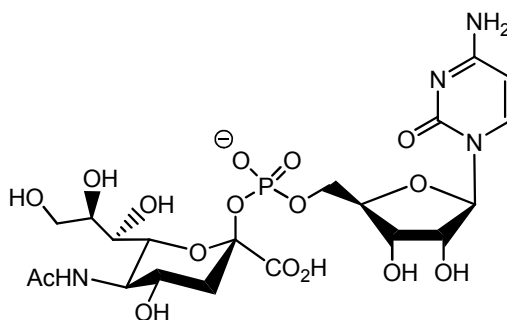
The major hindrance in resolving such arguments is the lack of information regarding mechanism and structure of these SOAE enzymes since there is only limited sequence information available^{48,50} and detailed information regarding structural differences between the two main types of SOAE enzyme (4- and 9-SOAE) is also somewhat limited.

1.1.6. Synthetic sialic acid derivatives towards SOATs

Previous research by Striecher *et al.* has included the development of potential substrates for SOAT enzymes for use as investigative tools for probing enzyme specificity and activity (see figure 12).⁶⁰ These substrates are α - and β -configured (the less common anomer) sialosides and were synthesised using established Koenigs-Knorr methodology.⁶⁰ The sialoside derivatives possessed a negatively charged group in addition to the anomeric carboxylate (speculated for successful enzyme recognition of the important sialyl donor CMP-Neu5Ac) and a fluorescent tag in order to aid conjugate detection during enzyme study. To date, these derivatives have not been used to investigate SOAT activity.



α - / β - sialosides for SOAT investigation



CMP-Neu5Ac

Figure 12. Potential synthetic substrates for SOAT enzymes and the important natural sialyldonor, CMP-*N*-acetylneuraminic acid (CMP-Neu5Ac).

I.2. Results and discussion

I.2.1. Project rationalisation

Being important biological molecules, *O*-acetylated sialic acids and their respective metabolising enzymes (SOAEs and SOATs) are of significant interest and are clear targets for investigation by the glycobiology community at large.

The burgeoning availability of these enzymes make systematic inhibition studies a viable possibility and potentially worthwhile endeavour. This is particularly as information about enzyme structure and properties is currently limited and has only begun to be studied in detail in mammalian systems.²⁶

As mentioned previously, infections relating to the HE activity of certain viral pathogens, though often mild and subclinical can be associated with severe human and animal disease. With the potential of future viral epidemics and the ability of certain viruses to exhibit animal to human transmission (for example, coronaviruses such as SARS),⁶¹ new treatment(s) and diagnostic tools for the investigation of various disease states where *O*-acetylated sialic acids and their metabolising enzymes are implicated would be of interest.

Highly conserved sites in the SOAE domains of HE(F)proteins of viral species compared to the archetypal domain of influenza C SOAE have been observed.^{46,48,50,59}

Therefore, with regards to viral activity the SOAE active site could be considered a logical target for broad-spectrum antivirals against sialate-*O*-acetylsterases of both orthomyxo- and coronaviruses and potential tools for investigation of SOAT enzymes.

I.2.1.1. Inhibitor design

Early studies into the nature of SOAEs have postulated that two pharmacophoric groups are essential for enzyme-substrate interaction. Firstly, the carboxylate group (at C2) is considered essential for esterase action and secondly, the 9-*O*- or 4-*O*-acetylated hydroxy group.^{4,49} The limited studies upon the specificity of SOATs also indicate that these functional groups are also most likely essential recognition components for successful enzyme catalysis.^{39,44,57}

With these structural prerequisites in mind, the synthesis of an α -glycosidically linked sialoside derivative (thus imitating the natural α -ketosidic anomeric linkage)^{4,62} was required and which could be synthetically manipulated to allow preferential access to the 4- and 9-hydroxy groups. The α -aglycone must be tolerated by and be chemically stable to other reactions involved in 4- and 9-hydroxy group functionalisation as well as having the capacity for further functionalisation or immobilisation (see figure 13).

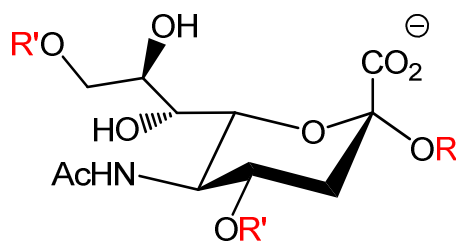


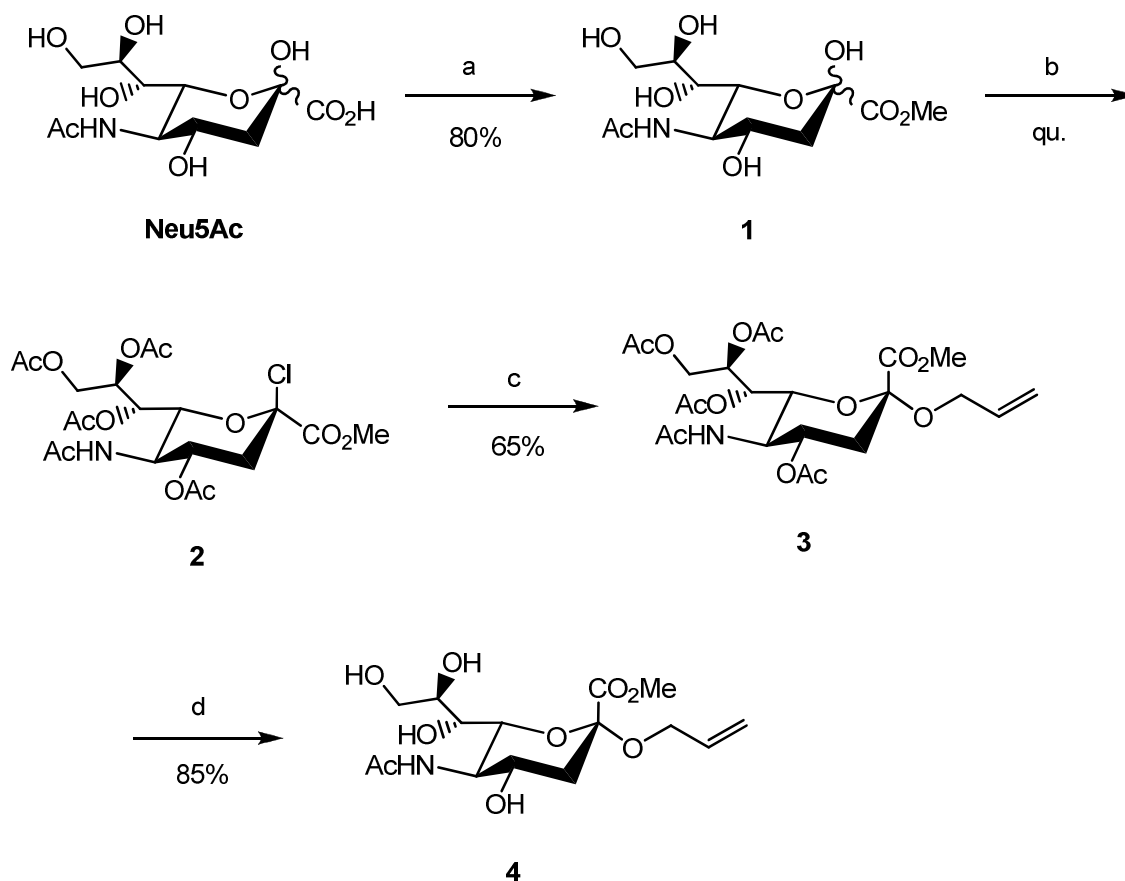
Figure 13. Requirements for potential SOAE and SOAT inhibitors. R = aglycone (with capacity for further modification); R' = inhibitor functionality for 4- or 9-SOAE/SOAT investigation at the 4-OH or 9-OH.

1.2.2. Synthesis of the α -sialoside precursor

The initial step towards α -allyl sialoside **4** is the protection of the carboxy functionality as a methyl ester, by treatment of Neu5Ac with MeOH and Amberlite IR-120 (H⁺) ion-exchange resin to yield compound **1**.

With compound **1** in hand, attention could be turned to forming a sialoside donor. The formation of a 2-chloro- β -sialoside **2** was achieved by the treatment of compound **1** with a solution of AcCl/AcOH and a small volume of MeOH (in order to generate HCl gas) and was isolated and used in subsequent steps without further purification. Other methods of sialoside donor formation are known, however chloro-donors are easily synthesised whilst generally giving good selectivity, usually with α -anomeric sialosides formed in higher ratio²⁰ than β -derivatives, which is synthetically useful for sialoside derivatives required in this project. Koenigs-Knorr sialylation of compound **2** with AgCO₃/AgClO₄ yielded the crude sialylated product with in an approximate 10:1 α : β ratio and gave compound **3** in good yield after purification. Subsequent Zemplen deprotection (NaOMe/MeOH) of compound **3** gave the desired α -allyl sialoside **4**.

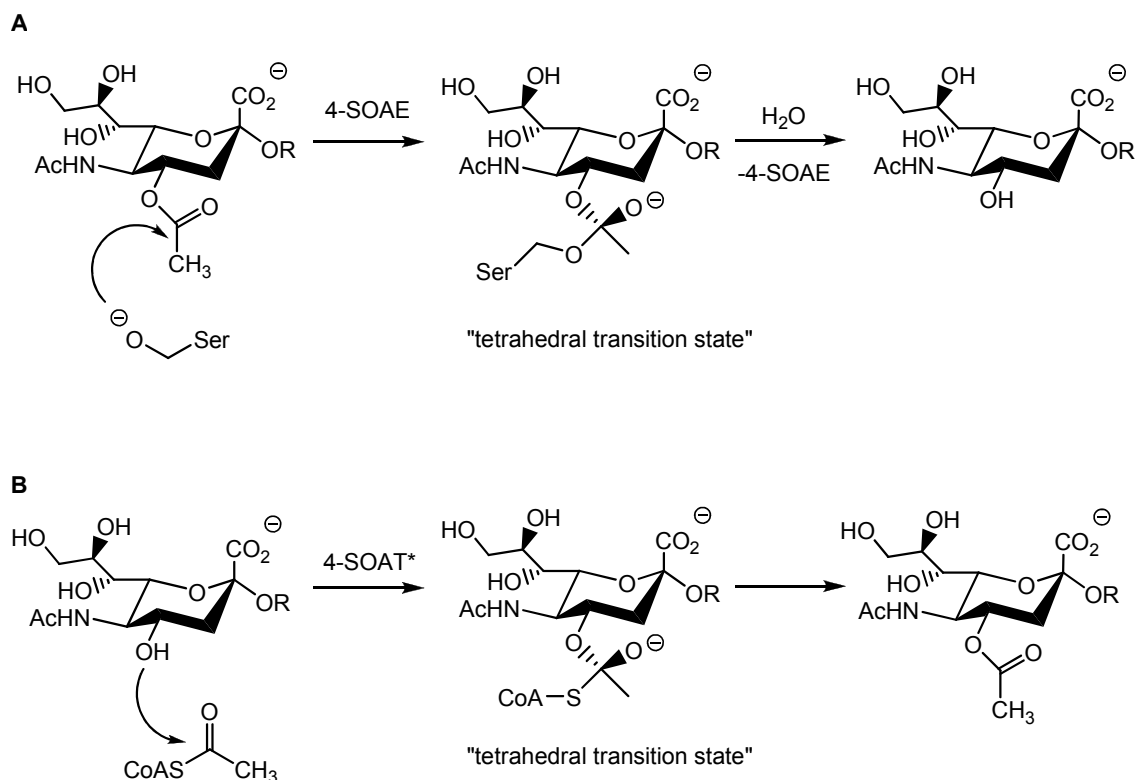
α -Allyl sialoside **4**, derived from per-acetylated precursor **3**, fulfilled the above requirements⁶³ and served as an intermediate for all syntheses towards 4-SOAE and 9-SOAE inhibitors and was conveniently synthesised in 3 steps from commercially available Neu5Ac using a established Koenigs-Knorr methodology (see scheme 5).^{64,63}



Scheme 5. Reagents and conditions; (a) IR-120(H⁺); MeOH; (b) AcCl, MeOH, AcOH, 0 °C; (c) Ag₂CO₃/AgClO₄, allyl alcohol; (d) i. MeOH/NaOMe, ii. Amberlite IR-120 (H⁺).

1.2.3. Potential inhibitors

As mentioned previously, studies on the SOAE active sites revealed the existence of an important carboxylate-stabilising arginine amino-acid residue and the “oxyanion hole” (suspected to stabilise the tetrahedral transition state formed during ester hydrolysis)^{54,49} which are thought to be essential for correct substrate binding and recognition. Speculatively, some of these sites may be present in the active sites of SOAT enzymes. These attributes can be used to the advantage of a potential inhibitor (see scheme 6).



Scheme 6. Potential mechanism for sialate deacetylation by SOAE enzyme (A) and the potential mechanism for sialate acetylation by a SOAT (B) (*using AcCoA as a co-factor or via a speculated “enzyme-complex”). A 4-*O*-acetylated α -sialoside is used as an example substrate.

In order to probe the active sites of both 4-SOAE and 9-SOAE two types of structural modification were introduced at the 4-OH and the 9-OH of sialic acid target compounds **5** to **8** (see Figure 14).

Methylation of the 4-hydroxy group resulting in compound **5** and the 9-OH resulting in compound **7** should provide information regarding the role of the respective hydroxy group as a hydrogen bond donor and moreover would provide information regarding the contribution of hydrophobic interactions to substrate binding within the enzyme active site.

Methylphosphonate groups were introduced as mimetics of the suspected tetrahedral transition state of acetyl hydrolysis. In theory, compounds **6** and **8** could interact with this polar transition state, including the “oxyanion hole”.

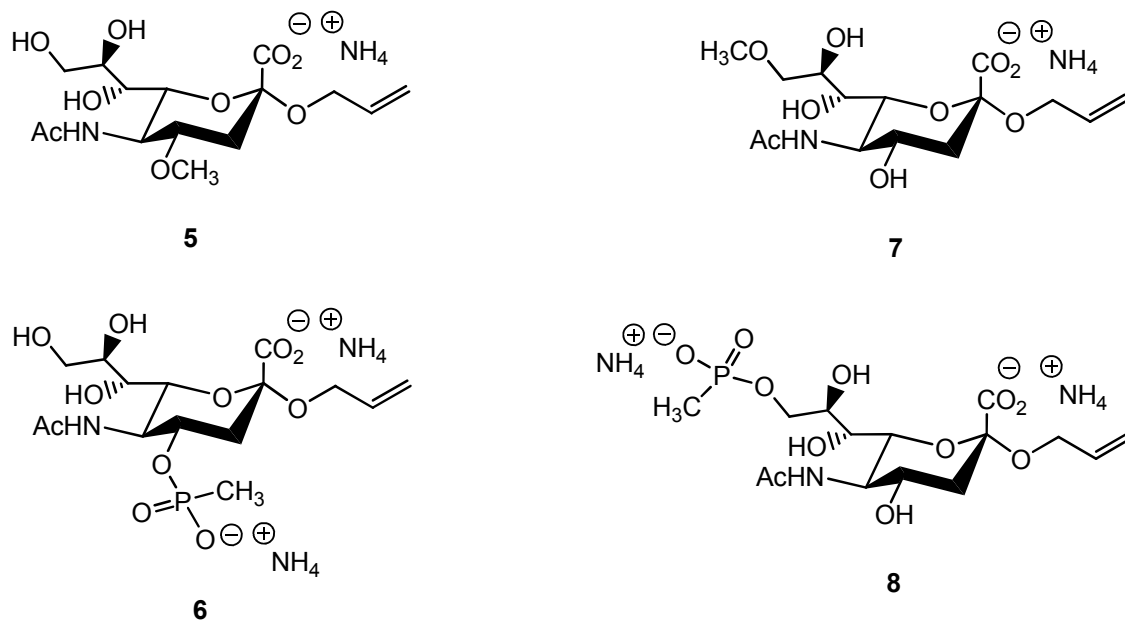
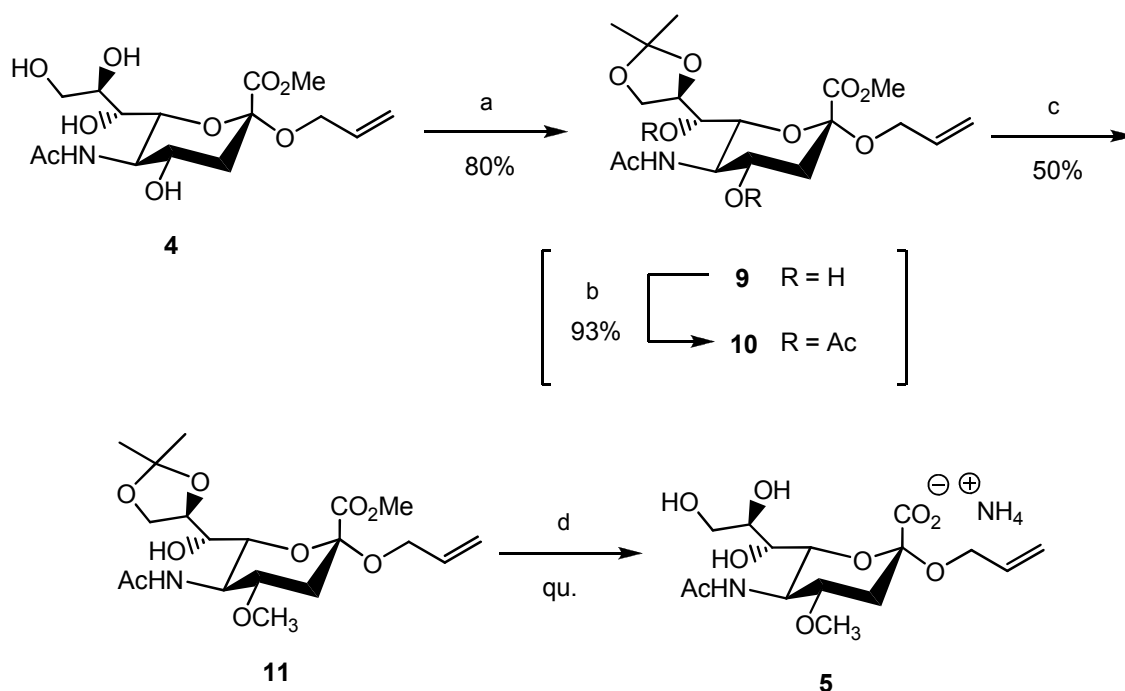


Figure 14. Targeted α -O-allyl sialosides containing methyl- (compounds **5** and **7**) or methylphosphonyl- (compounds **6** and **8**) functionality at the 4- or 9-hydroxy group.

1.2.4. Synthesis of 4-O-modified sialoside derivatives

1.2.4.1. Methylation of the 4-hydroxy group

Selective methylation of the 4-hydroxy group was achieved through the introduction of a cyclic isopropylidene ketal blocking the 8- and 9-hydroxy groups via an acid catalysed reaction of compound **4** with 2,2-dimethoxypropane to yield compound **9** in 85% yield (see scheme 7).



Scheme 7. Reagents and conditions; (a) DMP, acetone, TsOH; (b) pyridine, acetic anhydride; (c) dimethyl sulfate, NaH, acetonitrile, 0 °C; (d) i. 80% AcOH (aq.); ii. NaOH (0.1 M); iii. gel permeation chromatography.

Per-acetylation of compound **9** to give compound **10** aided in the ^1H NMR spectroscopic identification of compound **9**.

Initial methylation attempts of compound **9** with NaH and MeI were unsuccessful. The application of Williamson conditions⁶⁵ using dimethyl sulfate as the alkylating agent produced compound **11** in 50% yield. The reaction was extremely sensitive to the addition of NaH and pushing the reaction towards completion led initially to multiple product formation observed by TLC with the eventual increase in baseline spot concentration. Best results were achieved by adding the NaH in small portions rather than concurrently at the beginning of the reaction. A one-pot deprotection sequence using 80% AcOH to remove the cyclic ketal followed by methyl ester saponification with NaOH (aq.) gave compound **5** after gel permeation chromatography (see scheme 7).

1.2.4.2. Phosphonylation of the 4-hydroxy group

Introduction of a phosphonate moiety at the 4-hydroxy group was attempted with methyl methylphosphonylchloridate⁶⁶ and pyridine. These initial phosphonylation attempts were unsuccessful with compound **4** as the reaction conditions were sufficiently acidic (pH 1-2, indicator paper) to remove the isopropylidene protecting group without successful phosphonylation occurring.

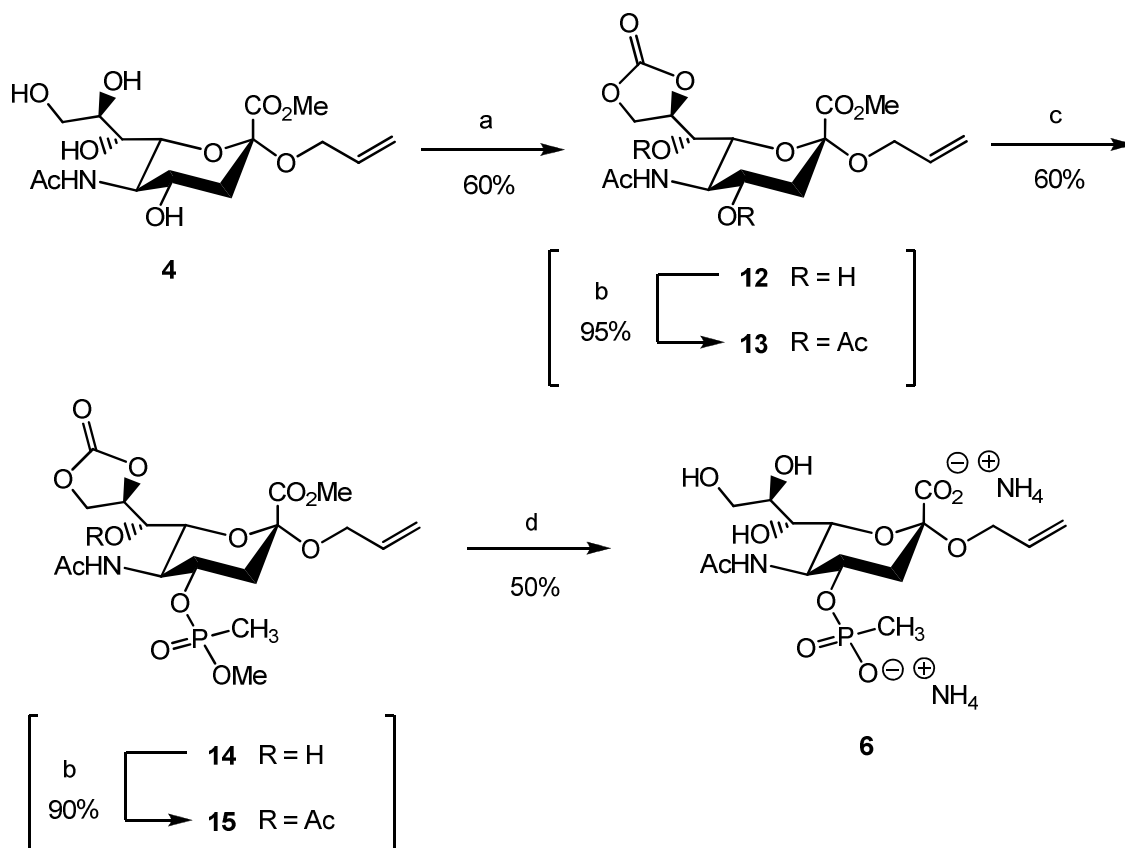
A base labile protecting group strategy was therefore pursued whereby the 8- and 9-hydroxy groups were protected as a cyclic carbonate. The protection step was initially carried out with carbonyl diimidazole using pyridine and pyridine/DCM mixtures but was unsuccessful.

The use of diphosgene and dimethylaminopyridine was successfully implemented to give compound **12** in 60% yield (see scheme 8). Per-acetylation of compound **12** to give compound **13** allowed for the unambiguous ¹H NMR spectroscopic determination of compound **12**.

Introduction of the phosphonate functionality was successfully achieved with methyl methylphosphonylchloridate and DIPEA to give compound **14**.

Compound **14** is obtained as a set of two diastereoisomers due to the chirality of the phosphorous centre. Two sets of resonances are consequently being observed in NMR spectroscopy. In ¹H NMR, the P-CH₃ and P-OCH₃ signals (doublets, respectively) are particularly useful for the determination of the ratio of the diastereoisomers. No attempt to separate the mixture of diastereoisomers has been made as this effect is only transient in the synthesis.

The position of the phosphonylation at the 4-hydroxy group was in part confirmed by acetylation of the remaining hydroxy group at the 7-hydroxy group to give mono-acetylated compound **15** (see scheme 8).



Scheme 8. *Reagents and conditions;* (a) Diphosgene, DMAP, DCM, 0 °C; (b) pyridine, acetic anhydride; (c) P(O)(OCH₃)CH₃Cl, DIPEA, DCM; (d) i. thiophenol, NEt₃, THF; ii. Py/NEt₃/H₂O; iii. gel permeation chromatography.

To yield the target compound **6**, deprotection of the phosphonate monoester and carboxy-methyl ester of compound **14** was initially undertaken using a variety of conditions. These included a reaction with 0.1 M NaOH (aq.), heating compound **14** to reflux in a 1:1:1 mixture of pyridine/triethylamine/H₂O and reaction with TMSBr.⁶⁷ These deprotection strategies were unsuccessful and led to a complex mixture of products which were not isolated or purified further. It is likely that these products were the result of mixed phosphonate ester cleavage under the deprotection conditions used.

Selective deprotection of the phosphonic acid methyl ester **14** using thiophenol and triethylamine⁶⁸ followed by basic hydrolysis of the carboxy-methyl ester with NaOH (aq.) was successfully used to generate target compound **6** after gel permeation chromatography in good yield (50%) (see scheme 8).

1.2.5. Synthesis of 9-O-modified sialoside derivatives

1.2.5.1. Methylation of the 9-hydroxyl group

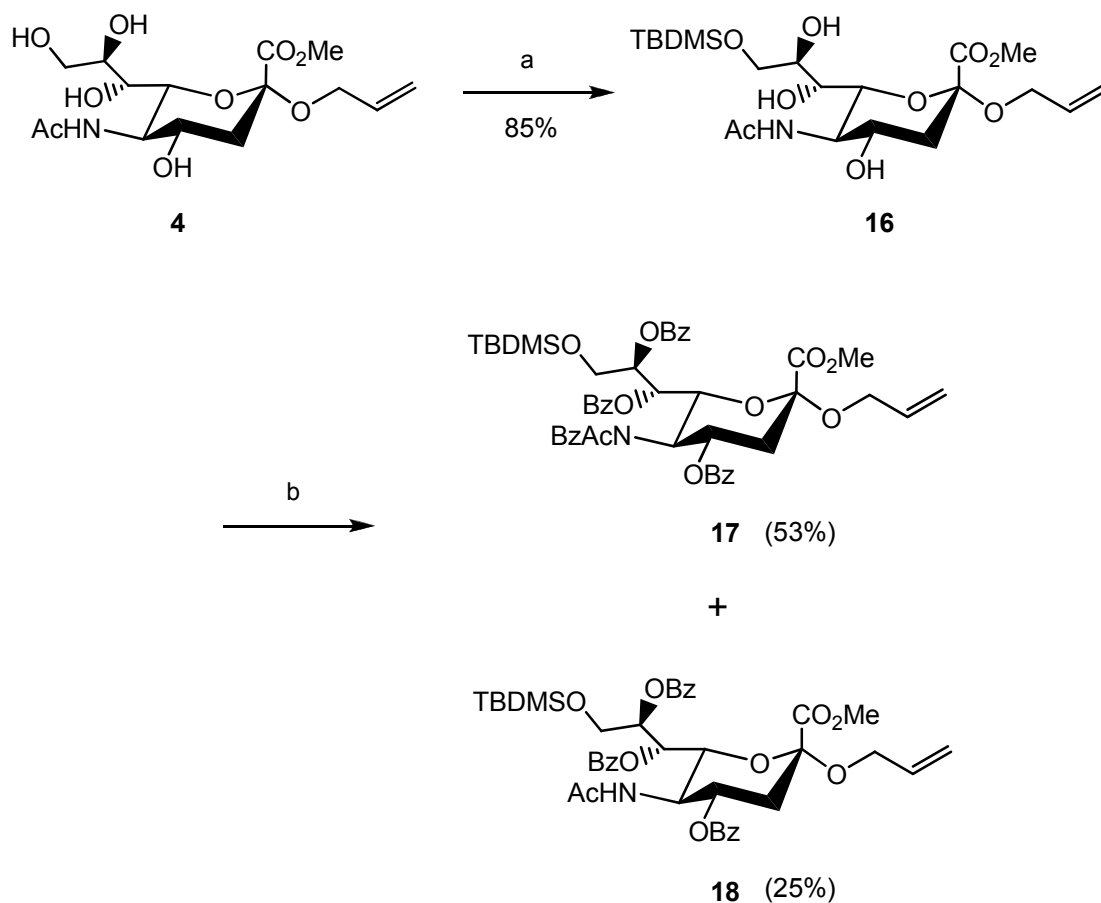
The methylation of the 9-hydroxy group using α -allyl sialoside **4** was initially approached using identical Williamson conditions as described in the synthesis of compound **11**, with the rationalisation that the slightly greater chemical reactivity of the primary 9-hydroxy group would allow for regioselective alkylation (over the secondary 4-, 7- and 8-hydroxy groups). The lack of protecting group manipulations would therefore lead to a more expedient synthesis of target compound **7**.

This approach was unsuccessful and generated a complex mixture of products which could not be purified successfully. Indeed, alkylation reactions at the glycerol side chains of sialic acid derivatives are known to be problematic.⁶⁹

In order to overcome this selectivity problem, syntheses were undertaken towards a suitably protected sialic acid derivative with access to the 9-hydroxy group for further functional group manipulation.

Compound **4** was protected selectively at the 9-hydroxy group as a silyl ether with TBDMSCl to give compound **16** (see scheme 9). Brief synthetic investigations were made into protecting the free 7- and 8-hydroxy groups with a cyclic ketal and as a cyclic carbonate in a similar vein to the intermediates towards target compounds **7** and **8**. This was however unsuccessful. It is speculated that the glycerol side chain may be too sterically demanding for this protection strategy, although carbonate protection of trans-diols is known in the literature.⁷⁰

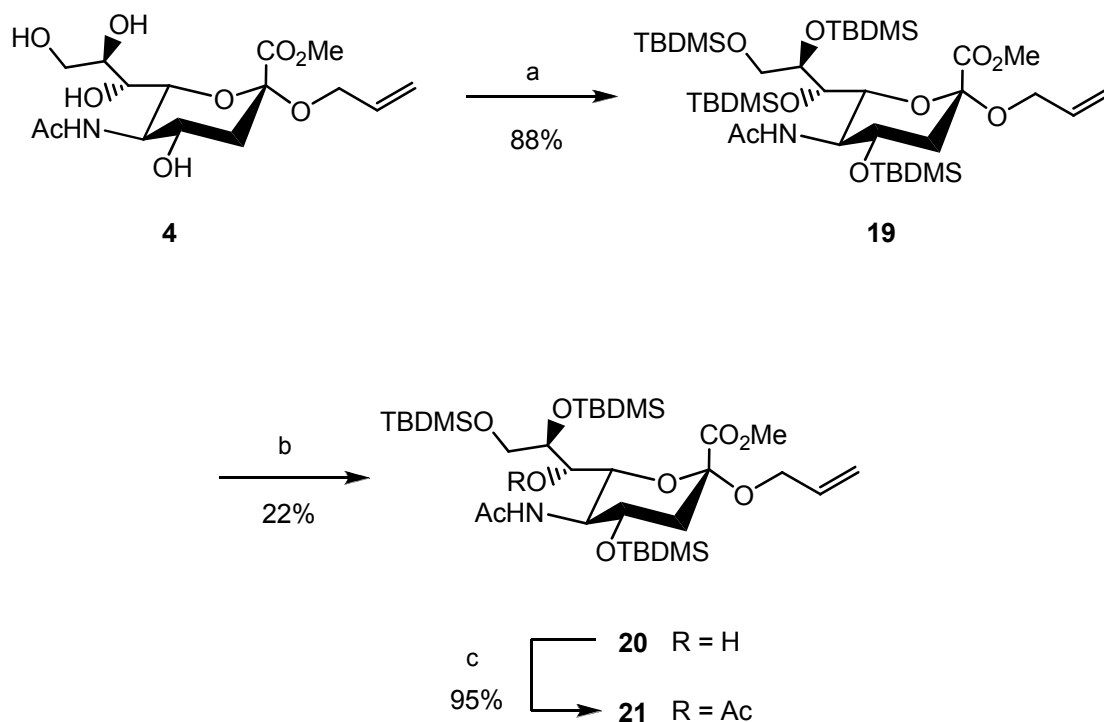
In a second strategy, compound **4** was per-benzoylated at the free 4-, 7- and 8-hydroxy groups, thus maintaining an orthogonal deprotection relationship between the protecting group patterns and avoiding the potential migratory issues often seen with acetyl protecting group strategies with sialic acid derivatives (see scheme 9).²



Scheme 9. Reagents and conditions; (a) TBDMSO, imidazole, DMF, 0 °C; (b) BzCl, DMAP, pyridine.

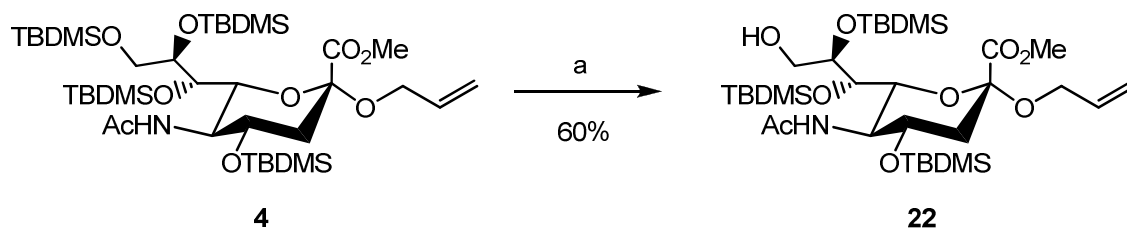
Compound **18** was obtained, but was not the major product formed in the reaction. Pushing the reaction towards product formation led to the formation of the unwanted side product **17** and as such this route was abandoned.

A third strategy towards selective access to the 9-hydroxy group involved the per-silylation of α -allyl sialoside **4** to give compound **19**, followed by selective deprotection of the primary 9-OTBDMS using catalytic amounts of carbon tetrabromide under photolytic conditions (see scheme 10).⁷¹



Scheme 10. Reagents and conditions; (a) TBDMSOTf, lutidine, DCM; (b) $h\nu$ (30 minutes), MeOH, CBr_4 ; (c) pyridine, acetic anhydride.

Initial studies using per-silylated compound **19** led to the formation of compound **20** and α -allyl sialoside **4** (via complete deprotection of compound **19**). It is suggested that the use of sodium hydrogen carbonate (NaHCO_3 (s)) in the work-up procedure led to the migration of a silyl protecting group to the 9-hydroxy group. Silyl group migration is known to occur under basic conditions.⁷⁰ Acetylation of the remaining free hydroxy group gave compound **21** (and led to the unambiguous spectroscopic identification of compound **20**) (see scheme 10). After the optimisation of reaction conditions (type and power of UV source, time of UV exposure and concentration of CBr_4) and work-up procedure (direct evaporation and subsequent chromatographic purification instead of basic NaHCO_3 work-up), compound **22** was synthesised in good yield of 60% (see scheme 11).

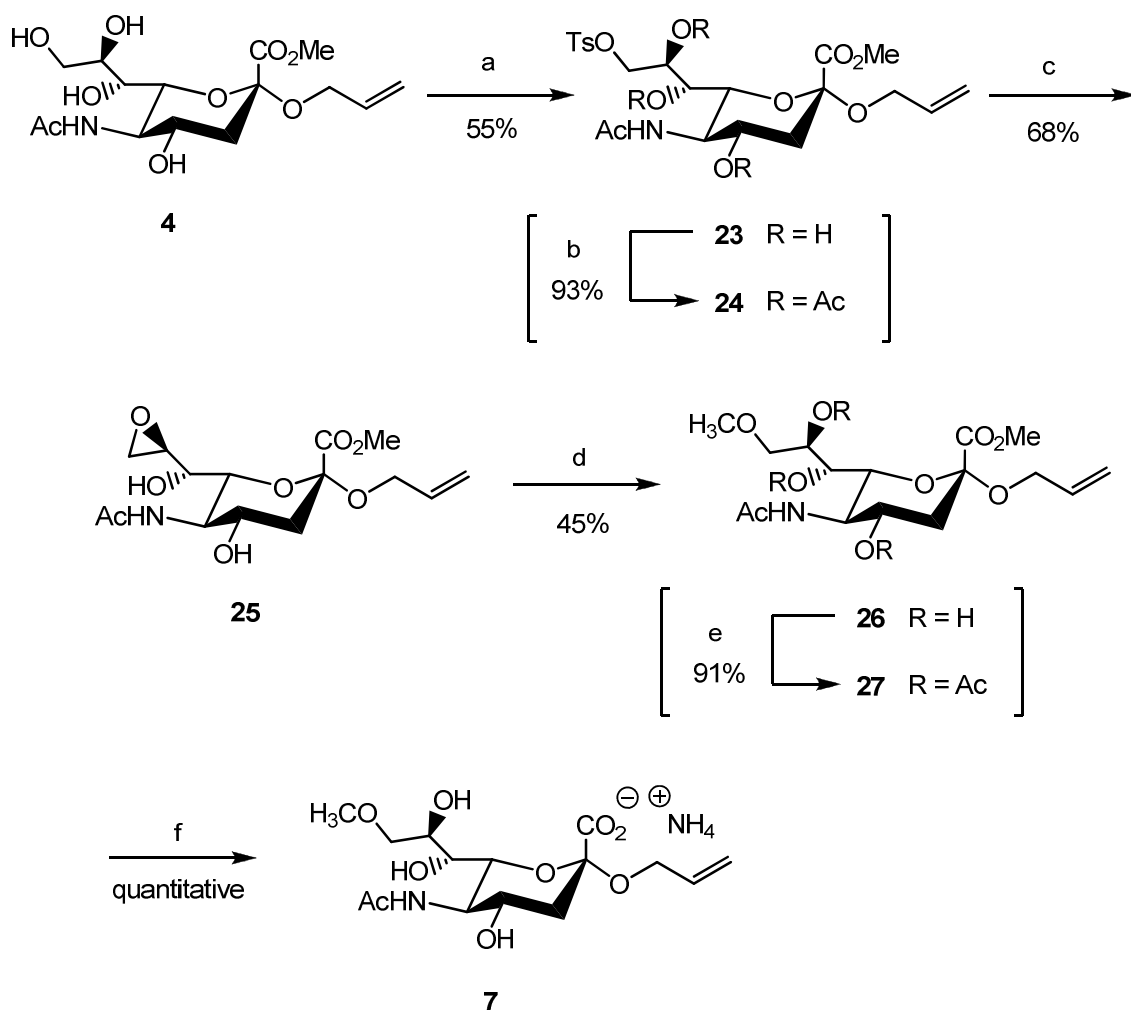


Scheme 11. Reagents and conditions; (a) $h\nu$ (10 minutes), MeOH, CBr_4 .

With compound **22** in hand methylation of the 9-hydroxy group was attempted but was unsuccessful using Williamson conditions.

The difficulties encountered when synthesising sialic acid derivatives with selective access to the 9-hydroxy group led to chemistry being conducted where possible directly from α -allyl sialoside **4** using limited protecting group manipulation in order to avoid time consuming and costly protection strategies.

Therefore an alternative route to target compound **7** was used whereby α -allyl sialoside **4** was tosylated with TsCl to give compound **23** (see scheme 12).⁷²



Scheme 12. Reagents and conditions; (a) TsCl, Pyridine, 0 °C; (b) pyridine, acetic anhydride; (c) NaOMe, MeOH; (d) Amberlite IR-120 (H⁺), MeOH; (e) pyridine, acetic anhydride; (f) i. NaOH (0.05M), dioxane; ii. gel permeation chromatography.

As with previous examples, per-acetylation of tosylated compound **23** gave compound **24** and was used in the spectroscopic identification of tosylated compound **23**. Compound **23** was subsequently treated with sodium methoxide in MeOH to give the 8,9-epoxide **25**.⁶⁹

Methylation at the 9-hydroxy group in moderate yield (45%) was achieved through the acid-mediated opening of the epoxide in MeOH with Amberlite ion-exchange resin (H⁺). Though the reaction can be carried out with compound **25** after purification, slightly better results were obtained when the methylation reaction was carried out directly *in situ* from the tosylated precursor **23**.

The per-acetylation of compound **26** generated compound **27** which aided in the unambiguous characterisation of compound **26**. Saponification of the methyl ester with

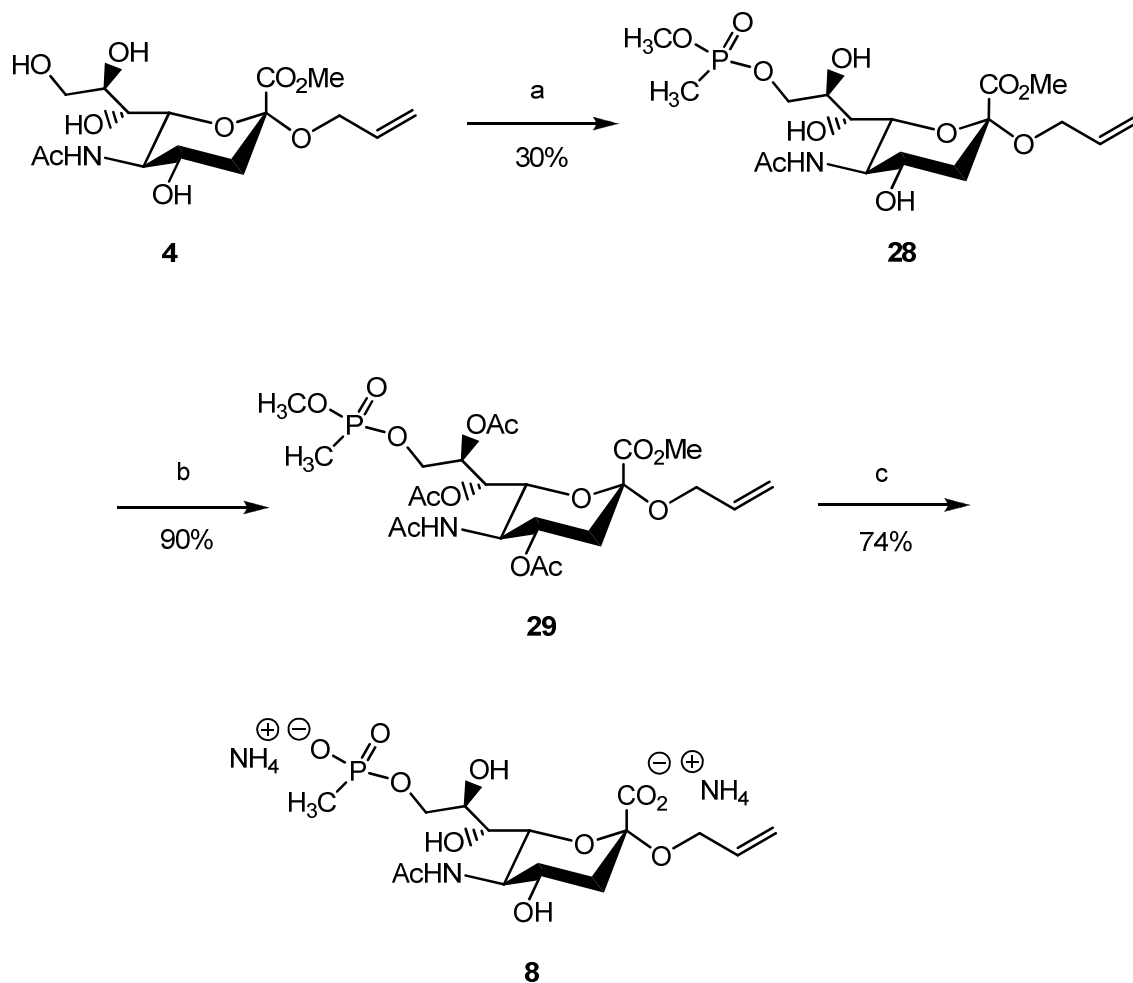
NaOH (aq.) and subsequent gel permeation chromatography yielded the desired target compound **7** (see scheme 12).

1.2.5.2. Phosphonylation of the 9-hydroxy group

As in the synthesis of compound **14**, the introduction of the phosphonate functionality at the 9-hydroxy group was attempted with compound **22** using methyl methylphosphonylchloridate and DIPEA. It was hoped that the use of a sialic acid derivative with access to the 9-hydroxy would prevent the formation of unwanted per-phosphonylated side products. However, the reaction was unsuccessful and did not lead to the formation of the desired 9-*O*-phosphonylated compound.

With the failure of the protecting group strategy to produce the desired phosphonylated intermediate, the direct reaction of α -allyl sialoside **4** with methyl methylphosphonylchloridate and DIPEA was successful and produced regioselectively compound **28** in moderate yield (30%) (see scheme 13). This route slightly improves the synthetic methodology towards 9-*O*-phosphonylated compounds (with particular reference to the ease of purification in comparison to alternative methods).⁷³

As described for compound **14**, the chiral phosphorous centre allows the formation of two diastereoisomers and consequently two signal sets in NMR. In contrast to the former, this was however not observed in the case of compound **28** with the most likely explanation being that only one isomer has been formed.



Scheme 13. Reagents and conditions; (a) $\text{P(O)(OCH}_3\text{)CH}_3\text{Cl}$, DIPEA, DCM, $-15\text{ }^\circ\text{C}$; (b) pyridine, acetic anhydride; (c) i. thiophenol, NEt₃, THF; ii. Py/NEt₃/H₂O; iii. gel permeation chromatography.

However, selectivity of phosphonylation becomes problematic when driving the reaction towards completion, as a diphosphonylated derivative (at the 8- and 9-hydroxy groups) appears to be formed (determined from ^1H NMR and ^1H - ^{31}P SED-NMR) but was not fully characterised. Starting material α -allyl sialoside **4** can (in part) be retained if the reaction is stopped before this point is reached.

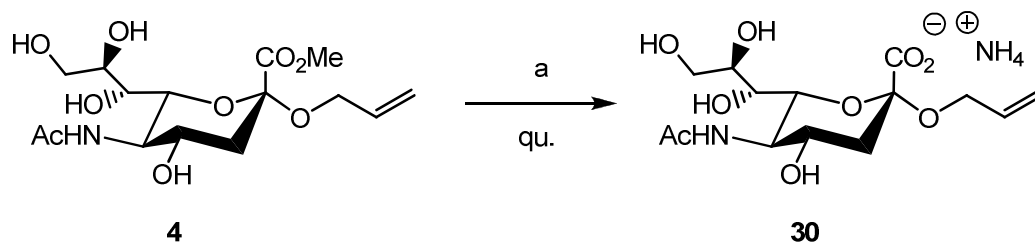
The selective deprotection of the phosphonate ester of compound **28** with thiophenol and triethylamine, followed by basic saponification of the methyl carboxylate ester (NaOH (aq.)) gave both the 9-O-methylphosphonate compound **8** and also the 8-O-methylphosphonate.

Per-acetylation and ^1H NMR analysis of the products formed after treatment with thiophenol/triethylamine indicated the presence of two products believed to be the 8- and 9-methylphosphonic acid intermediates (which then subsequently undergo basic hydrolysis). It is therefore speculated that the 8-hydroxy group is participating in an intramolecular transfer from the 9-hydroxy group to the 8-hydroxy group, leading to the

formation of the unwanted 8-*O*-methylphosphonate derivative, the exact mechanism of which has not been elucidated.

In order to avoid the formation of the unwanted 8-*O*-methylphosphonate, synthesis of compound **28** was followed by per-*O*-acetylation to give compound **29** (see scheme 13). The deprotection of compound **29** was then carried out with thiophenol and triethylamine, followed by basic saponification of the methyl carboxylate ester to give target compound **8** after gel permeation chromatography in 20% yield (4 steps).

As a control sample for SOAE or SOAT studies, compound **30** was synthesised from compound **4** by basic saponification and subsequent gel permeation chromatography (see scheme 14).



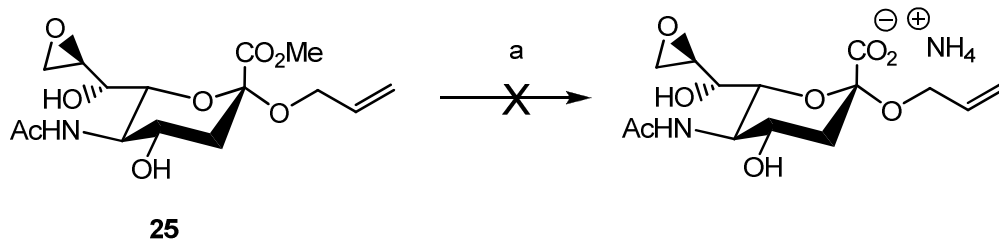
Scheme 14. Reagents and conditions; (a) i. NaOH (0.1 M); ii. gel permeation chromatography.

1.2.6. Towards non-competitive (irreversible) inhibitors

Synthesis was carried out towards an irreversible (suicide) inhibitor of SOAE and SOAT enzymes based upon the 8,9-epoxide compound **25**. For SOAE/SOAT studies, irreversible inhibitors need reactive functionality at the 9-hydroxy group (or 4-hydroxy group) in order to covalently bind to the nucleophilic serine residue in the active site. By trapping out the active site residues, more detailed information regarding enzyme structure and properties can be obtained.

The epoxide functionality is a potentially viable covalent (suicide) inhibitor for SOAE and SOAT applications but only if the methyl carboxylate ester of precursor **25** can be removed (thus providing access to the biologically active compound) without disturbing the chemical stability of the epoxide (see scheme 15).

Enzymatic cleavage of the carboxy-methyl ester of compound **25** appeared to be a selective method for methyl ester deprotection without compromising the 8,9-epoxide functionality. PLE (porcine liver esterase) has been shown to successfully cleave methyl carboxylate esters and *O*-acetylated moieties in good to moderate yields, and importantly, even in the presence of epoxide functionality.⁷⁴⁻⁷⁶



Scheme 15. Proposed enzymatic conversion of compound **25** to the deprotected epoxide, a potential suicide (non-competitive) inhibitor. (a) PLE (porcine liver esterase).

Initial studies involved assessing the stability of both the 8,9-epoxide derivative **25** and the α -O-allyl sialoside **4** in both D₂O and enzyme buffer solution (PBS, pH 8, made with D₂O). Both the α -O-allyl sialoside **4** and the 8,9-epoxide derivative **25** showed no sign of hydrolysis (or epoxide opening with respect to compound **25**).

The PLE reactions proved unsuccessful in hydrolysing the carboxy-methyl ester at all under any of the reaction conditions tested (see appendix 1: PLE experiments, page 259).

NMR analysis and TLC studies indicated that after prolonged reaction times the compounds tested failed to show any evidence of ester hydrolysis.

Enzymatic reactions with the methyl-ester sialoside **1** also showed no ester hydrolysis, indicating that enzymatic activity is independent of carboxy-functional group conformation at the anomeric centre.

Inactivity of the PLE enzyme was eliminated as a reason for unsuccessful enzymatic hydrolysis reactions by incubating 3-cyclohexene-1-carboxylic acid methyl ester with PLE to hydrolyse the substrate to the respective 3-cyclohexene-1-carboxylic acid. ¹H NMR indicated the hydrolysis was successful. (see appendix 1: PLE experiments, page 259).⁷⁷ The lack of PLE enzymatic activity with the α -O-allyl sialoside derivatives indicates that the α -O-allyl sialoside derivatives are not suitable PLE substrates. Other methods, both enzymatic and chemical have to be considered as alternatives for future work.

1.2.7. Investigation of the inhibitory activity against viral SOAEs

With target compounds **5** to **8** now available, a study was embarked upon in collaboration with Prof. R. Vlasak (Salzburg, Austria) with the aim of finding competitive inhibition with viral SOAE expressing enzymes.⁷⁸

Inhibition of the SOAE activity of three viruses, influenza C virus (INF-C),^{50,49} bovine coronavirus (BCoV)^{79, 80} and mouse hepatitis virus strain S (MHV-S).^{42,81} and of two

chimeric recombinant viral haemagglutinin esterases, from influenza C/Cal/78 virus (HE12-GFP) and sialodacryoadenitis virus (SDAV-HE) was investigated.³

The effectiveness of inhibitor compounds **7** and **8** toward the 9-SOAE activities of HE12-GFP, INFC virus and BCoV and of compounds **5** and **6** toward the 4-SOAE activity of SDAV-HE and MHV-S were determined by an pNPA assay. This assay is based upon the spectrophotometric detection of the enzymatic hydrolysis product of *p*-nitrophenyl acetate in the presence of an esterase inhibitor. Inhibition of esterase activity results in a reduction in the amount of hydrolysis product and as such a reduction in hydrolysis product detected, which is related to the concentration of esterase inhibitor present.⁷⁸

1.2.7.1. Results and discussion of inhibition studies

The sialate-*O*-acetylerases were incubated with the sialoside target compounds **5** to **8** (and negative control compound **30**) of different concentrations.

The 9-*O*-methyl sialoside compound **7** has been identified as a potential inhibitor of HE12-GFP. The 9-*O*-methyl sialoside compound **7** inhibited SOAE approximately 86% of SOAE activity (at 5mM concentration) (see table 2).⁷⁸ The negative control, α -allyl sialoside **30** did not show detectable inhibition of any of the enzymes investigated.

The inhibitory effect of compound **7** was reduced when using whole influenza C virus particles suggesting that the differing conformation of the haemagglutinin protein between HE12-GFP (monomeric) and whole virus particles (trimeric) may have an impact on the binding and therefore the inhibitory effect of compound **7**.

This is also the case with the 9-SOAE of BCoV, where compound **7** also showed reduced inhibitory activity in the fluorimetric assay. It has been suggested that BCoV is more dependent on the nature of the aglycone than the SOAE of influenza C virus which may provide an explanation for the reduced inhibitory activity observed.^{78,49}

Sialoside conc.	HE12-GFP		INF-C virus		BCoV	
	7	8	7	8	7	8
0.5 mM	22.95%	1.06%	7.01%	< 0%	2.86%	9.78%
1 mM	22.42%	6.08%	8.63%	3.85%	9.00%	2.70%
2 mM	33.03%	7.91%	7.05%	7.39%	< 0%	< 0%
5 mM	85.79%	-	-	-	-	-

Table 2. Inhibition (%) of viral 9-SOAEs by α -sialoside target compounds determined by the catalysed hydrolysis of *p*-nitrophenyl acetate (pNPA).

It is clear when comparing the results for inhibitory activities of compound **7** (9-*O*-methyl) to **8** (9-*O*-methylphosphonate) that the original reasoning for use of methylphosphonate functionality (mimicry of the proposed tetrahedral intermediate formed during acetyl hydrolysis) is not supported, as the charged methylphosphonate does not lead to improved binding and inhibition in comparison to the unmodified negative control, compound **30** (see table 2). The effect of the hydrophobic methyl group of compound **7** however shows a significant effect which could be exploited by further functional group modification at the 9-hydroxy group. It should also be mentioned that the results obtained in this initial study (for influenza C virus esterase) support those from an earlier investigation where a K_i of 4.2 mM was determined for a 9-acetamido-9-deoxy-sialic acid derivative.⁷²

Sialoside conc.	MHV-S		SDAV-HE	
	5	6	5	6
0.1 mM	4.00%	5.00%	2.13%	8.30%
0.5 mM	0%	2.36%	2.56%	2.89%
1 mM	8.31%	11.89%	0.51%	0.65%
2 mM	7.73%	7.81%	8.73%	10.96%

Table 3. Inhibition (%) of viral 4-SOAEs by α -sialoside target compounds determined by the catalysed hydrolysis of *p*-nitrophenyl acetate (pNPA).

Unfortunately no significant inhibition was observed in the pNPA assay when investigating the effects of the target compounds **5** (4-*O*-methyl) and **6** (4-*O*-methylphosphonate) towards the 4-SOAEs expressed by MHV-S and SDAV-HE (see Table 3). The fact that at higher inhibitor concentrations there was no inhibitory activity observed indicates that the scope for further functional group modification at the 4-hydroxy group is limited towards SOAE inhibition. It should be kept in mind however that the mode of action of 4-SOAEs may not be the same as 9-SOAEs.

1.2.8. Conclusion

To conclude, a set of structurally modified sialosides (compounds **5** to **8**) have been synthesised and have proved useful tools for studying the active sites of viral 4-SOAE and 9-SOAE enzymes investigated in preliminary assays. Though inhibition of 4-SOAEs was not observed, the 9-*O*-methyl derivative **7** showed inhibition of the recombinant SOAE from influenza C virus though not significantly with whole virus particles (as

mentioned above). Although it can be speculated that this is a result of it being a monomer rather than the native trimer, further studies are required with optimised inhibitors of higher affinity to corroborate this speculation.

Further studies based upon these inhibitors and variants thereof would be able to develop high-affinity inhibitors of the viral SOAE enzymes as potential drug lead compounds and investigative tools.

The sialosides developed are in no way limited to viral applications and could also be applied to SOAE and SOAT enzymes expressed by other organisms and disease states where *O*-acetylation of sialic acids are implicated.

1.2.9. Future scope

The synthesis of further α -*O*-allyl sialoside derivatives displaying functional group modifications at the 9-hydroxy are currently in the groups' pipeline. It is hoped that compounds displaying hydrophobic moieties of a varied chemical nature (for example, alkyl vs. aromatic substituents) at this position will be available to further investigate of the effect of hydrophobic substitution with regards to SOAE inhibition.

The continued development of the non-competitive suicide inhibitor based upon the 8,9-epoxide compound **25** is also of interest. Continuing the enzymatic route towards carboxy-methyl ester hydrolysis is an option using a different hydrolytic enzyme such as PPL (porcine pancreatic lipase), which also is considered a versatile enzyme for synthetic applications.^{74,77,75}

Chemical methods of methyl ester hydrolysis (in the presence of the epoxide moiety) will also need to be assessed. One particular method of interest is the use of trimethyltin hydroxide (SnMe_3OH) as a mild hydrolysis reagent.⁸²

It is also of interest for the α -*O*-allyl sialoside derivatives developed here to be investigated for their inhibitory potency of SOATs, particularly of mammalian SOAT systems where little structural information is known.

It may be the case that synthetic methodologies towards larger di-, tri-, multi-sialylated compounds containing the inhibitor functionalities seen in compounds **5** to **8** would need to be developed in order to investigate SOAT enzyme properties if simple α -*O*-allyl sialoside inhibitors are found to be unsuitable substrates (to the 9-SOAT).²⁷

The functionalisation of α -*O*-allyl sialoside derivatives onto solid supports/surfaces/quantum dots are another area which could be developed with the aim of synthesising SOAE/SOAT diagnostics.

Methodologies to conjugate the allyl group will therefore need to be investigated. One possible direction of research includes metathesis reactions because of the *O*-allyl functionality at the aglycone. Recent developments in the synthesis of novel dimers of *C*-

allyl sialosides⁸³ have utilised Grubbs-type catalysts in metathesis reactions with success and as such is a good indication that such methods may be applicable to α -*O*-allyl sialoside derivatives.

Thiol-ene coupling chemistry also lends itself to the functionalisation of α -*O*-allyl sialoside derivatives and also would allow a convenient method for bioconjugation⁸⁴ as well as other more conventional (amino-coupling chemistry) methods for linker ligation.⁶³

New Tools for the characterisation and investigation of influenza virus neuraminidases: towards novel influenza virus sensors

II.1. Introduction

II.1.1. Introduction to the Influenza Virus

Influenza viruses are enveloped, single-stranded RNA viruses belonging to the Orthomyxoviridae family. They are further classified into three serologically distinct types; influenza A, B, and C viruses.⁸⁵ However, only influenza virus A and B are considered highly pathogenic (causing seasonal and pandemic disease) towards the human population.^{86,87}

Influenza A viruses are divided again based upon the distinctive antigenic behaviour of the two main influenza virus surface proteins; a hemagglutinin (HA) and a neuraminidase (NA).^{85,88} With respect to Influenza A virus subtypes, these include 16 for Hemagglutinin (H1-H16) and 9 for neuraminidase (N1-N9).⁸⁸

A third membrane protein, the M2 protein, is present in small quantities in influenza A viruses but is not considered a significant factor towards viral pathogenicity.⁸⁹

II.1.1.1. Influenza A virus

Influenza A viruses have obtained a certain degree of notoriety having been the cause of all major human influenza pandemics.⁹⁰ The most deadly of which occurred in the twentieth century and resulted in the deaths of approximately 1% of the global population, the so-called “Spanish flu” pandemic of 1918 (influenza A H1N1). Other influenza pandemics have since occurred (for example, Asian flu, 1957 (H2N2) and Hong-Kong flu, 1968 (H3N2)) but have not had the same level of global impact to date.⁹¹ In humans, the influenza virus causes acute viral infection of the respiratory tract (more specifically, the epithelium lining the trachea) where common symptoms include fever, sore throat, muscular pain and fatigue.⁸⁹ It is the risk of secondary infection/complication (for example, pneumonia) or hypercytokinemia (“cytokine storm”)⁹² amongst at-risk populations (typically the very young and old) which give influenza infection high morbidity and mortality rates, particularly during pandemics and severe seasonal outbreaks.^{93,94}

Influenza A viruses are known to infect a wide range of host organisms and are believed to have originated among the avian population, of which wild birds (ducks, geese, swans, and shore birds) are considered to be a large natural repository of influenza viruses. It is noteworthy to point out that all of the known influenza A virus 16 HA and 9

NA subtypes have been found in these wild bird populations, however the jumping of subtypes from avian to mammalian species is rare.⁸⁹

The virus is asymptomatic in many avian species and as such they are referred to as low pathogenic avian influenza (LPAI) viruses. It is the adaptation of these viruses into new aggressive influenza strains which allow increased pathogenicity towards human populations and/or other host species.^{95,90}

This ability of cross-species transmission and subsequent rapid transmission and infection in the human population comes as a result of changes in the virus RNA genome. The evolution of an existing influenza virus through point mutations (“antigenic drift”) or the reassortment of RNA segments between influenza viruses of different species (“antigenic shift”) can lead to the creation of a new influenza subtype which has the potential of causing severe consequences for human health.^{96,90,97}

II.1.1.2. Pandemic influenza (H1N1, H5N1)

The most recent global influenza concerns have centred around the 2008-2009 influenza pandemic as a result of the pandemic H1N1 (“Swine Flu”, “Mexican Flu”) virus and the currently limited global outbreaks of the H5N1 (“bird flu”, “avian flu”) virus to which substantial fears of a future global pandemic have been attributed.

Though less deadly than initially feared and now moving into a post-pandemic period (as of April 2011), the pandemic H1N1 (“Swine Flu”, “Mexican Flu”) virus initially spread rapidly around the world through human-human transmission after early outbreaks in North America.^{98,99}

The pandemic H1N1 virus exhibited patterns of infectivity and mortality not normally attributed to seasonal influenza outbreaks, with a higher than expected proportion of deaths effecting younger, otherwise healthy individuals. As of 2009 the number of laboratory confirmed fatalities occurring as a result of the pandemic H1N1 virus is believed to be >16,000 cases.⁹⁹

Fortunately however, the pandemic H1N1 virus did not appear to develop any significant resistance to anti-viral prophylactic treatments (*vide infra*) and mutation did not lead to a more virulent form of the virus.¹⁰⁰

Considered to be a highly pathogenic avian influenza (HPAI) virus (as opposed to previously mentioned LPAI viruses), the recent emergence and spread of the H5N1 influenza virus subtype has heightened global concerns of a future influenza pandemic.^{90,101}

First identified in Hong-Kong (1997) and subsequently seen in limited outbreaks amongst avian populations (mostly localised to south-east Asia), human-human

transmission appears to be infrequent and occasional though the mortality rate of the H5N1 virus when contracted is associated with severe and often fatal outcomes.^{89, 96}

The H5N1 virus, though not classed as a pandemic, has met two of three relevant criteria; 1) the emergence of a virus strain to which there exists no natural immunity in the human population; 2) the successful transmission and infection of the virus strain to humans.^{89,101}

The spread of this influenza strain has become endemic in many poultry and wild bird populations in Asia which only serves to increase the chances of a successful virus variation (through “antigenic shift” or “antigenic drift”) towards the human population as a consequence of increased human-animal (avian) interactions.^{89,90}

This fear is exacerbated by clinical evidence which indicates the resistance of certain H5N1 variants to anti-viral treatments which may retain high levels of pathogenicity as seen in the wild-type virus in humans.^{102,103}

As of April 2011, The WHO (World Health Organization) confirmed 549 cases of H5N1 in humans globally, 320 of which were fatal.¹⁰⁴

The consequences of a severe influenza outbreak (such as the H5N1 subtype) and its obvious detrimental health and socioeconomic impact upon the global population mean that the WHO continues to monitor the disease globally and influenza research constitutes a global R&D investment in excess of \$7 billion in 2009.^{95,105}

II.1.2. The role of neuraminidase and hemagglutinin in influenza virus replication

As previously mentioned the influenza virus has two main surface proteins, HA and NA. Both surface proteins (the ratio of which is approximately 10:1 HA to NA respectively) play a major role in the replicative fitness of the influenza virus infection process.¹⁰⁶

Both the HA and NA are carbohydrate-recognising proteins (lectins) which utilise terminally-bound sialic acid (linked to an underlying galactose moiety on glycoproteins and glycolipids) as the main receptor determinant.¹⁰⁷

The influenza viruses follow a typical replicative path (see figure 15). The HA is primarily responsible for initial sialic acid mediated attachment of the virus to the host cell surface and is also responsible for viral entry into the host cell via endocytosis and fusion of the virus with the host cell.¹⁰⁸

The process of viral entry by the HA is critically helped by the M2 protein channels (previously mentioned) on the virus surface. These small membrane-bound structures act as proton channels, allowing the acidification of intracellular compartments of the host cell on HA binding therefore enabling viral uncoating and the escape of viral RNA into the host cell.¹⁰⁹

The viral RNA is then replicated within the nucleus of the host cell whereby new viral progeny are packaged and transported to the host cell surface where budding of virus particles occurs. Newly formed virus progeny are then released from the host cell surface. It is here that the NA comes into action by cleaving the glycosidic linkages of terminal sialic acids from the host cell surface which allows the newly generated viral progeny to be released unimpeded, thus allowing the viral infection to propagate.¹⁰⁸ Without the receptor-destroying function of NA, influenza infection would be limited and as such its disease-causing potential curtailed.¹⁰⁸ It has also been suggested that NA action aids viral infection of a host organism by hydrolysing sialic acid residues present on the mucin which lines epithelial cells in the respiratory tract of the host organism.¹¹⁰

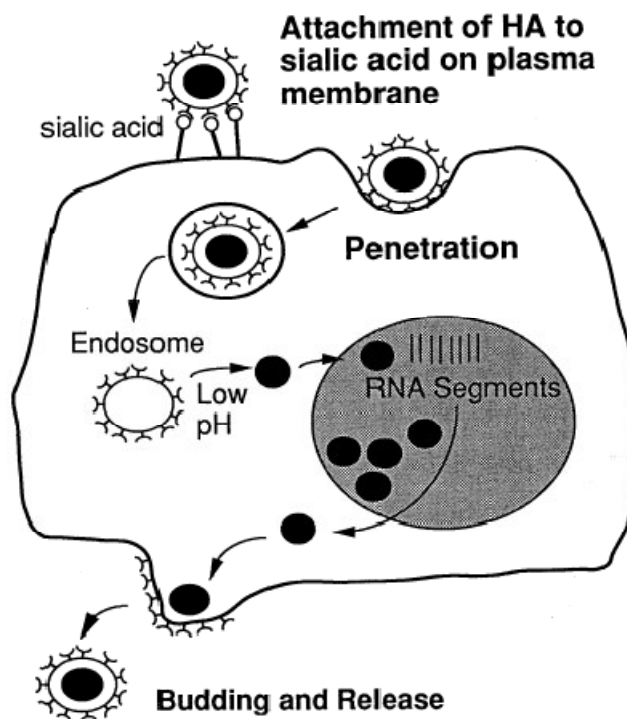


Figure 15. Influenza virus replicative cycle. Viral infection is started with hemagglutinin (HA) binding to sialylated cell surface structures. This induces the virus endocytosis and subsequent release and replication of RNA and viral proteins. The new virions bud from the cell surface and are released on cleavage of terminal sialic acid epitopes by the neuraminidase (NA). (Reprinted with permission from Springer+Business Media; *Analytical and Bioanalytical Chemistry* **2005**, 381, 156-164.)

II.1.2.1. Hemagglutinin

The binding interactions of HA to α -ketosidically linked sialic acids on glycoconjugates are multivalent in nature as the affinity for a single-receptor (monomeric sialic acid) is characterised by weak binding ($K_{\text{diss}} > 10^{-4}$ M).^{86,111}

The HA consists of three subunits and as such is classed as a trimer (see figure 16). It is roughly cylindrical in shape and is anchored to the virus via the viral lipid membrane.^{107,112} The surface of an influenza virion consists of approximately 300-500 trimeric subunits which are found to be equally distributed over the virion surface.¹¹³ It has been approximated that the distance between HAs on the same trimer is $\sim 40\text{\AA}$ and estimated that the distance between HAs of adjacent trimers to be $\leq 55\text{\AA}$.^{114,115}

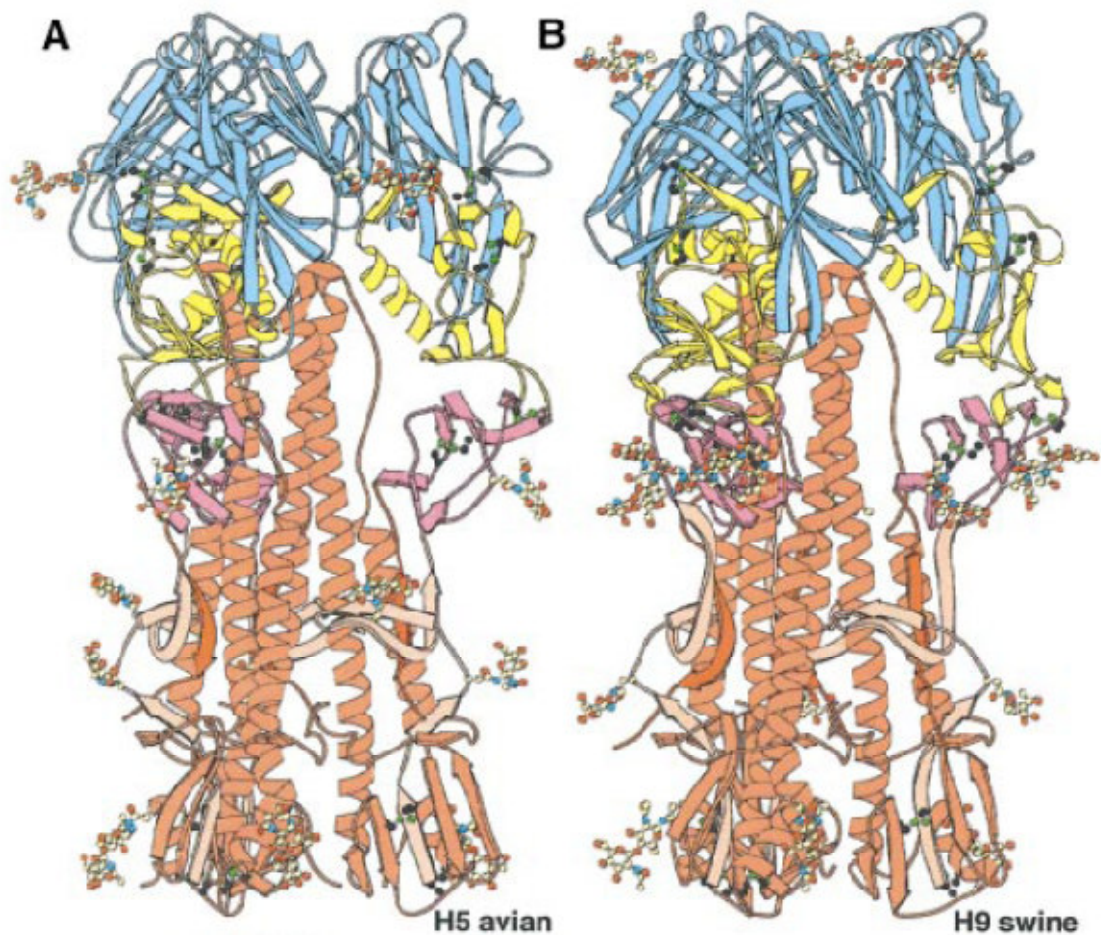


Figure 16. (A) Ribbon diagram of the trimer of an H5 (A/Dk/Sing/97) avian HA and (B) a ribbon diagram of an H3 swine (A/Sw/9/98) HA. The sialic acid binding domain is coloured blue. (Reprinted with permission from Macmillan Publishers Ltd.; *EMBO Journal* **2002**, 21, 865-875.)

Each subunit of HA consists of a further two subunits classed as HA1 and HA2 and overall the HA divided into two distinct regions; 1) A triple-stranded coiled area of α -helices anchored in the membrane by HA2. Both HA1 and HA2 are contained in this region. 2) A globular region (containing only HA1 subunits) consisting of anti-parallel β -sheets which is placed atop of the previous region. It is this second region which contains the sialic acid binding site and is also the location of antibody binding sites

(antigenic determinants) generated by the host-immune response to the viral infection.^{112,90,116}

It has been shown that the binding affinity of the HA to the host sialic acid allows for the host specificity of influenza A viruses.⁹⁰

This specificity is believed to arise from a limited number of amino acid substitutions within the HA receptor pocket which enable preferential binding of the HA to terminal sialylated glycosylated biological structures.^{97,96,90,117}

This receptor specificity can be best illustrated by comparing avian- and human-specific influenza viruses. Influenza strains with specificity towards humans bind to α -2,6-sialylgalactosides preferentially whereas avian (and equine) influenza viruses preferentially recognise α -2,3-sialylgalactosides (see figure 17). This comes as a consequence of the predominant expression of a particular sialylgalactoside regioisomer found in these particular species.^{89,90}

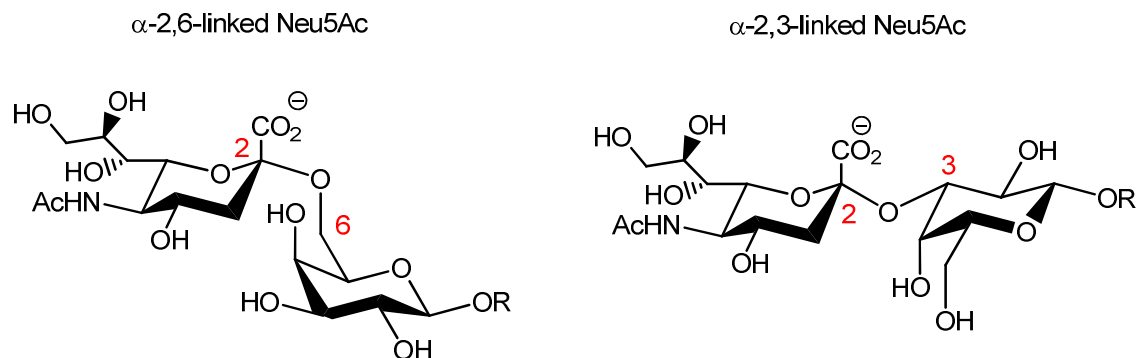


Figure 17. α -2,6-sialylgalactosides vs. α -2,3-sialylgalactosides (R = glycoconjugate).

This preference for receptor specificity in swine is often not as stringent. Swine are susceptible to both human and avian influenza viruses because the epithelial cells of the respiratory tract in these animals contain both types of sialylgalactoside linkage (α -2,6- and α -2,3-). Therefore, swine is considered a non-selective host for the evolution of new influenza strains (from the mixing of species specific influenza strains) and as such are considered a source of pandemic influenza strains towards the human population (for example pandemic H1N1 “swine flu”).^{89,90}

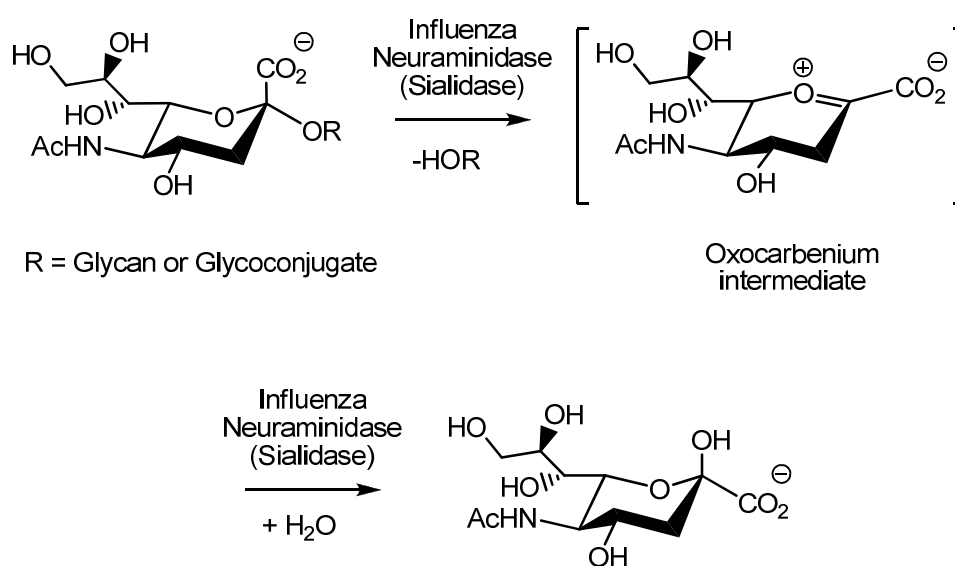
Significant differences in the binding conformations of α -2,6- and α -2,3-sialosides to HA have been observed^{118,119} and as such indicates that for successful viral adaptation to human populations from avian species, the virus must adapt to address these conformational changes in order to successfully infect and replicate. It is understood that the development of an avian influenza strain with the ability to bind preferentially to α -

2,6-sialylgalactosides is a major prerequisite in the generation of pandemic influenza strains with risk to human health.

Recent studies have added even further complexity to HA binding by indicating that the topology of α -sialylated glycans (the structural conformation presented on the host cell surface) is important for differentiation between influenza strains beyond the anomeric linkage.¹²⁰ More specifically, the binding of influenza HA to α -sialylated glycans displaying “umbrella” or “cone” conformations appears essential for the adaptation and transmission of influenza viruses between organisms.^{121,122,123}

II.1.2.2. Neuraminidase

The role played by the NA in the influenza life cycle can be described as that of a “receptor destroying enzyme” as it cleaves the sialic acid residues on the host cell surface (see scheme 16) which are needed for initial viral attachment (by the HA) but which also prevent the escape and subsequent infectivity of newly formed viral progeny.



Scheme 16. Simplified schematic of the hydrolysis reaction of the NA upon sialylated biological structures.

As alluded to earlier, influenza virus infectivity is a delicate balance between the HA and NA.¹⁰⁷

The determination of X-ray crystal structures of the NA glycoprotein has shown that a distinction can be drawn between the influenza A subtypes. These investigations have shown that the NA of influenza A viruses (subtypes N1-N9) can be separated into two phylogenetically and structurally distinct groups; group-1 (N1, 4, 5 and 8) and group-2 (N2, 3, 6, 7 and 9) NA.^{88,96,124,125,126}

The NA (of influenza A and B) is made up of four identical subunits and as such is referred to as a tetramer (see figure 18) and like the HA, is also attached to the viral membrane surface. But unlike the HA, the NA is not the major target site for the host immune system.⁹⁰ Each NA monomer subunit is arranged into a propeller formation through the arrangement of six anti-parallel β -sheets.⁸⁸ The surface of an influenza virion consists of approximately 50 tetrameric subunits (based on X31 H3N2) of a distance of approximately 45-50Å between each subunit and unlike HA are not equally distributed over the virion surface (neuraminidase patches).^{113,124}

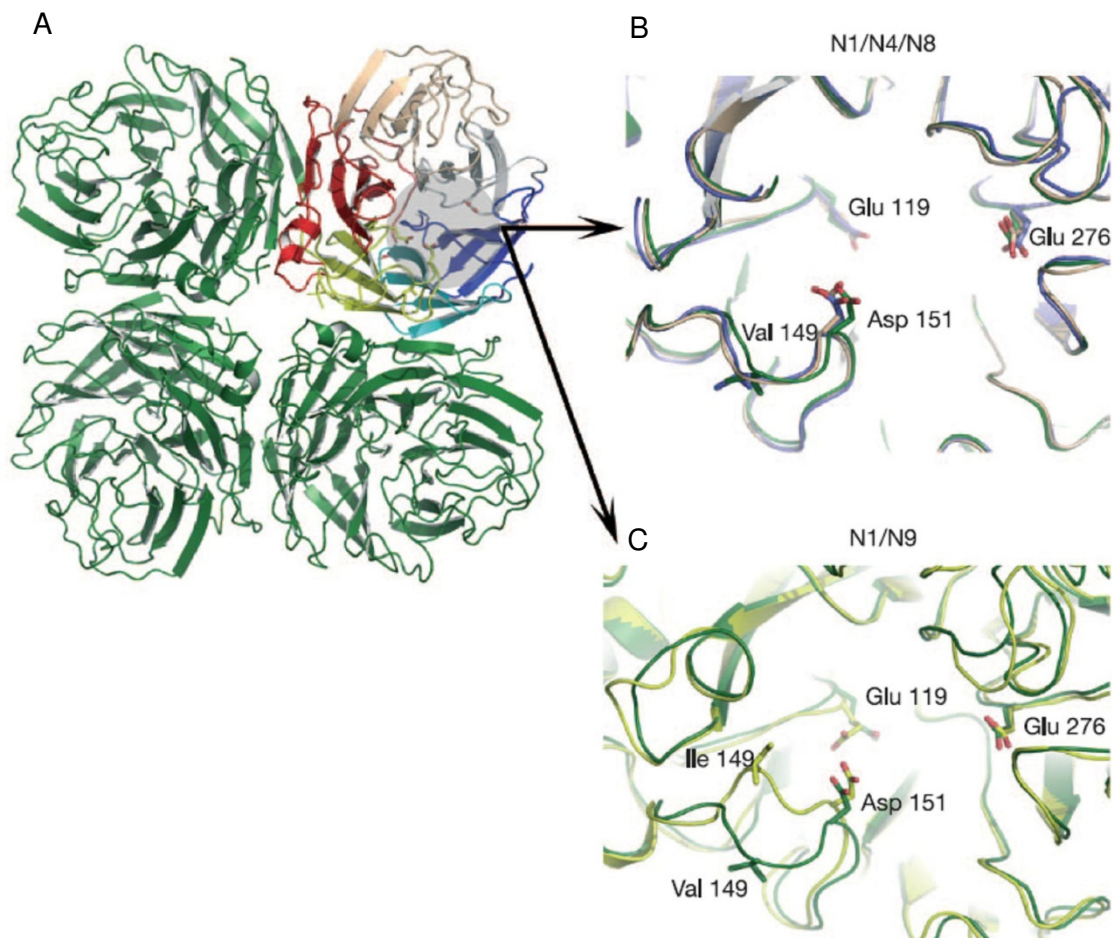


Figure 18. Ribbon diagrams of the group-1 (N1) neuraminidase tetramer (A). The upper right monomer (of the tetramer) is highlighted to emphasize the canonical six-bladed β -propeller structure. Expansions of the NA active site are shown (B and C). Superposition of the active sites of three NAs from group-1 (B), show the similarities between various influenza strains: N1, green, N4, gold, and N8, blue. The superposition of the active site of N1 (green) and N9 (yellow) NAs highlight the difference between the N9 and N1 HA in the 150-loop region. Conserved residues such as Glu 119, Asp 151 and Glu 276 and the hydrophobic residue at position 149 are shown in a stick representation. (Reprinted with permission from Macmillan Publishers Ltd.; *Nature* **2006**, 443, 45-49.)

The active sites of all influenza NA appear highly conserved, particularly between viruses of the same subtype.^{88,107} The highly conserved areas, in particular the amino acid residues in the enzyme active site which bind to sialic acid, are considered invariant (for example, the “arginine triad”).

Structural differences between group-1 and group-2 NA have been determined despite these similarities. These distinctive differences centre on the display of a flexible protein loop (referred to as the “150 loop”, between amino acid residues 147-152) and a hydrophobic cavity (referred to as the “150 cavity”) near the NA active site which is present in group-1 NA (and which is “closed” in group-2 NA).^{96,88}

The conformational rearrangement of the flexible “150-loop” from the “open” form (lower-energy in the *apo*-structure) to the “closed” form which occurs on binding of a NA inhibitor (oseltamivir, *vide infra*) is a slow process.⁸⁸

Recent theoretical research has indicated that the electrostatic interactions between the NA inhibitor pharmacophore and the amino-acid residues present on the “150-loop” are essential in determining the binding selectivity (with larger basic functional groups potentially favouring binding to the “open” conformation in group-1 NA).¹²⁷

This potentially can create new opportunities for NA-inhibitor drug design (based on existing NA based inhibitors) as a larger active site is presented as a result of this protein loop (increased width of approximately 5Å).^{96,88}

Such inhibitors could show greater specificity and activity towards group-1 NA and as such may serve as lead compounds to target the avian influenza A/H5N1 virus.⁸⁸ There has been recent synthetic work described in the literature towards compounds which exploit the “150 loop” for increased binding to NA.^{128,87,129}

With regards to substrate specificity towards α -2,3- and α -2,6-linked sialylgalactosides the preference for NA is less certain than the case with HA. The α -2,3- linkage seems to be preferentially cleaved by both avian and human influenza A viruses though the α -2,6-sialylgalactoside is also normally a substrate to some degree.^{107,130,131,132}

II.1.3. Influenza therapeutics

Options are available for the alleviation of the impact of influenza infection, with anti-viral treatments and vaccines being the first choice.

Vaccine production and vaccination are time consuming approaches with a limited shelf-life for the vaccine itself as well as having an initial inoculation period of approximately 1 month to be fully effective against the respective influenza strain/s.

Moreover, the “antigenic drift” and “antigenic shift” of influenza viruses inevitably lead to the redundancy of vaccines after each subsequent season of infection which means that during a severe influenza outbreak, vaccination is often not an immediate preventative

treatment option. The alternative to this strategy are anti-viral drug treatments, in particular NA inhibitors to combat influenza infection.^{91,103}

Many aspects of the influenza life cycle have been the target for chemotherapeutic intervention and accordingly, anti-influenza drugs and therapies can be divided into different classes depending on their mode of action. Some examples of which are outlined below.

II.1.3.1. Neuraminidase inhibitors

Targeting the NA function of influenza viruses has proved to be an effective strategy towards anti-influenza therapeutics (see figure 19).¹³³ The neuraminidase inhibitors work by interfering with the NA function of the influenza virus, preventing the successful release of viral progeny from infected host cells and thus preventing the further spread of infection.¹⁰⁸

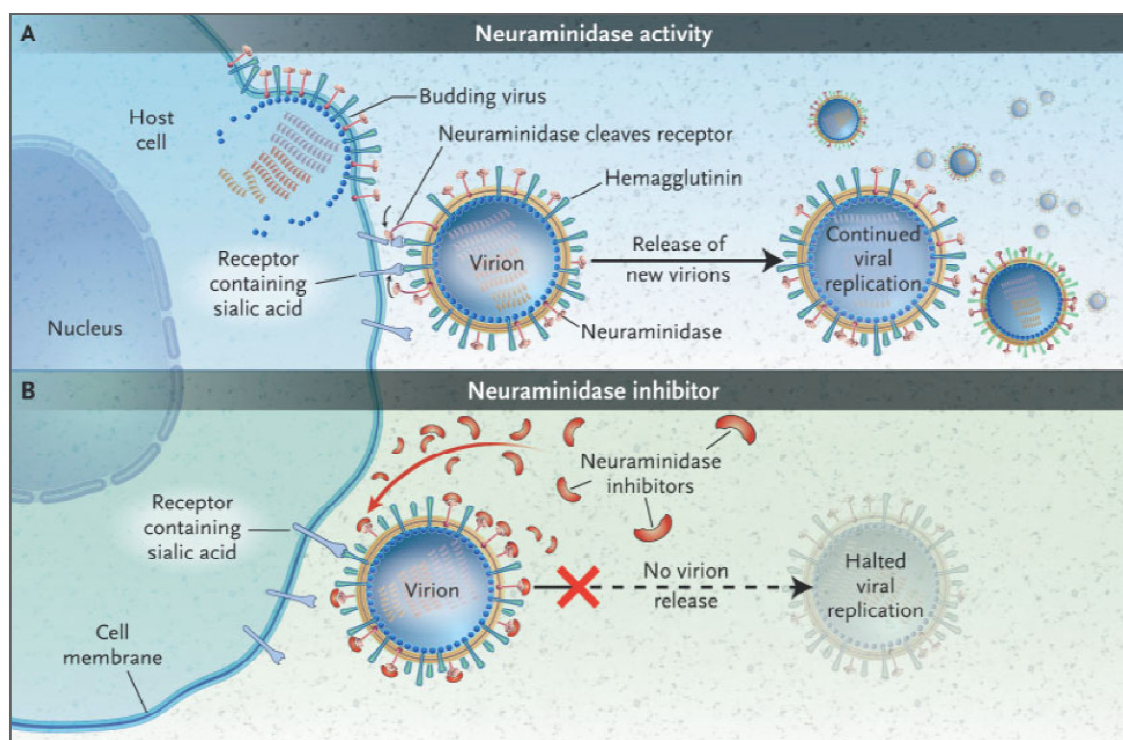


Figure 19. The mode of action by Neuraminidase Inhibitors. Neuraminidase is not inhibited, allowing the continued replication of influenza and therefore infection (A). The replication is blocked by neuraminidase inhibitors which prevent virions from being released from the surface of infected cells causing virion aggregation (B). (Reprinted with permission from Massachusetts Medical Society (MMS); *New England Journal of Medicine* **2005**, 353, 1363-1373.)

Such inhibitors are used as both prophylactics and therapeutics against all NA subtypes and by extension against all strains of influenza A and B viral infections.¹⁰⁸

The use of NA inhibitors comes with low toxicity and a decreased susceptibility to viral resistance. As such, NA inhibitors (oseltamivir, zanamivir and peramivir) are continually being developed and stockpiled as a first line of defence against future influenza outbreaks (see figure 20).¹⁰⁸

It is anticipated that the modes of inhibition displayed new types of NA inhibitors are altered significantly from those of the main (therapeutically used) NA inhibitors with respect to binding interactions within the neuraminidase active site. An example of which is the alternative hydrophobic binding approach of pyrrolidine-based NA inhibitors which render the C4 guanidino and amino substituents (of zanamivir and oseltamivir respectively) obsolete.^{134,135} Such compounds are therefore considered therapeutically useful as they may lack cross-resistance with the oseltamivir pharmacophore.^{136,137,138}

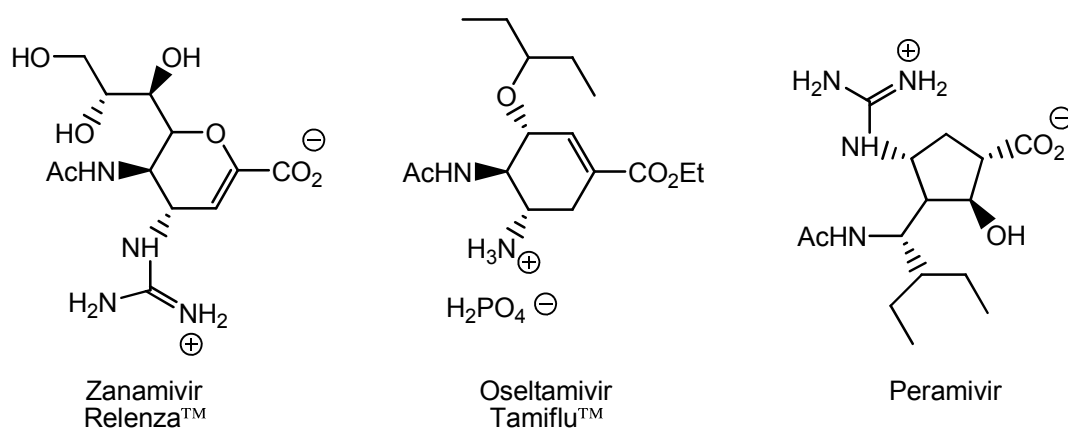


Figure 20. Structures of common NA inhibitors.

II.1.3.2. M2 protein blockers

M2 protein inhibitors such as the amantadine-derivatives (amantadine and rimantadine) combat influenza infection by interfering with the M2-proteins' role as a proton-channel (as previously mentioned, important in viral-host membrane fusion and viral replication) (see figure 21). These drugs are only active against influenza A viruses and though initially highly active, drug resistance to these inhibitors rapidly developed along with side effects relating to the CNS (central nervous system).^{97,133}

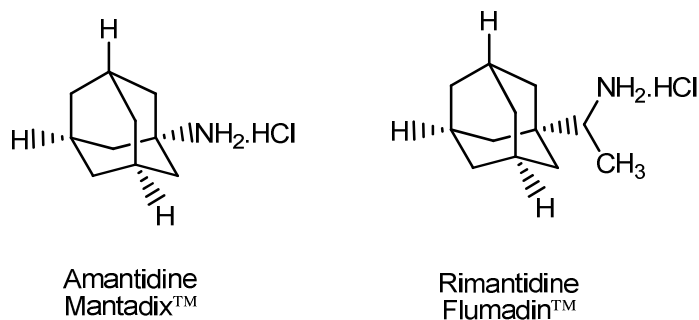


Figure 21. Structures of common M2 protein blockers.

II.1.3.3. IMP dehydrogenase inhibitors

Inosine 5'-monophosphate (IMP) dehydrogenase inhibitors (see figure 22) target an important enzyme (IMP dehydrogenase) involved in viral RNA synthesis.¹³³

Though having showed limited activity towards treatment of influenza A (H1N1) infection, Ribavirin and Viramidine (a ribavirin prodrug) is active against the H5N1 influenza subtype and is used as a preferred therapeutic method to treat acute influenza viral infection. However, the high doses required often lead to the break down of red-blood cells.^{97,133}

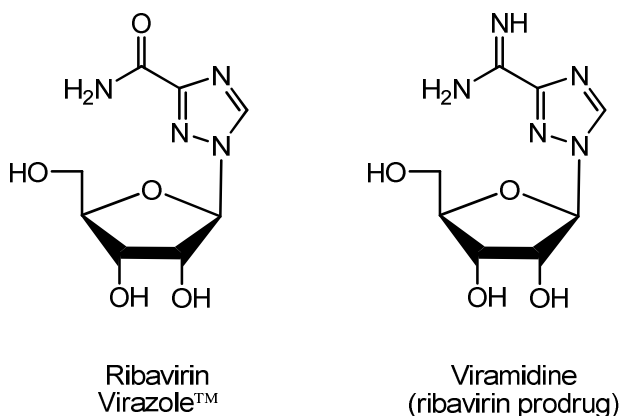


Figure 22. Structures of IMP dehydrogenase inhibitors.

II.1.3.4. RNA polymerase inhibitors

This activity of this type of inhibitor is based upon the recognition of the pyrazine derivatives (for example, T705 and flutimide) as nucleobases (see figure 23), which after conversion to a triphosphorylated ribonucleotide, is postulated to inhibit the influenza viral RNA polymerase enzyme competitively.⁹⁷ T705 has exhibited inhibitory activity towards influenza A, B and C *in vitro* and *in vivo*.^{133,97}

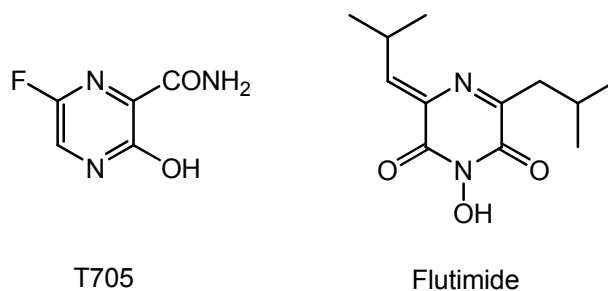


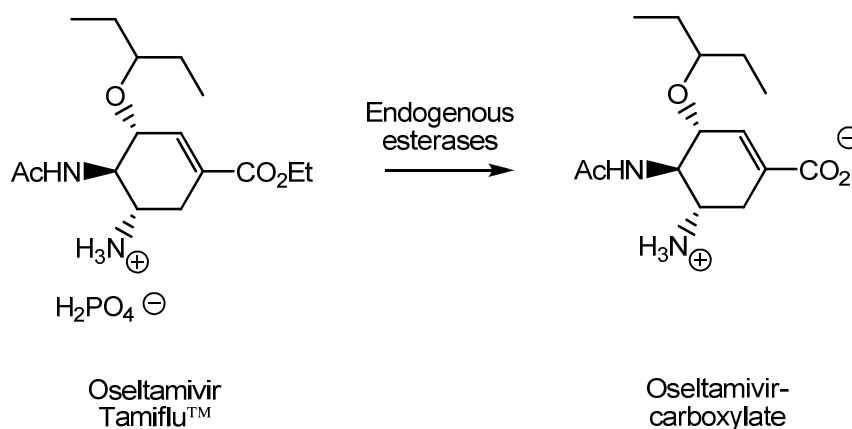
Figure 23. Structures of RNA polymerase inhibitors.

Other treatments under development for influenza viral infection include biological approaches such as, the application of interferons (natural proteins produced by the cells of the immune system) and siRNAs.⁹⁷

II.1.4. Oseltamivir: a neuraminidase inhibitor

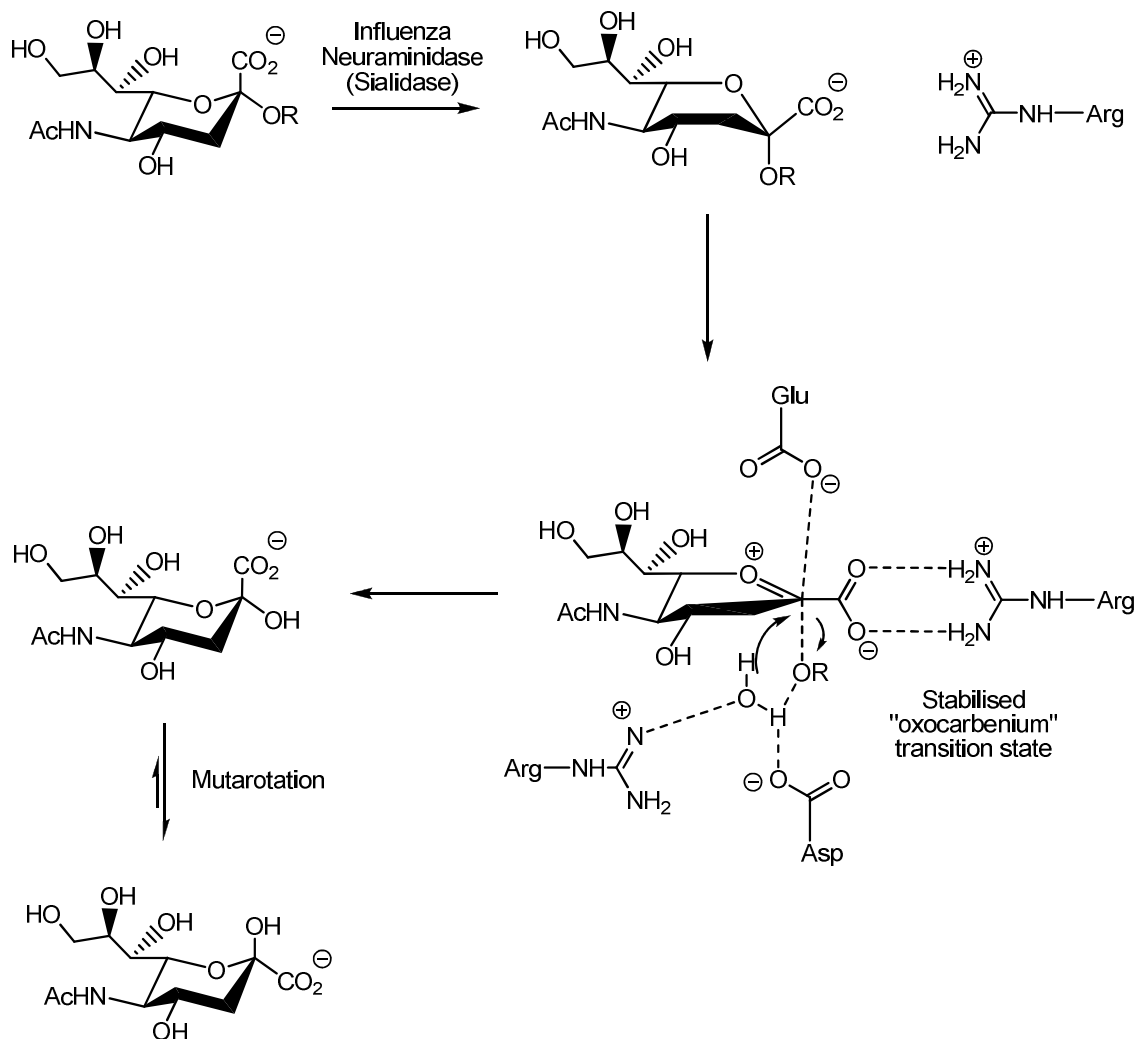
As mentioned above, the most widely used and applicable anti-influenza treatments are the NA inhibitors. The development of oseltamivir (as well as zanamivir, its forebear) was based upon successful structure-based inhibitor design methodology using the structural data of group-2 NA (and also NA of influenza B) obtained via X-ray crystallographic methods.^{124,125,129}

Developed by Gilead Sciences^{139,140,141} and marketed in a phosphate salt formulation by Hoffmann-La Roche under the trade name TamifluTM (the ethyl ester prodrug of oseltamivir carboxylate),^{142,76} oseltamivir was the first commercially developed orally active NA inhibitor for use against Influenza A and B viruses (see scheme 17).¹³³



Scheme 17. Oseltamivir, Tamiflu.

The mechanism of action displayed by these NA inhibitors is one of competitive inhibition within the NA active site. Oseltamivir mimics the proposed oxocarbenium intermediate formed during the enzymatic hydrolysis of the sialic acid receptor (at the glycosidic bond) by the by influenza virus neuraminidase (see scheme 18).^{133,107}



Scheme 18. Proposed mechanism of sialic acid hydrolysis by influenza NA. The enzyme active site stabilises the proposed oxocarbenium-intermediate.

The proposed mechanism of sialic acid hydrolysis by influenza virus neuraminidase is based upon several important steps.¹⁰⁷ The ²C₅ chair conformation of the α-sialoside is distorted to that of a boat conformation through the interaction of the carboxylate moiety with an arginine triad within the enzyme active site. Protonation of the glycosidic oxygen leads to glycosidic bond breakage and the reaction proceeding through a proposed enzyme-stabilised oxocarbenium cation intermediate (half-chair conformation). This

oxocarbenium intermediate in turn reacts stereoselectively with H₂O to generate α-sialic acid (which is then subject to mutarotation).^{143,144}

The effectiveness of oseltamivir (and structurally related molecules) to act as an inhibitor of influenza NA indicates that the formation of an oxocarbenium cation intermediate is a likely and important facet to the hydrolysis reaction at some stage during its progression.¹⁰⁷

Within the enzyme active site, interactions with oseltamivir are mainly electrostatic in nature and are primarily derived from the interaction of ionisable functional groups on the oseltamivir structural motif with charge-corresponding amino-acid residues (see figure 24).

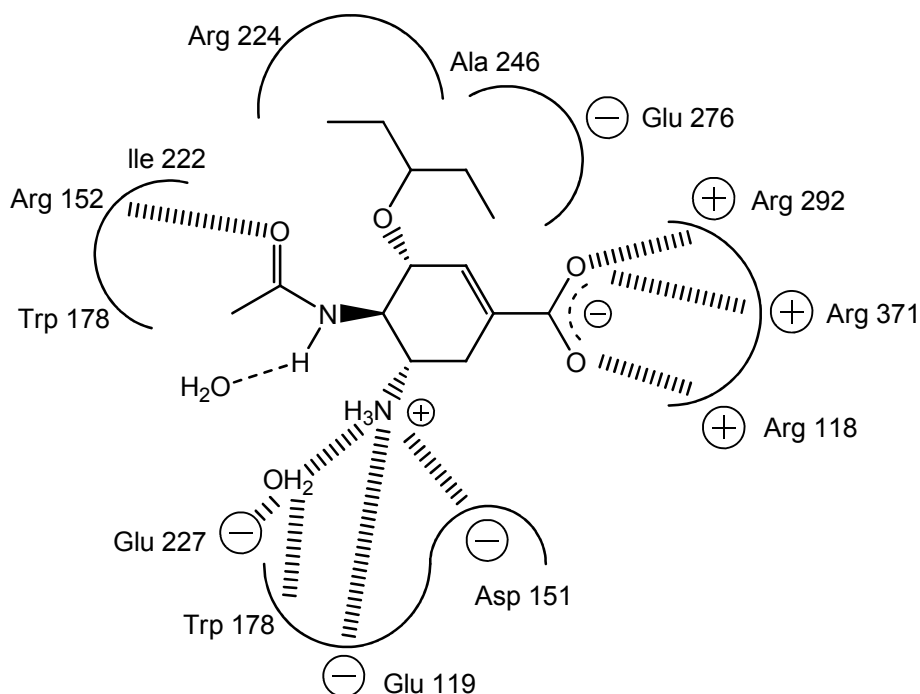


Figure 24. Oseltamivir carboxylate interactions in the neuraminidase active site.

Of primary importance is the interaction between the negatively charged carboxylate group with the positively charged “arginine triad” (consisting of Arg 118, Arg 292 and Arg 371). Of secondary importance is the interaction of the basic amino functionality (or guanidino functionality in zanamivir) with the negatively charged Glu 119, Glu 227 and Asp 151 residues. The remaining interactions are a result of a combination of hydrogen bonding, electrostatic and nonpolar interactions. These include the pentyl chain of the ether group with the residues Ile 222, Arg 224, Ala 246 and Glu 276 (hydrophobic contributions) and the hydrogen bond-donating and hydrogen bond-accepting

interactions of the charged amino and acetamido functionalities under physiological conditions.^{133,107}

II.1.4.1. Oseltamivir vs. influenza virus: emerging resistance

The highly conserved nature of NA active sites across various influenza strains and subtypes mean that the potential mutation of active-site amino acid residues would compromise NA activity and therefore reduce the replicative viability of the virus. However some active site mutations which render NA less susceptible to NA inhibitors are known to occur.

Some known point mutations which are known to occur in both group-1 and/or group-2 NA and correspond to mutations (isolated from influenza viruses) which show a high to intermediate level of resistance to oseltamivir include; 1) His274Tyr (H5N1, H1N1) 2) Asn294Ser (H3N1, H5N1) 3) Glu119Val (H3N2) 4) Arg292Lys (H3N2) 5) Tyr252His (H5N1) 6) Asn294Ser (H3N2, H5N1).^{103,145,133}

It seems logical that mutations in the active site residues involved in substrate binding can generate resistance to NA inhibitors. In particular, the mutations His274Tyr and Asn294Ser have been shown to reduce the inhibition caused by oseltamivir with respect to group-1 NA and a similar effect has been observed with the Arg292Lys mutation in group-2 NA.^{103,102,145}

It is worth mentioning that zanamivir resistant influenza strains (for example, containing the mutation Arg292Lys as observed in H3N2) are uncommon to date. It has been speculated that this is because of the poor viability of viruses in receipt of this mutation.^{133,145}

With regards to the His274Tyr mutation, this oseltamivir resistant trait has been found to be more readily transmissible than other NA active site mutations.¹³³ This is supported by the WHO, whose reports state that oseltamivir resistance observed in influenza virus strains remains mainly limited to seasonal H1N1 viruses with the His274Tyr mutation being the common resistance mutation in circulation.^{146,147}

It has been suggested that this mutation alters a hydrophobic pocket within the enzyme active site (essential for oseltamivir binding).¹⁰³

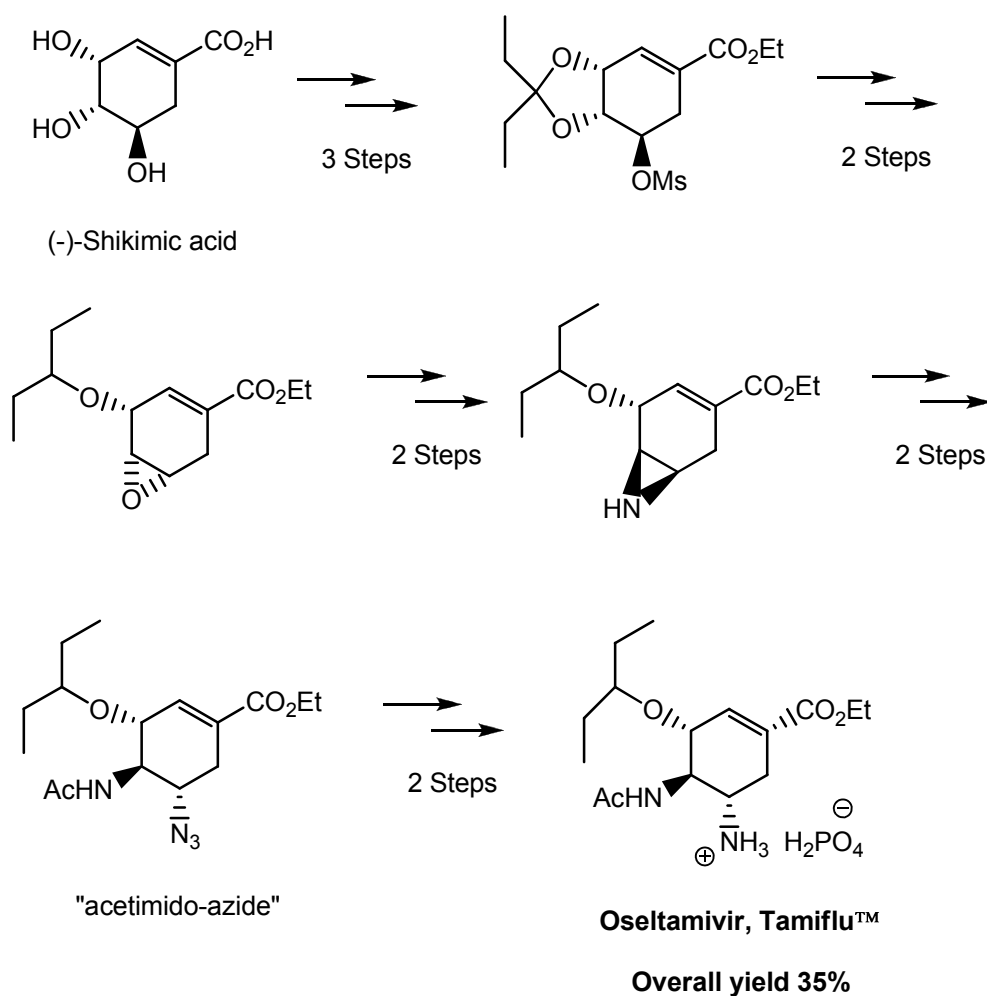
The fact that oseltamivir resistant mutations have also been found in resistant (and fatal) H5N1 influenza virus strains are a cause for concern. If mutations such as His274Tyr become common in avian H5N1 then the reasoning for using and stockpiling oseltamivir would be compromised. Studies also suggest that these mutations remain viable and stable in nature in the many subtypes of viruses where they are expressed (that is, their pathogenicity is not detrimentally affected).^{102,103,133}

II.1.4.2. Syntheses of oseltamivir

The use of oseltamivir as the NA inhibitor of choice for the treatment of influenza infection globally comes as a result of its superior bioavailability and all-round efficacy against influenza strains compared to its nearest competitors (zanamivir, peramivir).¹³³ It is produced annually on a several hundred metric tonne scale with sales in excess of \$2 billion.

The current industrial synthesis of oseltamivir (see scheme 19) by Hoffman-La Roche makes use of (-)-shikimic acid as starting material and in a 10 step sequence (overall yield 35%) to generate oseltamivir phosphate (Tamiflu™).^{76,142,148,149}

In brief, the synthesis proceeds via a 3,4-pentylidene 5-mesylyshikimate derivative of (-)-shikimic acid, which is then regioselectively reduced to the 4,5-epoxide intermediate. Stereoselective epoxide-opening results in the formation an aziridine derivative which is subsequently converted to the acetamido-azide derivative. Reduction of the azido-functionality, followed by formation of the phosphate salt gives oseltamivir phosphate.



Scheme 19. Industrial Tamiflu synthesis.

There have been many synthetic endeavours, from both academic and industrial laboratories towards refining and improving the synthesis of oseltamivir, some of the reasons for which include; 1) the limited availability of the shikimic acid starting material (isolated naturally from star anise (*Illicium verum*) or produced via recombinant *E.coli*), 2) the economic benefit gained from improved synthetic routes which are both economically and chemically efficient and 3) the recent emergence of a influenza virus pandemic strain (H1N1 “swine flu”) and the potential threat from avian H5N1 (“bird flu”).

Oseltamivir, though a small molecule, is densely functionalised and as such has posed a difficult synthetic target for laboratories specialising in natural product chemistry and total synthesis. As such, some interesting chemistry has been utilised recently towards oseltamivir synthesis.^{150,151,152}

II.1.4.3. A synthetic strategy towards phospho-isosteres of oseltamivir

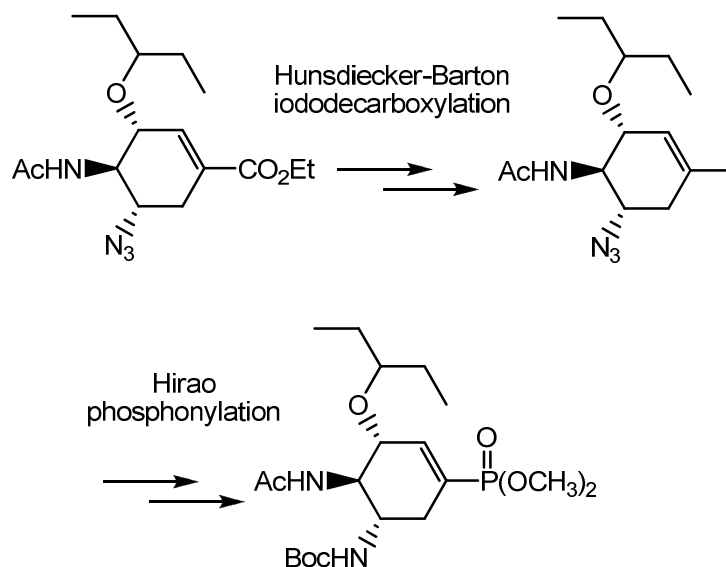
The phosphonate moiety is often used as a bio-isostere of carboxy-functional groups in drug design and synthesis and has been used in the synthesis of sialic acid phosphonate congeners.¹⁵³⁻¹⁵⁷

Though first reported by Shie *et al.*, the synthesis of the phosphonate congener of oseltamivir was heavily inspired by previous synthetic investigations by Streicher *et al.* based on a synthesis utilising chiral D- and L-xylose precursors^{153-155,158} and in a later synthetic approach via an azide-free synthesis.¹⁵⁹

The synthesis of the phosphonate congener of oseltamivir has been shown experimentally to be more potent than the original carboxylate congener against wild-type NAs of H1N1 and H5N1.¹⁵⁸

In molecular modelling and docking studies, phospho-oseltamivir exhibited a slightly stronger contribution to electrostatic binding within the enzyme active site which is attributed to the extra negative charge it presents and as such suggests a reason for its slightly increased potency.¹²⁷

Recent work in the Streicher lab has resulted in the development^{67,160,161} of an efficient synthesis of the cyclohexenephosphonate scaffold from chiral pool precursors via two key steps (see scheme 20); a modified Hunsdiecker-Barton iododecarboxylation and a Pd-mediated phosphite (Hiaro reaction) coupling step for the introduction of the phosphonate functionality.



Scheme 20. The two key synthetic steps towards phospho-isosteres of oseltamivir.

These two key steps provided access to various phospho-isosteres of oseltamivir, including the phospho-isostere of oseltamivir carboxylate itself, “tamiphosphor” or “phospha-oseltamivir”.

These phospho-isosteres are derived from the industrial oseltamivir “acetamido-azide” precursor, where a phosphonate or phosphonate monoester replaces the carboxylate without impairing the potency of the oseltamivir pharmacophore.⁶⁷

The monoester strategy developed by Streicher *et al.* allowed structural modification at the phosphonate ester and thus enabled the synthesis of a set of structurally diverse monoesters which retain the negative charge essential for activity under physiological conditions (see figure 25).^{67,161} As such, the pharmacophore was not compromised and all monoesters exhibited subnanomolar inhibition in the range of oseltamivir carboxylate. Of particular interest were the Phospha-oseltamivir derivatives synthesised as chemically stable mimetics of α -2,3- and α -2,6-linked sialylgalactosides which highlighted the preferential binding of certain NA subtypes to sialic acids of varying anomeric linkage to the underlying carbohydrate moiety.

In the absence of structural data, inhibition values for the sialoside mimetics cannot be directly correlated with substrate specificity of the virus. However, the inhibition values obtained indicate that the ratio between the respective inhibition constants (of the sialoside mimetics) should show some form of proportionality to the ratio of the binding constants of the respective α -2,3- and α -2,6-linked sialylgalactoside substrates.¹⁶¹

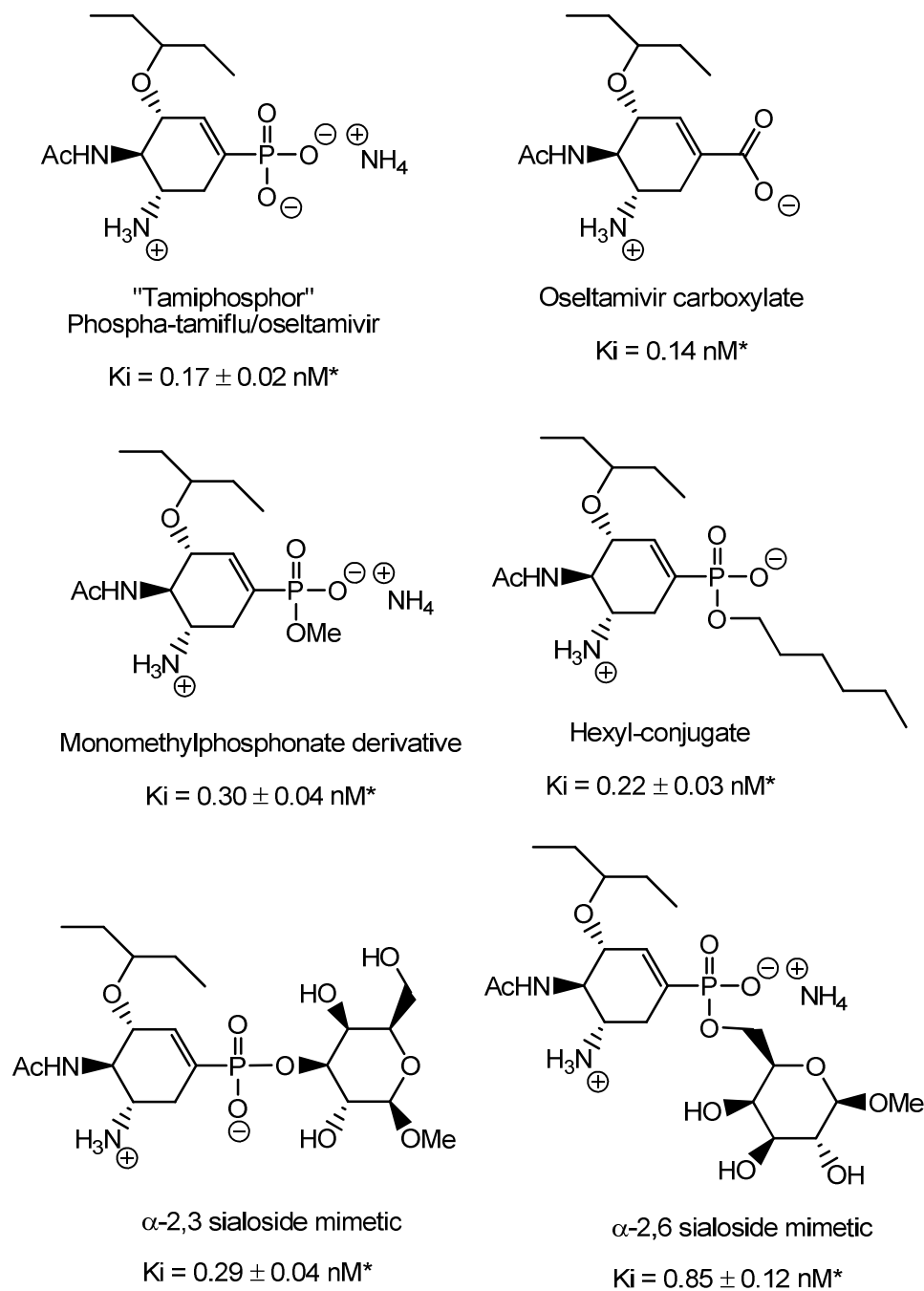


Figure 25. Previous NA inhibitors synthesised by Streicher *et al.*,^{67,161} phospha-isosteres of oseltamivir which retain the potency of the oseltamivir pharmacophore. (*for influenza A/Norway/1758/07 (H1N1)).

II.1.5. The concept of multivalency to achieve stronger binding

Qualitatively, multivalency can be employed for the achievement of strong ligand binding to a target substrate through the use of multiple ligand interactions. Such multivalent systems are known to often exhibit enhanced binding potency in comparison to monovalent ligands for a particular system. For a multiple-ligand displaying system the observed enhancement of interaction must be expressed on a “valence (ligand) corrected basis”.¹⁶² Put another way, it can be expressed as “a relative potency per ligand” compared to the monovalent analogue.¹⁶³

In biology, multivalent interactions are the foundation of many essential biological processes and interactions and a wide array of responses (as a result of multivalent binding) in biological systems are produced (for example, cellular activation, migration, and differentiation).^{164,1}

Synthetic multivalent ligand systems can be used to probe and interfere with such biological processes by acting as inhibitors or effectors of specific biological processes. Because of the increased complexity with which a multivalent ligand system can interact with a specific target in comparison to monovalent ligands, the mode of action attributed to a multivalent system can be tailored and optimised by altering the multivalent architecture of the ligand system.¹⁶⁵

The functioning of a multivalent system as an inhibitor results from the multiple presentation of specific ligands to a target which bind (ideally) with specificity and high-avidity. In comparison, the functioning of a multivalent system as an effector results from the inducement of a specific biological response in the target system (for example, clustering of biological macromolecules).¹⁶⁵ By changing the parameters of a synthetic multivalent system, the interaction and activity of that system with target is altered accordingly.^{165,163}

A good example of multivalent processes include carbohydrate-protein interactions, which are categorised by multiple copies of (individually) weak binding glycans exerting a stronger carbohydrate-protein binding interactions through high affinity multimeric interactions.^{163,164} This enhancement of ligand activity (in comparison to monovalent glycans) is referred to as the “cluster-glycoside effect”.¹⁶²

Multivalent ligands systems have been touted as providing new tools for the investigation of various biological problems and even potential drug-leads towards human diseases and infections where multivalent interactions play a role in the onset of sickness.¹⁶⁶

Common synthetic multivalency platforms in use include multivalent inhibitors based on functionalised organic frameworks (di-, tri-, tetra-, multi-), polymer architectures such as dendrimers, linear and branched polymers and nanoparticles.¹⁶³

II.1.5.1. Mechanisms of binding enhancement

The mechanisms by which multivalency exerts influence in biological systems are many and by no means is this section a thorough quantitative review of multivalent binding interactions. For illustrative purposes with regards to generic carbohydrate-protein binding interactions, multivalency mechanisms fall into two main classes; chelation effects and statistical (or proximity) binding effects.¹⁶³

II.1.5.2. Chelation effects

Chelation effects (see figure 26) are dependent on a target substrate possessing multiple ligand binding sites which can bind to a multivalent ligand-presenting platform. The binding potency of subsequent ligand interactions (compared to the initial ligand binding event) are enhanced as entropic penalties of interaction are accounted for on initial ligand binding, albeit whilst incurring a minor conformational entropy cost.^{162,164,166}

Where chelation effects are observed to increase the binding potency of a multivalent ligand system, enhancements in binding in the order of 10^3 - 10^6 have been observed. However, chelation effects are heavily dependent on the spacer functionality between the respective functionalised ligands (orientation and distance).¹⁶³

II.1.5.3. Statistical rebinding

Statistical (or proximity) binding effects (see figure 26) are best exemplified by statistical rebinding mechanisms which have multivalent origins. This binding mechanism arises in situations where only a single binding site is available for ligand-target interaction due to limitations of the spacer functionality. The spacer limitations thus prevent ligand interaction with other potential binding sites. Despite the physical binding limitation placed on the ligand system, multivalency effects are still observed and are attributed to the differences in binding rates between monomeric ligands and ligands as part of a multivalent platform. A net-increase in ligand affinity is observed for multivalent systems as a result of the slower dissociation rate (or “off-rate”) compared to monovalent ligands.¹⁶³ This decreased “off-rate” is a consequence of the increased proximity of other ligands which can undergo a binding interaction after the initial ligand dissociation.¹⁶³ Non-chelation effects are typically regarded as weaker multivalent interaction mechanisms where chelation binding is effective.

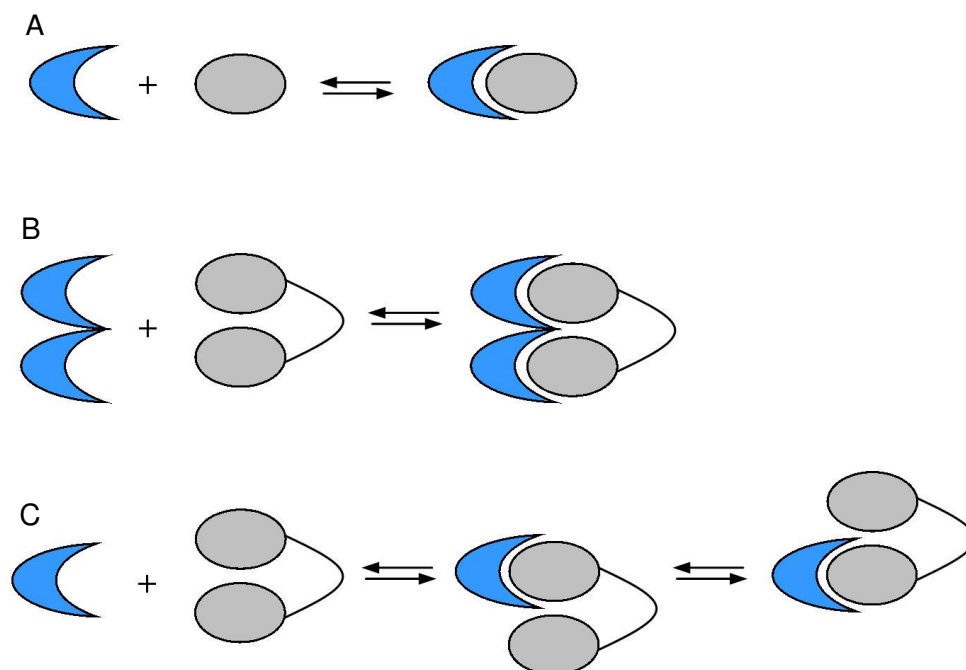


Figure 26. Simple mechanisms of ligand binding; (A) Monovalent binding, (B) divalent ligand binding via chelation and (C) divalent ligand binding via statistical rebinding. Adapted from; *Organic and Biomolecular Chemistry* **2009**, 7, 2013-2025.

II.1.6. Multivalency with regards to influenza

Monomeric sialic acids are bound by the HA with high selectivity but only with low affinity, as it is typical for carbohydrate-protein interactions.¹⁶⁷ Indeed, the interaction between the sialylated receptor determinants and the HA active site are considered weak.⁸⁶ As such, the interactions between the influenza HA and its sialylated receptor determinants is based upon the multivalent, cooperative interaction of sialylated glycans binding to the HA binding site. The high-avidity, multivalent nature of the interactions therefore compensate for the individually weak binding sialylated receptor determinants.^{121,166}

II.1.6.1. Synthetic platforms towards multivalency inhibitors of Influenza virus HA and NA

With regards to the application of synthetic multivalent platforms towards influenza viruses, the HA has been the main target for approaches using multivalent ligands as chemical probes or anchors for diagnostics and as possible therapeutic agents, for example, 'anti-adhesion therapy' (the inhibition of viral adhesion to the host cell with by

employing a soluble receptor analogue)¹⁶⁸ mainly because of the abundance of HA on the viral surface and its natural affinity for accessible sialic-containing derivatives.¹⁶⁶

Since the early 1990's, synthetic work towards multivalent sialoside inhibitors/effectors have been undertaken. The outcome of the majority of this research, particularly towards a multivalent therapeutic has been on the whole moderate.^{86,169}

Although selective binding and relatively high affinities have been obtained in many instances (as a result of the "glycoside cluster effect"), such approaches suffer from intrinsic disadvantages that come with the use of sialic acid as the ligand, for example; 1) susceptibility of *O*-sialosides to chemical and enzymatic hydrolysis, 2) the low affinity of sialic acid as a monovalent receptor, 3) the potential for cross-reactivity with other biological sialic acid processing machinery.

Below are some examples of multivalent systems which have been applied towards influenza viruses.

II.1.6.2. Multivalent sialic acid derivatives: low molecular weight scaffolds

A common approach towards HA inhibitors of influenza viruses are based on low molecular weight scaffolds of increasing multivalency. The inhibitory activities (determined from Hemagglutination inhibition assays) of divalent compounds (see figure 27) presenting α -sialosides were found to be heavily dependent on linker (spacer) length between the sialoside moieties, with longer linker lengths ($\sim 50\text{\AA}$) of moderate conformational restriction being relatively successful, with binding localised to individual virions HAs (non-clustering effects).¹⁷⁰

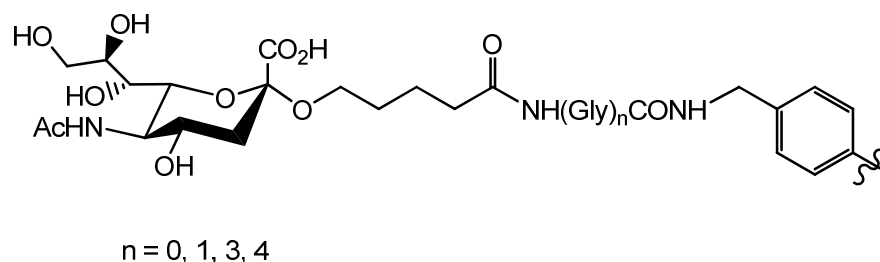


Figure 27. Example of a dimeric α -*O*-sialoside.

Another example of multivalent inhibitors of increasing valency includes α -sialoside presenting tetra-antennary peptides (see figure 28). These compounds exhibited binding to influenza virus and were able to inhibit viral adhesion 10^3 times more effectively than the native receptor, sialic acid.¹⁶⁹

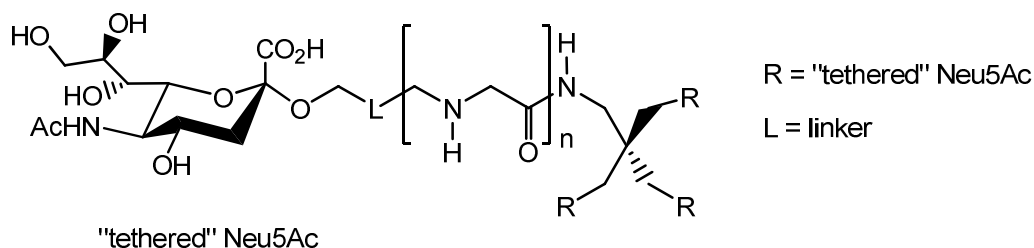


Figure 28. Example of a tetraivalent *O*-sialoside.

Other multivalent frameworks have also been used to increase the number of ligands presented by organic structures, a recent example for that are calixarenes.¹⁷¹ Calix[4]arene based *S*-sialoclusters (tetra- and octa-valent) have been shown to inhibit influenza virus adsorption (and as such, viral infectivity) to host cells at submillimolar concentrations (see figure 29). It has been speculated that the moderate results observed with these scaffolds come as a consequence of the "glycoside cluster effect".¹⁷²

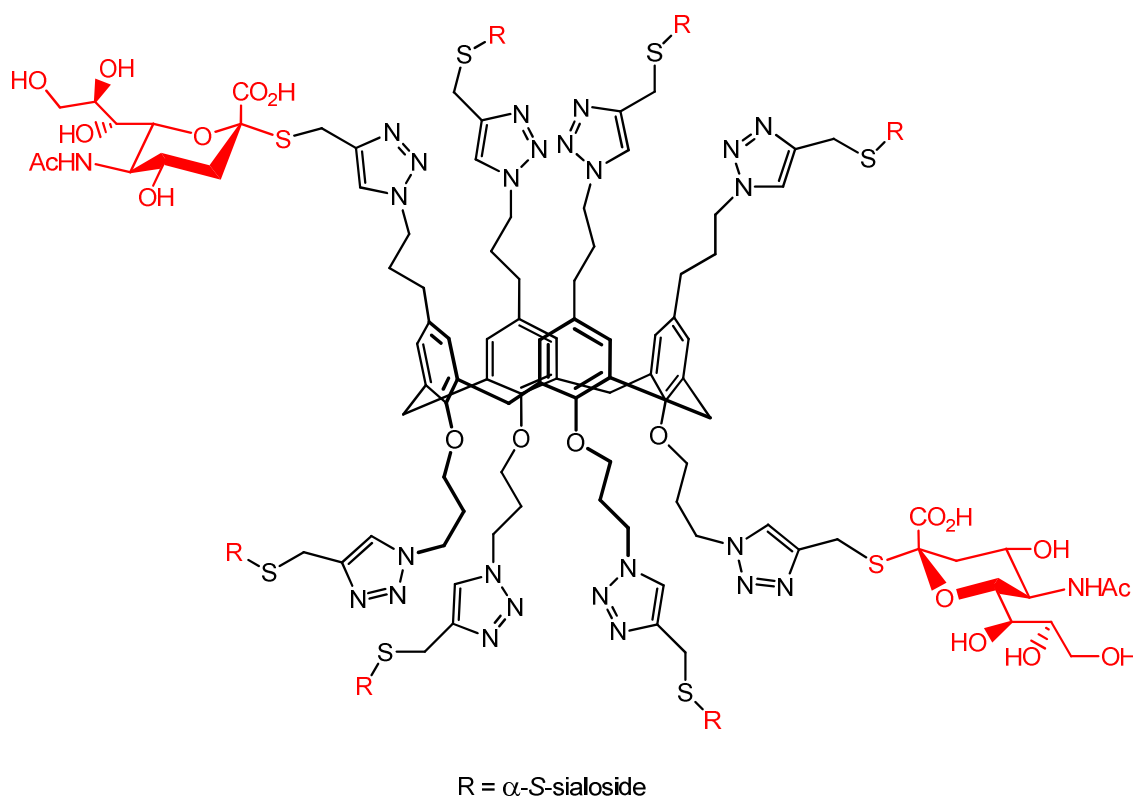


Figure 29. Example an octavalent calixarene scaffold functionalised with α -*S*-sialosides (red).

Inhibitors of increasing valency bound to relatively small organic frameworks highlight the importance of sialoside orientation and the distance between ligand functionalities in order to maximise binding to influenza viruses.¹⁶⁹

II.1.6.3. Multivalent sialic acid derivatives: polymeric scaffolds

As with di- and tetra-valent scaffolds, early synthetic research towards sialic-acid functionalised polymers and dendrimers applied towards influenza virus research and therapeutics began in the 1990's.¹⁶⁹

Dendrimers (typically globular, branched oligomers) are hyperbranched scaffolds which allow the multiple presentation of various ligand types, including α -sialosides.¹⁷³ Sialic acid decorated dendrimers have been shown to prevent erythrocyte agglutination (via a Hemagglutination inhibition assay) in the presence of influenza A (X31, H3N2) in the micromolar range.¹⁷³ The use of contrasting dendrimer architectures has led to observed differences in influenza (H2N2 and H3N2) hemagglutination inhibition (up to 5×10^4 times greater than Neu5Ac) and showed a dose-dependent reduction in influenza infection *in vitro* (see figure 30).¹⁷⁴

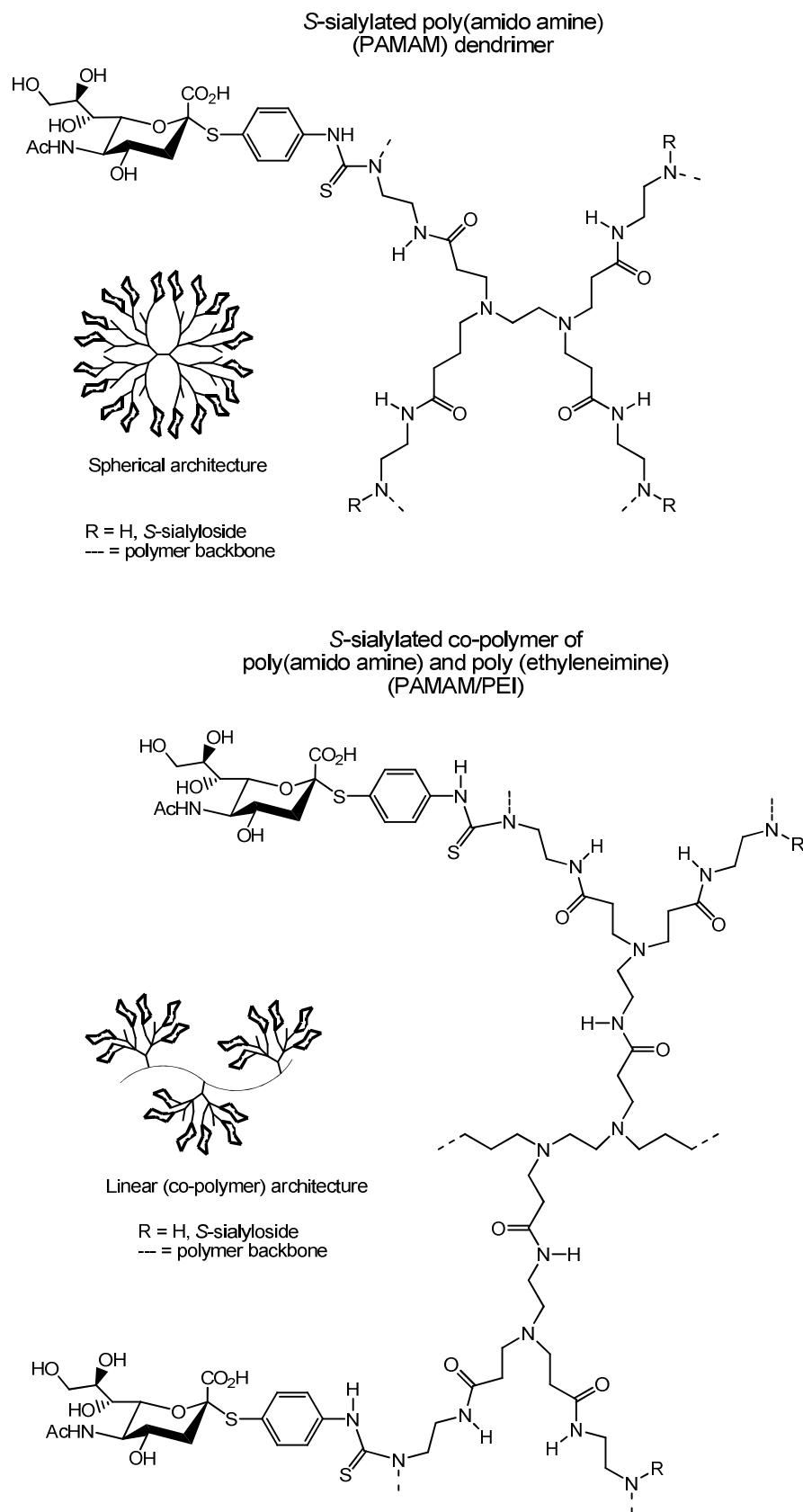


Figure 30. Examples of contrasting dendrimer architectures which exhibit inhibition of influenza virus (H2N2 and H3N2) via hemagglutinin binding.

More recently, the application of dendrimer-based nanoparticles has been applied towards influenza virus with the aim of developing “anti-adhesion” therapeutics (see figure 31). Hyperbranched polyglycerols are dendritic polyether-polyols (water-soluble) which when functionalised with α -sialosides (*O*- and *S*-sialosides) inhibited influenza A virus (X31) binding and fusion up to 80% (using nanoparticles of diameter ~ 100 nm). The optimisation of ligand density and nanoparticle size to match that of the influenza virus size and receptor multiplicity were found to be essential for good inhibitory activity. This ensured that biological surface interactions closely resembled multivalent binding events involved in virus-cell surface binding.¹⁷⁵

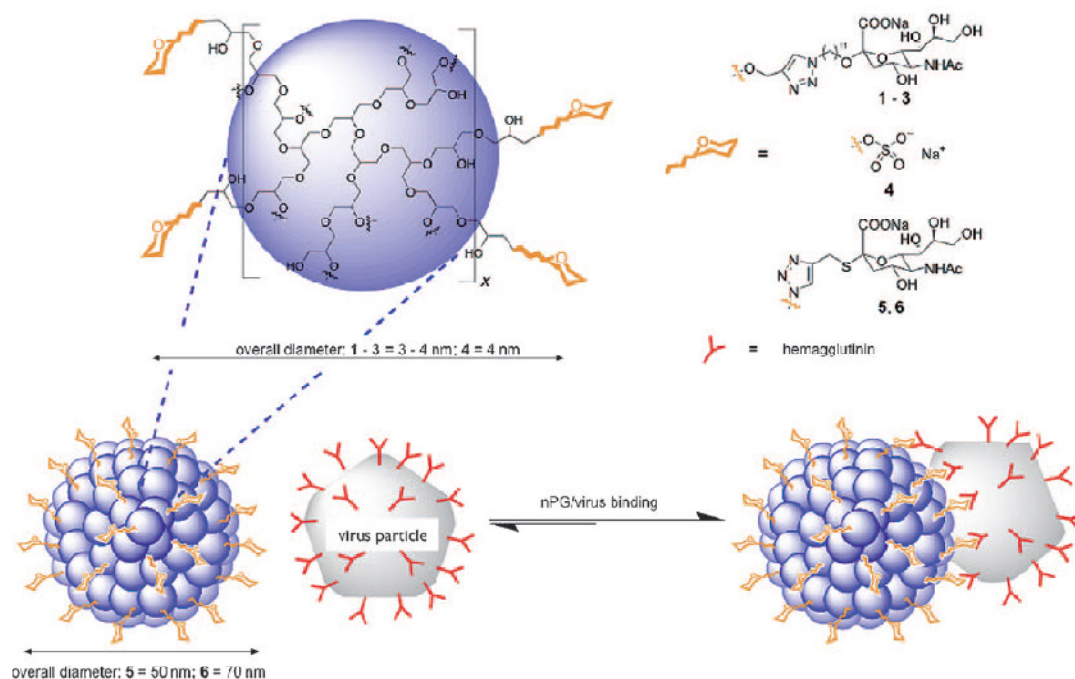


Figure 31. Schematic representation of dendrimer-based nanoparticles used to inhibit influenza viral infection. (Reprinted with permission from Wiley-VCH Verlag GmbH & Co. KGaA; *ChemBioChem* **2011**, 12 (6), 887–895.)

HA inhibitors based on polymeric α -sialoside-functionalised architectures have been developed over last two decades. Synthetic backbones, typically amorphous linear polymers the majority of which being copolymers of acrylic acid esters^{176,177} copolymers of acrylamide esters^{178,176} or other backbones.¹⁷⁹

Generally, polymeric sialic-acid bearing systems exhibit millimolar to nanomolar inhibition of hemagglutination by influenza viruses when the scaffold structures are optimised, particularly, the chemical structure and topology of the ligand, its content in the polymer, and the structure of the polymer side chains.^{177,176}

Polyacrylamide structures have tended to show greater inhibitory activity than highly branched dendrimeric structures but biological toxicity of the former is a concern.¹⁶⁹ The inhibitory activity of large polymeric multivalent platforms has been attributed to the “glycoside cluster effect” but also achieved through the steric stabilisation of the influenza virus surface or via changes in solution viscosity and viral particle aggregation.¹⁶⁹

More recently, a rapidly synthesised (1-step) polymeric chitosan functionalised with sialylated glycans (for example, free sialyl glycan (FSG)) has shown inhibitory activity against influenza virus infection (micromolar IC_{50} values obtained in inhibition assays with influenza A H1N1) in comparison to free glycans (see figure 32).¹⁸⁰

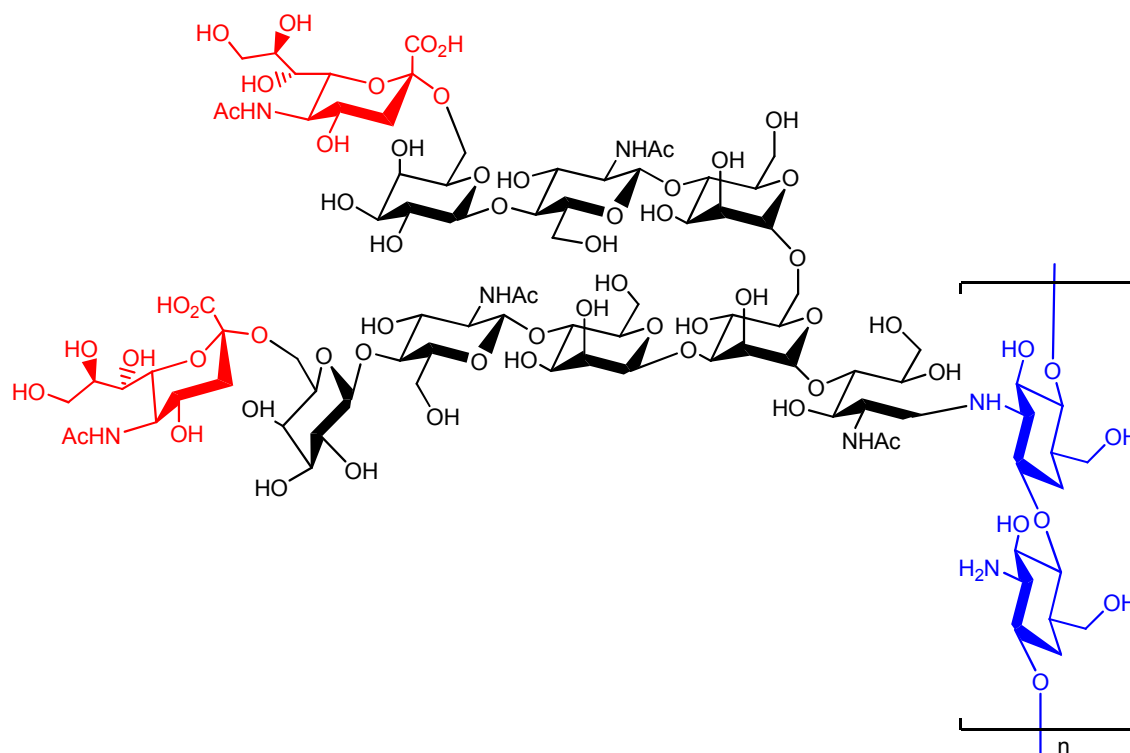


Figure 32. FSG-chitosan polymer, which exhibits inhibitory activity against influenza virus infection. The constituent parts of the polymer are highlighted; the terminal sialic acids (red), the underlying glycan structure (black) and the chitosan polymer backbone (blue).

II.1.6.4. Multivalent sialic acid derivatives: other scaffolds

Though not strictly speaking multivalent scaffolds in the same vein as those presented previously, recent examples have made use of multivalent α -sialoside-mediated interactions with influenza for the development of influenza detection methods. A biotin-labeled biantennary scaffold functionalised with α -sialosides (see figure 33) has been used to develop a reporter assay (based on the sandwich immunoassay method) using glycans only rather than virus-specific antibodies. The well-known biotin-

avidin/streptavidin interaction¹⁸¹ can therefore be used to immobilise the α -sialoside biantennary structure and through multivalent interaction with influenza HA, immobilise influenza virus. The position of ligand, orientation, density, linker length and ancillary groups influence the binding and selectivity to influenza.¹²⁰

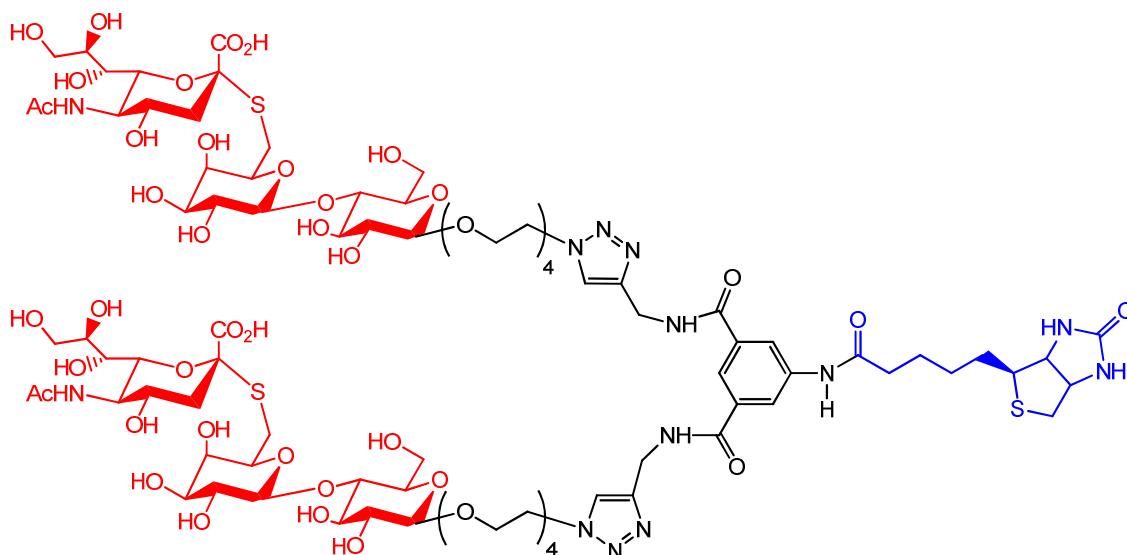


Figure 33. Biotin (blue)-labelled biantennary scaffold functionalised with a α -S-sialosides containing glycan (red).

II.1.6.5. Multivalency and influenza therapeutics: targeting the NA

With regards to the targeting of the HA of influenza viruses, to date no multi- or polyvalent α -sialoside scaffolds are used therapeutically for the treatment of influenza viral infection. This is due mainly to inconsistency problems and problems with the pharmacokinetics of polymer-based systems.^{169,168}

Many of these problems can be attributed to those outlined above regarding multivalent approaches to HA targeting. Though some problems associated to these approaches can be overcome (for example the use of *S*- and *C*-sialosides instead of *O*-sialosides)⁸⁶ the essential problem, that of increasing monovalent ligand affinity towards the HA, has remained challenging.

II.1.6.6. Multivalent sialylmimetics: low molecular weight scaffolds

Whilst the NA has so far prevailed against the HA as drug target it has not been utilised as frequently as a target for “anti-adhesion therapies”, mainly as a result of the non-participation of NA in viral hemagglutination.¹⁷⁰

Multivalency concepts have been applied to NA inhibitor scaffolds (mainly zanamivir) in the same vein as small organic molecule scaffolds (low molecular weight clusters) and polymeric scaffolds.^{182,183} The inhibitory potency and affinity of these sialylmimetics towards NA is significantly greater than the corresponding affinity of α -sialosides for HA and hence their appeal in multivalent applications.

The synthesis of divalent NA inhibitors based on the zanamivir structure (optimum linker length $\sim 20\text{\AA}$, ~ 10 -18 methylene linker units)¹⁸⁴ have shown *in vitro* and *in vivo* inhibition of influenza virus replication and were found to be approximately 100-fold more active than monovalent zanamivir (see figure 34). However, NA inhibition levels were compromised slightly. As such, improved influenza inhibition is attributed to multivalency effects (viral cross-linking and clustering) rather than improved NA inhibition.^{184,185} Such divalent inhibitors have exhibited a longer retention time and greater efficacy and thus potentially offer a low-dose therapeutic treatment for influenza infection.^{96,184,185,186}

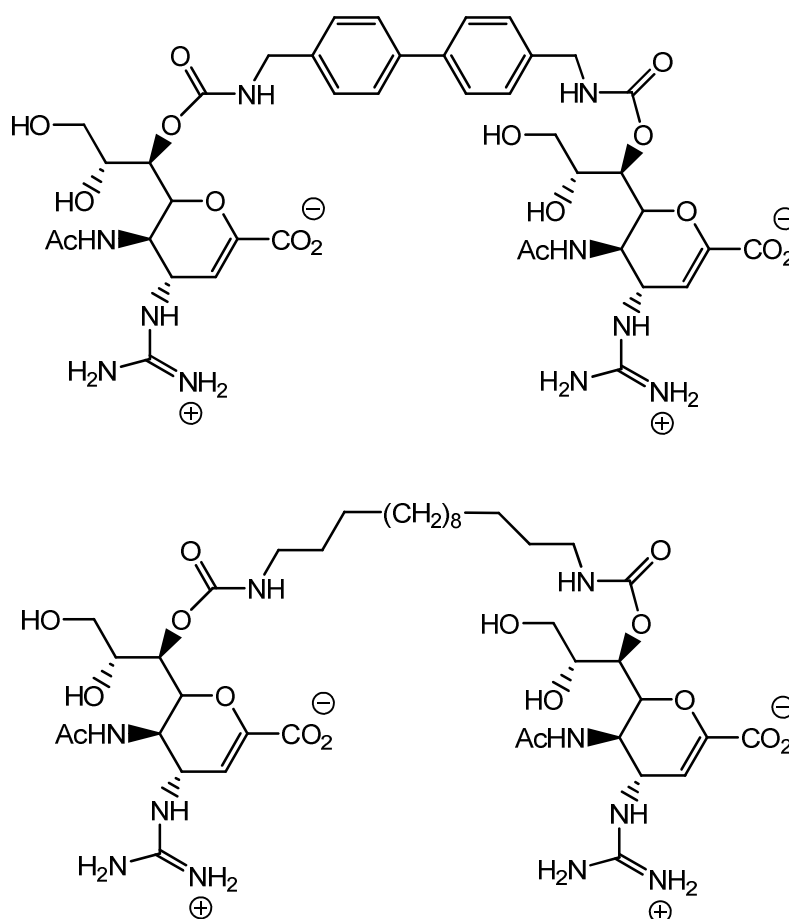


Figure 34. Examples of dimeric zanamivir structures.

A recent multivalent inhibitor presenting tetravalent zanamivir upon a porphyrin scaffold has shown decreased activity towards NA inhibition but inhibits influenza virus replication approximately 100 times more potently than monovalent zanamivir (see figure 35). The enhanced inhibition activity has been attributed to a photosensitisation process causing NA inactivation directly, as well as multivalency effects.¹⁸⁷

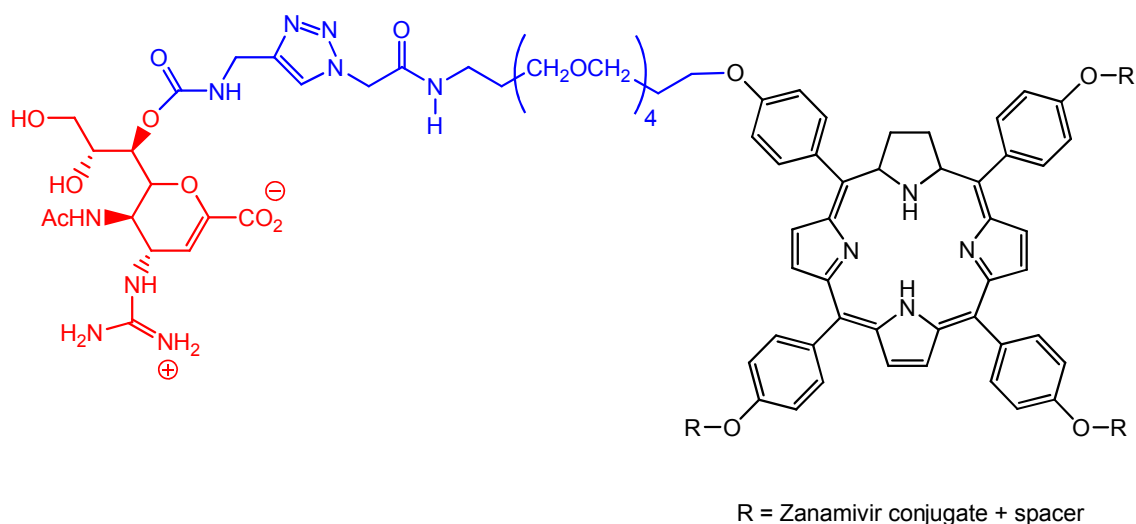


Figure 35. A tetravalent zanamivir-porphyrin structure. The zanamivir conjugate (red) and spacer (blue) and porphyrin scaffold (black) are highlighted.

II.1.6.7. Multivalent sialylmimetics: polymeric scaffolds

A recent example of zanamivir conjugated to poly-L-glutamine via a flexible linker (see figure 36) exhibits inhibition of group-2 NA influenza strains (both oseltamivir and zanamivir resistant) and wild-type viruses up to approximately 2×10^4 greater than monovalent zanamivir (during the plaque reduction and binding affinity assays). It is speculated that the polyvalent presentation of zanamivir compensates for reduced NA inhibition by monovalent zanamivir with resistant influenza strains.¹⁸⁸

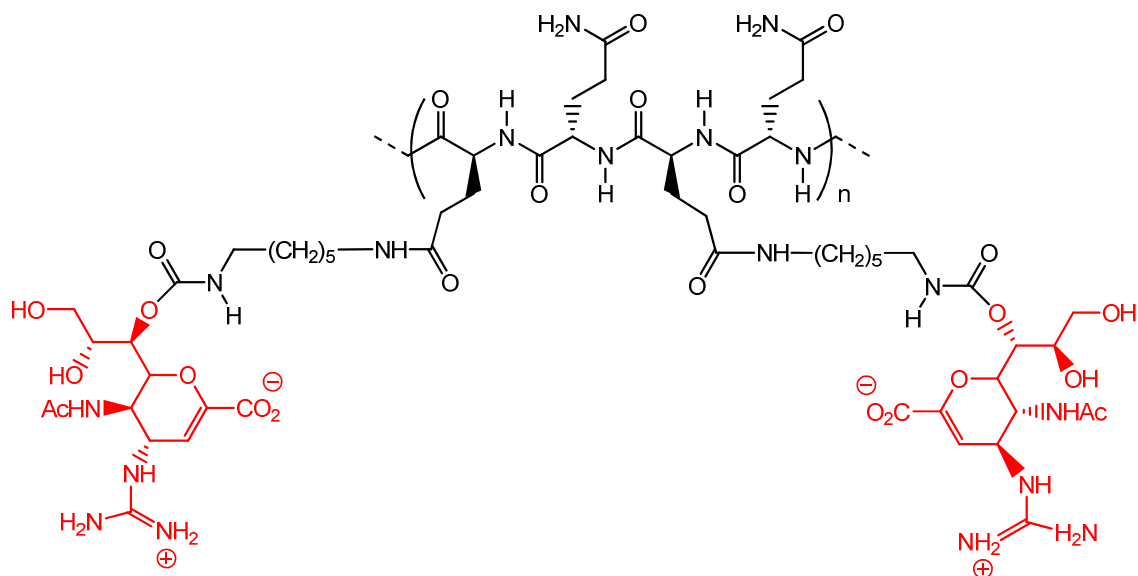


Figure 36. Polymeric (poly-L-glutamic acid) zanamivir. The zanamivir scaffold is highlighted (red).

II.1.6.8. Multivalent sialylmimetics: other scaffolds

Zanamivir appears the more applicable NA inhibitor for use in multivalent inhibitor platforms (as a result of the ease in conjugation without significant pharmacophore compromise). Oseltamivir functionalised materials are rare. An example of the use of the oseltamivir scaffold in a multivalent fashion is the attachment of the oseltamivir scaffold, modified at the traditional pentyl-ether linkage, to solid-phase resin beads (see figure 37) for application to affinity chromatography (towards influenza virus isolation and purification). Only minor binding events were observed with H1N1 NA but were not quantified. The lack of effective multivalent interactions and subsequent influenza binding is more likely a result of the compromised oseltamivir pharmacophore, resulting in a greatly reduced binding affinity to influenza NA.¹⁸⁹

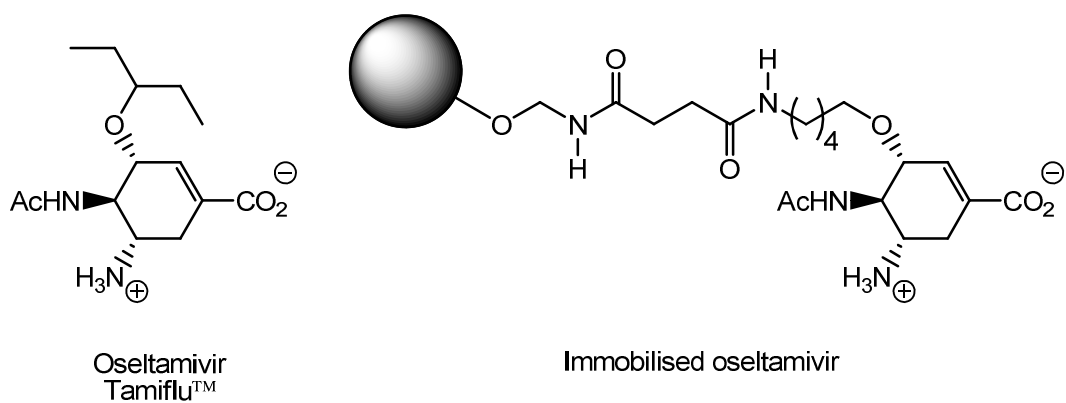


Figure 37. Immobilised osetamivir analogue. The osetamivir core is linked to an affinity-chromatographic resin via a short methylene spacer (right). Unfunctionalised osetamivir (left) is shown for comparison. Adapted from; *Tetrahedron Letters* **2009**, 50, 3205-3208.

II.1.7. Nanoparticles

Nanoparticle research has developed into a broad scientific discipline over the past two decades.¹⁹⁰

The significant interest generated by nanoparticle platforms comes as a result of the unusual physical and electronic properties and as a result of their structure, particularly “quantum size effects” (*vide infra*). Nanoparticle suspensions are best described as colloidal systems, though they are at the lower end of the colloidal range (1nm - 1 μ m) (see figure 38).¹⁹¹

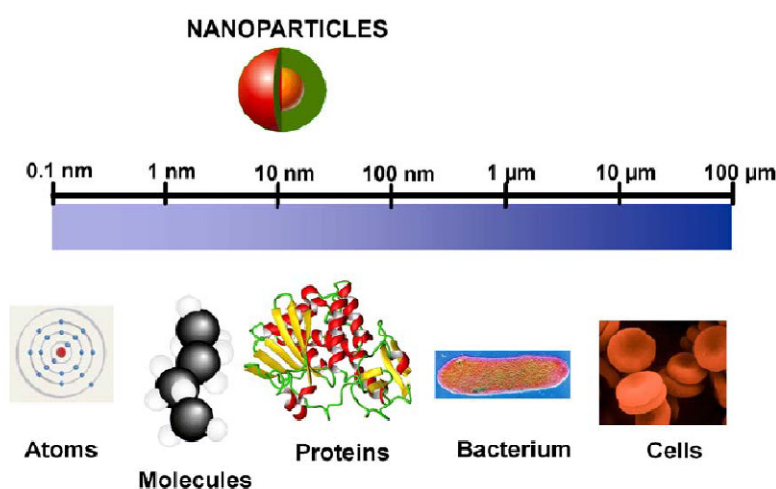


Figure 38. The size scale of nanoparticles. (Reprinted with permission from Elsevier; *Biochimica et Biophysica Acta (BBA)* **2006**, 1760, 636 - 651.)

A common method of inorganic nanoparticle stabilisation is the functionalisation of the metal surface with organic ligands, akin to self-assembled monolayers of 2D surfaces.^{192,193}

Self-assembled monolayers (or the ligand shell) simultaneously stabilise the nanoparticle surface (preventing core agglomeration) and present chemical functionality at the particle-solvent interface. As such, properties of nanoparticles are heavily determined by the nature of the surrounding ligand shell.^{193,194}

Inorganic nanoparticles have been constructed from a variety of elements and are not restricted to any particular metal. However, gold has become a standard platform for nanoparticle applications. It is a reasonably inert metal, is widely studied and is widely used as a platform in other spectroscopic and analytical methods.¹⁹³

As a consequence of the widespread use of gold as the nanoparticle core, sulfur-containing stabilising ligands (alkylthiolates derived from thiols or disulfides) are most

commonly used as the stabilising ligand shell because of the thiophilic nature of gold.^{193,195}

Nanoparticles have emerged as a popular scaffold for the presentation of multiple copies of bioactive motifs en route to developing novel tools and sensors for investigation biological systems and processes. Of particular interest to this project has been the use of nanoparticles as probes for the study of carbohydrate–protein and carbohydrate–carbohydrate interactions, providing an alternative to traditional multivalent ligand presenting platforms. This comes as a result of the advantage of using nanoparticle platforms to investigate multivalency effects as the three-dimensional globular structure can be used as a model system for the dense glycan coverage found on cell surfaces.^{196,197,198}

The properties of gold-nanoparticles (on account of their low-level of cellular toxicity)¹⁹³ in particular have led to many developments towards applications in towards biology and medicine, some recent examples of which include; cellular imaging,¹⁹⁹ antibacterial agents²⁰⁰ and potential therapeutics and therapeutic delivery agents.^{201,202}

II.1.7.1. Gold nanoparticles: quantum size effect

The physical properties of nanoparticles occupy a middle ground between that of bulk materials and molecular compounds and reflect the electronic band structure of nanoparticles of this size as predicted by quantum-mechanics, that is, unlike bulk metals there is a distinction between the valence and conduction bands. When the de Broglie wavelength of the valence band electrons is the same order as the nanoparticle size, then nanoparticles behave electronically as zero-dimensional “quantum dots”.¹⁹⁵

It is in part the behaviour of these zero-dimensional “quantum dots” which give rise to novel size- and shape-dependent optical and electronic properties (along with a high surface/volume ratio and varied surface functionalisation) which give nanoparticles their interesting properties and has led to many potential applications of colloidal nanoparticles (in comparison to bulk materials).^{203,190}

II.1.7.2. Gold nanoparticles: bonding

The nature of bonding between the stabilising sulphur-terminated ligands and the gold core is complicated but can be broadly categorised as thiolate-gold interactions of significant covalent character.^{204,195} Experimental evidence suggests that the formation of gold nanoparticles from thiols- or disulfides yield a monolayer coating of equivalent structure.¹⁹³

However, this bonding picture does indicate a significant degree of charge transfer from the gold to the sulphur moiety and not strictly speaking a gold (Au^{I}) sulphide interaction.^{193,195}

The surface stabilisation by sulphur-terminated ligands is a reversible process (energy barrier approximately -30 kcal/mol) and place-exchange reactions by other sulphur terminated ligands are possible though the process is not facile (*vide infra*).¹⁹³

Although the thiolate-bonding model is widely held, experimental and theoretical investigations into small gold-nanoparticle structures (less than 2 nm in diameter) have developed a bonding picture of greater complexity. Stabilising ligands are bonded to surrounding ligands and gold atoms in a bridging co-ordinated fashion. It is also apparent that the nanoparticle gold atoms are not strictly part of the core but exist as discrete co-ordinated “staple” structures as part of nanoparticle superstructure. Though this bonding picture has not been proved or developed for larger gold nanoparticles.^{205,190}

Other stabilising ligands with different functionalities to sulphur are known to stabilise gold nanoparticles. These include amines, phosphines, and carboxylates. However, these interactions are known to be weaker (thermodynamically)²⁰⁶ than the Au-S interaction (approximately -50 kcal/mol) and often the stability of other terminating ligands comes as a result of kinetic stabilisation only.^{195,207}

II.1.8. Gold nanoparticle synthesis and characterisation

The two most widely applied methodologies for the synthesis of gold nanoparticles are; 1) the *in situ* synthesis of gold nanoparticles from the reduction of Au^{III} by a reducing agent in the presence of a suitable sulphur-containing ligand (the Brüst-Shiffrin method)^{208,209} or 2) the synthesis of pre-formed gold nanoparticles from the reduction of Au^{III} by a mild reducing agent (the Turkevitch method) followed by ligand-exchange reaction upon the gold surface with thio-functionalised ligands.²¹⁰

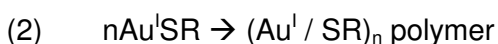
With regards to the Brüst-Shiffrin method, nucleation and gold cluster formation is achieved by rapid addition of reducing agent, whereas gold nanoparticles produced by the Turkevitch method rely upon the decomposition of the Au^{III} precursor at elevated temperatures.¹⁹³

II.1.8.1. Brüst-Shiffrin method

The Brüst-Shiffrin method allows the rapid synthesis of gold nanoparticles of reduced size and polydispersity, with particle diameters typically ranging from approximately 1 to 10 nm (depending on reaction conditions and reagents).¹⁹⁵

The limitation to small nanoparticle size distributions comes as a result of the slow rate of desorption of thiolate ligands on gold. The binding of thiolate ligands to the gold surface retards the growth of the surface through the stabilising influence of the ligands, thus defining nanoparticle size. The size of the nanoparticles obtained by this method can be altered therefore by the Au:thiolate-ligand ratio used and also by controlling the temperature and the rate at which the reducing agent (commonly sodium borohydride) is added. The manipulation of these variables alters the rate at which the gold precursors nucleate and grow to form nanoparticle clusters.^{195,193,211}

Originally based on a two-phase transfer method, initially involving the reaction of auric acid with tetraoctylammonium bromide (TOAB) followed by thiol or disulfide nanoparticle functionalisation,²⁰⁸ the Brüst-Shiffrin method was thought to follow this simplified reaction pathway; 1) The reduction of the Au^{III} precursor to Au^I by the stabilising ligand, 2) the formation of an Au^I polymeric structure bridged by thiolate-sulphur atoms and 3) the further reduction (by sodium borohydride) of the Au^I-SR to Au⁰ and the formation of stabilised gold clusters (see figure 39).



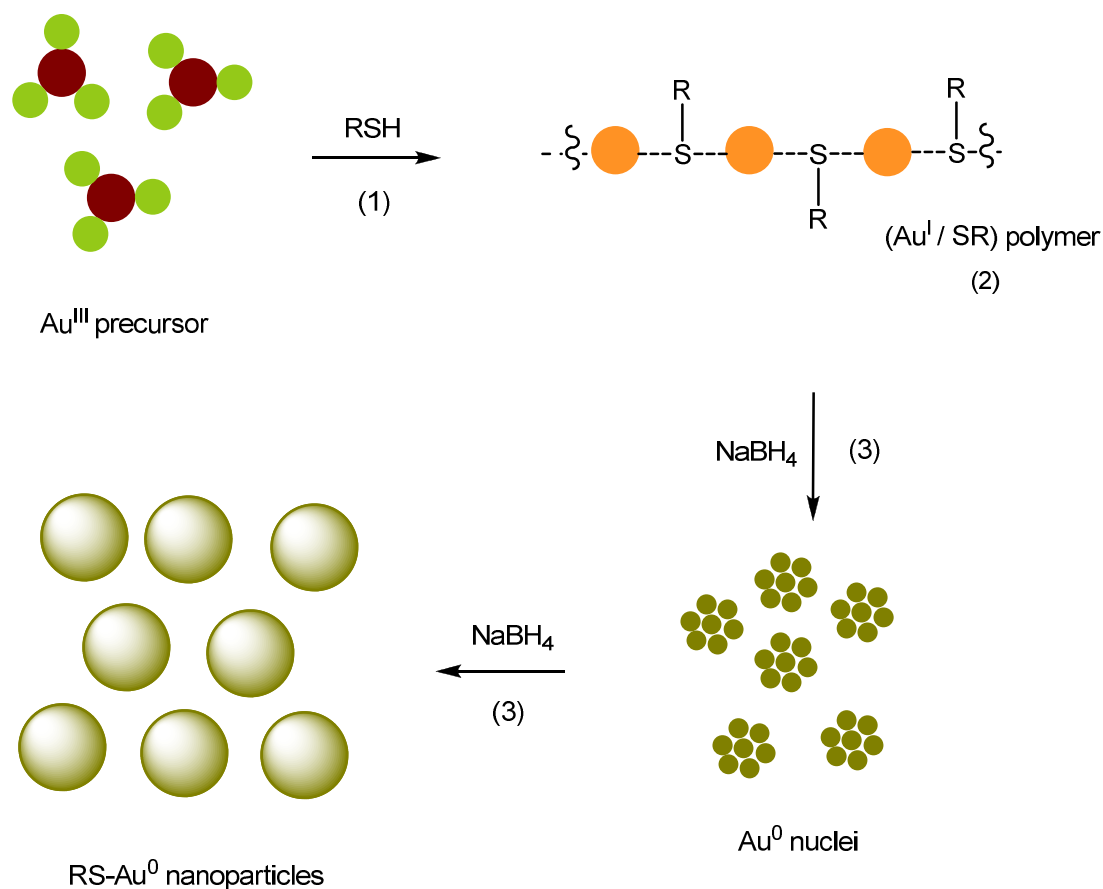


Figure 39. Simplified schematic depicting of gold nanoparticle synthesis via the Brüst-Shiffrin method. Numbers (1), (2) and (3) refer to the stages in nanoparticle synthesis as given by the equations above. Adapted from; *Chemistry: A European Journal* **2010**, 16, 1459-1463.

Recent research has demonstrated that this mechanistic picture is misleading when applied to the original two-phase Brüst-Shiffrin method as Au^{I} polymeric structures are not observed (by NMR) and that Au^{III} and Au^{I} tetraalkylammonium ($[\text{AuX}_2][\text{NR}_4]$ and $[\text{AuX}_4][\text{NR}_4]$) species are the precursors present in solution prior to the addition of reducing agent (see figure 40).²¹²

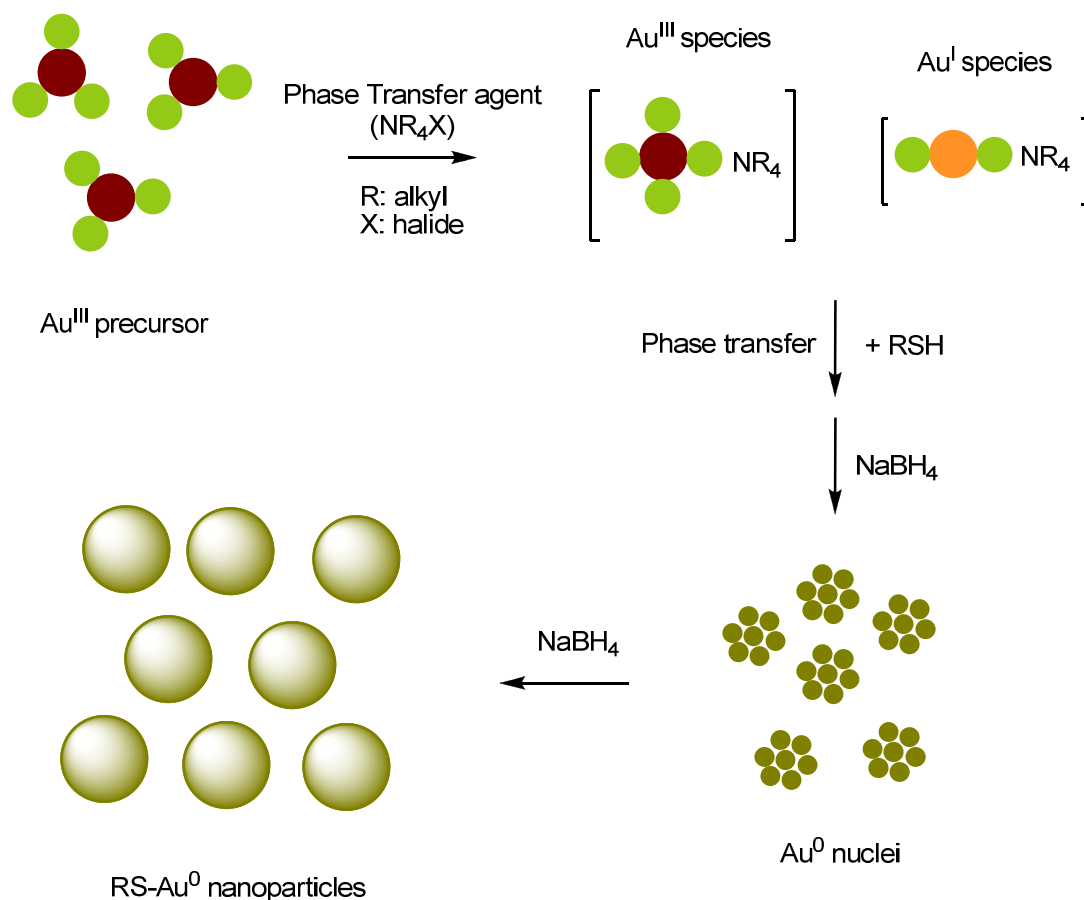


Figure 40. Simplified schematic depicting of gold nanoparticle synthesis via the Brüst-Shiffrin method including the formation of Au-tetraalkylammonium species.

Moreover, current research has corroborated this mechanistic correction (via Raman/DLS spectroscopy) and has indicated the formation of reverse-micelle structures in solution prior to reducing agent addition. These reverse-micelles encapsulate water and as such act as the repositories for the intermediate gold tetraalkylammonium species. Thiolate functionalisation of Au^0 subsequently proceeds (on the addition of reducing agent) via ligand diffusion through the micelle structure resulting in the formation of discrete Au-S bonds.²¹³

The original Brüst-Shiffrin method has been modified by carrying out the reaction in MeOH or MeOH/water mixtures and can tolerate considerable variation in stabilising ligand functionality beyond simple alkylthiol species in order to produce gold nanoparticles with the necessary attributes (for example, water solubility) for biological applications.^{209,214-217}

The use of ligands with ionisable groups often provides an electrostatic barrier to gold nanoparticle formation with irreversible aggregation of gold observed on the addition of

reducing agent. The decrease of solution pH during nanoparticle synthesis prevents core-core coalescence and is an essential adjustment to the Brüst-Shiffrin method when water-soluble gold nanoparticles are desired.²¹⁴ Mechanistically, the Brüst-Shiffrin method is believed to follow the originally proposed pathway in highly polar solvents (that is, the formation of intermediate Au^I polymeric structures as single-phase nanoparticle precursors). This is attributed to the prevention of gold-quaternary cation ion-pairs formation through solvent coordination effects.²¹²

II.1.8.2. Turkevitch method with ligand-exchange

The Turkevitch method (and Ligand-exchange) is generally considered the more popular method of gold nanoparticle synthesis¹⁹⁰ because of the larger diameter, lower polydispersity and heterogeneity of the nanoparticles produced (in comparison to the Brüst-Shiffrin method). It is based upon the formation of gold nanoparticles stabilised by weakly bound citrate molecules. The resulting gold colloid is stabilised via the electrostatic interaction between the citrate and the gold surface, however the stabilisation process initially requires elevated temperatures.¹⁹⁵ Maintaining elevated temperatures is critical to nanoparticle synthesis. Reducing the temperature during synthesis causes irregular shapes and larger diameters in the gold nanoparticles obtained.²¹⁸

The ratio of the reducing agent (usually trisodium citrate) and Au^{III} precursor is used to generate nanoparticles of approximately 10-20 nm in diameter.

The faster rate of desorption of weaker citrate co-ordinating ligands in comparison to the thiolate-ligands of the Brüst-Shiffrin method leads to larger nanoparticle sizes.¹⁹³

A recent mechanistic suggestion for gold nanoparticle synthesis by the citrate reduction method includes the following mechanistic processes (see figure 41); 1) a ligand exchange process with citrate, 2) a rate-determining ring-closure step where decarboxylation and Au^{III} to Au^I reduction occur and 3) the disproportionation of Au^I species which subsequently form the Au⁰ core of the nanoparticles.²¹⁹

The dicarboxyacetone formed is believed to form an extended molecular complex with Au^I species in solution and as such is heavily implicated in the disproportionation process. More specifically, it is suggested that the balance between the rate of Au⁰ nucleation and dicarboxyacetone degradation (generating acetone and carbon dioxide) affects the nanoparticle size obtained during the reaction, as well as the initial citrate/Au ratio.^{220,219}

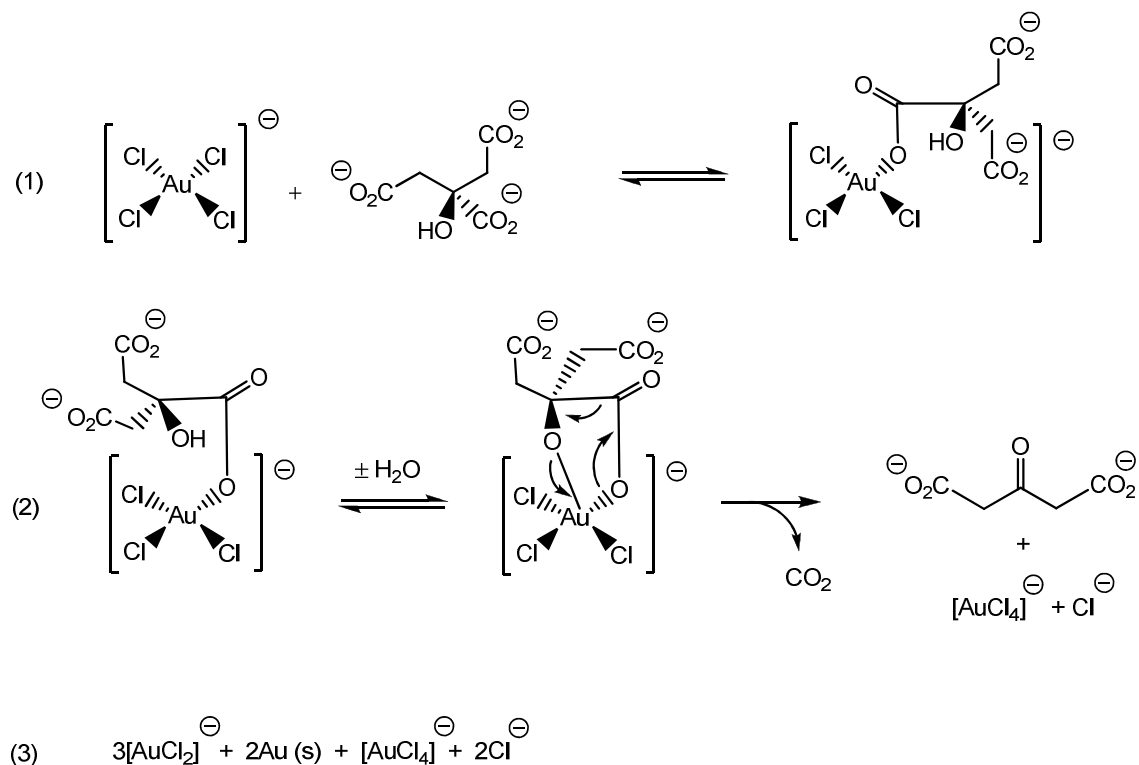


Figure 41. Proposed mechanism towards the formation of gold nanoparticles by the reduction of Au^{III} salts by trisodium citrate (Turkevitch method).

The loosely-affiliated citrate molecules which stabilise the gold core can be exchanged for stabilising ligands which have a greater affinity for gold (thio-functionalised ligands) and in this way the citrate can be exchanged from the nanoparticle surface. The exchange reaction can be assumed to reach completion with the use of excess stabilising ligand.¹⁹⁰

The main advantage offered by this technique is that gold nanoparticles can be rapidly functionalised displaying various ligand functionalities without impairing the characteristics of the gold core, which is a synthetic issue for the Brüst-Shiffrin method.¹⁹⁶

II.1.8.3. Place exchange reactions: further functionalisation

Alkylthiolate-stabilised gold nanoparticles can be subject to further place-exchange reactions by other sulphur-containing ligands after initial functionalisation. As such, place-exchange reactions open up gold nanoparticles to further functionalisation.

The rate of ligand exchange is heavily dependent on the nature of the ligands involved, more specifically, the ratio between the incoming- and outgoing-ligand, the linker lengths and steric bulk of the incoming- and outgoing-ligand.¹⁹⁵

Experimentally it has been determined that ligands bound at vertices and edges of gold nanoparticles have higher rate of exchange than ligands bound at planar faces²²¹ and an increased exchange rate is also observed with increasing positive charge on the nanoparticle core.²²²

Alkylthiolate place-exchange reactions have a characteristic 1:1 stoichiometry, are based on an associative mechanism, yield the displaced ligand in solution as a thiol and are known not to involve disulfides or oxidized sulfur species.²⁰⁴

II.1.9. Characterisation of gold nanoparticles

II.1.9.1. Gold nanoparticles: size and shape

Gold nanoparticles stabilised by thiolate ligands tend to adopt a roughly spherical shape with the exception of small nanoparticles (<1 nm diameter), which tend to exhibit octahedral or cubo-octahedral morphologies. The roughly spherical shape adopted by larger gold nanoparticles comes as a result of the similar affinity of thiolate ligands for all gold crystalline faces and as such the overall shape of the nanoparticle is not preferentially controlled by thiolate binding to gold.¹⁹³

It has also been observed that the ligand surface coverage of gold nanoparticles is greater than that observed with two dimensional self-assembled monolayers. It is understood that this high surface coverage results from higher ligand-to-gold binding ratios or nanoparticle core edges and vertices.¹⁹⁵

The degree of ligand organisation on the surface of a gold nanoparticle is very much dependent on the nature of the ligand itself (for example, ligand size, steric bulk and terminal functionality). In order to minimise the free energy of the ligand shell, the thiolate anchored ligands adopt conformations which enable inter-ligand interactions (for example, Van der Waal interactions or hydrogen bonding). Interactions of this type result in a secondary level of ligand organisation on a nanoparticle surface.¹⁹³

II.1.9.2. Stability of gold nanoparticles

The need for stabilising ligands upon gold nanoparticles is a result of the need to shield the gold cores from particle-particle agglomeration on the account of the high surface energy of the gold nanoparticle core.²²³

Brownian motion (the random movement of particles in a fluid due to continuous interaction from molecules of the surrounding medium) alone is insufficient to form dispersions capable of preventing such interactions. The physical barrier (stabilising ligands) is therefore required, and these barriers are typically based around electrostatic or steric stabilising processes.²²⁴

The stability of colloidal gold systems can be described qualitatively as being dependent on the type and nature of the forces used to stabilise the colloidal system, these forces can be quantified to some degree by DVLO (Derjaguin-Landau-Verwey-Overbeek) theory. Qualitatively, DVLO theory describes colloidal stability in terms of the total free energy of interaction (G) and is composed of the sum of the Van der Waal interactions and electrostatic interactions ($G = G_{VDW} + G_{electrostatic}$), where Van der Waal interactions (G_{VDW}) take on an attractive force as opposed to the repulsive force offered by electrostatic interactions ($G_{electrostatic}$). It is the balance between these two forces which determines the energy barrier needed to overcome colloidal stability.²²⁵

Though DVLO theory can be used in many cases to describe colloidal stability it cannot be used to accurately describe the interaction and stability of colloidal nanoparticle systems over small particle-particle distances because of the effects of non-DVLO forces also involved in colloidal stability. These forces include, hydrophobic, steric and solvation interactions, which can be stronger than DVLO forces depending on the nature or stabilisation method of the colloidal system (at both large and small particle separations).²²⁵

The balance between colloidal stabilising forces is no more sensitive and essential than in aqueous systems where water-soluble nanoparticles are of interest towards biological applications. The synthesis of functionalised gold nanoparticles containing ionisable ligand functionality (for example, amino- or carboxylate-groups) is challenging and problematic.²²⁶

The incorporation of ionisable ligands into nanoparticle systems can lead to the destabilisation of the colloid at physiological conditions. This takes the form of nanoparticle aggregation, which can be irreversible and/or reversible in nature depending on the nature of the interaction and the physical factors leading to the instability.^{227,228}

As previously mentioned, the properties and colloidal stability of gold nanoparticles are heavily dependent on the nature of the terminal functionality of the thiolate stabilising ligand. As such, the functionality of a terminal thiolate ligand has dramatic effects of nanoparticle stability in aqueous systems.

In many cases, the synthesis of water-soluble gold nanoparticles by the Brüst-Shiffrin method shows limited or mixed success (ligand dependent) with nanoparticles displaying limited colloidal stability over time.²²⁹ The situation is often pronounced for larger nanoparticles synthesised by ligand-exchange methodologies where it is a non-trivial process to maintain the electrostatic stability of a colloid and assemble a protective monolayer with a desired ligand (if the ligand is unable to form stabilising monolayer).²³⁰

It has often been observed that carboxy-terminated ligands show increased colloidal stability towards aggregation when used as nanoparticle stabilising ligands compared to amine-terminated ligands. The stability of such ligands in gold nanoparticle systems is heavily dependent on the ionic strength and pH of the surrounding medium in relation to the pKa of the ionisable functional groups.^{222,231} Changes in these conditions, particularly decreases in solution pH lead to ligand-induced nanoparticle aggregation through hydrogen-bonding networks (and subsequent nanoparticle aggregation through irreversible VDW interactions between the gold nanoparticle cores). The modulation of these conditions therefore overcomes the electrostatic repulsive forces which maintain colloidal stability (particularly when ionisable groups are involved).^{230,227,231}

Aggregation is also dependent to a large extent on the linker length between the anchoring thiolate and the terminal functionality. Longer linker lengths are equated with slower rates of aggregation in colloidal systems susceptible to such instabilities as a result of the higher energy barrier to aggregation (on account of favourable hydrophobic interactions between longer alkyl linkers). However, where ionisable ligands are involved, electrostatic forces often play the dominant role in determining colloidal stability.²²⁷

Unlike proteins where stability in aqueous systems can be maintained by protein folding and the subsequent energetic stabilisation of both hydrophobic and hydrophilic groups, nanoparticles which display ionisable ligands cannot rearrange to prevent unwanted electrostatic aggregation, particularly to prevent the attractive interactions from ammonium and carboxylate functionalities at physiological pH. It is therefore not surprising that gold nanoparticles are known to aggregate in aqueous solutions when thiol-containing amino acids/peptides are used as terminating ligands.²³²

Various synthetic methodologies (both novel and modifications to existing methodologies) have been developed to try and overcome these problems, often with success (towards a specific goal or application) but have yet to reach the simplicity of synthesis and the wide level of acceptance gained by the Brust-Shiffrin and Turkevitch/ligand-exchange methods for gold nanoparticle synthesis. Examples include; peptide-capped gold nanoparticle precursors,²³² a two-phase synthetic process, where the initial gold colloid is place-exchanged with intermediate anionic-stabilising ligands²³⁰ and alternative gold-precursor capping agents such as, DMAP, amino acids and Bunte salts (salts of S-alkylthiosulfuric acids).^{226,233,234}

II.1.9.3. Analysis of gold nanoparticles

The most common techniques to analyse gold nanoparticle preparations include electron microscopy techniques (TEM, HRTEM, SEM, AFM), light scattering methods (DLS,

SLS), X-ray diffraction and mass spectrometry (if applicable). Such methods are used for core visualisation and particle distribution analyses.¹⁹⁵ With regards to nanoparticle composition, other analytical methods such as elemental analysis, X-ray photoelectron spectroscopy or thermogravimetric analysis (TGA) are used.¹⁹⁵ These various techniques are often used in a complementary fashion to build up an overall picture of the nanoparticle preparation in order to overcome shortcomings with individual techniques.

Direct $^1\text{H}/^{13}\text{C}$ NMR analysis of gold nanoparticles particles often show a broadening or total absence of NMR resonance peaks (relative to the non-functionalised organic ligand) with increasing proximity to the Au-S bond.¹⁹²

The main reasons attributed to NMR resonance broadening include; 1) the difference in ligand packing density on the nanoparticle ($-\text{CH}_2-$ resonances closer to the Au-S bond experience faster spin relaxation effects from dipolar interactions), 2) the difference in ligand binding sites on highly faceted nanoparticles (vertices vs. edges vs. terraces) and 3) spin-spin relaxation (T2) broadening which is dependent of the rate of tumbling of nanoparticles in solution (analogous to large macromolecules or proteins rotating in solution).²³⁵

II.1.9.4. Surface plasmon resonance (SPR) band

As a result of the “quantum size effect” of gold nanoparticles, the absorption of electromagnetic radiation induces a collective electron oscillation of the free (metal-) valence electrons which gives rise to an enhanced electromagnetic field at the nanoparticle surface and subsequently a characteristic absorption band observable in the UV-Vis spectra of gold nanoparticles. This is termed the surface plasmon resonance band (SPR band) and is typically observed at approximately 520nm for particles approximately 5-20 nm in diameter. It is this SPR band which gives rise to the red-wine colour of gold nanoparticle preparations in this size range.^{195,224}

The excitation wavelength observed for gold nanoparticles is sensitive to a number of factors including the composition, particle size, particle shape, inter-particle distance and environment (dielectric properties) of the gold nanoparticles and surrounding solvent.^{195,224}

The SPR band is absent in gold nanoparticle preparations smaller than approximately 3nm in diameter. At these size ranges, gold nanoparticles are no longer considered “metallic” in nature (that is, they do not possess a mobile valence band of electrons) but can be treated quantum-mechanically as molecular entities (molecular-orbital description). Without the oscillation of free (metal-) valence electrons, the SPR band is not observed.²²⁴

The extinction coefficients of gold nanoparticles have been found to be high (up to $10^{11} \text{ M}^{-1} \text{ cm}^{-1}$) as a result of the SPR band, which makes them much more sensitive than standard spectroscopic probes used in UV-Vis applications.²²⁴

The SPR band is also an essential tool for understanding the stability of the gold nanoparticles in colloidal suspension. Aggregation of gold nanoparticles (as mentioned above in relation to ionisable ligands) results in the red-shifting of the SPR band. This is due to interactions of the plasmon resonances of individual gold nanoparticles which shift the absorbance to lower energies at reduced inter-particle distances (see figure 42).^{236,237}

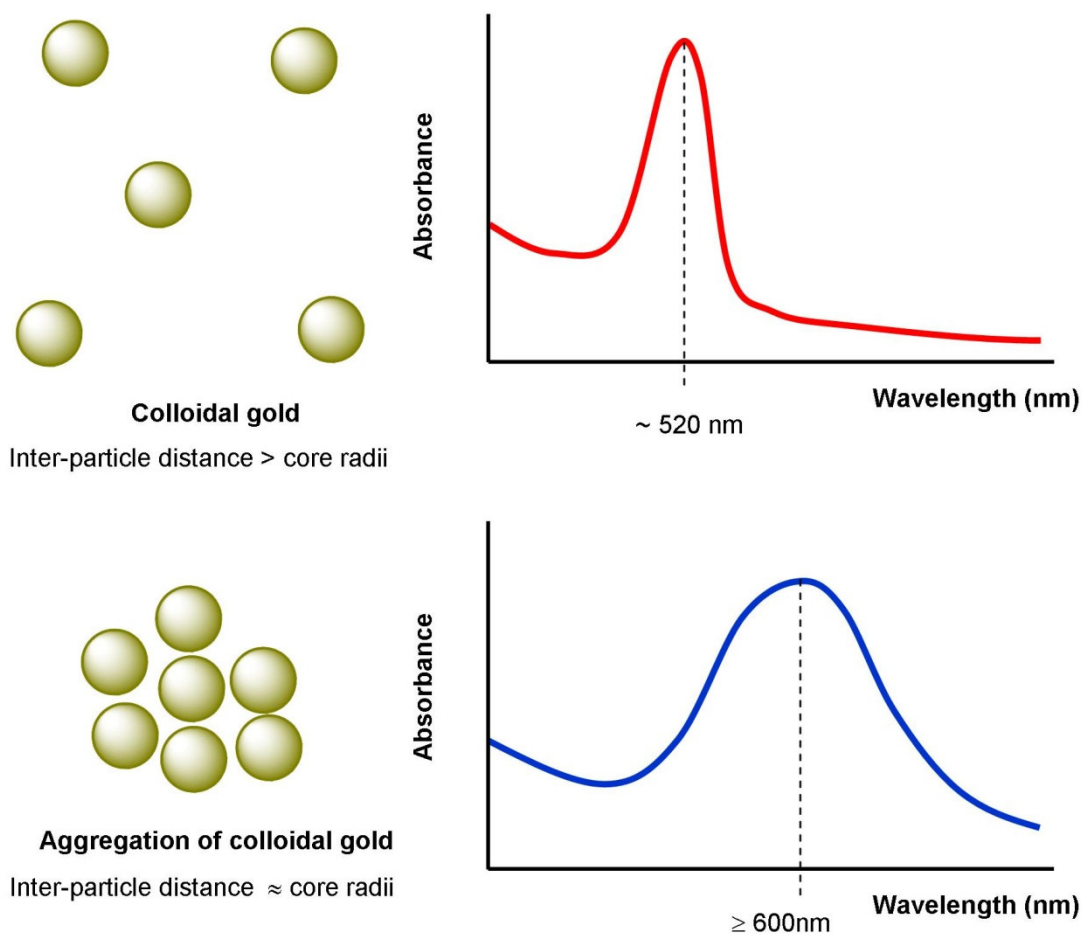


Figure 42. Schematic illustration of the effect of decreasing interparticle distance on the SPR band of gold nanoparticles. Reducing interparticle distance leads to a “red-shift” in the observed UV-Vis spectrum of gold nanoparticles.

With particular reference to gold nanoparticles, when the distance between the gold cores is small compared to the core radii, additional plasmon resonances occur at longer wavelengths than the resonances of the isolated gold nanoparticles (typically, ~600nm in

UV-Vis spectrum).²²⁷ The red-shifting of the SPR-band occurs concurrently with a change in the colour of the colloidal suspension as the SPR band moves to longer wavelengths (red-to-blue colour change observed).

It is the sensitivity of the SPR band of gold nanoparticles to their surroundings that makes gold nanoparticle systems the basis for novel labelling, detection, diagnostic and sensing probes for biological applications.^{195,224,238}

Colorimetric detection methods and assays follow the general principle of inducing nanoparticle aggregation through the specific binding (and recognition) interaction of functionalised ligands upon a nanoparticle with a target analyte.²³⁸

There are now many examples of such colorimetric assays for a wide range of purposes and biological applications, these include; the detection of DNA and biological proteins,^{239,240} the investigation of carbohydrate-protein and carbohydrate-carbohydrate interactions,^{237,241,217} the detection of biological toxins, bacteria and viruses,^{242,243,244} and the detection of various biological analytes.^{245,246}

II.1.10. Influenza and gold nanoparticles

With regards to influenza infection, common methods of detection utilising gold are based on 2D surfaces^{247,248,249} or gold nanoparticles^{250,251} but these methods are typically gold-immunoassays which target the HA and only rarely the NA.²⁵²

With particular reference to nanoparticle applications, gold nanoparticles are commonly used as scaffolds for various biological recognition elements (for example, antibodies or other biological molecules) and are only a minor part of often complicated, multi-sequence procedures towards influenza detection. As such, rather than being the exclusive detection element, gold nanoparticles are often non-participatory and of secondary importance to the main detection element of a particular assay or detection method.²⁵³

Nevertheless, an interesting example of influenza detection which makes use of gold nanoparticles includes a genomic microarray assay where oligonucleotide-functionalised gold nanoparticles (15nm in diameter) are used to bind (indirectly) to a complementary influenza viral (H5N1, H1N1, H3N2) RNA sequence (immobilised on a glass slide) through a sequence of complementary oligonucleotide interactions (see figure 43).²⁵⁴ The final detection of viral RNA is achieved using silver-staining (enhancement of nanoparticle light scattering) of the oligonucleotide-bound gold nanoparticle and subsequent detection of the scattered light. Although a sensitive technique it is multi-sequence assay, requires skilled personnel and can be sensitive to background interference because of its low detection limit.²⁵⁴

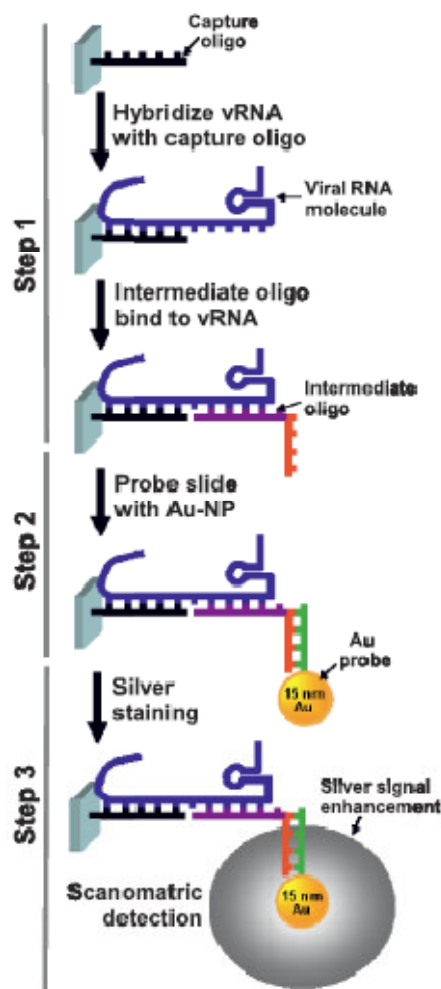


Figure 43. A simplified schematic of a gold-nanoparticle based microassay used to detect influenza (via viral RNA detection). The sequence of events includes; the capture of viral RNA to a complementary oligonucleotide sequence (step 1), the binding of gold nanoparticles to additional, complementary oligonucleotide sequences (step 2), and the enhancement of light scattering for detection of viral RNA via silver staining of the gold nanoparticle (step 3). (Reprinted with permission from BioMed Central Ltd.; *BMC Biotechnology*, 2010, 10, 74)

It is possible to say that the use of gold nanoparticles towards influenza detection is not uncommon if one includes immunoassay-based applications. However, the use of functionalised gold nanoparticles, independent of immunoassay methods with the aim of specific and discrete binding to whole influenza virions (and not viral RNA or isolated antigens) is not common.

Such an approach has been achieved only recently using a multivalency platform based upon α -sialoside functionalised gold nanoparticles targeting the influenza HA (as a potential anti-adhesion therapeutic).²⁵⁵

Though sialic acid functionalised gold nanoparticles have been synthesised by other groups,^{256,257} the research carried out by Papp *et al.* show the binding of sialic-acid-

terminated glycerol dendrimers to 14nm gold nanoparticles (see figure 44). The incubation of these nanoparticles with influenza A (X31) followed by visualisation with TEM and cryo-TEM (cryogenic transmission electron microscopy) indicated nanoparticle binding to the viral surface.²⁵⁵ The results obtained by this investigation indicated that for efficient HA binding, flexibility is required in the ligand presenting scaffold and the size of the gold nanoparticle platform is paramount.

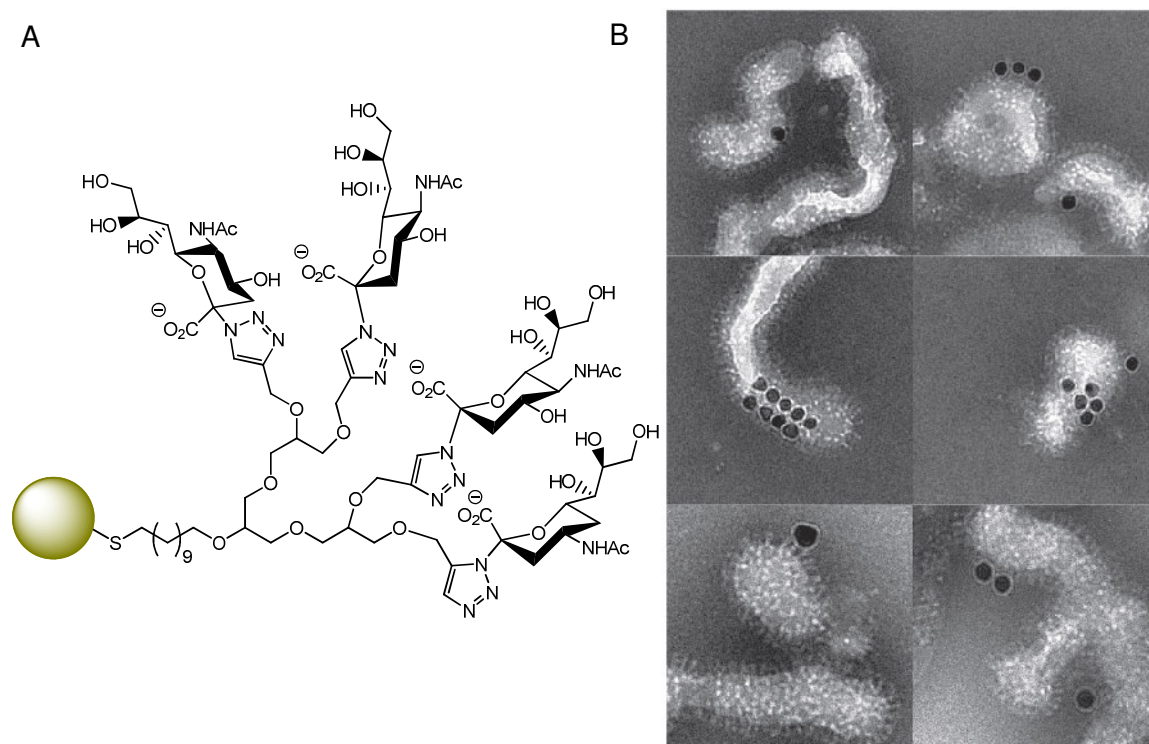


Figure 44. Schematic representation of sialic-acid-terminated glycerol dendrimers immobilised on gold nanoparticles (A). TEM images of the gold nanoparticles binding to influenza A virus via the HA (B). (Reprinted with permission from Wiley-VCH Verlag GmbH & Co. KGaA; *Small*, 2010, 6 (24), 2900–2906.)

Another recent study has used gold nanoparticles (~4nm in diameter) functionalised with simple anionic capped thiolate-ligands (mercaptoethansulfonate, MES, and mercaptosuccinic acid, MAS) to inhibit influenza virus infection (determined by ELISA and hemagglutination assays).²⁵⁸

The primary method of interaction here appears to be based upon electrostatic attraction between charged surfaces on the nanoparticle and the virus surface and not a high affinity, high specificity interaction with the influenza surface proteins. Although, counter-intuitively, the MES capped gold nanoparticles showed greater inhibitory potential than the MAS capped particles, which has a slightly higher surface charge (which suggests electrostatic charge may not be the sole determining factor for virus interaction).

The inhibitory activity observed is attributed to the blocking of viral attachment to the cell surface (via multivalency interactions) and the potential inhibition the viral fusion process with the host cell surface.²⁵⁸

Improving the selectivity and specificity (towards influenza viruses in the presence of other charged biological structures) based purely on generic electrostatic interactions would obviously be a difficult hurdle to overcome in terms of developing a selective therapeutic treatment.

II.1.11. Influenza and other nanoparticles

Other types of nanoparticles have also recently been applied towards influenza virus detection. As previously mentioned, dendrimeric-nanoparticles have been shown to bind to influenza virus (see page 92)¹⁷⁵ but also the use of magnetic iron-oxide nanoparticles as an alternative to the gold nanoparticle core.²⁵⁹

In another example of an immunoassay approach, these “electrically active” iron-oxide nanoparticles (coated with polyaniline and bound to immobilised anti-influenza HA antibodies) have been used as part of a multi-step, charge-transfer biosensor for the detection and (magnetic) separation of influenza HA (not whole influenza virus) from biological media (mouse serum matrix).²⁵⁹ The HA antibody is the recognition element and the polyaniline nanoparticle coating acts as an electrical transducer. Following HA binding, HA-bound nanoparticles are separated and a positive HA-detection result is elicited on completion of an electrical circuit.²⁵⁹

II.1.12. Novel colorimetric methods of influenza detection

The colorimetric detection of respiratory viruses such as influenza using functionalised gold-nanoparticles to date has not been achieved. The development of colorimetric methods to detect such biological pathogens is extremely attractive owing to the high sensitivity, rapid detection time and the lack of specialist equipment and instruments required for detection in comparison to standard clinical methods (or example, RNA/DNA based and immunoassay approaches).^{260,261}

With regards to influenza detection, the developments in colorimetric methods of detection have not made use of nanoparticle scaffolds but have used immobilised bilayer and polymeric systems.

The use of a glass-slide coated with a bilayer system composed of octadecylsilane and polydiacetylene and terminally functionalised with α -sialoside derivatives provides an example of a colorimetric method for influenza detection (see figure 45). Detection of influenza HA binding is signalled by a colorimetric transition caused by conformational

changes to the conjugated ene-yne polymer backbone on binding of influenza A (X31) (blue to red colour change observed).²⁶²

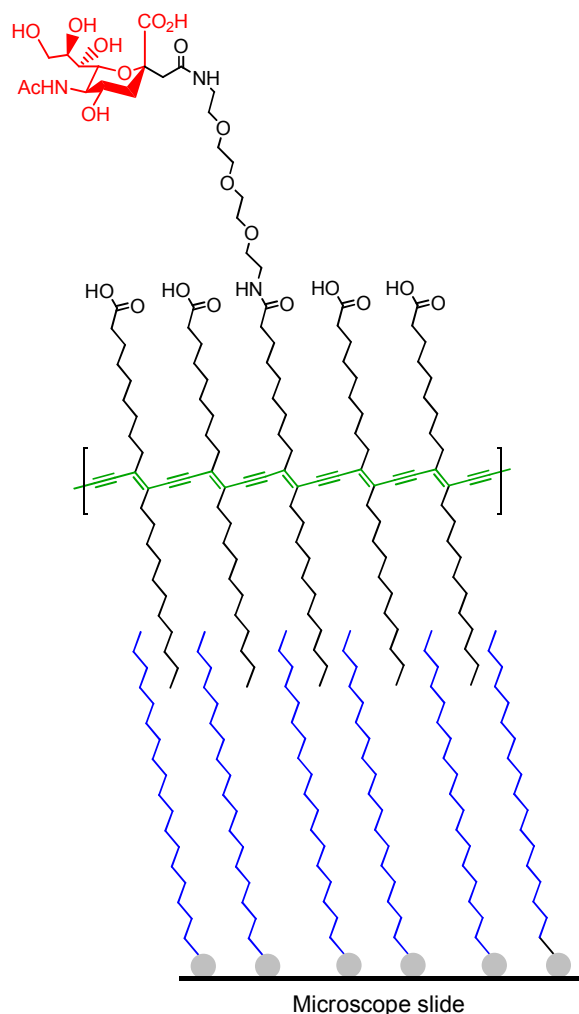


Figure 45. Novel colorimetric influenza detection system based upon an immobilised a bilayer system. The important elements of this system are highlighted; the influenza binding α -C-sialoside (red), the chromatic detection element (green) and the monolayer support (blue). Adapted from; *Science* **1993**, 261, 585-588.

Another approach towards colorimetric influenza detection was based upon the synthesis of water-soluble α -sialyl polythiophenes (see figure 46). On binding of influenza virus a red-shift was observed in the visible spectra as a result of the disruption of the intermolecular interactions which maintain the polymer conformation. Influenza binding converted the polymer backbone from a twisted conformation to a more planar conformation.²⁶³

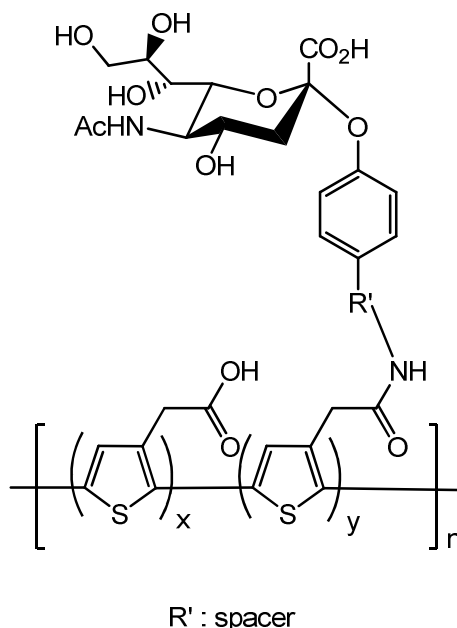


Figure 46. Structure of water soluble α -O-sialyl polythiophenes used in a colorimetric detection method for influenza virus.

As is common with research towards multivalent scaffolds (mentioned above) to inhibit influenza virus binding and infection, the use of sialic acid as the receptor ligand for influenza HA is also used in these approaches. As such, these approaches suffer from the same potential shortcoming and weaknesses in using this recognition ligand. However, these methodologies do show that colorimetric sensing/detection platforms are an achievable goal towards the influenza virus and could offer levels of sensitivity when optimised to complement traditional influenza laboratory-based (PCR assays and HI assays) and potentially rival clinical point-of-care kits (rapid influenza diagnostic tests, RIDTs).^{264,261}

II.2. Results and discussion

II.2.1. Project rationalisation

With a synthetic strategy towards phospho-isosteres of oseltamivir already established,^{161,67} research undertaken in this project is broadly based upon designing and synthesising novel influenza neuraminidase-specific materials and inhibitors presenting the oseltamivir phospho-isostere structural motif. As a target for multivalent binding strategies, the tetrameric NA should offer the same options as the commonly targeted trimeric HA but with the advantage that high-affinity, low molecular weight ligands are readily available in the form of influenza NA inhibitors.

Powerful sialidase inhibitors such as oseltamivir carboxylate (and as such their phospho-isosteres) are considered strongly-binding, high-affinity ligands for the influenza NA. Oseltamivir has a pharmacophore of decreased similarity to sialic acid (in comparison to zanamivir) and therefore exhibits minimal cross-reactivity with other proteins and biological molecules which use sialic acid as a receptor determinant in complex biological systems.²⁶⁵

Because of such structural characteristics and specificities, the development of these compounds and their potential application as new types of influenza diagnostic tools (for example, used in the detection and quantification of NA on influenza virus surface, the investigation of influenza neuraminidase topology and their ligation to useful reporter groups or solid supports) is of significant interest.

The main synthetic goal is directed towards nanoparticle synthesis and small molecule inhibitors (dimeric and conjugatable inhibitors) for displaying the phospho-oseltamivir motif.

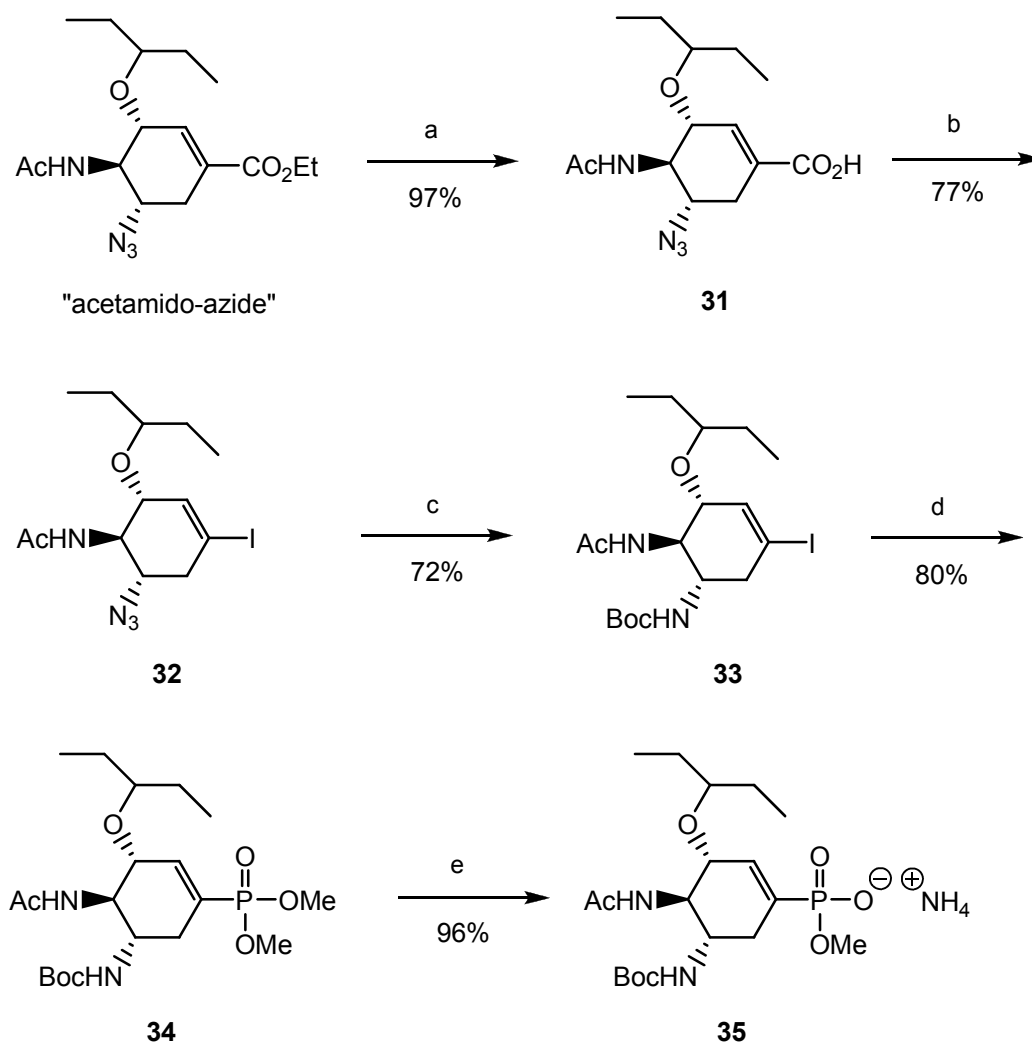
Gold nanoparticles have been chosen as a reference system for our approach to target the influenza virus via its NA due to their emergence as a popular scaffold for the presentation of multiple copies of bioactive motifs en route to the development of various sensors and diagnostics,²⁶⁶ particularly gold nanoparticles as colorimetric sensors.

With respect to small molecule inhibitors and their conjugation to useful reporter groups, the popularity of chemical ligation techniques such as the Huisgen-1,3-dipolar cycloaddition (an example of “click-chemistry”)²⁶⁷ or conjugation via more conventional amino-coupling chemistry, could be used to ligate the phospho-oseltamivir scaffold to other molecules such as biotin and fluorescent probes.

By incorporating conjugatable chemical handles into phospho-oseltamivir derivatives, these popular conjugation methodologies and the compounds that result from their application could be exploited to create widely applicable chemical research tools for influenza virology.

II.2.2. Strategies towards gold nanoparticles derivatised with phospho-oseltamivir

The industrial Tamiflu precursor “acetamido-azide” was the starting material for all of the chemical transformations towards the important monophosphonate precursor **35** (see scheme 21). The “acetamido-azide” was saponified with NaOH (aq.) to give the free acid in 97 % yield. The free acid **31** then underwent a radical halodecarboxylation procedure initially using the Vilsmeier reagent (generated by the reaction of a stoichiometric ratio of DMF and thionylchloride) to generate the acid chloride *in situ*, followed by the irradiation of the solution (using a broad spectrum, 300W UV lamp) in the presence of $\text{CF}_3\text{CH}_2\text{I}$ (the iodo-source), DMAP and 1-Hydroxypyridine-2-thione, to yield vinyl iodide **32** after purification in good yield 71% (based on recovered starting material).



Scheme 21. Reagents and conditions; (a) NaOH (0.5 M), dioxane; (b) i. Vilsmeier reagent, DCM; ii. *N*-hydroxypyridine-2-thione, DMAP, $\text{CF}_3\text{CH}_2\text{I}$, DCM, *h\nu*; (c) i. PMe_3 , THF, ii. BocON, THF iii. H_2O ; (d) dimethylphosphite, $\text{Pd}(\text{PPh}_3)_4$, NEt_3 , toluene; (e) NaOH (0.25 M), dioxane.

It is important to note that during the synthesis towards compound **32** the significance of using high purity 1-hydroxypyridine-2-thione was discovered. It was found that commercially available 1-hydroxypyridine-2-thione is oxidised to its respective disulfide over time (determined by NMR spectroscopy and HR-MS). As such, the use of this disulfide hinders the halodecarboxylation strategy significantly, with synthetic yields of compound **32** dropping to <5%. To ensure successful synthesis of important iodo-precursor **32**, freshly prepared 1-hydroxypyridine-2-thione (obtained by acidification of the commercially available 1-hydroxypyridine-2-thione sodium salt, followed by recrystallisation from EtOH/H₂O)²⁶⁸ was used in the halodecarboxylation.

The azido-moiety of compound **32** was then reduced and protected as a *tert*-butyl carbamate in a one-pot sequence using PMe₃ in THF (Staudinger reaction) followed by treatment with BocON to give compound **33** (72%).

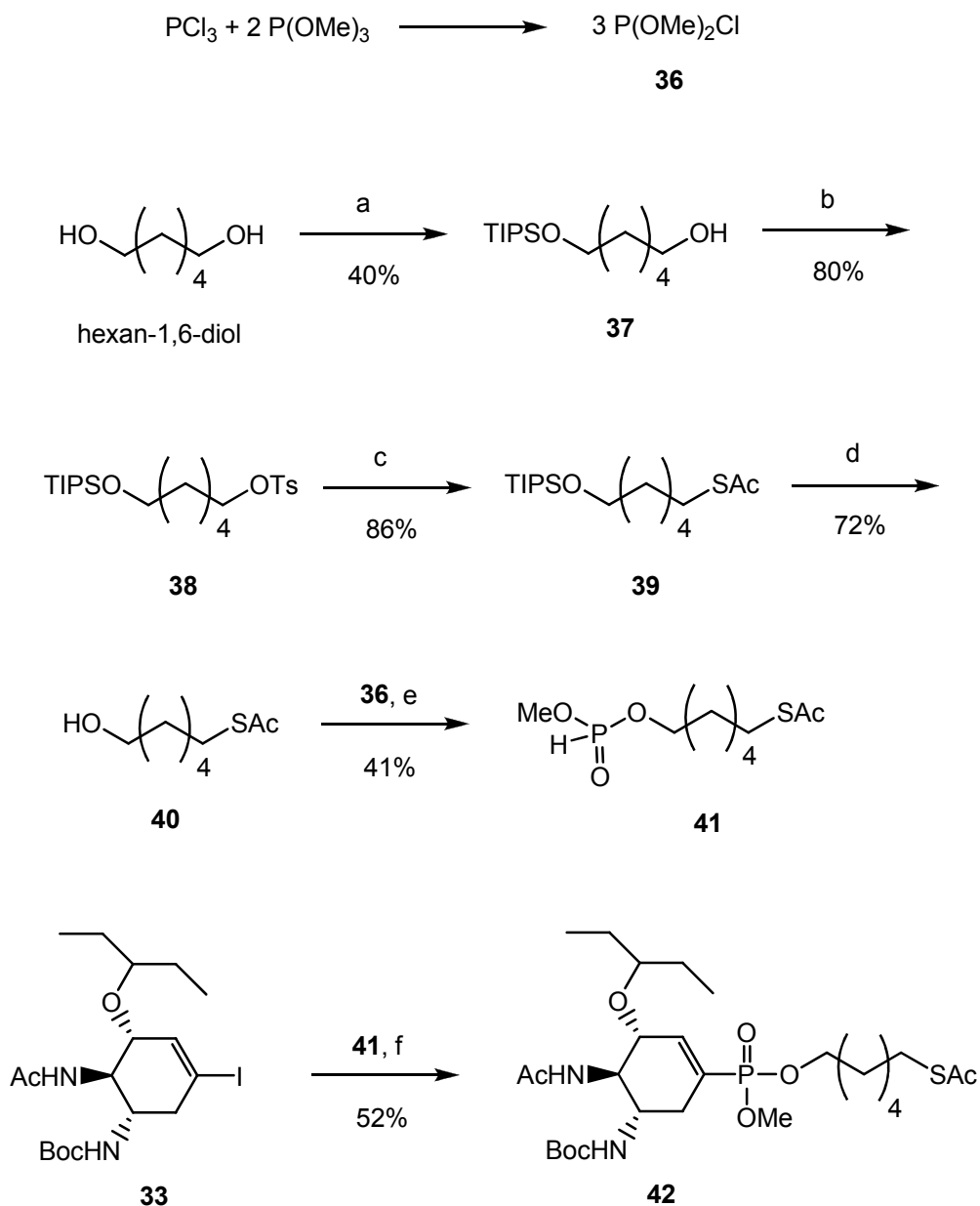
The palladium-mediated coupling step (Hirao reaction) of compound **33** with dimethylphosphite furnished the phosphonate diester **34** in 80% yield. Mono-saponification of compound **34** was then achieved using NaOH (aq.) to afford monoester **35** in 96% yield. Monoester **35** was the important precursor for all subsequent chemical modifications (41% overall yield over 5 steps).

II.2.2.1. Synthesis of dimeric phospho-oseltamivir

The synthesis of the dimeric phospho-oseltamivir constitutes a simple dimeric NA inhibitor. Subsequent investigation of its inhibitory potential would indicate whether any effects on observed NA inhibition are a result of enhanced substrate binding through multivalency effects or a result of purely statistical rebinding. Moreover, the disulfide could be directly applied to the synthesis of functionalised gold nanoparticles (*vide infra*). The length of the linker (6 methylene units) was incorporated into the phospho-oseltamivir derivatives. This is a compromise to provide adequate linker length (>10 methylene units for the dimeric derivative) to mimic the structure of successful dimeric zanamivir compounds¹⁸⁴ and to be short enough to maximise aggregation effects between gold nanoparticles (as longer linker lengths are known to cause functionalised colloidal gold nanoparticles to aggregate more slowly when subjected to conditions which induce aggregation) towards a potential influenza sensor.²²⁷ As such, with the development of a gold nanoparticle based influenza sensor in mind, the aggregation caused by nanoparticle-analyte interaction should be maximised (in part) by using a relatively short linker.

Linker compound **42**, used as a precursor to dimeric compound **45** has already been synthesised via a palladium mediated coupling of vinyl iodide **33** with *O*-methyl *O*-(ω -thioacetyl hexyl) phosphonic acid **41**, synthesised from dimethyl chlorophosphate, **36**

and compound **40**. Compound **40** itself was synthesised from hexan-1,6-diol in 4 steps (see scheme 22).²⁶⁹

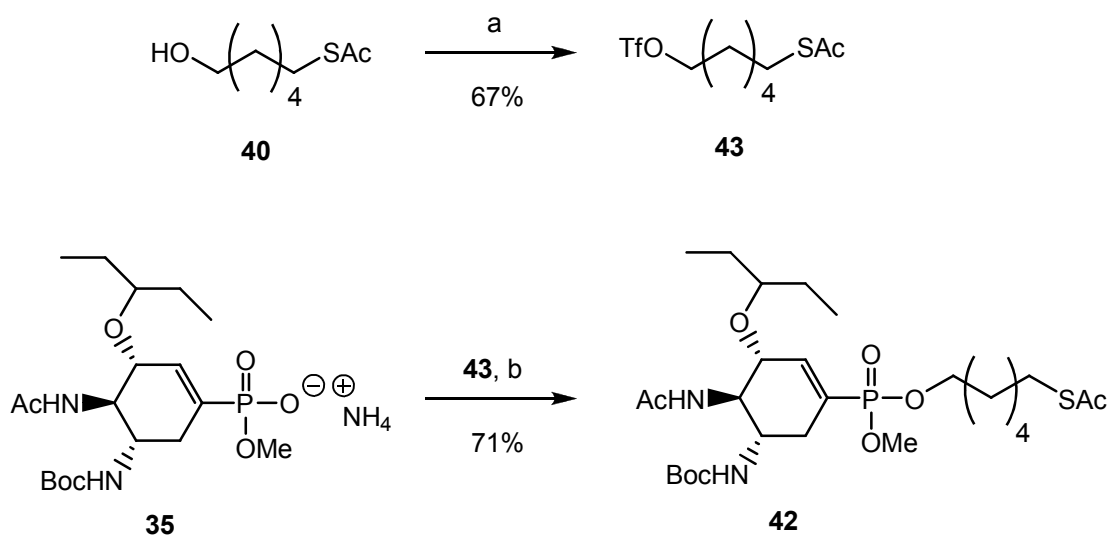


Scheme 22. Reagents and conditions; (a) imidazole, TIPSCl; (b) TsCl, DMAP, pyridine; (c) KSAc, pyridine; (d) TBAF, AcOH, THF; (e) chloro(dimethyl)phosphine **36**, DIPEA, DCM; (f) Pd(PPh₃)₄, NEt₃, toluene.

The synthetic yield of this palladium-mediated reaction was improved slightly in this work through a modified reaction procedure (specifically, the use a more stringent inert atmosphere and an optimised order of reagent addition) from a 36% to a 52% yield.

Although the coupling reaction developed for compound **42** had been improved, a highly pure analytical sample was difficult to obtain because of triphenylphosphine oxide impurities (originating from $\text{Pd}(\text{PPh}_3)_4$ as a result of the aqueous work-up procedure) which could not be completely removed. An alternative strategy was therefore used to form compound **42** which relied upon the alkylation of the monomethylphosphonate **35** with a suitably functionalised alkyl triflate (see scheme 23).

Triflate **43** was synthesised by the reaction of compound **40** with trifluoromethanesulfonic anhydride at reduced temperature. It was found that triflate **43** was not stable for prolonged periods of time and decomposed over the course of 48 to 72 hours ($-20\text{ }^\circ\text{C}$ refrigeration) and decomposed rapidly when heated to above moderate temperatures ($>30\text{ }^\circ\text{C}$).



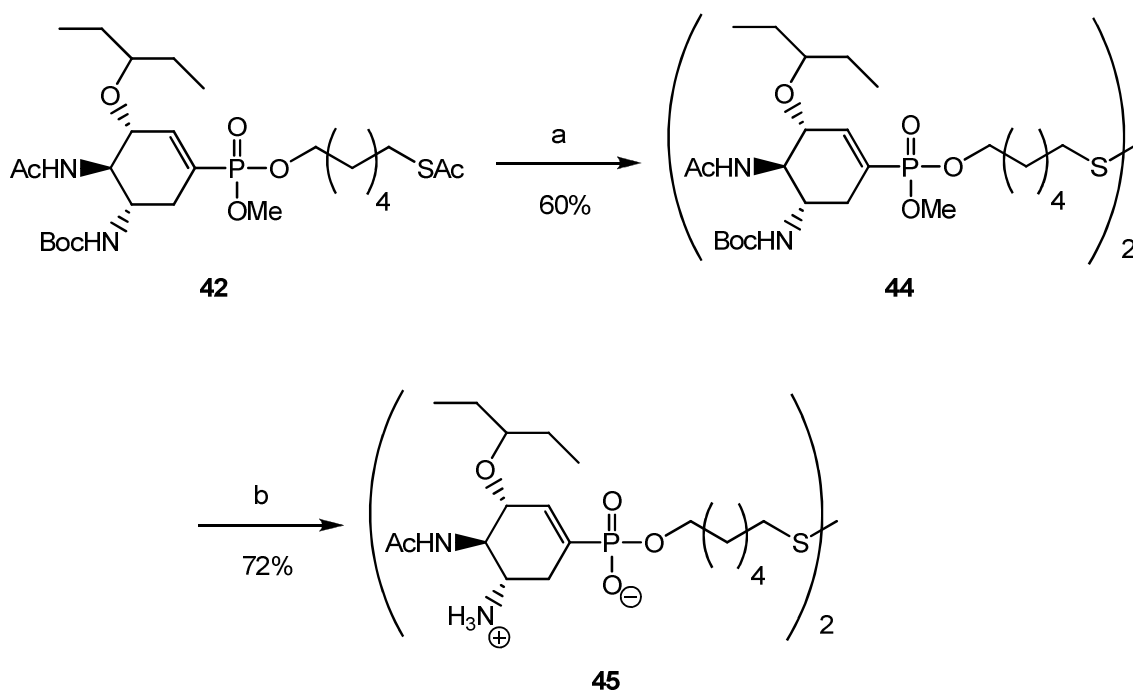
Scheme 23. *Reagents and conditions;* (a) Trifluoromethanesulfonic anhydride, lutidine, DCM, $-60\text{ }^\circ\text{C}$; (b) i. compound **37** lyophilised with NEt_3 ; ii. Acetonitrile, compound **43**.

Reactivity studies (via TLC) indicated that the triflate **43** decomposed rapidly (less than 5 minutes) when stirred in polar solvents necessary for the alkylation reaction (these included DMF, DMSO, and THF). Only in anhydrous acetonitrile was the decomposition of triflate **43** slow enough to allow the alkylation reaction to proceed in competition.

Both strategies yielded compound **42** in similar yields (when disregarding recovered starting material), however, the synthesis of compound **42** via the triflate alkylation method was safer (as it did not require the synthesis of compound **36**) and more economical (as it was palladium-free). Moreover, starting material from the triflate method could be reclaimed and reused.

The synthesis of disulfide **44** was achieved by dimerisation of compound **42** with sodium methoxide in MeOH in the presence of O₂(g) (see scheme 24).

Initial investigations towards deprotection of compound **44** included basic hydrolysis of the phosphonate methyl ester (attempted using both NaOH (aq.) and KOH (aq.), 0.1M) which was unsuccessful and led to mixed ester cleavage. A selective thiophenol/triethylamine phosphonate ester deprotection strategy was also unsuccessful. Successful deprotection of the phosphonate methyl ester of compound **44** was achieved using Finkelstein conditions (NaI in refluxing anhydrous acetone) followed by removal of the *tert*-butyl carbamate protecting group with 50% TFA/H₂O and 1,4-dioxane which resulted in compound **45** after gel permeation chromatography (72% yield).



Scheme 24. Reagents and conditions; (a) NaOMe/MeOH, O₂(g); (b) i. NaI, acetone, reflux; ii. TFA/H₂O (50%); iii. gel permeation chromatography.

II.2.2.2. Neuraminidase (NA) inhibition studies with dimeric phospho-oseltamivir

Compound **45** was investigated for NA inhibitory activity in collaboration with the NIMR (National Institute of Medical Research).

The inhibition constant K_i is obtained by measuring the effect of the inhibitor on the rate of MUNANA hydrolysis and is a standard assay widely used in influenza research.

compound 45	hexyl-conjugate	Oseltamivir
0.10 ± 0.01	0.22 ± 0.03	0.14 ± 0.02

Table 4. Inhibition constant (K_i [nM]) for target dimeric phospho-oseltamivir, compound **45** in comparison to known NA inhibitors.

(Inhibition of MUNANA hydrolysis catalysed by neuraminidase from influenza virus A/Norway/1758/07; inhibition constants were determined as described in experimental section; Inhibition of neuraminidase activity of influenza viruses from allantoic fluid from infected eggs; K_M for MUNANA = $6.4 \pm 0.6 \mu\text{M}$). For hexyl-conjugate, see figure 25, page 84).

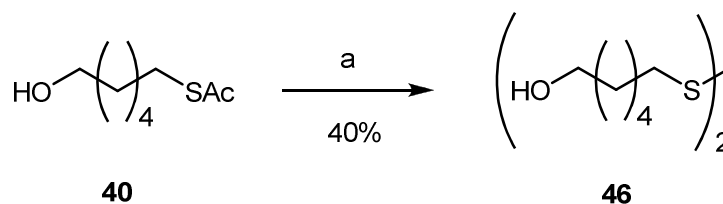
Improved inhibition was found for compound **45** ($K_i = 0.10 \pm 0.01 \text{ nM}$) compared to the hexyl-conjugate and to oseltamivir (see table 4) and indicates that the potency of inhibition is approximately twice that of the hexyl-conjugate ($K_i = 0.22 \pm 0.03 \text{ nM}$).⁶⁷ This suggests that the binding and subsequent inhibition of NA activity is a result of statistical rebinding of compound **45** with the NA opposed to multivalency effects.

II.2.3. Synthesis of functionalised gold nanoparticles

The synthesis of phospho-oseltamivir stabilised gold nanoparticles was pursued using two synthetic methodologies, a modified Brüst-Shiffrin protocol and a ligand-exchange procedure upon pre-synthesised gold nanoparticles via the Turkevitch protocol. Both methodologies are well-established and widely used to generate nanoparticles of varied size.

II.2.3.1. Brüst-Shiffrin method

Model compound **46** was synthesised initially from compound **40** (see scheme 25). The purpose of compound **46** was to allow preliminary gold nanoparticle synthetic studies to be carried out in preparation for the synthesis of phospho-oseltamivir gold nanoparticles. A modified Brüst-Shiffrin method^{198,217} using aqueous auric acid in a methanolic solution of disulfide **46** (3:1 molar equivalents compared to auric acid) followed by the addition of sodium borohydride, was used to synthesise small functionalised gold nanoparticles.



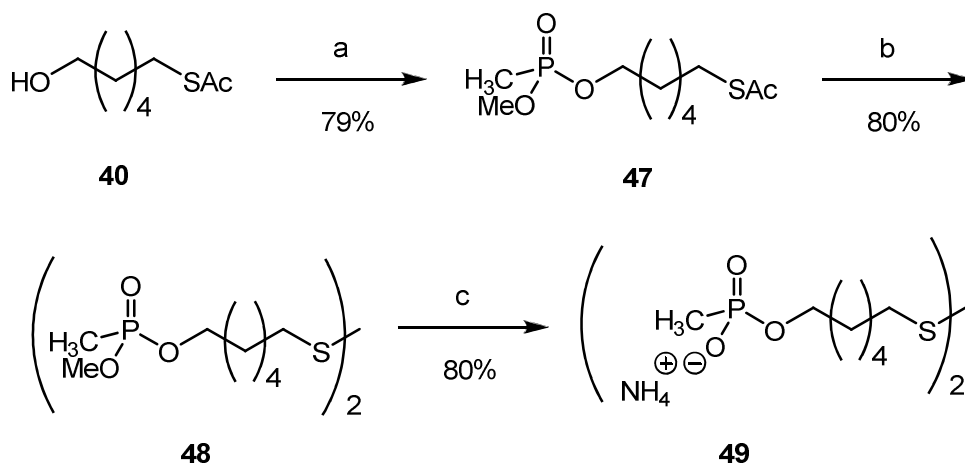
Scheme 25. Reagents and conditions; (a) NaOMe/MeOH, O₂(g).

Although a characteristic brown/black solution was formed on the addition of sodium borohydride, the purification of nanoparticles from excess disulfide **46** was problematic. A centrifugation-based purification procedure²¹⁷ was attempted unsuccessfully (small molecule impurities were present in the ¹H NMR following the centrifugation process). The nanoparticles synthesised were not highly water suspendible and as such methanolic nanoparticle solutions were used during centrifugation which leached small molecule impurities from the centrifugal filtration device. The lack of water suspendibility of the nanoparticles did not lend this system to optimising the Brüst-Shiffrin procedure towards phospho-tamiflu-stabilised gold particles (which were expected to form a suspension in water). As such, the development of compound **46** as a template for nanoparticle synthesis was abandoned.

II.2.3.2. “Small” methylphosphonate-stabilised gold nanoparticles as a control sample

With the aim of finding an alternative to nanoparticles synthesised from compound **46**, disulfide **49** was synthesised with two main objectives in mind (see scheme 26). Firstly, the spacered methylphosphonate compound **49** would provide a more suitable platform for attempting and optimising nanoparticle synthesis before using phospho-oseltamivir derivatives (because of the polar terminal methylphosphonate moiety). Secondly, monomethylphosphonate stabilised gold nanoparticles are a perfect platform as a control sample in inhibition studies (because the methylphosphonate moiety retains the negative

charge so important to phospho-oseltamivir binding but is devoid of the other essential recognition elements for successful NA inhibition).



Scheme 26. Reagents and conditions; (a) P(O)(OCH₃)(CH₃)Cl, DIPEA, DCM; (b) NaOMe/MeOH, O₂(g); (c) i. NaI, acetone, reflux; ii. gel permeation chromatography.

Compound **47** was synthesised from compound **40** and methyl methylphosphonochloridate⁶⁶ in good yield (79%). Dimerisation to give protected disulfide **48** and subsequent deprotection gave compound **49** and was achieved using the same reaction conditions as used in the synthesis of phospho-oseltamivir disulfide **45** in an overall yield of 64% over 3 steps (see scheme 26).

Methylphosphonate-stabilised gold nanoparticles were synthesised using the modified Brüst-Shiffrin procedure however, the procedure was unsuccessful and on the addition of sodium borohydride, an insoluble black solid was formed (assumed to be a result of the reduction of Au^{III} to Au⁰).

The use of a small quantity of acetic acid (30:1 molar equivalents compared to auric acid) was used to prevent the formation of this insoluble black solid (bulk Au⁰) by preventing the high pH induced irreversible gold core coalescence (in the presence of ionisable sulfur-containing ligands) under these experimental conditions.^{209,214} No sound physical basis or justification however has been provided in the literature for the use of acetic acid for this purpose beyond improving the solubility of nascent thiolate-capped gold nanoparticles (which have limited solubility in MeOH).

The methylphosphonate-stabilised gold nanoparticles obtained could be suspended in water (see figure 47) and were purified by a repeated centrifugation/resuspension procedure (until unreacted starting material **49** was no longer detected). Subsequently the methylphosphonate-stabilised gold nanoparticles underwent prolonged dialysis to remove small molecule impurities (see scheme 27).

Unreacted disulfide **49** was reclaimed and was chemically unchanged after the functionalisation procedure (determined by ^1H NMR).

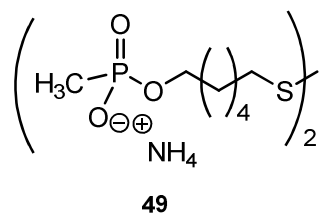
II.2.3.3. Phospha-oseltamivir-stabilised gold nanoparticles: “small TamiGold”

Using the same modified Brüst-Shiffrin methodology, phospha-oseltamivir-stabilised gold nanoparticles (henceforth referred to as “small TamiGold”) were synthesised (see scheme 28).

As was the case with “small” methylphosphonate-stabilised gold nanoparticles, unreacted starting material (in this case, disulfide **45**) was reclaimed and appeared chemically unaltered after the functionalisation procedure (determined by ^1H NMR).

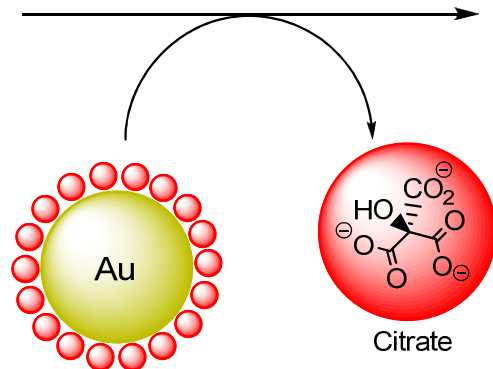


Figure 47. Images of gold nanoparticles synthesised by the Brüst-Shiffrin method; “small TamiGold”, ~0.5 mg/mL (left) and “small” methylphosphonate stabilised gold nanoparticles, ~1 mg/mL (right).



Modified Brust-Shiffrin Protocol

- i. $\text{HAuCl}_4 \cdot 3\text{H}_2\text{O}$,
MeOH, AcOH, 24hrs
- ii. Centrifugation/resuspension
- iii. Dialysis (MilliQ H_2O)

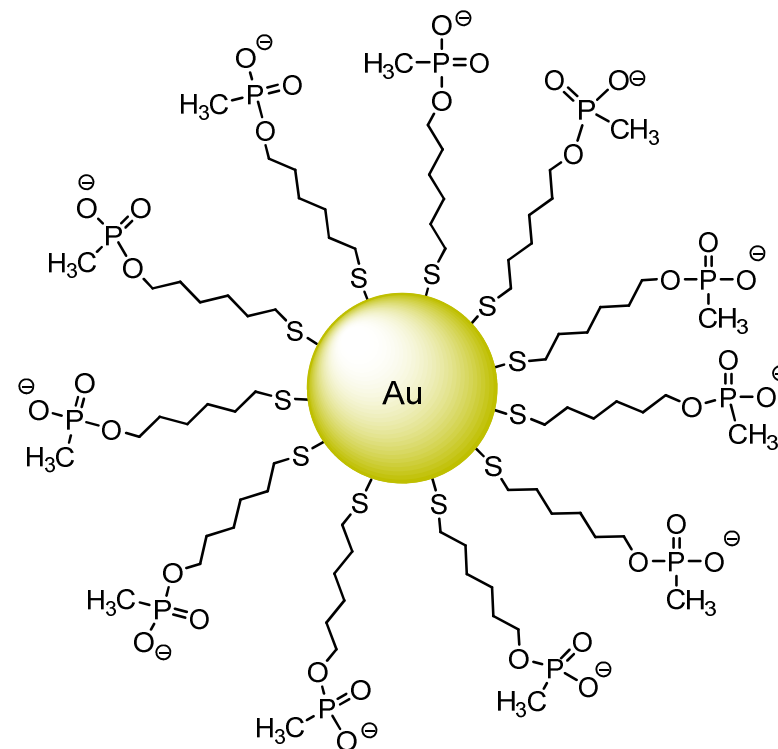


- i. Citrate-capped AuNPs
- ii. Centrifugation/Resuspension
- iii. Dialysis (phosphate buffer, 10mM, pH 7.6)

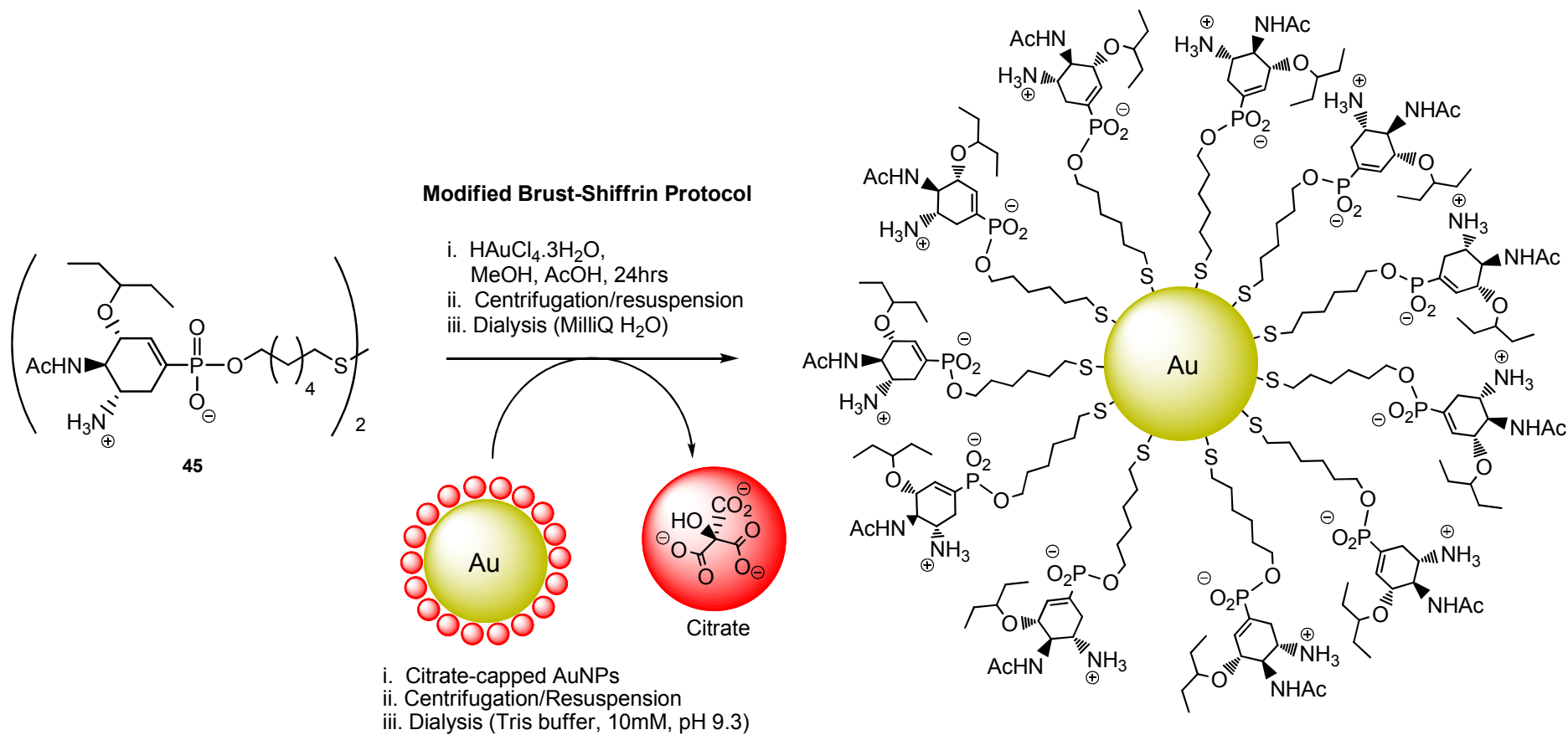
Turkevitch Protocol

Scheme 27. Synthesis of monomethylphosphonate stabilised gold nanoparticles.

Methylphosphonate-stabilised gold nanoparticles



Phospha-oseltamivir-stabilised gold nanoparticles
"TamiGold"



Scheme 28. Synthesis of "TamiGold"

II.2.3.4. Turkevitch method and ligand exchange

Citrate-capped nanoparticles were synthesised via the Turkevitch method using auric acid and trisodium citrate as described in the literature, forming a wine-red coloured colloidal gold solution and giving a characteristic SPR band at approximately 519 nm.²³⁸

II.2.3.5. “Large” methylphosphonate-stabilised gold nanoparticles as a control sample

Methylphosphonate-stabilised gold nanoparticles were synthesised using the citrate-capped gold nanoparticles generated from the Turkevitch method mentioned above (as a means of optimising nanoparticle synthesis and purification for phospho-oseltamivir stabilised gold nanoparticles).

Ligand exchange of compound **49** with freshly citrate-capped gold nanoparticles over 72 hours lead to the formation of methylphosphonate-stabilised gold nanoparticles.

The ligand-exchange process itself was easily carried out but initial attempts at purification using both gel permeation chromatography (10mM phosphate buffer, pH 7.6) and dialysis (against 10mM phosphate buffer, pH 7.6) were not sufficient to completely remove unfunctionalised compound **49** or excess citrate.²⁷⁰

Centrifugation/resuspension purification procedures were also initially unsuccessful with methylmonophosphonate stabilised gold nanoparticles. Ultracentrifugation as described in the purification of other functionalised gold nanoparticles²²⁷ often resulted in permanent aggregation of the nanoparticles (signified by a red to purple colour change of the resulting pellet). Prolonged dialysis (> 7 days) using deionised water (pH ~7) also resulted in the aggregation of the nanoparticle suspensions during purification. It was clear that the delicate colloidal stability of the methylphosphonate-stabilised gold nanoparticles required careful purification through a combination of methods to maintain stability. This was eventually achieved through gel permeation chromatography, a limited centrifugation/resuspension sequence and prolonged dialysis (10mM phosphate buffer, pH 7.6) to produce methylphosphonate-stabilised gold nanoparticles, which exhibited a characteristic SPR band at 524 nm and remained stable for prolonged lengths of time (months) with limited flocculation (at pH 7.6 during refrigeration at 4 °C in the absence of light).

II.2.3.6. Phospha-oseltamivir-stabilised gold nanoparticles: “large TamiGold”

The ligand exchange reaction of disulfide **45** generated phospha-oseltamivir stabilised gold nanoparticles henceforth referred to as “large TamiGold”. Lessons learned in the synthesis of methylphosphonate-stabilised gold nanoparticles were however not entirely applicable to “large TamiGold”.

The initial ligand exchange reaction was marked by aggregation of the gold nanoparticles (red to purple colour change, which was not observed in the synthesis of methylphosphonate-stabilised gold nanoparticles) which was only reversed by the addition of 0.1 M NaOH (aq.) over the course of the reaction (see figure 48)

As shown below, the aggregation of the gold nanoparticles occurs on addition of compound **45** resulting in a red-shift of the SPR band which can be reversed by the addition of NaOH (aq.). It is also important to point out that this behaviour is not observed with the citrate-capped control sample (same conditions but without compound **45**) and that increasing solution pH of citrate-capped gold nanoparticles appears to have no detrimental effect on colloidal stability or the SPR band.

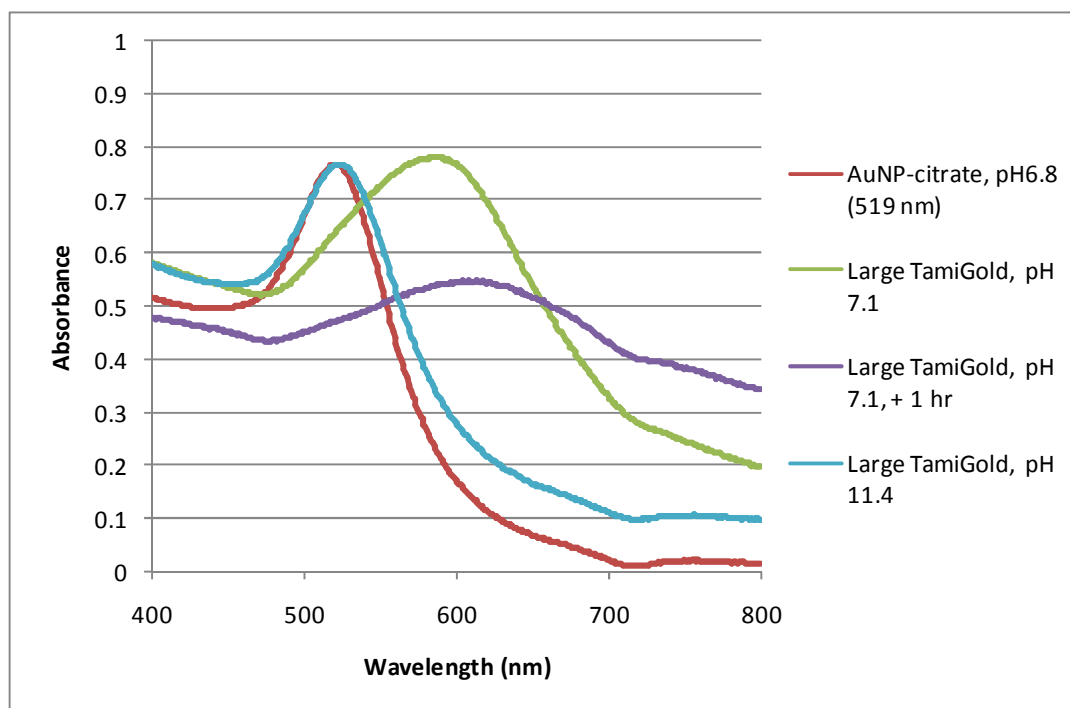


Figure 48. UV-Vis spectra of initial “large TamiGold” synthesis. The SPR band was returned to 525 nm on increasing solution pH.

The aggregation behaviour of “large TamiGold” observed during the initial syntheses did not appear to hinder the ligand exchange reaction as UV studies (*vide infra*) still

indicated a distinctive difference between the behaviour of non-thiolate functionalised citrate-capped gold nanoparticles and those reacted with phospho-oseltamivir disulfide **45**.

It is reasoned that this behaviour is attributed to the interaction of cationic functionality present on gold-immobilised ligands with neighbouring functionalised gold nanoparticles. It appears that this effect is pronounced with functionalised ligands of a zwitterionic or cationic nature because of their ability to act as nanoparticle cross-linking agents.²⁷⁰ This is the case in conditions where the pKa of capping ligand and solution pH is not optimised towards the stability of the gold capping agent in aqueous solution. In this example, at physiological pH (\sim pH 7.6) the primary amino-group (pKa \sim 12.5) is present as its conjugate acid and is speculated therefore to prevent gold nanoparticle colloidal stability through electrostatic interactions between other phospho-oseltamivir structures and the gold nanoparticles. Aqueous solution of pH $>$ 9 prevented this aggregation behaviour of “large TamiGold”.

This synthetic issue was overcome by first dissolving compound **45** in phosphate buffer (pH 7.6) then continuing the standard ligand exchange procedure.

The subsequent nanoparticle purification procedure was more straight forward and used a centrifugation/resuspension process followed by prolonged dialysis against Tris buffer (10 mM, pH 9.3) to give “large TamiGold”, which exhibited a characteristic SPR band at 525 nm and appeared red in colour (see figure 49).

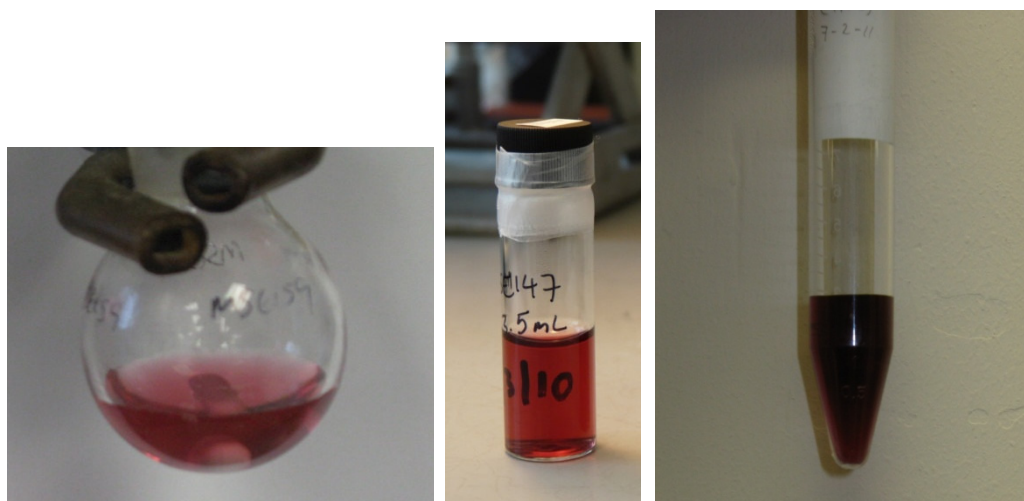


Figure 49. Images of gold nanoparticles synthesised by the ligand exchange/Turkevitch method; “large TamiGold” (left, right) and “large” methylphosphonate stabilised gold nanoparticles (middle).

II.2.4. Gold nanoparticle characterisation: “small TamiGold” and control sample

II.2.4.1. UV-Vis spectroscopy

UV-Vis spectroscopy revealed that both “small” methylphosphonate-stabilised gold nanoparticles and “small TamiGold” did not display an SPR band in their spectra. As previously mentioned, the SPR band is commonly displayed by gold nanoparticles of a larger particle diameter (typically greater than 5 nm) thus supporting the conclusion of successful gold nanoparticle synthesis with a particle diameter of less than 3 nm (see figure 50 and figure 51).²⁷¹

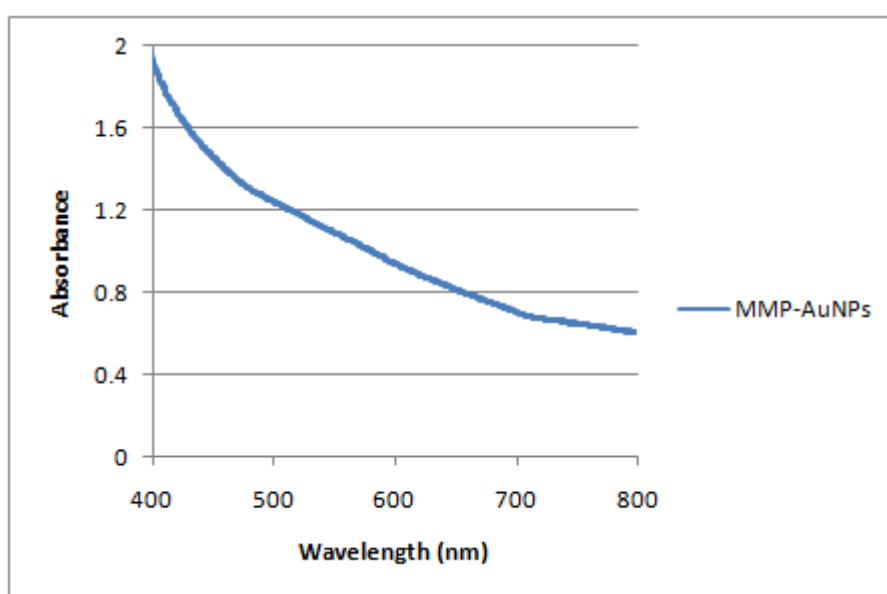


Figure 50. UV-Vis spectrum of “small” methylphosphonate-stabilised gold nanoparticles (~1 mg/mL).

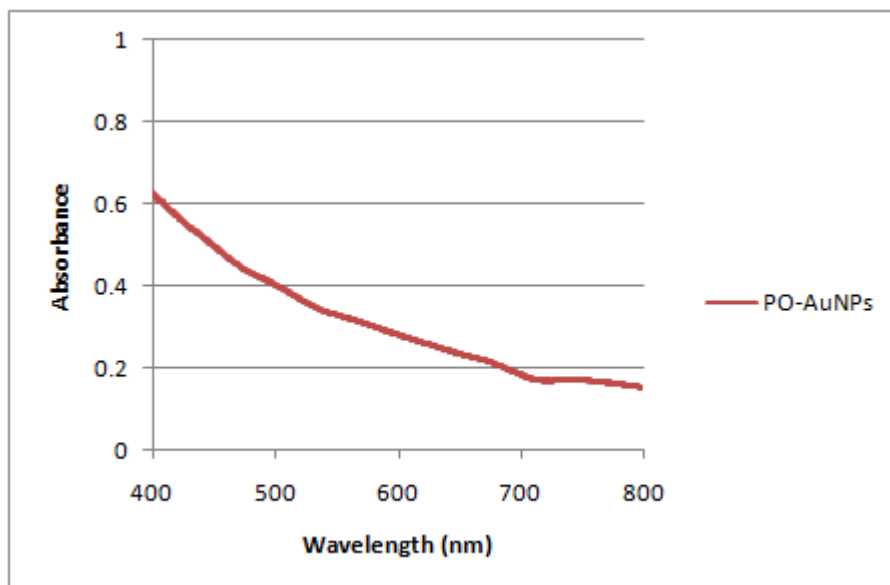


Figure 51. UV-Vis spectrum of “small TamiGold” (~ 0.5 mg/mL).

II.2.4.2. High resolution transmission electron microscopy (HRTEM)

High resolution transmission electron microscopy (HRTEM) of “small” methylphosphonate-stabilised gold nanoparticles gave an average particle diameter of 2.4 nm with a particle size range of 1 - 4 nm (see figure 52).

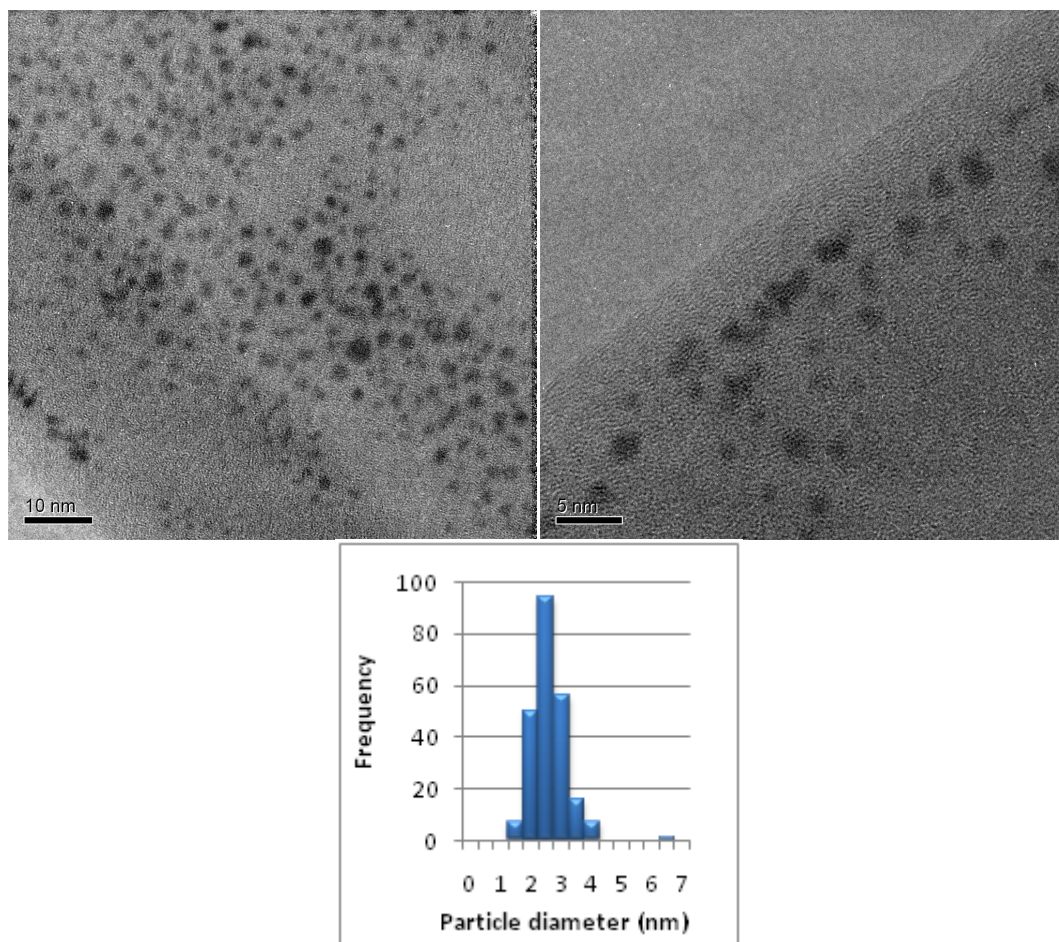


Figure 52. HRTEM images and size distribution histogram of “small” methylphosphonate-stabilised gold nanoparticles.

HRTEM analysis of “small TamiGold” gave an average particle diameter of 2.0 nm with a particle size range of 1 - 4 nm. This shows that both gold nanoparticle samples are of a similar size and distribution (see figure 53).

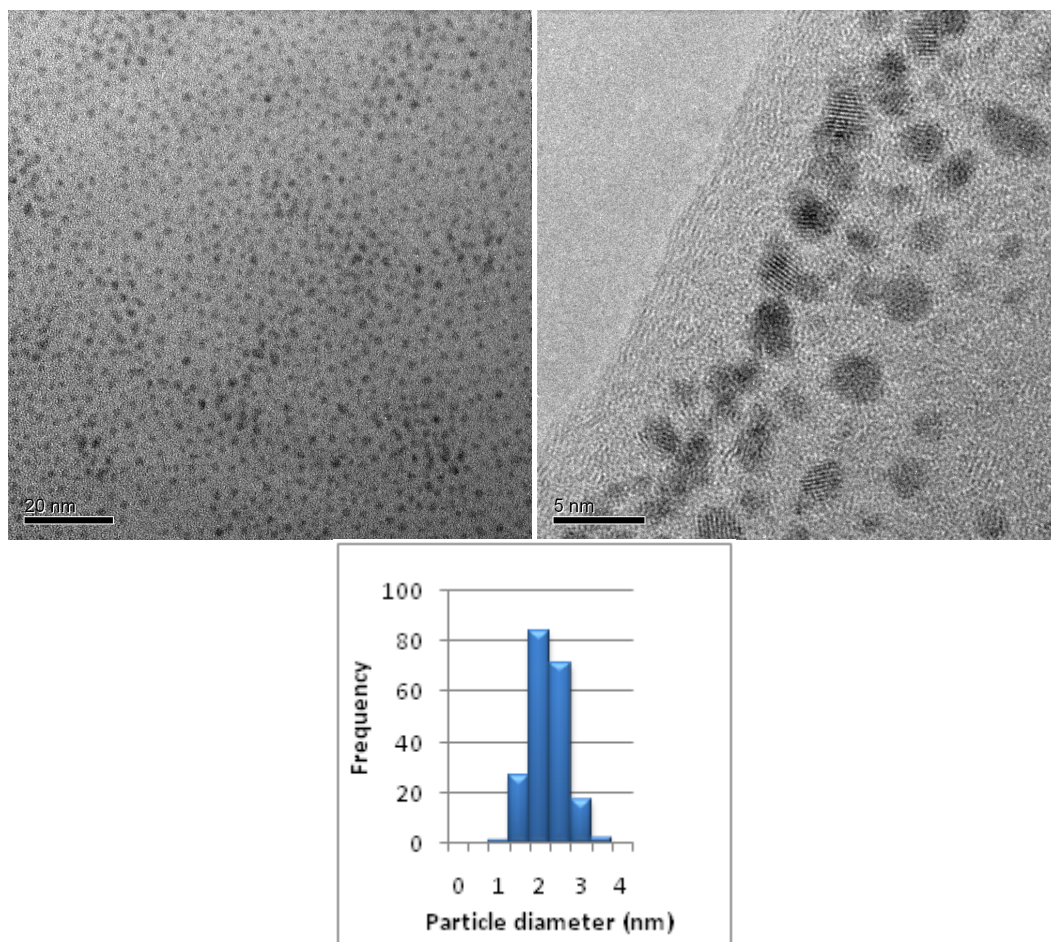


Figure 53. HRTEM images and size distribution histogram of “small TamiGold”.

In general, there may be some bias in particle counting and the resulting size distribution analysis resulting from limitations in HRTEM image acquisition of $<1\text{nm}$ particle populations (due to decreased particle image contrast compared to the carbon grid background).

Rudimentary visual inspection of the HRTEM images for “small” methylphosphonate-stabilised gold nanoparticles indicates some clustering of particles, accounting for the non-regular particle size distribution on the sample grid which is not observed for “small TamiGold” (where the particle distribution appears more regular). This irregularity associated with “small” methylphosphonate-stabilised gold nanoparticles may be due to the polar terminal methylphosphonate functionality. Although it must also be considered that these clustering observations may also be produced by the drying-down process and HRTEM sample preparation on the carbon grid.

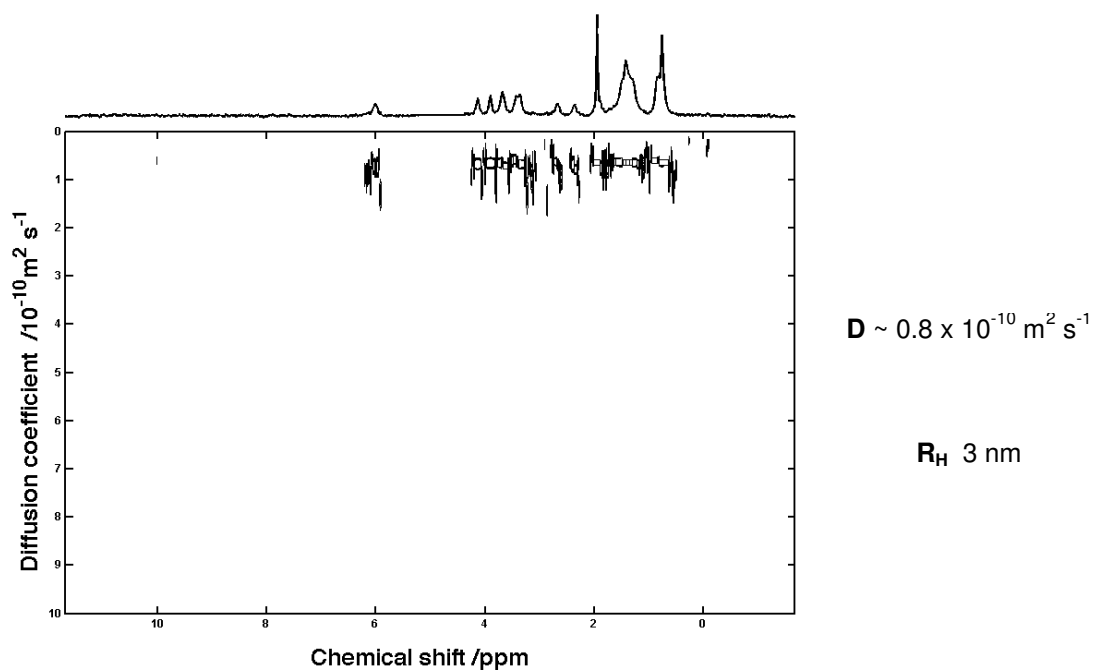
Lattice fringes related to the FCC 111 “bulk” gold crystal lattice (literature value 0.235 nm)²⁷² are observable from the HRTEM images of “small TamiGold” (observed value

0.239 nm). The deviation from the bulk gold is due to the small size of the gold nanoparticles produced by the Brüst-Shiffrin method, whereby there are typically more gold atoms at the gold nanoparticle surface rather than in the bulk which causes an alteration to the observed crystal structure.²⁷²

II.2.4.3. Diffusion ordered spectroscopy (DOSY) NMR

DOSY-NMR experiments with “small” methylphosphonate-stabilised gold nanoparticles gave a hydrodynamic radius (R_H) of approximately 5 nm and for “small TamiGold” a hydrodynamic radius (R_H) of approximately 3 nm (derived from estimated diffusion coefficients) (see figure 54).

A



B

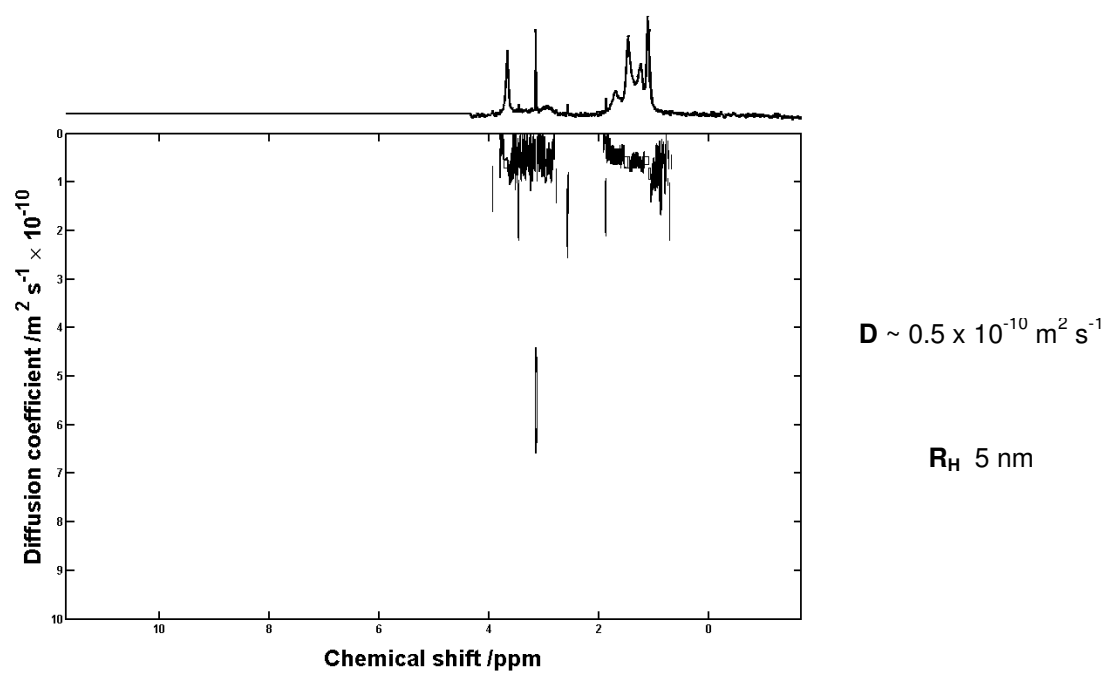


Figure 54. (A) DOSY-NMR spectra for "small TamiGold" and (B) DOSY-NMR spectra for "Small" methylphosphonate-stabilised gold nanoparticles; Solvent: D_2O (solvent signal suppressed).

This data supports the HRTEM results as particle diameters of a similar order of magnitude are obtained. The larger particle diameter obtained by the DOSY-NMR method is due to the incorporation of the surrounding ligand shell and the hydration sphere of the respective nanoparticle.

However, there is a larger difference in particle size of “small TamiGold” and “small” methylphosphonate-stabilised gold nanoparticles derived from DOSY-NMR data compared to those derived from HRTEM data. This can be explained by the different chemical nature of the terminating group, that is, phospho-oseltamivir versus terminal methylphosphonate, the latter of which may induce greater long-range ordering effects in solution which are accounted for by DOSY-NMR though not by HRTEM (where only the gold nanoparticle core is imaged).

II.2.4.4. ¹H NMR

¹H NMR spectra of “small” methylmonophosphonate stabilised gold nanoparticles and “small TamiGold” confirmed the slight upfield shift and broadening of resonances and the complete broadening of the -CH₂- signals adjacent to the S-Au bond which were no longer visible in comparison to the starting material (see figure 55). Such NMR effects are mainly attributed to the effect of ligand-Au bonding on NMR relaxation times.²³⁵

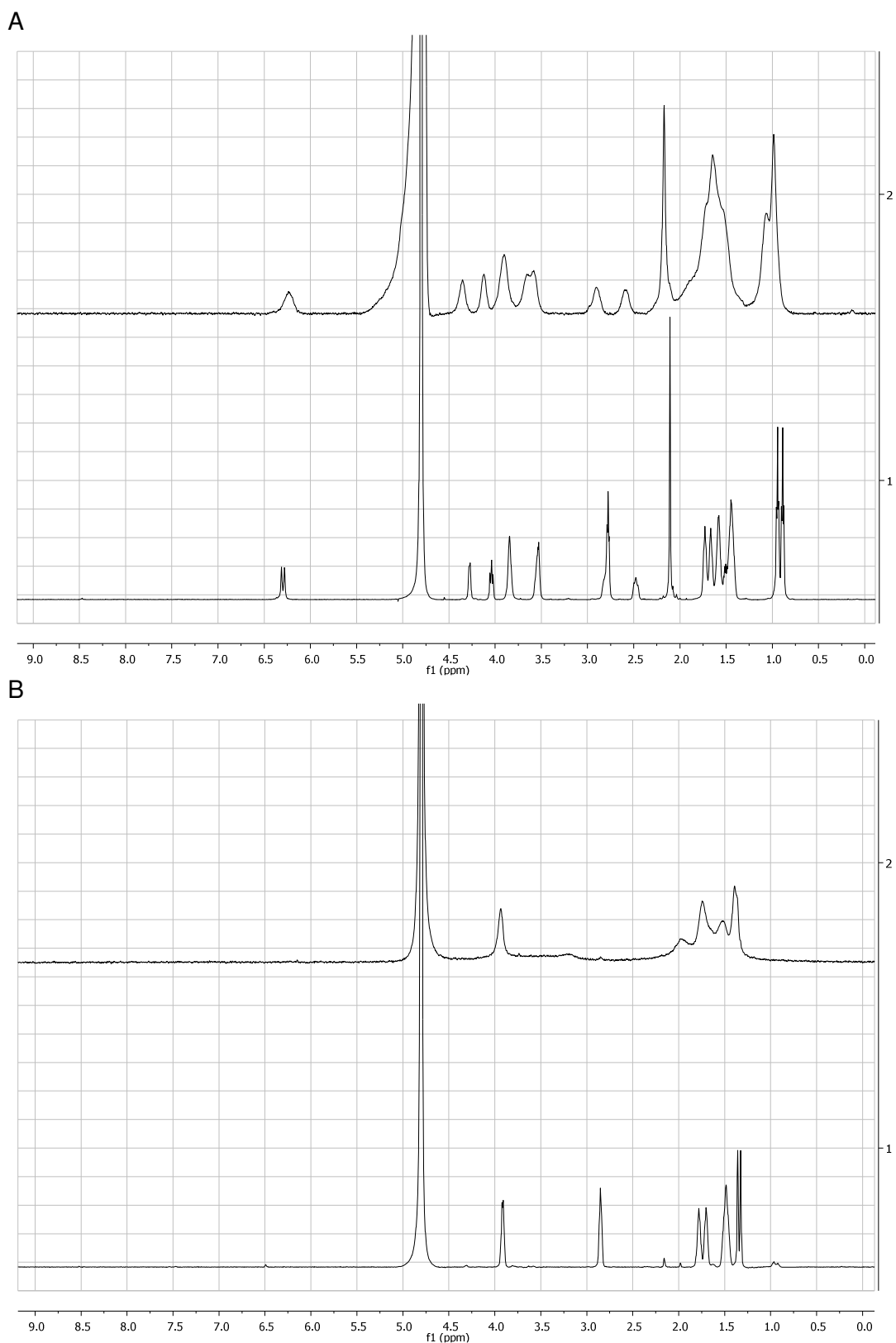


Figure 55. (A) ¹H-NMR-spectra overlay of “small TamiGold” with compound **45** and (B) ¹H-NMR-spectra overlay of small methylphosphonate-stabilised gold nanoparticles with compound **49**; Solvent: D₂O. Line broadening of 1.5 Hz was applied to the nanoparticle spectra.

II.2.4.5. Dynamic light scattering (DLS)

Dynamic light scattering (DLS) analysis of “small” methylphosphonate-stabilised gold nanoparticles and “small TamiGold” was not successful.

The intensity size distribution obtained for both samples indicated a polymodal distribution with scattering contributions from a significant population of large aggregates (above the 6000 nm threshold) even after 0.45 µm filtration.

Attempts to lower the concentration of the gold nanoparticle samples (with the intention of reducing interparticle interactions which may result in aggregate formation) did not completely reduce the large particle aggregates observed. Sample dilution to < 0.01 mg/mL led to a poor photon count rate which was insufficient for data collection and analysis.

It was not possible to gather significant and reliable data gathered for volume- and number-based distributions for these nanoparticle samples because values for the refractive index (n_R) and absorption (n_I) (specific to the gold nanoparticle samples) needed for the necessary data analysis were not known (see appendix 2: Dynamic light scattering (DLS), page 263).

II.2.4.6. Mass Spectrometry

MALDI-MS of “small TamiGold” (in collaboration with the John Innes Centre, UK) resulted in the detection of the monomer thiol fragment of the gold nanoparticle (see figure 56). Under the conditions used, fragmentation of “small TamiGold” occurs and the molecular ion species $[M+H]^+$ of the monomeric thiol ligand is consequently detected as the peak of highest intensity ($[M+H]^+$: m/z 436.946).

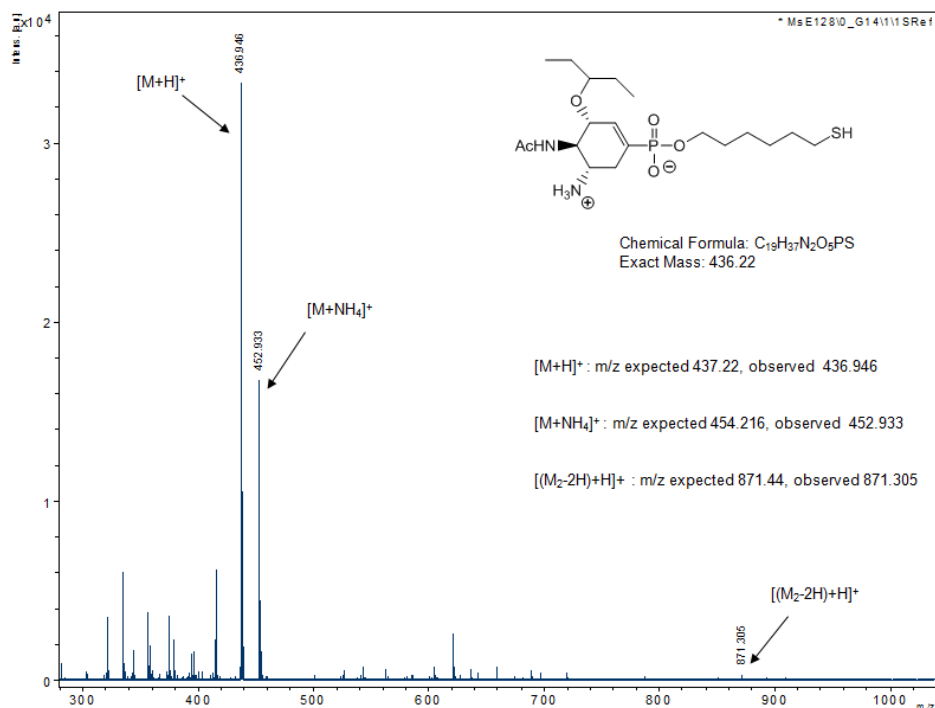


Figure 56. MALDI-MS of “small TamiGold”. Fragmentation leads to detection of monomeric thiol ligand.

The observation of the thiol fragment (and not the disulfide) is indicative of the successful formation of phospho-oseltamivir functionalisation on gold nanoparticles. MALDI-MS of “small” methylphosphonate stabilised gold nanoparticles did not detect the functionalised gold nanoparticles or the free methylphosphonate ligand because the [M+H]⁺ peak was obscured by the matrix used in the MALDI technique. ESI-MS was also unsuccessful in determining the mass of both of the gold nanoparticle samples owing to their inability to be ionised successfully by this method.

II.2.4.7. Energy dispersive X-ray (EDX) analysis

Energy dispersive X-ray (EDX) analysis (in collaboration with the John Innes Centre, UK) was used to analyse “small” methylphosphonate stabilised gold nanoparticles and “small TamiGold”.

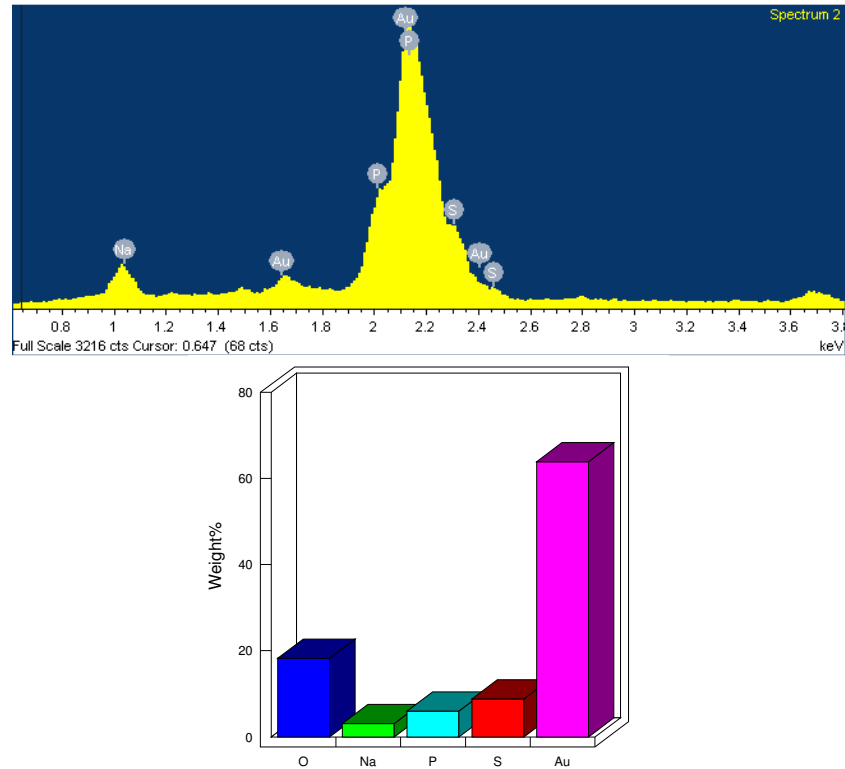


Figure 57. EDX analysis of small methylphosphonate-stabilised gold nanoparticles, resulting in a Au/S ratio of $\sim 1:1$.

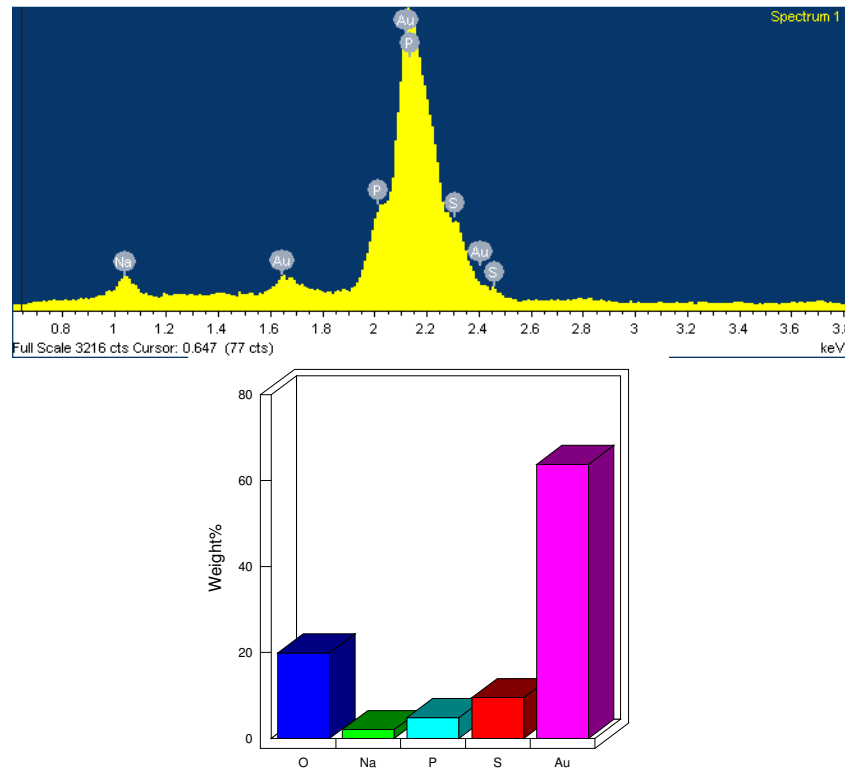


Figure 58. EDX analysis of "small TamiGold", resulting in a Au/S ratio of $\sim 1:1$.

For “small TamiGold” (see figure 58), EDX confirmed the presence of Au, S and P as major constituents of the nanoparticles synthesised. Semi-quantitative EDX analysis determined an approximate Au/S ratio of 60% Au/10% S (% mass) which results in a molar ratio of approximately 1:1. A similar result is obtained for “small” methylphosphonate-stabilised gold nanoparticles (see figure 57) and similar values for alkylthiol-functionalised gold nanoparticles obtained by EDX have been reported.²⁷³

The presence of sodium in the sample is not unusual or unexpected (even after prolonged dialysis with milliQ water) and has been reported elsewhere.²⁷⁴

The approximate 1:1 Au/S ratio was subsequently used as basis for the calculation of phospho-oseltamivir ligand concentration (upon gold nanoparticles) for use in inhibition assays (*vide infra*).

It should be noted that the Au/S ratio is likely to be an overestimate with respect to sulfur due to experimental error associated with small particle samples studied by EDX, which are known to be problematic.²⁷⁵

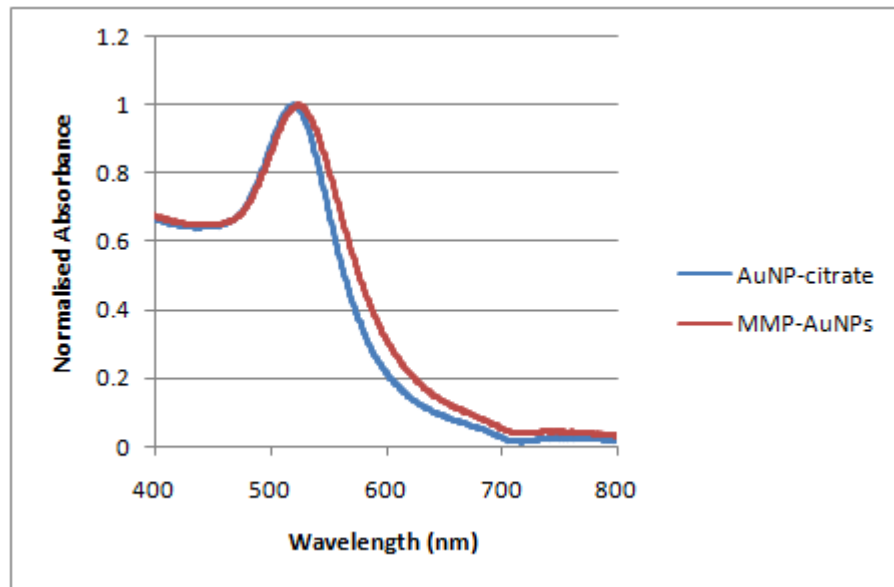
Peak overlap problems (poor detector resolution, non-Gaussian distributions, lack of calibration standards) leads to difficulties in the determination of peak amplitudes for various elements therefore leading to problems with quantification (and subsequent under/over-estimation of elemental analysis). This is a particular problem with Au/S/P since there is significant peak overlap of their characteristic X-ray emissions. As such, the associated error is estimated to be in the order of at least 10-20% with regards to the semi-quantitative data obtained.^{275,276}

II.2.5. Gold nanoparticle characterisation: “large TamiGold” and control sample

II.2.5.1. UV-Vis spectroscopy

UV-Vis spectroscopy indicated that both “large” methylphosphonate stabilised gold nanoparticles and “large TamiGold” displayed the characteristic SPR band in their respective spectra. Ligand exchange of citrate-capped (Turkevitch) particles by compound **49** and compound **45** resulted in a red-shift of the absorption band from 519 nm (citrate-capped gold nanoparticles) to 524 nm (“large” methylphosphonate stabilised gold nanoparticles) and 525 nm (“large TamiGold”) respectively (see figure 59).

A



B

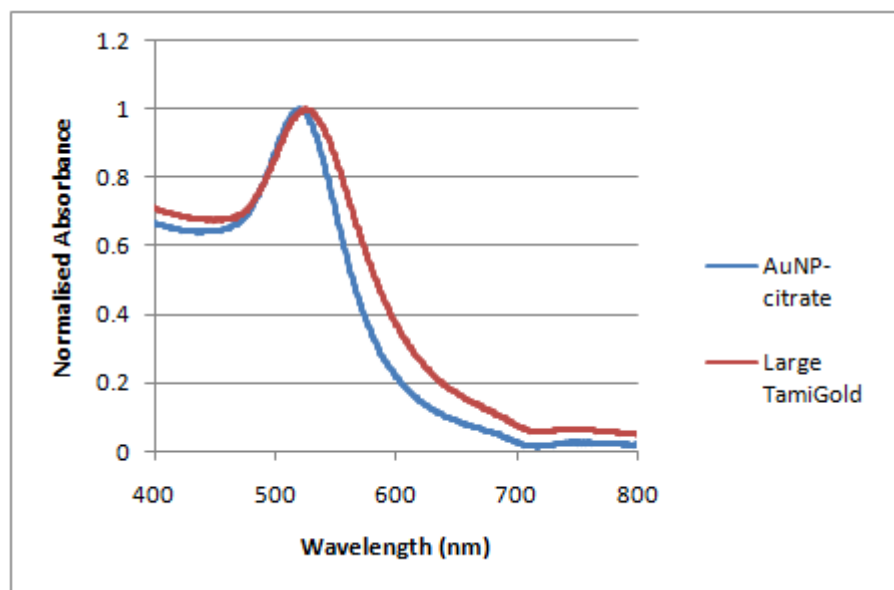


Figure 59. (A) Comparison of UV-VIS spectra of citrate-capped gold nanoparticles and “large” methylphosphonate stabilised gold nanoparticles. (B) Comparison of UV-VIS spectra of citrate-capped gold nanoparticles and “large TamiGold”. (AuNP-citrate = citrate-capped gold nanoparticles; MMP-AuNPs = “large” methylphosphonate stabilised gold nanoparticles)

UV studies were carried out to determine the behaviour of the functionalised gold nanoparticles by varying the pH of solution.

With respect to “large” methylphosphonate stabilised gold nanoparticles, the decrease of solution pH (pH 7.6 to ~pH 2) induces gold nanoparticle aggregation (through

hydrogen bonding networks between nanoparticle functionalised monophosphonate groups and Van der Waals attractive forces between the gold cores with decreasing interparticle distance).^{232,277}

However, once this pH adjustment has occurred it is difficult to resuspend “large” methylphosphonate stabilised gold nanoparticles by increasing the pH of the solution alone (see Figure 60). For successful “large” methylphosphonate gold nanoparticle resuspension the initial pH decrease must not be reduced to below pH 2-3. “Large” methylphosphonate stabilised gold nanoparticles can then regain the original SPR band (~524 nm) by a centrifugation and resuspension process (using a low volume of 0.1 M NaOH (aq.) and phosphate buffer, pH 7.6) (see figure 61).

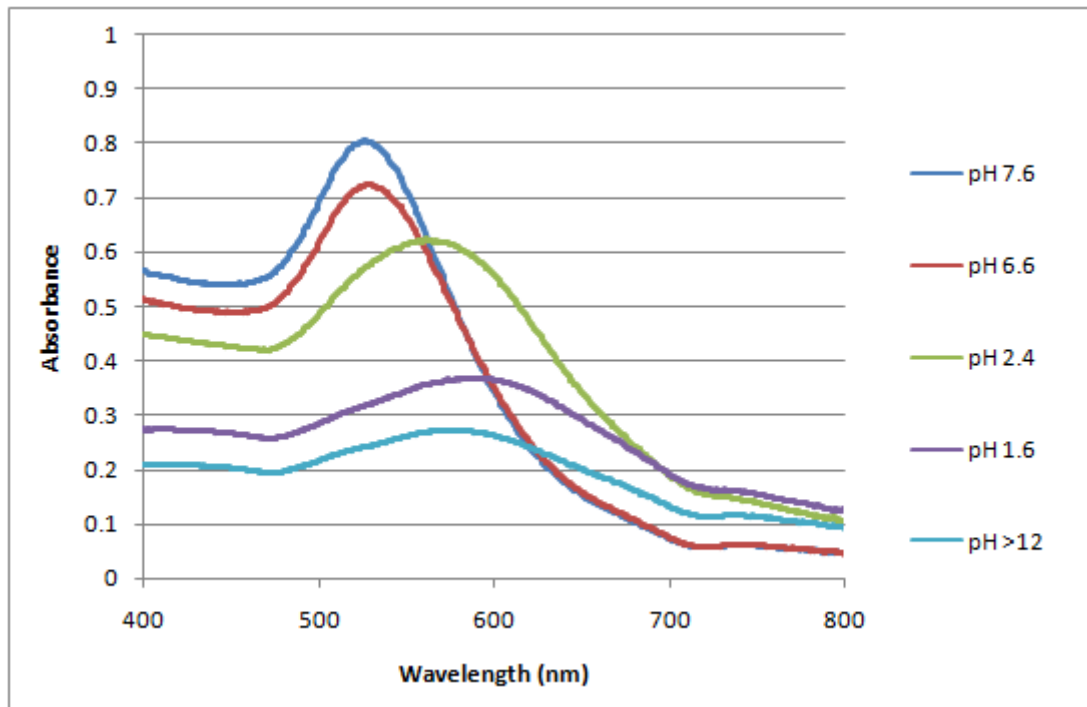


Figure 58. pH-dependent aggregation of “large” methylphosphonate stabilised gold nanoparticles. The original SPR band (~524 nm) is not regained on increasing pH.

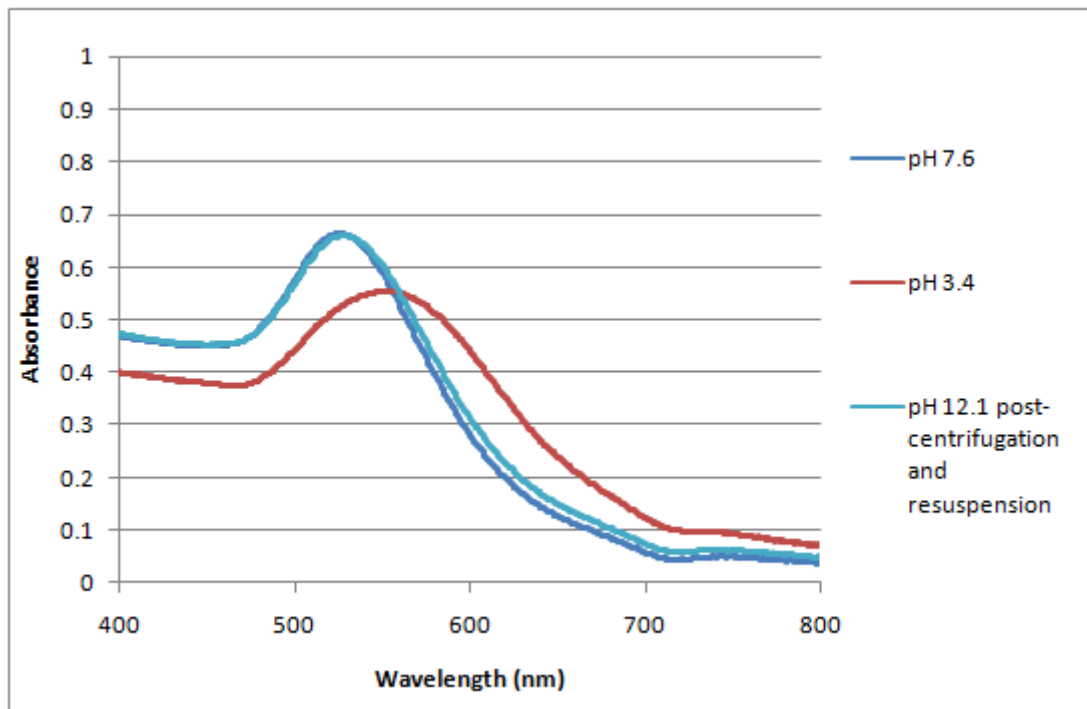
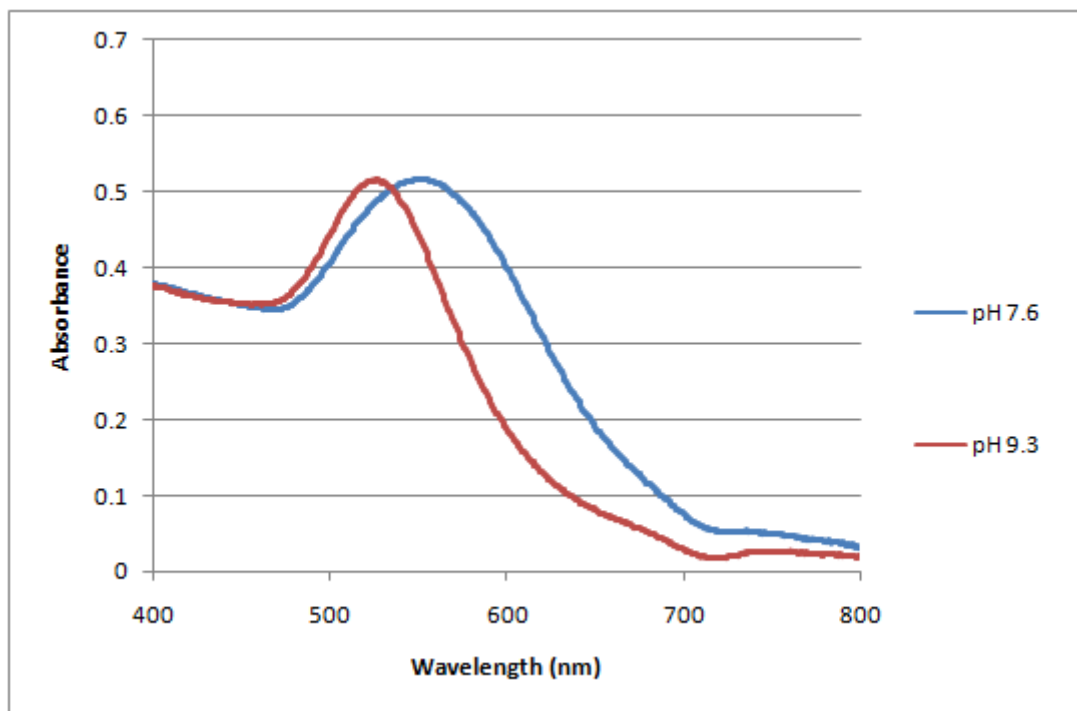


Figure 61. pH-dependent aggregation and resuspension of “large” methylphosphonate stabilised gold nanoparticles.

With respect to “Large TamiGold”, the SPR-absorption also undergoes a red-shift and band broadening in the physical pH-range from 525 nm (pH 9.3) to 553 nm (pH 7.6). Transmission electron microscopy (TEM) images of the decrease in solution pH (dialysis over 3 days) show the aggregation of gold nanoparticles occurring (see figure 62). The red-shift observed in the UV spectra of both “large” methylphosphonate stabilised gold nanoparticles and “large TamiGold” is indicative of a reduction in the interparticle distance which shifts the absorbance to lower energies.^{236,237}

A



B

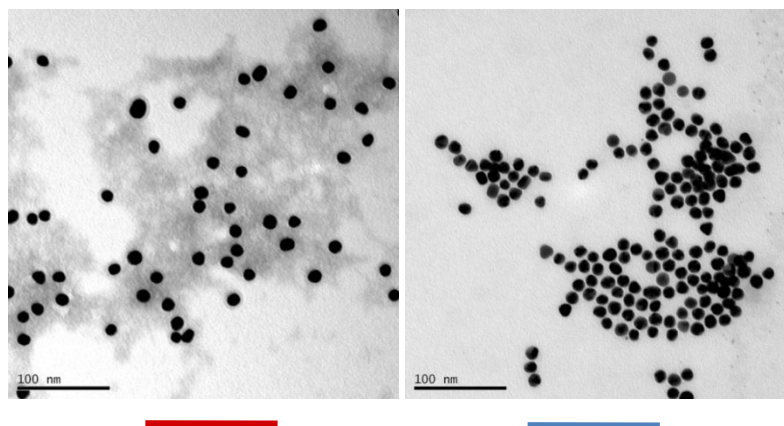


Figure 62. (A) UV-Vis spectra showing a “red-shift” of the SPR band after slow aggregation (3 days) of “large TamiGold” when dialysed against phosphate buffer at physiological pH (pH 7.6); (B) TEM images before and after aggregation as described under A.

As was the case with “large” methylphosphonate stabilised gold nanoparticles, this red-shift was entirely reversible when the solution pH was adjusted to pH > 9. No centrifugation and resuspension process was required (see figure 63).

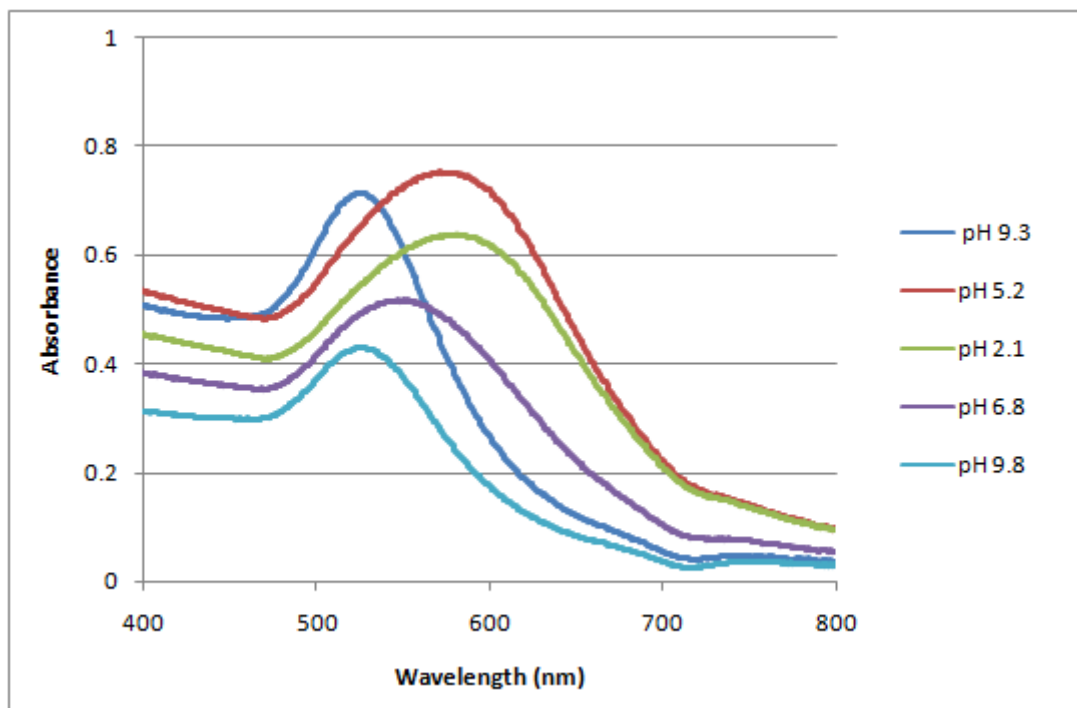


Figure 63. pH-dependent aggregation and resuspension of “large TamiGold”.

From these studies it was apparent that “large” methylphosphonate stabilised gold nanoparticles were more sensitive to changes in solution pH than “large TamiGold”. This may also be explained by the different chemical nature of the terminating group on each functionalised gold nanoparticle (as described in DOSY-NMR results).

The pH dependent behaviour of the SPR band of both “large” methylphosphonate-stabilised gold nanoparticles and “large TamiGold” also provides a confirmation of the change in gold surface functionalisation from citrate-capped (electrostatic) to methylphosphonate and phospho-oseltamivir functionalised (S-Au interaction of covalent character). A pH decrease results in irreversible aggregation of citrate-capped gold nanoparticles. As such it provides a qualitative way of telling whether the ligand exchange reaction has been successful in lieu of other spectroscopic data (see figure 64).

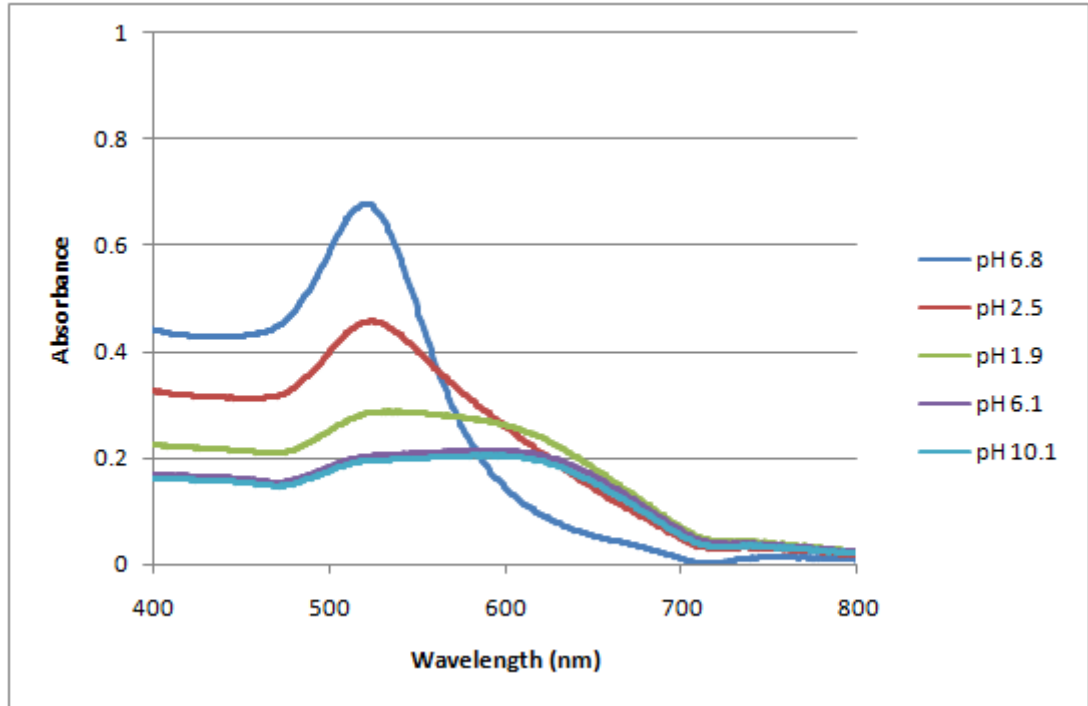


Figure 64. Irreversible aggregation of citrate-capped gold nanoparticles on decreasing the pH of the colloidal suspension.

II.2.5.2. Transmission electron microscopy (TEM)

Transmission electron microscopy (TEM) of “large” methylphosphonate-stabilised gold nanoparticles gave an average particle diameter of 14.4 nm with a particle size range of 12-18 nm (see figure 65).

TEM analysis of “large TamiGold” gave an average particle diameter of 13.9 nm with a particle size range of 12-17 nm (see figure 66). This shows that both gold nanoparticle samples are of a similar size and distribution (approximately 14 nm) and do not show significant changes in particle size compared to the citrate-capped gold nanoparticle precursor (particle diameter of 13.9 nm with a particle size range of 12-18 nm) (see figure 67).

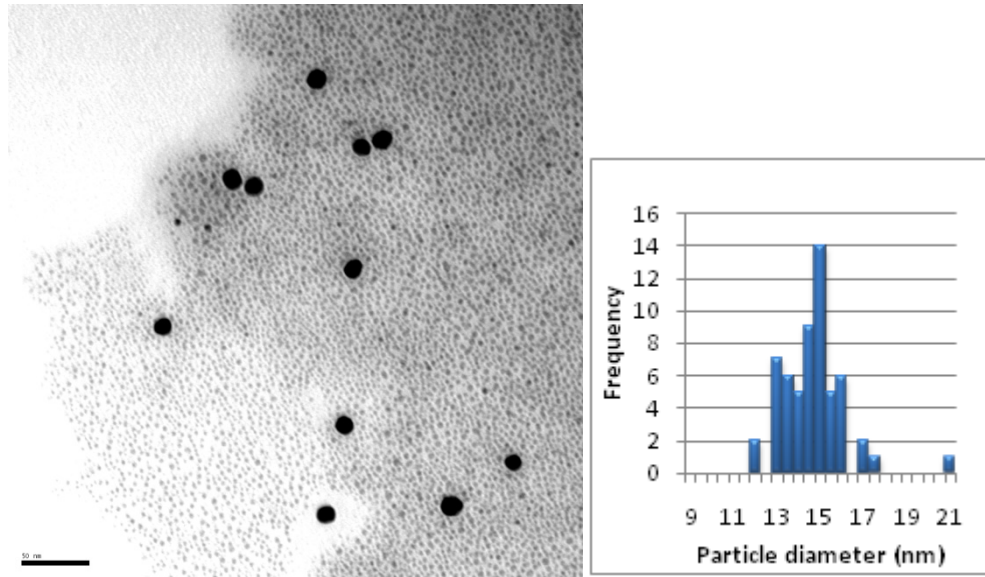


Figure 65. TEM image and size distribution histogram of “large” methylphosphonate-stabilised gold nanoparticles.

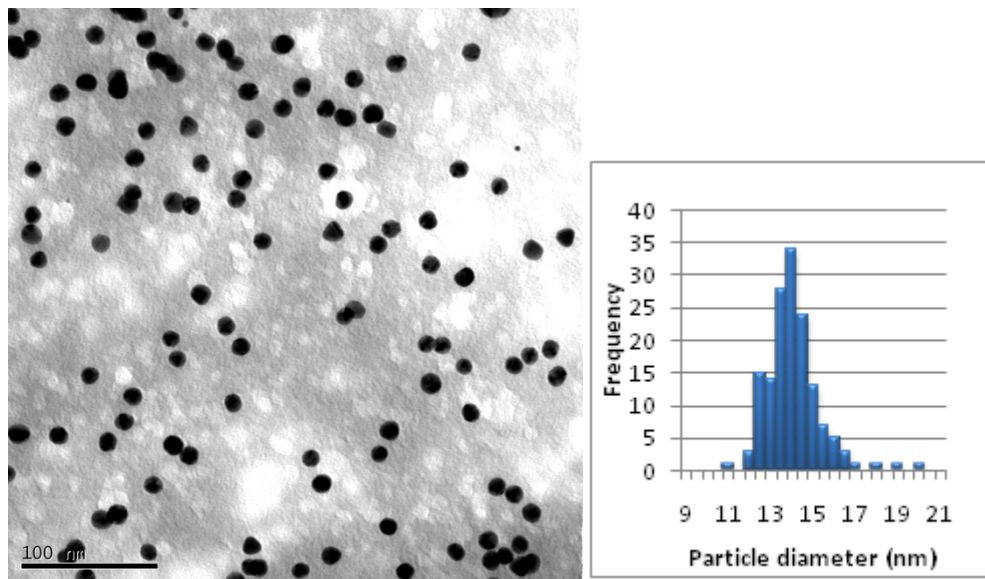


Figure 66. TEM image and size distribution histogram of “large TamiGold”.

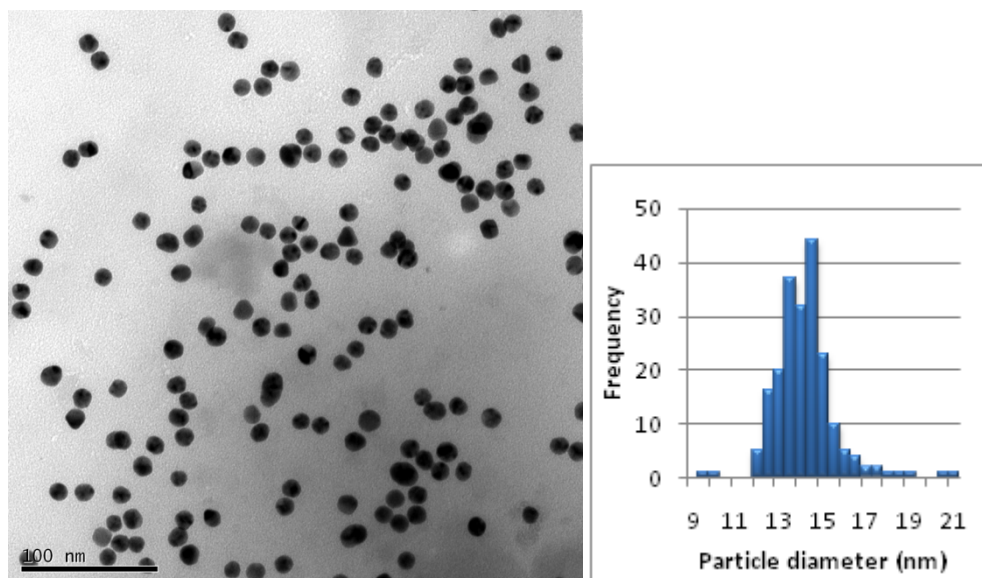
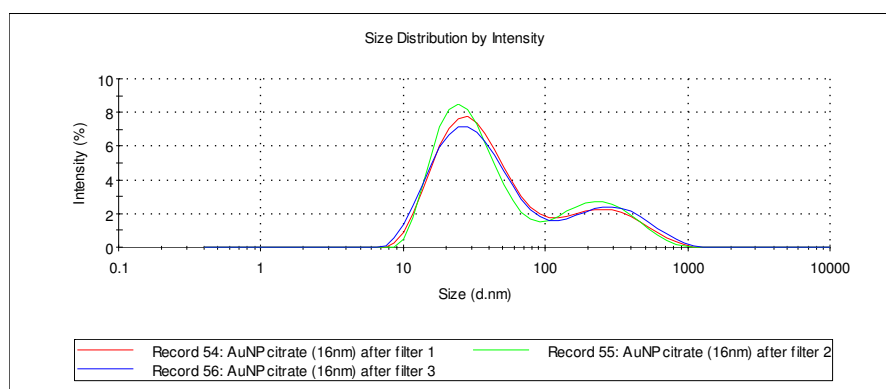


Figure 67. TEM image and size distribution histogram of citrate-capped gold nanoparticles.

II.2.5.3. Dynamic light scattering (DLS)

As a reference experiment, DLS analysis of the citrate-capped gold nanoparticles gave a bimodal intensity distribution with peak averages of 34.99 nm (74.6% intensity) and 294.4 nm (25.4% intensity) with a Z-average particle diameter of 32.00 nm with a polydispersity (PDI) of 0.445, indicative of a wide particle distribution and/or significant population of larger particle aggregates (see figure 68).

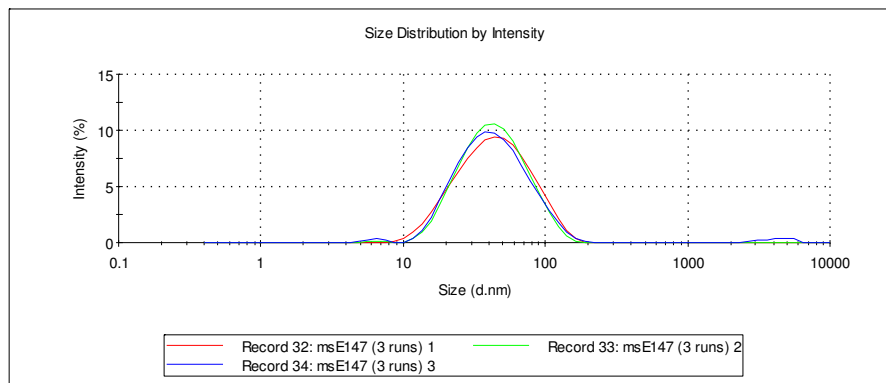


Z-average diameter (nm): 32.0 nm **Polydispersity Index (PDI):** 0.445

Figure 68. Dynamic light scattering analysis of citrate-capped gold nanoparticles.

DLS analysis of “large” methylphosphonate-stabilised gold nanoparticles resulted in a size analysis showing a broad mono-modal distribution with the majority of scattering

intensity from particles and/or particle aggregates with a peak mean of 48.79 nm (99%). The Z-average particle diameter is 36.61 nm with a polydispersity of 0.240 (see figure 69).



Z-average diameter (nm): 36.61 nm **Polydispersity Index (PDI):** 0.240

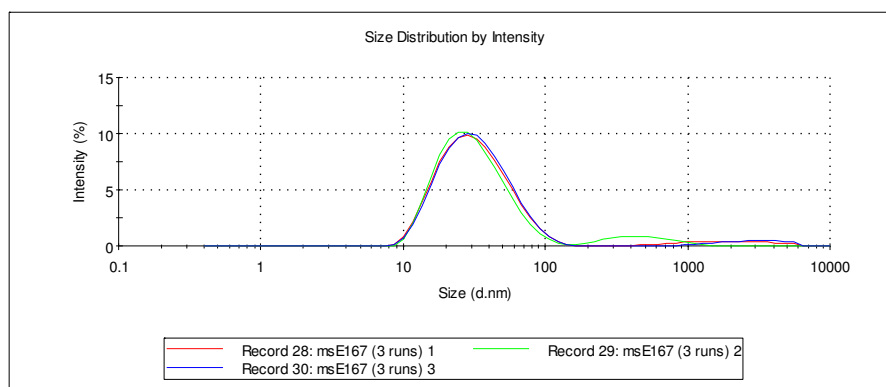
Figure 69. Dynamic light scattering analysis of “large” methylphosphonate stabilised gold nanoparticles.

Conversion to volume- and number-based distributions was problematic. Volume distribution and gave a polymodal distribution with peak means of 6.125 nm (25.9%), 21.59 nm (72.5%) and 4646 nm (1.6%).

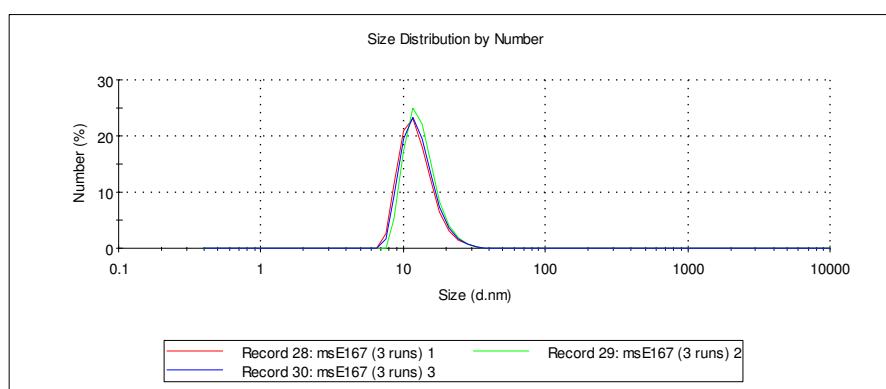
The number-based analysis gave a bi-modal distribution, with a peak mean of 5.9 nm (64.3%) and 13.4 nm (35.7%). The repeatability of the DLS experiments with “large” methylphosphonate-stabilised gold nanoparticles proved difficult with respect to volume and number distribution.

DLS analysis of “large TamiGold” resulted in intensity-distribution data also showing a broad monomodal distribution corresponding to a peak average of 34.90 nm (94%) with minor scattering contributions from larger aggregates with peak means of 598.6 nm (3.3%) and 2903 nm (2.6%) with a Z-average diameter of 28.19 nm with a polydispersity of 0.265 (see figure 70).

A



B



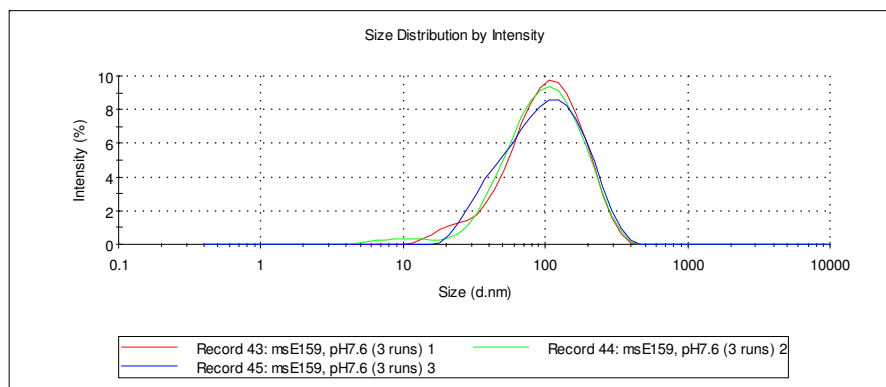
Z-average diameter (nm): 36.61 nm **Polydispersity Index (PDI):** 0.240

Figure 70. Dynamic light scattering analysis of “large TamiGold” (pH 9.3). (A) Intensity distribution and (B) number distribution.

Conversion to a volume-based distribution gives a mainly monomodal distribution with a peak mean of 17.70 nm (95.5% by volume). The number-based analysis (see figure 68) gave a mono-modal distribution, with a peak mean of 13.2 nm (100%). Result reproducibility was very good.

The number average particle size of “large TamiGold” (13.2 nm) is in good agreement with the TEM sizing (approximately 14nm) when considering the effect of data analysis on number-based particle size for nanoparticles (see appendix 2: Dynamic light scattering (DLS), page 263).

DLS analysis of “large TamiGold” at physiological pH (refer to figure 71) resulted in an intensity size distribution showing a broad mono-modal distribution corresponding to a peak average of 113.8 nm (100%) with a Z-average particle diameter of 79.45 nm with a polydispersity of 0.280.



Z-average diameter (nm): 79.45 nm **Polydispersity Index (PDI):** 0.280

Figure 71. Dynamic light scattering analysis of “large TamiGold” at physiological pH (pH 7.6).

The Z-average particle diameter (at pH 7.6, 79.45 nm) is significantly larger than the Z-average particle diameter at pH 9.3 (28.19 nm) due to nanoparticle aggregation. This corroborates the data obtained in UV-Vis and TEM studies regarding the aggregation of functionalised gold nanoparticles in solutions of varied pH.

DLS data supports the size estimates of the TEM analysis. There is no significant size difference between the functionalised gold nanoparticle samples or the citrate capped gold nanoparticles (precursor).

In comparing the DLS data of “large” methylphosphonate-stabilised gold nanoparticles to “large TamiGold” (Z-average diameters of 36.61 nm and 28.19 nm respectively) it is clear that both samples have a nanoparticle size of the same order of magnitude, however, the value for “large” methylphosphonate-stabilised gold nanoparticles is slightly larger. Considering the larger size of the phospho-oseltamivir moiety in comparison to the methylphosphonate group the opposite results may have been expected. But once again the nature of the terminating functional group (phospho-oseltamivir vs. methylphosphonate) is of importance in determining the average nanoparticle size population since the terminal methylphosphonate has an unhindered ability (in comparison to phospho-oseltamivir) to form long-range (hydrogen-bonded) networks within solution which would contribute to a large aggregate population (and as such a larger Z-average particle diameter) for the methylphosphonate stabilised gold nanoparticles.

Larger ligands (in comparison to those with small terminating groups) are known to disrupt the organisation of ligands on the gold surface and as such do not present the same degree of ligand packing or ligand directional orientation.¹⁹³

II.2.5.4. ¹H NMR

It was not possible to obtain ¹H NMR spectra of both “large” methylphosphonate-stabilised gold nanoparticles and “large TamiGold” due to the increased gold particle size (compared to gold nanoparticles produced by the Brüst-Shiffrin method). ¹H NMR resonances are broadened out completely through NMR relaxation effects and as such are not observed for large gold nanoparticles.

II.2.5.5. Physical observations

“Large” methylphosphonate-stabilised gold nanoparticles and “large TamiGold” are not easily isolated (and stable) once removed from their respective buffer solutions. Lyophilisation of both leads to a slight but noticeable red-shift in the SPR band of both functionalised nanoparticles, though “large TamiGold” seems to appear more robust in their tolerance of such conditions.

“Large TamiGold” in particular (but displayed by “large” methylphosphonate-stabilised gold nanoparticles to a lesser extent) displays hysteresis when the pH of the surrounding medium was varied. The final state of the gold nanoparticles (with regards to the SPR band) is only achieved when the nanoparticles pass an intermediate region of high pH. That is, the SPR band does not return to its original position (pre-pH variation) until the pH of the solution is increased beyond the optimal pH range for colloidal stabilisation. More specifically, “Large TamiGold” is a stable colloidal solution and an SPR band at 525 nm at pH 9.3 (in Tris buffer, as described above) but on solution acidification and subsequent SPR red-shift, the 525nm is not returned until the pH of solution initially increased to pH > 9.3 and subsequently dialysed against pH 9.3 (to return to initial solution pH).

This aspect of gold nanoparticle behaviour has only been investigated qualitatively here with respect to the handling of the functionalised gold nanoparticles but this behaviour has been discussed in the literature, particularly with respect to ligands of a cationic nature.²⁷⁸

There is a significant difference in the solubility and stability of “small/large TamiGold” and “small/large” methylphosphonate-stabilised gold nanoparticles. Both “small TamiGold” and “small” methylphosphonate-stabilised gold nanoparticles are suspendible in water whereas “large TamiGold” and “large” methylphosphonate-stabilised gold nanoparticles require a buffered aqueous solution (pH > 9 and pH >7 respectively). This difference in aqueous solution stability can be attributed to the degree of surface functionalisation of gold nanoparticles.

Large gold nanoparticles (because of the increased surface area available for ligand immobilisation) display a greater number of ligands on the particle surface. In this situation, the ionisable phosphonate- and amino-groups present within the phosphoseltamivir motif act to induce gold nanoparticle aggregation of “large TamiGold” (through hydrogen bond interactions and/or bridging of nanoparticles by ions present in solution) when the usually dominant electrostatic stabilising force of the ligands is lessened in aqueous solutions where the pH of solution is sub-optimal for colloidal stability.^{228,278,232}

The strength of these interactions is approximately equivalent to the number of bond made and as such, weak individual hydrogen bonding interactions are enhanced because of their multivalent nature. Ligand-ligand interactions between gold nanoparticles are therefore more significant with respect to the colloidal stability of large gold nanoparticles compared to small gold nanoparticles and explain why the large nanoparticle systems synthesised in this project show increased sensitivity to the surrounding aqueous environment.²⁰³ It has also been speculated in the literature that residual citrate also contributes to gold nanoparticle cross-linking and thus particle aggregation.²⁷⁰

II.2.5.6. Gold nanoparticle stability with respect to an application as an Influenza virus sensor

Typically, a broad bell-shaped pH profile range of enzyme activity is observed with NA of various subtypes. Enzymatic activity at high pH has been observed (pH>8). Therefore, the stability of “large TamiGold” in basic aqueous suspensions is not expected to severely compromise the binding affinity of the immobilised phosphoseltamivir ligands for the influenza NA. The arginine triad within the active site is arguably the most essential recognition component for the oseltamivir pharmacophore.^{133,107} The pH at which “large TamiGold” is stable to aggregation (pH ~ 9.3) should not detrimentally effect this important electrostatic interaction and as such substrate binding is expected to be maintained beyond optimum NA activity values (pH ~5-6).^{279,280}

II.2.6. Investigation into NA inhibition by functionalised gold nanoparticles: “small TamiGold”

“Small TamiGold” (and “small” methylphosphonate-stabilised gold nanoparticles as the control sample) were investigated in fluorescence-based inhibition assays with

seasonal and pandemic influenza A virus (H1N1) strains (both oseltamivir-resistant (R) and oseltamivir-sensitive (S)) in collaboration with the NIMR (National Institute of medical research) in order to assess the ability of the functionalised phospho-oseltamivir motif to bind to viral NA.²⁸¹

The particle size data obtained by HRTEM and the Au/S ratio determined by EDX analysis of “small” methylphosphonate gold nanoparticles and “small TamiGold” were used as a basis for the calculation of ligand (phospha-oseltamivir) concentration for the inhibition assays (see appendix 3: Gold nanoparticle inhibition assays: calculation of ligand surface coverage, page 266). The inhibitory values (IC_{50} values) determined refer to the estimated concentration of phospha-oseltamivir (not absolute values).

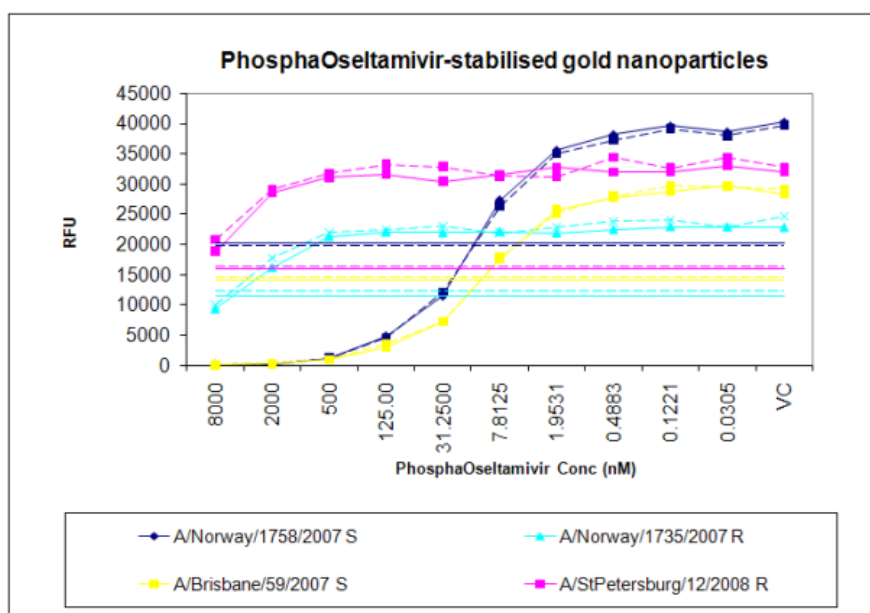


Figure 72. Inhibition of the neuraminidase activity of seasonal influenza virus strains (H1N1) by ‘small TamiGold’. Horizontal lines represent 50% inhibition for the individual experiments. IC_{50} values (nM) are 14.7 and 12.3 for wild-type influenza virus strains A/Norway/1758/2007 and A/Brisbane/59/2007, respectively. For the oseltamivir-resistant strains the IC_{50} values (nM) are 5.3×10^3 for A/Norway/1735/2007 and 14.1×10^3 nM for A/St. Petersburg/12/2008.

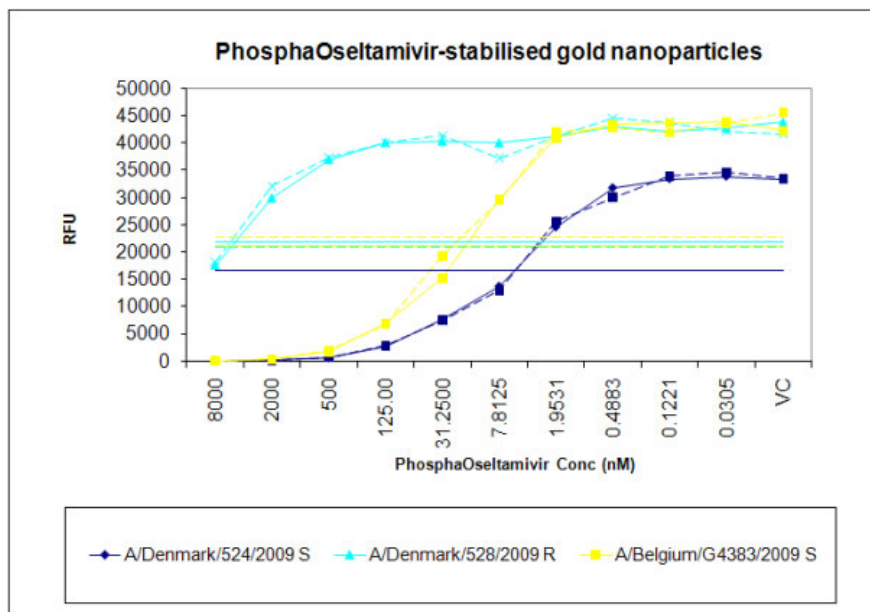


Figure 73. Inhibition of the neuraminidase activity of pandemic (2008) influenza virus strains (H1N1) by 'small TamiGold'. IC_{50} values (nM) are 5.2 and 18.6 for wild-type influenza virus strains A/Denmark/524/2009 and A/Belgium/4283/2009, respectively. For the oseltamivir-resistant strain A/Denmark/528/2009 the IC_{50} value (nM) is 5.5×10^3 .

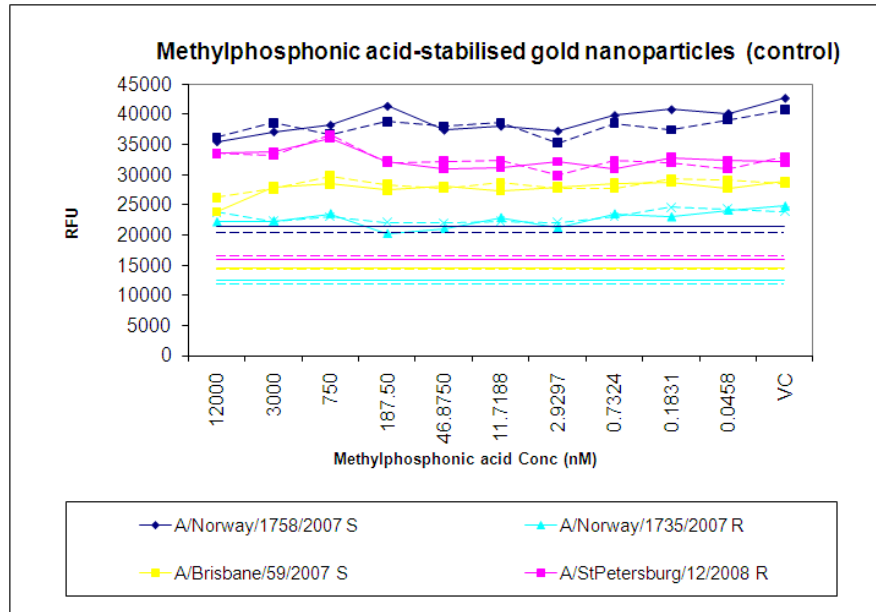
The seasonal strains A/Norway/1758/2007 and A/Brisbane/59/2007 (oseltamivir-sensitive) resulted in IC_{50} values of 14.7 nM and 12.3 nM respectively. This is in contrast to (oseltamivir-resistant) seasonal strains A/Norway/1735/2007 and A/StPetersburg/12/2008 which required higher nanoparticle concentrations for 50% inhibition which resulted in IC_{50} values of 5.3×10^3 nM and 14.1×10^3 nM, respectively (see figure 72).

It should be noted that the IC_{50} value of influenza virus strain H1N1 A/St. Petersburg/12/2008 was slightly outside the maximum particle concentration tested. The value given is an extrapolation of the data points obtained, indicating clear inhibition of the influenza virus.

Similar inhibitory results were obtained with the pandemic influenza virus strains investigated (see figure 73). The pandemic strains A/Denmark/524/2009 and A/Belgium/G4383/2009 (both oseltamivir-sensitive) resulted in IC_{50} values of 5.2 nM and 18.6 nM respectively whereas A/Denmark/528/2009 (oseltamivir-resistant) resulted in an IC_{50} value of 5.5×10^3 nM (therefore weaker inhibition).

The inhibition assays carried out with "small" methylphosphonate-stabilised gold nanoparticles and the same influenza virus strains show no inhibition of influenza virus NA activity (see figure 74).

A



B

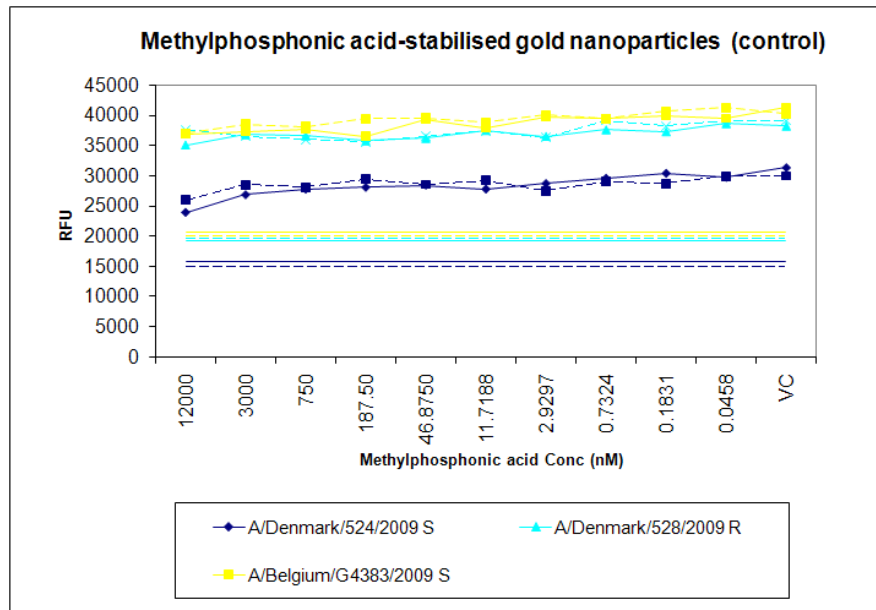


Figure 74. Inhibition of the neuraminidase activity of influenza virus strains (H1N1) by small methylphosphonate-stabilised gold nanoparticles. (A) Seasonal influenza virus strains (H1N1) and (B) pandemic influenza virus strains (H1N1). No inhibition was detected within the concentration range tested.

The results of the inhibition assays indicate strong and selective binding of “small TamiGold” to the influenza virus strains via the NA surface protein and that “small TamiGold” even binds to oseltamivir-resistant strains (albeit at higher concentrations). The lack of inhibition detected with the H1N1 influenza virus strains with “small” methylphosphonate-stabilised gold nanoparticles (control) over the concentration range

tested all but excludes unspecific interaction with the influenza virus strains as a cause of NA inhibition. The conclusion can therefore be drawn that the binding properties of “small TamiGold” are an approximate 1:1-translation of the specificity and affinity of the phospho-oseltamivir motif onto the gold nanoparticle.

The main contributing factors to the error in the inhibitory concentrations (IC_{50} values) of phospho-oseltamivir motifs on “small TamiGold” arise from three main factors; 1) not all phospho-oseltamivir moieties on a given gold nanoparticle are available for binding, 2) the error in the Au/S ratio determined by EDX analysis (mentioned above) and c) the assumptions made regarding the morphology of the gold nanoparticles.

II.2.7. Investigation into NA inhibition by functionalised gold nanoparticles: “large TamiGold”

II.2.7.1. TEM study with influenza A virus (H1N1)

A TEM study was carried out with deactivated influenza A virus (H1N1/PR8). The incubation of H1N1/PR8 with “large TamiGold” (~4 nM) at room temperature led to TEM images of “large TamiGold” binding to the surface of the virus (see figure 75).

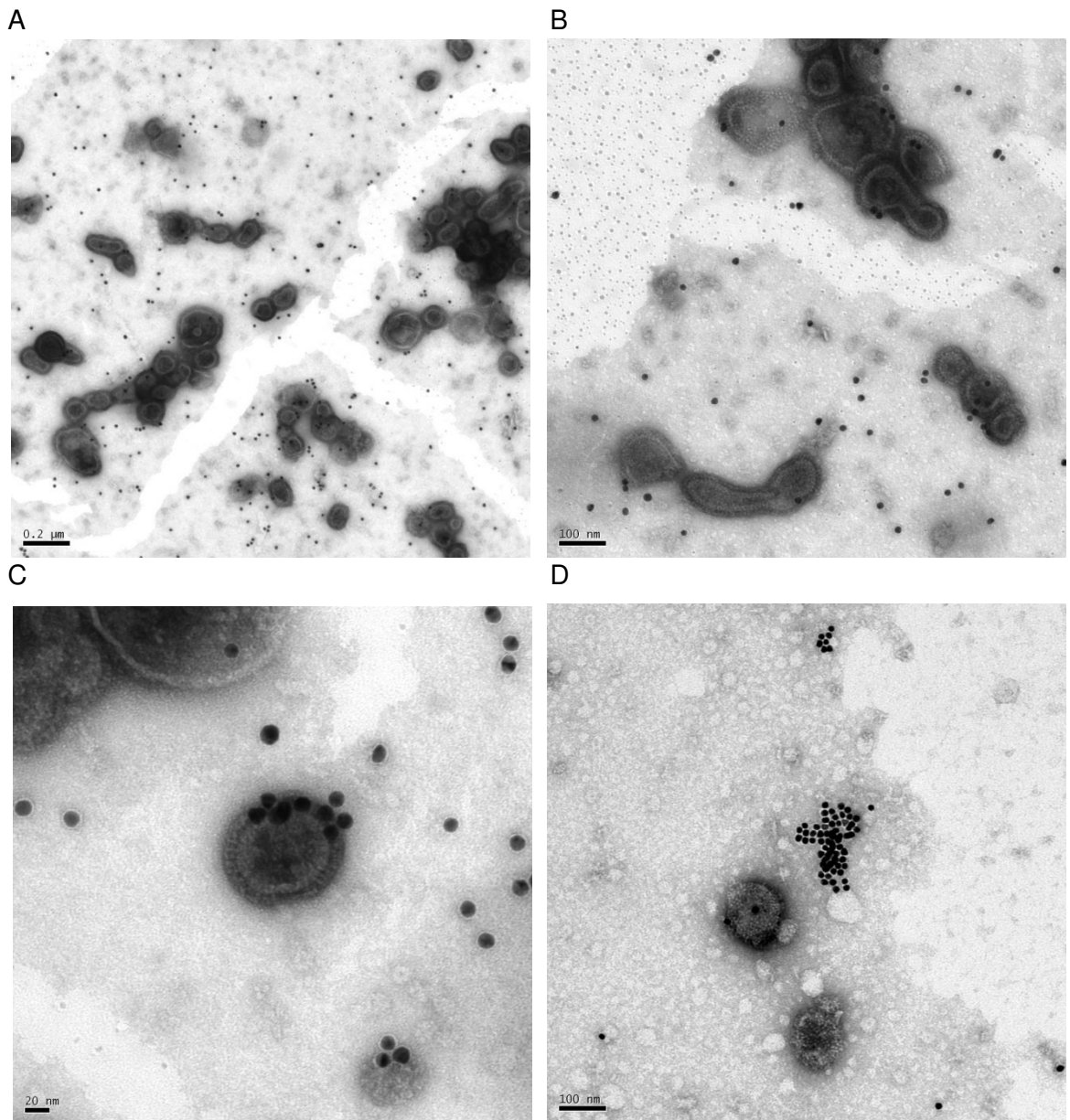


Figure 75. (A,B) TEM images of binding of 'large TamiGold' to influenza virus (PR8/H1N1). (C) TEM image showing clustering of 'large TamiGold' on the virus surface. (D) Aggregation of 'large TamiGold' in presence of monomeric inhibitor (monophosphonate derivative, $K_i = 0.30 \pm 0.04$ nM). The inhibitor is expected to saturate the neuraminidase active sites but may also impact on the aggregation due to changes in the ionic strength.

The negative staining of influenza virus was not as successful with the second set of images (see figure 76). Despite this lower image quality the binding of "large TamiGold" to the influenza virus particle is clear (in comparison to images obtained from blank grids and control samples (see figure 75).

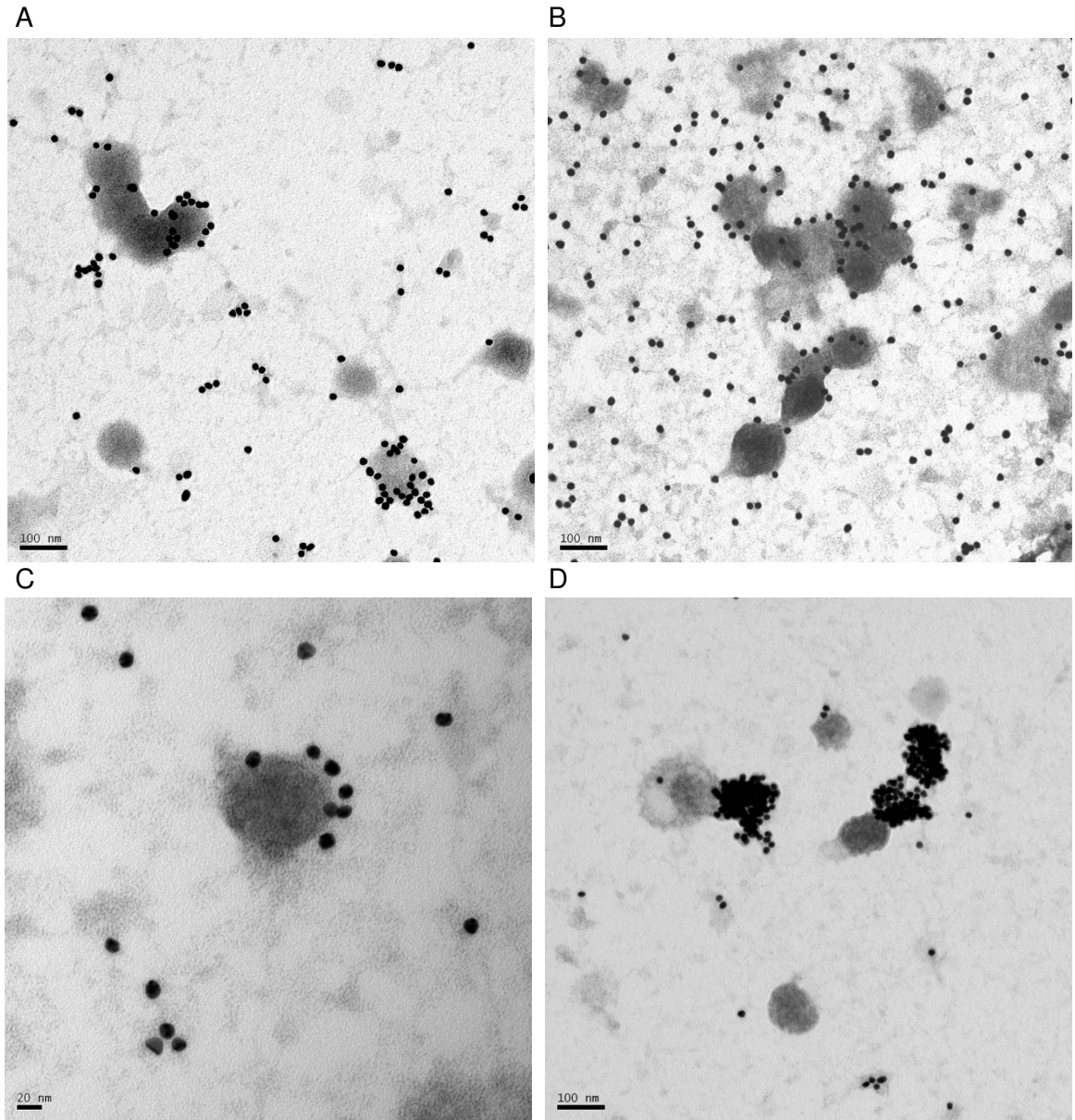


Figure 76. (A,B,C) TEM images of binding and clustering of 'large TamiGold' to influenza virus (PR8/H1N1). (D) Aggregation of 'large TamiGold' in presence of monomeric inhibitor (monophosphonate derivative, $K_i = 0.30 \pm 0.04$ nM). The source of poor virus resolution was not determined.

The selectivity of the binding was reversed by the addition of an excess of a known NA inhibitor (monophosphonate phospho-oseltamivir, $K_i: 0.30 \pm 0.04$ nM, 60 mM), which is expected to saturate the NA active sites. However, the concentration of the NA inhibitor was relatively high and appeared to impact on the aggregation of "large TamiGold" through changes in solution ionic strength and/or through inhibitor cross-linking with the nanoparticles (see figure 77, A).

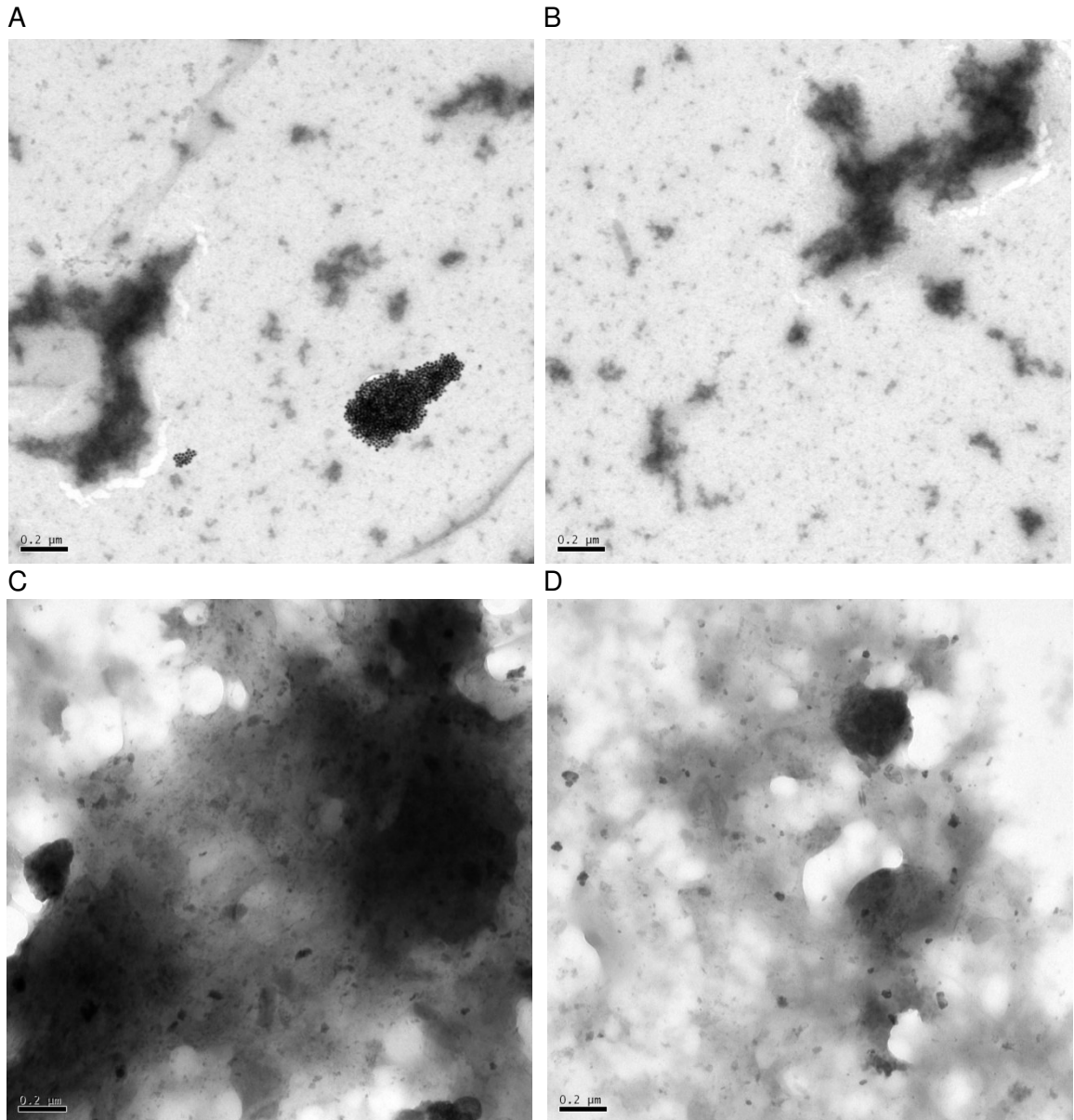


Figure 77. (A) TEM image of aggregated “large TamiGold” on addition of monomeric inhibitor in the absence of H1N1. (B,C,D) Natural aberrations present on the TEM grid (post-staining) which are distinctively different from the influenza A H1N1 containing TEM images with “large TamiGold”. B,C: Blank grid + Tris buffer (10mM, pH 9.3) + 2 % uranyl acetate.

To summarise, the TEM study confirmed the interaction of the functionalised phospho-seltamivir motif with the NA of influenza virus.

Unfortunately, due to a lack of availability of whole influenza virus, a similar TEM-study upon “large” methylphosphonate stabilised gold nanoparticles study was not carried out.

II.2.7.2. Preliminary UV-Vis study with influenza A virus (H1N1)

A qualitative assessment of the effect of virus on the wavelength of the SPR band of “large TamiGold” was carried out with the intention of assessing the potential for “large TamiGold” (~4 nM) to act as a prototype influenza virus sensor.

The deactivated virus suspension (~1mg/mL in PBS) was added in small aliquots to “large TamiGold” (Tris buffer, pH 9.3). UV-Vis spectra were then recorded to observe any potential changes in “large TamiGold” SPR band. As a control, “large TamiGold” was diluted with the same volume of PBS buffer (to exclude changes in solution concentration and pH unrelated to the influenza virus).

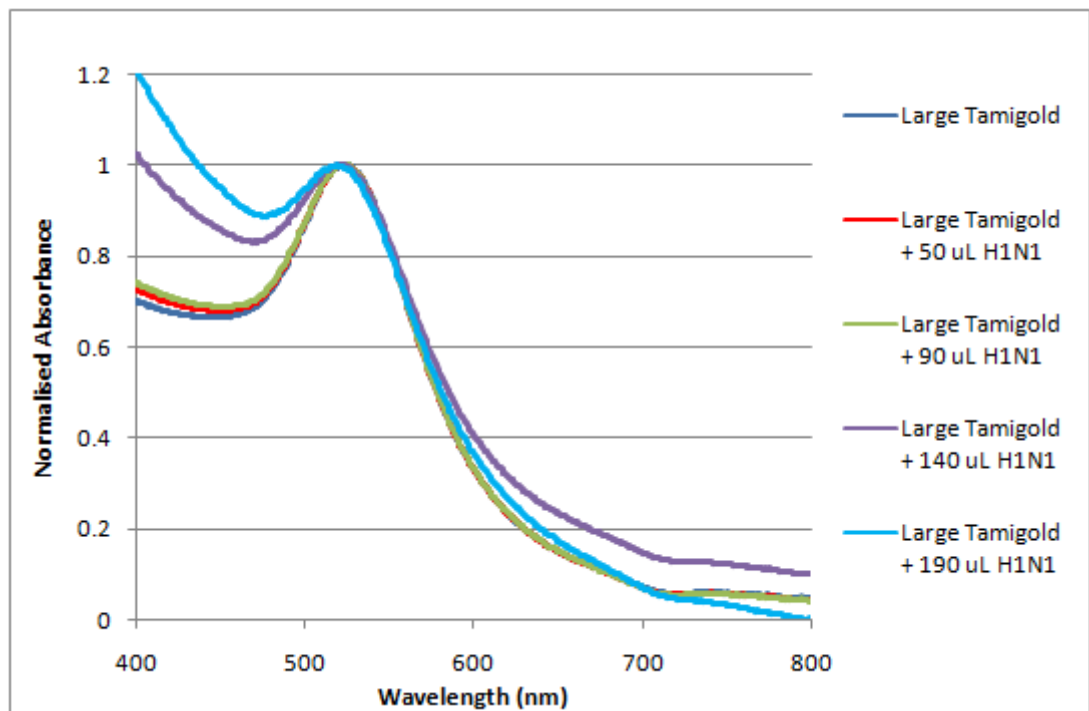


Figure 78. Addition of increasing amounts of influenza virus (H1N1/PR8, ~1mg/mL) to ‘large TamiGold’, resulting in a very slight blue-shift (~ 5 nm) of the absorption band.

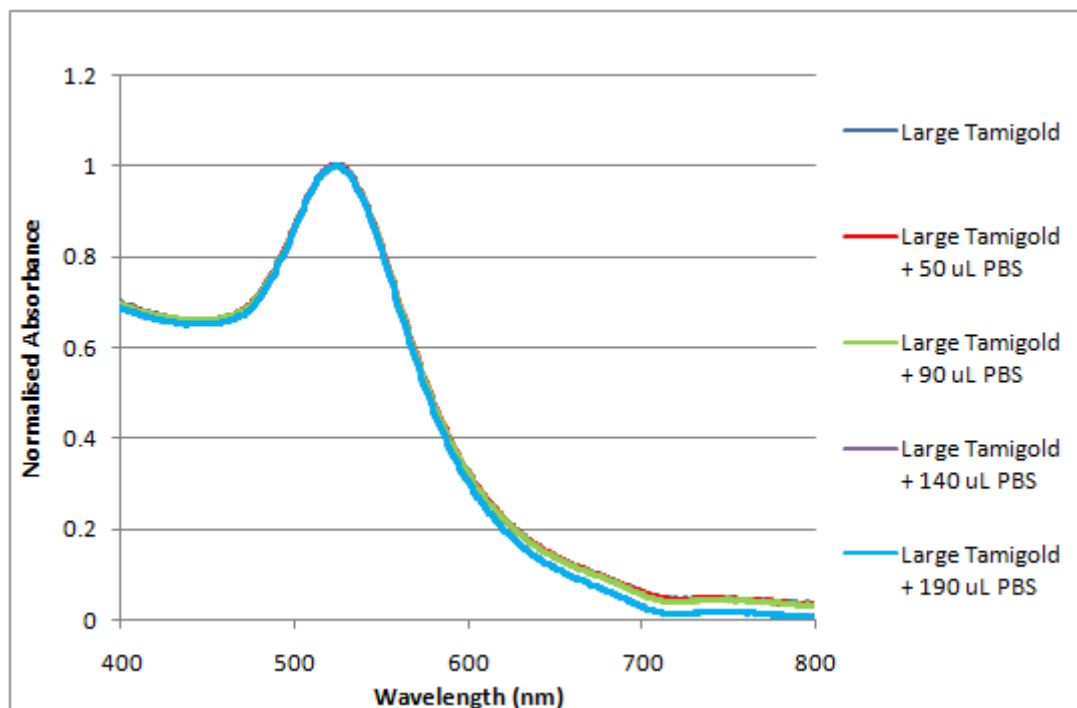


Figure 79. Dilution of a solution of ‘large TamiGold’ (same sample concentrations as in figure 76.) with PBS buffer. No blue-shift was observed under these conditions.

Addition of increasing amounts of virus resulted in a very slight blue-shift (and not the desired red-shift) in the SPR absorption band (see figure 78). This very slight blue-shift (~ 5nm) was not observed with the control (influenza virus-free) sample at this level of dilution and as such the blue-shift is attributed to the presence of the influenza virus in solution (see figure 79).

The source of this blue-shift has not been determined and deserves further study.

In this situation, it appears as though the overall effect of influenza virus addition is to screen or shield “large TamiGold” particles from interacting (through coupling of the surface plasmons). As such, a blue-shift is observed even though binding is occurring between the influenza virus and “large TamiGold” at a local level (observed in TEM images). However, it is worth noting that a “blue-shift” in the SPR bands of gold nanoparticles have been observed in the detection of cancer cells and is attributed to the saturation of gold nanoparticles at higher cell concentrations.²⁸² It can therefore be speculated that for optimal sensing of the virus (through an SPR band red-shift with concurrent visual nanoparticle aggregation) less disparity is required in terms of the size of the nanoparticles and the influenza virus (as well as optimised linker lengths).¹⁷⁵

Though the results of this UV study (blue-shift of the SPR band of “large TamiGold”) were not expected, the UV study indicates that the presence of influenza virus does influence the phospho-oseltamivir-stabilised gold nanoparticles and provides a method of observing that interaction (via the SPR band).

In conjunction with the TEM images, these data indicate that specific interaction does occur with “large TamiGold” and influenza NA. However, with regards to the development of an influenza sensor there are many practical hurdles to overcome.

As with the TEM studies with influenza virus (see above), the lack of availability of whole influenza virus prevented further colorimetric studies with “large” methylphosphonate stabilised gold nanoparticles. This prevents drawing any further conclusions from the nature of the interaction between influenza virus NA and “large TamiGold” for the time being.

II.2.8. Conclusions

The synthesis of a simple dimeric phospho-oseltamivir presenting structure, compound **45**, has given some insight into the effect of multimeric phospho-oseltamivir inhibitors on NA binding. Although the binding observed with compound **45** and NA was slightly improved compared to oseltamivir itself, this most likely comes as a result of statistical rebinding effects and not through multivalent interactions.

The syntheses and use of phospho-oseltamivir derivatives has been successfully implemented towards functionalised gold nanoparticles (“TamiGold”). Though not the first example of an immobilized oseltamivir analogue,¹⁸⁹ the work carried out in this project is the first example of an immobilised oseltamivir analogue functionalised to a solid support (gold nanoparticles) without compromising the oseltamivir pharmacophore.

Functionalised gold nanoparticles synthesised by the Brüst-Shiffrin method (“small TamiGold”) bind strongly and selectively to both seasonal and pandemic influenza virus strains investigated and at higher concentrations to oseltamivir-resistant strains and this binding is independent of non-specific binding effects.

The interaction of functionalised gold nanoparticles synthesised by the ligand-exchange/Turkevitch method (“large TamiGold”) have also shown to bind to influenza virus H1N1 (from TEM and qualitative UV studies), although a much better understanding of “TamiGold” binding and selectivity with influenza virus has yet to be achieved. The lack of availability of H1N1 proved a hindrance in the pursuit of further investigations of the binding interaction of “large TamiGold” with influenza virus.

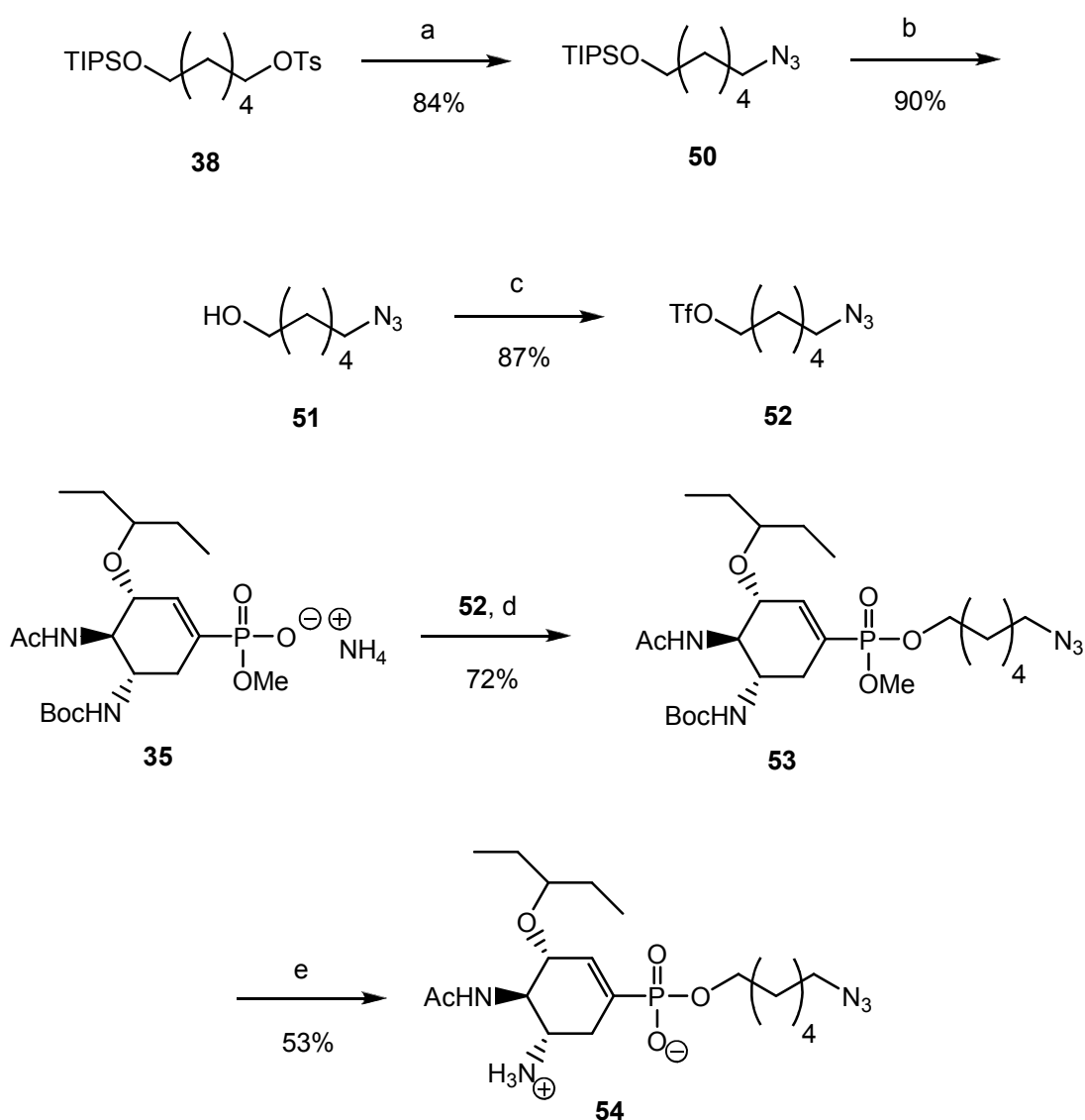
However, the influenza NA has been made available as a target for multivalent tools and diagnostics for influenza research, providing an alternative to HA-targeting strategies.

“TamiGold” may have a potential use as TEM image contrast agents for studying influenza viruses as well as serving as a prototype for novel virus sensors targeting the NA. However, it appears that biosensor systems based on functionalised gold nanoparticles (typically colorimetric in nature) are a complicated balance between a number of variables (nanoparticle size, size of detected analyte, the concentration of nanoparticles/analyte, pH, ionic strength). As such, more detailed studies of such variables are the next logical step for this research.

II.2.9. Towards phospho-oseltamivir based tools for the investigation of influenza virus neuraminidase

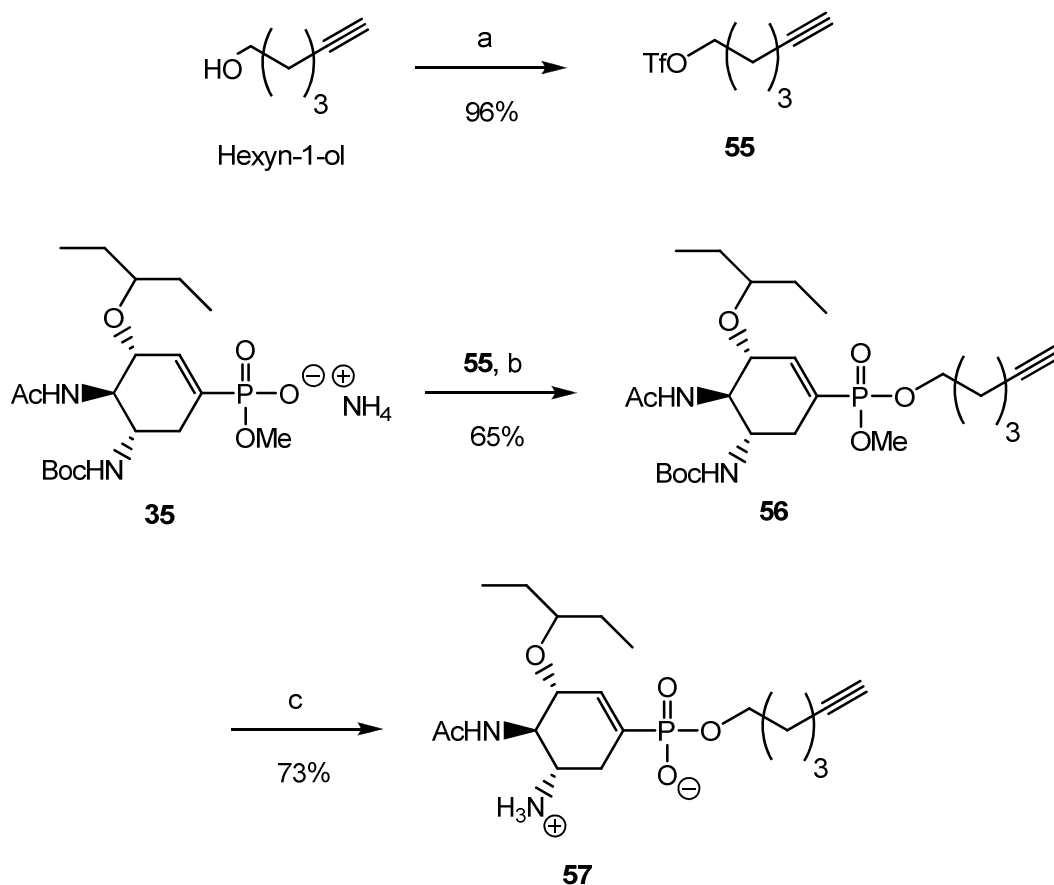
II.2.10. Synthesis of “clickable” phospho-oseltamivir derivatives

Using the same alkylation methodology as with phospho-oseltamivir derivative **42**, the ω -azido hexyl derivative **53** was synthesised from the alkylation reaction of the monomethyl phosphonate **35** with triflate **52** (itself synthesised in 3 steps (66%) from compound **38**). The resulting mixed diester could be fully deprotected using standard conditions to give the target ω -azido derivative **54** (see scheme 29).



Scheme 29. Reagents and conditions; (a) NaN_3 , DMF; (b) TBAF, AcOH, THF; (c) Trifluoromethanesulfonic anhydride, lutidine, DCM, $-60\text{ }^\circ\text{C}$; (d) acetonitrile, **52**; (e) i. NaI, acetone, reflux; ii. TFA/ H_2O (50%); iii. gel permeation chromatography.

In a similar fashion, the synthesis of ω -ethynylbutyl derivative **56** was achieved through the alkylation reaction of the monophosphonate **35** with triflate **55** (synthesised directly from commercially available hexyn-1-ol) in good yield (65%, based on recovered starting material) followed by deprotection to give target compound **57** (see scheme 30).



Scheme 30. *Reagents and conditions;* (a) Trifluoromethanesulfonic anhydride, lutidine, DCM, -60 °C; (b) acetonitrile and compound **55**; (c) i. NaI, acetone, reflux; ii. TFA/H₂O (50%); iii. gel permeation chromatography.

The introduction of these specific chemical handles (ω -azido and ω -ethynylbutyl) for ligation purposes provides freedom of application to the phospho-oseltamivir structure, whether via traditional amino-coupling chemistry (via reduction of the azido moiety to the corresponding primary amine) or, as mentioned, through “click” methodologies (considered rapid and high-yielding reactions, tolerant of a range of solvents conditions and often allowing orthogonality of reaction conditions)^{267,283} and therefore provides the rationale for the synthesis of compounds **54** and **57**.

This flexibility in conjugation methodology (provided by compounds **54** and **57**) enables the phospho-oseltamivir motif to accommodate any pre-existing ligation requirements of different chemical and biological systems without researchers having to rely upon a single conjugation method. As such, the availability of these compounds to influenza researchers with differing chemical/conjugation requirements is achieved.

At the time of submission, a dimeric “clicked” phospho-oseltamivir ($K_i = 0.04 \pm 0.01$ nM) had been synthesised by Streicher *et al.* using compound **53**.²⁸⁴

II.2.10.1. Neuraminidase (NA) inhibition studies

In conjunction with the NIMR, compounds **54** and **57** were tested for inhibition of the NA isolated from influenza X31 (H3N2) and were compared to the well-established and selective NA inhibitors oseltamivir-carboxylate and zanamivir.

54	57	Oseltamivir	Zanamivir
0.224 ± 0.037	0.234 ± 0.036	0.130 ± 0.032	0.268 ± 0.039

Table 5. Inhibition constants (K_i [nM]) for target phosphonates.

(Inhibition of MUNANA hydrolysis catalysed by neuraminidase from influenza virus X (H3N2); inhibition constants were determined as described in experimental section; K_M for MUNANA = 6.4 ± 0.6 μ M).

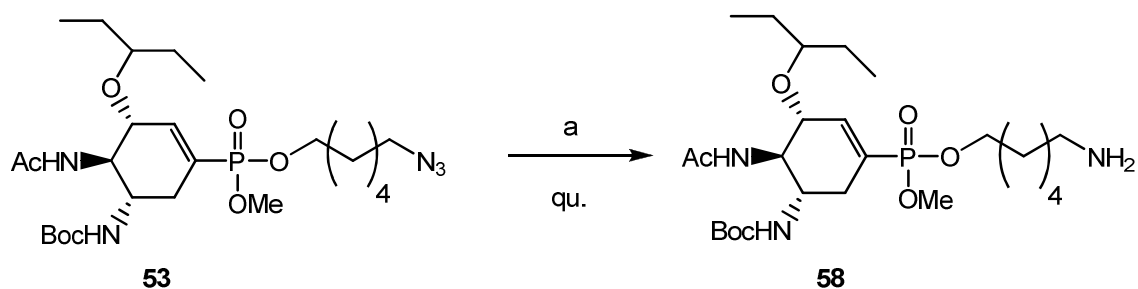
Both target compounds **54** and **57** are found to be subnanomolar inhibitors of MUNANA hydrolysis by the NA from influenza X31 (H3N2) and are of the same order of magnitude as the benchmark NA inhibitors (see table 5).

II.2.11. Conjugation to reporter groups

The ω -azido derivative **53** was used to synthesise phospho-oseltamivir derivatives conjugated to two types of reporter groups; biotin and fluorescein, widely used in biological research. Fluorescein represents a family of fluorophores widely used in biochemistry and virology (for example, the Alexfluor® group. The application of biotin is well-established and usually in conjunction with its interaction with avidin or streptavidin proteins.¹⁸¹

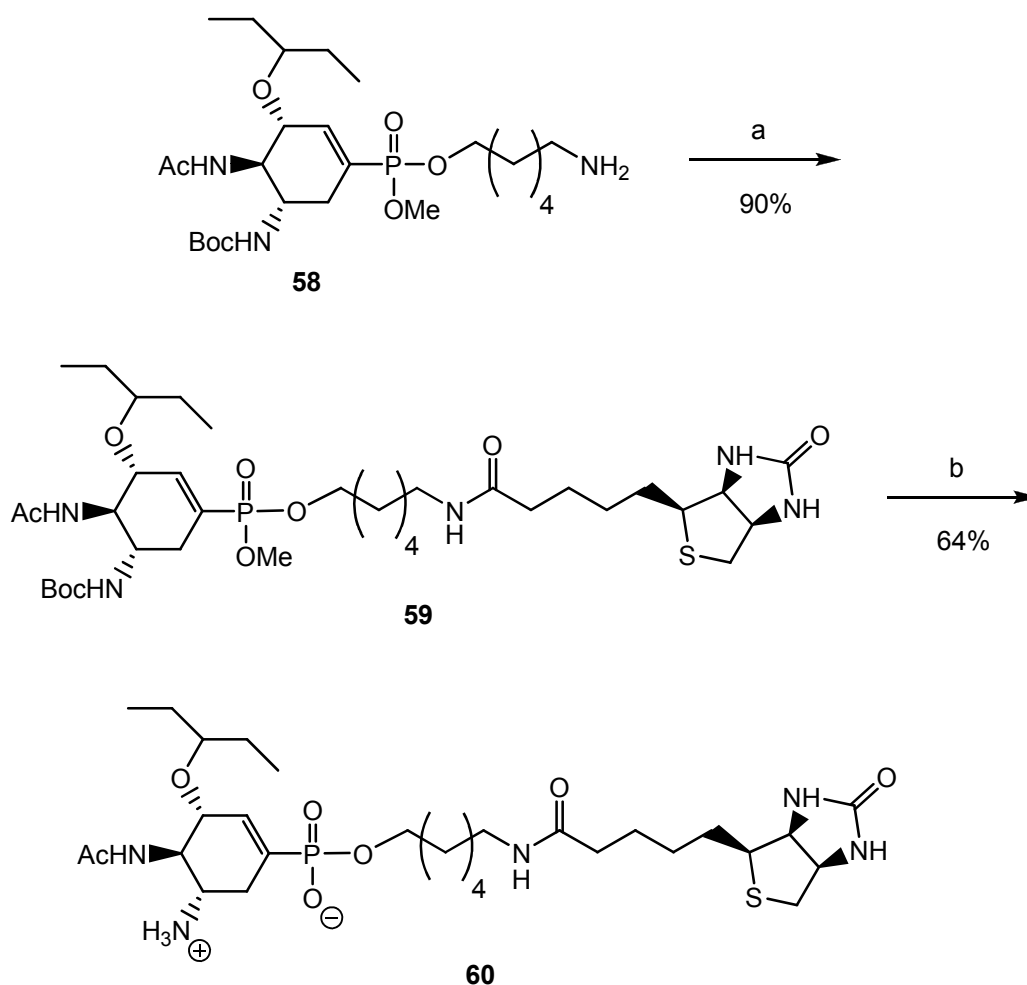
As the respective reporter groups were not readily available with the appropriate functionality to allow the Huisgen-1,3-dipolar cycloaddition reaction, the conjugation of these reporter groups was achieved through standard amino-coupling methods.

The reduction of the ω -azido derivative **53** was successfully achieved by a Staudinger reaction with PMe_3 in THF (1 M) followed by aqueous hydrolysis to give the amine **58**, which was then used as the precursor to the reporter group conjugates (see scheme 31).



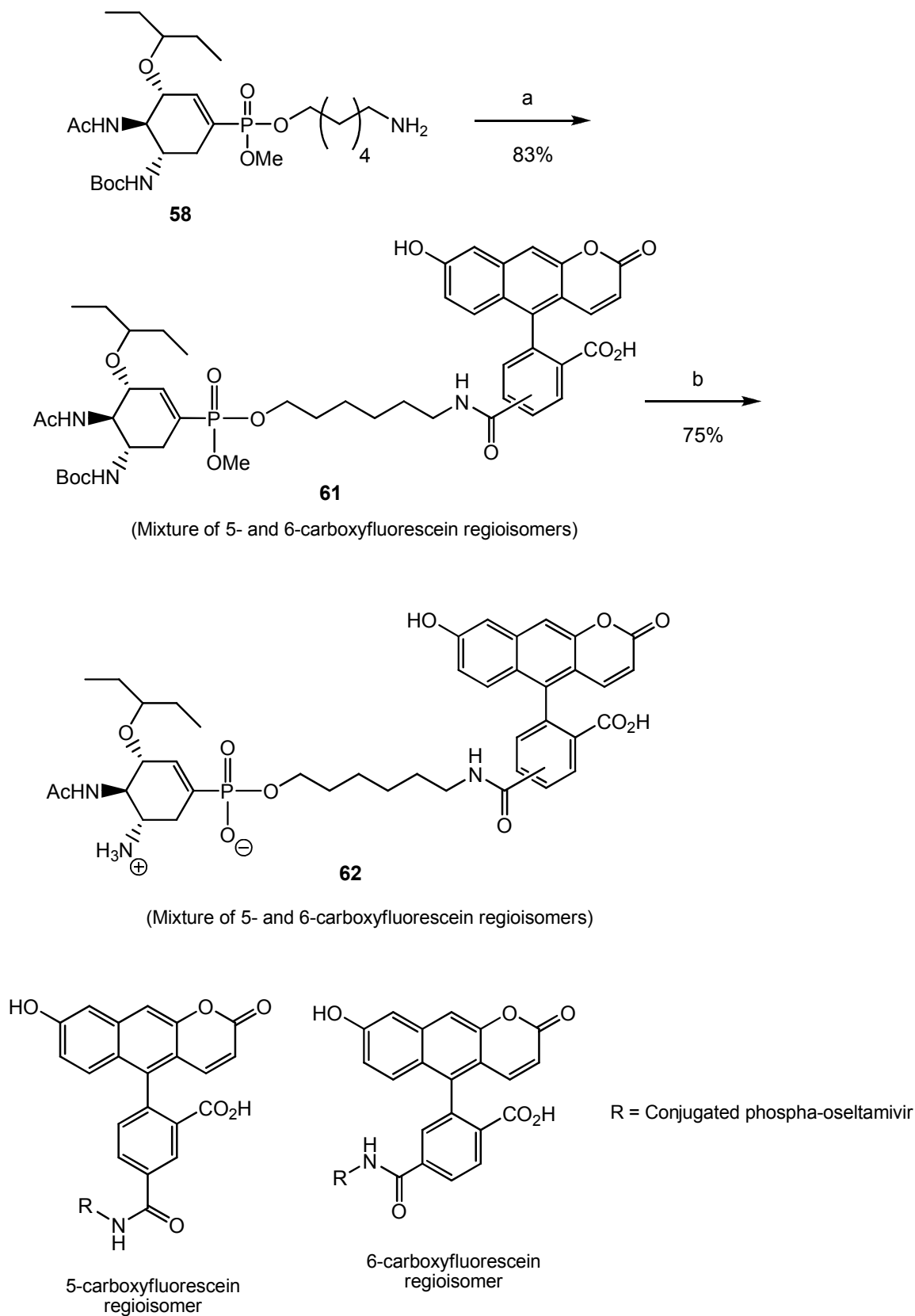
Scheme 31. Reagents and conditions; (a) i. PMe_3 , THF; ii. H_2O .

The (+)-biotin conjugate **60** was synthesised by coupling the amine **58** with (+)-biotin using benzotriazol-1-yl-oxypyrrolidinephosphonium hexafluorophosphate (PyBOP) as the condensing agent. Deprotection of the methylphosphonate ester using Finkelstein conditions followed by *tert*-butyl carbamate removal with trifluoroacetic acid yielded (+)-biotin conjugate **60** in good yield (64 %) (see scheme 32).



Scheme 32. *Reagents and conditions;* (a) d-biotin, PyBOP, DMF; (b) i. NaI, acetone, reflux; ii. TFA/H₂O (50%); iii. gel permeation chromatography.

In order to synthesise the target fluorescein conjugate **62**, the amine **58** was reacted with 5-/6-carboxyfluorescein succinimidyl ester (NHS-Fluorescein; used as the commercially available mixture of isomers) in the presence of triethylamine to give fluorescein conjugate **61** as a mixture of regioisomers (see scheme 33).



Scheme 33. Reagents and conditions; (a) NHS-Fluorescein, DIPEA, DMF; (b) i. NaI, acetone, reflux; ii. TFA/H₂O (50%); iii. reversed phase chromatography.

The separation of these isomers was not possible using standard chromatography techniques available and was never intended.

Using similar deprotection conditions as above, target fluorescein conjugate **62** was obtained (as the mixture of regioisomers). Purification of the fully deprotected fluorescein conjugate **62** (both regioisomers) was problematic by gel permeation chromatography due to reduced solubility in ammonium phosphate buffer. It was possible to obtain a purified sample via reverse phase chromatography. The use of DMSO/H₂O mixtures of fluorescein conjugate **62** (\geq 1:10 ratio) resulted in no solubility problems.

II.2.11.1. Neuraminidase (NA) inhibition studies

As with the “clickable” conjugates **54** and **57**, the (+)-biotin conjugate **60** and fluorescein conjugate **62** were tested for inhibition of the NA isolated from influenza X31 (H3N2) (NIMR collaboration).

60	62	Oseltamivir	Zanamivir
0.241 \pm 0.052	0.162 \pm 0.032	0.130 \pm 0.032	0.268 \pm 0.039

Table 6. Inhibition constants (K_i [nM]) for target phosphonates.

(Inhibition of MUNANA hydrolysis catalysed by neuraminidase from influenza virus X (H3N2); inhibition constants were determined as described in experimental section; K_M for MUNANA = 6.4 \pm 0.6 μ M)

Both the (+)-biotin conjugate **60** and fluorescein conjugate **62** are subnanomolar inhibitors of MUNANA hydrolysis by influenza NA (see table 6).

II.2.11.2. Fluorescence titrations with NA

Slightly stronger binding was observed for the fluorescein conjugate **62** and (in collaboration with the NIMR) prompted a preliminary study on the impact of fluorescence observed when fluorescein conjugate **62** binds with influenza NA (see figure 80).

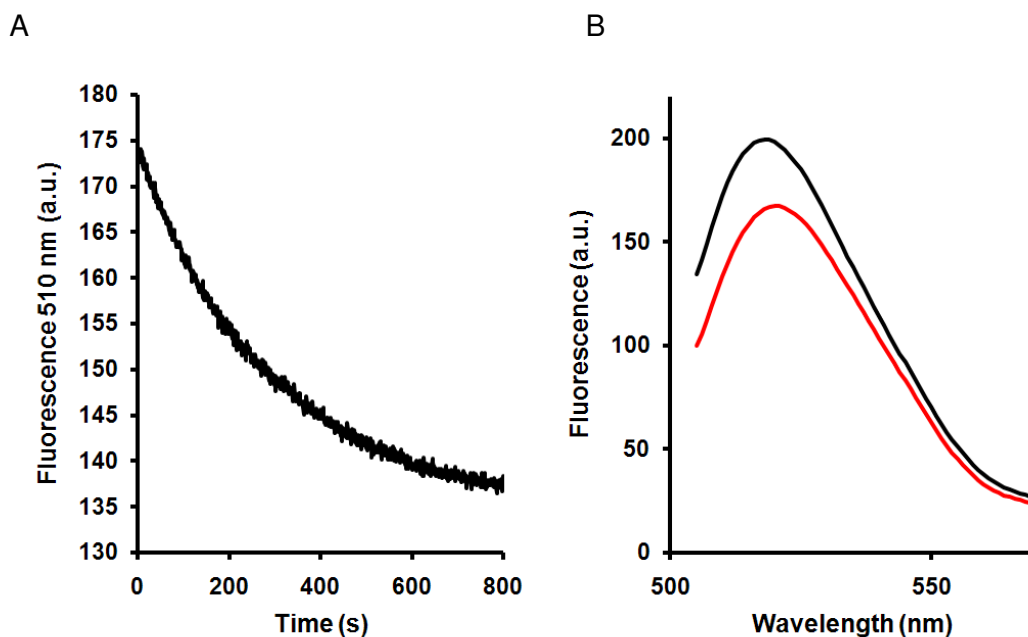


Figure 80. Decrease in fluorescence intensity (510 nm) of compound **62** upon binding to influenza virus NA (A). The binding experiment was carried out at 5 °C and concentrations of compound **62** and NA were comparable (9 nM and 12 nM, respectively). Red-shift and reduction of fluorescence maximum of compound **62** upon binding to influenza NA (B); Black line: Unbound compound **62**. Red line: compound **62** bound to NA.

A decrease in the fluorescence intensity of compound **62** (and a slight shift in the emission fluorescence maxima) was observed on binding to NA. Only a slight perturbation in the fluorescence maxima on NA binding is observed. Fluorescein (in comparison to other fluorescent probes) is not considered to be overly environmentally-sensitive fluorophore.²⁸⁵ As such, the change in fluorescence intensity observed is more than sufficient for binding studies.

A fluorescence-based binding titration with compound **62** and influenza virus X (H3N2) determined quantitatively the dissociation constant (K_i) for the interaction (0.23 ± 0.05 nM), which shows reasonable agreement to the value determined by inhibition of MUNANA hydrolysis (0.162 ± 0.032 nM) (see figure 81).

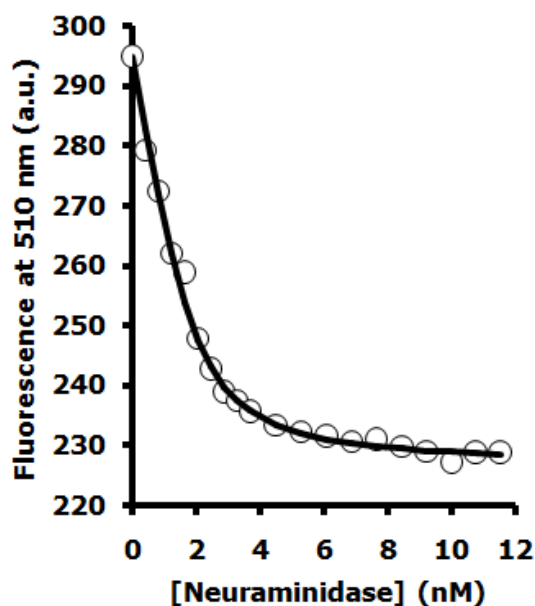


Figure 81. Fluorescence titration of compound **62** against NA (X31 N2). The dissociation constant determined for compound **62** was 0.23 ± 0.05 nM.

II.2.12. Conclusions

The successful syntheses of “clickable” phospho-oseltamivir derivatives along with the conjugation of the phospho-oseltamivir structural motif to biologically useful reporter groups (+)-biotin and fluorescein has been achieved.

These results expand upon previous synthetic work within the group and support the conclusion that manipulation at the phosphonate-ester by the introduction of “clickable” chemical handles and larger biologically useful reporter groups do not impair the binding affinity of the phospho-oseltamivir pharmacophore.

With regards to the “clickable” derivatives compound **54** and **57**, the potential of these compounds to act as precursors to multivalent chemical probes and phospho-oseltamivir functionalised surfaces by exploiting their conjugation chemistry is now within reach.

The (+)-biotin conjugate **60** may provide a new method of studying the binding of NA to immobilised phospho-oseltamivir. The use of biotin to immobilise or ligate bioactive compounds to various materials for biological study is well-established (for example, ELISA assay formats or Biacore systems) and a similar use has been proposed for zanamivir conjugates of biotin.²⁸⁶

Compound **60** could be developed to provide a stable influenza virus immobilisation platform to permit the investigation of the binding of polyvalent sugar derivatives to the

virus surface proteins. For such studies, the linker length of compound **60** may need optimisation. This is entirely possible using the chemistry that has been applied in this project.

The binding titration (see figure 81) illustrates that fluorescein conjugate **62** could be used to obtain small-molecule binding affinities with NA via a displacement titration and therefore provides a new alternative to the classical (but unselective) MUNANA based assay.

The clear interaction of fluorescein conjugate **62** with NA (and the subsequent effect on fluorescence) suggests the possibility of using the compound as a tool for the quantification of influenza NA directly or to provide the basis for a fluorimetric method of influenza virus detection independent of standard immunoassay methodologies.

Further experiments in collaboration with the NIMR are underway to investigate the fluorescence quenching effect on NA substrate binding and to assess the potential of fluorescein conjugate **62** towards applications such as the identification of irregular NA distribution (“neuraminidase patches”) on the virus surface and the distribution of NA on influenza virus subtypes.

II.2.13. Future scope

Although nanoparticle characterisation techniques have been applied to “TamiGold” (primarily for sizing purposes), further nanoparticle characterisation techniques are required in order to unequivocally determine the physical composition and characteristics of the gold nanoparticles. The determination of ligand surface coverage to a higher level of accuracy is of significant importance (with respect to determining the concentration of functionalised phospho-oseltamivir).

Therefore, the compositional analysis of “TamiGold” will need to be addressed by other analytical methods (for example, XPS (X-ray photoelectron spectroscopy) or TGA (thermogravimetric analysis)) in addition to EDX.¹⁹⁵

Further TEM studies with “large TamiGold” and also with “large” methylphosphonate-stabilised nanoparticles are required to further qualify the interaction of “large TamiGold” with influenza A H1N1 as selective and specific.

Other studies of gold nanoparticles utilised as detecting agents for larger biomolecules or biological superstructures showed limited or no effect on the nanoparticle SPR band without increasing the nanoparticle size (therefore observing stronger affinity between functionalised nanoparticles and the target analyte) or by increasing the affinity of the interaction through the use of molecular crowding agents.^{282,287}

Macromolecular crowding increases the association and extent of macromolecular interactions in solution.^{288,287} With respect to “large TamiGold” and its interaction with influenza NA, the use of a macromolecular crowding agent may promote the association of the two species and thus enhance the desired colorimetric observations (SPR red-shift) necessary for a novel sensor based on this interaction.

Further work will therefore include more detailed investigations into the variables which affect the ability of “large TamiGold” to act as an influenza virus sensor. This may be achieved by increasing the size of the nanoparticle presenting the phospho-oseltamivir motif, varying the linker length of the functionalised ligand and by altering the chemical equilibria that govern macromolecular interactions. All may improve the sensitivity of nanoparticle-virus interactions.

It is highly improbable that absolute selectivity is achieved regardless of the type of recognition system used for nanoparticle-analyte interactions. With respect to “TamiGold”, some limited non-selective binding will occur but is unlikely that such non-specific interactions would cause the same level of SPR perturbation (significant red-shift and particle aggregation) to “TamiGold”-NA binding once the nanoparticle sensor platform is fully optimised for influenza NA detection.

The multiple presentation of the phospho-oseltamivir motif is not limited to gold particles. Other types of nanoparticles tailored for specific experimental applications can be synthesised using phospho-oseltamivir disulfide **45**. Iron particles (for NMR studies) or semiconductor nanodots (for fluorescence studies and single virus detection) are a logical step forward regarding tools for the investigation of influenza NA.

Recent work by Streicher *et al.* has used the Huisgen-1,3-dipolar cycloaddition reaction (“click” chemistry) successfully with the ω -azido derivative **53**, as expected.²⁸⁴

The application of this chemistry will therefore be continued towards the synthesis of multimeric phospho-oseltamivir displaying molecules (trimer, tetramers, hexamers, dendrimers) with the aim of binding to influenza NA with increased potency through multivalent interactions with NA active sites. Chemistry which makes use of the ω -ethynylbutyl compounds **56** or **57**, with complementary “click” functionality, will also be developed further (particularly if the ω -azido derivatives **53** or **54** are not synthetically applicable to a specific application).

With regards to the (+)-biotin conjugate **60**, the optimisation of linker lengths to prevent unwanted steric interactions between the NA and avidin/streptavidin proteins is also in the pipeline. A biotin-containing conjugate with optimised linker lengths to prevent such

unwanted steric interactions allows the immobilisation of influenza virus on surfaces (as mentioned above). Avidin/streptavidin-coated quantum dots could be used to immobilise (+)-biotin conjugate **60** (or related analogues) thus also allowing further fluorescence based experiments (FRET (fluorescence resonance energy transfer) and single virus detection) to investigate binding of the phospho-isosteres of oseltamivir to influenza NA.

As mentioned above, further work with compound **62** is underway to investigate the fluorescence quenching effect on NA substrate binding and to assess the potential applications of the compound (for example, virus counting, NA distribution, etc.).

Using the chemistry developed herein, other types of fluorophores may be conjugated to the phospho-oseltamivir motif. Fluorescein is only one of a large number of structurally related fluorophores and is not always the most useful in fluorescent applications in comparison to other fluorophores, such as the Alexafluor group® (often used as standard in influenza virology) which often exhibit better properties (for example, improved water solubility and photo-stability) for fluorescence applications in biological research.²⁸⁵

The phospho-oseltamivir monoester methodology itself could be developed further with the aim of synthesising novel influenza NA inhibitors which exploit the “150-loop” in group-1 neuraminidases.⁸⁸ The exploitation of this flexible, hydrophobic cavity in the active site of group-1 neuraminidases would make possible the synthesis of NA inhibitors of increased inhibitory potency and affinity towards the pandemic A/H1N1, avian A/H5N1 influenza viruses.^{87,128,129}

III. Experimental section

III.1. General procedures

Where anhydrous solvents were required for reactions, MeOH and DMF were purchased (anhydrous) and used as received. DCM was doubly distilled (over CaH₂) before use and THF was obtained anhydrous and was used without further drying. All other solvents were dried using appropriate drying reagents. Fine chemicals were purchased from Aldrich-, Sigma- or Acros-Chemicals and were of the highest purity available. Reactions were monitored via thin layer chromatography (TLC) using pre-coated silica sheets with fluorescent indicator UV₂₅₄. Compound detection was achieved by UV absorption and by developing plates by staining with a molybdenum phosphate reagent (20 g ammonium molybdate and 0.4 g cerium^(IV) sulfate in 400 mL of 10% aqueous sulphuric acid) with subsequent heating.

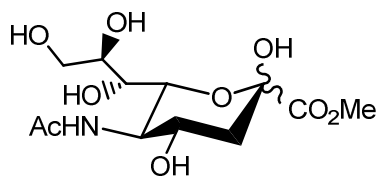
Chromatographic purification was performed using silica gel 60A 'Davisil' (particle size 35-70µm) from Fisher Scientific, UK and silica gel 100 C18 reversed phase (particle size 40-63µm from Fluka Analytical, UK. Silica-based MPLC chromatography was carried out on the Büchi Sepacore system equipped with glass columns packed with LiChroprep Si 60 (15-25µm) from Merck, Darmstadt, Germany. Solvents for chromatography were used as received except for toluene and ethyl acetate, which were distilled before use. Gel permeation chromatography was carried out in the 1-10 mg scale on a XK 16/70 column (bed volume 130 mL), from Amersham packed with Sephadex G-10 (particle size 40-120µm) and 0.1 M NH₄HCO₃ as buffer. Detection was achieved using a differential refractometer from Knauer, Berlin, Germany.

¹H NMR, ¹³C NMR, ³¹P NMR and all multidimensional spectra were recorded on Varian VNMR spectrometers (600 MHz, 500 MHz or 400 MHz). Chemical shifts in ¹H and ¹³C NMR spectra were referenced to the residual proton resonance of the respective deuterated solvents, CDCl₃ (7.26 ppm), D₂O (4.80 ppm) and CD₃OD (3.31 ppm) respectively. For ³¹P NMR spectra H₃PO₄ was used as external standard (0 ppm).

HR-ESI-MS spectra were recorded on a Bruker Daltonics Apex III in positive mode with MeOH and/or H₂O as solvent. Where possible, HR-ESI-MS has been used to characterise compounds which have been synthesised.

III.2. Synthetic procedures towards α -O-sialoside derivatives

Methyl 5-acetamido-3,5-dideoxy-*D*-glycero-*D*-galacto-2-nonulopyranosonate (1)



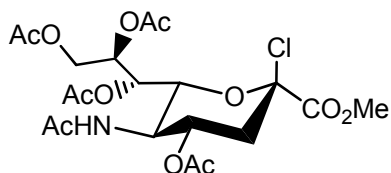
MeOH (230 mL) was added to 5-acetamido-3,5-dideoxy-*D*-glycero-*D*-galacto-2-nonulopyranosonicacid (Neu5Ac) (5.0 g, 16.0 mmol). To the resulting solution, Amberlite IR-120 ion-exchange resin (H⁺) was added. The solution was then vigorously shaken (mechanically) overnight. After shaking, the Amberlite IR-120 (H⁺) ion-exchange resin was filtered off, rinsed with MeOH and the resulting clear solution was then evaporated to dryness leaving a white crystalline solid, compound **1** (3.9 g, 75%) which was then dried extensively *in vacuo*.

Data corresponds to literature.⁶³

¹H NMR (500 MHz, MeOH-D₄) δ_{H} : 1.67 (0.1 H, dd, $J = 11.9, 12.0$ Hz, α -H_{3ax}), 1.89 (1 H, dd, $J = 12.0, 12.2$ Hz, β -H_{3ax}), 2.01 (s, 3H, -NCOCH₃), 2.22 (1 H, dd, $J = 4.5, 12.9$ Hz, β -H_{3eq}), 2.68 (0.1 H, dd, $J = 43.7, 12.5$ Hz, α -H_{3eq}), 3.48 (1 H, d, $J = 9.2$ Hz, H₇), 3.62 (1 H, dd, $J = 5.7, 11.3$ Hz, H₉), 3.70 (1 H, m, H₈), 3.78 (3 H, s, -CO₂CH₃), 3.77 – 3.82 (1 H, m, H₅, H₉), 4.00 (1 H, d, $J = 10.7$ Hz, H₆), 4.04 (1 H, m, H₄).

¹³C NMR (125.7 MHz, MeOH-D₄) δ_{C} : 22.64 (-NHCOCH₃), 40.75 (C3), 53.12 (-CO₂CH₃), 54.37 (C5), 64.88 (C9), 67.88 (C4), 70.26 (C7), 71.68 (C8), 72.14 (C6), 96.70 (C2), 171.78 (C1), 175.12 (-NCOCH₃).

Methyl (5-acetamido-3,5-dideoxy-4,7,8,9-tetra-*O*-acetyl- β -*D*-glycero-*D*-galacto-2-nonulopyranosylchloride)onate (2)



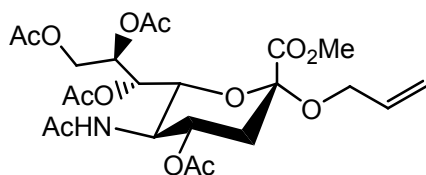
A solution of MeOH (0.60 mL) and AcCl (4.12 mL) was added to compound **1** (203.9 mg, 0.618 mmol) and cooled to 0 °C (ice-bath). AcOH (0.20 mL) was added and the

reaction was stirred at 0 °C for 15 hours (overnight). After the reaction was complete, the acidic solution was evaporated and the resulting product was co-evaporated with toluene several times, leaving a yellow-brown syrup which after filtering through a 0.2 μm syringe filter and on further drying under high vacuum yielded an off-white foam (322 mg, ~quantitative). R_f : 0.32 (EA). No further purification was carried out.

Data corresponds to literature.⁶³

^1H NMR (500 MHz, CDCl_3) δ_{H} : 1.90 – 2.16 (15 H, 5s, $-\text{NCOCH}_3$, 4 x $-\text{OCOCH}_3$), 2.29 (1 H, dd, $J = 11.7, 11.7$ Hz, $\text{H}_{3\text{ax}}$), 2.79 (1 H, dd, $J = 4.8, 13.9$ Hz, $\text{H}_{3\text{eq}}$), 3.87 – 3.89 (3 H, s, $-\text{CO}_2\text{CH}_3$), 4.00 – 4.24 (2 H, m, H_5, H_9), 4.35 (1 H, dd, $J = 1.6, 10.8$ Hz, H_6), 4.41 (1 H, ddd, $J = 1.5, 9.0, 12.4$ Hz, H_9), 5.18 (1 H, m, H_8), 5.23 – 5.34 (1 H, m, $-\text{NH}$), 5.41 (1 H, ddd, $J = 4.6, 10.7, 14.6$ Hz, H_4), 5.347 (1 H, d, $J = 7.0$ Hz, H_7). Toluene impurity present.

Methyl (allyl 5-acetamido-3,5-dideoxy-4,7,8,9-tetra-*O*-acetyl-*D*-glycero- α -*D*-galacto-2-nonulopyranosid)onate (3)



Ag_2CO_3 (2.55 g, 9.25 mmol) and AgClO_4 (191.8 mg, 0.925 mmol) were dried *in vacuo* for 3 hours in the absence of light and were then placed under an N_2 atmosphere. Dry allyl alcohol (5 mL) was then added via syringe, forming a suspension which was left to stir for 20 minutes. Compound **2** (943.8 mg, 1.85 mmol) was then dissolved in dry allyl alcohol (4 mL) and was quickly added to the stirring suspension and left to stir (under N_2 and in the absence of light) at room temperature for 20 hours (overnight). On completion, the resulting solution was filtered through celite filtering agent (with DCM), the celite being rinsed thoroughly with DCM. Subsequently, the solvent was evaporated *in vacuo* and after flash chromatography (EA), a clear oil was obtained, which on further drying *in vacuo* yielded a white crystalline foam, compound **3** (552.5 mg, 56 %). R_f : 0.30 (EA). Data corresponds to literature.⁶³

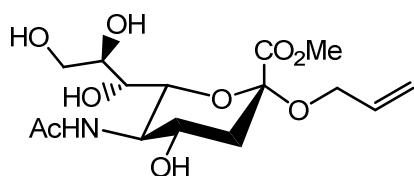
^1H NMR (500 MHz, CDCl_3) δ_{H} : 1.85, 2.00, 2.01, 2.11, 2.12 (15 H, 5s, $-\text{NHCOCH}_3$, 4 x $-\text{OCOCH}_3$), 1.95 (1 H, dd, $J = 12.6, 12.6$ Hz, $\text{H}_{3\text{ax}}$), 2.58 (1 H, dd, $J = 4.5, 12.8$ Hz, $\text{H}_{3\text{eq}}$), 3.75 (3 H, s, $-\text{CO}_2\text{CH}_3$), 3.85 (1 H, dd, $J = 5.8, 12.8$ Hz, $-\text{CHH}'-\text{CH}=\text{CH}_2$), 4.03 (1 H, dd, $J = 10.2, 10.3$ Hz, H_5), 4.05 – 4.11 (2 H, 2m, H_6, H_9), 4.22 – 4.31 (2 H, 2m, $\text{H}_9, -\text{CHH}'-$

CH=CH₂), 4.83 (1 H, ddd, J = 4.6, 9.7, 12.4 Hz, H₄), 5.09 (1 H, d, J = 9.5 Hz, -NH), 5.14 (1 H, dd, J = 1.1, 10.4 Hz, -CH₂-CH=CHH_{cis}), 5.26 (1 H, dd, J = 1.3, 17.2 Hz, -CH₂-CH=CHH_{trans}), 5.30 (1 H, dd, J = 1.8, 8.4 Hz, H₇), 5.40 (1 H, m, H₈), 5.84 (1 H, m, -CH₂-CH=CH₂).

¹³C NMR (125.7 MHz, CDCl₃) δ_C: 20.87, 20.94, 20.96, 21.23 (4s, 4 x -OCOCH₃), 23.30 (-NHCOCH₃), 38.20 (C3), 49.59 (C5), 52.77 (-CO₂CH₃), 62.55 (C9), 66.03 (-CH₂-CH=CH₂), 67.53 (C7), 68.79 (C8), 69.24 (C4), 72.68 (C6), 98.63 (C2), 117.35 (-CH₂-CH=CH₂), 133.71 (-CH₂-CH=CH₂), 168.50 (C1), 170.17, 170.25, 170.29, 170.72 (4 x -OCOCH₃), 171.10 (-NHCOCH₃).

HR-ESI-MS (m/z) calculated for C₂₃H₃₃NO₁₃ [M+Na]⁺ 554.1852, found 554.1849.

Methyl (allyl 5-acetamido-3,5-dideoxy-D-glycero-α-D-galacto-2-nonulopyranosid)onate (4)



Compound **3** (100mg, 0.224 mmol) was dissolved in anhydrous MeOH (1.5 mL) and freshly prepared NaOMe solution (0.6 mL, 0.33 M) was added. The resulting solution was left to stir for 4 hours. Once complete, the solution was neutralised with Amberlite IR-120 (H⁺) ion-exchange resin (mechanically shaken for 15 minutes). Subsequently, the resin was removed by filtration, rinsed with MeOH and the resulting clear solution was evaporated to dryness *in vacuo*. After flash chromatography purification (DCM:MeOH; 7:1), a clear oil was obtained which on further drying *in vacuo*, yielded a white crystalline foam compound **4** (69.2 mg, 85%). R_f: 0.16 (DCM:MeOH 7:1).

Data corresponds to literature.⁶³

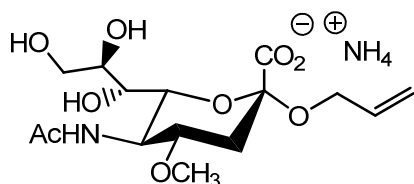
¹H NMR (500 MHz, MeOH-D₄) δ_H: 1.76 (1 H, dd, J = 12.5, 12.5 Hz, H_{3ax}), 2.00 (3 H, s, -NHCOCH₃), 2.70 (1 H, dd, J = 4.6, 12.8 Hz, H_{3eq}), 3.51 (1 H, d, J = 9.1 Hz, H₇), 3.58 (1 H, d, J = 10.5 Hz, H₆), 3.61 - 3.68 (2 H, m, H₄, H₉), 3.77 (1 H, dd, J = 10.0, 10.2 Hz, H₅), 3.83 (3 H, s, -CO₂CH₃), 3.84 - 3.87 (2 H, m, H₈, H₉), 3.99 (1 H, dd, J = 5.4, 12.6 Hz, -CHH'-CH=CH₂), 4.29 (1 H, dd, J = 5.2, 12.9 Hz, -CHH'-CH=CH₂), 5.12 (1 H, d, J = 10.3 Hz, -CHH'-CH=CHH_{cis}), 5.23 (1 H, d, J = 17.3 Hz, -CHH'-CH=CHH_{trans}), 5.87 (1 H, m, -CHH'-CH=CH₂).

¹³C NMR (125.7 MHz, MeOH-D₄) δ_C: 22.67 (-NHCOCH₃), 41.71 (C3), 53.35

(-CO₂CH₃), 53.84 (C5), 64.73 (C9), 66.22 (-CH₂CH=CH₂), 68.52 (C4), 70.23 (C7), 72.45 (C8), 74.96 (C6), 100.01 (C2), 116.94 (-CH₂CH=CH₂), 135.43 (-CH₂CH=CH₂), 171.00 (C1), 175.20 (-NHCOCH₃).

HR-ESI-MS (m/z) calculated for C₁₅H₂₅NO₉ [M+Na]⁺ 386.1421, found 386.1419.

Ammonium (allyl 5-acetamido-3,5-dideoxy-4-O-methyl-D-glycero- α -D-galacto-2-nonulopyranosidonate) (5)



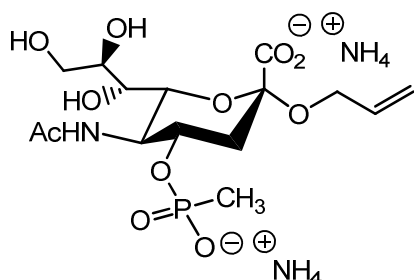
Compound **11** (19.9 mg, 0.0477 mmol) was dissolved in 80% AcOH_(aq.) (1.5 mL) and was stirred for 2 hours, after which, the AcOH_(aq.) solution was removed *in vacuo* and the oily product was then co-evaporated with toluene and dried *in vacuo*. NaOH_(aq.) (1.5 mL, 0.1 M) was then added to the oil and the resulting solution was left to stir for 2 hours. After completion, the solution was neutralised using Amberlite IR-120 (H+) ion-exchange resin, the resin was then removed and the solvent removed *in vacuo* yielding compound **5** (17.9 mg, ~quantitative). A sample of compound **5** (9.9 mg) was purified by gel permeation chromatography which was then lyophilised to give a white powder.

¹H NMR (600 MHz, D₂O) δ_{H} : 1.65 (1 H, dd, J = 12.0, 12.1 Hz, H_{3ax}), 2.10 (3 H, s, -NHCOCH₃), 2.99 (1 H, dd, J = 4.5, 12.6 Hz, H_{3eq}), 3.48 (3 H, s, -OCH₃), 3.52 (1 H, m, H₄), 3.65 (1 H, d, J = 8.9 Hz, H₇), 3.72 (1 H, m, H₉), 3.81 (1 H, dd, J = 1.5, 10.5 Hz, H₆), 3.91 – 4.00 (3 H, m, H₅, H₈, H₉), 4.12 (1 H, ddd, J = 1.2, 5.7, 12.2 Hz, CHH'-CH=CH₂), 4.33 (1 H, ddd, J = 1.1, 6.0, 12.1 Hz, CHH'-CH=CH₂), 5.30 (1 H, d, J = 10.3 Hz, -CH₂-CH=CHC_{is}H), 5.41 (1 H, dd, J = 1.4, 17.3 Hz, -CH=CHC_{trans}H), 6.02 (1 H, m, -CH₂-CH=CH₂).

¹³C NMR (150.8 MHz, D₂O) δ_{C} : 21.97 (-NHCOCH₃), 36.90 (C3), 50.22 (C5), 56.34 (-OCH₃), 62.68 (C9), 65.92 (-CH₂CH=CH₂), 68.19 (C7), 71.44 (C8), 72.77 (C6), 77.20 (C4), 100.38 (C2), 118.22 (-CH₂CH=CH₂), 133.67, (-CH₂CH=CH₂), 172.94 (C1), 174.93 (-NHCOCH₃).

HR-ESI-MS (m/z) calculated for C₁₅H₂₅NO₉ (acid form) [M+Na]⁺ 386.1422, found 386.1422.

Ammonium (allyl 5-acetamido-4-*O*-(*P*-methylphosphonyl)-3,5-dideoxy-*D*-glycero- α -*D*-galacto-2-nonulopyranosidonate) (6)



Compound **14** (18 mg, 0.0305 mmol) was placed under an N₂ (g) atmosphere and dissolved in anhydrous THF (0.7 mL). Triethylamine (60 μL, 0.427 mmol) was then added followed by a few minutes of stirring. Thiophenol (22 μL, 0.213 mmol) was then added and the solution was stirred overnight. Over the course of 4 days, gentle heating (35-40 °C) and a further 4 portions of triethylamine (60 μL, 0.427 mmol) and thiophenol (22 μL, 0.213 mmol) were added whilst maintaining the THF solvent volume (~ 0.5 - 0.7 mL). Once TLC analysis had indicated that the reaction had progressed no further, the solvent was directly evaporated *in vacuo* and purified on a short silica plug (EA:MeOH; 5:1 → DCM:MeOH; 1:1 → MeOH) to give the deprotected phosphonate intermediate which was lyophilised with dioxane/H₂O (9 mg, 96%). The deprotected phosphonate intermediate was then heated to 50 °C with Py:NEt₃:H₂O (1:1:1, 0.75 mL). After stirring overnight, the solvent was evaporated *in vacuo* and a crude NMR taken which indicated the presence of the desired product. The residue was then purified by gel permeation chromatography to afford compound **6** (9 mg, 76%) as a white solid after lyophilisation.

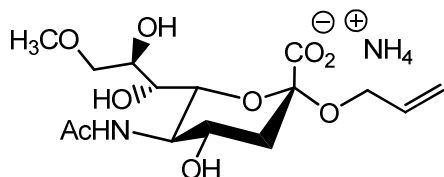
¹H NMR (600 MHz, MeOH-D₄) δ_H: 1.29 (1 H, d, J = 16.6 Hz, P-CH₃), 1.84 (1 H, dd, 12.1, 12.3 Hz, H_{3ax}), 2.03 (3 H, s, -NHCOCH₃), 2.91 (1 H, dd, J = 4.7, 12.6 Hz, H_{3eq}), 3.53 (1 H, dd, J = 1.5, 9.0 Hz, H₇), 3.57 (1 H, dd, J = 1.5, 10.4 Hz, H₆), 3.62 (1 H, dd, J = 5.8, 11.4 Hz, H₉), 3.74 (1 H, dd, J = 10.1, 10.2 Hz, H₅), 3.83 (1 H, dd, J = 2.5, 11.4 Hz, H₉), 3.86 (1 H, m, H₈), 4.01 (1 H, ddd, J = 1.2, 5.6, 12.6 Hz, -CHH'-CH=CH₂), 4.26 - 4.32 (2 H, m, H₄, -CHH'-CH=CH₂), 5.10 (1 H, dd, J = 1.4, 10.5 Hz, -CH₂-CH=CHH_{cis}), 5.25 (1 H, dd, J = 1.7, 17.3 Hz, -CH₂-CH=CHH_{trans}), 5.90 (1 H, m, -CH₂-CH=CH₂).

¹³C NMR (150.8 MHz, MeOH-D₄) δ_C: ~13.53 (d, J = 139.2 Hz, P-CH₃), 22.79 (-NHCOCH₃), 41.34 (C3), 53.53 (C5), 64.61 (C9), 66.36 (-CH₂CH=CH₂), 70.37 (C7), 71.34 (C4), 72.76 (C8), 75.13 (C6), 100.42 (C2), 116.77 (-CH₂CH=CH₂), 135.77 (-CH₂CH=CH₂), 172.61 (C1), 175.90 (-NHCOCH₃).

^{31}P NMR (242.7 MHz, MeOH- D_4) δ_{P} : 24.73 (s).

HR-ESI-MS (m/z) calculated for $\text{C}_{15}\text{H}_{26}\text{NOP}$ (acid form) $[\text{M}+\text{Na}]^+$ 450.1136, found 450.1131.

Ammonium (allyl 5-acetamido-3,5-dideoxy-9-O-methyl-D-glycero- α -D-galacto-2-nonulopyranosidonate) (7)



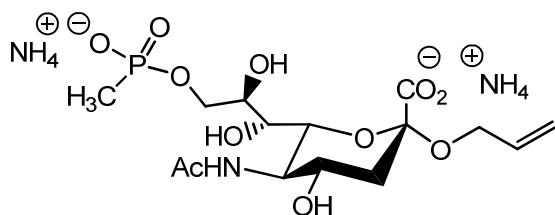
Compound **26** (5 mg, 0.0132 mmol) was dissolved in dioxane (0.5 mL) and was stirred. NaOH (0.05 M, 0.5 mL) was then added to the stirring solution. The resulting mixture was stirred for 2 hours at room temperature. The basic solution was then neutralised with Amberlite IR-120 (H+) ion-exchange resin, the resin removed and the solvent evaporated *in vacuo*. The residue was then purified by gel permeation chromatography to afford compound **7** (5 mg, qu.) as a lyophilised powder.

^1H NMR (600 MHz, D_2O) δ_{H} : 1.76 (1 H, dd, $J = 12.1, 12.3$ Hz, $\text{H}_{3\text{ax}}$), 2.11 (3 H, s, - NHCOCH_3), 2.82 (1 H, dd, $J = 4.6, 12.5$ Hz, $\text{H}_{3\text{eq}}$), 3.48 (3 H, s, - OCH_3), 3.61 – 3.68 (2 H, m, H_7, H_9), 3.72 – 3.83 (3 H, m, $\text{H}_4, \text{H}_6, \text{H}_9$), 3.90 (1 H, dd, $J = 10.1, 10.2$ Hz, H_5), 4.05 (1 H, dd, $J = 7.7, 7.7$ Hz, H_8), 4.10 (1 H, dd, $J = 5.8, 12.2$ Hz, - $\text{CHH}'\text{-CH}=\text{CH}_2$), 4.32 (1 H, dd, $J = 6.1, 12.1$ Hz, - $\text{CHH}'\text{-CH}=\text{CH}_2$), 5.30 (1 H, d, $J = 10.4$ Hz, - $\text{CH}_2\text{-CH}=\text{CH}_{\text{cis}}\text{H}$), 5.40 (1 H, d, $J = 17.4$ Hz, - $\text{CH}=\text{CH}_{\text{trans}}\text{H}$), 6.02 (1 H, ddd, $J = 6.0, 11.2, 16.6$ Hz, - $\text{CH}_2\text{-CH}=\text{CH}_2$).

^{13}C NMR (150.8 MHz, D_2O) δ_{C} : 21.94 (- NHCOCH_3), 40.40 (C3), 51.76 (C5), 58.35 (- OCH_3), 65.96 (- $\text{CH}_2\text{-CH}=\text{CH}_2$), 68.17, 68.19 (C4, C7), 70.03 (C8), 72.46 (C6), 73.14 (C9), 100.53 (C2), 118.14 (- $\text{CH}_2\text{-CH}=\text{CH}_2$), 133.67 (- $\text{CH}_2\text{-CH}=\text{CH}_2$), 173.38 (C1), 174.94 (- NHCOCH_3).

HR-ESI-MS (m/z) calculated for $\text{C}_{15}\text{H}_{25}\text{NO}_9$ (acid form) $[\text{M}+\text{Na}]^+$ 386.1422, found 386.1424.

Diammonium (allyl 5-acetamido-3,5-dideoxy-9-O-(*P*-methylphosphonyl)-*D*-glycero- α -*D*-galacto-2-nonulopyranosidonate) (8)



Compound **31** (14 mg, 0.0240 mmol) was placed under an N₂ (g) atmosphere and dissolved in anhydrous THF (0.7 mL). Triethylamine (47 μ L, 0.336 mmol) was then added followed by a few minutes of stirring. Thiophenol (17 μ L, 0.168 mmol) was then added and the solution was stirred overnight. Over the course of 4 days, a further 4 portions of triethylamine (47 μ L, 0.336 mmol) and thiophenol (17 μ L, 0.168 mmol) were added whilst maintaining the THF solvent volume (~ 0.5 - 0.7 mL). Once TLC analysis had indicated that the reaction had progressed no further, the solvent was directly evaporated *in vacuo* and purified on a short silica plug (DCM:MeOH; 5:1 \rightarrow 2:1 \rightarrow MeOH) to give the deprotected phosphonate intermediate which was lyophilised with dioxane/H₂O (10.2 mg, 74%). The deprotected phosphonate intermediate (10 mg) was then treated with a 1:1 mixture of dioxane and 0.05M NaOH (aq.) at approximately 4-5 $^{\circ}$ C for 2 hours after which the solution was neutralised with ion-exchange resin Amberlite IR-120. The solvent was removed and the residue was then purified by gel permeation chromatography to afford compound **8** (9.6 mg, ~qu.) after lyophilisation.

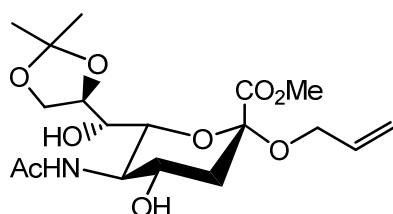
¹H NMR (600 MHz, D₂O) δ_{H} : 1.41 (3 H, d, J = 16.4 Hz, P-CH₃), 1.79 (1 H, dd, J = 12.1, 12.2 Hz, H_{3ax}), 2.11 (3 H, s, -NHCOCH₃), 2.80 (1 H, dd, J = 4.3, 12.5 Hz, H_{3eq}), 3.74 (1 H, d, J = 8.4 Hz, H₇), 3.76 – 3.82 (1 H, m, H₄), 3.87 (1 H, d, J = 10.3 Hz, H₆), 3.93 (1 H, dd, J = 9.9, 10.1 Hz, H₅), 4.02 – 4.09 (2 H, m, H₈, H₉), 4.12 (1 H, dd, J = 5.7, 12.0 Hz, -CHH'-CH=CH₂), 4.15 – 4.22 (1 H, m, H₉), 4.34 (1 H, dd, J = 6.1, 12.1 Hz, -CHH'-CH=CH₂), 5.31 (1 H, d, J = 10.2 Hz, -CH₂-CH=CH_{cis}H), 5.41 (1 H, d, J = 17.3 Hz, -CH=CH_{trans}H), 6.01 (1 H, ddd, J = 5.7, 11.3, 16.1 Hz, -CH₂-CH=CH₂).

¹³C NMR (150.8 MHz, D₂O) δ_{C} : ~10.80 (d, J = 137 Hz, P-CH₃), 22.07 (-NHCOCH₃), 40.02 (C3), 51.83 (C5), 65.04 (d, J = 5 Hz, C9), 65.90 (-CH₂-CH=CH₂), 67.64 (C7), 68.01 (C4), 70.13 (d, J = 7 Hz, C8), 72.62 (C6), 99.96 (C2), 118.33 (-CH₂-CH=CH₂), 133.57 (-CH₂-CH=CH₂), 172.61 (C1), 174.95 (-NHCOCH₃).

³¹P NMR (161.7 MHz, D₂O) δ_{P} : 28.45 (s).

HR-ESI-MS (m/z) calculated for C₁₅H₂₆NO₃ (acid form) [M+Na]⁺ 450.1136, found 450.1135.

Methyl (allyl 5-acetamido-3,5-dideoxy-8,9-O-isopropylidene-D-glycero- α -D-galacto-2-nonulopyranosid)onate (9)



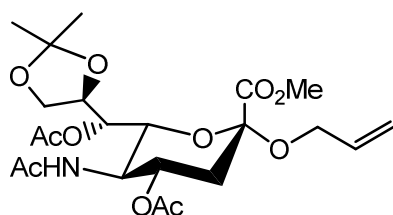
Compound 4 (56 mg, 0.154 mmol) was dissolved in dry acetone (1.85 mL) under N₂(g). DMP (200 μ L) was then added to the resulting solution via syringe, followed by p-TsOH.H₂O (7mg). The solution was then left to stir at room temperature, under N₂ for 2 hours. Once complete, NEt₃ (few drops) was added to the solution to neutralise the reaction and the solvent was evaporated to dryness. After flash chromatography (Tol:Acetone; 1:1), a clear oil was obtained, which after further drying *in vacuo* yielded a white foam compound **9** (53 mg, 85%). R_f: 0.52 (Tol:Acetone; 1:1).

¹H NMR (500 MHz, CDCl₃) δ _H: 1.34, 1.38 (6 H, 2s, -C(CH₃)₂), 1.79 (1 H, dd, J = 12.0, 12.2 Hz, H_{3ax}), 2.02 (3 H, s, -NHCOCH₃), 2.69 (1 H, dd, J = 4.7, 12.8 Hz, H_{3eq}), 3.43 (1 H, d, J = 10.4 Hz, H₆), 3.60 (1 H, dd, J = 5.6, 5.7 Hz, H₇), 3.69 (1 H, m, H₄), 3.74 – 3.81 (1 H, m, H₅, -CO₂CH₃), 3.98 – 4.11 (4 H, m, H₉, H_{9'}, -OH, -CHH'-CH=CH₂), 4.14 (1 H, d, J = 5.7 Hz, -OH), 4.21 – 4.27 (2 H, m, -CHH'-CH=CH₂, H₈), 5.13 (1 H, ddd, J = 1.1, 1.4, 10.5 Hz, -CH₂-CH=CH_{cis}H), 5.23 (1 H, ddd, J = 1.4, 1.6, 17.2 Hz, -CH=CH_{trans}H), 5.83 (1 H, ddd, J = 5.6, 10.6, 16.3 Hz, -CH₂-CH=CH₂), 6.59 (1 H, d, J = 8.0 Hz, -NH).

¹³C NMR (125.7 MHz, CDCl₃) δ _C: 23.31 (-NHCOCH₃), 25.65, 26.93 (-C(CH₃)₂), 40.62 (C3), 52.68, 53.19, 53.54 (-CO₂CH₃, C5), 65.54 (-CH₂CH=CH₂), 66.55 (C9), 67.95 (C4), 69.79 (C7), 74.67 (C6), 75.88 (C8), 99.15 (C2), 108.75 (-C(CH₃)₂), 117.27 (-CH₂CH=CH₂), 134.02, (-CH₂CH=CH₂), 169.17 (C1), 173.50 (-NHCOCH₃).

HR-ESI-MS (m/z) calculated for C₁₈H₂₉NO₃Na [M+Na]⁺ 426.1734, found 426.1734.

Methyl (allyl 5-acetamido-3,5-dideoxy-4,7-di-O-acetyl-8,9-O-isopropylidene-D-glycero- α -D-galacto-2-nonulopyranosid)onate (10)



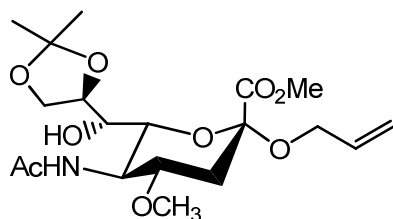
Compound **9** (15.2 mg, 0.037 mmol) was stirred overnight in a solution of pyridine (0.5 mL) and acetic anhydride (0.5 mL). The solvent was then evaporated *in vacuo* and purified by flash chromatography (EA) to give compound **10**. (16.5 mg, 93%). R_f : 0.92 (Tol:Acetone; 1:1).

$^1\text{H NMR}$ (500 MHz, CDCl_3) δ_{H} : 1.34, 1.35 (6 H, 2s, $-\text{C}(\text{CH}_3)_2$), 1.88 (3 H, s, $-\text{COCH}_3$), 1.97 (1 H, dd, $J = 12.3, 12.5$ Hz, $\text{H}_{3\text{ax}}$), 2.03 (3 H, s, $-\text{COCH}_3$), 2.14 (3 H, s, $-\text{COCH}_3$), 2.67 (1 H, dd, $J = 4.9, 12.9$ Hz, $\text{H}_{3\text{eq}}$), 3.82 (3 H, s, $-\text{CO}_2\text{CH}_3$), 3.92 (1 H, dd, $J = 1.8, 10.7$ Hz, H_6), 3.96 – 4.04 (3 H, m, $\text{H}_9, \text{H}_5, -\text{CHH}'-\text{CH}=\text{CH}_2$), 4.08 (1 H, m, H_9), 4.25 (1 H, ddd, $J = 1.3, 5.3, 12.6$ Hz, $\text{CHH}'-\text{CH}=\text{CH}_2$), 4.37 (1 H, m, H_8), 4.99 (1 H, m, H_4), 5.13 – 5.21 (2 H, m, $-\text{NH}$, $-\text{CH}_2-\text{CH}=\text{CH}_{\text{cis}}\text{H}$), 5.28 (1 H, dd, $J = 1.5, 17.2$ Hz, $-\text{CH}=\text{CH}_{\text{trans}}\text{H}$), 5.39 (1 H, m, H_7), 5.87 (1 H, ddd, $J = 5.4, 10.6, 16.5$ Hz, $-\text{CH}_2-\text{CH}=\text{CH}_2$);

$^{13}\text{C NMR}$ (125.7 MHz, CDCl_3) δ_{C} : 21.03, 21.09, 23.37, 25.48 (3 x $-\text{COCH}_3$, $-\text{NHCOCH}_3$), 26.53 ($-\text{C}(\text{CH}_3)_2$), 37.72 (C3), 50.11 (C5), 52.93 ($-\text{CO}_2\text{CH}_3$), 65.70, 65.76 (C9, $-\text{CH}_2-\text{CH}=\text{CH}_2$), 68.84 (C7), 69.02 (C8), 73.79 (C6), 76.17 (C4), 99.08 (C2), 108.59 ($-\text{C}(\text{CH}_3)_2$), 117.44 ($-\text{CH}_2-\text{CH}=\text{CH}_2$), 133.62 ($-\text{CH}_2-\text{CH}=\text{CH}_2$), 168.50 (C1), 170.36, 170.54, 171.03 ($-\text{NHCOCH}_3$, 2 x $-\text{COCH}_3$).

HR-ESI-MS (m/z) calculated for $\text{C}_{22}\text{H}_{33}\text{NO}_{11}$ $[\text{M}+\text{Na}]^+$ 510.1922, found 510.1930.

Methyl (allyl 5-acetamido-3,5-dideoxy-4-O-methyl-8,9-O-isopropylidene-D-glycero- α -D-galacto-2-nonulopyranosid)onate (11)



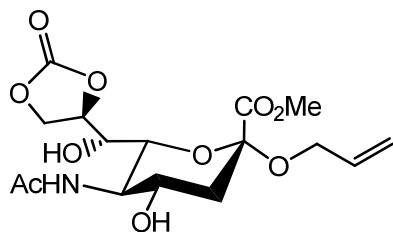
Compound **9** (56 mg, 0.138 mmol) was dissolved in dry CH₃CN (0.7 mL), under N₂ (g) and was cooled to 0 °C (ice bath). DMSO₄ (24.5 μL, 0.259 mmol) was then added to the solution followed by NaH_(s) (6.6 mg, 0.276 mmol). The resulting suspension was allowed to stir for 4 hours at 0 °C, at which point, more DMSO₄ (24.5 μL, 0.259 mmol) was added and the suspension was left to stir overnight. On completion, excess NH₄Cl_(s) was added to quench the reaction and the solution was diluted with DCM (3 mL) and filtered over celite and the solvent was evaporated to dryness. After flash chromatography (Tol:Acetone; 1:1) a clear oil, compound **11**, was obtained (29 mg, 50%). R_f: 0.24 (Tol:Acetone; 2:1).

¹H NMR (600 MHz, CDCl₃) δ_H: 1.36, 1.39 (6 H, 2s, -C(CH₃)₂), 1.73 (1 H, dd, J = 12.1, 12.2 Hz, H_{3ax}), 2.05 (3 H, s, -NHCOCH₃), 2.87 (1 H, dd, J = 4.5, 12.8 Hz, H_{3eq}), 3.34 (3 H, s, -OCH₃), 3.37 (1 H, d, J = 10.5 Hz, H₆), 3.42 (1 H, ddd, J = 4.5, 10.7, 10.9, H₄), 3.56 (1 H, dd, J = 5.6, 5.7 Hz, H₇), 3.78 (3 H, s, -CO₂CH₃), 3.87 (1 H, m, H₅), 4.04 – 4.13 (3 H, m, H₉, H_{9'}, -CHH'-CH=CH₂), 4.28 – 4.33 (2 H, m, H₈, CHH'-CH=CH₂), 4.42 (1 H, d, J = 4.9 Hz, -OH), 5.15 (1 H, d, J = 10.5 Hz, -CH₂-CH=CH_{cis}H), 5.25 (1 H, d, J = 17.2 Hz, -CH=CH_{trans}H), 5.39 (1 H, d, J = 7.4 Hz, -NH), 5.86 (1 H, ddd, J = 55.6, 10.7, 16.4 Hz, -CH₂-CH=CH₂).

¹³C NMR (150.8 MHz, CDCl₃) δ_C: 23.47 (-NHCOCH₃), 25.75, 26.99 (-C(CH₃)₂), 36.42 (C₃), 51.27 (C₅), 52.54 (-CO₂CH₃), 55.57 (-OCH₃), 65.47 (-CH₂CH=CH₂), 66.93 (C₉), 69.86 (C₇), 74.76 (C₆), 75.44 (C₈), 75.94 (C₄), 99.21 (C₂), 108.71 (-C(CH₃)₂), 117.31 (-CH₂CH=CH₂), 134.03, (-CH₂CH=CH₂), 169.20 (C₁), 173.85 (-NHCOCH₃).

HR-ESI-MS (m/z) calculated for C₁₉H₃₁NO₉ [M+Na]⁺ 440.1891, found 440.1898.

Methyl (allyl 5-acetamido-3,5-dideoxy-8,9-O-carbonate-D-glycero-α-D-galacto-2-nonulopyranosid)onate (12)



Compound **4** (345 mg, 0.949 mmol) and DMAP (278 mg, 2.28 mmol) were dried *in vacuo* for approximately 1 hour and then placed under an atmosphere of N_{2(g)}. Dry DCM (20 mL) was then added via syringe and the resulting suspension formed was ultrasonicated for a few minutes then cooled to approximately 0 °C. Diphosgene (152

μL , 1.23 mmol) was then added via microsyringe to the white suspension with vigorous stirring. On completion, the reaction was quenched by pouring the solution into 40 mL of cold 10% KH_2PO_4 . The DCM layer was separated and the aqueous layer was extracted with ethyl acetate (4 x 25 mL). The organic phases were then dried over MgSO_4 and the solvents were removed.

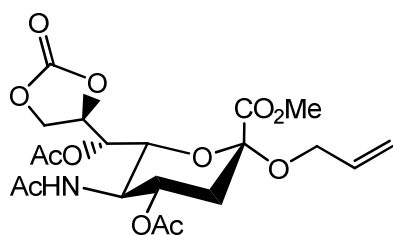
After flash chromatography (EA:MeOH; 15:1) and the removal of organic solvents *in vacuo*, a clear oil, compound **12**, was obtained (220 mg, 60%). R_f : 0.63 (EA:MeOH; 5:1).

^1H NMR (500 MHz, MeOH- D_4) δ_{H} : 1.74 (1 H, dd, $J = 12.3, 12.3$ Hz, $\text{H}_{3\text{ax}}$), 2.01 (3 H, s, - NHCOCH_3), 2.66 (1 H, dd, $J = 4.6, 12.8$ Hz, $\text{H}_{3\text{eq}}$), 3.53 (1 H, d, $J = 10.5$ Hz, H_6), 3.61 (1 H, ddd, $J = 4.5, 10.6, 12.9$ Hz, H_4), 3.75 - 3.79 (1 H, m, H_5), 3.80 (3 H, s, $-\text{CO}_2\text{CH}_3$), 3.93 (1 H, m, H_7), 3.97 (1 H, dd, $J = 5.3, 12.6$ Hz, $-\text{CHH}'\text{-CH}=\text{CH}_2$), 4.19 (1 H, dd, $J = 4.2, 12.8$ Hz, $-\text{CHH}'\text{-CH}=\text{CH}_2$), 4.55 (1 H, dd, $J = 8.4, 8.4$ Hz, H_9), 4.70 (1 H, dd, $J = 7.2, 7.9$ Hz, H_9), 4.95 (1 H, m, H_8), 5.14 (1 H, d, $J = 10.5$ Hz, $-\text{CHH}'\text{-CH}=\text{CH}_{\text{cis}}$), 5.26 (1 H, d, $J = 17.4$ Hz, $-\text{CHH}'\text{-CH}=\text{CH}_{\text{trans}}$), 5.86 (1 H, dddd, $J = 1.08, 5.2, 10.5, 16.8$, $-\text{CHH}'\text{-CH}=\text{CH}_2$).

^{13}C NMR (100.5 MHz, MeOH- D_4) δ_{C} : 22.76 ($-\text{NHCOCH}_3$), 41.46 (C3), 53.10 (C5), 53.66 ($-\text{CO}_2\text{CH}_3$), 66.29 ($-\text{CH}_2\text{CH}=\text{CH}_2$), 67.24 (C9), 68.17 (C4), 69.22 (C7), 76.20 (C6), 79.63 (C8), 100.49 (C2), 116.94 ($-\text{CH}_2\text{CH}=\text{CH}_2$), 135.21 ($-\text{CH}_2\text{CH}=\text{CH}_2$), 157.38 ($-\text{O}-\text{C}(\text{O})-\text{O}-$), 169.90 (C1), 175.10 ($-\text{NHCOCH}_3$).

HR-ESI-MS (m/z) calculated for $\text{C}_{16}\text{H}_{23}\text{NO}_{10}$ $[\text{M}+\text{Na}]^+$ 412.1214, found 412.1219.

Methyl (allyl 5-acetamido-4,7-di-*O*-acetyl-3,5-dideoxy-8,9-*O*-carbonate-*D*-glycero- α -*D*-galacto-2-nonulopyranosid)onate (13)



Compound **12** (16 mg, 0.041 mmol) was placed into a flask. Pyridine (0.5 mL) and acetic anhydride (0.5 mL) were then added. The flask was stoppered and allowed to stir overnight. Once the reaction was complete, the solvent was removed directly *in vacuo*. Co-evaporation with toluene several times followed by flash chromatography

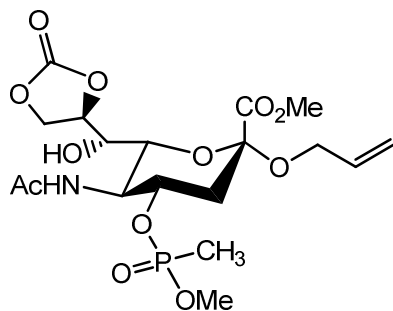
(EA:MeOH 20:1 → 5:1) gave the desired product, compound **13** (19 mg, 95%). R_f : 0.54 (EA:MeOH; 10:1).

^1H NMR (500 MHz, CDCl_3) δ_{H} : 1.86 (3 H, s, $-\text{NHCOCH}_3$), 1.95 (1 H, dd, $J = 12.4, 12.4$ Hz, $\text{H}_{3\text{ax}}$), 2.01 (3 H, s, $-\text{OCOCH}_3$), 2.16 (3 H, s, $-\text{OCOCH}_3$), 2.66 (1 H, dd, $J = 4.7, 12.8$ Hz, $\text{H}_{3\text{eq}}$), 3.81 (3 H, s, $-\text{CO}_2\text{CH}_3$), 3.93 (1 H, dd, $J = 5.2, 12.7$ Hz, $-\text{CHH}'\text{-CH}=\text{CH}_2$), 3.97 - 4.05 (2 H, m, H_5, H_6), 4.14 (1 H, dd, $J = 4.6, 12.6$ Hz, $-\text{CHH}'\text{-CH}=\text{CH}_2$), 4.51 (1 H, dd, $J = 8.5, 8.7$ Hz, H_9), 4.60 (1 H, dd, $J = 7.4, 8.2$ Hz, H_9), 4.92 (1 H, m, H_4), 5.03 (1 H, m, H_8), 5.18 (1 H, d, $J = 10.5$ Hz, $-\text{CHH}'\text{-CH}=\text{CHH}_{\text{cis}}$), 5.26 (1 H, d, $J = 17.2$ Hz, $-\text{CHH}'\text{-CH}=\text{CHH}_{\text{trans}}$), 5.58 (1 H, d, $J = 8.4$ Hz, $-\text{NH}$), 5.82 (1 H, ddd, $J = 5.3, 10.4, 16.5$ Hz, $-\text{CH}_2\text{-CH}=\text{CH}_2$).

^{13}C NMR (100.5 MHz, CDCl_3) δ_{C} : 20.92 ($-\text{COCH}_3$), 21.04 ($-\text{COCH}_3$), 23.33 ($-\text{NHCOCH}_3$), 37.54 (C3), 49.62 (C5), 53.25 ($-\text{CO}_2\text{CH}_3$), 65.79 ($-\text{CH}_2\text{-CH}=\text{CH}_2$), 66.22 (C9), 68.16 (C7), 68.90 (C4), 73.72 (C6), 76.66 (C8), 99.33 (C2), 117.63 ($-\text{CH}_2\text{-CH}=\text{CH}_2$), 133.33 ($-\text{CH}_2\text{-CH}=\text{CH}_2$), 154.59 ($-\text{O-C(O)-O-}$), 168.33, 170.25, 170.81, 170.93 (C1, $-\text{NHCOCH}_3$, 2 x $-\text{OCOCH}_3$).

HR-ESI-MS (m/z) calculated for $\text{C}_{20}\text{H}_{27}\text{NO}_{12}$ $[\text{M}+\text{Na}]^+$ 496.1425, found 496.1428.

Methyl (allyl 5-acetamido-3,5-dideoxy-4-*O*-(*O,P*-dimethylphosphonyl)-8,9-*O*-carbonate-*D*-glycero- α -*D*-galacto-2-nonulopyranosid)onate (14)



Compound **12** (75 mg, 0.193 mmol) was placed in a flask under an N_2 (g) atmosphere. Dry DCM (2 mL) was then added via syringe resulting in a suspension of compound **12** which required ultrasonication. *N,N*-diisopropylethylamine (67 μL , 0.386 mmol) was added to the suspension followed by further ultrasonication. With continuous stirring, the suspension was cooled to approximately -15°C . Once acclimatised to the temperature, methyl methylphosphonochloridate (27 μL , 0.270 mmol) was added dropwise to the solution. The reaction was allowed to come up to room temperature where it was then stirred overnight. The reaction was again then cooled to -15°C , where a further portion of *N,N*-diisopropylethylamine (67 μL , 0.386 mmol) and methyl

methylphosphonochloridate (27 μ L, 0.270 mmol) was added. Once TLC monitoring of the reaction had indicated completion, the reaction was quenched by the addition of MeOH (1 mL) and a small spatula of NaHCO₃ (s). After stirring for 10 minutes, the solvent was removed directly *in vacuo* and the product was directly purified by flash chromatography (EA:MeOH; EA \rightarrow 7:1 \rightarrow 5:1) to give compound **14** (57 mg, 60%). R_f: 0.21 (EA:MeOH; 10:1).

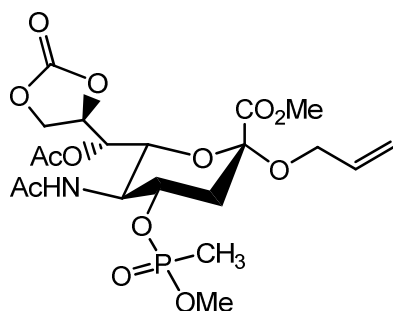
¹H NMR (500 MHz, CDCl₃) δ _H: 1.53, 1.47 (3 H, 2d, J = 17.7, 17.8 Hz, P-CH₃), 2.01 (1 H, m, H_{3ax}), 2.06 (3 H, s, -NHCOCH₃), 2.73, 2.78 (1 H, 2dd, J = 5.0, 12.8, 4.9, 12.9 Hz, H_{3eq}), 3.25 (1 H, d, J = 10.3 Hz, H₆), 3.66, 3.75 (3 H, 2d, J = 11.5, 11.2 Hz, P-OCH₃), 3.81, 3.82 (3 H, 2s, -CO₂CH₃), 3.83 - 3.92 (1 H, m, H₅), 4.02 (1 H, dd, J = 5.4, 12.4 Hz, -CHH'-CH₂=CH₂), 4.22 (1 H, dd, J = 5.1, 12.6 Hz, CHH'-CH₂=CH₂), 4.40, 4.53 (1 H, m, H₄), 4.49 (1 H, dd, J = 8.5 Hz, H₉), 4.65 (1 H, m, H₉), 4.74 (1 H, bs, -OH), 4.87 (1 H, m, H₈), 5.16 (1 H, d, J = 10.5 Hz, -CH₂-CH=CHH_{cis}), 5.24 (1 H, d, J = 17.3 Hz, -CH₂-CH=CHH_{trans}), 5.82 (1 H, ddd, J = 5.4, 10.5, 16.1 Hz, -CH₂-CH=CH₂), 7.43 (1 H, m, -NH).

¹³C NMR (125.7 MHz, CDCl₃) δ _C: ~10.69, ~11.01 (2d, J = 143.41, 146.06 Hz, P-CH₃), 23.04, 23.07 (-NHCOCH₃), 38.81 (m, C3), 51.90 (C5), ~52.15 (d, J = 7.4 Hz, P-OCH₃), 52.99, 53.05 (-CO₂CH₃), 65.51 (-CH₂-CH=CH₂), 66.66, 66.69 (C9), 68.82 (C7), ~70.41 (d, J = 6.6 Hz, C4), ~71.46 (d, J = 5.0 Hz, C4), 74.89 (C6), 75.99, 76.05 (C8), 98.91, 99.01 (C2), 117.40 (-CH₂-CH=CH₂), 133.47 (-CH₂-CH=CH₂), 155.11 (-O-C(O)-O-), 168.28, 168.30 (C1), 174.02, 174.12 (-NHCOCH₃).

³¹P NMR (161.7 MHz, CDCl₃) δ _P: 34.63 (s), 35.82 (s).

HR-ESI-MS (m/z) calculated for C₁₈H₂₈NO₁₂P [M+Na]⁺ 504.1218, found 504.1241.

Methyl (allyl 5-acetamido-3,5-dideoxy-7-O-acetyl-4-O-(P-methylphosphonyl)-8,9-O-carbonate-D-glycero- α -D-galacto-2-nonulopyranosid)onate (15)



Compound **14** (11 mg, 0.0228 mmol) was placed into a flask. Pyridine (0.5 mL) and acetic anhydride (0.5 mL) were then added. The flask was stoppered and allowed to

stir overnight. Once the reaction was complete, the solvent was removed directly *in vacuo*. Co-evaporation with toluene several times followed by flash chromatography (EA:MeOH 20:1 → 5:1) gave the desired product, compound **15** (10.5 mg, 90%). R_f : 0.50 (EA:MeOH; 10:1).

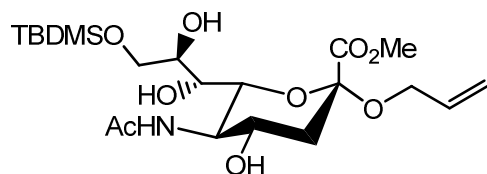
^1H NMR (500 MHz, CDCl_3) δ_{H} : 1.41, 1.46 (3 H, 2d, $J = 17.4, 17.7$ Hz, P- CH_3), 1.93, 1.94 (3 H, 2s, $-\text{OCOCH}_3$), 2.02 (1 H, m, $\text{H}_{3\text{ax}}$), 2.16 (3 H, s, $-\text{NHCOCH}_3$), 2.76 (1 H, m, $\text{H}_{3\text{eq}}$), 3.62, 3.67 (3 H, 2d, $J = 11.3, 11.4$ Hz, P- OCH_3), 3.82 (3 H, s, $-\text{CO}_2\text{CH}_3$), 3.85 (1 H, m, H_6), 3.96 (1 H, m, $-\text{CHH}'\text{-CH}=\text{CH}_2$), 4.01 (1 H, dd, $J = 10.1, 10.1$ Hz, H_5), 4.16 (1 H, ddd, $J = 2.0, 3.4, 5.0$ Hz, $-\text{CHH}'\text{-CH}=\text{CH}_2$), 4.39 – 4.53 (1 H, m, H_4), 4.49 (1 H, dd, $J = 8.6, 8.6$ Hz, H_9), 4.58 (1 H, m, H_9), 4.97 (1 H, m, H_8), 5.19 (1 H, dd, $J = 0.8, 10.4$ Hz, $-\text{CH}_2\text{-CH}=\text{CH}_{\text{cis}}$), 5.27 (1 H, dd, $J = 1.3, 17.2$ Hz, $-\text{CH}_2\text{-CH}=\text{CH}_{\text{trans}}$), 5.48 (1 H, m, H_7), 5.83 (1 H, ddd, $J = 5.4, 10.6, 16.0$ Hz, $-\text{CH}_2\text{-CH}=\text{CH}_2$), 6.19, (1 H, d, $J = 9.4$ Hz, $-\text{NH}$).

^{13}C NMR (100.5 MHz, CDCl_3) δ_{C} : ~10.60, ~11.10 (2d, $J = 144, 146$ Hz), 20.72, 20.75 ($-\text{NHCOCH}_3$), 23.28, 23.31 ($-\text{OCOCH}_3$), 39.11, 39.21 (2d, $J = 2.9, 4.0$ Hz, C3), 49.99, 50.13 (2d, $J = 2.7, 3.4$ Hz, C5), 52.28, 52.31 (2d, $J = 6.3, 6.7$ Hz, P- OCH_3), 53.01, 53.05 ($-\text{CO}_2\text{CH}_3$), 65.54, 65.56 ($-\text{CH}_2\text{CH}=\text{CH}_2$), 66.00, 66.02 (C9), 67.94 (C7), 71.06, 71.65 (2d, $J = 6.1, 7.2$ Hz, C4), 73.38, 73.41 (C6), 76.02, 76.09 (C8), 99.00, 99.08 (C2), 117.44, 117.46 ($-\text{CH}_2\text{CH}=\text{CH}_2$), 133.09, 133.11 ($-\text{CH}_2\text{CH}=\text{CH}_2$), 154.13 ($-\text{O}-\text{C}(\text{O})-\text{O}-$), 168.02, 168.04, 170.01, 170.04 (C1, $-\text{OCOCH}_3$), 171.05, 171.06 ($-\text{NHCOCH}_3$).

^{31}P NMR (400 MHz, CDCl_3) δ_{P} : 31.70 (s), 33.38 (s).

HR-ESI-MS (m/z) calculated for $\text{C}_{20}\text{H}_{30}\text{NO}_{13}\text{P}$ [$\text{M}+\text{Na}$] $^+$ 546.1346, found 546.1330.

Methyl (allyl 5-acetamido-3,5-dideoxy-9-*O*-*tert*-butyldimethylsilyl-*D*-glycero- α -*D*-galacto-2-nonulopyranosid)onate (16)



Compound **4** (197 mg, 0.542 mmol) and imidazole (92 mg, 1.35 mmol) were dried *in vacuo* for an hour and then placed under an N_2 (g) atmosphere. Dry DMF (2.25 mL) was then added and the resulting suspension was cooled to 0°C . TBDMSCl (98 mg, 0.650 mmol) was then quickly added to the stirring solution and the solution was allowed to stir for a further 5 hours. Once TLC analysis had indicated that the reaction

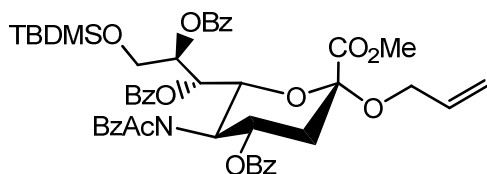
had reached completion, saturated NaHCO₃ (aq.) (0.4 mL) was added to the solution and stirred. The DMF was then removed *in vacuo* and the product was purified by flash chromatography (Tol:EA; 2:1 → 1:10) to yield compound **16** (220 mg, 85%). R_f: 0.68 (EA:MeOH; 5:1).

¹H NMR (500 MHz, MeOH-D₄) δ_H: 0.09 (6 H, 2s, 2 x -Si-CH₃), 0.92 (9 H, s, -Si-C(CH₃)₃), 1.75 (1 H, dd, J = 12.3, 12.3 Hz, H_{3ax}), 1.99 (3 H, s, -NHCOCH₃), 2.70 (1 H, dd, J = 4.7, 12.9 Hz, H_{3eq}), 3.55 (1 H, d, J = 10.3 Hz, H₆), 3.59 (1 H, d, J = 8.9 Hz, H₇), 3.66 (1 H, m, H₄), 3.75 (1 H, dd, J = 10.1, 10.2 Hz, H₅), 3.79 - 3.84 (2 H, m, H₉, H₉'), 3.82 (3 H, s, -CO₂CH₃), 3.90 (1 H, d, J = 8.7 Hz, H₈), 3.99 (1 H, dd, J = 5.6, 12.8 Hz, -CHH'-CH=CH₂), 4.28 (1 H, dd, J = 5.3, 12.8 Hz, -CHH'-CH=CH₂), 5.11 (1 H, d, J = 10.4 Hz, -CH₂-CH=CH_{cis}), 5.23 (1 H, d, J = 17.2 Hz, -CH₂-CH=CH_{trans}), 5.87 (1 H, ddd, J = 5.4, 10.6, 16.1 Hz, -CH₂-CH=CH₂).

¹³C NMR (125.7 MHz, MeOH-D₄) δ_C: -5.04, -4.99 (-Si-CH₃), 22.81 (-NHCOCH₃), 19.47 (-Si-C(CH₃)₃), 26.64 (-Si-C(CH₃)₃), 41.88 (C3), 53.47 (-CO₂CH₃), 54.09 (C5), 65.86 (C8), 66.38 (-CH₂-CH=CH₂), 68.54 (C4), 69.60 (C7), 72.69 (C9), 75.17 (C6), 100.18 (C2), 117.08 (-CH₂-CH=CH₂), 135.61 (-CH₂-CH=CH₂), 171.13 (C1), 175.33 (-NHCOCH₃).

HR-ESI-MS (m/z) calculated for C₂₁H₃₉NO₉Si [M+Na]⁺ 500.2286, found 500.2268.

Methyl (allyl 5-(*N*-acetyl-*N*-benzoyl)-amido-3,5-dideoxy-4,7,8-tri-*O*-benzoyl-9-*O*-*tert*-butyldimethylsilyl-*D*-glycero- α -*D*-galacto-2-nonulopyranosid)onate (17)



Compound **16** (99 mg, 0.208 mmol) was placed under an N₂ (g) atmosphere and pyridine (3 mL) was added. The solution was then cooled to 0 °C and BzCl (97 μL, 0.832 mmol) was added dropwise via microsyringe with stirring. The reaction was left to stir overnight where then a further portion of BzCl (48 μL, 0.416 mmol) was added. Once TLC analysis had indicated that the reaction had progressed no further, saturated NaHCO₃ (aq.) (0.5 mL) was added to the solution and stirred. The pyridine was evaporated *in vacuo* and the resulting product was suspended in DCM (10 mL) and washed with semi-saturated NH₄Cl (aq.), NaHCO₃ (aq.) and brine. The organic phase was then dried over MgSO₄ and the solvent was evaporated *in vacuo*. Flash

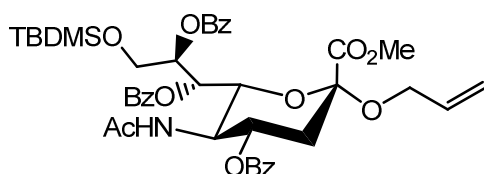
chromatography (Tol:EA; 20:1 → 2:1) gave compound **17** (87 mg, 53%). R_f : 0.81 (Tol:EA; 2:1).

^1H NMR (500 MHz, CDCl_3) δ_{H} : -0.18, -0.15 (6 H, 2s, -Si- CH_3), 0.72 (9 H, s, -Si- $\text{C}(\text{CH}_3)_3$), 1.64 - 1.83 (3 H, 2bs, - NHCOCH_3), 2.01 (1 H, dd, $J = 11.4, 11.6$ Hz, $\text{H}_{3\text{ax}}$), 3.01 (1 H, dd, $J = 4.8, 12.8$ Hz, $\text{H}_{3\text{eq}}$), 3.49 (3 H, s, - CO_2CH_3), 3.82 (1 H, dd, $J = 3.8, 11.7$ Hz, H_9), 4.05 - 4.09 (1 H, m, - $\text{CHH}'\text{-CH=CH}_2$), 4.12 (1 H, dd, $J = 5.7, 12.9$ Hz, H_9), 4.47 (1 H, dd, $J = 4.4, 12.8$ Hz, - $\text{CHH}'\text{-CH=CH}_2$), 5.02 (1 H, dd, $J = 9.2, 9.7$ Hz, H_5), 5.15 - 5.20 (1 H, m, H_6), 5.18 (1 H, d, $J = 10.0$ Hz, - $\text{CH}_2\text{-CH=CHH}_{\text{cis}}$), 5.32 (1 H, dd, $J = 1.3, 17.3$ Hz, - $\text{CH}_2\text{-CH=CHH}_{\text{trans}}$), 5.62 (1 H, m, H_8), 5.75 - 5.89 (2 H, m, H_4, H_7), 5.94 (1 H, ddd, $J = 5.4, 10.6, 16.1$ Hz, - $\text{CH}_2\text{-CH=CH}_2$), 7.13 - 8.17 (20 H, m, - COPh).

^{13}C NMR (125.7 MHz, CDCl_3) δ_{C} : -5.45, -5.42 (-Si- CH_3), 18.29 (-Si- $\text{C}(\text{CH}_3)_3$), 25.86 (-Si- $\text{C}(\text{CH}_3)_3$), 27.11, 28.17 (- NHCOCH_3), 39.11 (C_{30}), 52.64 (- CO_2CH_3), 56.25 (C_5), 61.50 (C_9), 65.78 (- $\text{CH}_2\text{-CH=CH}_2$), 68.22, 69.05 (C_4, C_7), 70.44 (C_6), 72.25 (C_8), 98.93 (C_2), 116.85 (- $\text{CH}_2\text{-CH=CH}_2$), 128.48, 128.66, 129.07, 129.26, 129.86, 130.02, 130.11, 130.32, 130.67 (- COPh), 132.98, 133.33, 134.59 (- $\text{CH}_2\text{-CH=CH}_2$), 168.42, 165.33, 165.68, (- COPh), 173.66 (C_1), 174.13 (- NHCOCH_3).

HR-ESI-MS (m/z) calculated for $\text{C}_{49}\text{H}_{55}\text{NO}_{13}\text{Si}$ [$\text{M}+\text{Na}$] $^+$ 916.3335, found 916.3277.

Methyl (allyl 5-acetamido-3,5-dideoxy-4,7,8-tri-O-benzoyl-9-O-tert-butylidimethylsilyl-D-glycero- α -D-galacto-2-nonulopyranosid)onate (18)



Compound 16 (254 mg, 0.531 mmol) and DMAP (65 mg, 0.531 mmol) were placed under an N_2 (g) atmosphere and pyridine (3mL) was added. The solution was then cooled to 0 °C and BzCl (432 μL , 3.72 mmol) was added dropwise via syringe with stirring. The reaction was left to stir overnight where then a further portion of BzCl (62 μL , 0.533 mmol) was added. Once TLC analysis had indicated that the reaction had progressed no further, a few small spatulas of NaHCO_3 (s) were added to the solution and stirred. The pyridine was evaporated *in vacuo* and the resulting product was suspended in DCM (20 mL) and washed successively with semi-saturated NH_4Cl (aq.), NaHCO_3 (aq.) and brine. The organic phase was then dried over MgSO_4 , co-evaporated with toluene (2 x 5 mL) and the solvent was evaporated *in vacuo*. Flash

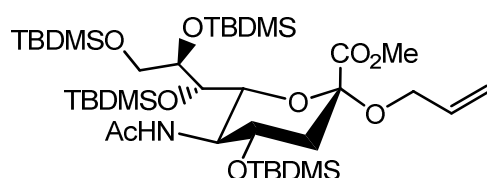
chromatography (cyclohexane:EA; 10:1 → 5:1 → EA)) gave compound **18** (106 mg, 25%). R_f : 0.72 (cyclohexane:EA; 1:1).

^1H NMR (500 MHz, CDCl_3) δ_{H} : -0.12, -0.10 (6 H, 2s, 2 x -Si-CH₃), 0.77 (9 H, s, -Si-C(CH₃)₃), 1.85 (3 H, s, -NHCOCH₃), 1.99 (1 H, dd, J = 12.2, 12.2 Hz, H_{3ax}), 2.79 (1 H, dd, J = 4.8, 12.8 Hz, H_{3eq}), 3.48 (3 H, s, -CO₂CH₃), 3.83 - 3.93 (2 H, m, H₅, H₉), 4.01 - 4.06 (2 H, m, H₉, -CHH'-CH=CH₂), 4.40 (1 H, dd, J = 5.1, 12.9 Hz, -CHH'-CH=CH₂), 4.57 (1H, dd, J = 1.2, 10.7 Hz, H₆), 5.16 (1 H, dd, J = 0.8, 10.5 Hz, -CH₂-CH=CHH_{cis}), 5.29 (1 H, dd, J = 1.2, 17.5 Hz, -CH₂-CH=CHH_{trans}), 5.42 (1 H, dd, J = 4.8, 11.5 Hz, H₄), 5.52 (1 H, d, J = 8.9 Hz, -NH), 5.66 (1 H, m, H₈), 5.80 (1 H, dd, J = 1.3, 7.9 Hz, H₇), 5.90 (1 H, ddd, J = 5.4, 10.6, 16.2 Hz, -CH₂-CH=CH₂), 7.34 - 8.09 (15 H, m, -COPh).

^{13}C NMR (125.7 MHz, CDCl_3) δ_{C} : -5.34 (-Si-CH₃), 18.32 (-Si-C(CH₃)₃), 23.56 (-NHCOCH₃), 25.89 (-Si-C(CH₃)₃), 38.39 (C3), 51.24 (C5), 52.65 (-CO₂CH₃), 62.11 (C9), 65.95 (-CH₂-CH=CH₂), 69.07 (C7), 69.51 (C4), 72.31 (C6), 77.60 (C8), 98.94 (C2), 117.03 (-CH₂-CH=CH₂), 128.56, 128.60, 128.71, 129.77, 129.99, 130.04, 130.10, 130.18, 130.35, 130.72, 133.12, 133.42, 133.43 (-COPh), 134.45 (-CH₂-CH=CH₂), 165.79, 165.88, 166.36 (-COPh), 168.79 (C1), 170.32 (-NHCOCH₃).

HR-ESI-MS (m/z) calculated for C₄₂H₅₁NO₁₂Si [M+Na]⁺ 812.3072, found 812.3051.

Methyl (allyl 5-acetamido-3,5-dideoxy-4,7,8,9-tetra-*O*-*tert*-butyldimethylsilyl-*D*-glycero- α -*D*-galacto-2-nonulopyranosid)onate (19)



Compound **4** (102 mg, 0.282 mmol) was placed under an N₂ (g) atmosphere and dry DCM (1.8 mL) and lutidine (264 μL , 2.27 mmol) were added. TBDMSOTf (292 μL , 1.27 mmol) was added to the solution with stirring. After 7 hours, a further portion of TBDMSOTf (70 μL , 0.340 mmol) was added and the reaction was allowed to stir overnight. The solvent was removed *in vacuo* and the resulting crude material was purified by flash chromatography directly (hexane:EA; 10:1 → 5:1 → 1:1) to give compound **19** as a clear oil (203 mg, 88%). R_f : 0.51 (hexane:EA; 4:1).

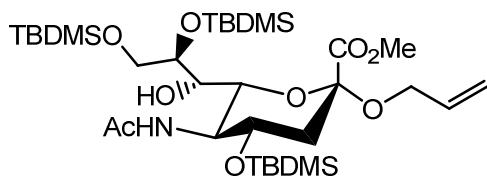
^1H NMR (500 MHz, CDCl_3) δ_{H} : -0.02, 0.03, 0.05, 0.07, 0.08, 0.15 (24 H, 6s, -Si-CH₃), 0.84, 0.87, 0.90 (36 H, s, -Si-C(CH₃)₃), 1.68 (1 H, dd, J = 12.0, 12.2 Hz, H_{3ax}), 1.87 (3 H, s, -NHCOCH₃), 2.56 (1 H, dd, J = 4.6, 12.7 Hz, H_{3eq}), 3.28 (1 H, m, H₅), 3.52 (1 H,

dd, $J = 7.5, 10.3$ Hz, H_9), 3.77 (3 H, s, $-\text{CO}_2\text{CH}_3$), 3.87 - 3.90 (2 H, m, H_7, H_8), 3.96 - 4.05 (3 H, m, $H_4, H_9, -\text{CHH}'\text{-CH=CH}_2$), 4.07 (1 H, dd, $J = 2.3, 10.7$ Hz, H_6), 4.24 (1 H, dddd, $J = 1.4, 2.5, 6.5, 12.6$ Hz, $-\text{CHH}'\text{-CH=CH}_2$), 5.10 (1 H, dd, $J = 1.2, 10.5$ Hz, $-\text{CH}_2\text{-CH=CHH}_{\text{cis}}$), 5.22 (1 H, dd, $J = 1.6, 17.3$ Hz, $-\text{CH}_2\text{-CH=CHH}_{\text{trans}}$), 5.40 (1 H, d, $J = 7.7$ Hz, $-\text{NH}$), 5.82 (1 H, ddd, $J = 5.6, 10.6, 16.2$ Hz, $-\text{CH}_2\text{-CH=CH}_2$).

^{13}C NMR (125.7 MHz, CDCl_3) δ_{C} : -5.09, -5.01, -4.82, -4.72, -4.37, -4.34, -4.28, -3.64 ($-\text{Si-CH}_3$), 18.07, 18.45, 18.71, 18.75 ($-\text{Si-C}(\text{CH}_3)_3$), 24.07 ($-\text{NHCOCH}_3$), 25.86, 26.24, 26.29, 26.37, 27.15 ($-\text{Si-C}(\text{CH}_3)_3$), 41.46 (C3), 52.48 ($-\text{CO}_2\text{CH}_3$), 55.80 (C5), 65.11, 65.21 (C9, $-\text{CH}_2\text{-CH=CH}_2$), 67.87, 74.40, 76.33 (C6, C7, C8), 98.91 (C2), 117.17 ($-\text{CH}_2\text{-CH=CH}_2$), 134.34 ($-\text{CH}_2\text{-CH=CH}_2$), 169.11 (C1), 169.74 ($-\text{NHCOCH}_3$).

HR-ESI-MS (m/z) calculated for $\text{C}_{39}\text{H}_{81}\text{NO}_9\text{Si}_4$ $[\text{M}+\text{Na}]^+$ 842.4881, found 842.4860.

Methyl (allyl 5-acetamido-3,5-dideoxy-4,8,9-tri-*O*-*tert*-butyldimethylsilyl-*D*-glycero- α -*D*-galacto-2-nonulopyranosid)onate (20)

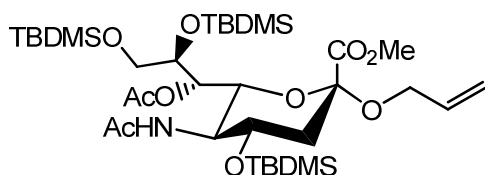


Compound **19** (110.3 mg, 0.134 mmol) was placed under an N_2 (g) atmosphere and dissolved in anhydrous MeOH (0.9 mL). The resulting solution was then transferred to a quartz reaction vessel (suitable for UV applications), also under an N_2 (g) atmosphere and the solution was stirred. A solution of CBr_4 (~2.7 mg, 0.00814 mmol added as 10 mg/mL solution) in anhydrous MeOH was quickly transferred to the stirring methanolic solution of compound **19**. The solution was then exposed for 20 minutes to a 6W UV lamp ($\lambda \sim 254$ nm), enclosed in a dark reaction container. After this time, the lamp was switched off and the reaction was monitored by TLC for a further 45 minutes to 1 hour. Once the reaction was complete, a small spatula of NaHCO_3 (s) was added, the methanol was removed directly from the reaction vessel and the vessel itself was rinsed well with MeOH. The solvent was then evaporated *in vacuo* and the product was purified directly by flash chromatography (hexane:EA; 2:1) to give compound **20** (21.2 mg, 22%). R_f : 0.42 (cyclohexane/EA; 4:1).

^1H NMR (500 MHz, CDCl_3) δ_{H} : 0.04 - 0.11 (18 H, 7s, $-\text{Si-CH}_3$), 0.86, 0.89, 0.90 (27 H, s, $-\text{Si-C}(\text{CH}_3)_3$), 1.84 (1 H, dd, $J = 11.0, 11.0$ Hz, $H_{3\text{ax}}$), 1.96 (3 H, s, $-\text{NHCOCH}_3$), 2.53 (1 H, dd, $J = 4.4, 12.9$ Hz, $H_{3\text{eq}}$), 3.58 - 3.67 (2 H, m, $H_{6/7, -\text{OH}}$), 3.77 (3 H, s, -

CO₂CH₃), 3.79 – 3.92 (5 H, m, H₄, H₅, H_{6/7}, H₉, H_{9'}), 4.01 (1 H, dd, J = 5.9, 12.6 Hz, -CHH'-CH=CH₂), 4.31 (1 H, dd, J = 5.4, 12.7 Hz, -CHH'-CH=CH₂), 5.13 (1 H, dd, J = 1.3, 10.5 Hz, -CH₂-CH=CHH_{cis}), 5.19 (1 H, d, J = 8.0 Hz, -NH), 5.24 (1 H, dd, J = 1.5, 17.2 Hz, -CH₂-CH=CHH_{trans}), 5.87 (1 H, ddd, J = 5.5, 10.7, 16.9 Hz, -CH₂-CH=CH₂);
¹³C NMR (100.5 MHz, CDCl₃) δ_C: -5.22, -4.63, -4.53, -4.13, -3.89 (-Si-CH₃), 1.17 (unknown), 17.99, 18.44, 18.48 (-Si-C(CH₃)₃), 23.47 (-NHCOCH₃), 25.72, 26.11, 26.25 (-Si-C(CH₃)₃), 29.86 (unknown), 41.67 (C3), 52.41 (-CO₂CH₃), 54.04 (C5), 65.04, 65.31 (C9, -CH₂-CH=CH₂), 68.20, 70.70, 73.13, 73.92 (C4, C6, C7, C8), 98.60 (C2), 117.01 (-CH₂-CH=CH₂), 134.43 (-CH₂-CH=CH₂), 169.20, 169.57, 171.19 (C1, -NHCOCH₃).
 HR-ESI-MS (m/z) calculated for C₃₃H₆₈NO₉Si₃ [M+H]⁺ 706.4196, found 706.4214.

Methyl (allyl 5-acetamido-3,5-dideoxy-7-O-acetyl-4,8,9-tetra-O-tert-butylidimethylsilyl-D-glycero-α-D-galacto-2-nonulopyranosid)onate (21)



Compound **20** (15 mg, 0.021 mmol) was placed into a flask. Pyridine (0.5 mL) and acetic anhydride (0.5 mL) were then added and the solution was stirred overnight. Once the reaction was complete, the solvent was removed directly *in vacuo*. Co-evaporation with toluene several times followed by flash chromatography (EA:MeOH 20:1 → 5:1) gave the desired product, compound **21** (15.1 mg, 95%). R_f: 0.24 (hexane/EA; 4:1).

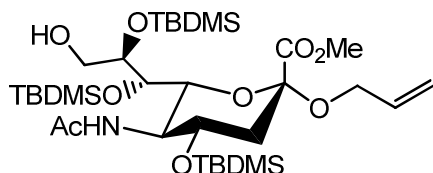
¹H NMR (500 MHz, CDCl₃) δ_H: -0.1 – 0.11 (18 H, 7s, -Si-CH₃), 0.85, 0.87, 0.90 ((27 H, s, -Si-C(CH₃)₃), 1.68 (1 H, dd, J = 11.8, 12.5 Hz, H_{3ax}), 1.91 (3 H, s, -NHCOCH₃), 2.13 (3 H, s, -COCH₃), 2.35 (Toluene), 2.59 (1 H, dd, J = 4.6, 12.8 Hz, H_{3eq}), 2.92 (1 H, dd, J = 9.6, 9.7 Hz, H₅), 3.59 (1 H, dd, J = 6.5, 6.7 Hz, H₉), 3.80 (3 H, s, -CO₂CH₃), 3.93 – 4.06 (3 H, m, H₈, H₉, -CHH'-CH=CH₂), 4.23 – 4.41 (3 H, m, H₄, H₆, -CHH'-CH=CH₂), 5.11 – 5.18 (2 H, m, H₇, -CH₂-CH=CHH_{cis}), 5.26 (1 H, dd, J = 1.3, 17.2 Hz, -CH₂-CH=CHH_{trans}), 7.13 – 7.28 (Toluene);

¹³C NMR (100.5 MHz, CDCl₃) δ_C: -5.17, -4.86, -4.79, -4.54, -4.11 (-Si-CH₃), 18.03, 18.25, 18.50 (-Si-C(CH₃)₃), 21.30 (-COCH₃), 23.88 (-NHCOCH₃), 25.79, 26.02, 26.15 (-Si-C(CH₃)₃), 29.85 (unknown), 42.01 (C3), 52.50 (-CO₂CH₃), 56.03 (C5), 64.64 (C9), 65.37 (-CH₂-CH=CH₂), 66.25 (C4), 71.19 (C6), 73.39, 73.54 (C8, C7), 98.73 (C2),

117.08 ($-\text{CH}_2-\text{CH}=\underline{\text{C}}\text{H}_2$), 134.25 ($-\text{CH}_2-\underline{\text{C}}\text{H}=\text{CH}_2$), 168.60 (C1), 170.04, 171.41 ($-\underline{\text{C}}\text{OCH}_3$, $-\text{NH}\underline{\text{C}}\text{OCH}_3$).

HR-ESI-MS (m/z) calculated for $\text{C}_{35}\text{H}_{70}\text{NO}_{10}\text{Si}_3$ $[\text{M}+\text{H}]^+$ 748.4302, found 748.4307.

Methyl (allyl 5-acetamido-3,5-dideoxy-4,7,8,-tri-*O*-*tert*-butyldimethylsilyl-*D*-glycero- α -*D*-galacto-2-nonulopyranosid)onate (22)



Compound **19** (173 mg, 0.211 mmol) was placed under an N_2 (g) atmosphere and dissolved in anhydrous MeOH (1.4 mL). The resulting solution was then transferred to a quartz reaction vessel (suitable for UV applications), also under an N_2 (g) atmosphere and the solution was stirred. A solution of CBr_4 (~4.2 mg, 0.0127 mmol added as 10 mg/mL solution) in anhydrous MeOH was quickly transferred to the stirring methanolic solution of compound **19**. The solution was then exposed for 10 minutes to a 6W UV lamp (λ ~254 nm), enclosed in a dark reaction container. After this time, the lamp was switched off and the reaction was monitored by TLC for a further 45 minutes to 1 hour. Once the reaction was complete, the methanol was removed directly from the reaction vessel and the vessel itself was rinsed with a small amount of DCM (1 mL). The solvent was then evaporated *in vacuo* and the product was purified directly by flash chromatography (hexane:EA; 2:1) to give compound **19** as a white foam on further drying (88 mg, 60%). R_f : 0.18 (hexane:EA; 4:1).

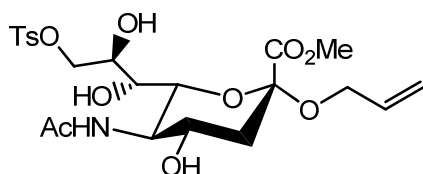
^1H NMR (500 MHz, CDCl_3) δ_{H} : -0.01, 0.03, 0.05, 0.08, 0.09, 0.10, 0.15 (18 H, 7s, $-\text{Si}-\underline{\text{C}}\text{H}_3$), 0.84, 0.89, 0.91 (27 H, s, $-\text{Si}-\underline{\text{C}}(\underline{\text{C}}\text{H}_3)_3$), 1.71 (1 H, dd, $J = 11.7, 11.7$ Hz, $\text{H}_{3\text{ax}}$), 1.90 (3 H, s, $-\text{NHCO}\underline{\text{C}}\text{H}_3$), 2.52 (1 H, dd, $J = 6.7, 6.8$ Hz, $-\text{OH}$), 2.57 (1 H, dd, $J = 4.6, 12.8$ Hz, $\text{H}_{3\text{eq}}$), 3.36 (1 H, m, H_5), 3.57 (1 H, m, H_9), 3.79 (3 H, s, $-\text{CO}_2\underline{\text{C}}\text{H}_3$), 3.82 (1 H, ddd, $J = 1.7, 5.1, 6.8$ Hz, H_8), 3.88 - 3.93 (1 H, m, H_9), 3.94 - 4.00 (3 H, m, $\text{H}_4, \text{H}_7, -\underline{\text{C}}\text{H}\text{H}'-\text{CH}=\text{CH}_2$), 4.10 (1 H, m, H_6), 4.25 (1 H, dddd, 1.3, 5.4, 6.8, 12.4 Hz, $-\underline{\text{C}}\text{H}\text{H}'-\text{CH}=\text{CH}_2$), 5.12 (1 H, dd, $J = 1.3, 10.4$ Hz, $-\text{CH}_2-\text{CH}=\underline{\text{C}}\text{H}_{\text{cis}}$), 5.19 (1 H, d, $J = 7.9$ Hz, $-\text{NH}$), 5.24 (1 H, ddd, $J = 1.4, 3.0, 17.2$ Hz, $-\text{CH}_2-\text{CH}=\underline{\text{C}}\text{H}_{\text{trans}}$), 5.83 (1 H, ddd, $J = 5.7, 10.7, 16.3$ Hz, $-\text{CH}_2-\underline{\text{C}}\text{H}=\text{CH}_2$).

^{13}C NMR (125.7 MHz, CDCl_3) δ_{C} : -4.92, -4.71, -4.57, -4.30, -3.64 ($-\text{Si}-\underline{\text{C}}\text{H}_3$), 18.06, 18.51, 18.74 ($-\text{Si}-\underline{\text{C}}(\underline{\text{C}}\text{H}_3)_3$), 23.96 ($-\text{NHCO}\underline{\text{C}}\text{H}_3$), 25.82, 26.24 ($-\text{Si}-\underline{\text{C}}(\underline{\text{C}}\text{H}_3)_3$), 41.42 (C3),

52.75 (-CO₂CH₃), 56.89 (C5), 63.59 (C9), 65.35 (-CH₂-CH=CH₂), 67.53, 74.93 (C4, C7), 74.42 (C6), under CHCl₃ resonance (C8), 99.07 (C2), 117.35 (-CH₂-CH=CH₂), 134.09 (-CH₂-CH=CH₂), 169.10 (C1), 169.90 (-NHCOCH₃).

HR-ESI-MS (m/z) calculated for C₃₃H₆₇NO₉Si₃ [M+Na]⁺ 728.4016, found 728.4028.

Methyl (allyl 5-acetamido-3,5-dideoxy-9-O-tosyl-D-glycero- α -D-galacto-2-nonulopyranosid)onate (23)



Compound **4** (560 mg, 1.54 mmol) was co-evaporated with dry pyridine and was then suspended in dry pyridine (12 mL) under N₂(g). The resulting suspension was cooled to below 0 °C and *p*-toluenesulfonyl chloride (293 mg, 1.54 mmol) was added quickly to the stirring solution.

After a short time the solution was allowed to warm up to room temperature and was subsequently stirred for a further 5 hours after which another portion of toluenesulfonyl chloride (293 mg, 1.54 mmol) was added. The solution was left to stir overnight.

Once completed, solvent was removed *in vacuo* and the crude product was purified directly by flash chromatography (EA → EA:MeOH; 5:1) to yield a white foam, compound **23** (470 mg, 59%). R_f: 0.70 (EA:MeOH; 4:1).

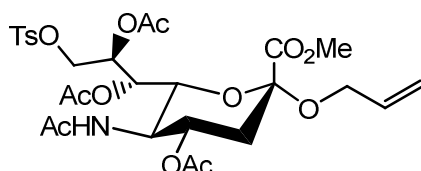
¹H NMR (500 MHz, CDCl₃) δ_H: 1.81 (1 H, dd, J = 11.7, 11.9 Hz, H_{3ax}), 2.01 (3 H, s, -NHCOCH₃), 2.41 (3 H, s, -C_{aryl}CH₃), 2.74 (1 H, dd, J = 3.8, 13.8 Hz, H_{3eq}), 3.40 (1 H, d, J = 9.2 Hz, H₆), 3.45 (1 H, d, J = 8.8 Hz, H₇), 3.64 – 3.75 (2 H, m, H₄, H₅), 3.65 – 3.77 (1 H, bs, -OH), 3.77 (3 H, s, -CO₂CH₃), 3.86 (1 H, dd, J = 5.7, 12.6 Hz, -CHH'-CH=CH₂), 3.91 (1 H, bs, -OH), 4.04 (1 H, m, H₈), 4.12 – 4.20 (2 H, m, H₉, -CHH'-CH=CH₂), 4.29 (1 H, m, H_{9'}), 4.68 (1 H, bs, -OH), 5.10 (1 H, dd, J = 0.8, 10.5 Hz, -CH₂-CH=CHH_{cis}), 5.18 (1 H, dd, J = 1.1, 17.3 Hz, -CH₂-CH=CHH_{trans}), 5.77 (1 H, ddd, J = 5.6, 10.8, 16.2 Hz, -CH₂-CH=CH₂), 6.61 (1 H, d, J = 7.0 Hz, -NH), 7.32 (2 H, d, J = 8.2 Hz, -C_{aryl}H), 7.75 (2 H, d, J = 8.3 Hz, -SC_{aryl}-C_{aryl}H).

¹³C NMR (125.7 MHz, CDCl₃) δ_C: 21.76 (-C_{aryl}-CH₃), 23.15 (-NHCOCH₃), 40.52 (C3), 52.92 (C5), 53.49 (-CO₂CH₃), 65.42 (-CH₂CH=CH₂), 67.62 (C4), 68.63 (C7), 69.22 (C8), 72.15 (C9), 73.65 (C6), 98.69 (C2), 117.43 (-CH₂CH=CH₂), 128.06, 130.12 (H₃C-

$\underline{C}_{\text{aryl}}-\underline{C}_{\text{aryl}}(\text{H})-$, $\text{H}_3\text{C}-\underline{C}_{\text{aryl}}-\underline{C}_{\text{aryl}}(\text{H})-$), 132.54 ($-\text{S}-\underline{C}_{\text{aryl}}-\underline{C}_{\text{aryl}}(\text{H})-$), 133.61 ($-\text{CH}_2-\underline{\text{C}}\text{H}=\text{CH}_2$), 145.21 ($-\text{S}-\underline{C}_{\text{aryl}}-\underline{C}_{\text{aryl}}(\text{H})-$), 169.82 (C1), 174.15 ($-\text{NH}-\underline{\text{C}}\text{OCH}_3$).

HR-ESI-MS (m/z) calculated for $\text{C}_{22}\text{H}_{31}\text{NO}_{11}\text{S}$ $[\text{M}+\text{Na}]^+$ 540.1510, found 540.1507.

Methyl (allyl 5-acetamido-3,5-dideoxy-4,7,8-tri-O-acetyl-9-O-tosyl-D-glycero- α -D-galacto-2-nonulopyranosid)onate (24)



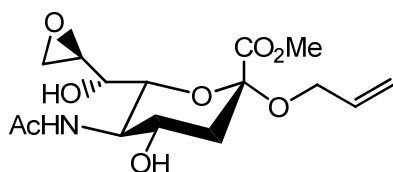
Compound **23** (20 mg, 0.0386 mmol) was stirred overnight in a solution of pyridine (0.5 mL) and acetic anhydride (0.5 mL). The solvent was then evaporated under high vacuum and purified by flash chromatography (Tol \rightarrow Tol:EA; 1:1) to give compound **24** (23 mg, 93 %). R_f : 0.71 (EA:MeOH, 10:1).

^1H NMR (500 MHz, CDCl_3) δ_{H} : 1.87 (3 H, s, $-\text{COCH}_3$), 1.95 (1 H, dd, $J = 12.4, 12.6$ Hz, $\text{H}_{3\text{ax}}$), 2.02 (3 H, s, $-\text{NHCOCH}_3$), 2.07, 2.08 (6 H, 2s, 2 x $-\text{COCH}_3$), 2.44 (3 H, s, Ph-CH_3), 2.62 (1 H, dd, $J = 4.5, 12.8$ Hz, $\text{H}_{3\text{eq}}$), 3.79 (3 H, s, $-\text{CO}_2\text{CH}_3$), 3.85 (1 H, dd, $J = 5.6, 12.7$ Hz, $-\text{CHH}'-\text{CH}=\text{CH}_2$), 3.91 – 4.10 (3 H, m, $\text{H}_5, \text{H}_9, \text{H}_6$), 4.22 (1 H, dd, $J = 5.1, 12.7$ Hz, $-\text{CHH}'-\text{CH}=\text{CH}_2$), 4.35 (1 H, d, $J = 11.1$ Hz, H_9), 4.80 (1 H, dd, $J = 4.5, 11.8$ Hz, H_4), 5.09 – 5.20 (2 H, m, $-\text{NH}$, $-\text{CH}_2\text{CH}=\text{CHH}_{\text{cis}}$), 5.23 – 5.38 (3 H, m, $\text{H}_7, \text{H}_8, -\text{CH}_2\text{CH}=\text{CH}_{\text{trans}}\text{H}$), 5.83 (1 H, ddd, $J = 5.7, 11.0, 16.7$ Hz, $-\text{CH}_2\text{CH}=\text{CH}_2$), 7.33 (2 H, d, $J = 8.0$ Hz, $-\text{C}_{\text{aryl}}-\text{H}$), 7.77 (1 H, d, $J = 8.0$ Hz, $-\text{C}_{\text{aryl}}-\text{H}$);

^{13}C NMR (100.5 MHz, CDCl_3) δ_{C} : 20.83, 20.97, 21.08, 23.34 (3 x $-\text{COCH}_3$, $-\text{NHCOCH}_3$), 21.76 ($\text{C}_{\text{aryl}}-\text{CH}_3$), 38.12 (C3), 49.61 (C5), 52.86 ($-\text{CO}_2\text{CH}_3$), 66.01 ($-\text{CH}_2-\text{CH}=\text{CH}_2$), 67.50 (C8/7), 67.81 (C9), 68.86 (C8/7), 69.09 (C4), 72.74 (C6), 98.74 (C2), 117.36 ($-\text{CH}_2\text{CH}=\text{CH}_2$), 128.15, 129.94 (2 x $\text{C}_{\text{aryl}}-\text{H}$), 133.02, 133.65 ($-\text{CH}_2-\text{CH}=\text{CH}_2$), 145.01, 168.36 (C1), 170.00, 170.17, 170.42, 171.03.

HR-ESI-MS (m/z) calculated for $\text{C}_{28}\text{H}_{37}\text{NO}_{14}\text{S}$ $[\text{M}+\text{Na}]^+$ 666.1826, found 666.1842.

Methyl (allyl 5-acetamido-3,5-dideoxy-8,9-anhydro-*D*-glycero- α -*D*-galacto-2-nonulopyranosid)onate (25)



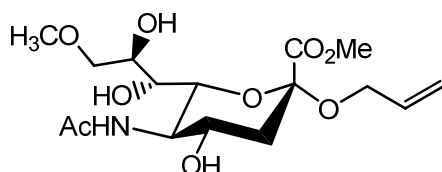
Compound **23** (194 mg, 0.375 mmol) was dissolved in anhydrous MeOH (2.4mL). Freshly prepared NaOMe (in anhydrous MeOH) (0.3 mL, 0.5 M) was added dropwise to the stirring solution. Further 0.1mL portions of NaOMe (0.5 M) were added as required (a total of 0.7 mL NaOMe was used). The reaction was monitored by TLC. On completion, a small amount of Amberlite IR-120 ion-exchange resin (H⁺) was added to the solution and was agitated until the pH was neutral. The resin was removed by filtration and the solvent was removed *in vacuo*. Flash chromatography of the crude material (EA:MeOH; 15:1 + 0.5% NEt₃) gave compound **25** as a white foam (87 mg, 68%). R_f: 0.34 (EA:MeOH; 10:1).

¹H NMR (500 MHz, CDCl₃) δ_H: 1.81 (1 H, dd, J = 12.1, 12.3 Hz, H_{3ax}), 2.00 (3 H, s, -NHCOCH₃), 2.71 (1 H, dd, J = 4.6, 12.7 Hz, H_{3eq}), 2.77 (1 H, dd, J = 2.5, 5.1 Hz, H₉), 2.83 (1 H, dd, J = 4.3, 4.6 Hz, H₉), 3.24 (1 H, m, H₈), 3.38 (1 H, dd, J = 4.8, 4.8 Hz, H₇), 3.55 (1 H, dd, J = 0.9, 10.4 Hz, H₆), 3.65 (1 H, m, H₄), 3.76 - 3.82 (1 H, m, H₅), 3.93 (1 H, bs, -OH), 3.96 (1 H, dd, J = 5.9, 12.6 Hz, -CHH'-CH=CH₂), 4.25 (1 H, m, -CHH'-CH=CH₂), 4.27 (1 H, d, J = 5.7 Hz, -OH), 5.12 (1 H, dd, J = 1.3, 10.5 Hz, -CH₂-CH=CHH_{cis}), 5.21 (1 H, dd, J = 1.5, 17.2 Hz, -CH₂-CH=CHH_{trans}), 5.82 (1 H, ddd, J = 5.6, 10.8, 16.1 Hz, -CH₂-CH=CH₂), 6.57 (1 H, d, J = 7.7 Hz, -NH).

¹³C NMR (125.7 MHz, CDCl₃) δ_C: 23.24 (-NHCOCH₃), 40.83 (C3), 46.08 (C9), 51.99 (C8), 52.85 (C5), 53.03 (-CO₂CH₃), 65.57 (-CH₂CH=CH₂), 67.84 (C4), 69.48 (C7), 75.37 (C6), 99.04 (C2), 117.28 (-CH₂CH=CH₂), 134.00 (-CH₂CH=CH₂), 169.22 (C1), 173.65 (-NHCOCH₃).

HR-ESI-MS (m/z) calculated for C₁₅H₂₃NO₈ [M+Na]⁺ 368.1315, found 368.1309.

Methyl (allyl 5-acetamido-3,5-dideoxy-9-O-methyl-D-glycero- α -D-galacto-2-nonulopyranosid)onate (26)



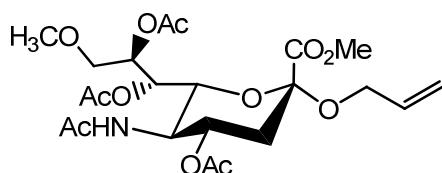
To a stirred solution of compound **25** (50 mg, 0.0966 mmol) in methanol (1.2 mL) was added freshly prepared methanolic NaOMe (~0.640 M, 0.2 mL). After stirring for 15 minutes, methanolic NaOMe solution was again added (until the solution had a resulting pH~10 as observed on indicator paper). The reaction was monitored by TLC, observing the formation of the resulting epoxide *in situ*. Once formation of the epoxide reached completion, the mixture was acidified (to ~pH 2) with Amberlite IR-120 ion-exchange resin (H⁺), the resin was filtered off and the solvent evaporated from the solution to leave an oily residue. The crude product was purified by flash chromatography directly (EA → EA:MeOH; 5:1) to yield (**X**) (16.4 mg, 45%). R_f: 0.38 (EA:MeOH; 5:1).

¹H NMR (500 MHz, CDCl₃) δ_H: 2.04 (3 H, s, -NHCOCH₃), 1.96 (1 H, dd, J = 11.7, 12.2 Hz, H_{3ax}), 2.74 (1 H, bs, -OH), 2.81 (1 H, dd, J = 4.3, 13.3 Hz, H_{3eq}), 3.39 – 3.43 (1 H, m, H₆), 3.43 (3 H, s, -OCH₃), 3.53 (1 H, dd, J = 3.3, 9.0 Hz, H₇), 3.65 – 3.80 (5 H, m, H₄, H₅, H₉, H_{9'}, -OH), 3.85 (3 H, s, -CO₂CH₃), 3.92 (1 H, dd, J = 5.9, 12.5 Hz, -CHH'-CH=CH₂), 4.01 (1 H, dd, J = 3.5, 8.7 Hz, H₈), 4.27 (1 H, dd, J = 5.4, 12.6 Hz, -CHH'-CH=CH₂), 4.67 (1 H, bs, -OH), 5.15 (1 H, d, J = 10.5 Hz, CH₂-CH=CH_{cis}H), 5.23 (1 H, dd, J = 1.0, 17.2 Hz, -CH=CH_{trans}H), 5.83 (1 H, ddd, J = 5.7, 10.8, 16.3 Hz, -CH₂-CH=CH₂), 6.73 (1 H, d, J = 6.8 Hz, -NH).

¹³C NMR (100.5 MHz, CDCl₃) δ_C: 23.07 (-NHCOCH₃), 40.79 (C3), 53.33, 53.42 (C5, -CO₂CH₃), 59.21 (-OCH₃), 65.42 (-CH₂-CH=CH₂), 68.15 (C4), 68.79 (C7), 69.98 (C8), 73.86, 73.87 (C6, C9), 98.58 (C2), 117.46 (-CH₂-CH=CH₂), 133.73 (-CH₂-CH=CH₂), 169.82 (C1), 173.72 (-NHCOCH₃).

HR-ESI-MS (m/z) calculated for C₁₆H₂₁NO₉ [M+Na]⁺ 400.1578, found 400.1576.

Methyl (allyl 5-acetamido-3,5-dideoxy-4,7,8-tri-*O*-acetyl-9-*O*-methyl-*D*-glycero- α -*D*-galacto-2-nonulopyranosid)onate (27)



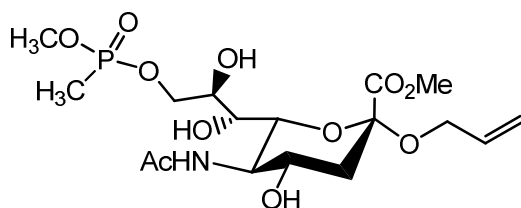
Compound **26** (5 mg, 0.0132 mmol) was stirred overnight in a solution of pyridine (0.5 mL) and acetic anhydride (0.5 mL). The solvent was then evaporated *in vacuo* and purified by flash chromatography (EA) to give compound **27** (6 mg, 91%). R_f : 0.23 (EA).

$^1\text{H NMR}$ (500 MHz, CDCl_3) δ_{H} : 2.01, 2.12, 2.14 (9 H, 3s, $-\text{OCOCH}_3$), 1.86 (3 H, s, $-\text{NHCOCH}_3$), 1.96 (1 H, dd, $J = 12.5, 12.6$ Hz, $\text{H}_{3\text{ax}}$), 2.59 (1 H, dd, $J = 4.6, 12.8$ Hz, $\text{H}_{3\text{eq}}$), 3.29 (3 H, s, $-\text{OCH}_3$), 3.36 (1 H, dd, $J = 4.6, 10.8$ Hz, H_9), 3.58 (1 H, dd, $J = 2.5, 10.7$ Hz, H_9), 3.76 (3 H, s, $-\text{CO}_2\text{CH}_3$), 3.87 (1 H, dd, $J = 5.8, 12.8$ Hz, $-\text{CHH}'-\text{CH}=\text{CH}_2$), 4.02 - 4.11 (2 H, m, H_5, H_6), 4.28 (1 H, dd, $J = 5.1, 12.7$ Hz, $-\text{CHH}'-\text{CH}=\text{CH}_2$), 4.86 (1 H, ddd, $J = 4.5, 9.9, 12.3$ Hz, H_4), 5.07 (1 H, d, $J = 9.7$ Hz, $-\text{NH}$), 5.14 (1 H, d, $J = 10.5$ Hz, $-\text{CH}_2-\text{CH}=\text{CH}_{\text{cis}}$), 5.25 - 5.36 (3 H, m, $\text{H}_7, \text{H}_8, -\text{CH}_2-\text{CH}=\text{CH}_{\text{trans}}$), 5.84 (1 H, ddd, $J = 5.6, 10.8, 16.7$ Hz, $-\text{CH}_2-\text{CH}=\text{CH}_2$).

$^{13}\text{C NMR}$ (100.5 MHz, CDCl_3) δ_{C} : 21.11, 21.51 ($-\text{OCOCH}_3$), 23.47 ($-\text{NHCOCH}_3$), 29.93, 38.33 (C3), 49.71 (C5), 52.87 ($-\text{CO}_2\text{CH}_3$), 59.38 ($-\text{OCH}_3$), 66.12 ($-\text{CH}_2-\text{CH}=\text{CH}_2$), 68.03 (C8), 69.22 (C7), 69.32 (C4), 71.37 (C9), 77.83 (C6), 98.65 (C2), 117.43 ($-\text{CH}_2-\text{CH}=\text{CH}_2$), 133.88 ($-\text{CH}_2-\text{CH}=\text{CH}_2$), 168.60 (C1), 170.33, 170.41, 171.21 ($-\text{OCOCH}_3, -\text{NHCOCH}_3$).

HR-ESI-MS (m/z) calculated for $\text{C}_{21}\text{H}_{32}\text{NO}_{12}$ $[\text{M}+\text{H}]^+$ 504.2076, found 504.2088.

Methyl (allyl 5-acetamido-3,5-dideoxy-9-*O*-(*O,P*-dimethylphosphonyl)-*D*-glycero- α -*D*-galacto-2-nonulopyranosid)onate (28)



Compound **4** (77 mg, 0.212 mmol) was placed in a flask under an N₂ (g) atmosphere. Dry DCM (2 mL) was then added which required ultrasonication. *N,N*-diisopropylethylamine (81 μ L, 0.466 mmol) was added to the suspension followed by further ultrasonication. With continuous stirring, the suspension was cooled to approximately -15 °C and methyl methylphosphonochloridate (29 μ L, 0.297 mmol) was added dropwise to the solution via microsyringe. After 5 hours the reaction was again then cooled to -15°C, where a further portion of *N,N*-diisopropylethylamine (81 μ L, 0.466 mmol) and methyl methylphosphonochloridate (29 μ L, 0.297 mmol) was added. The reaction was left to stir overnight. Once TLC monitoring of the reaction had indicated completion, the reaction was quenched by the addition of MeOH (1 mL) and a small spatula of NaHCO₃ (s). After stirring for 10 minutes, the solvent was removed directly *in vacuo* and the product was directly purified by flash chromatography (EA:MeOH; EA \rightarrow 10:1 \rightarrow 5:1) to give compound **28** (27 mg, 30%). R_f: 0.25 (EA:MeOH; 10:1).

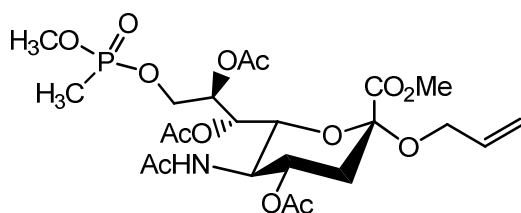
¹H NMR (500 MHz, CDCl₃) δ _H: 1.54 (3 H, dd, J = 2.2, 17.6 Hz, P-CH₃), 1.75 (1 H, dd, J = 12.2, 12.3 Hz, H_{3ax}), 2.00 (3 H, s, -NHCOCH₃), 2.69 (1 H, dd, J = 4.6, 12.8 Hz, H_{3eq}), 3.52 (1 H, ddd, J = 1.4, 9.9, 10.1 Hz, H₇), 3.62 (1 H, dd, J = 1.4, 10.5 Hz, H₆), 3.66 (1 H, m, H₄), 3.75 (3 H, dd, J = 1.7, 11.2 Hz, P-OCH₃), 3.75 - 3.80 (1 H, m, H₅), 3.98 - 4.02 (1 H, m, H₈), 3.98 - 4.02 (1 H, m, -CHH'-CH=CH₂), 4.15 (1 H, m, H₉), 4.26 - 4.33 (1 H, m, -CHH'-CH=CH₂), 4.26 - 4.33 (1 H, m, H₉), 5.12 (1 H, dd, J = 1.1, 10.5 Hz, -CH₂-CH=CHH_{cis}), 5.24 (1 H, dd, J = 1.7, 17.2 Hz, -CH₂-CH=CHH_{trans}), 5.87 (1 H, ddd, J = 5.5, 10.6, 16.2 Hz, -CH₂-CH=CH₂).

¹³C NMR (100.5 MHz, CDCl₃) δ _C: ~9.15, ~10.29 (2d, J = 144 Hz, P-CH₃), 22.68 (-NHCOCH₃), 41.69 (C3), ~52.91, 53.83, 53.85 (s, m, C5, P-OCH₃), 53.28 (-CO₂CH₃), 66.26 (-CH₂-CH=CH₂), 68.46 (C4), 69.12, 69.30 (2d, J = 6.3, 6.4 Hz, C9), 69.80, 69.94 (C7), 70.80, 70.90 (2d, J = 6.4, 6.8 Hz, C8), 74.70 (C6), 100.12 (C2), 116.94 (-CH₂-CH=CH₂), 135.47 (-CH₂-CH=CH₂), 170.84 (C1), 175.16 (-NHCOCH₃).

³¹P NMR (161.7 MHz, CDCl₃) δ _P: 34.24 (s), 34.34 (s).

HR-ESI-MS (m/z) calculated for C₁₇H₃₀NO₁₁P [M+Na]⁺ 478.1449, found 478.1449.

Methyl (allyl 5-acetamido-3,5-dideoxy-4,7,8-tri-O-acetyl-9-O-(*O,P*-dimethylphosphonyl)-*D*-glycero- α -*D*-galacto-2-nonulopyranosid)onate (29)



Compound **28** (23 mg, 0.0520 mmol) was placed into a flask. Pyridine (0.5 mL) and acetic anhydride (0.5 mL) were then added and the solution was stirred overnight. Once the reaction was complete, the solvent was removed directly *in vacuo*. Co-evaporation with toluene several times followed by flash chromatography (EA:MeOH 20:1 \rightarrow 10:1) gave the desired product, compound **29** (26 mg, 90%). R_f : 0.45 (EA:MeOH; 10:1).

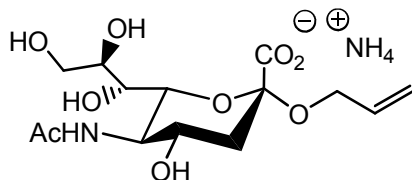
^1H NMR (500 MHz, CDCl_3) δ_{H} : 1.45 (1 H, dd, $J = 3.4, 17.6$ Hz, P- CH_3), 1.85, 2.12 - 2.14 (9 H, s,m, 3 x - OCOCH_3), 2.00 (3 H, s, - NHCOCH_3), 1.95 (1 H, dd, $J = 12.4, 12.6$ Hz, $\text{H}_{3\text{ax}}$), 2.60 (1 H, dd, $J = 4.6, 12.8$ Hz, $\text{H}_{3\text{eq}}$), 3.68, 3.72 (3 H, 2d, $J = 11.1, 11.2$ Hz, P- OCH_3), 3.87 (1 H, dd, $J = 5.9, 12.8$ Hz, - $\text{CHH}'\text{-CH}=\text{CH}_2$), 3.95 - 4.13 (3 H, m, $\text{H}_5, \text{H}_6, \text{H}_9$), 4.21 - 4.33 (2 H, m, H_9' , - $\text{CHH}'\text{-CH}=\text{CH}_2$), 4.87 (1 H, m, H_4), 5.14 (1 H, dd, $J = 1.4, 10.4$ Hz, - $\text{CH}_2\text{-CH}=\text{CH}_{\text{cis}}$), 5.22 (1 H, d, $J = 10.0$ Hz, - NH), 5.26 (1 H, d, $J = 17.2$ Hz, - $\text{CH}_2\text{-CH}=\text{CH}_{\text{trans}}$), 5.30 (1 H, m, H_7), 5.37 (1 H, m, H_8), 5.84 (1 H, ddd, $J = 5.5, 10.7, 16.1$ Hz, - $\text{CH}_2\text{-CH}=\text{CH}_2$).

^{13}C NMR (100.5 MHz, CDCl_3) δ_{C} : ~10.49, ~10.57 (2d, $J = 145.1, 145.4$ Hz, P- CH_3), 21.00, 21.27, 23.35 (3 x - OCOCH_3 , - NHCOCH_3), 38.17 (C3), 49.69, 49.73 (C5), ~52.31 (m, P- OCH_3), 52.83 (- CO_2CH_3), 63.88 (m, C9), 66.02 (- $\text{CH}_2\text{-CH}=\text{CH}_2$), 67.54 (C7), 69.18, 69.23 (C4), ~69.60, ~69.82 (2d, $J = 6.5, 6.5$ Hz, C8), 72.65, 72.68 (C6), 98.70 (C2), 117.38 (- $\text{CH}_2\text{-CH}=\text{CH}_2$), 133.76 (- $\text{CH}_2\text{-CH}=\text{CH}_2$), 168.49, 168.52 (C1), 170.16, 170.25, 170.35, 171.07 (3 x - OCOCH_3 , - NHCOCH_3).

^{31}P NMR (161.7 MHz, CDCl_3) δ_{P} : 32.51 (s), 32.73 (s).

HR-ESI-MS (m/z) calculated for $\text{C}_{23}\text{H}_{36}\text{NO}_{14}\text{P}$ [$\text{M}+\text{Na}$] $^+$ 604.1766, found 604.1756.

Methyl (allyl 5-acetamido-3,5-dideoxy-*D*-glycero- α -*D*-galacto-2-nonulopyranosidonate) (30)



Compound **4** (10 mg, 0.0275 mmol) was dissolved in dioxane (0.5 mL) with stirring. NaOH (aq.) (0.1 M, 0.5 mL) was then added to the solution which was stirred for 2 hours. The solution was then neutralised with Amberlite IR-120 ion-exchange resin (H⁺) and the solvent removed *in vacuo*. The crude residue was then purified by gel permeation chromatography and then lyophilised to give a white powder (9 mg, ~quantitative). Data corresponds to literature.⁶³

¹H NMR (500 MHz, D₂O) δ_{H} : 1.74 (1 H, dd, *J* = 12.1, 12.1 Hz, H_{3ax}), 2.11 (3 H, s, -NHCOCH₃), 2.83 (1 H, dd, *J* = 4.4, 12.4 Hz, H_{3eq}), 3.66 (1 H, d, *J* = 8.9 Hz, H₇), 3.69 – 3.82 (3 H, m, H₄, H₆, H₉), 3.85 – 3.99 (3 H, m, H₅, H₈, H_{9'}), 4.09 (1 H, dd, *J* = 5.7, 12.0 Hz, -CHH'-CH=CH₂), 4.32 (1 H, dd, *J* = 6.2, 12.0 Hz, -CHH'-CH=CH₂), 5.30 (1 H, d, *J* = 10.4 Hz, -CH₂-CH=CH_{cis}-H), 5.40 (1 H, d, *J* = 17.3 Hz, -CH=CH_{trans}-H), 6.02 (1 H, ddd, *J* = 5.9, 11.4, 16.5 Hz, -CH₂-CH=CH₂).

¹³C NMR (100.5 MHz, D₂O) δ_{C} : 22.01 (-NHCOCH₃), 40.45 (C3), 51.88 (C5), 62.60 (C9), 65.95 (-CH₂CH=CH₂), 68.21 (C4, C7), 71.69 (C8), 72.65 (C6), 100.59 (C2), 118.19 (-CH₂CH=CH₂), 133.76, (-CH₂CH=CH₂), 173.42 (C1), 175.06 (-NHCOCH₃).

HR-ESI-MS (*m/z*) calculated for C₁₄H₂₃NO₉ (acid form) [M+Na]⁺ 372.1265, found 372.1280.

III.3. SOAE Inhibition assays

III.3.1. Viruses and recombinant viral sialate-O-acetyl esterases

Influenza C virus C/JJ/50 was grown in embryonated chicken eggs. Bovine coronavirus (BCoV) was grown in Madin-Darby bovine kidney (MDBK) cells and mouse hepatitis virus strain S (MHV-S) was grown in mouse L cells.

The INF-C virus HEF and SDAV-HE were expressed as chimeric recombinant influenza C/Cal/78 virus and sialodacryoadenitis virus haemagglutinin esterase, respectively, fused in frame to enhanced green fluorescent protein (HE12-GFP and SDAV-HE). Both HE12-GFP and SDAV-HE were expressed in insect Sf9 cells in serum-free media by recombinant baculoviruses.

III.3.2. Enzyme and inhibitors

The three different viruses (INF-C virus, BCoV and MHV-S) were concentrated and purified by ultracentrifugation through a 3 ml cushion of 20 % sucrose for 1.5 hours at 4 °C at 26,000 rpm (110.000 x g) in a Beckman SW 41 rotor. The virus pellets were resuspended in 500 µl PBS (phosphate buffered saline) pH 7.4.

The recombinant enzymes (HE12-GFP and SDAV-HE) were recovered from cell culture supernatants by ultracentrifugation for 1.5 hours at 4 °C at 26,000 rpm.

Target sialosides (compounds **5 - 8**) were dissolved in ddH₂O to a final concentration of 10 mM. Stock solutions of *p*-nitrophenyl acetate (100 mM) were prepared in acetonitrile, and 3,4-Dichloroisocoumarin (positive control) was dissolved in dimethylsulfoxide to a final concentration of 10 mM.

III.3.3. *p*-nitrophenylacetate (pNPA) Inhibition assay

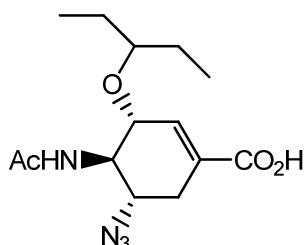
The esterase activities of all viruses and recombinant proteins were determined with pNPA as described in the literature.⁴⁶

One milliunit of viral esterase activity was defined as the amount of enzymatic activity resulting in the hydrolysis of 1 nmol of pNPA per minute.

An esterase activity was incubated in the presence of a sialoside at room temperature for 30 min. For control inhibition reactions, 100 µM 3,4-Dichloroisocoumarin was incubated with the different esterase activities 10 µl pNPA and PBS pH 7.4 was added to 1 ml and the A₄₀₀ was monitored.

III.4. Synthetic procedures towards phospho-oseltamivir derivatives

(3*R*,4*R*,5*S*)-4-acetamido-5-azido-3-(1-ethylpropoxy)-1-cyclohexene-1-carboxylic acid (**31**)



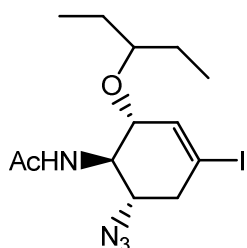
Tamiflu precursor (“acetamido-azide”) (1 g, 2.95 mmol) was dissolved in dioxane (6 mL), a NaOH-solution (0.5 M, 6 mL) was added and the mixture was stirred overnight. The mixture was neutralized with Amberlite IR-120 (H⁺), filtered and lyophilized. The residue was purified by flash chromatography (Tol:EA; 1:1: +0.5% AcOH) to afford the free acid, compound **31** (889 mg, 97% yield) as a colourless solid. *R*_f: 0.27 (Tol:EA; 1:1).

¹H NMR (500 MHz, MeOH-D₄) δ_H: 0.86 (3 H, t, J = 7.4 Hz, -OCH(CH₂CH₃)₂), 0.88 (3 H, t, J = 7.4 Hz, -OCH(CH₂)₂(CH₃)₂), 1.40 – 1.55 (4 H, m, -OCH(CH₂CH₃)₂), 1.97 (3 H, s, -NHCOCH₃), 2.16 (1 H, m, H_{6ax}), 2.78 (1 H, dd, J = 5.4, 16.8 Hz, H_{6ax}), 3.31 – 3.37 (1 H, m, -OCH(CH₂)₂(CH₃)₂), 3.70 – 3.80 (2 H, m, H₄, H₅), 4.17 (1 H, d, J = 7.6 Hz, H₃), 6.75 (1 H, m, H₂);

¹³C NMR (125.8 MHz, MeOH-D₄) δ_C: 9.56, 9.89 (-OCH(CH₂CH₃)₂), 23.05 (-NHCOCH₃), 26.73, 27.24 (-OCH(CH₂CH₃)₂), 31.36 (C₆), 56.98 (C₅), 60.12 (C₄), 76.43 (C₃), 83.70 (-OCH(CH₂CH₃)₂), 126.90 (C₁), 139.27 (C₂), 168.96 (-CO₂H), 173.79 (-NHCOCH₃).

HR-ESI-MS (m/z) calculated for C₁₄H₂₂N₄O₄ (M+Na)⁺ 333.1533, found 333.1533.

(3*R*,4*R*,5*S*)-4-acetamido-5-azido-3-(1-ethylpropoxy)-1-iodocyclohexene (**32**)



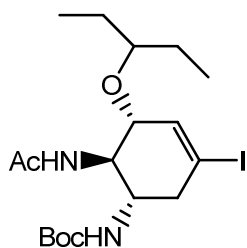
Under an atmosphere of dry nitrogen, the free acid **31** (250 mg, 0.81 mmol) and (chloromethylene)dimethyliminium chloride (Vilsmeier reagent, 124 mg, 0.97 mmol) were dissolved in dry DCM (2 mL) and the mixture was stirred for 40 min at room temperature. Simultaneously, using a quartz tube, *N*-hydroxypyridine-2-thione (144 mg, 0.97 mmol), DMAP (50 mg, 0.4 mmol) and 2-iodo-1,1,1-trifluoroethane (0.317 mL, 3.22 mmol) were dissolved in dry DCM (2 mL) under an atmosphere of dry nitrogen using an ultrasonic bath. The mixture was irradiated and heated to reflux with a 250W flood lamp for 5 minutes, followed by addition of the acyl chloride mixture. Irradiation and refluxing was then continued for a further 30 min. After evaporation of the solvent, the mixture was purified by flash chromatography (Tol:EA; 5:1 → 2:1) to give the iodo derivative **32** (129 mg, (41% (77% based on consumed starting material)) as a pale yellow crystalline solid. R_f : 0.53 (Tol:EA; 1:1).

^1H NMR (500 MHz, CDCl_3) δ_{H} : 0.87 (6 H, m, $-\text{OCH}(\text{CH}_2\text{CH}_3)_2$), 1.46 (4 H, m, $-\text{OCH}(\text{CH}_2\text{CH}_3)_2$), 2.02 (3 H, s, $-\text{NHCOCH}_3$), 2.55 (1 H, dd, $J = 9.1, 17.0$ Hz, $\text{H}_{6\text{ax}}$), 2.90 (1 H, dd, $J = 4.3, 17.4$ Hz, $\text{H}_{6\text{eq}}$), 3.25 (1 H, m, $-\text{OCH}(\text{CH}_2\text{CH}_3)_2$), 3.46 (1 H, m, H_4), 4.21 (1 H, dd, $J = 9.6, 14.6$ Hz, H_5), 4.28 (1 H, d, $J = 5.4$ Hz, H_3), 6.27 (1 H, s, H_2), 6.41 (1 H, bs, $-\text{NH}$);

^{13}C NMR (150.9 MHz, CDCl_3) δ_{C} : 9.37, 9.68 ($-\text{OCH}(\text{CH}_2\text{CH}_3)_2$), 23.55 ($-\text{NHCOCH}_3$), 25.75, 26.34 ($-\text{OCH}(\text{CH}_2\text{CH}_3)_2$), 44.71 (C6), 56.99 (C4), 58.33 (C5), 76.08 (C3), 82.23 ($\text{OCH}(\text{CH}_2\text{CH}_3)_2$), 92.18 (C1), 139.03 (C2), 171.43 ($-\text{NHCOCH}_3$).

HR-ESI-MS (m/z) calculated for $\text{C}_{13}\text{H}_{21}\text{IN}_4\text{O}_2$ $[\text{M}+\text{Na}]^+$ 415.0601, found 415.0609.

(3*R*,4*R*,5*S*)-4-acetamido-5-*N*-*tert*-Butoxycarbonyl-amino-3-(1-ethylpropoxy)-1-iodocyclohexene (33)



Under an atmosphere of dry nitrogen, the azido compound **32** (236 mg, 0.6 mmol) was dissolved in dry THF, PMe_3 was added (0.661 mL of 1 M solution in THF, 0.66 mmol) and the mixture was stirred at room temperature for 1 hour. When TLC indicated the absence of starting material, the mixture was cooled to -16 °C and a solution of 2-(*tert*-Butoxycarbonyloxyimino)-2-phenylacetonitrile (BocON, 222 mg, 0.9 mmol) in THF (1

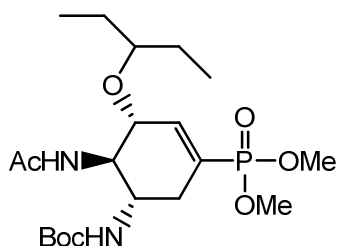
mL) was added via cannula. The mixture was then stirred for 3.5 hours, during which it was allowed to come to room temperature. Water (2 mL) was added and the solution was stirred for additional few minutes. The solution was extracted with DCM (30 mL) and then washed with saturated aqueous NaCl (2x20 mL). The organic phase was dried over MgSO₄, concentrated and the residue was purified by flash chromatography (Tol:EA; 5:1 → 1:1) to afford compound **33** (202 mg, 72%) as a pale yellow crystalline solid. R_f: 0.39 (Tol:EA; 1:1).

¹H NMR (500 MHz, CDCl₃) δ_H: 0.88 (6 H, m, -OCH(CH₂CH₃)₂), 1.42 (9 H, s, -NHCO(CH₃)₃), 1.44 – 1.53 (4 H, m, -OCH(CH₂CH₃)₂), 1.98 (3 H, s, -NHCOCH₃), 2.62 (1 H, dd, J = 8.2, 17.7 Hz, H_{6ax}), 2.87 (1 H, dd, J = 4.7, 18.0 Hz, H_{6eq}), 3.30 (1 H, p, J = 5.4, 5.6 Hz, -OCH(CH₂CH₃)₂), 3.77 (1 H, dd, J = 5.9 Hz, H₃), 3.84 (1 H, ddd, J = 5.3, 8.7, 14.1 Hz, H₅), 4.10 (1 H, dd, J = 8.8, 8.9 Hz, H₄), 5.27 (1 H, d, J = 8.7 Hz, -NHCO(CH₃)₃), 5.54 (1 H, d, J = 8.9 Hz, -NHCOCH₃), 6.33 (1 H, s, H₂);

¹³C NMR (100.5 MHz, CDCl₃) δ_C: 9.38, 9.62 (-OCH(CH₂CH₃)₂), 23.43 (-NHCOCH₃), 25.88, 26.26 (-OCH(CH₂CH₃)₂), 28.47 (-NHCO(CH₃)₂), 45.13 (C₆), 50.60 (C₅), 53.28 (C₄), 77.67 (C₃), 79.80 (-NHCO(CH₃)₂), 82.14 (-OCH(CH₂CH₃)₂), 94.92 (C₁), 138.14 (C₂), 156.12 (-NHCO(CH₃)₂), 170.95 (-NHCOCH₃).

HR-ESI-MS (m/z) calculated for C₁₈H₃₁N₂O₄ [M+Na]⁺ 489.1221, found 489.1218.

Dimethyl (3*R*,4*R*,5*S*)-4-acetamido-5-*N*-*tert*-Butoxycarbonyl-amino-3-(1-ethylpropoxy)-1-cyclohexene-1-phosphonate (34**)**



Under an atmosphere of dry nitrogen, tetrakis(triphenylphosphine) palladium (230 mg, 0.2 mmol) and vinyl iodide **33** (620 mg, 1.33 mmol) were dissolved in anhydrous toluene (10 mL). Triethylamine (0.74 mL, 5.32 mmol) and dimethylphosphite (0.49 mL, 5.32 mmol) were added to the solution and the mixture was stirred at 80 °C for 90 minutes. After cooling to room temperature, the reaction was quenched by addition of saturated aqueous NH₄Cl (10 mL). DCM (50 mL) was added and the organic phase was extracted with NH₄Cl (10 mL), washed with brine (2x10 mL), dried over MgSO₄ and evaporated. Purification by flash chromatography (EA:MeOH; 1:0 → 5:1) gave the

desired vinyl phosphonate **34** (475 mg, 80%) a white glassy solid. R_f : 0.42 (EA:MeOH; 6:1).

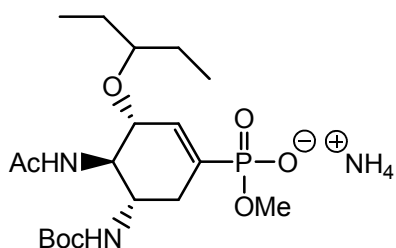
^1H NMR (500 MHz, CDCl_3) δ_{H} : 0.86 (6 H, m, $-\text{OCH}(\text{CH}_2\text{CH}_3)_2$), 1.40 (9 H, s, $-\text{NHCO}(\text{CH}_3)_3$), 1.48 (4 H, m, $-\text{OCH}(\text{CH}_2\text{CH}_3)_2$), 1.97 (3 H, s, $-\text{NHCOCH}_3$), 2.21 (1 H, m, $\text{H}_{6\text{ax}}$), 2.58 (1 H, m, $\text{H}_{6\text{eq}}$), 3.34 (1 H, p, $J = 5.1, 5.9$ Hz, $-\text{OCH}(\text{CH}_2\text{CH}_3)_2$), 3.70 (6 H, 2d, $J = 10.9$ Hz, $\text{P}-\text{OCH}_3$), 3.78 (1 H, m, H_5), 3.93 (1 H, s, H_3), 4.05 (1 H, dd, $J = 8.8, 17.9$ Hz, H_4), 5.21 (1 H, d, $J = 8.5$ Hz, $-\text{NHCOCH}_3$), 6.08 (1 H, d, $J = 8.4$ Hz, $-\text{NHCO}(\text{CH}_3)_3$), 6.59 (1 H, d, $J_{\text{P-2}} = 21.8$ Hz, H_2);

^{13}C NMR (100.5 MHz, CDCl_3) δ_{C} : 9.27, 9.64 ($-\text{OCH}(\text{CH}_2\text{CH}_3)_2$), 23.38 ($-\text{NHCOCH}_3$), 25.71, 26.22 ($-\text{OCH}(\text{CH}_2\text{CH}_3)_2$), 28.45 ($-\text{NHCO}(\text{CH}_3)_2$), ~ 31.2 (d, $J = 9.6$ Hz, C6), 49.21, 49.32 (C5), ~ 52.7 (m, $-\text{P}(\text{OCH}_3)_2$), 54.37 (C4), ~ 76.1 (m, C3), 79.78 ($-\text{NHCO}(\text{CH}_3)_2$), 82.28 ($-\text{OCH}(\text{CH}_2\text{CH}_3)_2$), ~ 126.5 (d, $J = 182$ Hz, C1), ~ 142.4 (d, $J = 7.8$ Hz, C2), 156.34 ($-\text{NHCO}(\text{CH}_3)_2$), 171.08 ($-\text{NHCOCH}_3$);

^{31}P NMR (161.7 MHz, CDCl_3) δ_{P} : 19.59 (s).

HR-ESI-MS (m/z) calculated for $\text{C}_{20}\text{H}_{37}\text{N}_2\text{O}_7\text{P}$ $[\text{M}+\text{Na}]^+$ 471.2231, found 471.2237.

Ammonium (Methyl [(3*R*,4*R*,5*S*)-4-acetamido-5-*N*-*tert*-Butoxycarbonyl-amino-3-(1-ethylpropoxy)-1-cyclohexene]-1-phosphonic acid]) (35)



Dimethyl phosphonate **34** (100 mg, 0.22 mmol) was dissolved in dioxane (2 mL), NaOH solution (0.25 M, 2 mL) was added and the mixture was stirred overnight at room temperature, neutralised with Amberlite IR-120 ion-exchange resin (H^+) and lyophilised. Purification by flash chromatography (EA:MeOH; 6:1 \rightarrow 1:2) yielded phosphonic acid compound **35** as a white powder after gel permeation chromatography and subsequent lyophilisation (93 mg, 96%). R_f : 0.29 (DCM:MeOH, 2:1).

^1H NMR (500 MHz, D_2O) δ_{H} : 0.91 (3 H, t, $J = 7.1$ Hz, $-\text{OCH}(\text{CH}_2\text{CH}_3)_2$), 0.97 (3 H, t, $J = 6.8$ Hz, $-\text{OCH}(\text{CH}_2\text{CH}_3)_2$), 1.50 (3 H, s, $-\text{NHCO}(\text{CH}_3)_3$), 1.63 (4 H, m, $-\text{OCH}(\text{CH}_2\text{CH}_3)_2$), 2.09 (3 H, s, $-\text{NHCOCH}_3$), 2.30 (1 H, dd, $J = 11.7, 13.5$ Hz, $\text{H}_{6\text{ax}}$), 2.62 (1 H, m, $\text{H}_{6\text{eq}}$), 3.55 – 3.62 (1 H, bm, $-\text{OCH}(\text{CH}_2\text{CH}_3)_2$), 3.58 (3 H, d, $J = 10.8$ Hz,

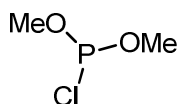
P-OCH₃), 3.81 (1 H, m, H₅), 3.89 (1 H, dd, J = 9.2, 10.5 Hz, H₄), 4.31 (1 H, bm, H₃), 6.38 (1 H, d, J_{P-2} = 19.7 Hz, H₂);

¹³C NMR (100.5 MHz, D₂O) δ_C: 8.57, 8.67, -OCH(CH₂CH₃)₂, 22.25 (-NHCOCH₃), 25.34, 25.66 (-OCH(CH₂CH₃)₂), 27.62 (-NHCO(CH₃)₂), 31.24 (d, J = 9.6 Hz, C₆), 49.32 (d, J = 14.1 Hz, C₅), 51.68 (d, J = 5.0 Hz, -P(OCH₃)₂), 55.60 (C₄), 76.80 (m, C₃), 80.97 (-NHCO(CH₃)₂), 84.13 (-OCH(CH₂CH₃)₂), ~131.1 (d, J = 172 Hz, C₁), 136.91 (m, C₂), 157.58 (-NHCO(CH₃)₂), 174.18 (-NHCOCH₃);

³¹P NMR (161.7 MHz, D₂O) δ_P: 15.23 (s).

HR-ESI-MS (m/z) calculated for C₁₉H₃₅N₂O₇P [M+(2Na-H)]⁺ 479.1894, found 479.1917.

Chloro(dimethyl)phosphine (36)

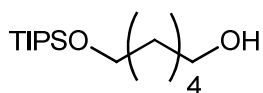


Under an atmosphere of nitrogen, P(OMe)₃ (16.2 mL, 137 mmol) was added dropwise to PCl₃ (6 mL, 68.6 mmol) at 0 °C. The colourless solution turned slightly orange as soon as the mixture was heated up gradually to 90 °C. The mixture was stirred at 90 °C for 1 hour and 30 min. The residue was then distilled under reduced pressure (34 °C, 42 Torr).

¹H NMR (500 MHz, CDCl₃) δ_H: 3.70 (6 H, d, J = 10.9 Hz);

³¹P NMR (161.7 MHz, CDCl₃) δ_P: 169.46 (s) (+ small impurity at 181.02 (s)).

O-Triisopropylsilylhexane-1,6-diol (37)



1,6-Hexanediol (2 g, 0.0169 mmol) and imidazole (3.46 g, 0.0507 mmol) were dried *in vacuo* in a round-bottomed flask for 1 hour, then placed under an N₂ (g) atmosphere. Dry DCM (7 mL) was added and the resulting suspension was briefly sonicated. The suspension was cooled to 0 °C (ice-bath) and TIPSCI (4.4 mL, 0.0253 mmol) was then added dropwise. Once TLC had indicated that the reaction was no longer progressing, the solvent was evaporated to dryness and the crude product was purified by column

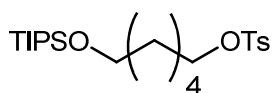
chromatography (Tol/EA; 1:0 → 10:1) to give compound **37** as a clear oil (1.82 g, 40%).
 R_f : 0.23 (Tol/EA; 10:1).

^1H NMR (500 MHz, CDCl_3) δ_{H} : 1.02 – 1.11 (21 H, m, $-\text{Si}(\underline{\text{C}}\text{H}(\text{CH}_3)_2)_3$, $-\text{Si}(\text{CH}(\underline{\text{C}}\text{H}_3)_2)_3$),
 1.38 (4 H, m, $-\text{CH}_2\text{CH}_2\text{CH}_2\text{CH}_2\text{OSi}-$), 1.57 (4 H, m, $\text{HOCH}_2\text{CH}_2\text{CH}_2\text{CH}_2\text{CH}_2\text{CH}_2\text{O}-$),
 3.62 – 3.70 (4 H, m, HOCH_2- , $-\text{CH}_2\text{OSi}-$);

^{13}C NMR (125.7 MHz, CDCl_3) δ_{C} : 12.21 ($-\text{Si}(\underline{\text{C}}\text{H}(\text{CH}_3)_2)_3$), 18.19 ($-\text{Si}(\text{CH}(\underline{\text{C}}\text{H}_3)_2)_3$),
 25.74, 25.82 ($\text{HOCH}_2\text{CH}_2\text{CH}_2\text{CH}_2\text{CH}_2\text{CH}_2\text{O}-$), 32.99, 33.13
 ($\text{HOCH}_2\text{CH}_2\text{CH}_2\text{CH}_2\text{CH}_2\text{CH}_2\text{O}-$), 63.18, 63.51 (HOCH_2- , $-\text{CH}_2\text{OSi}-$).

HR-ESI-MS (m/z) calculated for $\text{C}_{15}\text{H}_{34}\text{O}_2\text{Si}$ $[\text{M}+\text{Na}]^+$ 297.2220, found 297.2218.

***O*-Toluenesulfonyl-*O*-triisopropylsilylhexane-1,6-diol (**38**)**

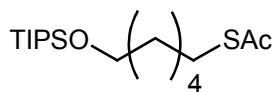


Under an atmosphere of dry nitrogen, alcohol **37** (3.86 g, 14.06 mmol) was dissolved in dry pyridine (12 mL). DMAP (172 mg, 1.41 mmol) and *p*-toluenesulfonyl chloride (4.02 g, 21.09 mmol) were added to the solution and the mixture stirred at 0 °C for 4 hours. The reaction was quenched by addition of saturated aqueous NH_4Cl (5 mL). After evaporation to dryness, the residue was dissolved in DCM (15 mL) which was then extracted with NH_4Cl (5 mL), washed with brine (2 x 5 mL), the organic phase was dried over MgSO_4 and the solvent evaporated. Purification by flash chromatography (cyclohexane/DE; 10:1) gave compound **38** (4.79 g, 80%) as a clear oil. R_f : 0.27 (cyclohexane/DE; 10:1).

^1H NMR (500 MHz, CDCl_3) δ_{H} : 1.00 - 1.10 (21 H, m, $-\text{Si}(\underline{\text{C}}\text{H}(\text{CH}_3)_2)_3$, $-\text{Si}(\text{CH}(\underline{\text{C}}\text{H}_3)_2)_3$),
 1.27 – 1.35 (4 H, m, $\text{HOCH}_2\text{CH}_2\text{CH}_2\text{CH}_2-$), 1.48 (2 H, m, $-\text{CH}_2\text{CH}_2\text{OSi}-$), 1.64 (2 H, m, $-\text{CH}_2\text{CH}_2\text{OTs}$), 2.44 (3 H, s, $\text{H}_3\text{C}-\text{Ph}-$), 3.63 (2 H, t, $J = 6.4$ Hz, $-\text{CH}_2\text{OSi}-$), 4.02 (2 H, t, $J = 6.4, 6.5$ Hz, $\text{Ts}-\text{OCH}_2-$), 7.33 (2 H, d, $J = 8.0$ Hz, H_{Aryl}), 7.78 (2 H, d, $J = 8.1$ Hz, H_{Aryl});

^{13}C NMR (125.7 MHz, CDCl_3) δ_{C} : 12.15 ($-\text{Si}(\underline{\text{C}}\text{H}(\text{CH}_3)_2)_3$), 18.16 ($-\text{Si}(\text{CH}(\underline{\text{C}}\text{H}_3)_2)_3$), 21.73 ($\text{CH}_3-\text{Ph}-$), 25.36, 25.40 ($\text{TsOCH}_2\text{CH}_2\text{CH}_2\text{CH}_2\text{CH}_2\text{CH}_2\text{O}-$), 29.01, 32.86 ($\text{TsOCH}_2\text{CH}_2\text{CH}_2\text{CH}_2\text{CH}_2\text{CH}_2\text{O}-$), 63.31 ($-\text{CH}_2\text{OSi}-$), 70.75 (TsOCH_2-), 128.00, 129.91 (CH_{Aryl}), 133.50, 144.71 (C_{Aryl});

HR-ESI-MS (m/z) calculated for $\text{C}_{22}\text{H}_{40}\text{O}_4\text{SSi}$ $[\text{M}+\text{Na}]^+$ 451.2296, found 451.2309.

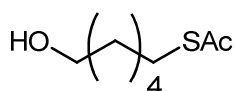
6-Triisopropylsilyloxy-S-acetyl-hexan-1-thiol (39)

Compound **38** (4.792 g, 0.011 mol) was dissolved in pyridine (65 mL) and KSAc (3.83 g, 0.033 mol) was then added to the solution. The mixture was stirred for 5 hours at room temperature. Pyridine was removed under high vacuum and the residue was dissolved in DCM (50 mL). The solution was washed with saturated aqueous NH_4Cl (2x15 mL), NaCl (20 mL), the organic phase was dried over MgSO_4 and the solvent evaporated. Purification by flash chromatography (Tol) afforded compound **39** (3.208 g, 86%) as a clear oil. R_f : 0.46 (Tol).

^1H NMR (500 MHz, CDCl_3) δ_{H} : 1.02 – 1.12 (21 H, s, $-\text{Si}(\text{CH}(\text{CH}_3)_2)_3$), $-\text{Si}(\text{CH}(\text{CH}_3)_2)_3$), 1.37 (4 H, m, $-\text{CH}_2\text{CH}_2\text{CH}_2\text{CH}_2\text{S}-$), 1.50 – 1.62 (4 H, m, $-\text{OCH}_2\text{CH}_2-$, $-\text{SCH}_2\text{CH}_2-$), 2.32 (3 H, s, $-\text{SCOCH}_3$), 2.87 (2 H, t, $J = 6.9, 7.1$ Hz, $-\text{SCH}_2-$), 3.67 (2 H, t, $J = 6.2, 6.3$ Hz, $-\text{OCH}_2-$);

^{13}C NMR (125.7 MHz, CDCl_3) δ_{C} : 12.20 ($-\text{Si}(\text{CH}(\text{CH}_3)_2)_3$), 18.20 ($-\text{Si}(\text{CH}(\text{CH}_3)_2)_3$), 25.56, 28.82 ($-\text{CH}_2\text{CH}_2\text{CH}_2\text{CH}_2\text{S}-$), 29.29 ($-\text{CH}_2\text{S}-$), 29.88 ($-\text{CH}_2\text{CH}_2\text{S}-$), 30.77 ($-\text{SCOCH}_3$), 33.00 ($-\text{CH}_2\text{CH}_2\text{O}-$), 63.47 ($-\text{CH}_2\text{O}-$);

HR-ESI-MS (m/z) calculated for $\text{C}_{17}\text{H}_{36}\text{O}_2\text{SSi}$ $[\text{M}+\text{Na}]^+$ 355.2097, found 355.2091.

6-Hydroxy-S-acetyl-hexan-1-thiol (40)

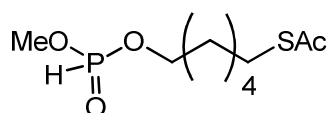
Compound **39** (0.874 g, 2.63 mmol) was dissolved in THF (20 mL), then AcOH (1 mL) and TBAF (3.32 g, 10.51 mmol) were successively added. The mixture was stirred overnight. The solution was washed with saturated aqueous NaHCO_3 (2x15 mL), NaCl (20 mL), the organic phase was dried over MgSO_4 and the solvent evaporated. Purification by flash chromatography (Tol) afforded compound **40** (0.333 g, 72%) as a clear oil. R_f : 0.17 (Tol:EA; 5:1).

^1H NMR (500 MHz, CDCl_3) δ_{H} : 1.33 (4 H, m, $-\text{CH}_2\text{CH}_2\text{CH}_2\text{CH}_2\text{SAc}$), 1.51 (4 H, m, $-\text{OCH}_2\text{CH}_2-$, $-\text{CH}_2\text{CH}_2\text{SAc}$), 2.26 (3 H, s, $-\text{SCOCH}_3$), 2.81 (2 H, t, $J = 7.3$ Hz, $-\text{SCH}_2-$), 3.56 (2 H, t, $J = 6.6$ Hz, $-\text{OCH}_2-$);

^{13}C NMR (125.7 MHz, CDCl_3) δ_{C} : 25.26, 28.53, 29.03, 29.47 ($-\underline{\text{C}}\text{H}_2\underline{\text{C}}\text{H}_2\underline{\text{C}}\text{H}_2\underline{\text{C}}\text{H}_2\text{SAc}$), 30.62 ($-\text{SCO}\underline{\text{C}}\text{H}_3$), 32.53 ($-\text{OCH}_2\underline{\text{C}}\text{H}_2-$), 62.63 ($-\text{O}\underline{\text{C}}\text{H}_2-$), 196.18 ($-\text{SCO}\underline{\text{C}}\text{H}_3$).

HR-ESI-MS (m/z) calculated for $\text{C}_8\text{H}_{16}\text{O}_2\text{S}$ $[\text{M}+\text{Na}]^+$ 199.0763, found 199.0768.

O-methyl O-(6-Acetylthiohex-1-yl) phosphonic acid (41)



Under an atmosphere of nitrogen, compound **40** (333 mg, 1.89 mmol) was dissolved in dry DCM (5 mL) at 0°C . DIPEA (0.99 mL, 5.67 mmol) was added to the solution. Chloro(dimethyl)phosphine **36** (0.6 mL) was added dropwise, the reaction mixture was allowed to come up to room temperature and stirred overnight. Solid NaHCO_3 (one spatula) was added to the reaction mixture, followed by MeOH (2 mL) and silica (a few spatulas). The mixture was evaporated to dryness. Purification by flash chromatography (Tol:EA ; 5:1 \rightarrow 1:3) gave compound **41** (208 mg, 41%) as a yellowish liquid/oil. R_f : 0.15 (Tol:EA; 1:1).

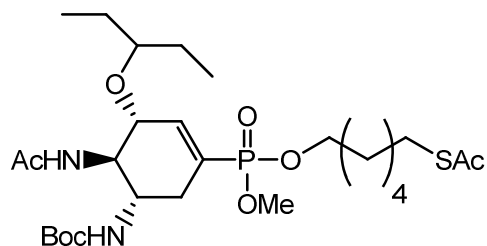
^1H NMR (500 MHz, CDCl_3) δ_{H} : 1.38 – 1.43 (4 H, m, $-\underline{\text{C}}\text{H}_2\underline{\text{C}}\text{H}_2\underline{\text{C}}\text{H}_2\underline{\text{C}}\text{H}_2\text{SAc}$), 1.55 – 1.62 (2 H, m, $-\underline{\text{C}}\text{H}_2\underline{\text{C}}\text{H}_2\text{SAc}$), 1.66 – 1.73 (2 H, m, $-\text{POCH}_2\underline{\text{C}}\text{H}_2-$), 2.32 (3 H, s, $-\text{SCO}\underline{\text{C}}\text{H}_3$), 2.87 (2 H, t, $J = 7.3$ Hz, $-\text{CH}_2\underline{\text{C}}\text{H}_2\text{SAc}$), 3.77 (3 H, d, $J = 11.9$ Hz, $\text{P}-\text{O}\underline{\text{C}}\text{H}_3$), 4.03 – 4.11 (2 H, m, $-\text{O}\underline{\text{C}}\text{H}_2\underline{\text{C}}\text{H}_2-$), ~ 6.78 (1 H, d, $J = 695$ Hz, $\text{P}-\underline{\text{H}}$);

^{13}C NMR (125.7 MHz, CDCl_3) δ_{C} : 25.10, 25.16, 28.34, 38.38 ($-\underline{\text{C}}\text{H}_2\underline{\text{C}}\text{H}_2\underline{\text{C}}\text{H}_2\underline{\text{C}}\text{H}_2\text{SAc}$), 29.07 ($-\underline{\text{C}}\text{H}_2\text{SAc}$), 29.52 ($-\underline{\text{C}}\text{H}_2\underline{\text{C}}\text{H}_2\text{SAc}$), ~ 30.4 (d, $J = 6.1$ Hz, $-\text{OCH}_2\underline{\text{C}}\text{H}_2-$), 30.76 ($-\text{SCO}\underline{\text{C}}\text{H}_3$), ~ 52.1 (d, $J = 5.7$ Hz, $\text{P}-\text{O}\underline{\text{C}}\text{H}_3$), ~ 54.3 (d, $J = 5.8$ Hz, $\text{P}-\text{O}\underline{\text{C}}\text{H}_3$), ~ 65.8 (d, $J = 6.1$ Hz, $-\text{O}\underline{\text{C}}\text{H}_2\underline{\text{C}}\text{H}_2-$), ~ 67.9 (d, $J = 6.0$ Hz, $-\text{O}\underline{\text{C}}\text{H}_2\underline{\text{C}}\text{H}_2-$), 195.98 ($-\text{SCO}\underline{\text{C}}\text{H}_3$);

^{31}P NMR (161.7 MHz, CDCl_3) δ_{P} : 9.08.

HR-ESI-MS (m/z) calculated for $\text{C}_9\text{H}_{19}\text{O}_4\text{PS}$ $[\text{M}+\text{Na}]^+$ 277.0634, found 277.0631.

(6'-Acetylthiohex-1'-yl) methyl [(3*R*,4*R*,5*S*)-4-acetamido-5-(1,1-dimethylethyloxycarbonylamino)-3-(1-ethylpropoxy)-1-cyclohexene-1-phosphonate] (**42**)



Palladium-mediated coupling

Tetrakis(triphenylphosphine) palladium (14 mg, 0.012 mmol) and vinyl iodide **32** (37 mg, 0.078 mmol) were added to the phosphinic acid **41** under an atmosphere of dry nitrogen. The mixture was dissolved in anhydrous toluene (3 mL) followed by the addition of triethylamine (8.8 μ L, 0.063 mmol). The mixture was heated to 80 °C, stirred and maintained at this temperature for 3 hours. After cooling to room temperature, the reaction was quenched by addition of saturated aqueous NH_4Cl (3 mL). DCM (15 mL) was added to the solution which was then extracted with NH_4Cl (3 mL), washed with brine (2x3 mL), the organic phase was dried over MgSO_4 and the solvent evaporated. Purification by flash chromatography (EA:MeOH ; 1:0 \rightarrow 5:1) gave the desired vinyl phosphonate **42** (17 mg, 0.0287 mmol, 52%). R_f : 0.51 (EA).

Alkylation strategy

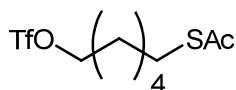
Compound **43** (49 mg, 0.177 mmol) was placed under an N_2 (g) atmosphere and dry acetonitrile (1.5 mL) was added. Compound **35** (70 mg, 0.131 mmol), previously lyophilised with NEt_3 (1 eq.) was then quickly added to the stirring solution. After stirring overnight, TLC analysis indicated the reaction had not progressed any further and that triflate **43** had degraded in solution. The solvent was evaporated *in vacuo* and the residue was directly purified by flash chromatography (Tol:EA; 1:1 \rightarrow EA \rightarrow EA:MeOH; 5:1 \rightarrow MeOH) to give compound **42** (31 mg, 71% based on recovered starting material). R_f : 0.51 (EA).

^1H NMR (500 MHz, CDCl_3) δ_{H} : 0.86 (6 H, m, $-\text{OCH}(\text{CH}_2\text{CH}_3)_2$), 1.37 (4 H, m, $-\text{CH}_2\text{CH}_2\text{CH}_2\text{CH}_2\text{S}-$), 1.40 (9 H, s, $-\text{NHCO}(\text{CH}_3)_3$), 1.48 (4 H, m, $-\text{OCH}(\text{CH}_2\text{CH}_3)_2$), 1.56 (2 H, m, $-\text{SCH}_2\text{CH}_2-$), 1.64 (2 H, m, $-\text{OCH}_2\text{CH}_2-$), 1.96 (3 H, s, $-\text{NHCOCH}_3$), 2.20 (1 H, m, $\text{H}_{6\text{ax}}$), 2.30 (3 H, m, $-\text{SCOCH}_3$), 2.59 (1 H, m, $\text{H}_{6\text{eq}}$), 2.85 (2 H, dd, $J = 1.4, 7.8$ Hz, $-\text{SCH}_2-$), 3.33 (1 H, m, $-\text{OCH}(\text{CH}_2\text{CH}_3)_2$), 3.68 (3 H, 2d, $J = 11.0$ Hz, $\text{P}-\text{OCH}_3$), 3.78 (1 H,

m, H₅), 3.88 – 4.09 (4 H, m, -OCH₂-, H₃, H₄), 5.16 (1 H, dd, J = 8.8, 9.3 Hz, -NHCOCH₃), 5.88 (1 H, d, J = 9.2 Hz, -NHCOCH₃), 6.58 (1 H, d, J_{P-2} = 22.1 Hz, H₂);
¹³C NMR (100.5 MHz, CDCl₃) δ_C: 9.25, 9.67 (-OCH(CH₂CH₃)₂), 23.45 (-NHCOCH₃), 25.16, 26.22 (-CH₂CH₂CH₂CH₂S-), 25.70 (-OCH(CH₂CH₃)₂), 28.32, 28.35, 28.45 (-NHCOCH₃), 29.02, 29.05 (-SCH₂-), 29.49 (-SCH₂CH₂-), 30.38 (m, -OCH₂CH₂-), 30.74 (-SCOCH₃), ~31.31 (m, C₆), ~49.29 (m, C₅), 52.54, 52.64 (2d, J = 5.3, 5.8 Hz, P-OCH₃), 54.55 (m, C₄), ~66.10 (2d, J = 5.8, 6.1 Hz, P-OCH₃), ~76.32 (m, C₃), 79.89 (-NHCOCH₃), 82.27 (-OCH(CH₂CH₃)₂), ~126.93 (d, J_{P-1} = 182 Hz, C₁), 142.15 (m, C₂), 156.36, 156.41 (-NHCOCH₃), 174.91 (-NHCOCH₃), 196.14 (-SCOCH₃);
³¹P NMR (161.7 MHz, CDCl₃) δ_P: 18.28 (s).

HR-ESI-MS (m/z) calculated for C₂₇H₄₉N₂O₈PS [M+Na]⁺ 615.2839, found 615.2837.

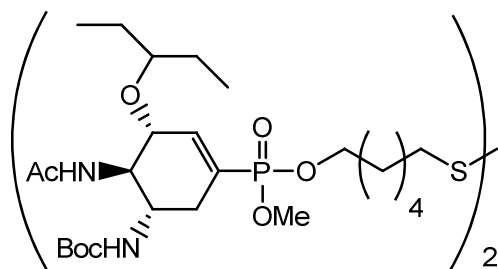
6-Trifluoromethanesulfonyloxy-S-acetyl-hexan-1-thiol (**43**)



Compound **40** (77 mg, 0.437 mmol) was placed under an N₂ (g) atmosphere and suspended in dry DCM (1mL). Lutidine (94 μL, 0.874 mmol) was then added and the solution was cooled to -60 °C. Triflic anhydride (96 μL, 0.568 mmol) was added to dry DCM (1mL), cooled to -60 °C for a few minutes and then added dropwise to the stirring solution of compound **40**. The reaction was stirred at this temperature for 45 minutes by which time the reaction was complete. The DCM solution was then poured into a separating funnel containing cold saturated KH₂PO₄ (aq.) and washed. The organic layer was separated, dried over MgSO₄ and the solvent evaporated (no heating). The crude material was then passed over a short silica plug (DCM). The solvent was evaporated *in vacuo* giving triflate **43** as a yellowish oil (135 mg, 67 %). R_f : 0.64 (cyclohexane:DE; 1:1). The compound was used without further characterisation.

¹H NMR (500 MHz, CDCl₃) δ_H: 1.37 – 1.49 (4 H, m, -OCH₂CH₂CH₂CH₂CH₂CH₂S-), 1.59 (2 H, m, -CH₂CH₂S-), 1.83 (2 H, m, -OCH₂CH₂-), 2.32 (3 H, s, -SCOCH₃), 2.86 (2 H, t, J = 7.0, 7.6 Hz), 4.52 (2 H, t, J = 6.4, 6.5 Hz).

6',6'-Dithiobis (hex-1'-yl methyl [(3*R*,4*R*,5*S*)-4-acetamido-5-(1,1-dimethylethoxy)carbonylamino]-3-(1-ethylpropoxy)-1-cyclohexene-1-phosphonate]) (44)



Compound **42** (28 mg, 0.0472 mmol) was placed under an O₂ (g) atmosphere and was dissolved in anhydrous MeOH (3.5 mL). A methanolic NaOMe solution (~350 μL, 0.1M) was then added dropwise to the stirring solution of compound **42**, ensuring that the O₂ (g) was bubbling through the solution and that indicator paper indicated a pH ~10. After stirring overnight, the solvent was evaporated *in vacuo* and the residue was directly purified by flash chromatography (EA:MeOH; 10:1) to give compound **44** (16 mg, 60%). R_f: 0.71 (EA:MeOH; 5:1).

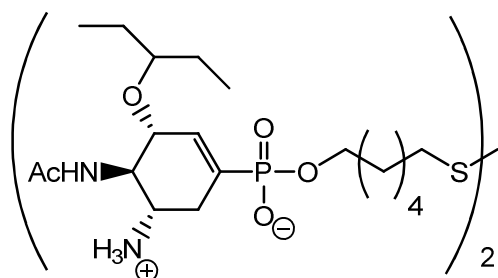
¹H NMR (500 MHz, CDCl₃) δ_H: 0.88 (m, 6H, -OCH(CH₂CH₃)₂), 1.42 (s, 13H, (-NHCO(CH₃)₃), -OCH₂CH₂CH₂CH₂CH₂CH₂S-), 1.46 – 1.55 (m, 4H, -OCH(CH₂CH₃)₂), 1.64 – 1.73 (m, 4H, -OCH₂CH₂-, -SCH₂CH₂-), 1.98 (s, 3H, -NHCOCH₃), 2.22 (m, 1H, H_{6ax}), 2.60 (m, 1H, H_{6eq}), 2.68 (dd, 2H, J = 7.2, 7.5 Hz, -CH₂-SAc), 3.34 (m, 1H, -OCH(CH₂CH₃)₂), 3.70 (d, 3H, J = 10.9 Hz, P-OCH₃), 3.80 (m, 1H, H₅), 3.93 (m, 1H, H₇), 4.02 (m, 3H, H₄, -OCH₂-), 5.10 - 5.25 (m, 1H, -NH COCH₃), 5.82 - 5.94 (m, 1H, -NHCOCH₃), 6.60 (d, 1H, J_{P-2} = 21.8 Hz, H₂).

¹³C NMR (100.5 MHz, CDCl₃) δ_C: 9.29, 9.73 (-OCH(CH₂CH₃)₂), 23.52 (-NHCOCH₃), 25.31, 25.72, 26.34 (-OCH(CH₂CH₃)₂), -OCH₂CH₂CH₂CH₂CH₂S-, 28.13, 28.48 29.15 (-NHCO(CH₃)₃), 30.50 (m, -OCH₂CH₂-, -SCH₂CH₂-), ~31.37 (m, C₆), 39.04, 39.10 (-CH₂S-), 49.31 (C₅), 52.67 (2d, J = 5.5, 5.5 Hz, P-OCH₃), 54.64 (C₄), 66.13 (m, -OCH₂-), 76.36 (m, C₃), 79.86 (-NHCO(CH₃)₃), 82.33 (-OCH(CH₂CH₃)₂), ~ 126.87 (d, J_{P-1} = 182 Hz, C₁), 142.23 (m, C₂), 156.44 (-NHCO(CH₃)₃), 171.00 (-NHCOCH₃).

³¹P NMR (161.7 MHz, CDCl₃) δ_P: 18.28 (s), 18.32 (s).

HR-ESI-MS (m/z) calculated for C₅₀H₉₂N₄O₁₄P₂S₂ [M+Na]⁺ 1121.5419, found 1121.5437.

6',6'-Dithiobis (hex-1'-yl [(3*R*,4*R*,5*S*)-4-acetamido-5-amino-3-(1-ethylpropoxy)-1-cyclohexene-1-phosphonic acid]) (45)



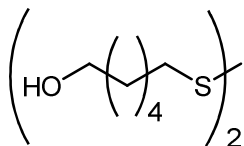
Compound **44** (8.2 mg, 0.00746 mmol) and NaI (4.9 mg, 0.0328 mmol) was placed under an N₂ (g) atmosphere in a reflux condenser and dissolved in dry acetone (1.5mL). The solution was heated to reflux for 8 hour periods over 3 days, with the addition of a further 2 portions of NaI (4.9 mg, 0.0328 mmol) and acetone to maintain the original volume. Once TLC analysis confirmed the reaction was complete, the solvent was evaporate *in vacuo* and the residue was purified by flash chromatography (EA:MeOH; 5:1 → 2:1 → 1:1 → MeOH) to yield the desired demethylated intermediate (6.5 mg, 80%). The residue was then treated with dioxane (0.5 mL) and 50% TFA/H₂O (0.5 mL) for 36 hours. The solvent was then evaporated *in vacuo* and the residue was purified by gel permeation chromatography to afford compound **45** (5.7 mg, 90%).

¹H NMR (500 MHz, D₂O) δ_H: 0.92 (6 H, 2t, J = 7.1, 7.3 Hz, -OCH(CH₂CH₃)₂), 1.38 – 1.53 (4 H, m, -CH₂CH₂CH₂CH₂S-), 1.54 – 1.62 (4 H, m, -OCH(CH₂CH₃)₂), 1.67 (2 H, m, -OCH₂CH₂-), 1.73 (2 H, m, -SCH₂CH₂-), 2.11 (3 H, s, -NHCOCH₃), 2.48 (1 H, dd, J = 12.0, 13.3 Hz, H_{6ax}), 2.78 (1 H, dd, J = 7.0, 7.0 Hz, -SCH₂-), 2.77 – 2.84 (1 H, m, H_{6eq}), 3.50 – 3.60 (2 H, m, H₅, -OCH(CH₂CH₃)₂), 3.85 (2 H, m, -OCH₂-), 4.04 (1 H, dd, J = 10.0, 10.2 Hz, H₄), 4.28 (1 H, d, J = 6.9 Hz, H₃), 6.30 (1 H, d, J_{P-2} = 19.3 Hz, H₂);

¹³C NMR (150.8 MHz, D₂O) δ_C: 8.63, 8.91 (-OCH(CH₂CH₃)₂), 22.36 (-NHCOCH₃), 24.91, 25.26, 25.70, 27.57 (-CH₂CH₂CH₂CH₂S-, -OCH(CH₂CH₃)₂), 28.50 (-SCH₂CH₂-), 29.55 (m, C₆), ~30.00 (d, J = 6.7 Hz, -OCH₂CH₂-), 38.38 (-SCH₂-), ~49.59 (d, J = 14.7 Hz, C₅), 53.24 (C₄), 65.27 (-OCH₂-), ~75.89 (1 H, d, J = 18.2 Hz, C₃), 83.71 (-OCH(CH₂CH₃)₂), ~130.43 (1 H, d, J_{P-1} = 173 Hz, C₁), 135.17 (m, C₂), 174.91 (-NHCOCH₃);

³¹P NMR (242.7 MHz, D₂O) δ_P: 12.33 (s).

HR-ESI-MS (m/z) calculated for C₃₈H₇₂N₄O₁₀P₂S₂ [M+Na]⁺ 893.4057, found 893.4084.

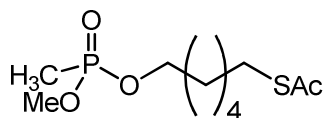
6',6'-Dithiobis (hex-1'-anol) (46)

Compound **40** (35mg, 0.198 mmol) was placed under an O₂ (g) atmosphere and was dissolved in anhydrous MeOH (3.0 mL). A methanolic NaOMe solution (~350 μL, 0.1M) was then added dropwise to the stirring solution of compound **40**, ensuring that O₂ (g) was bubbling through the solution and that indicator paper indicated pH ~10. After stirring overnight, the reaction had not reached completion. However, the solvent was evaporated *in vacuo* and the residue was directly purified by flash chromatography (DE:cyclohexane; 3:1 → 10:1) to give compound **46** (16 mg, 40%). R_f : 0.15 (DE:cyclohexane; 3:1).

¹H NMR (500 MHz, CDCl₃) δ_H: 1.37 (4 H, m, -CH₂CH₂CH₂CH₂S-), 1.53 (2 H, dd, J = 6.7, 13.4 Hz, -OCH₂CH₂-), 1.65 (2 H, dd, J = 7.1, 14.3 Hz, -SCH₂CH₂-), 1.86 (1 H, bs, -OH), 2.65 (2 H, dd, J = 6.7, 7.6 Hz, -S-CH₂-), 3.59 (2 H, dd, J = 6.2, 6.2 Hz, -OCH₂-).

¹³C NMR (125.7 MHz, CDCl₃) δ_C: 25.55, 28.42 (-CH₂CH₂CH₂CH₂S-), 29.30 (-SCH₂CH₂-), 32.72 (-OCH₂CH₂-), 39.23 (-SCH₂-), 62.91 (-OCH₂-).

HR-ESI-MS (m/z) calculated for : C₁₂H₂₆O₂S₂ [M+Na]⁺ 289.1266. Found: 289.1247.

(6-Acetylthio-hexy-1-yl) methyl (methylphosphonate) (47)

Compound **40** (112 mg, 0.635 mmol) was placed under an N₂ (g) atmosphere. Dry DCM (5 mL) was added followed by dry DIPEA (221 μL, 1.27 mmol). The resulting solution was cooled to -15 °C (ice/salt bath) and methyl methylphosphonochloridate (82 μL, 0.825 mmol) was added dropwise. The reaction was allowed to warm to room temperature over the course of 3 hours after which time TLC analysis confirmed the completion of the reaction. MeOH (2 mL) was then added and the solution was stirred for a further 10 minutes. The solvent was removed under vacuum and the crude product was purified directly by flash chromatography (EA) to give compound **47** as an oil (135 mg, 79%).

R_f: 0.31 (EA).

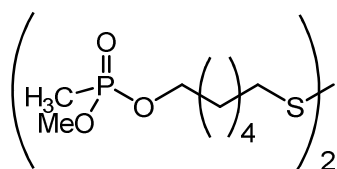
¹H NMR (500 MHz, CDCl₃) δ_H: 1.37 (4 H, m, -CH₂CH₂CH₂CH₂SAc), 1.44 (3 H, d, J = 17.5 Hz, P-CH₃), 1.55 (2 H, m, -SCH₂CH₂-), 1.64 (2 H, m, -OCH₂CH₂-), 2.29 (3 H, s, -SCOCH₃), 2.83 (3 H, t, J = 7.3 Hz, -SCH₂-), 3.69 (3 H, d, J = 11.0 Hz, P-OCH₃), 3.98 (2 H, m, -OCH₂-);

¹³C NMR (125.7 MHz, CDCl₃) δ_C: ~10.53 (d, J = 144 Hz, P-CH₃), 25.15, 28.36 (-CH₂CH₂CH₂CH₂SAc), 29.04 (-CH₂S-), 29.49 (-CH₂CH₂S-), ~30.43 (d, J = 6.2 Hz, -OCH₂CH₂-), 30.70 (-SCOCH₃), ~52.15 (d, J = 6.4 Hz, P-OCH₃), ~65.58 (d, J = 6.4 Hz, -OCH₂-), 195.92 (-SCOCH₃);

³¹P NMR (161.7 MHz, CDCl₃) δ_P: 31.81

HR-ESI-MS (m/z) calculated for C₁₀H₂₁O₄PS [M+Na]⁺ 291.0790, found 291.0787.

6',6'-Dithiobis (hex-1'-yl methyl methylphosphonate) (**48**)



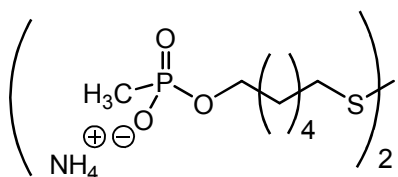
Compound **47** (41 mg, 0.155 mmol) was placed under an O₂ (g) atmosphere and was dissolved in anhydrous MeOH (1.5mL). A methanolic NaOMe solution (1.55 mL, 0.1 M) was then added dropwise to the stirring solution of compound **47**, ensuring that the O₂ (g) was bubbling through the solution and that indicator paper indicated a pH ~10. After stirring overnight, the solvent was evaporated *in vacuo* and the residue was directly purified by flash chromatography (EA:MeOH; 10:1) to give compound **48** as an oil (32 mg, 80%). R_f: 0.13 (EA:MeOH; 10:1).

¹H NMR (500 MHz, CDCl₃) δ_H: 1.38 – 1.46 (8 H, m, -CH₂CH₂CH₂CH₂S-), 1.47 (6 H, d, J = 17.5 Hz, P-CH₃), 1.69 (8 H, m, -OCH₂CH₂CH₂CH₂CH₂CH₂S-), 2.67 (4 H, t, J = 7.4 Hz, -SCH₂-), 3.72 (6 H, d, J = 11.1 Hz, P-OCH₃), 4.02 (4 H, m, -OCH₂-);

¹³C NMR (125.7 MHz, CDCl₃) δ_C: ~10.59 (d, J = 144 Hz, P-CH₃), 25.34, 28.16 (-OCH₂CH₂-CH₂CH₂-CH₂CH₂S-), 29.18 (-CH₂CH₂S-), ~30.54 (d, J = 6.2 Hz, -OCH₂CH₂-), 39.03 (-CH₂S-), ~52.22 (d, J = 6.3 Hz, P-OCH₃), ~65.67 (d, J = 6.5 Hz, -OCH₂-);

³¹P NMR (161.7 MHz, CDCl₃) δ_P: 31.87 (s).

HR-ESI-MS (m/z) calculated for C₁₆H₃₆O₆P₂S₂ [M+Na]⁺ 473.1321, found 473.1325.

6',6'-Dithiobis (ammonium [hex-1'-yl methyl methylphosphonate]) (49)

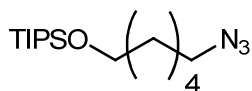
Compound **48** (80 mg, 0.178 mmol) and sodium iodide (269 mg, 1.78 mmol) were dried under vacuum in the absence of light for 20 minutes and then placed under an N₂ (g) atmosphere. Dry acetone (2 mL) was then added to the reaction flask followed by ultrasonication. The solution was then refluxed over 48 hours by which time TLC had indicated the absence of starting material and the formation of a new baseline spot. The solvent was removed under vacuum and purified by flash chromatography (EA:MeOH; 5:1 → MeOH) to give compound **49** as a white solid after subsequent gel permeation chromatography and lyophilisation (60 mg, 80%). R_f: 0.26 (EA/MeOH; 1:1).

¹H NMR (500 MHz, MeOH-D₄) δ_H: 1.22 (6 H, d, J = 16.4 Hz, P-CH₃), 1.43 (8 H, m, -CH₂CH₂CH₂CH₂S-), 1.62 (4 H, tt, J = 6.4, 7.0 Hz, -OCH₂CH₂-), 1.69 (4 H, p, J = 7.0 Hz, -CH₂CH₂S-), 2.69 (4 H, t, J = 7.1, 7.3 Hz, -CH₂S-), 3.83 (4 H, dt, J = 6.5, 6.5 Hz, -OCH₂-);

¹³C NMR (100.5 MHz, MeOH-D₄) δ_C: ~12.43 (d, J = 137 Hz, P-CH₃), 26.59, 29.22 (-CH₂CH₂-CH₂CH₂S-), 30.20 (-CH₂-CH₂S-), ~31.98 (d, J = 6.8 Hz, -OCH₂CH₂-), 39.63 (-CH₂S-), ~64.88 (d, J = 5.6 Hz, -OCH₂-);

³¹P NMR (161.7 MHz, MeOH-D₄) δ_P: 24.19 (s).

HR-ESI-MS (m/z) calculated for C₁₄H₃₂O₆P₂S₂ [M+3Na]⁺ 489.0647, found 489.0645.

6-Azido-O-triisopropylsilylhexane-1-ol (50)

Compound **38** (59 mg, 0.138 mmol) was placed under an N₂ (g) atmosphere and dissolved in DMF (1.0 mL). The solution was cooled to 0 °C and NaN₃ (27 mg, 0.414 mmol) was then quickly added. The solution was stirred for 4 hours at which time the reaction was complete. The DMF was evaporated *in vacuo* and the resulting residue was suspended in DCM and washed with cold H₂O, semi-saturated NH₄Cl (aq.) and

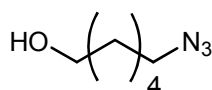
brine. The organic phase was dried over MgSO_4 and purified by flash chromatography to give azide **50** as an oily liquid (35 mg, 84%). R_f : 0.84 (DE:cyclohexane; 1:10).

^1H NMR (500 MHz, CDCl_3) δ_{H} : 1.03, 1.04 (21 H, 2s, $-\text{Si}(\text{CH}(\text{CH}_3)_2)_3$), 1.38 (4 H, m, $-\text{CH}_2\text{CH}_2\text{CH}_2\text{CH}_2\text{N}_3$), 1.53 (2 H, m, $-\text{OCH}_2\text{CH}_2-$), 1.60 (2 H, m, $\text{N}_3\text{CH}_2\text{CH}_2-$), 3.24 (2 H, t, $J = 7.0$ Hz, N_3CH_2-), 3.66 (2 H, t, 6.4 Hz, $-\text{OCH}_2-$);

^{13}C NMR (125.7 MHz, CDCl_3) δ_{C} : 12.27, 18.25 $-\text{Si}(\text{CH}(\text{CH}_3)_2)_3$, 25.67 ($-\text{CH}_2\text{CH}_2\text{CH}_2\text{CH}_2\text{N}_3$), 26.80 ($-\text{Si}(\text{CH}(\text{CH}_3)_2)_3$), 29.09 ($\text{N}_3\text{CH}_2\text{CH}_2-$), 33.05 ($-\text{OCH}_2\text{CH}_2-$), 51.69 (N_3CH_2-), 63.46 ($-\text{OCH}_2-$);

HR-ESI-MS (m/z) calculated for $\text{C}_{15}\text{H}_{33}\text{N}_3\text{OSi}$ [$\text{M}+\text{Na}$] $^+$ 322.2285, found 322.2286.

6-Azido-1-hexanol (51)



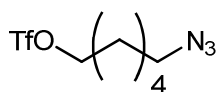
Compound **50** (489 mg, 1.63 mmol) was dissolved in THF (11.0 mL), then AcOH (0.1 mL) and TBAF. $3\text{H}_2\text{O}$ (1.54 g, 4.89 mmol) were added to the solution and stirred overnight. On completion of the reaction, the solvent was evaporated *in vacuo* and the residue was suspended in DCM, washed with NaHCO_3 (aq.) and brine. The organic phase was dried over MgSO_4 , the solvent was removed and the residue was purified by flash chromatography to give compound **51** as an oil (212 mg, 90%). R_f : 0.17 (Tol:EA; 10:1).

^1H NMR (500 MHz, CDCl_3) δ_{H} : 1.35 (bm, 4H, $-\text{CH}_2\text{CH}_2\text{CH}_2\text{CH}_2\text{N}_3$), 1.53 (m, 2H, $-\text{OCH}_2\text{CH}_2-$), 1.57 (m, 2H, $\text{N}_3\text{CH}_2\text{CH}_2-$), 1.88 (bs, 1H, $-\text{OH}$), 3.22 (t, 2H, $J = 6.8, 6.9$ Hz, N_3CH_2-), 3.58 (t, 2H, $J = 6.6$ Hz, $-\text{OCH}_2-$).

^{13}C NMR (125.7 MHz, CDCl_3) δ_{C} : 25.47, 26.66 ($-\text{OCH}_2\text{CH}_2\text{CH}_2\text{CH}_2\text{CH}_2\text{N}_3$), 28.94 ($\text{N}_3\text{CH}_2\text{CH}_2-$), 32.66 ($-\text{OCH}_2\text{CH}_2-$), 51.52 (N_3CH_2-), 62.78 ($-\text{OCH}_2-$).

HR-ESI-MS (m/z) calculated for $\text{C}_6\text{H}_{13}\text{N}_3\text{O}$ [$\text{M}+\text{Na}$] $^+$ 166.0951, found 166.0952.

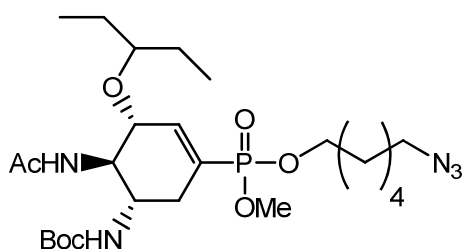
6-Azido-O-trifluoromethanesulfonyl-hexan-1-ol (52)



Compound **51** (55.9 mg, 0.390 mmol) was placed under an N₂ (g) atmosphere and suspended in dry DCM (1 mL). Lutidine (90 μ L, 0.780 mmol) was then added and the solution was cooled to -40 °C. Triflic anhydride (86 μ L, 0.507 mmol) was added to dry DCM (1 mL), cooled to -40 °C for a few minutes and then added dropwise to the stirring solution of compound **51**. The reaction was stirred at this temperature for 30 minutes by which time the reaction was complete. The DCM solution was then poured into a separating funnel containing cold saturated KH₂PO₄ (aq.) and washed. The organic layer was separated, dried over MgSO₄ and the solvent evaporated to give the desired triflate **52** as brown oil (94 mg, 87%) which was used without further purification.

¹H NMR (500 MHz, CDCl₃) δ_{H} : 1.46 (4 H, m, -CH₂CH₂CH₂CH₂N₃), 1.62 (2 H, tt, J = 6.8, 7.3 Hz, -CH₂CH₂N₃), 1.85 (2 H, tt, J = 6.5, 6.9 Hz, -CH₂CH₂OTf), 3.29 (2 H, t, J = 6.6 Hz, -CH₂N₃), 4.54 (2 H, t, J = 6.5 Hz, -CH₂OTf).

Methyl (6-azidohex-1-yl) [(3R,4R,5S)-4-acetamido-5-(1,1-dimethylethyloxycarbonylamino)-3-(1-ethylpropoxy)-1-cyclohexene-1-phosphonate] (53)



Monoester **35** was converted into the triethylammonium salt by treatment with Amberlite IR-120 ion exchange resin (H⁺) in water, filtration, addition of triethylamine and lyophilisation. The triethylammonium salt of compound **35** (35 mg, 0.0653 mmol) was then placed under an N₂ (g) atmosphere and dry acetonitrile (0.4 mL) was added. Azido triflate **52** (21 mg, 0.763 mmol) was dissolved in dry acetonitrile (0.3 mL) under an N₂ (g) atmosphere and then quickly added to the stirring solution of the triethylammonium salt of compound **35**. After an hour, TLC analysis indicated the reaction had not progressed any further and that the azide triflate was degrading in solution. The solvent was evaporated *in vacuo* and the residue was directly purified by flash chromatography (Tol:EA; 1:1 → EA → MeOH) to give compound **53** (17.0 mg, 72% based on recovered starting material). R_f: 0.54 (EA).

¹H NMR (500 MHz, CDCl₃) δ_{H} : 0.85 (6 H, dd, J = 7.5, 14.9 Hz, -OCH(CH₂CH₃)₂), 1.37 - 1.42 (13 H, s/bm, -NHCO(CH₃)₃, -OCH₂CH₂CH₂CH₂N₃), 1.47 (4 H, m, -

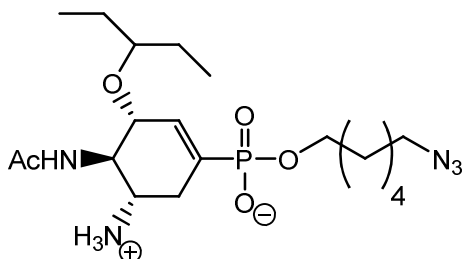
OCH(CH₂CH₃)₂), 1.58 (2 H, dd, J = 6.3, 12.9 Hz, N₃CH₂CH₂-), 1.66 (2 H, m, -OCH₂CH₂-), 1.96 (3 H, s, -NHCOCH₃), 2.17 (1 H, m, H_{6ax}), 2.58 (1 H, ddd, J = 5.9, 12.3, 17.3 Hz, H_{6eq}), 3.25 (2 H, dd, J = 6.8, 6.8 Hz, -CH₂N₃), 3.31 (1 H, dd, J = 5.5, 11.1 Hz, -OCH(CH₂CH₃)₂), 3.68 (3 H, dd, J = 1.8, 11.0 Hz, P-OCH₃), 3.77 (1 H, ddd, J = 5.3, 9.8, 15.0 Hz, H₅), 3.90 (1 H, m, H₃), 3.94 - 4.08 (3 H, m, H₄, -OCH₂-), 5.17 (1 H, d, J = 8.4 Hz, -NHCO(CH₃)₃), 5.94, 6.00 (1 H, 2d, J = 9.0 Hz, -NHCOCH₃), 6.58 (1 H, d, J_{P-2} = 21.7 Hz, H₂).

¹³C NMR (100.5 MHz, CDCl₃) δ_C: 9.26, 9.68 (-OCH(CH₂CH₃)₂), 23.48 (-NHCOCH₃), 25.26, 25.71, 26.24, 26.42 (-OCH₂CH₂CH₂CH₂CH₂CH₂N₃, -OCH(CH₂CH₃)₂), 28.46 (-NHCO(CH₃)₃), 28.86 (N₃CH₂CH₂-), 30.46 (d, J = 6.0 Hz, -OCH₂CH₂-), 31.44 (d, J = 9.3 Hz, C₆), 49.35 (d, J = 14.6 Hz, C₅), 51.46 (-CH₂N₃), 52.48-52.77 (m, P-OCH₃), 54.60 (m, C₄), 66.02 (d, J = 6.0 Hz, -OCH₂-), 76.28, 76.50 (C₃), 79.87 (-NHCO(CH₃)₂), 82.31 (-OCH(CH₂CH₃)₂), ~126.9 (d, J_{P-1} = 182 Hz, C₁), 142.20 (d, J_{P-2} = 6.8 Hz, C₂), 156.40 (-NHCO(CH₃)₃), 170.97 (-NHCOCH₃);

³¹P NMR (161.7 MHz, CDCl₃) δ_P: 18.29 (s), 18.32 (s).

HR-ESI-MS (m/z) calculated for C₂₅H₄₆N₅O₇P [M+Na]⁺ 582.3027, found 582.3058.

(6-Azido hexyl) (3R,4R,5S)-4-acetylamino-5-amino-3-(1-ethylpropoxy)-1-cyclohexene-1-phosphonic acid (54)



Azido-conjugate **53** (18 mg, 0.0322 mmol) and sodium iodide (50 mg, 0.333 mmol) were dried *in vacuo* in the absence of light for 20 minutes and then placed under an N₂ (g) atmosphere. Dry acetone (1 mL) was then added to the reaction flask followed by ultrasonication. The solution was then refluxed over 24 hours by which time TLC had indicated the absence of starting material and the formation of a new baseline spot. The resulting crude product was purified over a short silica plug (EA → EA/MeOH; 1:1) to give the demethylated product (10 mg, 58%). This deprotected intermediate (10 mg, 0.0183 mmol) was then stirred in a solution of TFA/H₂O (1:1) (1.2 mL) and 1,4-dioxane (0.8 mL) overnight. The solvent was then evaporated *in vacuo* and the residue was

purified by gel permeation chromatography to afford target compound **54** (7.4 mg, 91%).

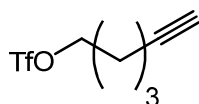
^1H NMR (600 MHz, D_2O) δ_{H} : 0.87 (3 H, t, $J = 7.4$ Hz, $-\text{OCH}(\text{CH}_2\text{CH}_3)_2$), 0.92 (3 H, t, $J = 7.4$ Hz, $-\text{OCH}(\text{CH}_2\text{CH}_3)_2$), 1.40 – 1.45 (4 H, bm, $-\text{CH}_2\text{CH}_2\text{CH}_2\text{CH}_2\text{N}_3$), 1.46 – 1.52, 1.53 – 1.61 (4 H, m, $-\text{OCH}(\text{CH}_2\text{CH}_3)_2$), 1.54 – 1.61 (4 H, m, $-\text{OCH}_2\text{CH}_2^-$, $\text{N}_3\text{CH}_2\text{CH}_2^-$), 2.10 (3 H, s, $-\text{NHCOCH}_3$), 2.40 (1 H, m, $\text{H}_{6\text{ax}}$), 2.75 (1 H, m, $\text{H}_{6\text{eq}}$), 3.35 (2 H, t, $J = 6.9$ Hz, $\text{N}_3\text{CH}_2\text{CH}_2^-$), 3.40 – 3.50 (1 H, m, H_5), 3.55 (1 H, dd, $J = 5.6, 11.4$ Hz, $-\text{OCH}(\text{CH}_2\text{CH}_3)_2$), 3.83 (2 H, m, $-\text{OCH}_2^-$), 4.00 (1 H, m, H_4), 4.26 (1 H, m, H_3), 6.35 (1 H, d, $J_{\text{P-2}} = 19.3$ Hz, H_2);

^{13}C NMR (150.8 MHz, D_2O) δ_{C} : 8.47, 8.54 ($-\text{OCH}(\text{CH}_2\text{CH}_3)_2$), 22.26 ($-\text{NHCOCH}_3$), 24.55, 25.14, 25.47, 25.56, 27.82, 29.70, 29.75 ($-\text{OCH}_2\text{CH}_2\text{CH}_2\text{CH}_2\text{CH}_2\text{N}_3$, $-\text{OCH}(\text{CH}_2\text{CH}_3)_2$, $\text{N}_3\text{CH}_2\text{CH}_2^-$, $-\text{OCH}_2\text{CH}_2^-$), ~ 30.81 (m, C6), ~ 49.6 (d, $J = 13.7$ Hz, C5), 51.07 (N_3CH_2^-), 54.61 (C4), 65.17 (m, $-\text{OCH}_2^-$), ~ 76.2 (m, C3), ~ 84.0 (m, $-\text{OCH}(\text{CH}_2\text{CH}_3)_2$), ~ 130.6 (d, $J_{\text{P-1}} = 171.6$ Hz, C1), 136.25 (m, C2), 160.15, 174.94 ($-\text{NHCOCH}_3$);

^{31}P NMR (242.7 MHz, D_2O) δ_{P} : 12.77 (s).

HR-ESI-MS (m/z) calculated for $\text{C}_{19}\text{H}_{36}\text{N}_2\text{O}_5\text{P}$ $[\text{M}+\text{Na}]^+$ 468.2346, found 468.2355.

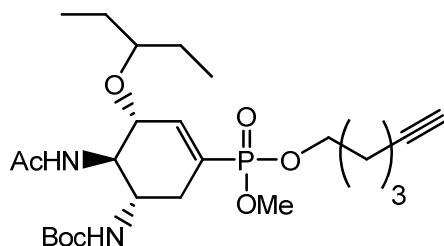
O-Trifluoromethanesulfonylhex-5-yn-1-ol (**55**)



5-Hexyn-1-ol (55.2 μL , 0.509 mmol) was placed under an N_2 (g) atmosphere and suspended in dry DCM (1 mL). Lutidine (118 μL , 1.02 mmol) was then added and the solution was cooled to -60°C . Triflic anhydride (103 μL , 0.611 mmol) was added to dry DCM (1 mL), cooled to -60°C for a few minutes and then added dropwise to the stirring solution of the alcohol. The reaction was stirred at this temperature for 1 hour by which time the reaction was complete. The DCM solution was then poured into a separating funnel containing cold saturated KH_2PO_4 (aq.) and washed. The organic layer was separated, dried over MgSO_4 and the solvent evaporated to give the desired triflate **55** as a slightly coloured oil (113 mg, 96%) which was used without further purification.

^1H NMR (500 MHz, CDCl_3) δ_{H} : 1.64 – 1.73 (2 H, m, $-\text{CH}_2\text{CH}_2\text{C}\equiv\text{CH}$), 1.94 – 2.02 (3 H, m, $-\text{OCH}_2\text{CH}_2\text{CH}_2\text{CH}_2\text{C}\equiv\text{CH}$), 2.29 (2 H, m, $-\text{CH}_2\text{CH}_2\text{C}\equiv\text{CH}$), 4.48 (2 H, t, $J = 6.2$ Hz, $-\text{OCH}_2\text{CH}_2^-$), 5.30 (s, residual DCM).

Methyl (hex-5-yn-1-yl) [(3*R*,4*R*,5*S*)-4-acetamido-5-(1,1-dimethylethyloxycarbonylamino)-3-(1-ethylpropoxy)-1-cyclohexene-1-phosphonate] (56)



Hexyne-triflate **55** (51 mg, 0.221 mmol) was placed under an N₂ (g) atmosphere and dry acetonitrile (0.7 mL) was added. The triethylammonium salt of **35** (80 mg, 0.184 mmol, prepared as described for compound **42**) was then quickly added to the stirring solution. After an hour, TLC analysis indicated the reaction had not progressed any further and that the hexyne-triflate was degrading in solution. The solvent was evaporated *in vacuo* and the residue was directly purified by flash chromatography (Tol:EA; 1:1 → EA → MeOH) to give compound **56** (30.5 mg, 65% based on recovered starting material). R_f: 0.40 (EA).

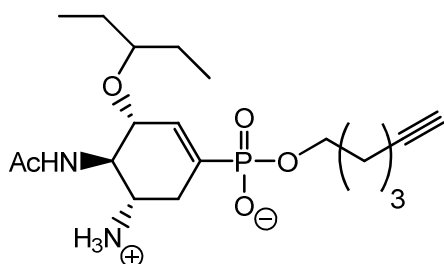
¹H NMR (500 MHz, CDCl₃) δ_H: 0.87 (6 H, m, -OCH(CH₂CH₃)₂), 1.40 (9 H, s, -NHCO(CH₃)₃), 1.49 (4 H, m, -OCH(CH₂CH₃)₂), 1.61 (2 H, m, -CH₂CH₂C≡CH), 1.79 (2 H, m, -OCH₂CH₂-), 1.92 (1 H, bs, -CH₂C≡CH), 1.97 (3 H, s, -NHCOCH₃), 2.16-2.25 (3 H, m, -CH₂C≡CH, H_{6ax}), 2.59 (1 H, m, H_{6eq}), 3.33 (1 H, d, J = 5.0 Hz, -OCH(CH₂CH₃)₂), 3.69 (3 H, 2d, J = 10.9 Hz, P-OCH₃), 3.79 (1 H, m, H₅), 3.91 (1 H, m, H₃), 3.98 – 4.09 (3 H, m, -OCH₂CH₂-, H₄), 5.11 (1 H, d, J = 7.1 Hz, -NHCOCH₃), 5.85 (1 H, m, -NHCO(CH₃)₃), 6.59 (1 H, d, J_{P-2} = 21.8 Hz, H₂);

¹³C NMR (100.5 MHz, CDCl₃) δ_C: 9.27, 9.67 (-OCH(CH₂CH₃)₂), 18.07 (-CH₂CH₂C≡CH), 23.46 (-NHCOCH₃), 24.60 (-CH₂CH₂C≡CH), 25.71, 26.23 (-OCH(CH₂CH₃)₂), 28.46 (-NHCO(CH₃)₂), ~29.5 (m, -OCH₂CH₂-), ~31.3 (d, J = 8.7 Hz, C₆), ~49.3 (m, C₅), ~52.6 (m, -P(OCH₃)₂), ~54.5 (m, C₄), ~65.6 (m, -OCH₂-), 69.01, 69.07 (-C≡CH), ~76.3 (m, C₃), 79.85 (-NHCO(CH₃)₂), 82.30 (-OCH(CH₂CH₃)₂), 83.83 (-C≡CH), ~126.8 (2d, J_{P-1} = 182 Hz, C₁), ~142.2 (d, J_{P-2} = 7.9 Hz, C₂), 156.39 (-NHCO(CH₃)₂), 170.97 (-NHCOCH₃);

³¹P NMR (161.7 MHz, CDCl₃) δ_P: 18.30 (s).

HR-ESI-MS (m/z) calculated for C₂₅H₄₃N₂O₇P [M+Na]⁺ 537.2700, found 537.2709.

(Hex-5-yn-1-yl) (3*R*,4*R*,5*S*)-4-acetamido-5-amino-3-(1-ethylpropoxy)-1-cyclohexene-1-phosphonic acid (**57**)



Hexyne-conjugate **56** (15 mg, 0.0291 mmol) and sodium iodide (44 mg, 0.291 mmol) were dried *in vacuo* in the absence of light for 20 minutes and then placed under an N₂ (g) atmosphere. Dry acetone (1 mL) was then added to the reaction flask followed by ultrasonication. The solution was then refluxed over 24 hours by which time TLC had indicated the absence of starting material and the formation of a new baseline spot. The resulting crude product was purified over a short silica plug (EA → EA/MeOH; 1:1) to give the demethylated product (12.5 mg, 86%). This deprotected intermediate (6 mg, 0.0120 mmol) was then stirred in a solution of TFA/H₂O (1:1) (1 mL) and 1,4-dioxane (0.2 mL) overnight. The solvent was then evaporated *in vacuo* and the residue was purified by gel permeation chromatography to afford compound target compound **57** (4.1 mg, 85%).

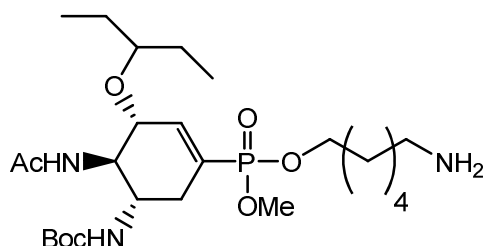
¹H NMR (600 MHz, MeOH-D₄) δ_H: 0.85 – 0.95 (6 H, m, -OCH(CH₂CH₃)₂), 1.47 – 1.57 (4 H, m, -OCH(CH₂CH₃)₂), 1.58 – 1.65 (2 H, m, -CH₂CH₂C≡CH), 1.70 – 1.77 (1 H, m, -OCH₂CH₂-), 2.03 (3 H, s, -NHCOCH₃), 2.15 – 2.27 (3 H, m, -CH₂C≡CH, -CH₂C≡CH), 2.39 (1 H, m, H_{6ax}), 2.78 (1 H, m, H_{6eq}), 3.36 – 3.45 (2 H, m, -OCH(CH₂CH₃)₂, H₅), 3.81 (2 H, dt, J = 6.2, 6.4 Hz, -OCH₂CH₂-), 3.95 (1 H, dd, J = 8.6, 8.6 Hz, H₄), 4.10 (1 H, d, J = 7.3 Hz, H₃), 6.40 (1 H, d, J = 18.7 Hz, H₂);

¹³C NMR (150.8 MHz, MeOH-D₄) δ_C: 9.58, 9.89 (-OCH(CH₂CH₃)₂), 18.75 (-CH₂C≡CH), 23.12 (-NHCOCH₃), 26.20 (-CH₂CH₂C≡CH), 26.64, 27.31 (-OCH(CH₂CH₃)₂), 30.62 (d, J = 10.5 Hz, C₆), 31.03 (d, J = 7.1 Hz, -OCH₂CH₂-), 51.49 (d, J = 13.2 Hz, C₅), 54.63 (C₄), 65.03 (d, J = 5.3 Hz, -OCH₂-), 69.73 (-C≡CH), 76.39 (d, J = 18.8 Hz, C₃), 83.28 (-OCH(CH₂CH₃)₂), 84.78 (-C≡CH), ~132.4 (d, J_{P-1} = 174 Hz, C₁), 136.34 (d, J_{P-2} = 6.4 Hz, C₂), 174.66 (-NHCOCH₃);

³¹P NMR (242.7 MHz, MeOH-D₄) δ_P: 8.05 (s).

HR-ESI-MS (m/z) calculated for C₁₉H₃₃N₂O₅P [M+Na]⁺ 423.2019, found 423.2038.

(6-amino hexyl) (3*R*,4*R*,5*S*)-4-acetamido-5-amino-3-(1-ethylpropoxy)-1-cyclohexene-1-phosphonate (58)



Azido-conjugate **53** (26 mg, 0.0473 mmol) was placed under an N₂ (g) atmosphere and dry THF (1 mL) was added. PMe₃ (1 M stock solution in THF, 61.5 μL) was then added dropwise to the stirring azido-conjugate solution. The reaction was monitored by TLC over the course of 4 hours after which time the reaction was complete. Deionised water (0.5 mL) was then added and the solution was stirred for an additional 30 minutes. The solvent was then removed directly *in vacuo* and the crude product was purified by flash chromatography (DCM/MeOH; 10:1 +3% NEt₃) to give the isolated amino-conjugate (qu.). ¹H NMR (MeOH-D₄) indicates the upfield shifting of -CH₂N- resonance with respect to compound **42**, and a poorly resolved spectrum in CDCl₃. R_f : 0.26 (DCM:MeOH; 10:1 + 3% NEt₃).

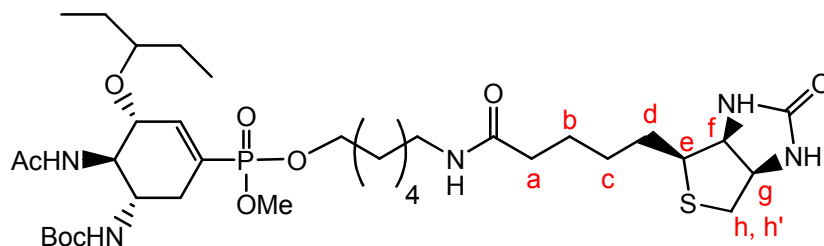
¹H NMR (500 MHz, MeOH-D₄) δ_H: 0.83 – 0.95 (6 H, m, -OCH(CH₂CH₃)₂), 1.43 (9 H, bs, -NHCOCH(CH₃)₃), 1.32 – 1.59 (12 H, bm, -CH₂CH₂CH₂CH₂NH₂, -OCH(CH₂CH₃)₂, -CH₂CH₂NH₂), 1.67 – 1.75 (2 H, m, -CH₂CH₂O-), 1.96 (3 H, s, -NHCOCH₃), 2.23 (1 H, m, H_{6ax}), 2.51 (1 H, m, H_{6eq}), 2.65 – 2.71 (2 H, m, -CH₂NH₂), 3.38 – 3.44 (1 H, m, -OCH(CH₂CH₃)₂), 3.74 (3 H, d, J = 11.1 Hz, P-OCH₃), 3.68 – 3.78 (1 H, m, H₅), 3.86 (1 H, dd, J = 8.9 Hz, H₄), 4.06 (2 H, dt, J = 6.1, 6.2 Hz, -OCH₂-), 4.09 – 4.14 (1 H, m, H₃), 6.58 (1 H, d, J_{P-2} = 22.0 Hz, H₂);

¹³C NMR (100.5 MHz, MeOH-D₄) δ_C: 9.62, 9.91 (-OCH(CH₂CH₃)₂), 22.9 (-NHCOCH₃), 26.42, 26.79, 27.27, 27.35 (-OCH₂CH₂CH₂CH₂CH₂N₃, -OCH(CH₂)₂(CH₃)₂), 28.72 (-NHCOCH(CH₃)₃), ~31.36 (d, J = 5.9 Hz, -OCH₂CH₂-), ~32.10 (d, J = 8.7 Hz, C₆), 32.78 (-NH₂CH₂CH₂-), 42.13 (-CH₂NH₂), 50.32, 50.47 (C₅), ~53.37 (m, P-OCH₃), ~56.04 (m, C₄), 67.62 (bm, -OCH₂-), 77.27, 77.49 (m, C₃), 80.30 (-NHCOCH(CH₃)₂), 83.77 (-OCH(CH₂CH₃), ~127.43(2d, J_{P-1} = 182 Hz, C₁), ~144.13 (m, C₂), 157.93 (-NHCOCH(CH₃)₃), 173.71 (-NHCOCH₃);

³¹P NMR (161.7 MHz, MeOH-D₄) δ_P: 18.46 (s).

HR-ESI-MS (m/z) calculated for C₂₅H₄₈N₃O₇P [M+H]⁺ 534.3303, found 534.3284.

Methyl (6-d-biotinamido-hex-1-yl) [(3R,4R,5S)-4-acetamido-5-(1,1-dimethylethoxy-carbonylamino)-3-(1-ethylpropoxy)-1-cyclohexene-1-phosphonate] (59)



Azido-conjugate **58** (26 mg, 0.0473 mmol) was placed under an N₂ (g) atmosphere and dry THF (1 mL) was added. PMe₃ (1 M stock solution in THF, 61.5 μL) was then added dropwise to the stirring azido-conjugate solution. The reaction was monitored by TLC over the course of 4 hours after which time the reaction was complete. Deionised water (0.5 mL) was then added and the solution was stirred for an additional 30 minutes. The solvent was then removed directly *in vacuo* and the crude product was placed on a short silica plug (DCM/MeOH; 10:1 +3% NEt₃) to give the isolated amino-conjugate without additional purification. d-Biotin (15.5 mg, 0.0633 mmol) and PyBOP (33 mg, 0.0633 mmol) were dried *in vacuo* and then placed under an N₂ (g) atmosphere. Dry DMF (1 mL) was then added followed by DIPEA (16 μL, 0.0974 mmol). The reaction flask was then sonicated briefly and cooled to 0 °C (ice-bath). After a few minutes the isolated amino-conjugate (25 mg, 0.0487 mmol) was dissolved in dry DMF (1 mL) and was added dropwise to the stirring d-Biotin solution. The solution was allowed to warm slowly to room temperature over 5 hours after which time TLC indicated the reaction was complete. The solvent was evaporated directly *in vacuo* and then purified by chromatography (EA/MeOH; 10:1 + 2% AcOH → 2:1 + 2% AcOH) to give protected target compound **59** (23 mg, 90%). R_f: 0.36 (DCM/MeOH + 3% AcOH).

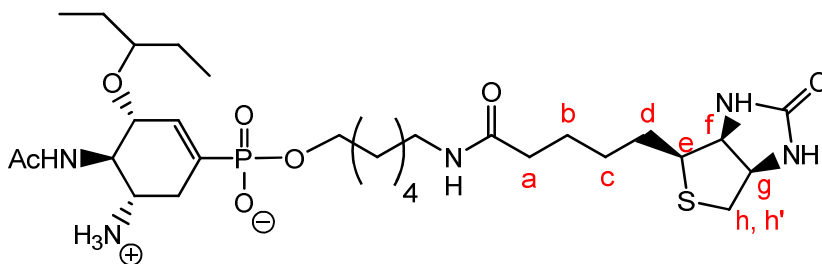
¹H NMR (500 MHz, MeOH-D₄) δ_H: 0.88, 0.92 (6 H, 2t, J = 7.1 Hz, -OCH(CH₂CH₃)₂), 1.43 (9 H, s, -NHCO(CH₃)₃), 1.34 – 1.78 (18 H, m, -OCH(CH₂CH₃)₂, H_b, H_c, H_d, -OCH₂CH₂-CH₂CH₂-CH₂CH₂NH-), 1.96 (3 H, s, -NHCOCH₃), 2.20 (2 H, dd, J = 6.9, 7.0 Hz, H_a), 2.18 – 2.27 (1 H, m, H_{6ax}), 2.51 (1 H, m, H_{6eq}), 2.71 (1 H, d, J = 12.7 Hz, H_{h'}), 2.93 (1 H, dd, J = 4.7, 12.6 Hz, H_h), 3.15-3.24 (3 H, m, -CH₂CH₂NH-, H_e), 3.41 (1 H, m, -OCH(CH₂CH₃)₂), 3.70 – 3.78 (1 H, m, H₅), 3.74 (3 H, d, J = 11.0 Hz, P-OCH₃), 3.86 (1 H, dd, J = 9.5, 9.7 Hz, H₄), 4.01 – 4.08 (2 H, m, -OCH₂CH₂-), 4.11 (1 H, m, H₃), 4.30, (1 H, dd, J = 4.3, 7.4 Hz, H_f), 4.49 (1 H, dd, J = 5.8, 6.0 Hz, H_g), 6.57 (1 H, d, J_{P-2} = 21.8 Hz, H₂);

^{13}C NMR (100.5 MHz, MeOH- D_4) δ_{C} : 9.63, 9.93 (-OCH(CH $_{2\text{C}}$ H $_{3\text{C}}$) $_{2\text{C}}$), 22.98 (-NHCOCH $_{3\text{C}}$), 26.34, 26.81, 26.94, 29.55, 29.80, 30.32 (Cb, Cc, Cd, -OCH $_{2\text{C}}$ CH $_{2\text{C}}$ -CH $_{2\text{C}}$ CH $_{2\text{C}}$ -CH $_{2\text{C}}$ CH $_{2\text{C}}$ NH-), 27.28, 27.46 (-OCH(CH $_{2\text{C}}$ CH $_{3\text{C}}$) $_{2\text{C}}$), 28.73 (-NHCOCH(CH $_{3\text{C}}$) $_{2\text{C}}$), ~31.4 (d, J = 5.9 Hz, -OCH $_{2\text{C}}$ CH $_{2\text{C}}$ -), ~32.1 (m, C6), 36.86 (Ca), 40.23 (-CH $_{2\text{C}}$ CH $_{2\text{C}}$ NH-), 41.07 (Ch,h'), ~50.4 (m, C5), ~53.4 (d, J = 5.8 Hz, -P(OCH $_{3\text{C}}$) $_{2\text{C}}$), 56.10 (m, C4), 57.05 (Ce), 61.62 (Cg), 63.42 (Cf), 67.69 (m, -OCH $_{2\text{C}}$ CH $_{2\text{C}}$ -), ~77.4 (m, C3), 80.35 (-NHCOCH(CH $_{3\text{C}}$) $_{2\text{C}}$), 83.82 (-OCH(CH $_{2\text{C}}$ CH $_{3\text{C}}$) $_{2\text{C}}$), 124.29, ~127.4 (d, $J_{\text{P-1}}$ = 183 Hz, C1), 144.17 (m, C2), 157.99 (-NHCOCH(CH $_{3\text{C}}$) $_{2\text{C}}$), 166.07 (-NHCH(O)NH-), 173.75 (-NHCOCH $_{3\text{C}}$), 175.90 (-CH $_{2\text{C}}$ CH(O)NH-CH $_{2\text{C}}$);

^{31}P NMR (161.7 MHz, MeOH- D_4) δ_{P} : 22.77 (s).

HR-ESI-MS (m/z) calculated for $\text{C}_{35}\text{H}_{62}\text{N}_5\text{O}_9\text{PS}$ [$\text{M}+\text{Na}$] $^{+}$ 782.3898, found 782.3900.

(6-*d*-Biotinamido-hex-1-yl) (3*R*,4*R*,5*S*)-4-acetamido-5-amino-3-(1-ethylpropoxy)-1-cyclohexene-1-phosphonic acid (60)



Protected biotin-conjugate **59** (8.4 mg, 0.0110 mmol) and sodium iodide (30 mg, 0.200 mmol) were dried *in vacuo* in the absence of light and then placed under an N_2 (g) atmosphere. Dry acetone (1 mL) was then added to the reaction flask followed by ultrasonication. The solution was then refluxed over 36 hours (maintaining the volume of acetone in the reaction flask) by which time TLC had indicated the absence of starting material. The resulting crude product was purified over a short silica plug (DCM/MeOH; 10:1 + 3% AcOH) to give the demethylated product (7 mg, 87%). This deprotected intermediate (7 mg, 0.00938 mmol) was then stirred in a solution of TFA/ H_2O (1:1) (1 mL) overnight. The solvent was then evaporated *in vacuo* and the residue was purified by gel permeation chromatography to afford target compound **60** (5 mg, 74%).

^1H NMR (600 MHz, MeOH- D_4) δ_{H} : 0.87, 0.92 (6 H, 2t, J = 7.4 Hz, -OCH(CH $_{2\text{C}}$ CH $_{3\text{C}}$) $_{2\text{C}}$), 1.34 – 1.79 (18 H, m, -OCH(CH $_{2\text{C}}$ CH $_{3\text{C}}$) $_{2\text{C}}$, Hb, Hc, Hd, -OCH $_{2\text{C}}$ CH $_{2\text{C}}$ CH $_{2\text{C}}$ CH $_{2\text{C}}$ CH $_{2\text{C}}$ CH $_{2\text{C}}$ NH-), 2.11 (3 H, s, -NHCOCH $_{3\text{C}}$), 2.27, (2 H, t, J = 7.1 Hz, Ha), 2.48 (1 H, m, H $_{6\text{ax}}$), 2.77 – 2.84

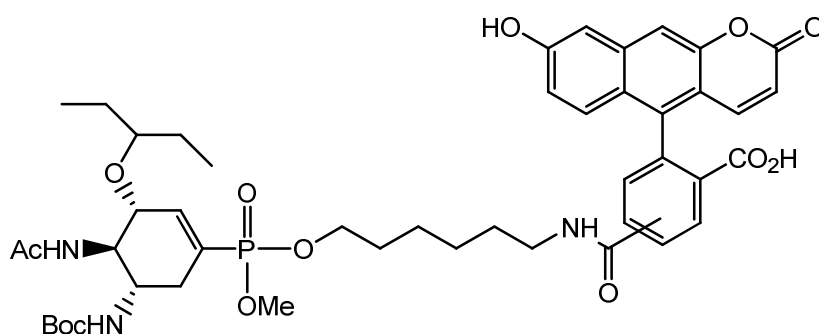
(1 H, m, H_{6eq}), 2.81 (1 H, d, J = 13.1 Hz, Hh'), 3.02 (1 H, dd, J = 5.0, 13.2 Hz, Hh), 3.21 (2 H, t, J = 6.8 Hz, -CH₂CH₂NH-), 3.36 (1 H, dd, J = 4.7, 4.8 Hz, He), 3.54 – 3.61 (2 H, m, H₅, -OCH(CH₂CH₃)₂), 3.83 (2 H, m, -OCH₂CH₂-), 4.07 (1 H, dd, J = 9.0, 9.2 Hz, H₄), 4.28 (1 H, d, J = 8.5 Hz, H₃), 4.45 (1 H, dd, J = 4.4, 4.5 Hz, Hf), 4.64 (1 H, dd, J = 4.9, 5.0 Hz, Hg), 6.35 (1 H, d, J_{P-2} = 19.3 Hz, H₂);

¹³C NMR (150.8 MHz, MeOH-D₄) δ_C: 8.46, 8.60 (-OCH(CH₂CH₃)₂), 22.28 (-NHCOCH₃), 24.76, 25.12, 25.18, 25.50, 25.77, 27.66, 27.84, 28.22 (Cb, Cc, Cd, -OCH₂CH₂CH₂CH₂CH₂NH-, -OCH(CH₂CH₃)₂), 29.25 (m, C6), 29.84 (-OCH₂CH₂-), 35.48 (Ca), 39.20 (-CH₂CH₂NH-), 39.63 (Ch, h'), ~49.6 (d, J = 14.2 Hz, C5), 52.93 (C4), 55.39 (Ce), 60.17 (Cg), 62.06 (Cf), 65.35 (m, -OCH₂CH₂-), ~75.8 (m, C3), 84.05 (-OCH(CH₂CH₃)₂), ~130.0 (d, J_{P-1} = 174 Hz, C1), 135.80 (C2), 165.25 (-NH-C(O)-NH-), 175.12 (-NHCOCH₃), 176.48 (-CH₂-C(O)NH-CH₂-);

³¹P NMR (242.7 MHz, MeOH-D₄) δ_P: 12.44 (s).

HR-ESI-MS (m/z) calculated for C₂₉H₅₂N₅O₇PS [M+Na]⁺ 668.3217, found 668.3244.

Methyl (6-(fluoresceinyl-5,6-carboxylamino)-hex-1-yl) [(3R,4R,5S)-4-acetamido-5-(1,1-dimethylethoxy)carbonylamino)-3-(1-ethylpropoxy)-1-cyclohexene-1-phosphonate] (61)



Azido-conjugate **58** (16 mg, 0.0293 mmol) was placed under an N₂ (g) atmosphere and dry THF (1 mL) was added. PMe₃ (1M stock solution in THF, 40 μL) was then added dropwise to the stirring azido-conjugate solution. The reaction was monitored by TLC over the course of 4 hours after which time the reaction was complete. Deionised water (0.5 mL) was then added and the solution was stirred for an additional 30 minutes. The solvent was then removed directly *in vacuo* and the crude product was placed on a short silica plug (DCM/MeOH; 10:1 +3% NEt₃) to give the isolated amino-conjugate without additional purification. The amino-conjugate (10 mg, 0.0187 mmol) and NHS-Fluorescein (9 mg, 0.0206 mmol) were dried *in vacuo* in the absence of light then

placed under an N₂ (g) atmosphere. Dry DMF (0.6 mL) was added to the flask (strong yellow coloured solution) to which was added dry triethylamine (~10 µL, 0.0748 mmol) (forming an orange coloured solution of pH~9). The solution was allowed to stir in the absence of light over 4 hours after which time the solvent was removed directly *in vacuo* (no heating). Chromatography of the crude product (EA + 3% AcOH → EA/MeOH; 10:1 + 3% AcOH) gave the desired protected target compound **61** as a yellow solid (15 mg, 83%). R_f: 0.58 (EA/MeOH; 10:1 + 3% AcOH).

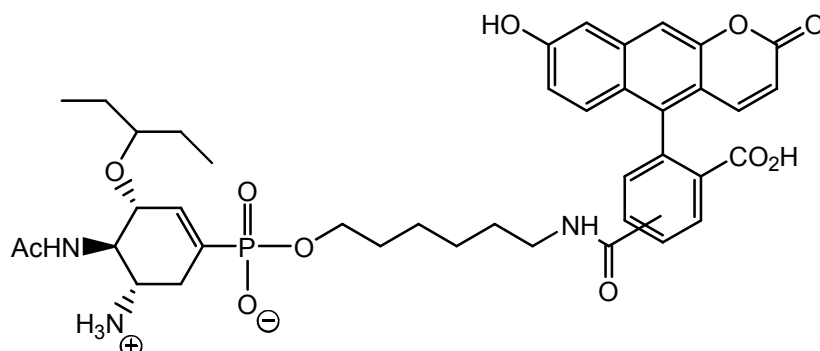
¹H NMR (500 MHz, MeOH-D₄) δ_H: 0.82 – 0.93 (6 H, m, -OCH(CH₂CH₃)₂), 1.41 (9 H, s, -NHCO(CH₃)₃), 1.30 – 1.55 (8 H, bm, -OCH(CH₂CH₃)₂, -CH₂CH₂CH₂CH₂NH-), 1.55 – 1.78 (4 H, m, -OCH₂CH₂CH₂CH₂CH₂CH₂NH-), 1.93 – 1.95 (3 H, 2s, -NHCOCH₃), 2.23 (1 H, m, H_{6ax}), 2.52 (1 H, m, H_{6eq}), 3.23 – 3.36, 3.42 – 3.48 (2 H, bm, -CH₂CH₂NH- (partially under MeOH resonance), 3.36 – 3.42 (1 H, m, -OCH(CH₂CH₃)₂), 3.66 – 3.80 (3 H, 2d, J = 11.3 Hz, P-OCH₃), 3.66 – 3.80 (1 H, m, H₅), 3.86 (1 H, dd, J = 9.5, 10.4 Hz, H₄), 3.98 – 4.16 (3 H, m, -OCH₂CH₂-, H₃), 6.35 – 6.76 (7 H, m, H₂, H-Fluorescein), 7.24 – 8.48 (3 H, m, H-Fluorescein);

¹³C NMR (100.5 MHz, MeOH-D₄) δ_C: 9.61, 9.92 (-OCH(CH₂CH₃)₂), 22.98 (NHCOCH₃), 26.33, 26.39, 26.79, 27.27, 27.51 (-OCH₂CH₂CH₂CH₂-, -OCH(CH₂CH₃)₂), 28.72 (-NHCO(CH₃)₂), 30.19, 30.32, 31.28, 31.34, 31.40 (-OCH₂CH₂CH₂CH₂CH₂CH₂NH-), 32.11 (d, J = 9.2 Hz, C6), 41.06, 41.10 (-CH₂CH₂NH-), 50.37 (m, C5), 53.36 (m, -P(OCH₃)₂), 56.08 (m, C4), 67.69, 67.70, 67.74 (m, -OCH₂CH₂-), 77.29, 77.51 (C3), 80.34 (-NHCO(CH₃)₂), 83.76, 83.79 (-OCH(CH₂CH₃)₂), 103.70 (C-H (Fluorescein)), ~111.6 (m), ~114.9 (m), ~124.9 ~125.5, ~126.5, ~126.9, ~128.4 (C1, C-H (Fluorescein)), 130.12, 130.18, 130.45, 130.65 (C-H (Fluorescein)), ~134.6 (m), 137.93, ~144.1 (m, C2), ~154.8 (m), 157.96 (-NHCO(CH₃)₂), 168.16, 168.41, 170.95, 173.76 (-NHCOCH₃, -CH₂-C(O)NH-CH₂-);

³¹P NMR (242.7 MHz, MeOH-D₄) δ_P: 18.91, 18.96, 18.98 (s).

HR-ESI-MS (m/z) calculated for C₄₆H₅₈N₃O₁₃P [M+Na]⁺ 914.3599, found 914.3603.

(6-(Fluoresceinyl-5,6-carboxylamino)-hex-1-yl) (3R,4R,5S)-4-acetylamino-5-amino-3-(1-ethylpropoxy)-1-cyclohexene-1-phosphonic acid (62)



Protected fluorescein-conjugate **61** (9 mg, 0.0101 mmol) and sodium iodide (15 mg, 0.0101 mmol) were dried *in vacuo* in the absence of light and then placed under an N₂ (g) atmosphere. Dry acetone (1 mL) was then added to the reaction flask followed by ultrasonication. The solution was then refluxed overnight by which time TLC had indicated the absence of starting material. The resulting crude product was purified over a short silica plug (EA/MeOH; 10:1 + 3% AcOH → 1:1 + 3% AcOH) to give the demethylated product (7 mg, 80%). This deprotected intermediate (6 mg, 0.00673 mmol) was then stirred in a solution of TFA/H₂O (1:1) (1 mL) overnight. The solvent was then evaporated *in vacuo* and the residue was purified by reversed-phase silica chromatography (short-plug) (MeOH/H₂O; 1:1 → 3:1) to afford target compound **62** (5 mg, 94%).

¹H NMR (600 MHz, MeOH-D₄) δ_H: 0.87 (6 H, m, -OCH(CH₂CH₃)₂), 1.40-1.60 (8 H, m, -OCH(CH₂CH₃)₂, -OCH₂CH₂CH₂CH₂CH₂CH₂NH-), 1.61 – 1.70 (4 H, m, -OCH₂CH₂-CH₂CH₂CH₂CH₂NH-), 1.97, 2.00 (3 H, 2s, -NHCOCH₃), 2.38 (1 H, m, H_{6ax}), 2.76 (1 H, m, H_{6eq}), 3.26 – 3.45 (2 H, bm, -CH₂CH₂NH- (partially obscured by MeOH)), 3.35 - 3.45 (2 H, m, H₇, H₅), 3.73 – 3.83 (2 H, m, -OCH₂CH₂-), 3.94 (1 H, m, H₄), 4.08 (1 H, m, H₃), 6.38 (1 H, m, H₂), 6.50 – 8.42 (9 H, m, H-Fluorescein);

¹³C NMR (150.8 MHz, MeOH-D₄) δ_C: 9.58, 9.53 (-OCH(CH₂CH₃)₂), 23.14 (-NHCOCH₃), 26.25, 27.32, 27.69, 30.32, 30.35, 31.86 (-OCH₂CH₂CH₂CH₂CH₂CH₂NH-, -OCH(CH₂CH₃)₂), 30.73 (m, C₆), 41.13 (-CH₂CH₂NH-), ~51.5 (d, J = 12.0 Hz, C₅), 54.67 (C₄), 65.46 (-OCH₂CH₂-), ~76.5 (m, C₃), 83.26 (-OCH(CH₂CH₃)₂), 103.66 (CH(Fluorescein)), 111.40, 114.51 (CH(Fluorescein)), 124.49, 125.26, 126.21, 126.67 (CH(Fluorescein)), 130.37, 131.91, 133.06, 134.85 (C₁, CH(Fluorescein)), ~136.3 (m, C₂), 137.97, 154.54, 168.42 (-C(O)NH-CH₂-), 170.81, 174.65 (-NHCOCH₃);

³¹P NMR (242.7 MHz, MeOH-D₄) δ_P: 8.14 (s).

HR-ESI-MS (m/z) calculated for $C_{40}H_{48}N_3O_{11}P$ $[M+Na]^+$ 800.2919, found 800.2919;
calculated for $C_{40}H_{48}N_3O_{11}P$ $[M+(2Na-H)]^+$ 822.2738, found 822.2767.

III.5. Nanoparticle syntheses

“Small” phospho-oseltamivir stabilised gold nanoparticles (“small TamiGold”)

Disulfide **45** (3.5 mg, 4.02×10^{-3} mmol) was dissolved in MeOH (0.4 mL). The methanolic solution was added to an aqueous solution of 0.025M $\text{HAuCl}_4 \cdot 3\text{H}_2\text{O}$ (1.34×10^{-3} mmol) followed by acetic acid (5.4 μL , 0.0938 mmol). Vigorous stirring over 15 minutes was followed by subsequent addition of freshly prepared aqueous 1M sodium borohydride (0.0268 mmol) in two portions over 5 minutes. The resulting brown/black solution was stirred overnight in the absence of light. The solvent was removed *in vacuo* to near dryness where the resulting waxy product was co-evaporated with MilliQ water (x2). MilliQ water (low volume) was added to the residue to aid the solubility of the nanoparticles for transfer to an eppendorf tube. Cycles of centrifugation ($\sim 12000g$) and resuspension with ethyl acetate/methanol (10:1 \rightarrow 5:1) were repeated until the supernatant showed no starting material (by TLC). The black/brown particulate suspension was resuspended in MilliQ water and dialysed against MilliQ water over 7 days (7 x 1 L).

“Small” monomethylphosphonate-stabilised gold nanoparticles (control)

A procedure identical to that of phospho-oseltamivir-stabilised gold nanoparticles described above was used, with disulfide **49** as ligand. The black/brown residue formed in the reaction showed a lower solubility in MeOH as compared to “small TamiGold”. Ethyl acetate/methanol ratios used in the centrifugation process were adjusted accordingly.

“Large” phospho-oseltamivir-stabilised gold nanoparticles (“large TamiGold”)

Freshly prepared citrate-capped gold nanoparticles (for synthesis, see below) (~ 3 nM, 10 mL) were added to a solution of disulfide **45** (6 mg, 0.00689 mmol) in 10mM phosphate buffer (pH ~ 7.6) (1 mL). After 30 minutes, UV spectroscopy confirmed a slight red-shift of the gold nanoparticle suspension (519 nm to 525 nm). The solution was stirred vigorously for a further 72 hours in the absence of light to ensure the place exchange reaction reached completion. The volume of the AuNP solution was then reduced *in vacuo* (no heating) to ~ 4 mL. The red coloured solution was then transferred to a 50 mL centrifuge tube and acidified to pH 2-3 (indicator paper) with 0.1 M HCl (aq.) in order to induce nanoparticle aggregation (red to purple colour change). The solution was then centrifuged after which the supernatant was removed carefully. Deionised H_2O (acidified to \sim pH 3) was added to the purple aggregate which was then

agitated, followed by further centrifugation. This process was repeated until disulfide **45** was no longer detected (TLC and ^1H NMR of supernatant residue). A few drops of 0.1 M NaOH (aq.) were added to the purple aggregate (which turned red) followed by 1 mL of Tris buffer (10 mM, pH 9.3) (2 mL). If necessary another drop of 0.1 M NaOH (aq.) was added to ensure all aggregated particles were resuspended (solution \sim pH 9.5 – 10, indicator paper). The resulting red solution was diluted with Tris buffer (final volume 5 mL) and underwent prolonged dialysis with Tris buffer (10 mM, pH 9.3) (2 L x 7 days). A final solution pH of \sim 9.3 was confirmed with the use of a pH meter.

“Large” methylphosphonate-stabilised gold nanoparticles

A procedure identical to that of “large TamiGold” described above was used, with disulfide **49** as ligand.

Synthesis of citrate-capped gold nanoparticles

A 100 mL aqueous solution of $\text{HAuCl}_4 \cdot 3\text{H}_2\text{O}$ (13.8 mg, 0.0350 mmol) was continuously stirred and heated to 60 °C. A 50 mL aqueous trisodium citrate solution (55.5 mg, 0.215 mmol) was heated to 60 °C and then rapidly added to the stirring chloroauric acid solution. Heating and vigorous stirring was maintained for \sim 2 hours until a wine red solution was obtained with characteristic UV band (\sim 519 nm).

III.6. Nanoparticle characterisation

Transmission electron microscopy (TEM and HR-TEM)

Transmission electron microscopy (TEM) and high resolution transmission electron microscopy (HR-TEM) were carried out using a Hitachi-7100 Transmission Electron Microscope (accelerating voltage of 100kV) and a JEOL 4000EX HREM (accelerating voltage of 400kV) respectively. Samples were prepared by dropping aqueous nanoparticle suspensions on Formvar-coated holey copper grids (TEM) or lacey carbon grids (HRTEM) and allowing the samples to air-dry. Samples for HRTEM were baked on a 60 W lamp before imaging. Staining was carried out using uranyl acetate (2%). Electron micrograph images were analysed using ImageJ (Rasband, W.S., ImageJ, U. S. NIH, Bethesda, Maryland, USA, <http://rsb.info.nih.gov/ij/>, 1997-2011). Images underwent limited editing to improve contrast for counting purposes where necessary. Particles were counted with the automated particle analysis tool or manually where necessary (by measuring the longest vertical particle diameter). All image analysis was carried out by the same operator using ~100-250 particles for statistical analysis.

Diffusion Ordered Spectroscopy (DOSY) NMR

Stokes-Einstein equation for the calculation of the hydrodynamic radius of a spherical particle from its diffusion coefficient:

$$D = kT / 6 \pi \eta r_H$$

D = diffusion coefficient from DOSY experiment

η (viscosity) = 8.9×10^{-4} Pa s (for H₂O at 298 K)

k = Boltzmann's constant

r_H ~ hydrodynamic radius

The data was acquired with the Oneshot sequence (M.D. Pelta, G.A. Morris, M.J. Stchedroff, and S.J. Hammond, A one-shot sequence for high resolution diffusion-ordered spectroscopy, 2002, *Magn. Reson. Chem.*, 40, S147-S152) and processed using the DOSY Toolbox (M. Nilsson, et al., The DOSY Toolbox: A new tool for processing PFG NMR diffusion data, 2009, *J. Mag. Res.*, 200, 296-302).

Energy dispersive X-ray analysis (EDX)

Energy dispersive x-ray analysis (EDX) was performed using an Oxford INCA Energy 200 Premium instrument connected to a JEOL JSM 5900LV scanning electron microscope. The solid sample was deposited onto an aluminium pin stub using double-sided adhesive carbon discs (Agar Scientific Ltd). The sample was viewed using 3 kV primary beam accelerating voltage and an in-lens distance of 5 mm. Data recording from the selected positions was performed over a period of 50 seconds.

Dynamic light scattering (DLS)

Size measurements were performed using dynamic light scattering (DLS) on a Malvern Zetasizer Nano-S (Malvern Instruments, Malvern, UK). Samples were irradiated with red light (HeNe laser, wavelength $\lambda = 632.8$ nm) and the intensity fluctuations of the scattered light (detected at a backscattering angle of 173°) was analysed (avalanche photodiode (APD) detector) to obtain an autocorrelation function. The software (DTS v5.00) provided both the size mean and polydispersity, using the cumulants analysis and a size distribution using a regularization scheme by intensity (and by volume and number where applicable). Samples were filtered before analysis, once over a cotton plug followed by a disposable $0.45\mu\text{m}$ filter to remove any unwanted contaminants and large aggregates.

The following assumptions were made in the analysis: the solution viscosity was assumed to be that of water, corrected for temperature ($\eta = 0.8872$ mPa.s); the solution refractive index was that of water ($n = 1.33$); the refractive index of the particle was selected to be $n_R = 0.34$ with absorption of $n_I = 2.37$. Samples were measured in disposable Eppendorf UVette 50-2000 μL polystyrene cuvettes at a temperature of 25°C , and this temperature was actively maintained within 0.1°C . Data were acquired in automatic mode (3 measurements \times 12 runs), ensuring enough photons were accumulated for the result to be statistically relevant. The software incorporated a 'data quality report' that indicated good quality for all data obtained.

UV-Visible spectroscopy

UV-Visible spectra were recorded on a Varian Cary 50 Scan spectrometer using the fast scan setting. Spectra of nanoparticle suspensions were recorded with deionised water, Tris buffer (10 mM, pH 9.3) or phosphate buffer (10 mM, pH 7.6) as a blank reference in a 1 mL cuvette (1 cm path length).

III.7. Inhibition of neuraminidase (NA) activity

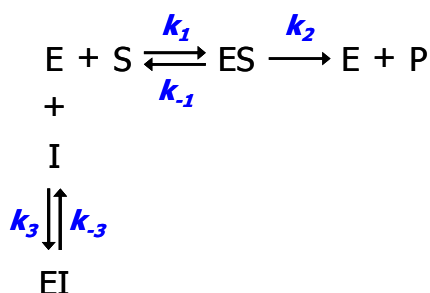
A whole virus assay using allantoic fluid from infected eggs was used to assess the inhibition of NA by compound **45** and isolated NA (purified NA from influenza virus X31 (H3N2)) was used to assess the inhibition of NA by compounds **54**, **57**, **60** and **62**.

In brief, neuraminidase (NA) enzymatic activity was studied using the fluorescent substrate 2'-4-methylumbelliferyl)- α -D-N-acetylneuraminic acid (MUNANA). Measurements were made at 37 °C in 32.5 mM MES (pH 6.5) + 4 mM CaCl₂ using a JASCO FP-6300 fluorimeter with excitation at 365 nm and emission at 450 nm.

Compound **45**: Michaelis-Menten constants for the enzyme, $K_m = (k_2 + k_{-1})/k_1$, were determined using standard initial rate measurements with estimated neuraminidase concentrations in the range 0.1 to 0.5 nM and MUNANA concentrations in the range 2 to 200 μ M.

Compounds **54**, **57**, **60** and **62**: Michaelis-Menten constants for the enzyme, $K_m = (k_2 + k_{-1})/k_1$, were determined by measuring the extent to which different concentrations of inhibitor (8, 16, 24 nM) reduced the steady-state rate of MUNANA hydrolysis (25 μ M MUNANA, 0.16 nM NA).

Inhibition constants (K_i) were determined by measuring the extent to which different concentrations of inhibitor reduced the steady-state rate of MUNANA hydrolysis. The data were interpreted using the following simple model for competitive inhibition in which E, S, and I represent neuraminidase, MUNANA, and inhibitor, respectively:



The reduced rate of hydrolysis of MUNANA observed in the presence of inhibitor is predicted by the following equation (Rameix-Welti *et al.*):⁸⁷

$$V_I = \frac{V_0([S] + K_m)}{[S] + K_m \left(1 + \frac{[I]}{K_I} \right)}$$

where V_I is the steady-state rate for MUNANA hydrolysis in the presence of inhibitor at concentration $[I]$, V_0 is the steady-state rate for MUNANA hydrolysis in the absence of inhibitor, $[S]$ is the MUNANA concentration, K_m is the Michaelis-Menten constant for hydrolysis of MUNANA, and K_I is the dissociation constant for the enzyme-inhibitor complex. Because these inhibitors show a slow approach to the new steady state rate²⁸⁷ it was necessary to confirm that the new steady-state rate had been reached; this was done by demonstrating that the first derivative of the fluorescence change (proportional to the NA activity) became constant at long times.

III.8. Fluorescence experiments

The fluorescence binding experiment was carried out at 5 °C, using a JASCO FP-6300 fluorimeter and concentrations of compound **62** and NA were comparable (9 nM and 12 nM, respectively).

III.8.1. Fluorescence titration

The binding experiment was carried out at 37 °C, using a JASCO FP-6300 fluorimeter by titrating compound **62** (2 nM) with X31 N2 in 32.5 mM MES (pH 6.5) + 100 mM NaCl. The dissociation constant determined using standard non-linear least-squares methods was 0.23 ± 0.05 nM, in reasonable agreement with the value determined by inhibition of MUNANA hydrolysis.

IV. References

- (1) Traving, C.; Schauer, R. *Cell. Mol. Life Sci.* **1998**, *54*, 1330-1349.
- (2) Chen, X.; Varki, A. *ACS Chem. Biol.* **2010**, *5*, 163-176.
- (3) Strasser, P.; Unger, U.; Strobl, B.; Vilas, U.; Vlasak, R. *Glycoconj. J.* **2003**, *20*, 551-561.
- (4) Schauer, R.; Reuter, G.; Stoll, S. *Biochimie* **1988**, *70*, 1511-1519.
- (5) Schauer, R. *Glycoconj. J.* **2000**, *17*, 485-499.
- (6) Schauer, R. *Zoology* **2004**, *107*, 49-64.
- (7) Guo, C.-T.; Sun, X.-L.; Kanie, O.; Shortridge, K. F.; Suzuki, T.; Miyamoto, D.; Hidari, K. I.-P. J.; Wong, C.-H.; Suzuki, Y. *Glycobiology* **2002**, *12*, 183-190.
- (8) Varki, A. *Glycoconj. J.* **2009**, *26*, 231-245-245.
- (9) Vimr, E. R.; Kalivoda, K. A.; Deszo, E. L.; Steenbergen, S. M. *Microbiol. Mol. Biol. Rev.* **2004**, *68*, 132-153.
- (10) Angata, T.; Varki, A. *Chem. Rev.* **2002**, *102*, 439-470.
- (11) Tiralongo, J.; Schauer, R. *Trends Glycosci. Glyc.* **2004**, *16*, 1-15.
- (12) Shen, Y.; Tiralongo, J.; Kohla, G.; Schauer, R. *Biol. Chem.* **2004**, *385*, 145-152.
- (13) Schauer, R. *Curr. Opin. Struct. Biol.* **2009**, *19*, 507-514.
- (14) Ogasawara, Y.; Namai, T.; Yoshino, F.; Lee, M.-C.-il; Ishii, K. *FEBS Lett.* **2007**, *581*, 2473-2477.
- (15) Tao, F.; Zhang, Y.; Ma, C.; Xu, P. *Appl. Microbiol. Biotechnol.* **2010**, *87*, 1281-1289.
- (16) Schauer, R.; Schmid, H.; Pommerencke, J.; Iwersen, M.; Kohla, G. *Advances in Experimental Medicine and Biology: Metabolism and role of O-acetylated sialic acids*; Molecular Immunology of Complex Carbohydrates 2; Kluwer Academic/Plenum Publishers, New York, 2001; Vol. 491.
- (17) Cornforth, J. W.; Firth, M. E.; Gottschalk, A. *Biochem. J.* **1958**, *68*, 57-61.
- (18) Danishefsky, S. J.; DeNinno, M. P.; Chen, S. H. *J. Am. Chem. Soc.* **1988**, *110*, 3929-3940.
- (19) Kiefel, M. J.; von Itzstein, M. *Chem. Rev.* **2002**, *102*, 471-490.
- (20) Ress, D. K.; Linhardt, R. J. *Curr. Org. Synth.* **2004**, *1*, 31-46.
- (21) Ando, H.; Imamura, A. *Trends Glycosci. Glyc.* **2004**, *16*, 293-303.

- (22) Boons, G.-J.; Demchenko, A. V. *Chem. Rev.* **2000**, *100*, 4539-4566.
- (23) Orlova, A. V.; Shpirt, A. M.; Kulikova, N. Y.; Kononov, L. O. *Carbohydr. Res.* **2010**, *345*, 721-730.
- (24) Hsu, C.-H.; Chu, K.-C.; Lin, Y.-S.; Han, J.-L.; Peng, Y.-S.; Ren, C.-T.; Wu, C.-Y.; Wong, C.-H. *Chem. Eur. J.* **2010**, *16*, 1754-1760.
- (25) Sinha, D.; Chatterjee, M.; Mandal, C. *Trends Glycosci. Glyc.* **2000**, *12*, 17-33.
- (26) Srinivasan, G.; Schauer, R. *Glycoconj. J.* **2008**, *26*, 935-944.
- (27) Houliston, R. S.; Endtz, H. P.; Yuki, N.; Li, J. Jarrell,; H. C. Koga,; M. van Belkum, A.; Karwaski, M.-F.; Wakarchuk, W. W.; Gilbert, M. *J. Biol. Chem.* **2006**, *281*, 11480-11486.
- (28) Iwersen, M.; Dora, H.; Kohla, G.; Gasa, S.; Schauer, R. *Biol. Chem.* **2003**, *384*, 1035-1047.
- (29) Schauer, R.; Tiralongo, J.; Shen, Y.; Guido Kohla, A. L. L.; Kamerling, J. P. *Eur. J. Biochem.* **2004**, *271*, 281-290.
- (30) Ghosh, S.; Bandyopadhyay, S.; Mukherjee, K.; Mallick, A.; Pal, S.; Mandal, C. Bhattacharya, D. K.; Mandal, C. *Glycoconj. J.* **2007**, *24*, 17-24.
- (31) Zanetta, J.-P.; Pons, A.; Iwersen, M.; Mariller, C.; Leroy, Y.; Timmerman, P.; Schauer, R. *Glycobiology* **2001**, *11*, 663 -676.
- (32) Varki, A. *Glycobiology* **1992**, *2*, 25-20.
- (33) van Lenthe, J. H.; den Boer, D. H. W.; Havenith, R. W. A.; Schauer, R.; Siebert, H.-C. *J. Mol. Struct.-Theochem.* **2004**, *677*, 29-37.
- (34) Higa, H. H.; Butor, C.; Diaz, S.; Varki, A. *J. Biol. Chem.* **1989**, *264*, 19427 - 19434.
- (35) Claus, H.; Borrow, R.; Achtman, M.; Morelli, G.; Kantelberg, C.; Longworth, E.; Frosch, M.; Vogel, U. *Mol. Microbiol.* **2004**, *51*, 227-239.
- (36) Lrhorfi, L. A.; Srinivasan, G. V.; Schauer, R. *Biol. Chem.* **2007**, *388*, 297-306.
- (37) Lewis, A. L.; Cao, H.; Patel, S. K.; Diaz, S.; Ryan, W.; Carlin, A. F.; Thon, V.; Lewis, W. G.; Varki, A.; Chen, X.; Nizet, V. *J. Biol. Chem.* **2007**, *282*, 27562-27571.
- (38) Lewis, A. L.; Hensler, M. E.; Varki, A.; Nizet, V. *J. Biol. Chem.* **2006**, *281*, 11186 -11192.
- (39) Bergfeld, A. K.; Claus, H.; Lorenzen, N. K.; Spielmann, F.; Vogel, U.; Mühlenhoff, M. *J. Biol. Chem.* **2009**, *284*, 6 -16.

- (40) Martin, L. T.; Marth, J. D.; Varki, A.; Varki, N. M. *J. Biol. Chem.* **2002**, *277*, 32930 -32938.
- (41) Schauer, R.; Shukla, A. *Glycoconj. J.* **2008**, *25*, 625-632.
- (42) Wurzer, W. J.; Obojes, K.; Vlasak, R. *J. Gen. Virol.* **2002**, *83*, 395-402.
- (43) Sjoberg, E. R.; Leland D. Powell; Klein, A.; Varki, A. *J. Cell. Biol.* **1994**, *126*, 549-562.
- (44) Cariappa, A.; Takematsu, H.; Liu, H.; Diaz, S.; Haider, K.; Boboila, C.; Kalloo, G.; Connole, M.; Shi, H. N.; Varki, N.; Varki, A.; Pillai, S. *J. Exp. Med.* **2009**, *206*, 125 -138.
- (45) Surolia, I.; Pirnie, S. P.; Chellappa, V.; Taylor, K. N.; Cariappa, A.; Moya, J.; Liu, H.; Bell, D. W.; Driscoll, D. R.; Diederichs, S.; Haider, K.; Netravali, I.; Le, S.; Elia, R.; Dow, E.; Lee, A.; Freudenberg, J.; De Jager, P. L.; Chretien, Y.; Varki, A.; MacDonald, M. E.; Gillis, T.; Behrens, T. W.; Bloch, D.; Collier, D.; Korzenik, J.; Podolsky, D. K.; Hafler, D.; Murali, M.; Sands, B.; Stone, J. H.; Gregersen, P. K.; Pillai, S. *Nature* **2010**, *466*, 243-247.
- (46) Vlasak, R.; Muster, T.; Lauro, A. M.; Powers, J. C.; Palese, P. *J. Virol.* **1989**, *63*, 2056-2062.
- (47) Rangarajan, E. S.; Ruane, K. M.; Proteau, A.; Schrag, J. D.; Valladares, R.; Gonzalez, C. F.; Gilbert, M.; Yakunin, A. F.; Cygler, M. *Protein Sci.* **2011**.
- (48) Smits, S. L.; Gerwig, G. J.; van Vliet, A. L. W.; Lissenberg, A.; Briza, P.; Kamerling, J. P.; Vlasak, R.; de Groot, R. J. *J. Biol. Chem.* **2005**, *280*, 6933-6941.
- (49) Mayr, J.; Haselhorst, T.; Langereis, M.; Dyason, J.; Huber, W.; Frey, B.; Vlasak, R.; de Groot, R.; von Itzstein, M. *Glycoconj. J.* **2008**, *25*, 393-399.
- (50) Rosenthal, P. B.; Zhang, X.; Formanowski, F.; Fitz, W.; Wong, C.-H.; Meier-Ewert, H.; Skehel, J. J.; Wiley, D. C. *Nature* **1998**, *396*, 92-96.
- (51) Garcia-Sastre, A.; Villar, E.; Manuguerra, J. C.; Hannoun, C.; Cabezas, J. A. *Biochem. J.* **1991**, *273*, 435-441.
- (52) Zeng, Q.; Langereis, M. A.; van Vliet, A. L. W.; Huizinga, E. G.; de Groot, R. J. *Proc. Natl. Acad. Sci. USA* **2008**, *105*, 9065 -9069.
- (53) Strobl, B.; Vlasak, R. *Virology* **1993**, *192*, 679-682.
- (54) de Groot, R. *Glycoconj. J.* **2006**, *23*, 59-72.
- (55) Hofling, K.; Klenk, H. D.; Herrler, G. *J. Gen. Virol.* **1997**, *78*, 567-570.
- (56) Hellebo, A.; Vilas, U.; Falk, K.; Vlasak, R. *J. Virol.* **2004**, *78*, 3055-3062.
- (57) Arbour, N.; Day, R.; Newcombe, J.; Talbot, P. J. *J. Virol.* **2000**, *74*, 8913-8921.

- (58) St-Jean, J. R.; Jacomy, H.; Desforges, M.; Vabret, A.; Freymuth, F.; Talbot, P. *J. J. Virol.* **2004**, *78*, 8824-8834.
- (59) Langereis, M. A.; Zeng, Q.; Gerwig, G. J.; Frey, B.; Itzstein, M. von; Kamerling, J. P.; de Groot, R. J.; Huizinga, E. G. *Proc. Natl. Acad. Sci. USA* **2009**, *106*, 15897-15902.
- (60) Eleuterio, I.; Streicher, H. *J. Chem. Res.* **2010**, *October*, 562-564.
- (61) Li, W.; Shi, Z.; Yu, M.; Ren, W.; Smith, C.; Epstein, J. H.; Wang, H.; Cramer, G.; Hu, Z.; Zhang, H.; Zhang, J.; McEachern, J.; Field, H.; Daszak, P.; Eaton, B. T.; Zhang, S.; Wang, L.-F. *Science* **2005**, *310*, 676-679.
- (62) Reinhard, B.; Becker, A.; Rothermel, J.; Faillard, H. *Biol. Chem. Hoppe Seyler* **1992**, *373*, 63-68.
- (63) Roy, R.; Laferriere, C. A. *Can. J. Chem.* **1990**, *68*, 2045-2054.
- (64) McAuliffe, J. C.; Rabuka, D.; Hindsgaul, O. *Org. Lett.* **2002**, *4*, 3067-3069.
- (65) Liav, A. *Carbohydr. Res.* **1995**, *271*, 241-245.
- (66) Xu, Y.; Lee, S. A.; Kutateladze, T. G.; Sbrissa, D.; Shisheva, A.; Prestwich, G. D. *J. Am. Chem. Soc.* **2006**, *128*, 885-897.
- (67) Carbain, B.; Collins, P. J.; Callum, L.; Martin, S. R.; Hay, A. J.; McCauley, J.; Streicher, H. *ChemMedChem* **2009**, *4*, 335-337.
- (68) Busse, H.; Hakoda, M.; Stanley, M.; Streicher, H. *J. Carb. Chem.* **2007**, *26*, 159-194.
- (69) Kiefel, M. J.; Wilson, J. C.; Bennett, S.; Gredley, M.; von Itzstein, M. *Bioorg. Med. Chem.* **2000**, *8*, 657-664.
- (70) Greene, T. W.; Wuts, P. G. M. *Protective Groups in Organic Synthesis*; third edition. John Wiley & Sons, Inc., **1999**.
- (71) Chen, M.-Y.; Patkar, L. N.; Lu, K.-C.; Lee, A. S.-Y.; Lin, C.-C. *Tetrahedron* **2004**, *60*, 11465-11475.
- (72) Fitz, W.; Rosenthal, P. B.; Wong, C.-H. *Bioorg. Med. Chem.* **1996**, *4*, 1349-1353.
- (73) Martin, R.; Witte, K. L.; Wong, C.-H. *Bioorg. Med. Chem.* **1998**, *6*, 1283-1292.
- (74) Reidel, A.; Waldmann, H. *J. Prakt. Chem.* **1993**, *335*, 109-127.
- (75) Tamm, C. *Pure Appl. Chem.* **1992**, *64*, 1187-1191.
- (76) Abrect, S.; Harrington, P.; Iding, H.; Karpf, M. R. T.; Wirz, B.; Zutter, U. *Chimia* **2004**, *58*, 621-629.
- (77) Tanyeli, C.; Turkut, E. *Tetrahedron: Asymmetry* **2004**, *15*, 2057-2060.

- (78) Stanley, M.; Mayr, J.; Huber, W.; Vlasak, R.; Streicher, H. *Eur. J. Med. Chem.* **2011**, *46*, 2852-2860.
- (79) Schultze, B.; Wahn, K.; Klenk, H.-D.; Herrler, G. *Virology* **1991**, *180*, 221-228.
- (80) Vlasak, R.; Luytjes, W.; Spaan, W.; Palese, P. *Proc. Natl. Acad. Sci. USA* **1988**, *85*, 4526-4529.
- (81) Regl, G.; Kaser, A.; Iwersen, M.; Schmid, H.; Kohla, G.; Strobl, B.; Vilas, U. Schauer, R.; Vlasak, R. *J. Virol.* **1999**, *73*, 4721-4727.
- (82) Nicolaou, K. C.; Estrada, A. A.; Zak, M.; Lee, S. H.; Safina, B. S. *Angew. Chem. Int. Ed.* **2005**, *44*, 1378-1382.
- (83) Meinke, S.; Thiem, J. *Carbohydr. Res. Synth. Chem.* **2008**, *343*, 1824-1829.
- (84) Hoyle, C. E.; Bowman, C. N. *Angew. Chem. Int. Ed.* **2010**, *49*, 1540-1573.
- (85) WHO *Bull. WHO* **1980**, *58*, 585-591.
- (86) Matrosovich, M.; Klenk, H.-D. *Rev. Med. Virol.* **2003**, *13*, 85-97.
- (87) Mohan, S.; McAtamney, S.; Haselhorst, T.; von Itzstein, M.; Pinto, B. M. *J. Med. Chem.* **2010**, *53*, 7377-7391.
- (88) Russell, R. J.; Haire, L. F.; Stevens, D. J.; Collins, P. J.; Lin, Y. P.; Blackburn, G. M.; Hay, A. J.; Gamblin, S. J.; Skehel, J. J. *Nature* **2006**, *443*, 45-49.
- (89) de Jong, M. D.; Hien, T. T. *J. Clin. Virol.* **2006**, *35*, 2-13.
- (90) Sandrock, C.; Kelly, T. *Crit. Care* **2007**, *11*, 209.
- (91) Magano, J. *Chem. Rev.* **2009**, *109*, 4398-4438.
- (92) Loo, Y.-M.; Gale, M. *Nature* **2007**, *445*, 267-268.
- (93) WHO; Influenza (Seasonal) Fact Sheet No. 211, <http://www.who.int/mediacentre/factsheets/fs211/en/>, 2011 **2009**.
- (94) Zambon, M. C. *Rev. Med. Virol.* **2001**, *11*, 227-241.
- (95) Oxford, J.; Lambkin-Williams, R.; Mann, A. *Antivir. Chem. Chemother.* **2007**, *18*, 71-74.
- (96) von Itzstein, M. *Curr. Opin. Chem. Biol.* **2008**, *12*, 102-108.
- (97) De Clercq, E.; Neyts, J. *Trends Pharmacol. Sci.* **2007**, *28*, 280-285.
- (98) Health Protection Agency HPA, Virus Reference Department (VRD), Seasonal Influenza; Frequently asked questions on influenza, http://www.hpa.org.uk/servlet/Satellite?c=HPAweb_C&cid=1195733745991&pageName=HPAweb%2FHPAwebStandard, 2011.

- (99) WHO, Global Alert and Response (GAR)/Influenza. <http://www.who.int/csr/disease/influenza/en/>.
- (100) WHO Media Centre H1N1 in post-pandemic period, H1N1 in post-pandemic period, http://www.who.int/mediacentre/news/statements/2010/h1n1_vpc_20100810/en/index.html **2010**.
- (101) Stöhr, K. *N. Engl. J. Med.* **2005**, *352*, 405-407.
- (102) Yen, H.-L.; Ilyushina, N. A.; Salomon, R.; Hoffmann, E.; Webster, R. G.; Govorkova, E. A. *J. Virol.* **2007**, *81*, 12418-12426.
- (103) Collins, P. J.; Haire, L. F.; Lin, Y. P.; Liu, J.; Russell, R. J.; Walker, P. A.; Skehel, J. J.; Martin, S. R.; Hay, A. J.; Gamblin, S. J. *Nature* **2008**, *453*, 1258-1261.
- (104) WHO, Cumulative Number of Confirmed Human Cases of Avian Influenza A/(H5N1) Reported to WHO, http://www.who.int/csr/disease/avian_influenza/country/cases_table_2011_04_11/en/index.html **2011**.
- (105) Global Pandemic Influenza Preparedness Market Forecast 2010-2015, Market Research Media, <http://www.marketresearchmedia.com/2009/04/24/pandemic-influenza-market/>, **2011**.
- (106) Mitnaul, L. J.; Matrosovich, M. N.; Castrucci, M. R.; Tuzikov, A. B.; Bovin, N. V.; Kobasa, D.; Kawaoka, Y. *J. Virol.* **2000**, *74*, 6015-6020.
- (107) Rich, J.; Dietmar, G.; von Itzstein, M. *Comprehensive Glycoscience: Design and synthesis of sialidase inhibitors for influenza virus infections*; Elsevier, 2007; Vol. 1.
- (108) Moscona, A. *N. Engl. J. Med.* **2005**, *353*, 1363-1373.
- (109) Fiorin, G.; Carnevale, V.; DeGrado, W. F. *Science* **2010**, *330*, 456-458.
- (110) Matrosovich, M. N.; Matrosovich, T. Y.; Gray, T.; Roberts, N. A.; Klenk, H.-D. *J. Virol.* **2004**, *78*, 12665-12667.
- (111) Newhouse, E. I.; Xu, D.; Markwick, P. R. L.; Amaro, R. E.; Pao, H. C.; Wu, K. J.; Alam, M.; McCammon, J. A.; Li, W. W. *J. Am. Chem. Soc.* **2009**, *131*, 17430-17442.
- (112) Wilson, I. A.; Skehel, J. J.; Wiley, D. C. *Nature* **1981**, *289*, 366-373.
- (113) Murti, K. G.; Webster, R. G. *Virology* **1986**, *149*, 36-43.
- (114) Weis, W.; Brown, J. H.; Cusack, S.; Paulson, J. C.; Skehel, J. J.; Wiley, D. C. *Nature* **1988**, *333*, 426-431.
- (115) Glick, G. D.; Knowles, J. R. *J. Am. Chem. Soc.* **1991**, *113*, 4701-4703.

- (116) Ha, Y.; Stevens, D. J.; Skehel, J. J.; Wiley, D. C. *EMBO J.* **2002**, *21*, 865-875.
- (117) Meng, B.; Marriott, A. C.; Dimmock, N. J. *Influenza Other Respi. Viruses* **2010**, *4*, 147-153.
- (118) Eisen, M. B.; Sabesan, S.; Skehel, J. J.; Wiley, D. C. *Virology* **1997**, *232*, 19-31.
- (119) Skehel, J. J.; Wiley, D. C. *Annu. Rev. Biochem.* **2011**, *69*, 531-569.
- (120) Kale, R. R.; Mukundan, H.; Price, D. N.; Harris, J. F.; Lewallen, D. M.; Swanson, B. I.; Schmidt, J. G.; Iyer, S. S. *J. Am. Chem. Soc.* **2008**, *130*, 8169-8171.
- (121) Viswanathan, K.; Chandrasekaran, A.; Srinivasan, A.; Raman, R.; Sasisekharan, V.; Sasisekharan, R. *Glycoconj. J.* **2010**, *27*, 561-570.
- (122) Chandrasekaran, A.; Srinivasan, A.; Raman, R.; Viswanathan, K.; Raguram, S.; Tumpey, T. M.; Sasisekharan, V.; Sasisekharan, R. *Nat. Biotech.* **2008**, *26*, 107-113.
- (123) Bewley, C. A. *Nat. Biotech.* **2008**, *26*, 60-62.
- (124) Varghese, J. N.; Laver, W. G.; Colman, P. M. *Nature* **1983**, *303*, 35-40.
- (125) Baker, A. T.; Varghese, J. N.; Laver, W. G.; Air, G. M.; Colman, P. M. *Proteins* **1987**, *2*, 111-117.
- (126) Xu, X.; Zhu, X.; Dwek, R. A.; Stevens, J.; Wilson, I. A. *J. Virol.* **2008**, *82*, 10493-10501.
- (127) Wang, P.; Zhang, J. Z. H. *J. Phys. Chem. B.* **2010**, *114*, 12958-12964.
- (128) Albohy, A.; Mohan, S.; Zheng, R. B.; Mario Pinto, B.; Cairo, C. W. *Bioorg. Med. Chem.* **2011**, *19*, 2817-2822.
- (129) Rudrawar, S.; Dyason, J. C.; Rameix-Welti, M.-A.; Rose, F. J.; Kerry, P. S.; Russell, R. J. M.; van der Werf, S.; Thomson, R. J.; Naffakh, N.; von Itzstein, M. *Nat. Commun.* **2010**, *1*, 113.
- (130) Kobasa, D.; Kodihalli, S.; Luo, M.; Castrucci, M. R.; Donatelli, I.; Suzuki, Y.; Suzuki, T.; Kawaoka, Y. *J. Virol.* **1999**, *73*, 6743-6751.
- (131) Baigent, S. J.; Bethell, R. C.; McCauley, J. W. *Virology* **1999**, *263*, 323-338.
- (132) Katinger, D.; Mochalova, L.; Chinarev, A.; Bovin, N.; Romanova, J. *Arch. Vir.* **2004**, *149*, 2131-2140.
- (133) De Clercq, E. *Nat. Rev. Drug Discov.* **2006**, *5*, 1015-1025.
- (134) Maring, C. J.; Stoll, V. S.; Zhao, C.; Sun, M.; Krueger, A. C.; Stewart, K. D.; Madigan, D. L.; Kati, W. M.; Xu, Y.; Carrick, R. J.; Montgomery, D. A.; Kempf-

- Grote, A.; Marsh, K. C.; Molla, A.; Steffy, K. R.; Sham, H. L.; Laver, W. G.; Gu, Y.-gui; Kempf, D. J.; Kohlbrenner, W. E. *J. Med. Chem.* **2005**, *48*, 3980-3990.
- (135) Abed, Y.; Nehm, B.; Baz, M.; Boivin, G. *Antiviral Res.* **2008**, *77*, 163-166.
- (136) Wang, G. T.; Chen, Y.; Wang, S.; Gentles, R.; Sowin, T.; Kati, W.; Muchmore, S.; Giranda, V.; Stewart, K.; Sham, H.; Kempf, D.; Laver, W. G. *J. Med. Chem.* **2001**, *44*, 1192-1201.
- (137) Stoll, V.; Stewart, K. D.; Maring, C. J.; Muchmore, S.; Giranda, V.; Gu, Y.-gui Y.; Wang, G.; Chen, Y.; Sun, M.; Zhao, C.; Kennedy, A. L.; Madigan, D. L.; Xu, Y.; Saldivar, A.; Kati, W.; Laver, G.; Sowin, T.; Sham, H. L.; Greer, J.; Kempf, D. *Biochemistry* **2003**, *42*, 718-727.
- (138) Zhang, J.; Wang, Q.; Fang, H.; Xu, W.; Liu, A.; Du, G. *Bioorg. Med. Chem.* **2008**, *16*, 3839-3847.
- (139) Kim, C. U.; Lew, W.; Williams, M. A.; Liu, H.; Zhang, L.; Swaminathan, S.; Bischofberger, N.; Chen, M. S.; Mendel, D. B.; Tai, C. Y.; Laver, W. G.; Stevens, R. C. *J. Am. Chem. Soc.* **1997**, *119*, 681-690.
- (140) Kim, C. U.; Lew, W.; Williams, M. A.; Wu, H.; Zhang, L.; Chen, X.; Escarpe, P. A.; Mendel, D. B.; Laver, W. G.; Stevens, R. C. *J. Med. Chem.* **1998**, *41*, 2451-2460.
- (141) Rohloff, J. C.; Kent, K. M.; Postich, M. J.; Becker, M. W.; Chapman, H. H.; Kelly, D. E.; Lew, W.; Louie, M. S.; McGee, L. R.; Prisbe, E. J.; Schultze, L. M.; Yu, R. H.; Zhang, L. *J. Org. Chem.* **1998**, *63*, 4545-4550.
- (142) Abrect, S.; Federspiel, M. C.; Estermann, H.; Fischer, R.; Karpf, M.; Mair, H. J.; Oberhauser, T.; Rimmler, G.; Trussardi, R.; Zutter, U. *Chimia* **2007**, *61*, 93-99.
- (143) Chong, A. K. J.; Pegg, M. S.; Taylor, N. R.; von Itzstein, M. *Eur. J. Biochem.* **1992**, *207*, 335-343.
- (144) Taylor, N. R.; von Itzstein, M. *J. Med. Chem.* **1994**, *37*, 616-624.
- (145) Klenk, H.-D.; Matrosovich, M. N.; Stech, J. *Avian influenza*; Karger Publishers, 2008.
- (146) WHO, WHO/ECDC frequently asked questions for Oseltamivir Resistance, http://www.who.int/csr/disease/influenza/oseltamivir_faqs/en/ **2008**.
- (147) Ciancio, B. C.; Meerhoff, T. J.; Kramarz, P.; Bonmarin, I.; Borgen, K.; Boucher, C. A.; Buchholz, U.; Buda, S.; Dijkstra, F.; Dudman, S.; Duwe, S.; Hauge, S. H.; Hungnes, O.; Meijer, A.; Mossong, J.; Paget, W. J.; Phin, N.; van der Sande, M.; Schweiger, B.; Nicoll, A. *Eurosurveillance* **2009**, *14*.
- (148) Federspiel, M.; Fischer, R.; Hennig, M.; Mair, H.-J.; Oberhauser, T.; Rimmler, G.; Albiez, T.; Bruhin, J.; Estermann, H.; Gandert, C.; Göckel, V.; Götzö, S.;

- Hoffmann, U.; Huber, G.; Janatsch, G.; Lauper, S.; Röckel-Stäbler, O.; Trussardi, R.; Zwahlen, A. G. *Org. Process Res. Dev.* **1999**, *3*, 266-274.
- (149) Harrington, P. J.; Brown, J. D.; Foderaro, T.; Hughes, R. C. *Org. Process Res. Dev.* **2004**, *8*, 86-91.
- (150) Yamatsugu, K.; Yin, L.; Kamijo, S.; Kimura, Y.; Kanai, M.; Shibasaki, M. *Angew. Chem. Int. Ed.* **2009**, *48*, 1070-1076.
- (151) Wichienukul, P.; Akkarasamiyo, S.; Kongkathip, N.; Kongkathip, B. *Tetrahedron Lett.* **2010**, *51*, 3208-3210.
- (152) Ishikawa, H.; Suzuki, T.; Hayashi, Y. *Angew. Chem. Int. Ed.* **2009**, *48*, 1304-1307.
- (153) Streicher, H.; Meisch, J.; Bohner, C. *Tetrahedron* **2001**, *57*, 8851-8859.
- (154) Streicher, H.; Bohner, C. *Tetrahedron* **2002**, *58*, 7573-7581.
- (155) Streicher, H.; Busse, H. *Bioorg. Med. Chem.* **2006**, *14*, 1047-1057.
- (156) Wallimann, K.; Vasella, A. *HCA* **1990**, *73*, 1359-1372.
- (157) Chan, T.-H.; Xin, Y.-C.; von Itzstein, M. *J. Org. Chem.* **1997**, *62*, 3500-3504.
- (158) Shie, J.-J.; Fang, J.-M.; Wang, S.-Y.; Tsai, K.-C.; Cheng, Y.-S. E.; Yang, A.-S.; Hsiao, S.-C.; Su, C.-Y.; Wong, C.-H. *J. Am. Chem. Soc.* **2007**, *129*, 11892-11893.
- (159) Shie, J.-J.; Fang, J.-M.; Wong, C.-H. *Angew. Chem. Int. Ed.* **2008**, *47*, 5788-5791.
- (160) Carbain, B.; Hitchcock, P. B.; Streicher, H. *Tetrahedron Lett.* **2010**, *51*, 2717-2719.
- (161) Carbain, B.; Martin, S. R.; Collins, P. J.; Hitchcock, P. B.; Streicher, H. *Org. Biomol. Chem.* **2009**, *7*, 2570-2575.
- (162) Lundquist, J. J.; Toone, E. J. *Chem. Rev.* **2002**, *102*, 555-578.
- (163) Pieters, R. J. *Org. Biomol. Chem.* **2009**, *7*, 2013-2025.
- (164) Kiessling, L. L.; Gestwicki, J. E.; Strong, L. E. *Curr. Opin. Chem. Biol.* **2000**, *4*, 696-703.
- (165) Gestwicki, J. E.; Cairo, C. W.; Strong, L. E.; Oetjen, K. A.; Kiessling, L. L. *J. Am. Chem. Soc.* **2002**, *124*, 14922-14933.
- (166) Mammen, M.; Choi, S.-K.; Whitesides, G. M. *Angew. Chem. Int. Ed.* **1998**, *37*, 2754-2794.
- (167) Watowich, S. J.; Skehel, J. J.; Wiley, D. C. *Structure* **1994**, *2*, 719-731.

- (168) Bovin, N. V.; Tuzikov, A. B.; Chinarev, A. A.; Gambaryan, A. S. *Glycoconj. J.* **2004**, *21*, 471-478.
- (169) Carlescu, I.; Scutaru, D.; Popa, M.; Uglea, C. *Med. Chem. Res.* **2009**, *18*, 477-494.
- (170) Glick, G. D.; Toogood, P. L.; Wiley, D. C.; Skehel, J. J.; Knowles, J. R. *J. Biol. Chem.* **1991**, *266*, 23660-23669.
- (171) Dondoni, A.; Marra, A. *Chem. Rev.* **2010**, *110*, 4949-4977.
- (172) Marra, A.; Moni, L.; Pazzi, D.; Corallini, A.; Bridi, D.; Dondoni, A. *Org. Biomol. Chem.* **2008**, *6*, 1396-1409.
- (173) Roy, R.; Zanini, D.; Meunier, S. J.; Romanowska, A. *J. Chem. Soc., Chem. Commun.* **1993**, 1869-1872.
- (174) Reuter, J.; D. Myc, A.; Hayes, M. M.; Gan, Z.; Roy, R.; Qin, D.; Yin, R.; Piehler, L. T.; Esfand, R.; Tomalia, D. A.; Baker, J. R. *Bioconj. Chem.* **1999**, *10*, 271-278.
- (175) Papp, I.; Sieben, C.; Sisson, A. L.; Kostka, J.; Böttcher, C.; Ludwig, K.; Herrmann, A.; Haag, R. *ChemBioChem* **2011**, *12*, 887-895.
- (176) Mammen, M.; Dahmann, G.; Whitesides, G. M. *J. Med. Chem.* **1995**, *38*, 4179-4190.
- (177) Choi, S.-K.; Mammen, M.; Whitesides, G. M. *J. Am. Chem. Soc.* **1997**, *119*, 4103-4111.
- (178) Roy, R.; Andersson, F. O.; Harms, G.; Kelm, S.; Schauer, R. *Angew. Chem. Int. Ed.* **1992**, *31*, 1478-1481.
- (179) Suzuki, K.; Sakamoto, J.-I.; Koyama, T.; Yingsakmongkon, S.; Suzuki, Y.; Hatano, K.; Terunuma, D.; Matsuoka, K. *Bioorg. Med. Chem. Lett.* **2009**, *19*, 5105-5108.
- (180) Umemura, M.; Makimura, Y.; Itoh, M.; Yamamoto, T.; Mine, T.; Mitani, S.; Simizu, I.; Ashida, H.; Yamamoto, K. *Carbohydr. Polym.* **2010**, *81*, 330-334.
- (181) Wilchek, M.; Bayer, E. A. *Anal. Biochem.* **1988**, *171*, 1-32.
- (182) Reece, P. A.; Watson, K. G.; Wu, W.-Y.; Jin, B.; Krippner, G. Y. Method and novel compounds for use therein, **1997**, WO/1998/021243.
- (183) Honda, T.; Yoshida, S.; Arai, M.; Masuda, T.; Yamashita, M. *Bioorg. Med. Chem. Lett.* **2002**, *12*, 1929-1932.
- (184) Macdonald, S. J. F.; Watson, K. G.; Cameron, R.; Chalmers, D. K.; Demaine, D. A.; Fenton, R. J.; Gower, D.; Hamblin, J. N.; Hamilton, S.; Hart, G. J.; Inglis, G. G. A.; Jin, B.; Jones, H. T.; McConnell, D. B.; Mason, A. M.; Nguyen, V.;

- Owens, I. J.; Parry, N.; Reece, P. A.; Shanahan, S. E.; Smith, D.; Wu, W.-Y.; Tucker, S. P. *Antimicrob. Agents Chemother.* **2004**, *48*, 4542-4549.
- (185) Macdonald, S. J. F.; Cameron, R.; Demaine, D. A.; Fenton, R. J.; Foster, G.; Gower, D.; Hamblin, J. N.; Hamilton, S.; Hart, G. J.; Hill, A. P.; Inglis, G. G. A.; Jin, B.; Jones, H. T.; McConnell, D. B.; McKimm-Breschkin, J.; Mills, G.; Nguyen, V.; Owens, I. J.; Parry, N.; Shanahan, S. E.; Smith, D.; Watson, K. G.; Wu, W.-Y.; Tucker, S. P. *J. Med. Chem.* **2005**, *48*, 2964-2971.
- (186) Watson, K. G.; Cameron, R.; Fenton, R. J.; Gower, D.; Hamilton, S.; Jin, B.; Krippner, G. Y.; Luttick, A.; McConnell, D.; MacDonald, S. J. F.; Mason, A. M.; Nguyen, V.; Tucker, S. P.; Wu, W.-Y. *Bioorg. Med. Chem. Lett.* **2004**, *14*, 1589-1592.
- (187) Wen, W.-H.; Lin, M.; Su, C.-Y.; Wang, S.-Y.; Cheng, Y.-S. E.; Fang, J.-M.; Wong, C.-H. *J. Med. Chem.* **2009**, *52*, 4903-4910.
- (188) Weight, A. K.; Haldar, J.; Álvarez de Cienfuegos, L.; Gubareva, L. V.; Tumpey, T. M.; Chen, J.; Klibanov, A. M. *J. Pharm. Sci.* **2011**, *100*, 831-835.
- (189) Kimura, Y.; Yamatsugu, K.; Kanai, M.; Echigo, N.; Kuzuhara, T.; Shibasaki, M. *Tetrahedron Lett.* **2009**, *50*, 3205-3208.
- (190) Sardar, R.; Funston, A. M.; Mulvaney, P.; Murray, R. W. *Langmuir* **2009**, *25*, 13840-13851.
- (191) de la Fuente, J. M.; Penades, S. *Biochim. Biophys. Acta* **2006**, *1760*, 636-651.
- (192) Badia, A.; Singh, S.; Demers, L.; Cuccia, L.; Brown, G. R.; Lennox, R. B. *Chem. Eur. J.* **1996**, *2*, 359-363.
- (193) Love, J. C.; Estroff, L. A.; Kriebel, J. K.; Nuzzo, R. G.; Whitesides, G. M. *Chem. Rev.* **2005**, *105*, 1103-1170.
- (194) Drechsler, U.; Erdogan, B.; Rotello, V. M. *Chem. Eur. J.* **2004**, *10*, 5570-5579.
- (195) Daniel, M.-C.; Astruc, D. *Chem. Rev.* **2004**, *104*, 293-346.
- (196) Larsen, K.; Thygesen, M. B.; Guillaumie, F.; Willats, W. G. T.; Jensen, K. J. *Carbohydr. Res. Synth. Chem.* **2006**, *341*, 1209-1234.
- (197) Rojo, J.; Díaz, V.; de la Fuente, J. M.; Segura, I.; Barrientos, A. G.; Riese, H. H.; Bernad, A.; Penadés, S. *ChemBioChem* **2004**, *5*, 291-297.
- (198) Barrientos, Á. G.; de la Fuente, J. M.; Rojas, T. C.; Fernández, A.; Penadés, S. *Chem. Eur. J.* **2003**, *9*, 1909-1921.
- (199) Sun, I.-C.; Lee, S.; Koo, H.; Kwon, I. C.; Choi, K.; Ahn, C.-H.; Kim, K. *Bioconj. Chem.* **2010**, *21*, 1939-1942.
- (200) Zhao, Y.; Tian, Y.; Cui, Y.; Liu, W.; Ma, W.; Jiang, X. *J. Am. Chem. Soc.* **2010**, *132*, 12349-12356.

- (201) Saada, M.-C.; Montero, J.-L.; Vullo, D.; Scozzafava, A.; Winum, J.-Y.; Supuran, C. T. *J. Med. Chem.* **2011**, *54*, 1170-1177.
- (202) Cheng, Y.; Meyers, J. D.; Broome, A.-M.; Kenney, M. E.; Basilion, J. P.; Burda, C. *J. Am. Chem. Soc.* **2011**, *133*, 2583-2591.
- (203) Stark, W. J. *Angewandte Chemie International Edition* **2011**, *50*, 1242-1258.
- (204) Templeton, A. C.; Wuelfing, W. P.; Murray, R. W. *Acc. Chem. Res.* **2000**, *33*, 27-36.
- (205) Jadzinsky, P. D.; Calero, G.; Ackerson, C. J.; Bushnell, D. A.; Kornberg, R. D. *Science* **2007**, *318*, 430-433.
- (206) Kumar, A.; Mandal, S.; Selvakannan, P.; Pasricha, R.; Mandale, A. B.; Sastry, M. *Langmuir* **2003**, *19*, 6277-6282.
- (207) Leff, D. V.; Brandt, L.; Heath, J. R. *Langmuir* **1996**, *12*, 4723-4730.
- (208) Brust, M.; Walker, M.; Bethell, D.; Schiffrin, D. J.; Whyman, R. *J. Chem. Soc., Chem. Commun.* **1994**, 801-802.
- (209) Brust, M.; Fink, J.; Bethell, D.; Schiffrin, D. J.; Kiely, C. *J. Chem. Soc., Chem. Commun.* **1995**, 1655-1656.
- (210) Turkevich, J.; Stevenson, P. C.; Hillier, J. *Discuss. Faraday Soc.* **1951**, *11*, 55-75.
- (211) Jana, N. R.; Gearheart, L.; Murphy, C. J. *Chem. Mater.* **2001**, *13*, 2313-2322.
- (212) Goulet, P. J. G.; Lennox, R. B. *J. Am. Chem. Soc.* **2010**, *132*, 9582-9584.
- (213) Li, Y.; Zaluzhna, O.; Xu, B.; Gao, Y.; Modest, J. M.; Tong, Y. J. *J. Am. Chem. Soc.* **2011**, *133*, 2092-2095.
- (214) Templeton, A. C.; Chen, S.; Gross, S. M.; Murray, R. W. *Langmuir* **1999**, *15*, 66-76.
- (215) de Paz, J.-L.; Ojeda, R.; Barrientos, A. G.; Penades, S.; Martin-Lomas, M. *Tetrahedron: Asymmetry* **2005**, *16*, 149-158.
- (216) Bowman, M.-C.; Ballard, T. E.; Ackerson, C. J.; Feldheim, D. L.; Margolis, D. M.; Melander, C. *J. Am. Chem. Soc.* **2008**, *130*, 6896-6897.
- (217) de la Fuente, J. M.; Barrientos, A. G.; Rojas, T. C.; Rojo, J.; Cañada, J.; Fernández, A.; Penadés, S. *Angew. Chem. Int. Ed.* **2001**, *40*, 2257-2261.
- (218) Kimling, J.; Maier, M.; Okenve, B.; Kotaidis, V.; Ballot, H.; Plech, A. *J. Phys. Chem. B.* **2006**, *110*, 15700-15707.
- (219) Ojea-Jiménez, I.; Romero, F. M.; Bastús, N. G.; Puentes, V. *J. Phys. Chem. C.* **2010**, *114*, 1800-1804.

- (220) Kumar, S.; Gandhi, K. S.; Kumar, R. *Ind. Eng. Chem. Res.* **2007**, *46*, 3128-3136.
- (221) Schlenoff, J. B.; Li, M.; Ly, H. *J. Am. Chem. Soc.* **1995**, *117*, 12528-12536.
- (222) Shon, Y.-S.; Choo, H. *C. R. Chim.* **2003**, *6*, 1009-1018.
- (223) Christian, P.; von der Kammer, F.; Baalousha, M.; Hofmann, T. *Ecotoxicology* **2008**, *17*, 326-343.
- (224) Boisselier, E.; Astruc, D. *Chem. Soc. Rev.* **2009**, *38*, 1759-1782.
- (225) Zhou, J.; Ralston, J.; Sedev, R.; Beattie, D. A. *J. Colloid Interface Sci.* **2009**, *331*, 251-262.
- (226) Rucareanu, S.; Gandubert, V. J.; Lennox, R. B. *Chem. Mater.* **2006**, *18*, 4674-4680.
- (227) Weisbecker, C. S.; Merritt, M. V.; Whitesides, G. M. *Langmuir* **1996**, *12*, 3763-3772.
- (228) Shipway, A. N.; Lahav, M. Gabai, R.; Willner, I. *Langmuir* **2000**, *16*, 8789-8795.
- (229) Ackerson, C. J.; Jadzinsky, P. D.; Kornberg, R. D. *J. Am. Chem. Soc.* **2005**, *127*, 6550-6551.
- (230) Lin, S.-Y.; Tsai, Y.-T.; Chen, C.-C.; Lin, C.-M.; Chen, C.-hsien *J. Phys. Chem. B.* **2004**, *108*, 2134-2139.
- (231) Aryal, S. K.C., R. B.; Bhattarai, N.; Kim, C. K.; Kim, H. Y. *J. Colloid Interface Sci.* **2006**, *299*, 191-197.
- (232) Lévy, R.; Thanh, N. T. K.; Doty, R. C.; Hussain, I.; Nichols, R. J.; Schiffrin, D. J.; Brust, M.; Fernig, D. G. *J. Am. Chem. Soc.* **2004**, *126*, 10076-10084.
- (233) Selvakannan, P.; Mandal, S.; Phadtare, S.; Pasricha, R.; Sastry, M. *Langmuir* **2003**, *19*, 3545-3549.
- (234) Lohse, S. E.; Dahl, J. A.; Hutchison, J. E. *Langmuir* **2010**, *26*, 7504-7511.
- (235) Hostetler, M. J.; Wingate, J. E.; Zhong, C.-J.; Harris, J. E.; Vachet, R. W.; Clark, M. R.; Londono, J. D.; Green, S. J.; Stokes, J. J.; Wignall, G. D.; Glish, G. L.; Porter, M. D.; Evans, N. D.; Murray, R. W. *Langmuir* **1998**, *14*, 17-30.
- (236) Westcott, S. L.; Oldenburg, S. J.; Lee, T. R.; Halas, N. J. *Chem. Phys. Lett.* **1999**, *300*, 651-655.
- (237) Hone, D. C.; Haines, A. H.; Russell, D. A. *Langmuir* **2003**, *19*, 7141-7144.
- (238) Schofield, C. L.; Haines, A. H.; Field, R. A.; Russell, D. A. *Langmuir* **2006**, *22*, 6707-6711.

- (239) Elghanian, R.; Storhoff, J. J.; Mucic, R. C.; Letsinger, R. L.; Mirkin, C. A. *Science* **1997**, *277*, 1078-1081.
- (240) Lacerda, S. H. D. P.; Park, J. J.; Meuse, C.; Pristinski, D.; Becker, M. L.; Karim, A.; Douglas, J. F. *ACS Nano* **2010**, *4*, 365-379.
- (241) Reynolds, A. J.; Haines, A. H.; Russell, D. A. *Langmuir* **2006**, *22*, 1156-1163.
- (242) Schofield, C. L.; Field, R. A.; Russell, D. A. *Anal. Chem.* **2007**, *79*, 1356-1361.
- (243) Wang, S.; Singh, A. K.; Senapati, D.; Neely, A.; Yu, H.; Ray, P. C. *Chem. Eur. J.* **2010**, *16*, 5600-5606.
- (244) Shawky, S. M.; Bald, D.; Azzazy, H. M. E. *Clin. Biochem.* **2010**, *43*, 1163-1168.
- (245) Jiang, Y.; Zhao, H.; Lin, Y.; Zhu, N.; Ma, Y.; Mao, L. *Angew. Chem. Int. Ed.* **2010**, *49*, 4800-4804.
- (246) Wu, S.-H.; Wu, Y.-S.; Chen, C.-hsien *Anal. Chem.* **2008**, *80*, 6560-6566.
- (247) Oh, S. Y.; Cornell, B.; Smith, D.; Higgins, G.; Burrell, C. J.; Kok, T. W. *Biosens. Bioelectron.* **2008**, *23*, 1161-1165.
- (248) Diouani, M. F.; Helali, S.; Hafaid, I.; Hassen, W. M.; Snoussi, M. A.; Ghram, A.; Jaffrezic-Renault, N.; Abdelghani, A. *Mater. Sci. Eng. C* **2008**, *28*, 580-583.
- (249) Kim, S. A.; Byun, K. M.; Kim, K.; Jang, S. M.; Ma, K.; Oh, Y.; Kim, D.; Kim, S. G.; Shuler, M. L.; Kim, S. J. *Nanotechnology* **2010**, *21*, 355503.
- (250) Peng, F.; Wang, Z.; Zhang, S.; Wu, R.; Hu, S.; Li, Z.; Wang, X.; Bi, D. *Clin. Vaccine Immunol.* **2008**, *15*, 569-574.
- (251) Chang, Y.-F.; Wang, S.-F.; Huang, J. C.; Su, L.-C.; Yao, L.; Li, Y.-C.; Wu, S.-C.; Chen, Y.-M. A.; Hsieh, J.-P.; Chou, C. *Biosens. Bioelectron.* **2010**, *26*, 1068-1073.
- (252) Ackerson, C. J.; Jadzinsky, P. D.; Jensen, G. J.; Kornberg, R. D. *J. Am. Chem. Soc.* **2006**, *128*, 2635-2640.
- (253) Cheng, X.-D.; yuan, Q.; yue, Q.-H.; Zheng, Q.-B.; Ma, Y.-Y.; Yang, B.-C.; Zhang, R.; Chen, Y.-X.; Su, M.-Q.; Zhang, J.; Xia, N.-S.; Hao, X.-K. *J. Clin. Virol.* **2011**, *50*, 153-155.
- (254) Zhao, J.; Tang, S.; Storhoff, J.; Marla, S.; Bao, Y. P.; Wang, X.; Wong, E.; Ragupathy, V.; Ye, Z.; Hewlett, I. *BMC Biotechnology* **2010**, *10*, 74.
- (255) Papp, I.; Sieben, C.; Ludwig, K.; Roskamp, M.; Böttcher, C.; Schlecht, S.; Herrmann, A.; Haag, R. *Small* **2010**, *6*, 2900-2906.
- (256) Zhang, L.; Wei, G.; Du, Y. *Carbohydr. Res.* **2009**, *344*, 2083-2087.

- (257) Bondioli, L.; Costantino, L.; Ballestrazzi, A.; Lucchesi, D.; Boraschi, D.; Pellati, F.; Benvenuti, S.; Tosi, G.; Vandelli, M. A. *Biomaterials* **2010**, *31*, 3395-3403.
- (258) Sametband, M.; Shukla, S.; Meningher, T.; Hirsh, S.; Mendelson, E.; Sarid, R.; Gedanken, A.; Mandelboim, M. *MedChemComm* **2011**, *2*, 421-423.
- (259) Kamikawa, T. L.; Mikolajczyk, M. G.; Kennedy, M.; Zhang, P.; Wang, W.; Scott, D. E.; Alcocilja, E. C. *Biosens. Bioelectron.* **2010**, *26*, 1346-1352.
- (260) Halfpenny, K. C.; Wright, D. W. *Wiley Interdiscip. Rev. Nanomed. Nanobiotechnol.* **2010**, *2*, 277-290.
- (261) Amano, Y.; Cheng, Q. *Anal. Bioanal. Chem.* **2005**, *381*, 156-164.
- (262) Charych, D.; Nagy, J.; Spevak, W.; Bednarski, M. *Science* **1993**, *261*, 585-588.
- (263) Baek, M.-G.; Stevens, R. C.; Charych, D. H. *Bioconj. Chem.* **2000**, *11*, 777-788.
- (264) Gavin, P. J.; Thomson, R. B. *Clin. Appl. Immunol. Rev.* **2004**, *4*, 151-172.
- (265) Hata, K.; Koseki, K.; Yamaguchi, K.; Moriya, S.; Suzuki, Y.; Yingsakmongkon, S.; Hirai, G.; Sodeoka, M.; von Itzstein, M.; Miyagi, T. *Antimicrob. Agents Chemother.* **2008**, *52*, 3484-3491.
- (266) Giljohann, D. A.; Seferos, D. S.; Daniel, W. L.; Massich, M. D.; Patel, P. C.; Mirkin, C. A. *Angew. Chem. Int. Ed.* **2010**, *49*, 3280-3294.
- (267) Kolb, H. C.; Finn, M. G.; Sharpless, K. B. *Angew. Chem. Int. Ed.* **2001**, *40*, 2004-2021.
- (268) Lobana, T. S.; Bhatia, P. K. *J. Chem. Soc., Dalton Trans.* **1992**, 1407-1410.
- (269) Carbain, B. A convenient synthesis of bioactive cyclohexenephosphonates. Doctoral thesis, University of Sussex, 2010.
- (270) Ojea-Jiménez, I.; Puentes, V. *J. Am. Chem. Soc.* **2009**, *131*, 13320-13327.
- (271) Alvarez, M. M.; Khoury, J. T.; Schaaff, T. G.; Shafigullin, M. N.; Vezmar, I.; Whetten, R. L. *J. Phys. Chem. B.* **1997**, *101*, 3706-3712.
- (272) Personal communication from Dr L. Karlsson, Oxford Materials, University of Oxford. **2010**.
- (273) López-Cartes, C.; Rojas, T. C.; Litrán, R.; Martínez-Martínez, D.; de la Fuente, J. M.; Penadés, S.; Fernández, A. *J. Phys. Chem. B.* **2005**, *109*, 8761-8766.
- (274) Fiurasek, P.; Reven, L. *Langmuir* **2007**, *23*, 2857-2866.
- (275) Geiss, R. Eds.; Brundle, R. C.; Evans, C. A.; Wilson, S. In *Encyclopedia of Materials Characterisation, Surfaces, Interfaces, Thin Films*; Elsevier: Netherlands, 1992; Vol. 3.1, pp. 120-121.

- (276) Hassellöv, M.; Readman, J.; Ranville, J.; Tiede, K. *Ecotoxicology* **2008**, *17*, 344-361-361.
- (277) Wang, D.; Nap, R. J.; Lagzi, I.; Kowalczyk, B.; Han, S.; Grzybowski, B. A.; Szleifer, I. *J. Am. Chem. Soc.* **2011**, *133*, 2192-2197.
- (278) Wang, D.; Kowalczyk, B.; Lagzi, I.; Grzybowski, B. A. *J. Phys. Chem. Lett.* **2010**, *1*, 1459-1462.
- (279) Mountford, C. E.; Grossman, G.; Holmes, K. T.; O'Sullivan, W. J.; Hampson, A. W.; Raison, R. L.; Webster, R. *Mol. Immunol.* **1982**, *19*, 811-816.
- (280) Takahashi, T.; Suzuki, Y.; Nishinaka, D.; Kawase, N.; Kobayashi, Y.; Hindari, K. I.-P. J.; Miyamoto, D.; Guo, C.-T.; Shortridge, K. F.; Suzuki, T. *J. Biochem.* **2001**, *130*, 279 -283.
- (281) SOP No 25/C2, Fluorescent (MUNANA) neuraminidase inhibition assay for influenza virus drug susceptibility determination, Division of Virology and WHO Collaborating Centre for Influenza Reference and Research, Mill Hill, London, UK. **2010**.
- (282) Medley, C. D.; Smith, J. E.; Tang, Z.; Wu, Y.; Bamrungsap, S.; Tan, W. *Anal. Chem.* **2008**, *80*, 1067-1072.
- (283) Meldal, M.; Tornø, C. W. *Chem. Rev.* **2008**, *108*, 2952-3015.
- (284) Stanley, M.; Martin, S. R.; Birge, M.; Carbain, B.; Streicher, H. *Org. Biomol. Chem.* **2011**, *9*, 5625-5629.
- (285) Johnson, I. D.; Pawley, J. B. In *Handbook of Biological Confocal Microscopy*; Plenum: New York, 2006; Vol. Chapter 17, pp. 353-367.
- (286) McKimm-Breschkin, J. L.; Colman, P. M.; Jin, B.; Krippner, G. Y.; McDonald, M.; Reece, P. A.; Tucker, S. P.; Waddington, L.; Watson, K. G.; Wu, W.-Y. *Angew. Chem. Int. Ed.* **2003**, *42*, 3118-3121.
- (287) Niikura, K.; Nagakawa, K.; Ohtake, N.; Suzuki, T.; Matsuo, Y.; Sawa, H.; Ijio, K. *Bioconj. Chem.* **2009**, *20*, 1848-1852.
- (288) Goodrich, G. P.; Helfrich, M. R.; Overberg, J. J.; Keating, C. D. *Langmuir* **2004**, *20*, 10246-10251.

V. Appendices

V.1. Appendix 1. PLE experiments

α -sialoside substrate	Method of analysis	PLE conc. ⁺	pH [#]	Temp. (°C)	Total time of experiment (hrs)	Results
4	¹ H NMR	400 mU	8	RT	168	No hydrolysis
25	¹ H NMR	400 mU	8	RT	168	No hydrolysis
4	¹ H NMR	1 U	8	30	120	No hydrolysis
4	¹ H NMR	10 U	8	30	120	No hydrolysis
4	¹ H NMR	100 U	8	30	120	No hydrolysis
25	¹ H NMR	1 U	8	30	120	No hydrolysis
25	¹ H NMR	10 U	8	30	120	No hydrolysis
25	¹ H NMR	100 U	8	30	120	No hydrolysis
4	TLC	54 U	6	35	168	No hydrolysis
4	TLC	54 U	7	35	168	No hydrolysis
4	TLC	54 U	8	35	168	No hydrolysis
4	TLC	54 U	9	35	168	No hydrolysis
25	TLC	54 U	6	35	168	No hydrolysis
25	TLC	54 U	7	35	168	No hydrolysis
25	TLC	54 U	8	35	168	No hydrolysis
25	TLC	54 U	9	35	168	No hydrolysis

* Substrate concentration given as percentage of total volume of PBS buffer.

1% substrate concentration (all experiments).

+ The amount of PLE is expressed in Units (1 U = 1 $\mu\text{mol min}^{-1}$). PLE used as a lyophilised powder (measured activity of 27 Umg^{-1})

pH (monitored by indicator paper range 7-11). pH 8 is the unmodified pH of PBS buffer solution

Table A1. Table of experimental conditions used in the unsuccessful hydrolysis of the methyl ester of compound **4** and compound **25**

Experimental comments

NMR experiments

PLE was suspended in deuterated PBS buffer. Reference ^1H NMR (32 scans) were taken of the substrates (α -*O*-allyl sialoside **4** and 8,9-epoxide derivative **25**) in PBS alone and PBS incubated with PLE. ^1H NMR spectra (32 scans) were taken over the course of the reaction (every 30 minutes then hourly, then daily). Conditions were varied for different experiments (amount of PLE, pH and incubation temperature).

No reduction was observed in the methyl-ester ^1H NMR resonance (δ 3.85 ppm in D_2O for α -*O*-allyl sialoside **4** and 8,9-epoxide derivative **25**) in any experiment.

TLC experiments

The pH of solution was varied (by addition of 0.5 M $\text{HCl}_{(\text{aq})}$ or $\text{NaOH}_{(\text{aq})}$) for PLE hydrolysis reactions with α -*O*-allyl sialoside **4** and 8,9-epoxide derivative **25**.

The reactions were monitored over time by spotting TLC plates at appropriate intervals and eluting with an appropriate TLC solvent system (EA/MeOH 5:1 for α -*O*-allyl sialoside **4** and EA/MeOH 10:1 8,9-epoxide derivative **25**).

No hydrolysis product was observed by TLC analysis for α -*O*-allyl sialoside **4** and 8,9-epoxide derivative **25**.

PLE enzymatic hydrolysis of 3-cyclohexene-1-carboxylic acid methyl ester to 3-cyclohexene-1-carboxylic acid determined by ^1H NMR

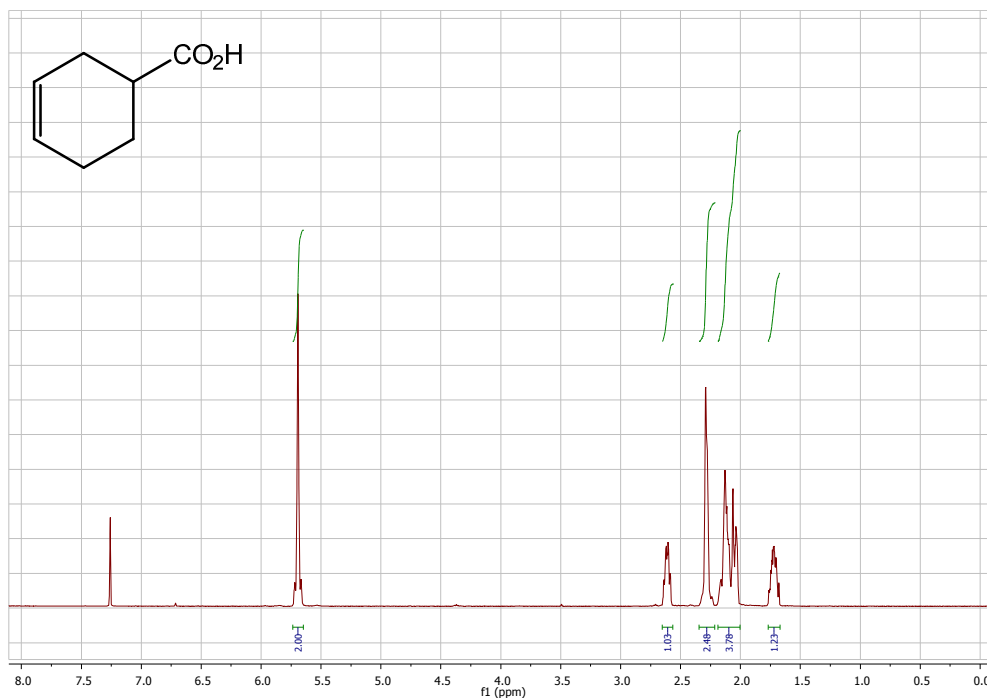


Figure A1. ^1H NMR of 3-cyclohexene-1-carboxylic acid (reference sample).
NMR solvent: CDCl_3

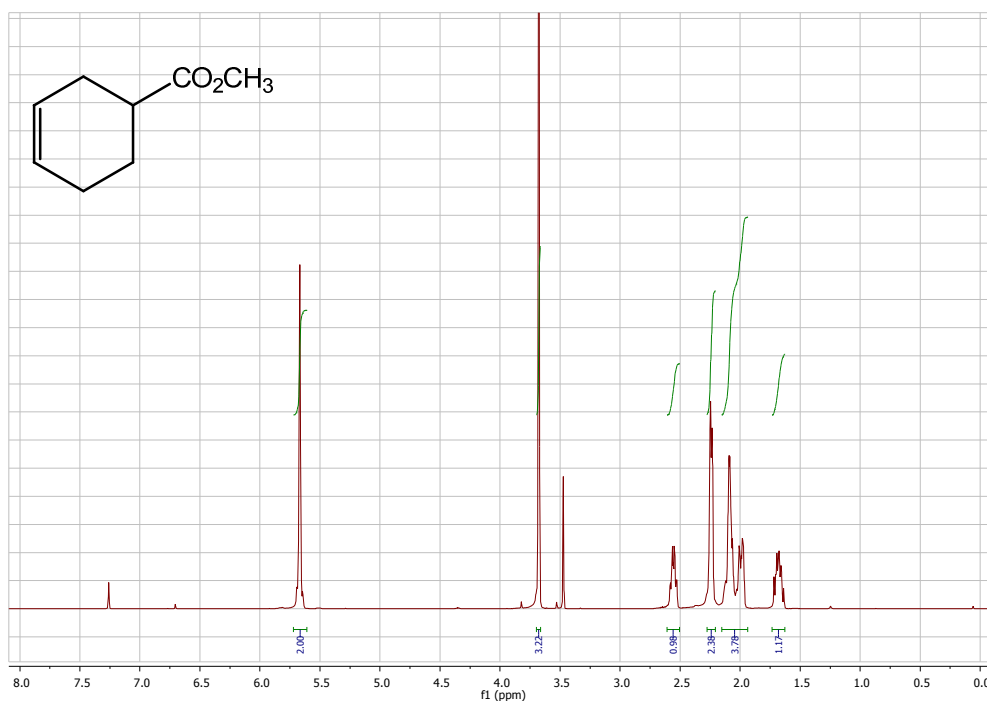


Figure A2. ^1H NMR of 3-cyclohexene-1-carboxylic acid methyl ester (pre-PLE hydrolysis). The methyl-ester ($-\text{CO}_2\text{CH}_3$) resonance is observed at δ 3.68 ppm (s). NMR solvent: CDCl_3

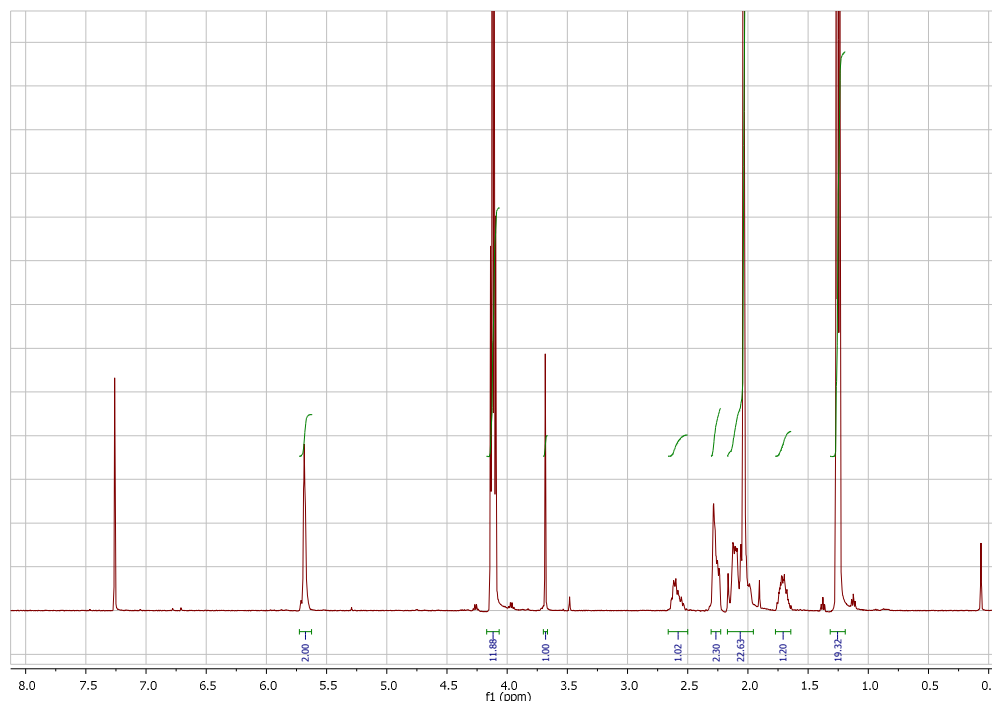


Figure A3. ^1H NMR of hydrolysis product. The hydrolysis of 3-cyclohexene-1-carboxylic acid methyl ester as observed by the reduction in the methyl-ester ($-\text{CO}_2\text{CH}_3$) ^1H resonance (δ 3.68 ppm (s)). Ethyl acetate impurity present in NMR spectrum (δ 4.12 ppm (q), 2.04 ppm (s) and 1.25 ppm (t)). NMR solvent: CDCl_3

Rudimentary ^1H NMR analysis (see **figure A3**) indicated that PLE hydrolysis of 3-cyclohexene-1-carboxylic acid methyl ester led to the formation of 3-cyclohexene-1-carboxylic acid. This was determined from the reduction in intensity of the methyl-ester ^1H resonance (δ 3.68 ppm) in comparison to other relevant ^1H resonance signals for the 3-cyclohexene-1-carboxylic acid scaffold. This indicates that the PLE enzyme is active.

The amount of product formed by this hydrolysis reaction and their diastereomeric determination were not carried out. The importance of this experiment was to observe the PLE enzyme working upon a known substrate. The lack of enzymatic hydrolysis with α -O-allyl sialoside **4** and the 8,9-epoxide derivative **25** suggests that these α -sialosides are not suitable PLE substrates.

V.2. Appendix 2. Dynamic light scattering (DLS)

Introduction

Dynamic light scattering (DLS) is a non-invasive technique which can be used for measuring the size of nanoparticles in a dispersion.^{1,2,3} The technique measures the time-dependent fluctuations in the intensity of scattered light from a suspension of particles undergoing Brownian motion.¹

The DLS instrument measures the intensity of light scattered from the nanoparticle over time (δt) and then correlates the detected light intensity at the t_0 (initial time or “time zero”) with $[t_0 + \delta t]$ as an “autocorrelation function”. As such, small particles lose their correlation more rapidly than larger particles due to a faster rate of diffusion.^{2,4}

The “autocorrelation function” ($g(\tau)$) of scattered light intensity is given by the relation;

$$g(\tau) = |G(\tau) - \langle I \rangle^2 / \gamma|^{1/2} = Ae^{-2\Gamma\tau}$$

$G(\tau)$: field autocorrelation function

$\langle I \rangle^2$: base line

γ : coherence factor

A : instrument specific constant

Γ : decay rate

τ : delay time

The diffusion coefficient for a nanoparticle (D) can be determined using the relation;

$$D = \Gamma/q^2 \quad \dots \text{where, } q: \text{ wave vector}$$

$$q = 4\pi\eta \sin(\pi/4)/\lambda$$

η : refractive index of surrounding medium

λ : wavelength of incident light

Therefore, analysis of the intensity fluctuations (obtained by plotting the intensity of scattered light as an “autocorrelation function”) allows for the determination of the nanoparticle diffusion coefficient (D), which in turn yields the particle size (i.e., the hydrodynamic radius (R_h)) through the Stokes- Einstein equation;

$$R_h = kT / 6\pi\eta D$$

k: Boltzmann's constant

T: Absolute temperature

Dynamic light scattering is a low resolution technique with the ability to resolve materials with a factor of three difference in their sizes. It is therefore not possible to resolve different sized peaks for various particle species (i.e. single particle, two particles and multiple-particle aggregates).³

Data obtained from DLS

The direct output from the DLS experiment is a distribution by intensity, that is, the area of each of the modes is related to the intensity of light scattered. The result obtained, the Z-average diameter (the mean hydrodynamic diameter) and the polydispersity index (an estimate of the sample distribution width) are intensity-weighted values and will therefore be sensitive to any larger size species in the sample.^{1,3}

For an ideal monodisperse sample, the peak in the intensity distribution is expected to be very close to the Z-average size from the Cumulant fit (Cumulants analysis being a mathematical tool to extract useful information from the autocorrelation function). As a consequence of sample polydispersity, the mean size of the peak by intensity is different from the Cumulant size. The Z-average is an intensity weighted average, therefore any polydispersity or breadth of particle size distribution will bias the Z-average toward the larger particle sizes^{3,5} as the scattering intensity of a nanoparticle suspension is proportional to R^6 (where R is the nanoparticle radius). As a result, a small population of large particulates can dictate the appearance of the intensity distribution obtained therefore making the particle distribution misleading.^{6,5}

The intensity distribution may be further manipulated mathematically to transform the result into a volume and a number distribution.⁴ Correct material properties (refractive index and absorption) are required to obtain accuracy in the results relating to volume and number distributions. Interpretation of DLS data beyond the intensity distribution is problematic. Along with the inherent uncertainty introduced to the DLS intensity data from band spreading (due to the mathematically ill-defined problem of deconvoluting the autocorrelation function) and the assumptions of nanoparticle morphology (homogenous and spherical), the mathematical conversion from intensity to volume and/or number-based distributions derived from intensity data typically skews particle

size to some degree.⁷ For accuracy of results, information about the optical properties of the dispersing medium and the dispersed phase is needed for the mathematical transformation. The effect is that for particle sizes below approximately 100 nm, the volume and number averages are smaller than the intensity average. As such, volume and number distributions derived from DLS measurements are best implemented for comparison purposes and do not correspond to absolute values.^{7,8}

DLS in relation to TEM imaging

For polydisperse samples, results obtained from DLS analysis will be larger than those obtained from TEM imaging due to the contribution of scattering from the larger particle aggregates. Number based metrologies are typically microscopy techniques, such as TEM, where particle images are counted and sorted into size bins. Again, when comparing size results obtained using electron microscopy, it must be noted that the corresponding size distribution for comparison is the number distribution.^{3,9}

References

- (1) Pecora, R. Dynamic light scattering measurement of nanometer particles in liquids. *J. Nanoparticle Res.* **2000**, *2*, 123-131.
- (2) Hassellöv, M. Readman, J. Ranville, J.; Tiede, K. Nanoparticle analysis and characterization methodologies in environmental risk assessment of engineered nanoparticles. *Ecotoxicology* **2008**, *17*, 344-361-361.
- (3) Characterisation of Colloidal Gold using Dynamic Light Scattering, Zetasizer Nano application note, MRK556-01, Malvern Instruments Ltd., <http://www.malvern.com/>, **2010**.
- (4) Dynamic Light Scattering: An introduction, DLS Technical note, MRK556-01, Malvern Instruments Ltd., <http://www.malvern.com/>, **2010**.
- (5) FAQ. What is the Z-average?, Malvern Instruments Ltd., <http://www.malvern.com/>, **2010**.
- (6) FAQ. How Accurate is the DLS Volume Distribution?, Malvern Instruments Ltd., <http://www.malvern.com/>, **2010**.
- (7) FAQ. Calculating Volume Distributions from Dynamic Light Scattering Data, Malvern Instruments Ltd., <http://www.malvern.com/>, **2010**.
- (8) Nobbmann, U.; Morfesis, A. Light Scattering and Nanoparticles. *Materials Today* *12*, 52-54.
- (9) FAQ. How different are the Z-average and TEM sizes?, Malvern Instruments Ltd., <http://www.malvern.com/>, **2010**.

V.3. Appendix 3.

Calculation of concentration of 'small TamiGold' and phospho-oseltamivir moieties in inhibition assays

Ratio (Au/phospho-oseltamivir moiety) = 1:1 based on EDX-analysis of the Au/S ratio.

Number of Au atoms/particle for a diameter of 2 nm: ~ 200.¹

Calculation of the number of gold atoms in a spherical nanoparticle;

$$n_{\text{Au}} = 4\pi (d/2)^3/3V_g$$

d: diameter of particle

V_g : volume of gold atom (fcc) = 17 Å³

This results in an estimate of 200 Au atoms and 200 phospho-oseltamivir moieties per particle, thus allowing calculation of the molecular weight per particle (m_{Particle});

$$m_{\text{Particle}} = 126500 \text{ Da} (200 \times m_{\text{Au}} + 200 \times (m_{\text{Compound 4}})/2).$$

m_{Au} : molecular weight of gold

m_{Compound} : molecular weight of phospho-oseltamivir derivative

Concentrations of 'small TamiGold' and phospho-oseltamivir moieties in stock solution used for inhibition assays;

Particle concentration: 1 mg/mL (particle) = 7.9×10^{-6} mM/mL (particle).

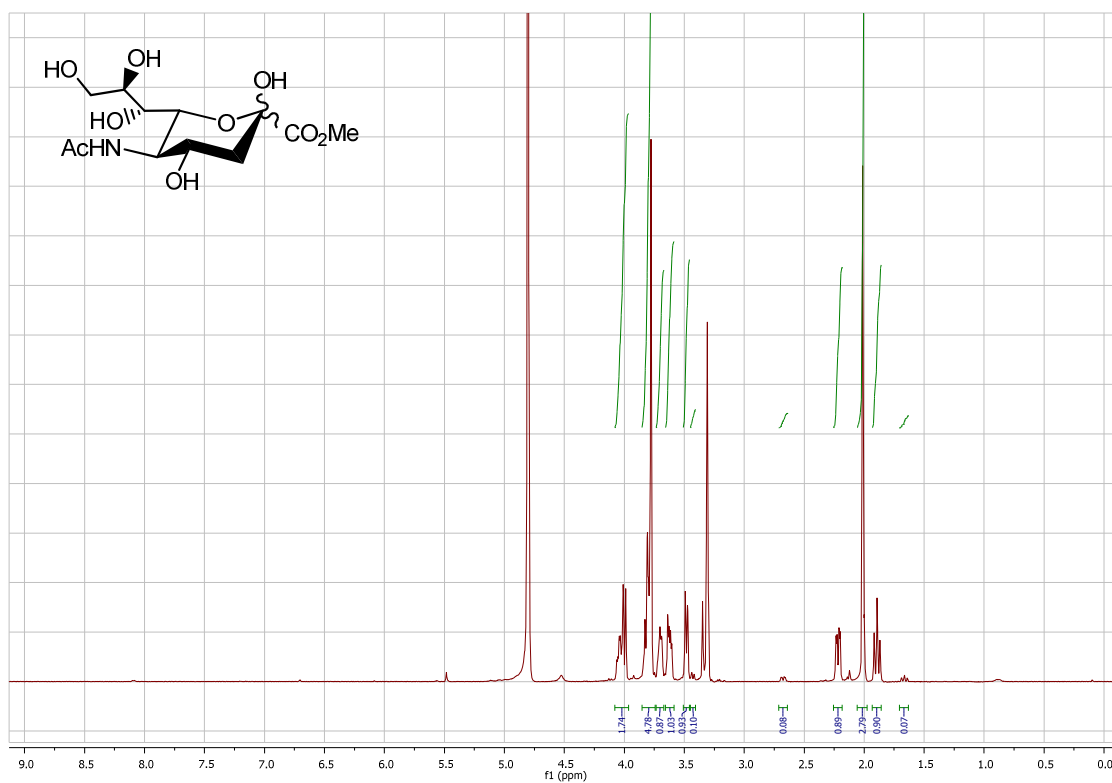
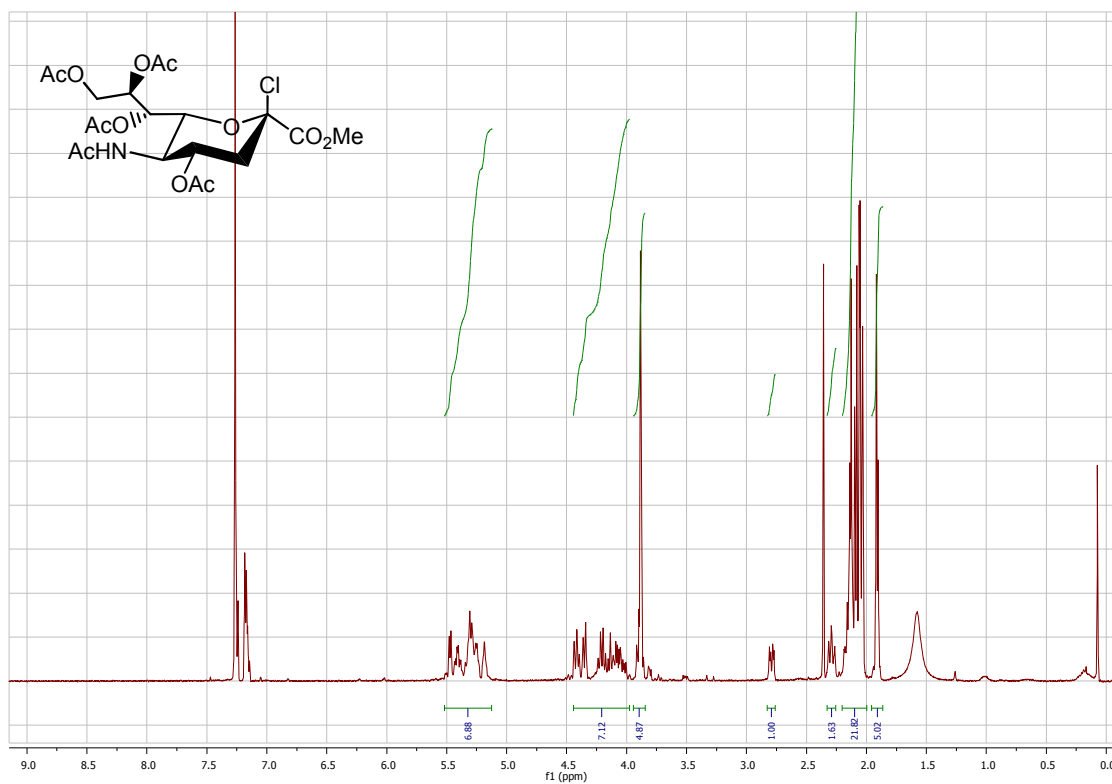
Phospho-oseltamivir concentration for 1 mg/mL (particle) = 1.6×10^{-3} mM/mL
= **1.6 mM**

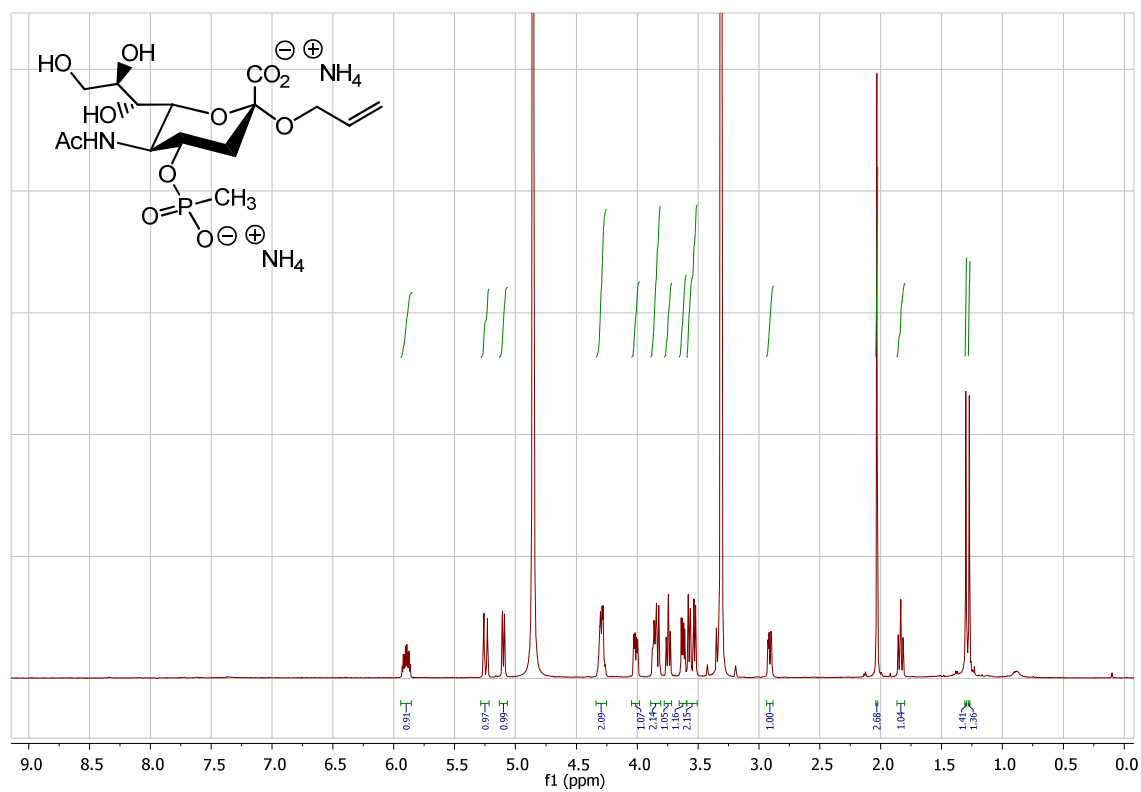
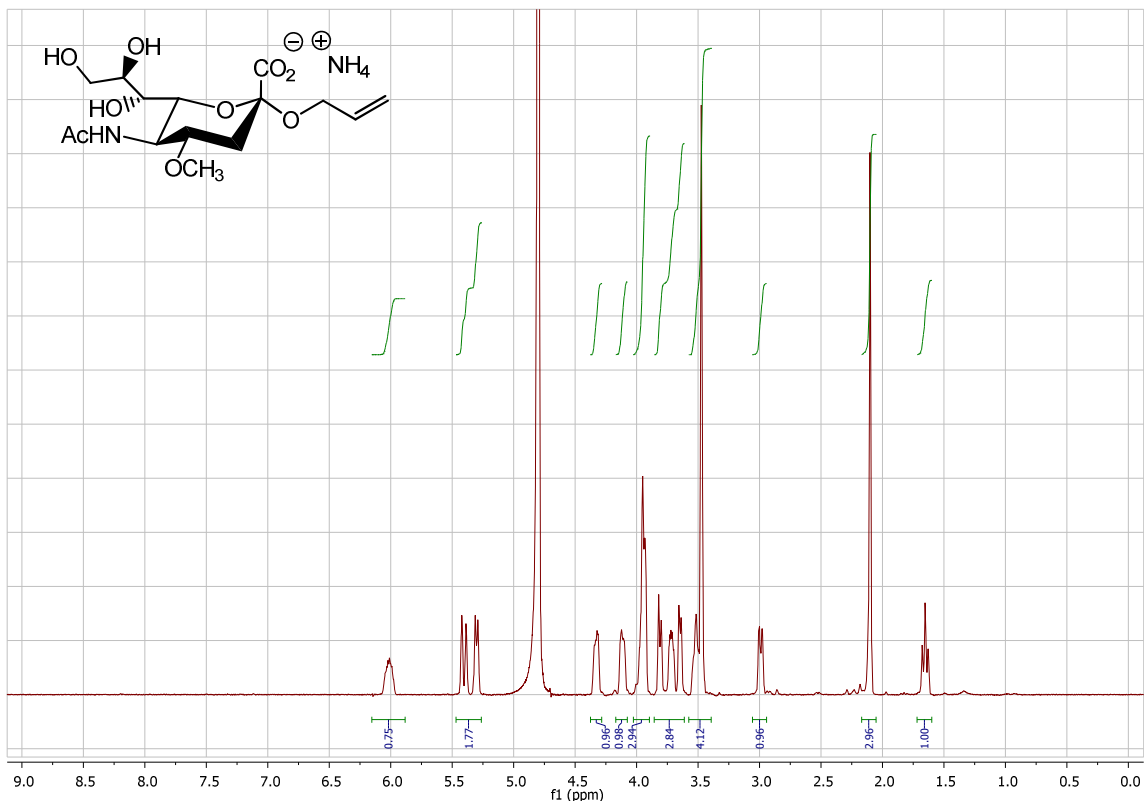
The same assumptions and calculations were used for the methylphosphonate-stabilised control particles, resulting in a **2.3 mM** stock solution.

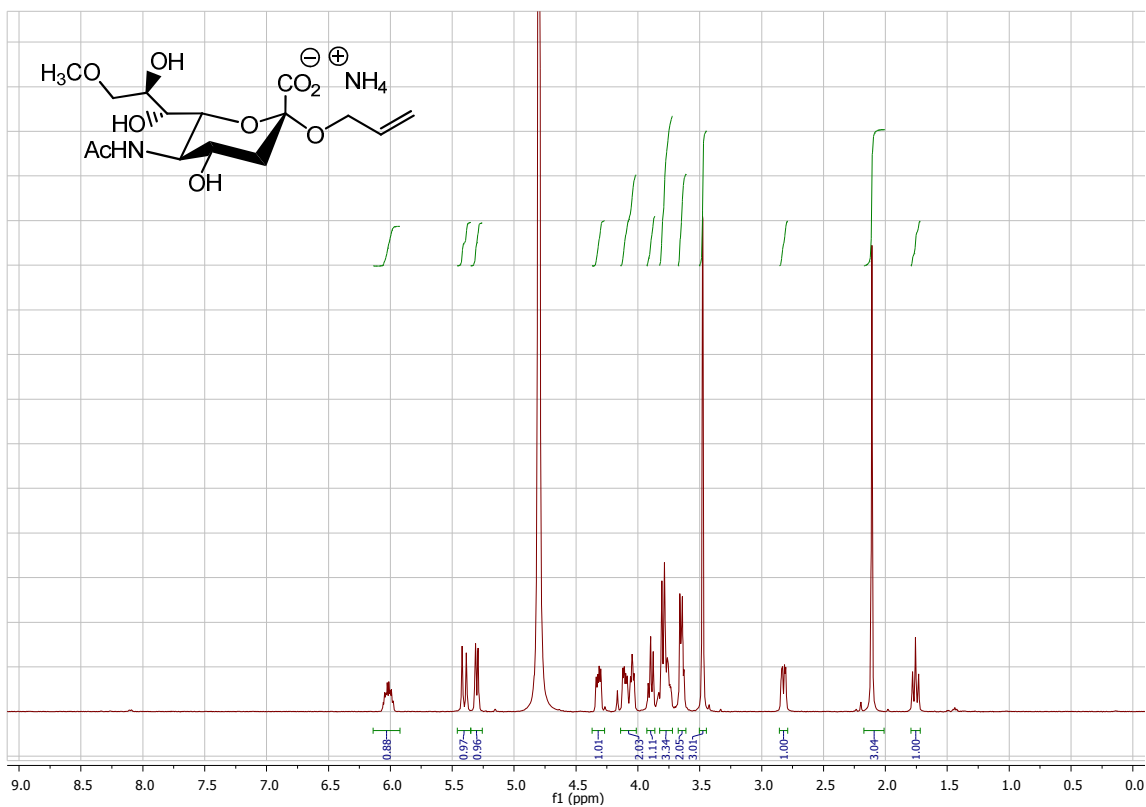
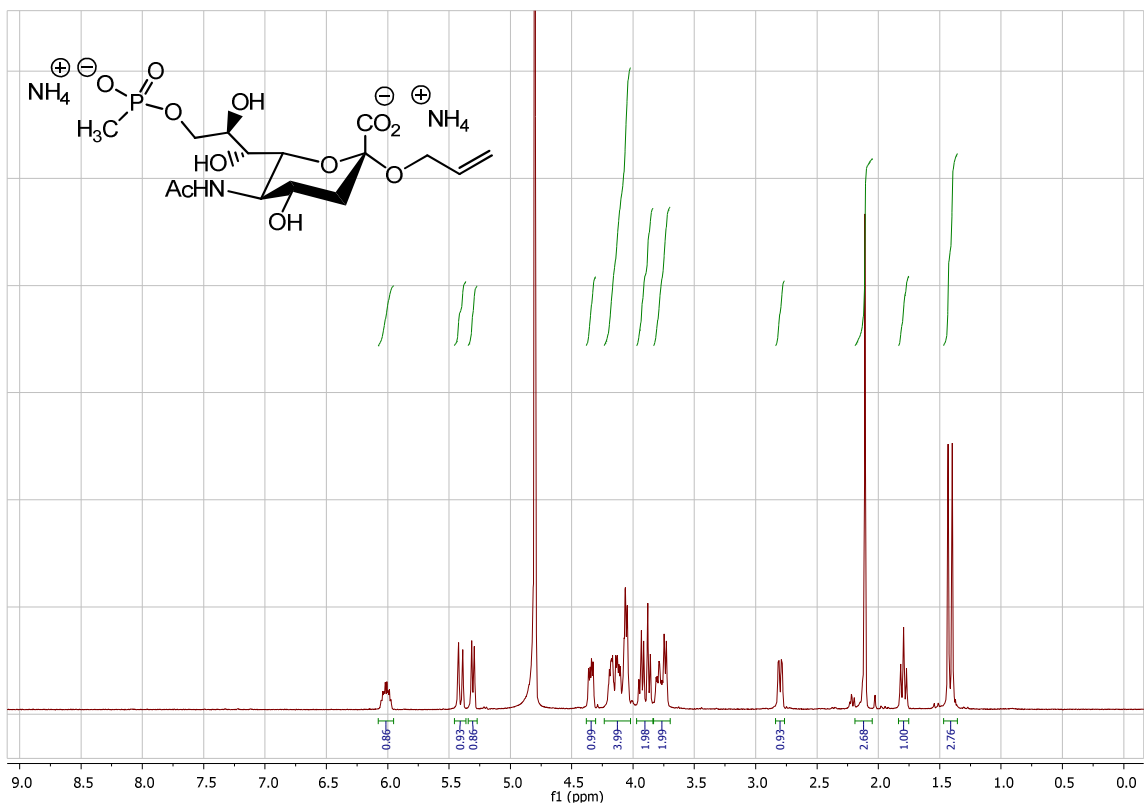
References

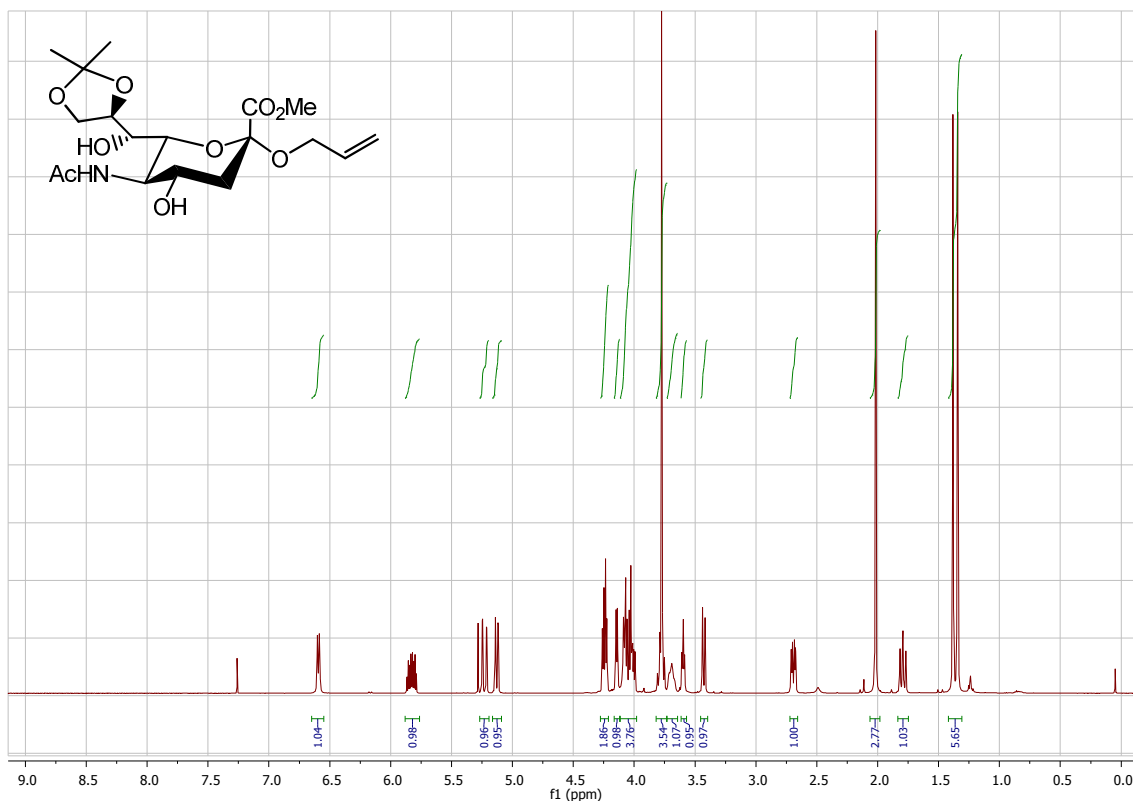
- (1) Daniel, M.-C.; Astruc, D. *Chemical Reviews* **2004**, *104*, 293-346.

V.4. NMR data

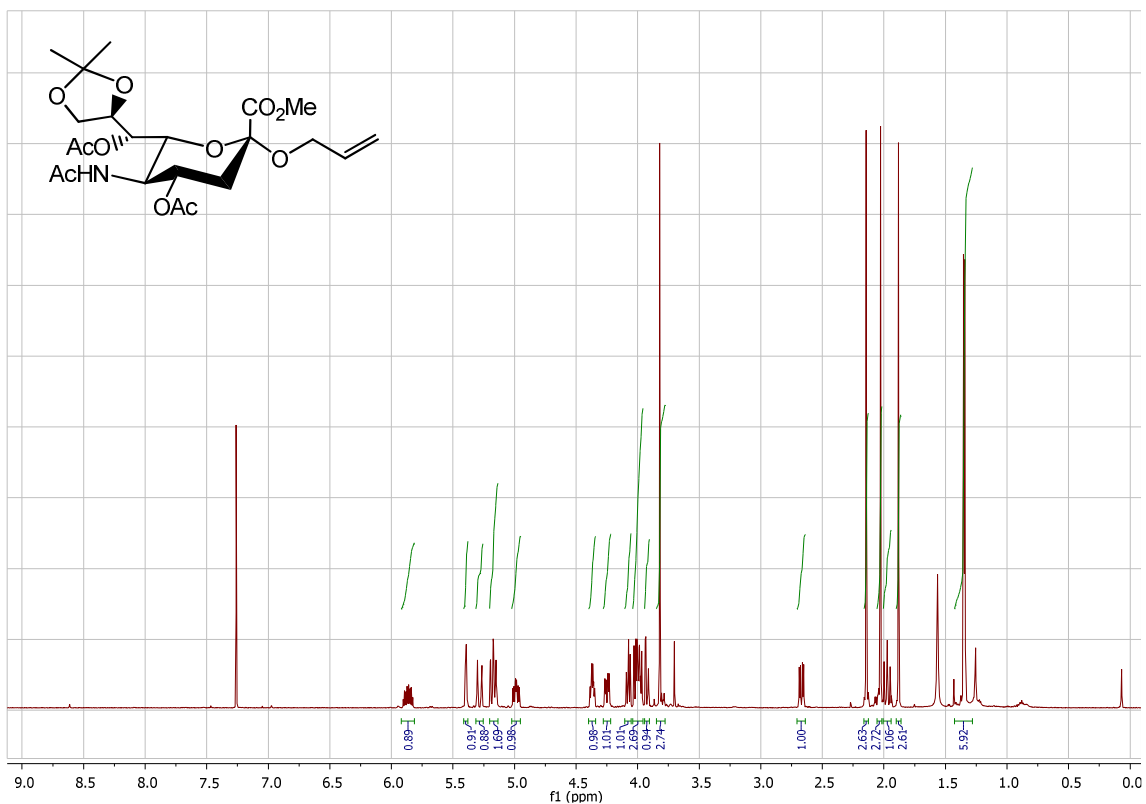
V.4.1. ^1H NMR ^1H NMR (500 MHz, MeOH- D_4) of compound 1 ^1H NMR (500 MHz, CDCl_3) of compound 2



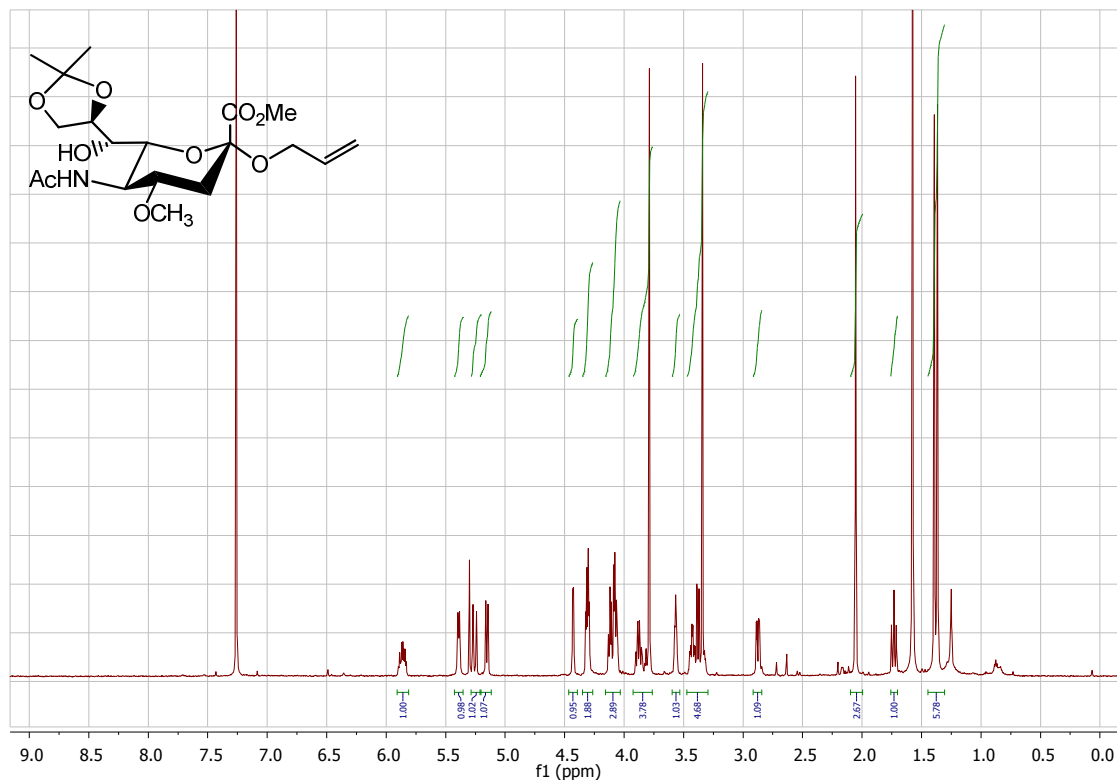
 ^1H NMR (600 MHz, D_2O) of compound 7 ^1H NMR (600 MHz, D_2O) of compound 8



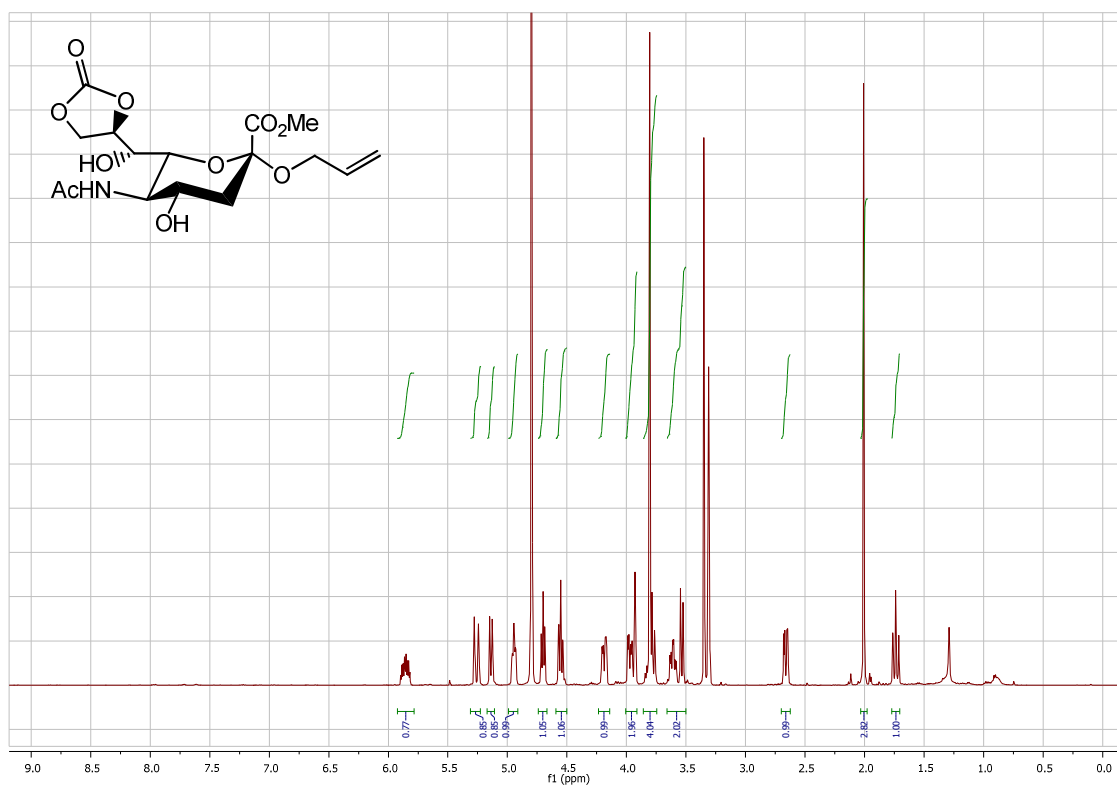
¹H NMR (500 MHz, CDCl₃) of compound 9



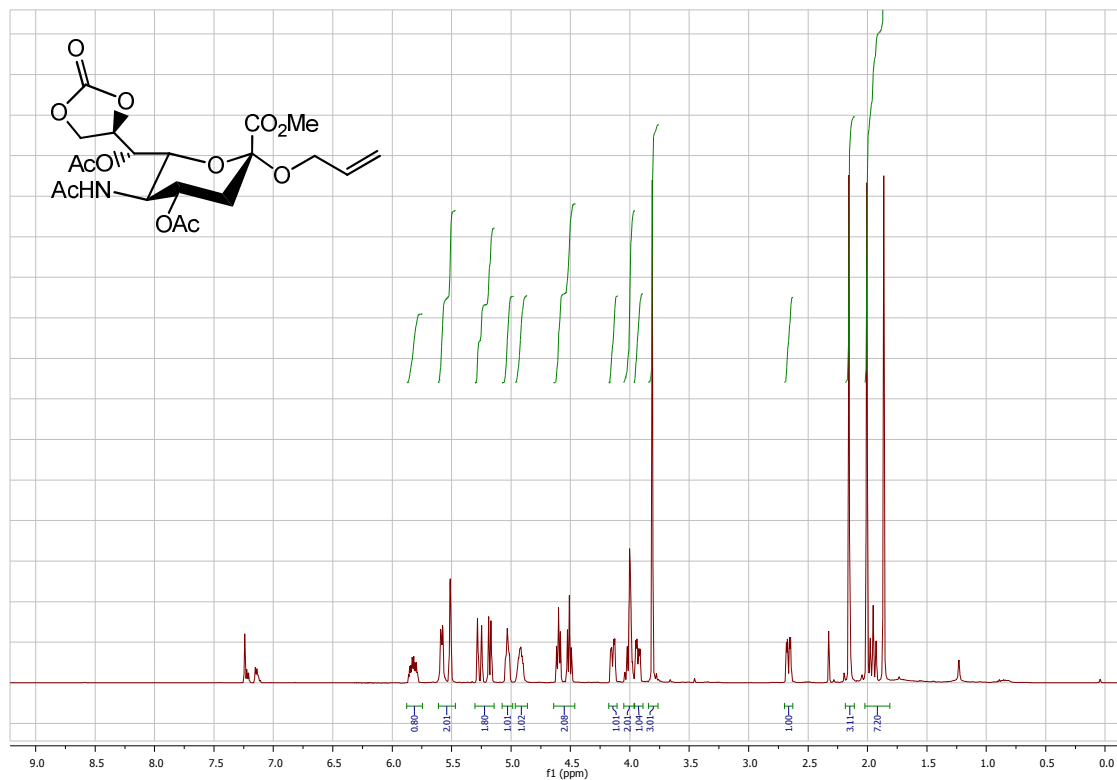
¹H NMR (500 MHz, CDCl₃) of compound 10



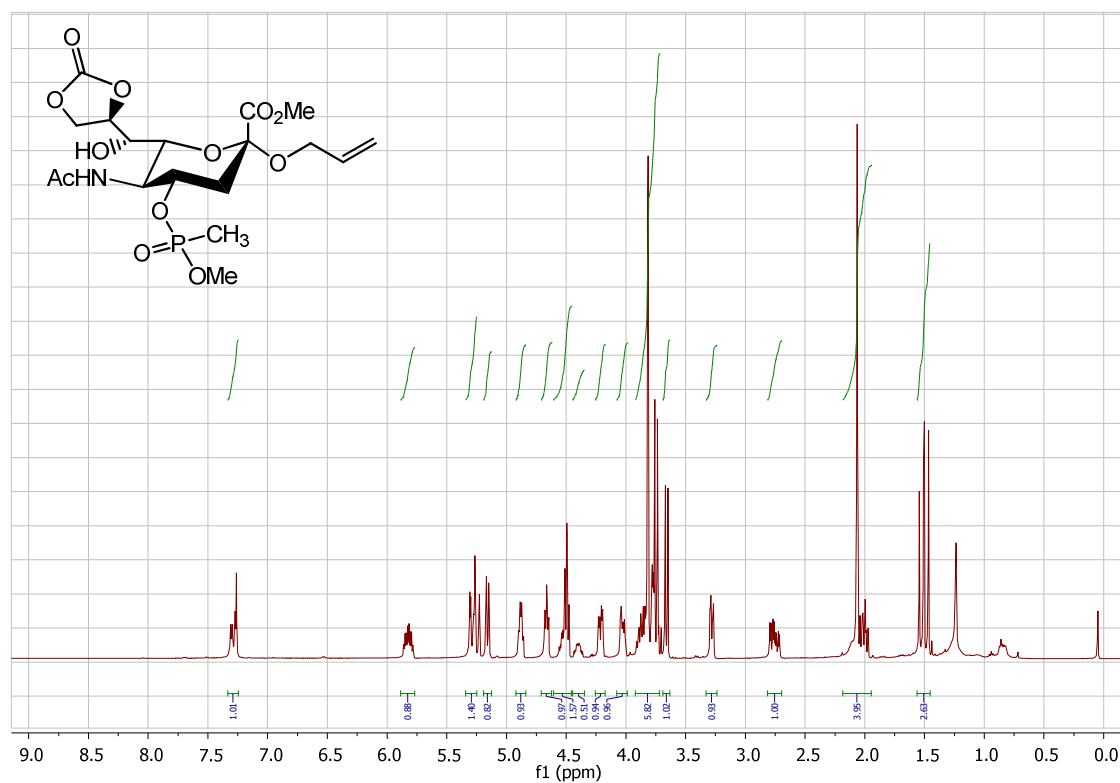
¹H NMR (600 MHz, CDCl₃) of compound 11



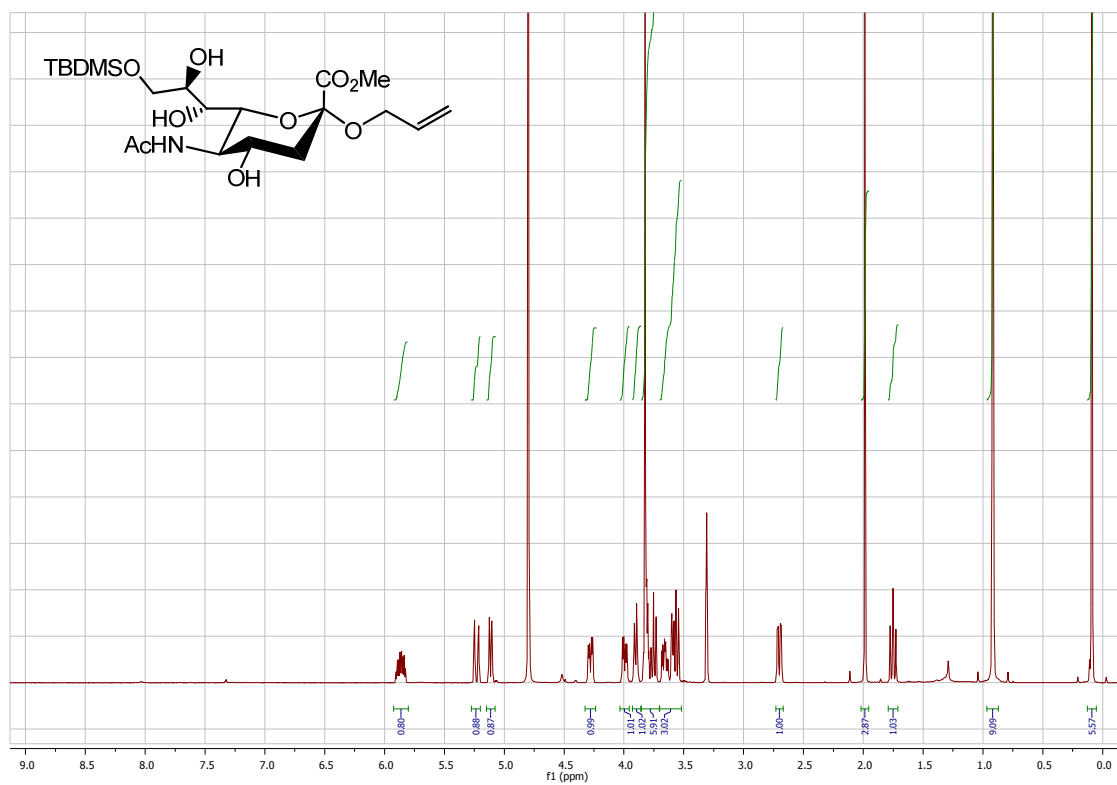
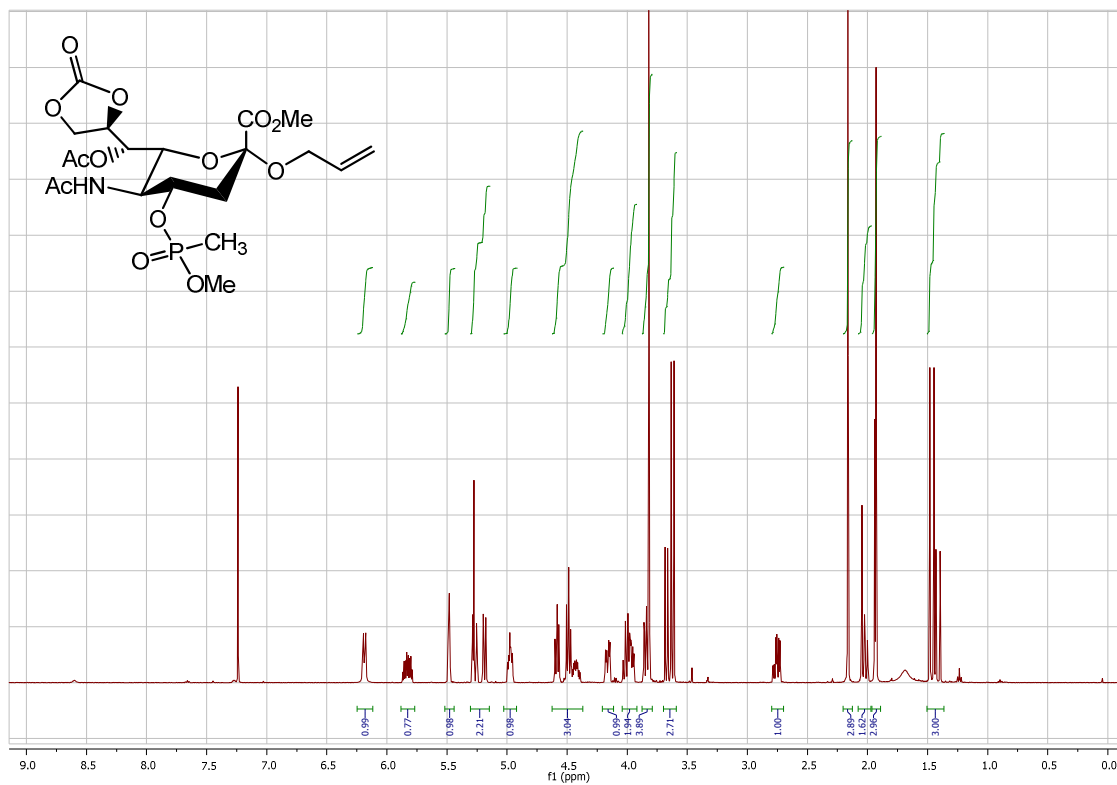
¹H NMR (500 MHz, MeOH-D₄) of compound 12

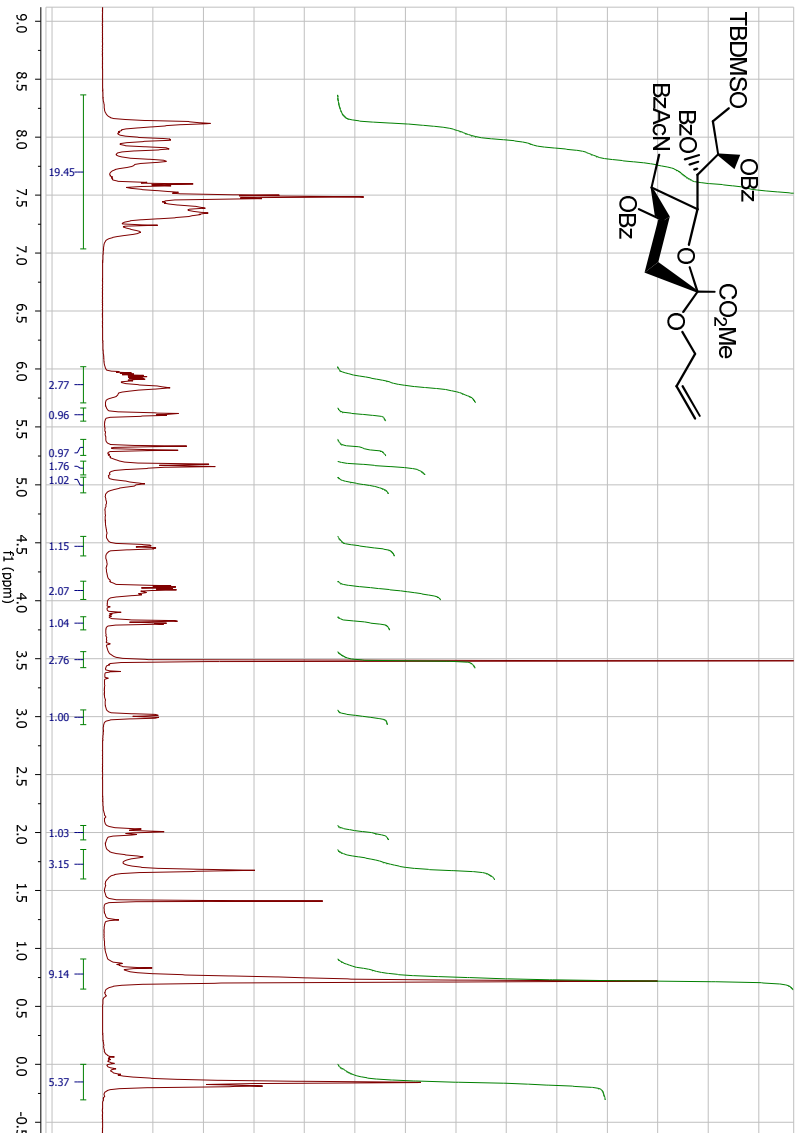
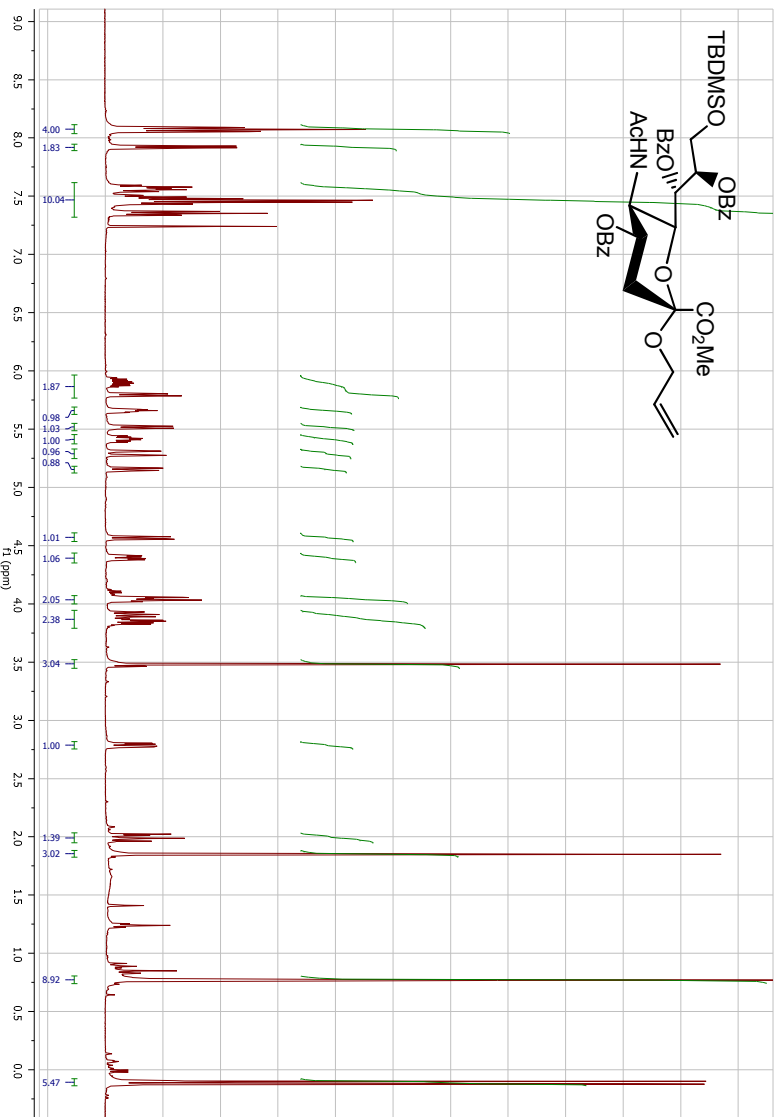


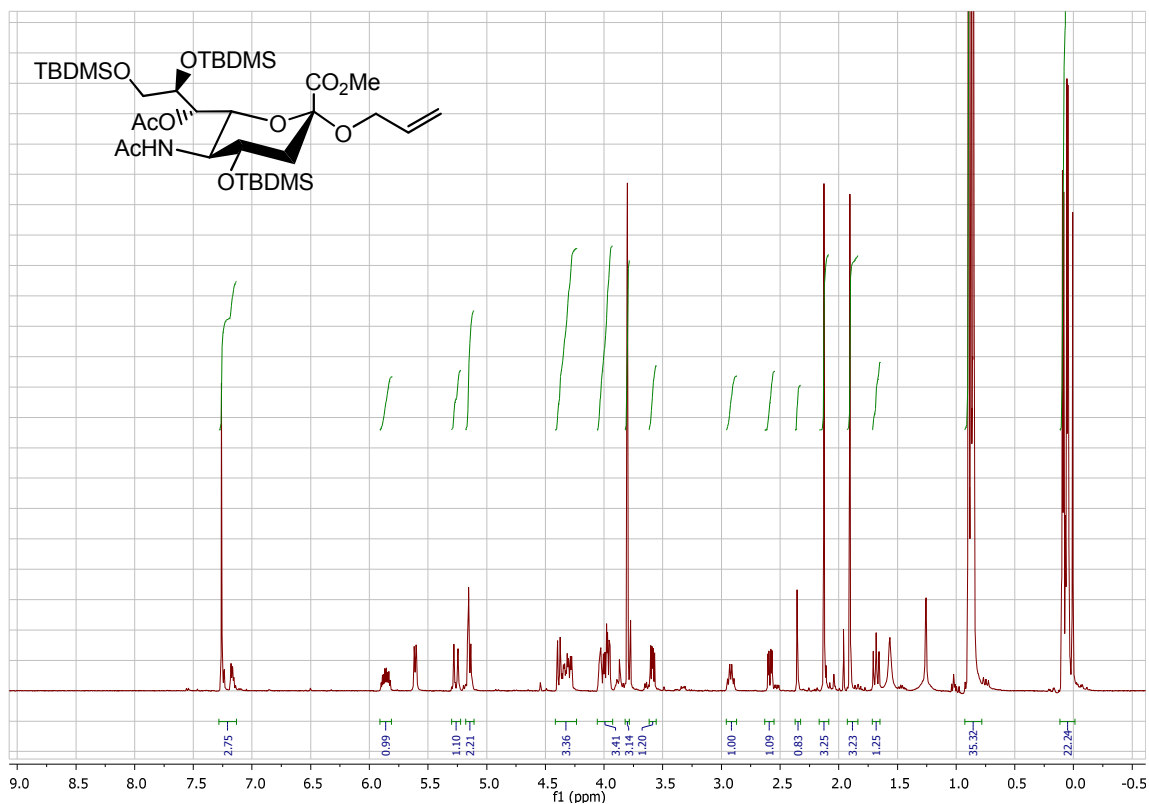
¹H NMR (500 MHz, CDCl₃) of compound 13



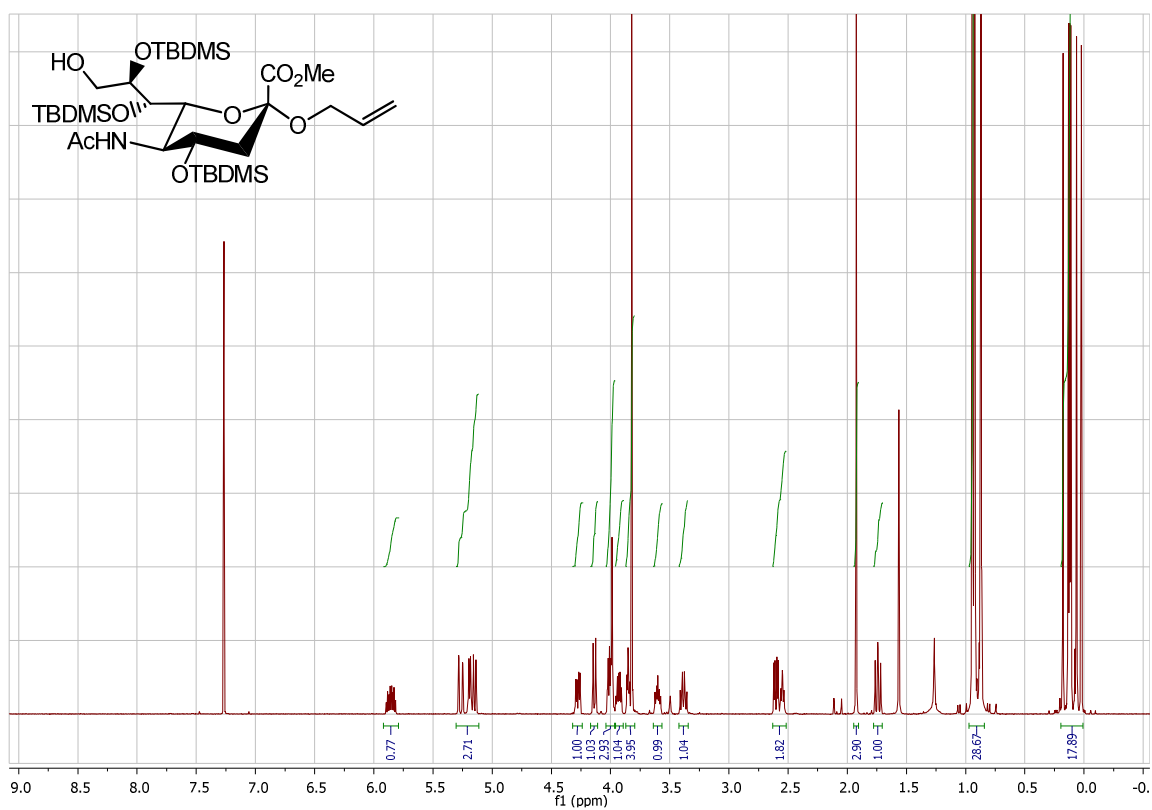
¹H NMR (500 MHz, CDCl₃) of compound 14



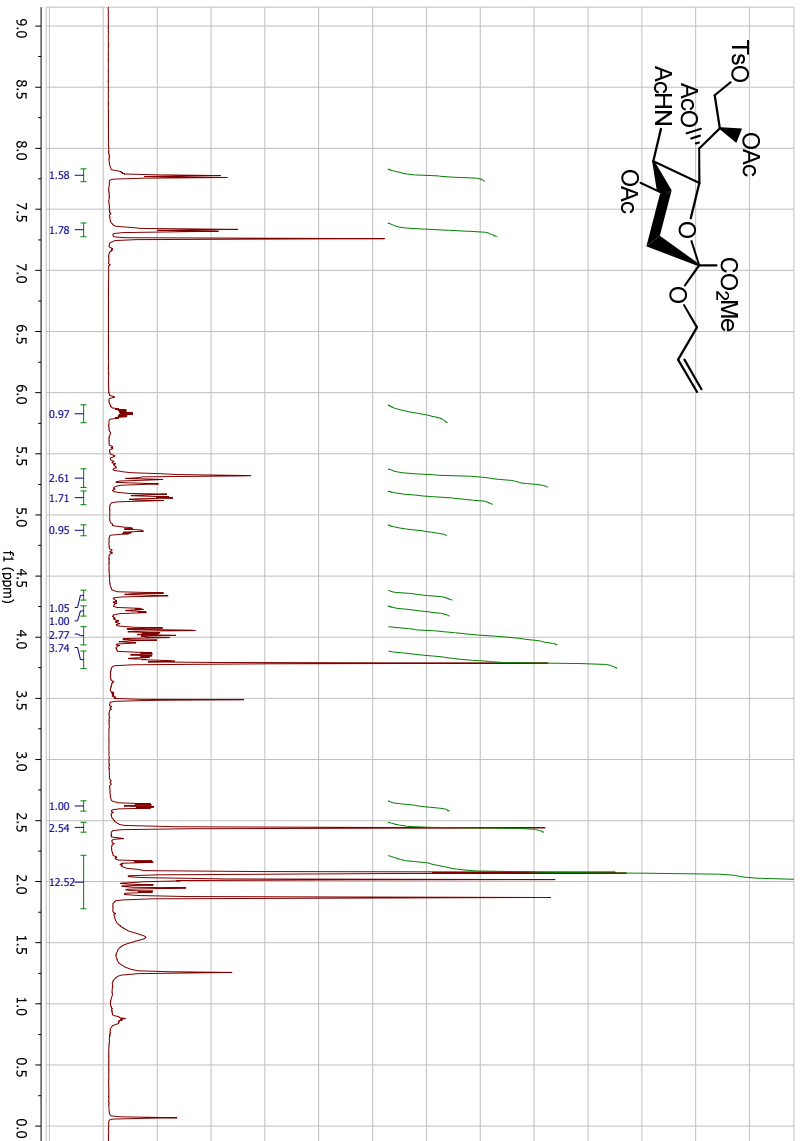
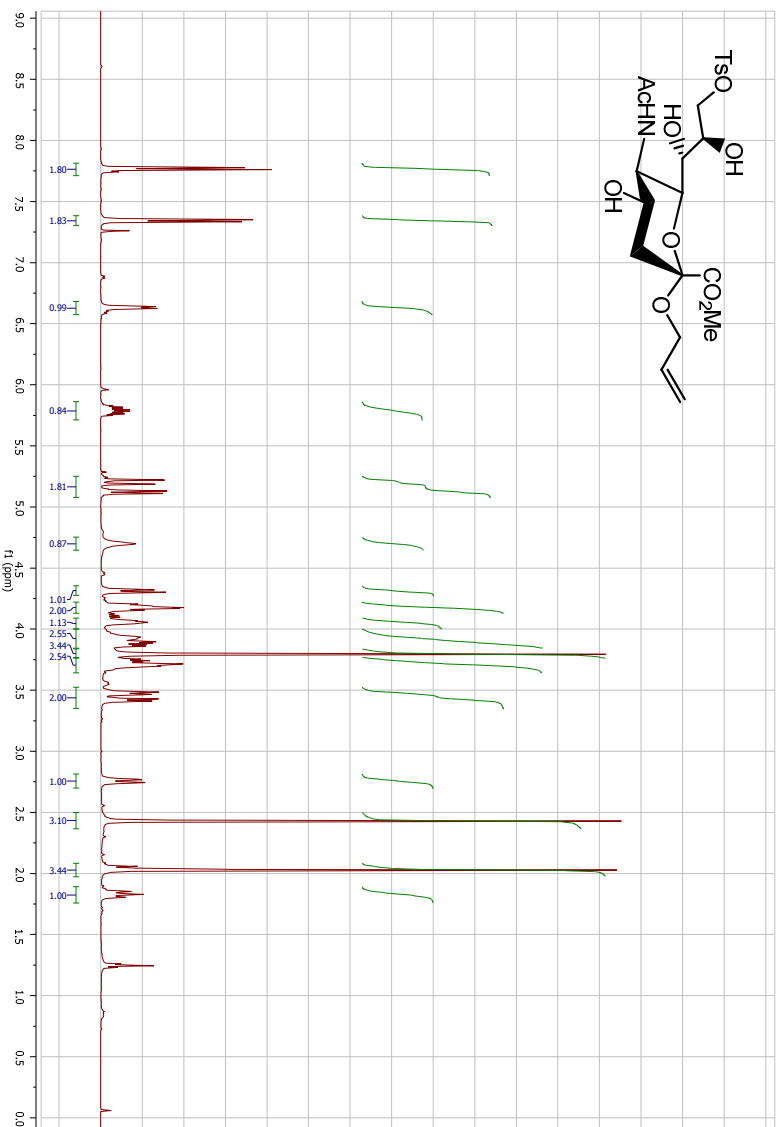
¹H NMR (500 MHz, CDCl₃) of compound **17**¹H NMR (500 MHz, CDCl₃) of compound **18**



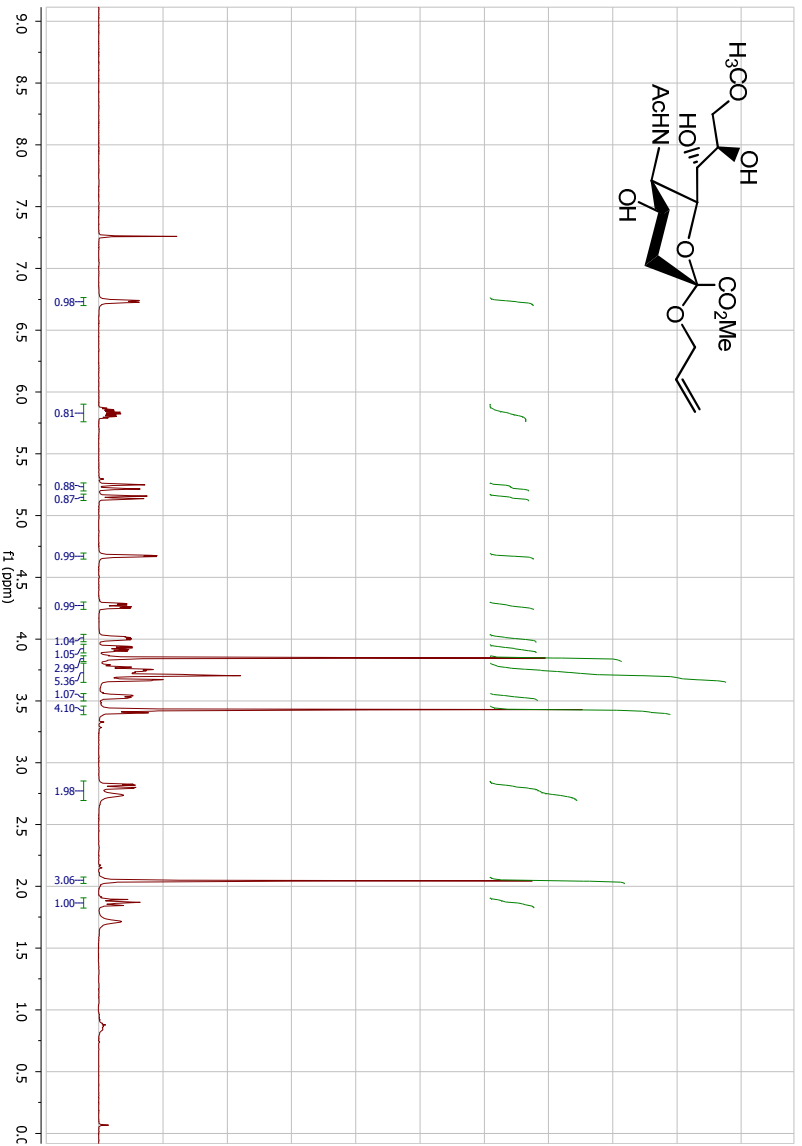
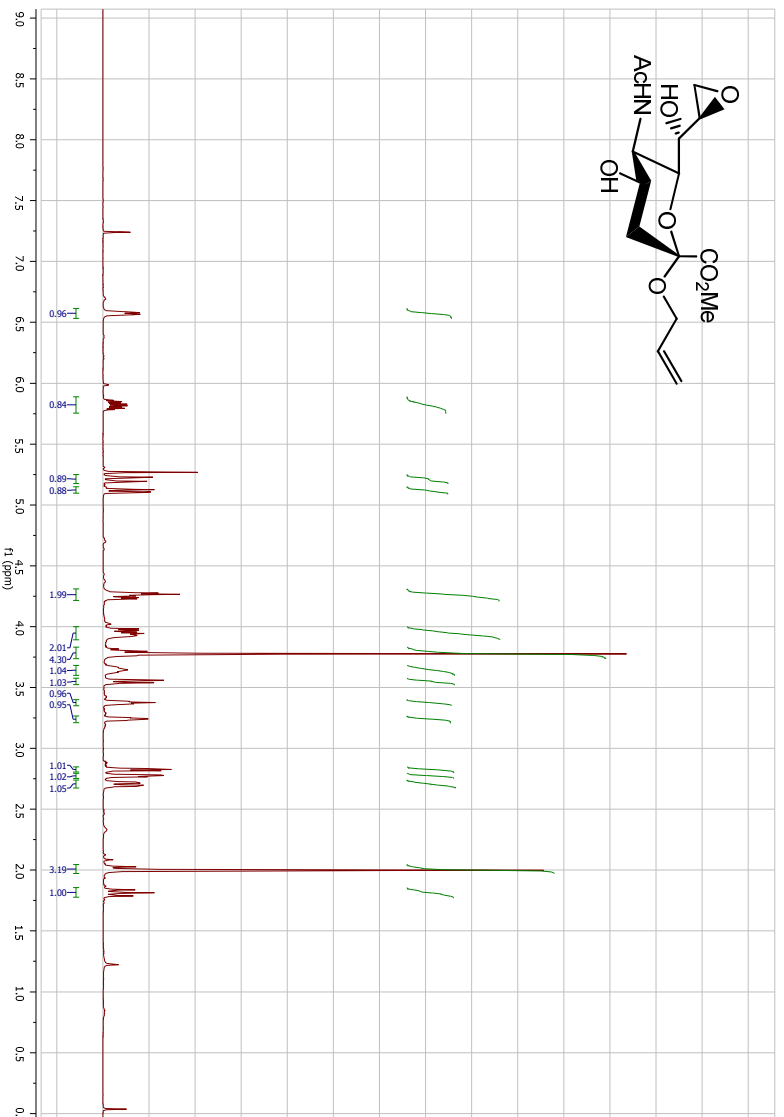
¹H NMR (500 MHz, CDCl₃) of compound 21

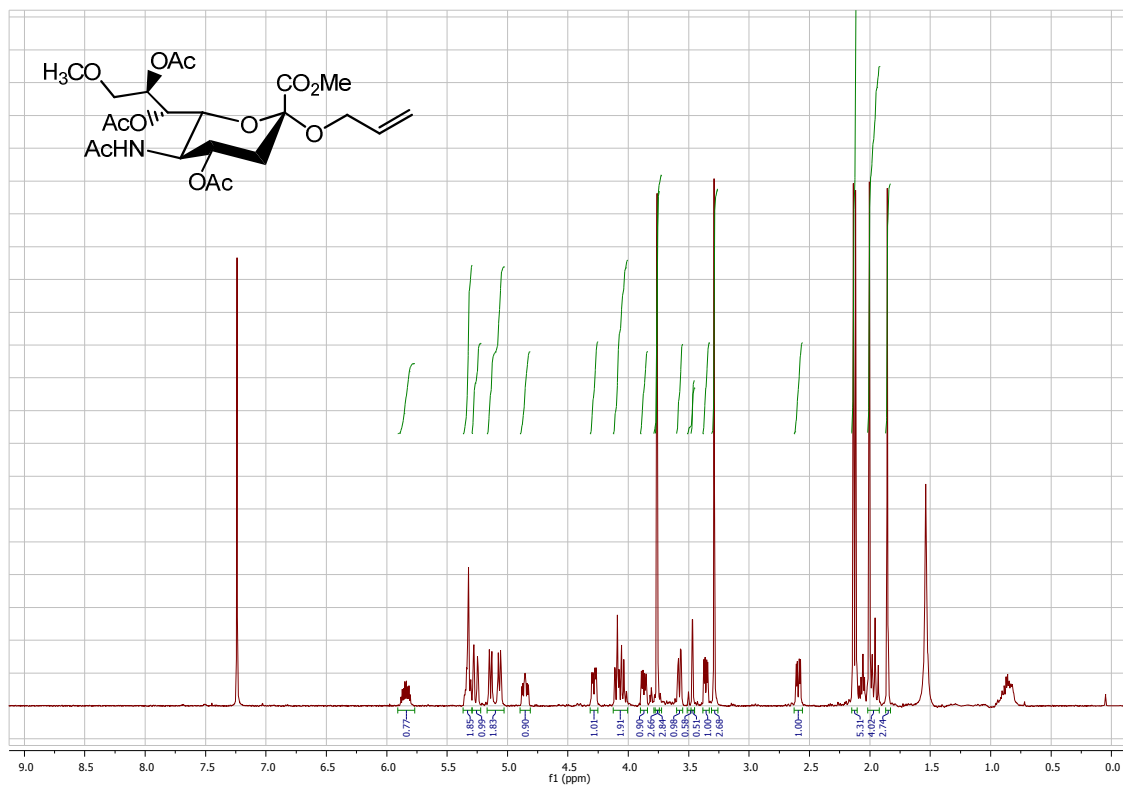


¹H NMR (500 MHz, CDCl₃) of compound 22

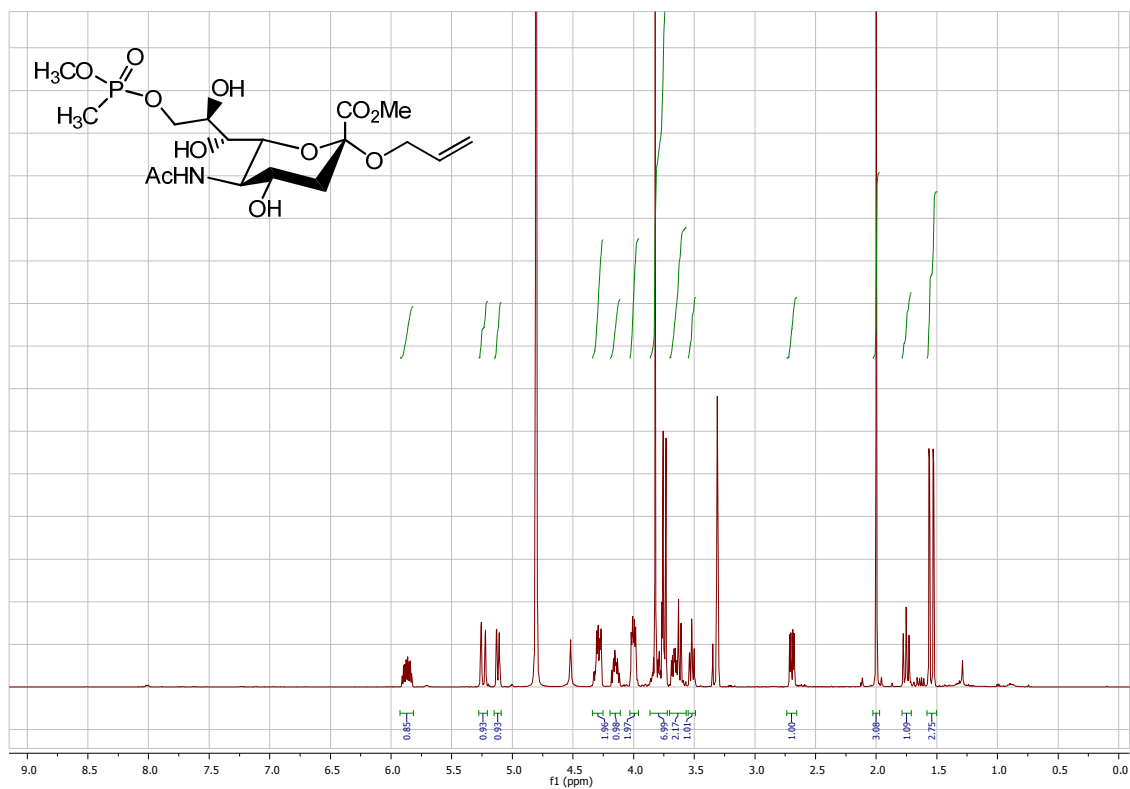


¹H NMR (500 MHz, CDCl₃) of compound **24**

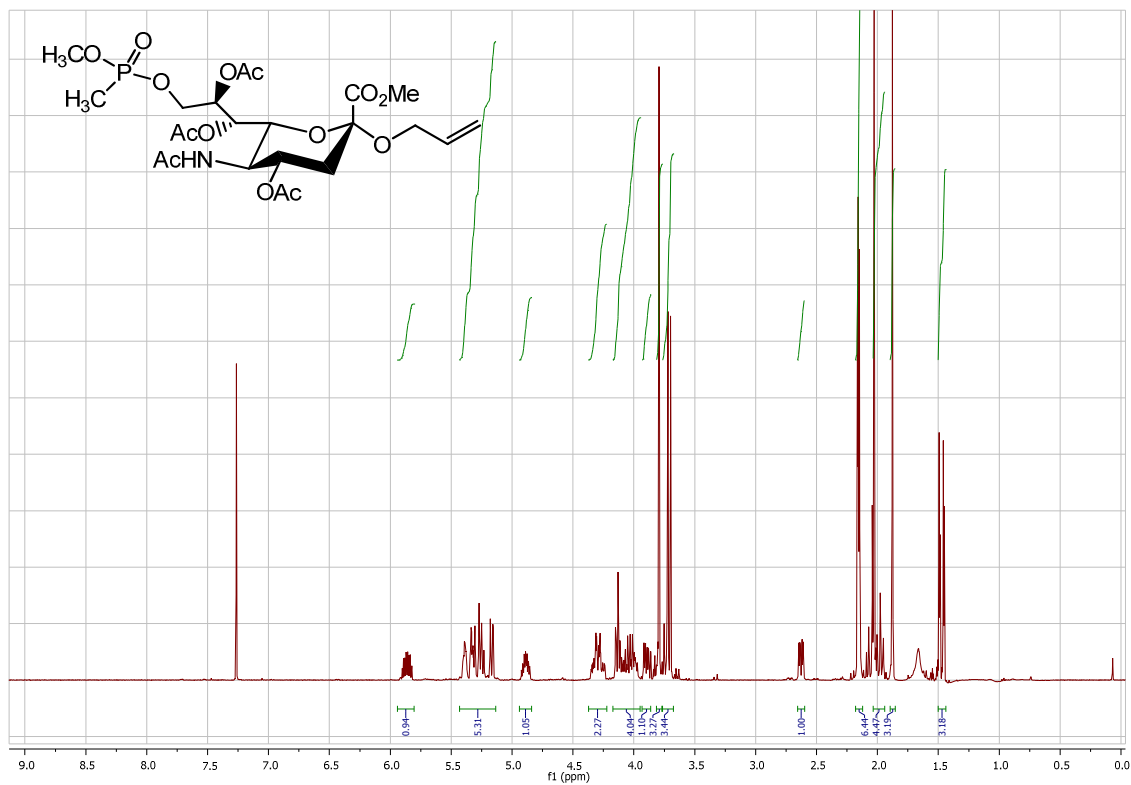




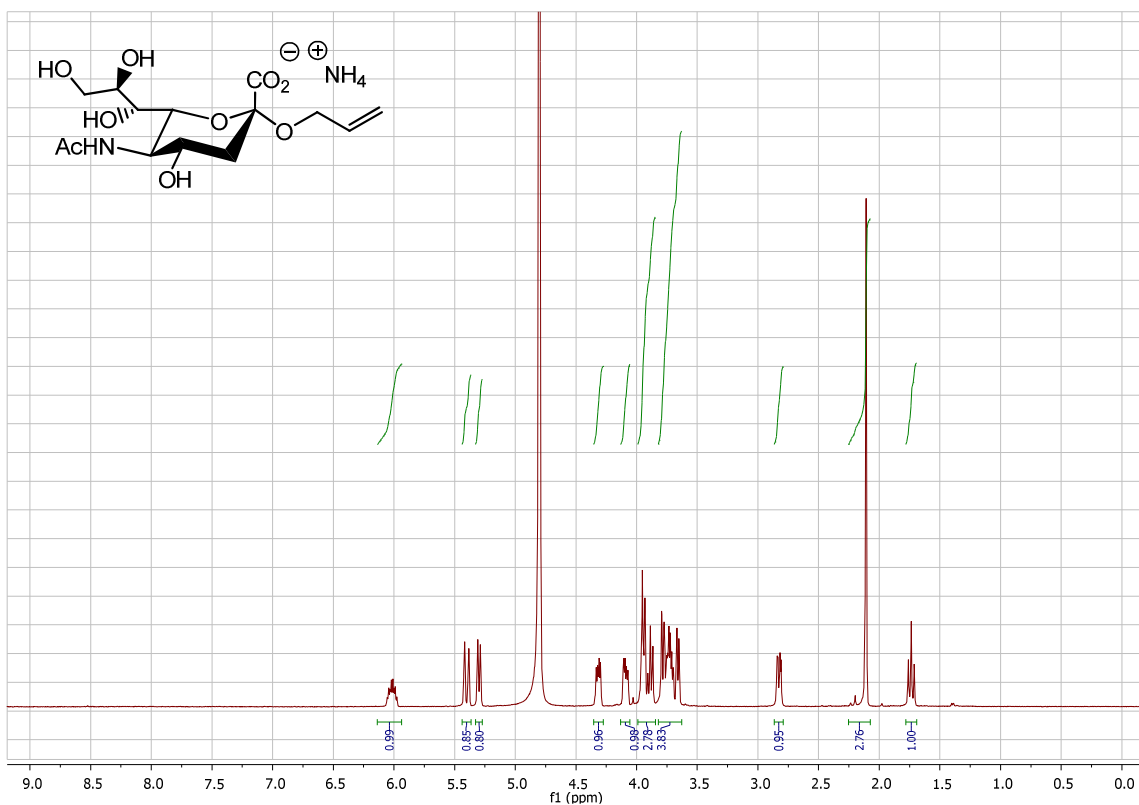
¹H NMR (500 MHz, CDCl₃) of compound 27



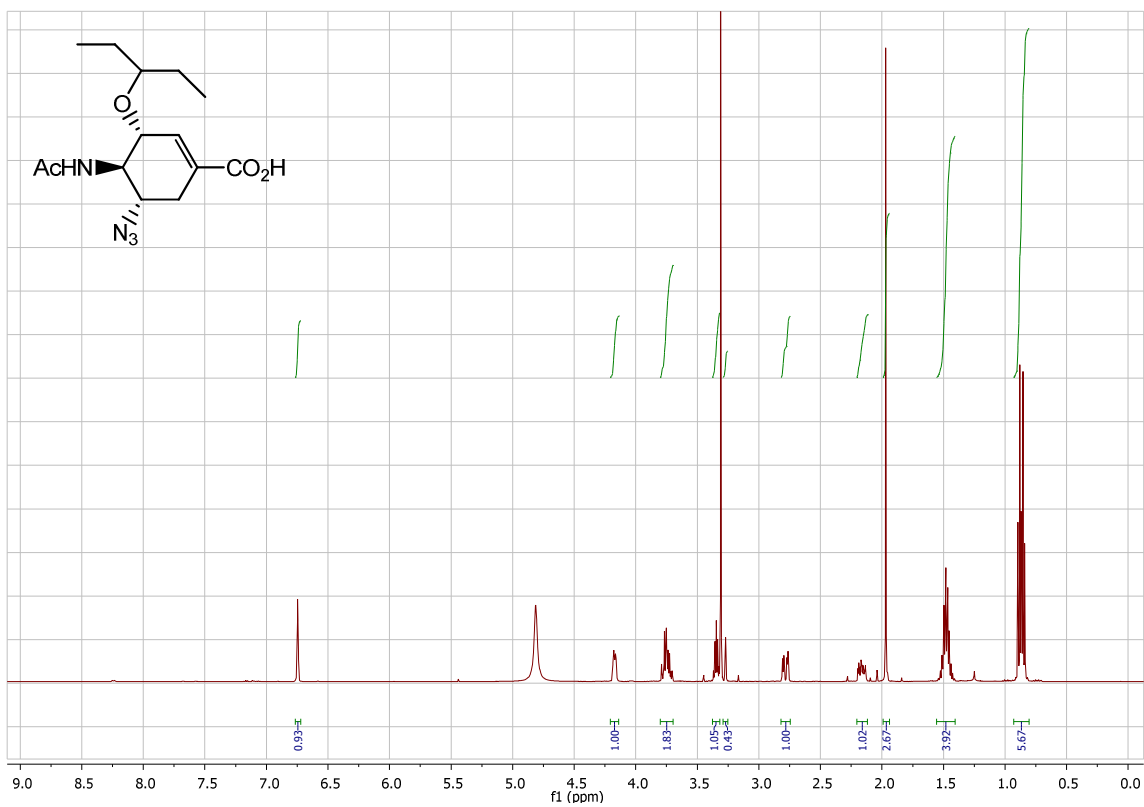
¹H NMR (500 MHz, CDCl₃) of compound 28



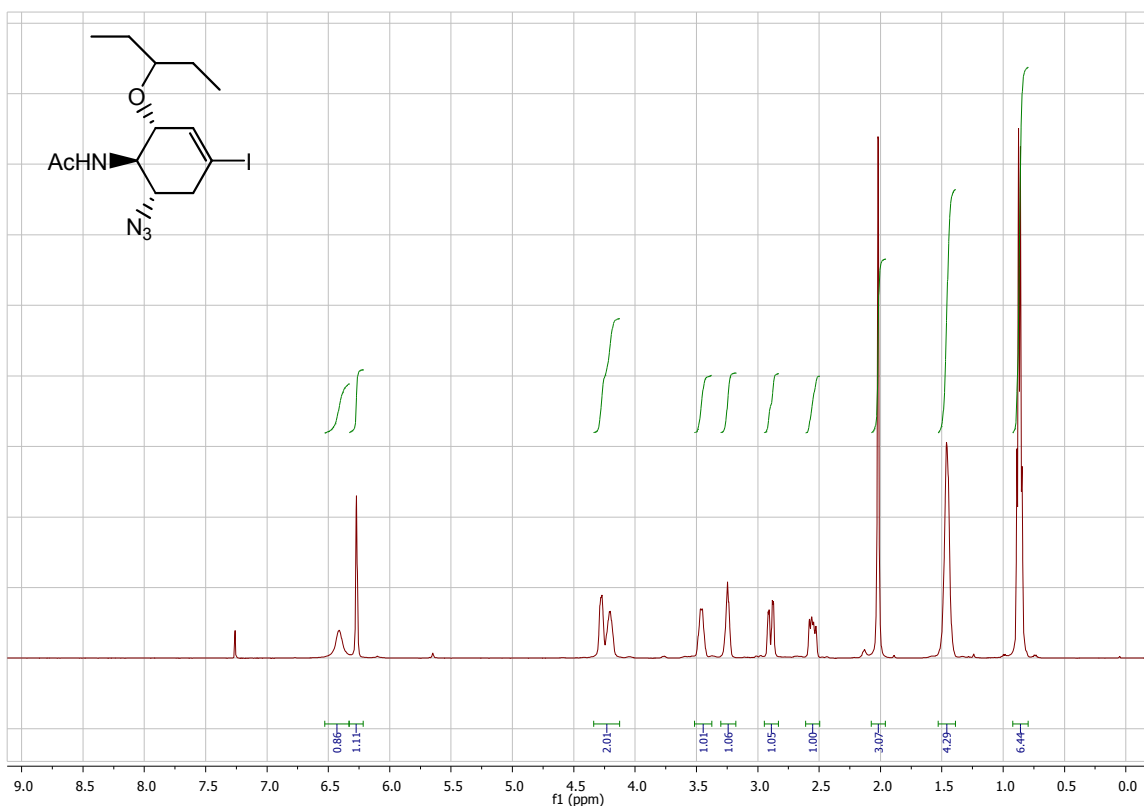
¹H NMR (500 MHz, CDCl₃) of compound **29**



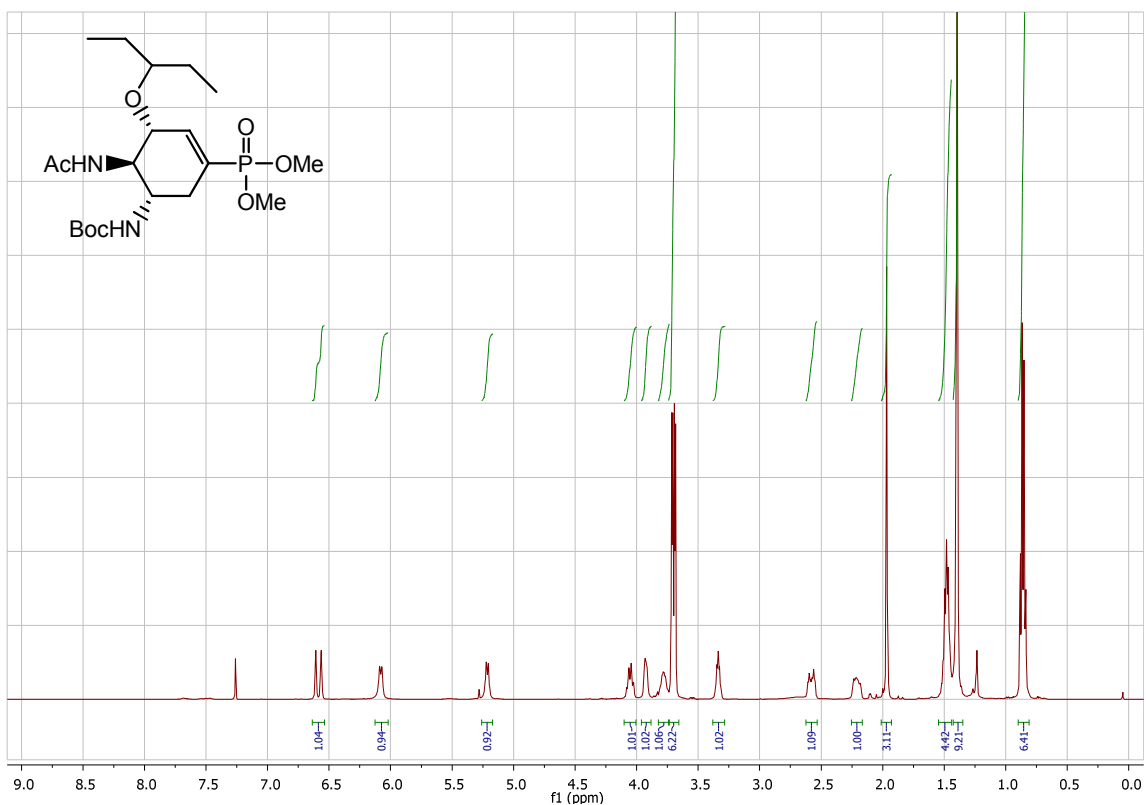
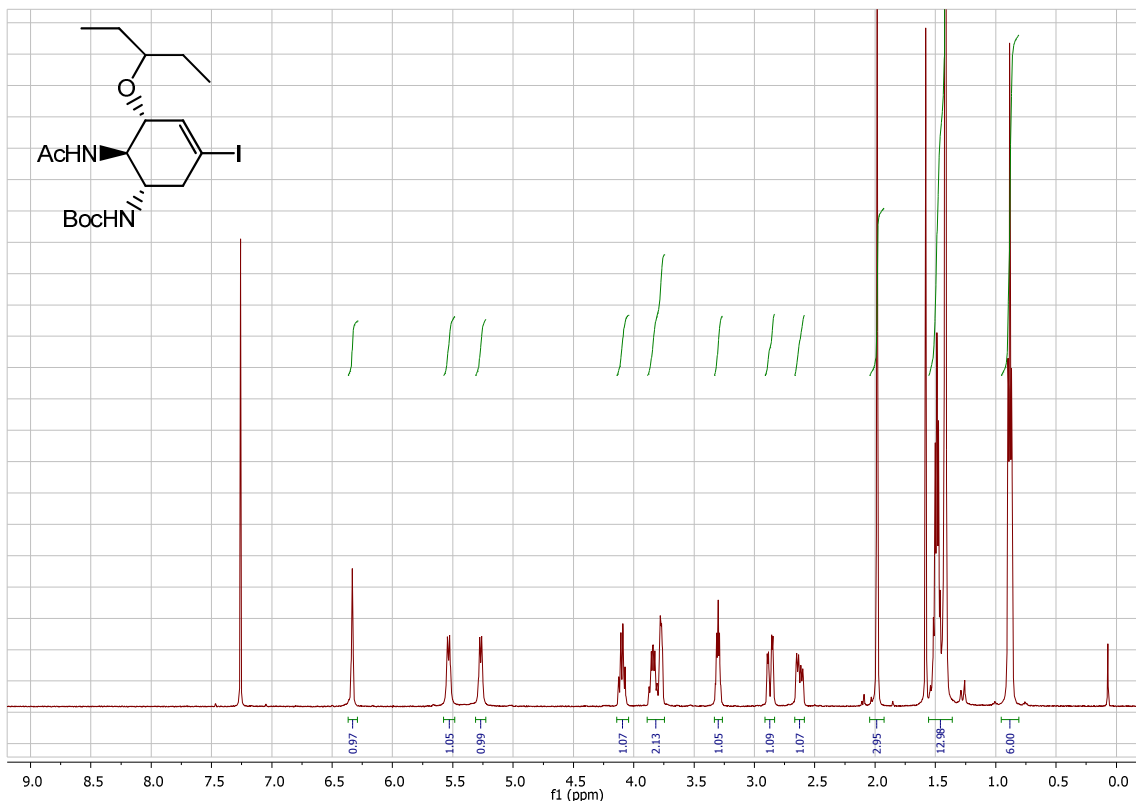
¹H NMR (500 MHz, D₂O) of compound **30**

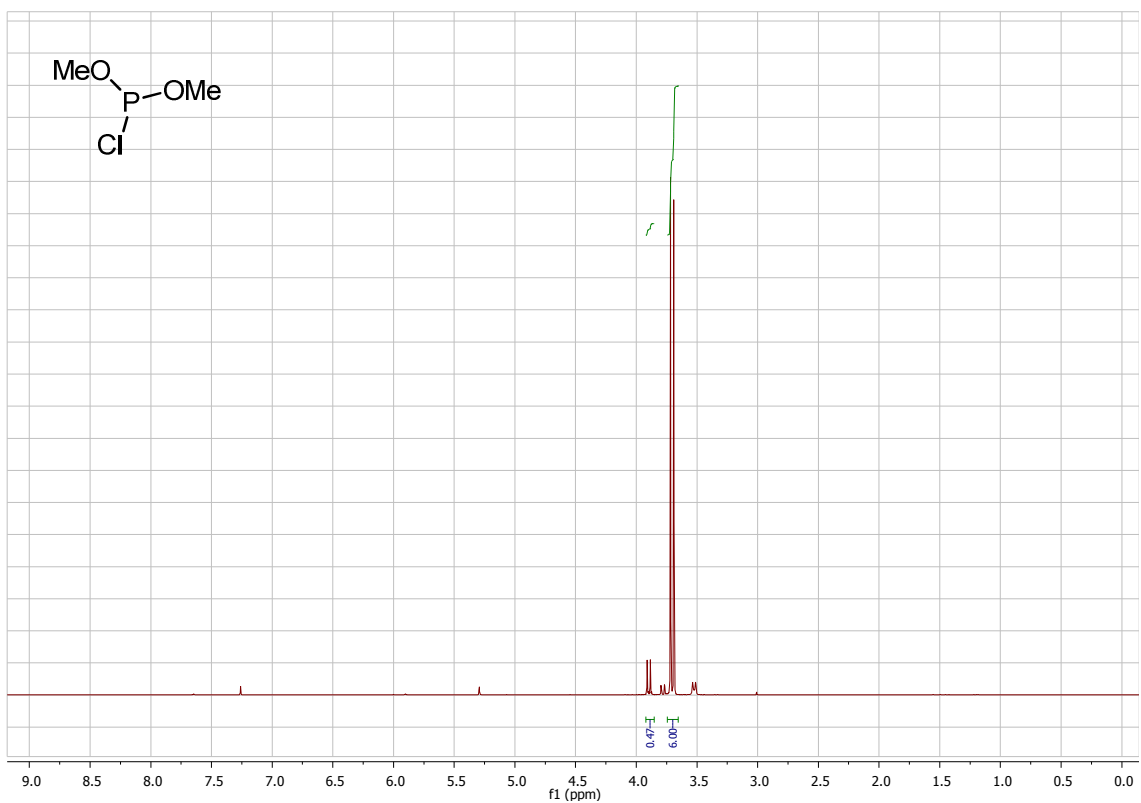
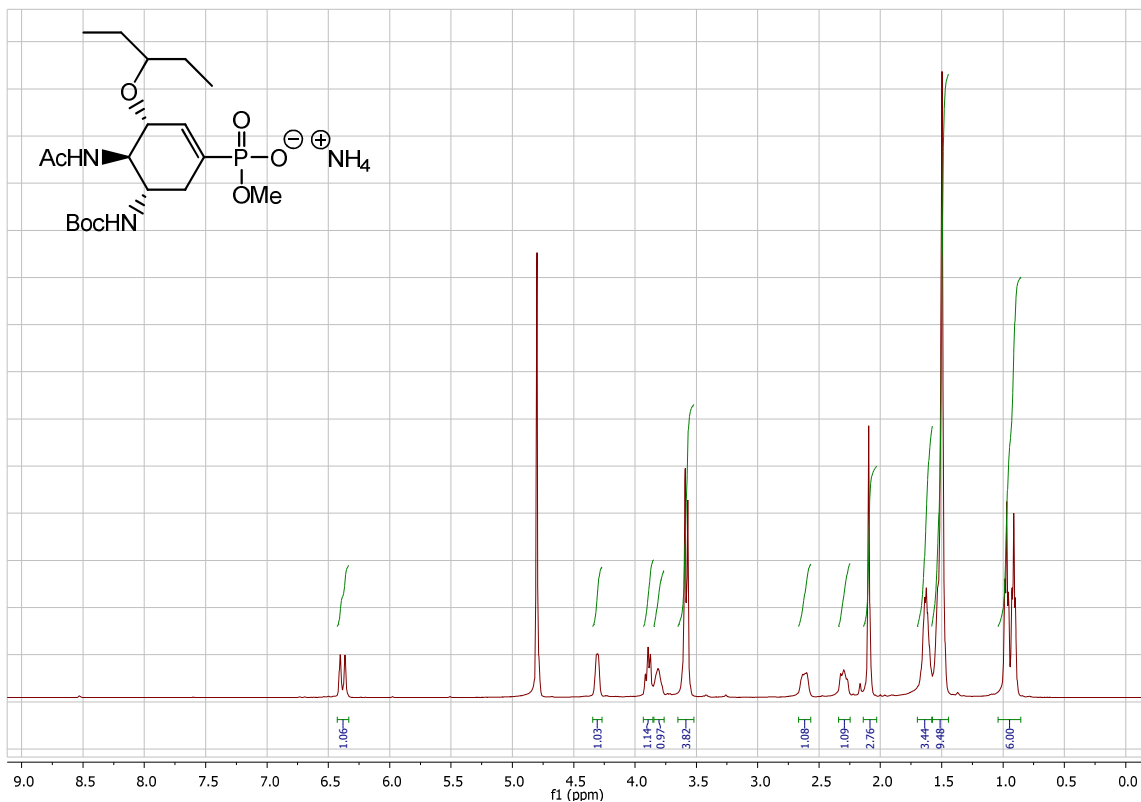


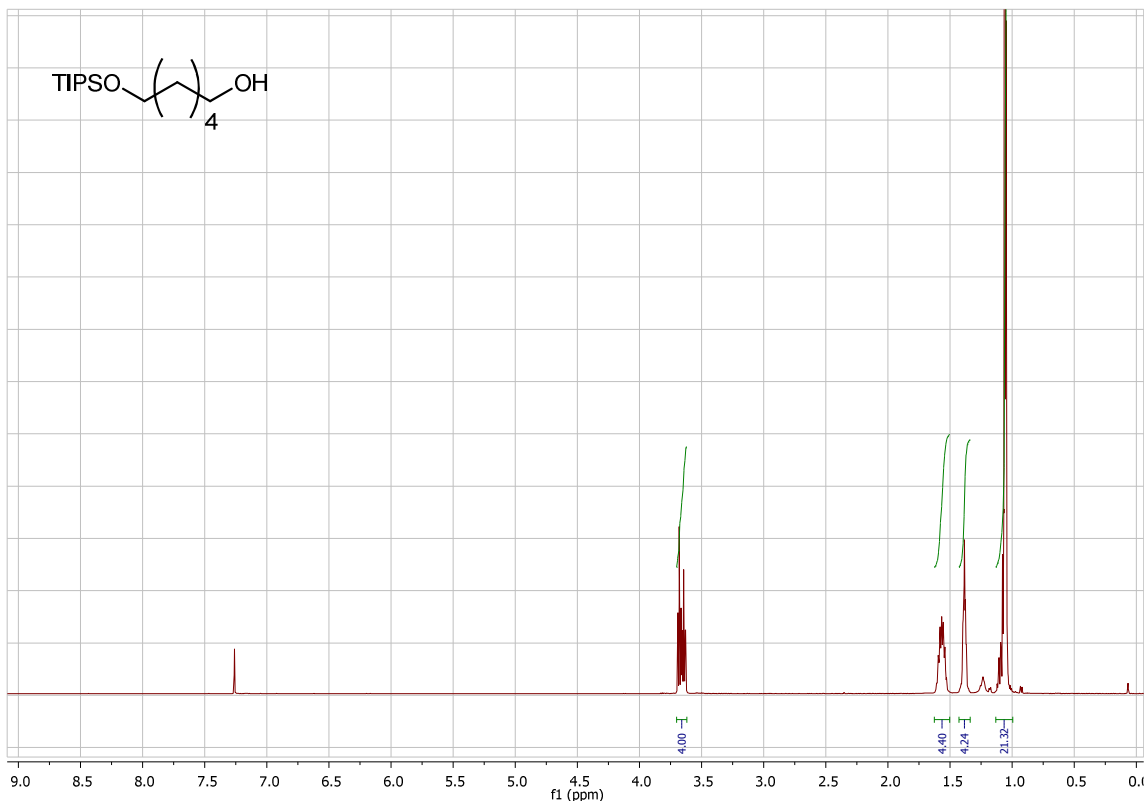
¹H NMR (500 MHz, MeOH-D₄) of compound **31**



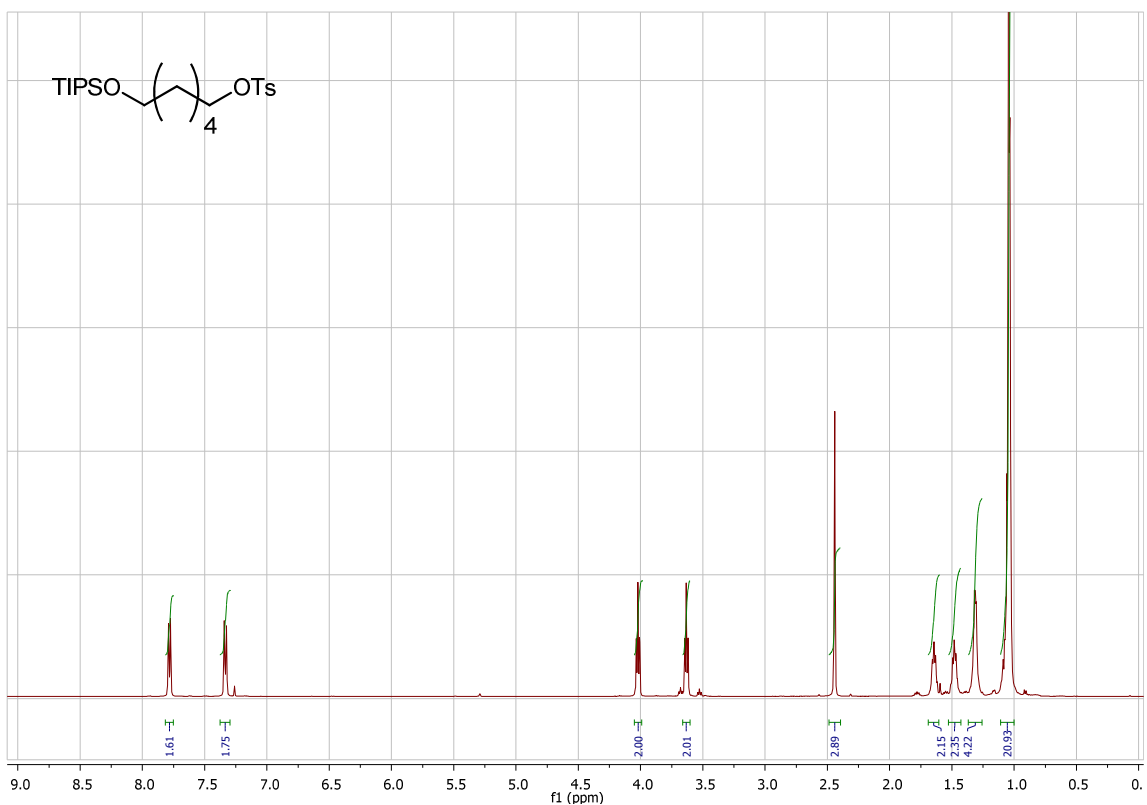
¹H NMR (500 MHz, CDCl₃) of compound **32**



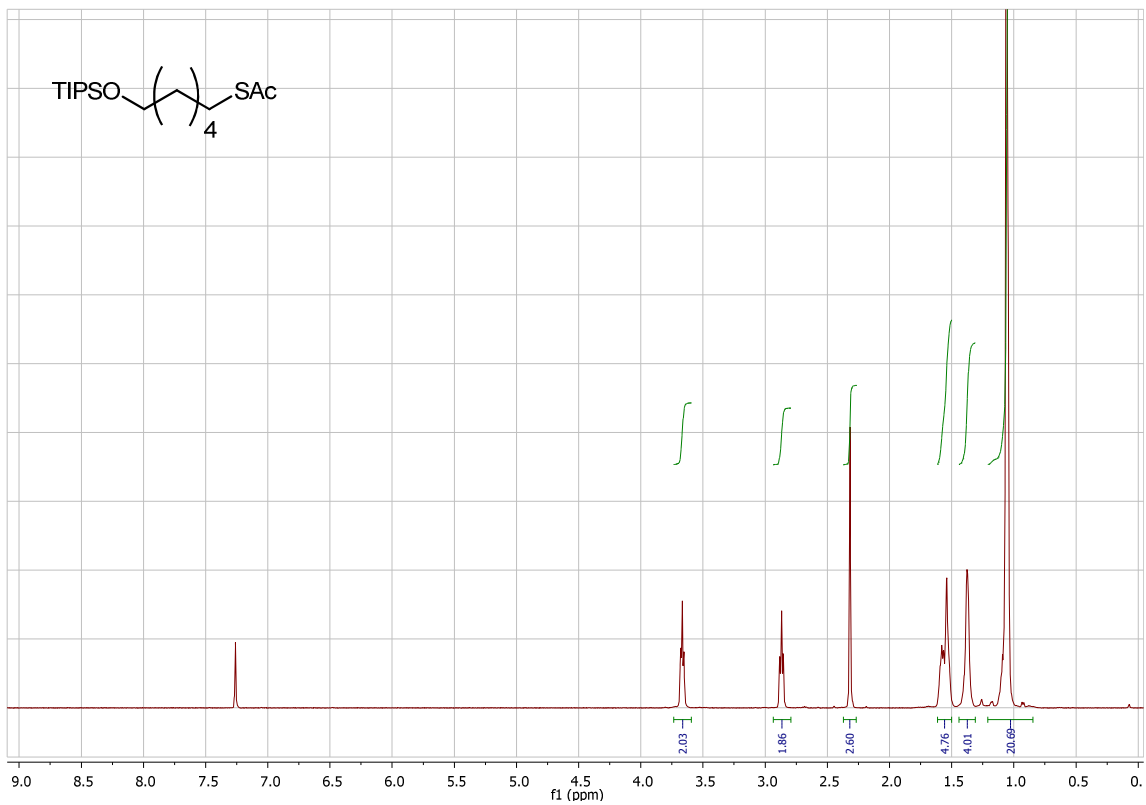




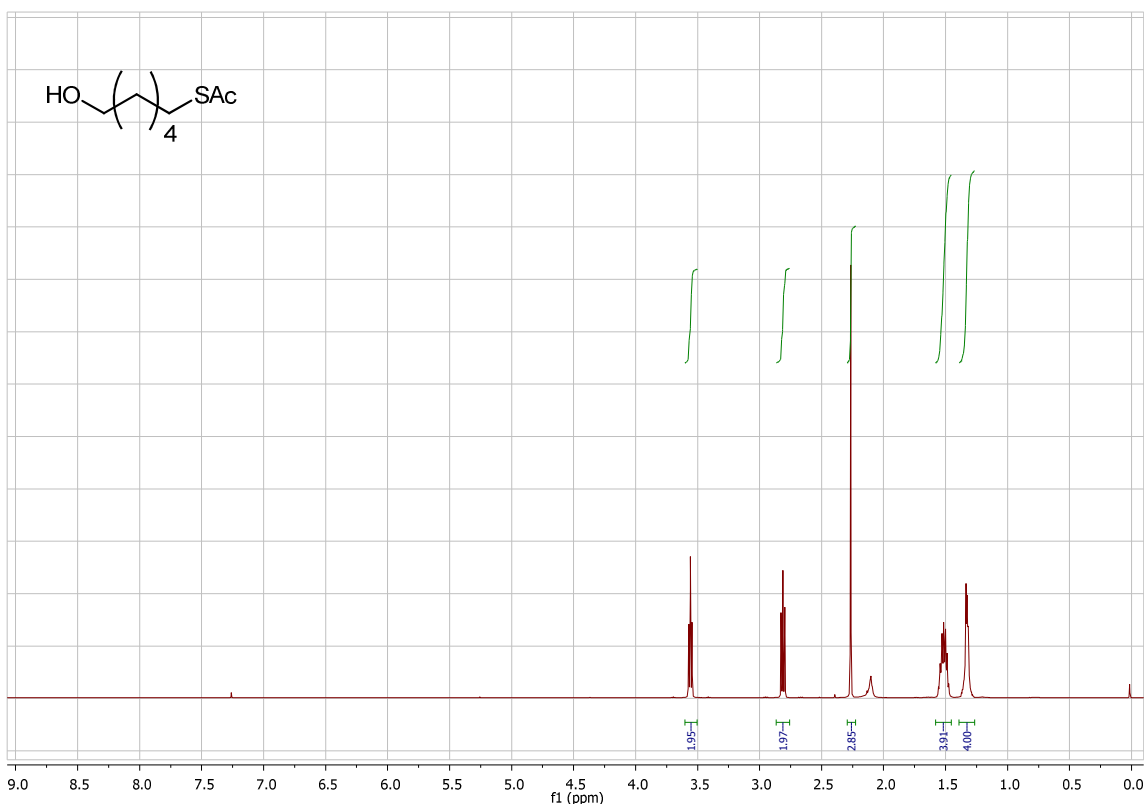
¹H NMR (500 MHz, CDCl₃) of compound **37**



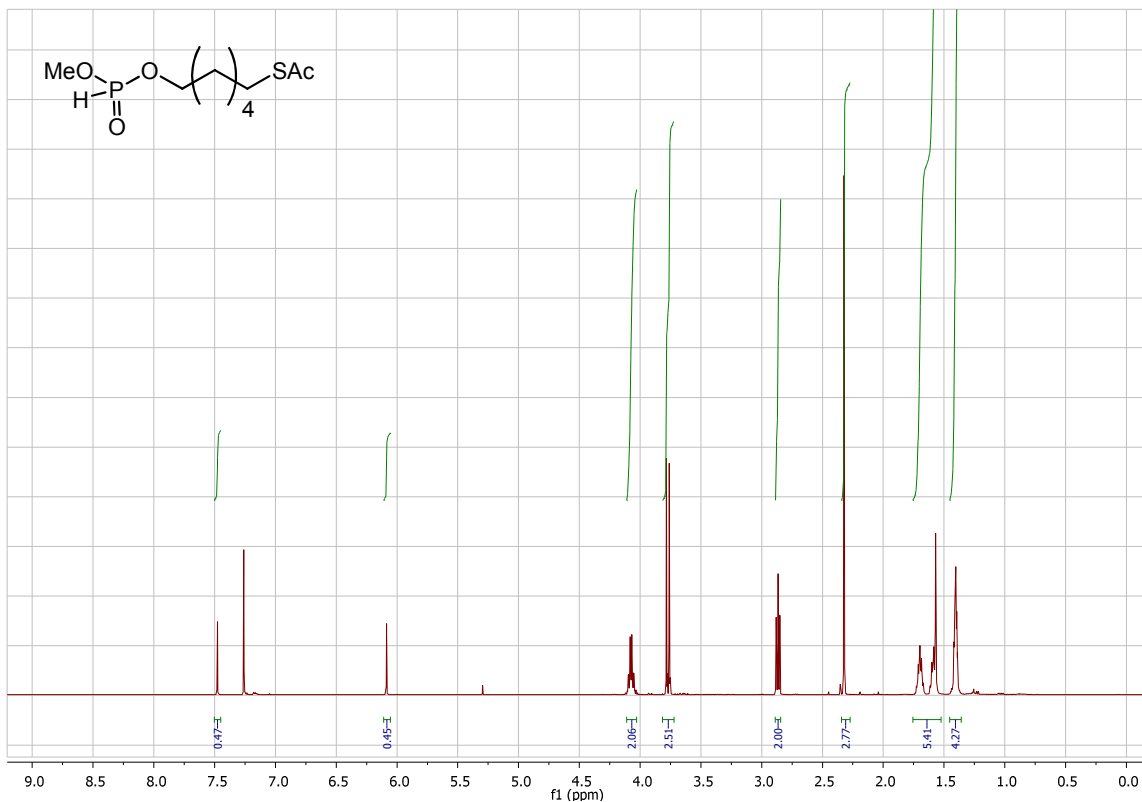
¹H NMR (500 MHz, CDCl₃) of compound **38**



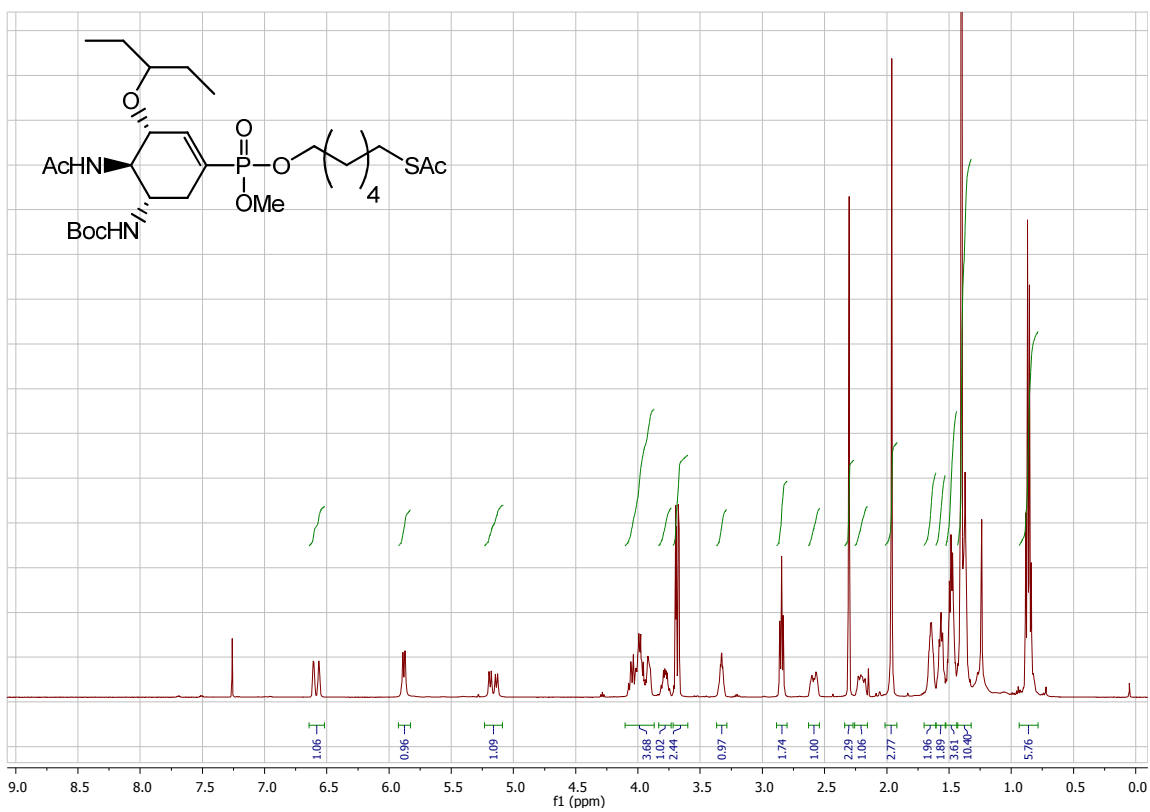
^1H NMR (500 MHz, CDCl_3) of compound **39**



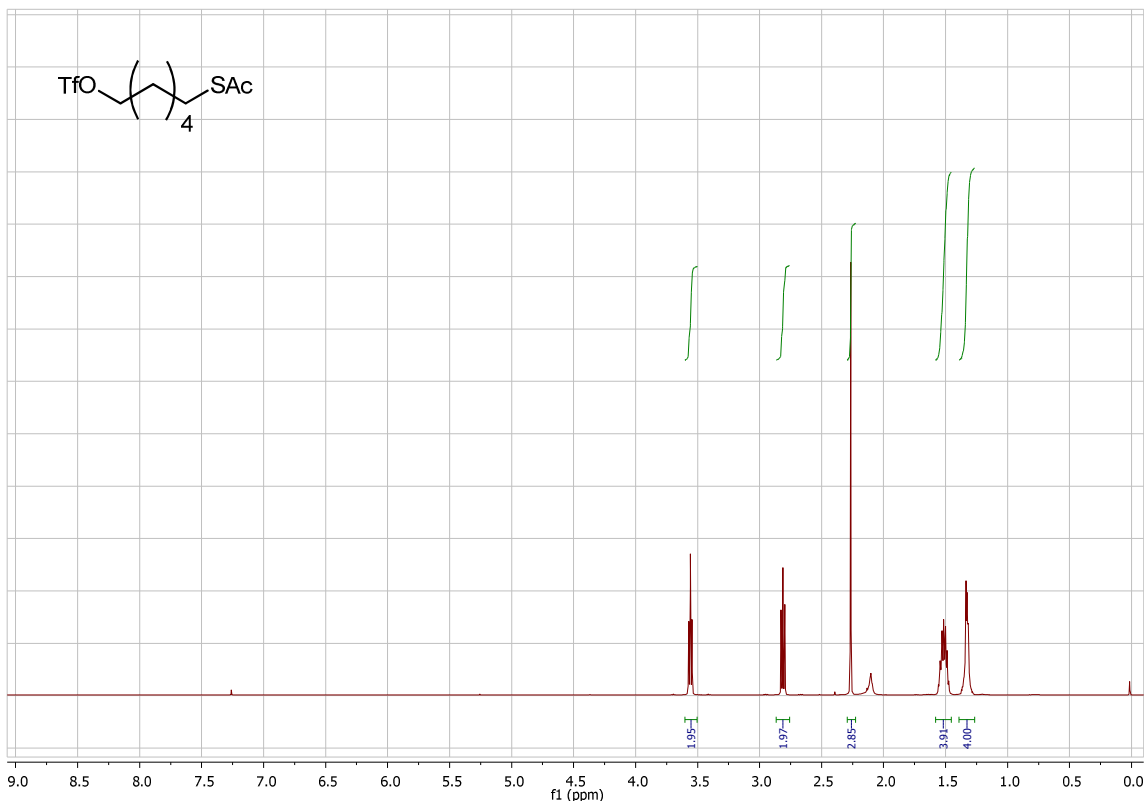
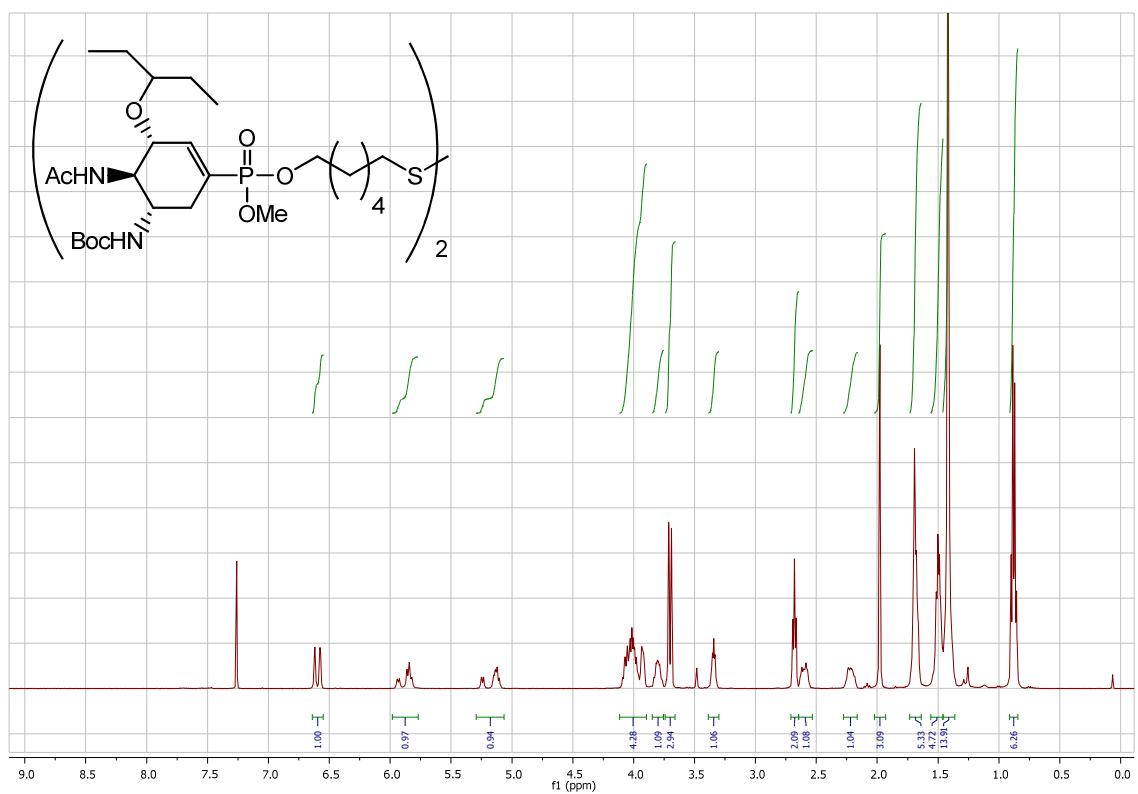
^1H NMR (500 MHz, CDCl_3) of compound **40**

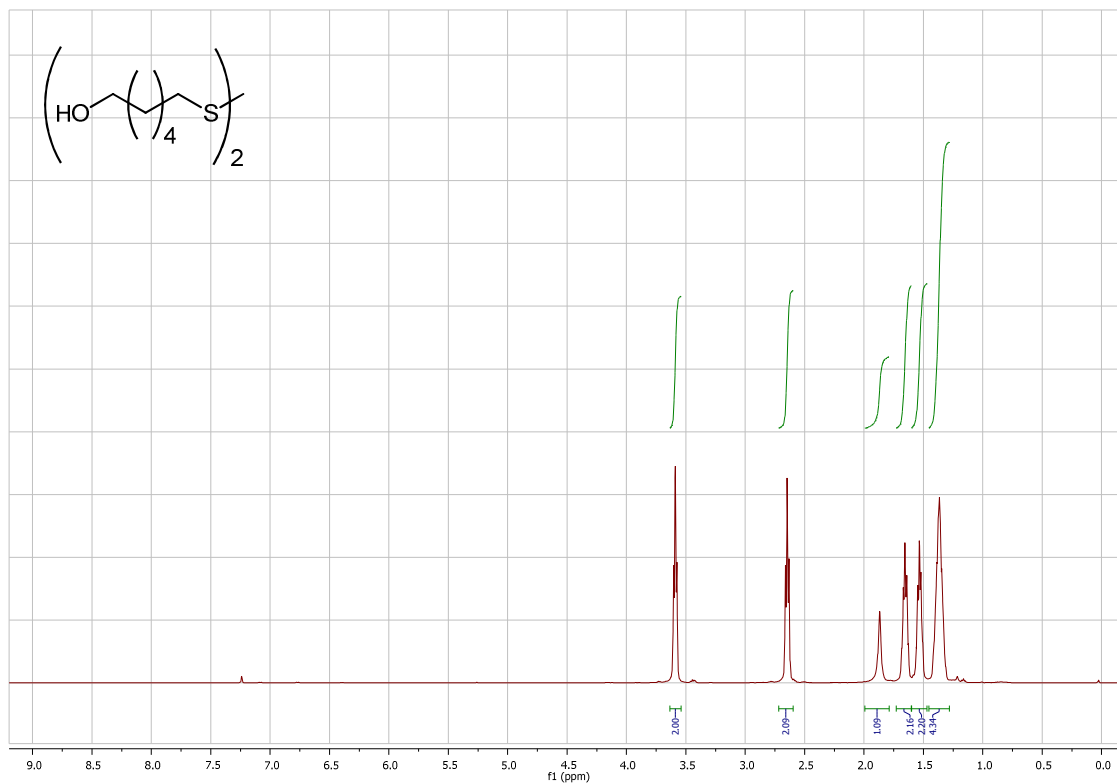
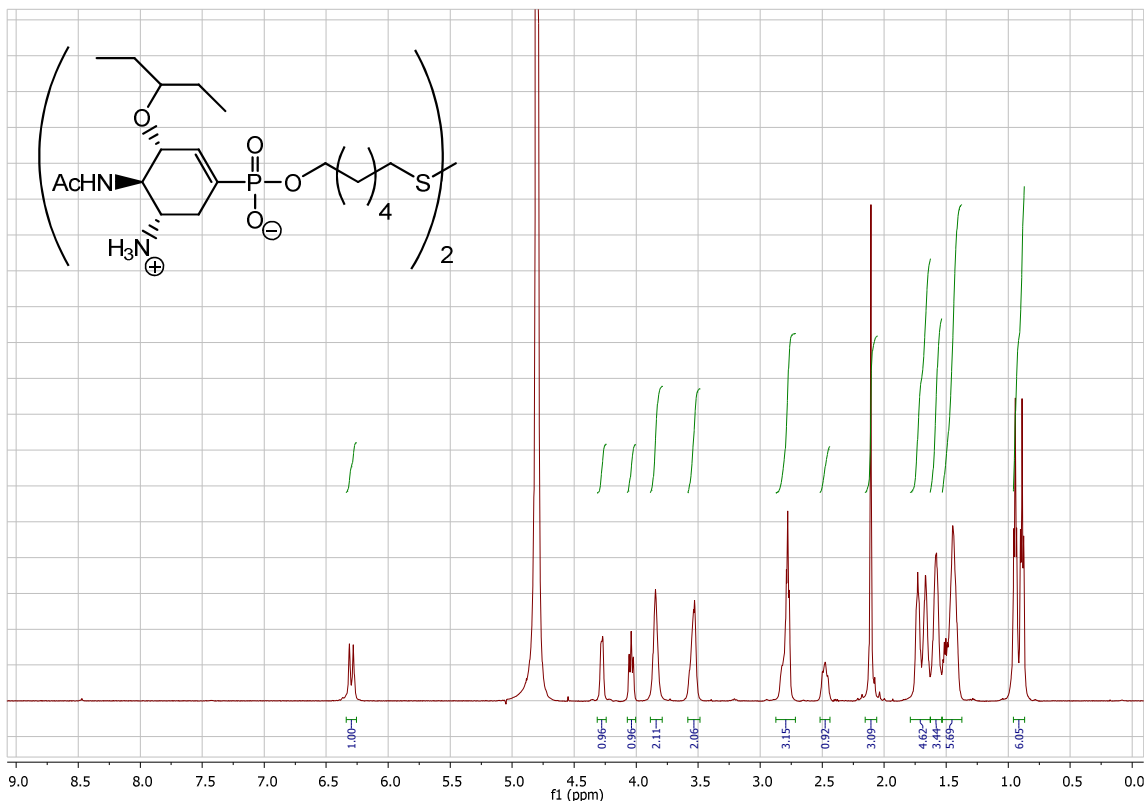


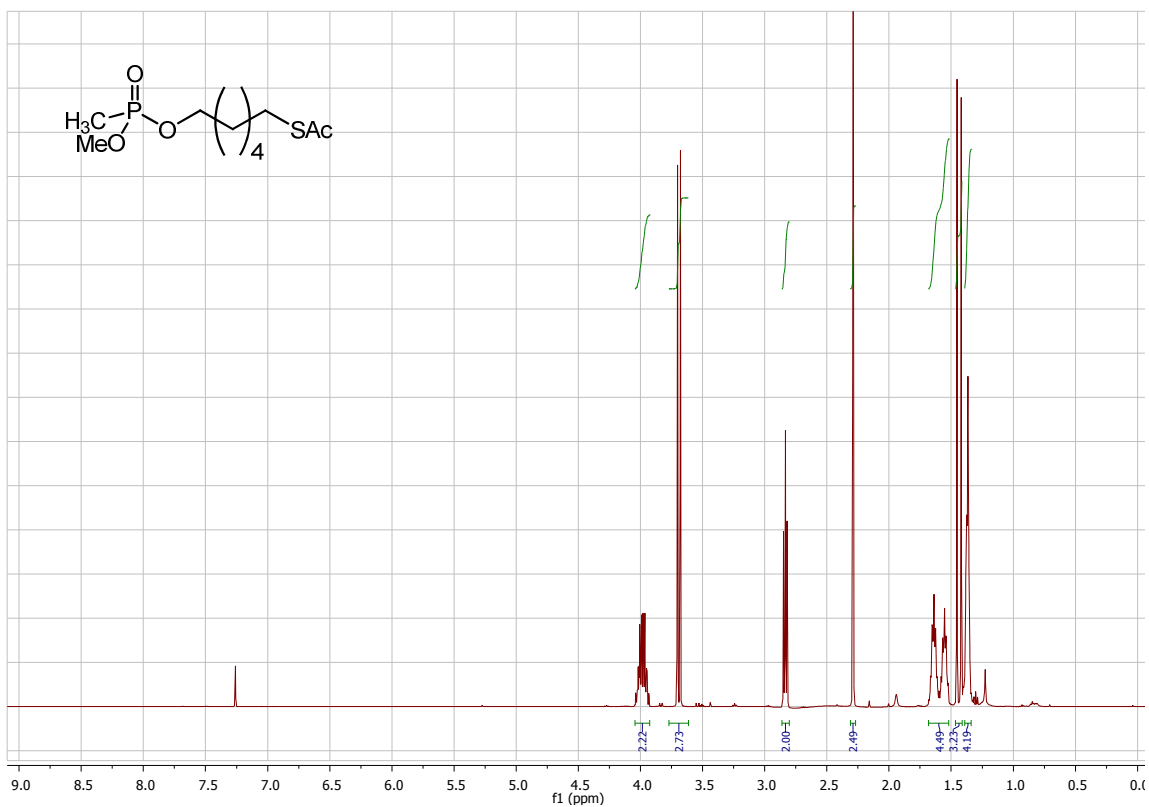
¹H NMR (500 MHz, CDCl₃) of compound 41



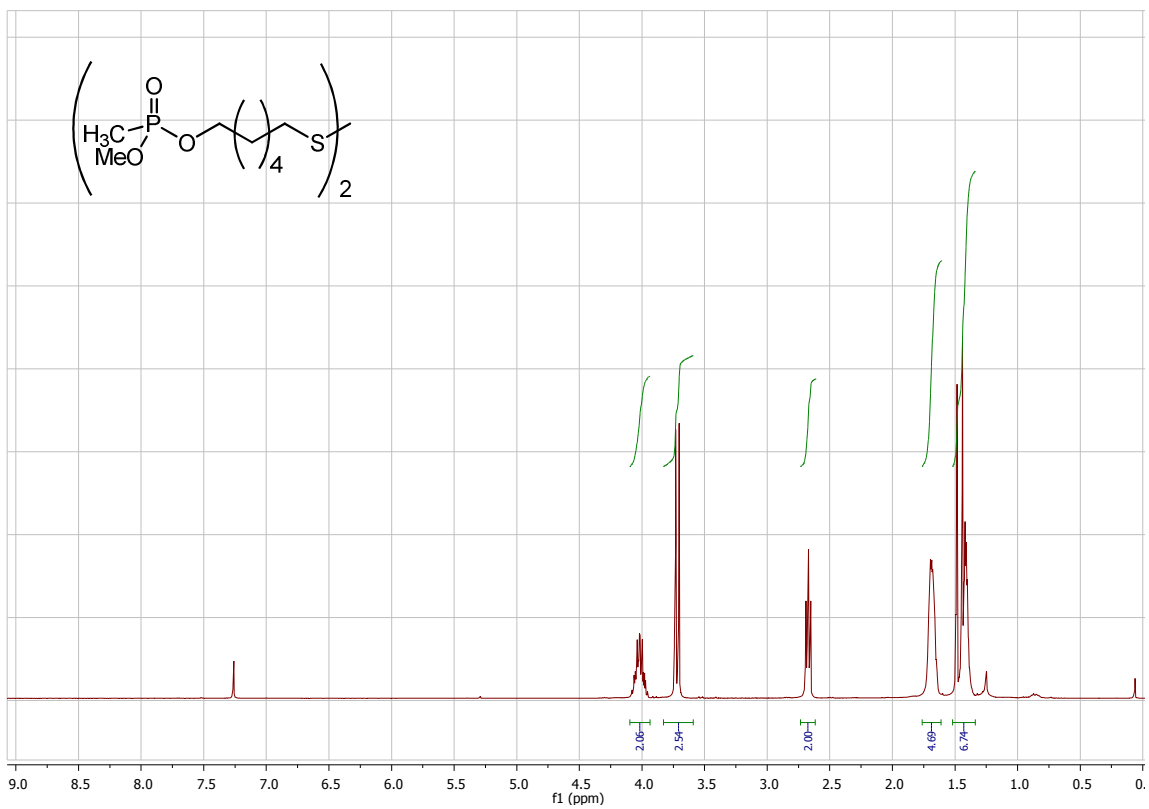
¹H NMR (500 MHz, CDCl₃) of compound 42

 $^1\text{H NMR}$ (500 MHz, CDCl_3) of compound 43 $^1\text{H NMR}$ (500 MHz, CDCl_3) of compound 44

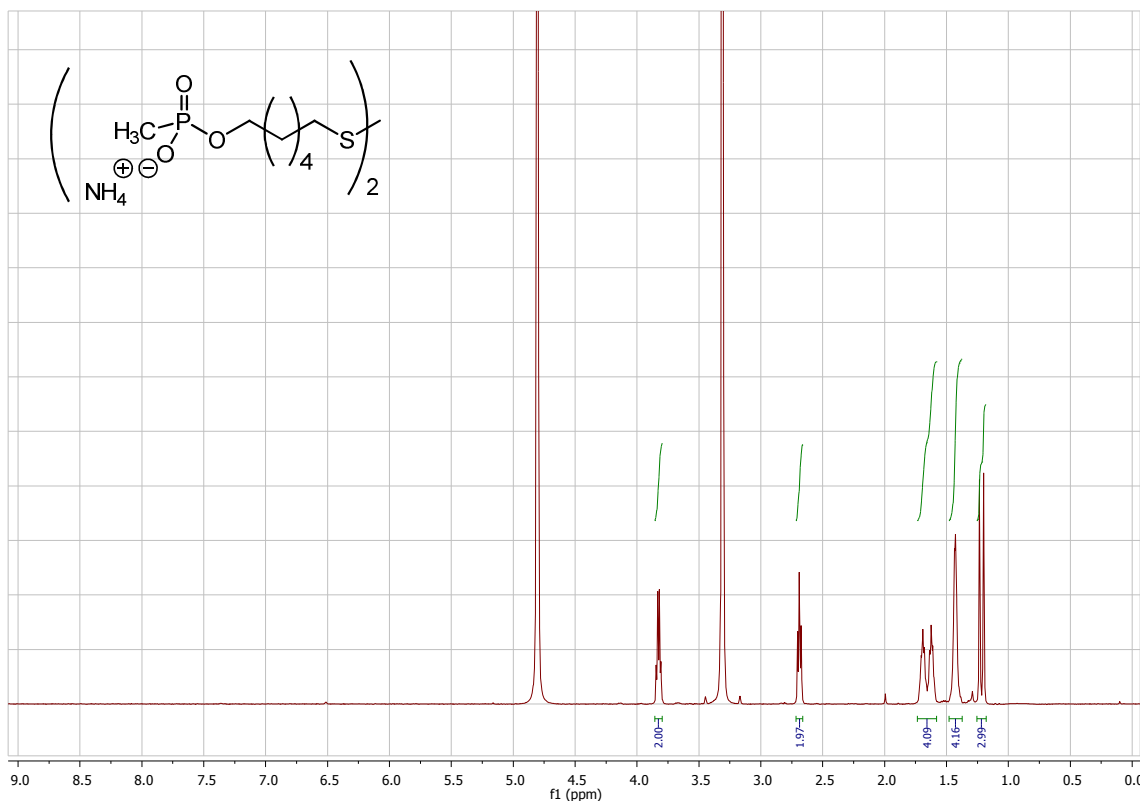




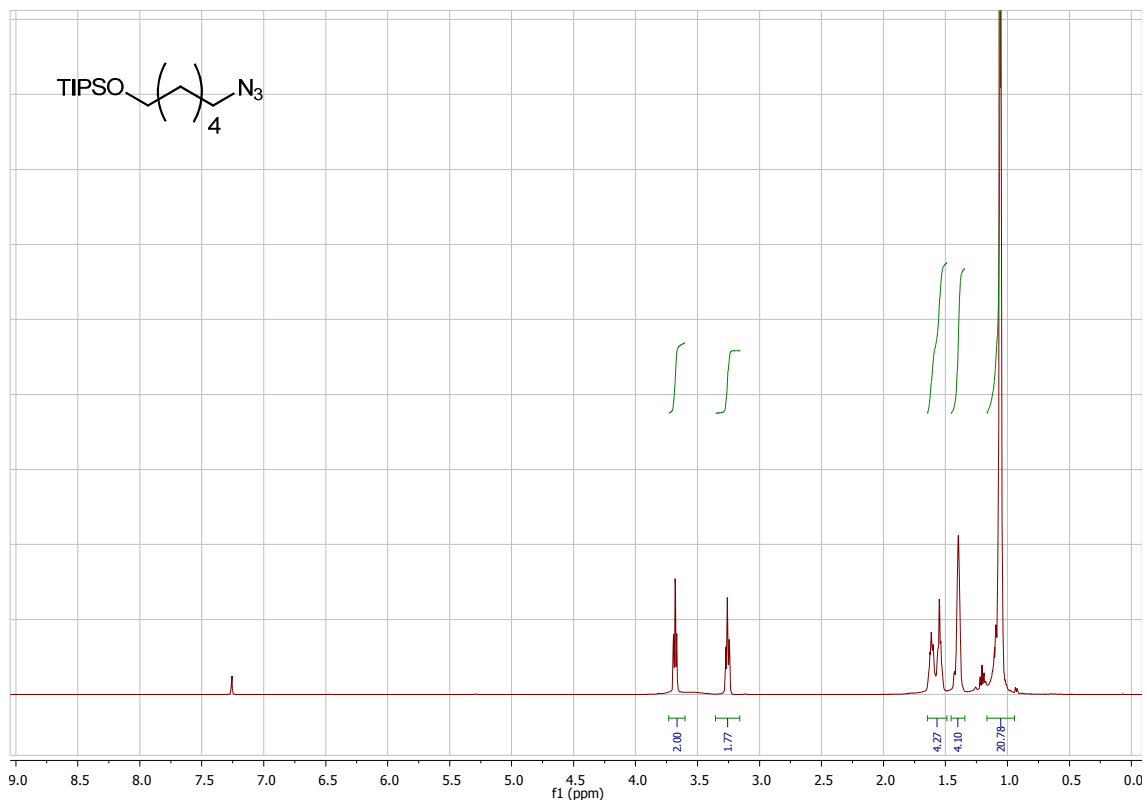
¹H NMR (500 MHz, CDCl₃) of compound 47



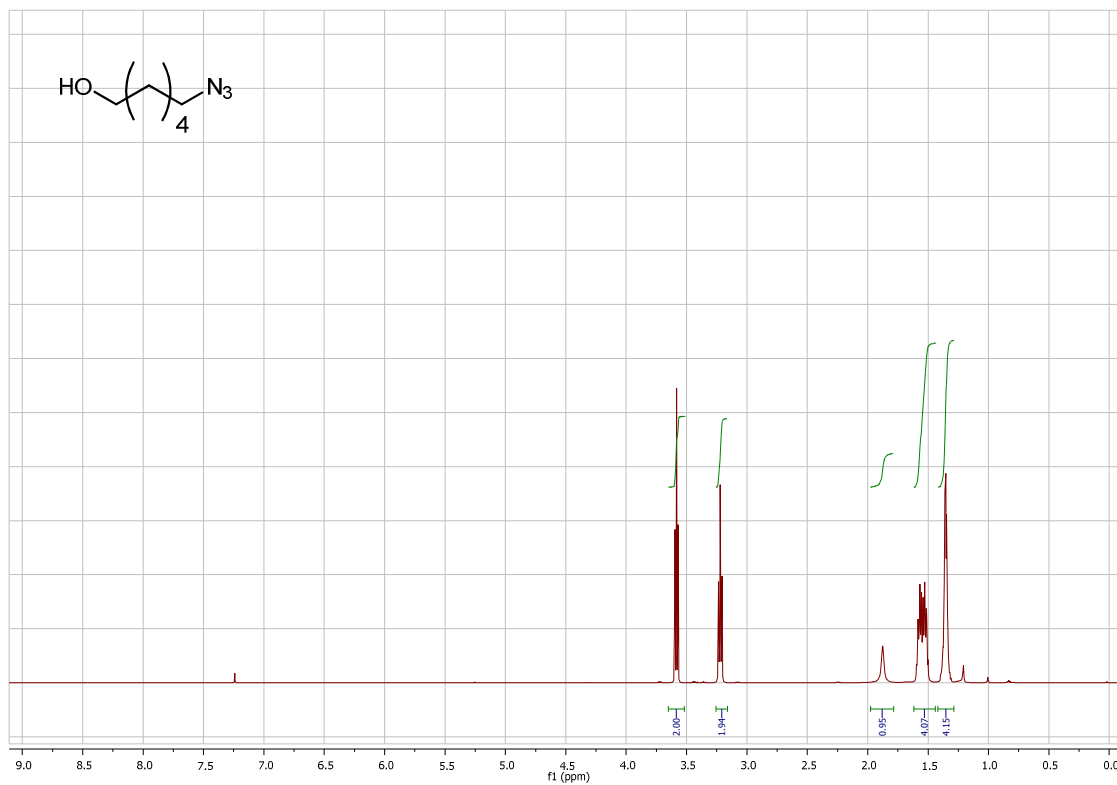
¹H NMR (500 MHz, CDCl₃) of compound 48



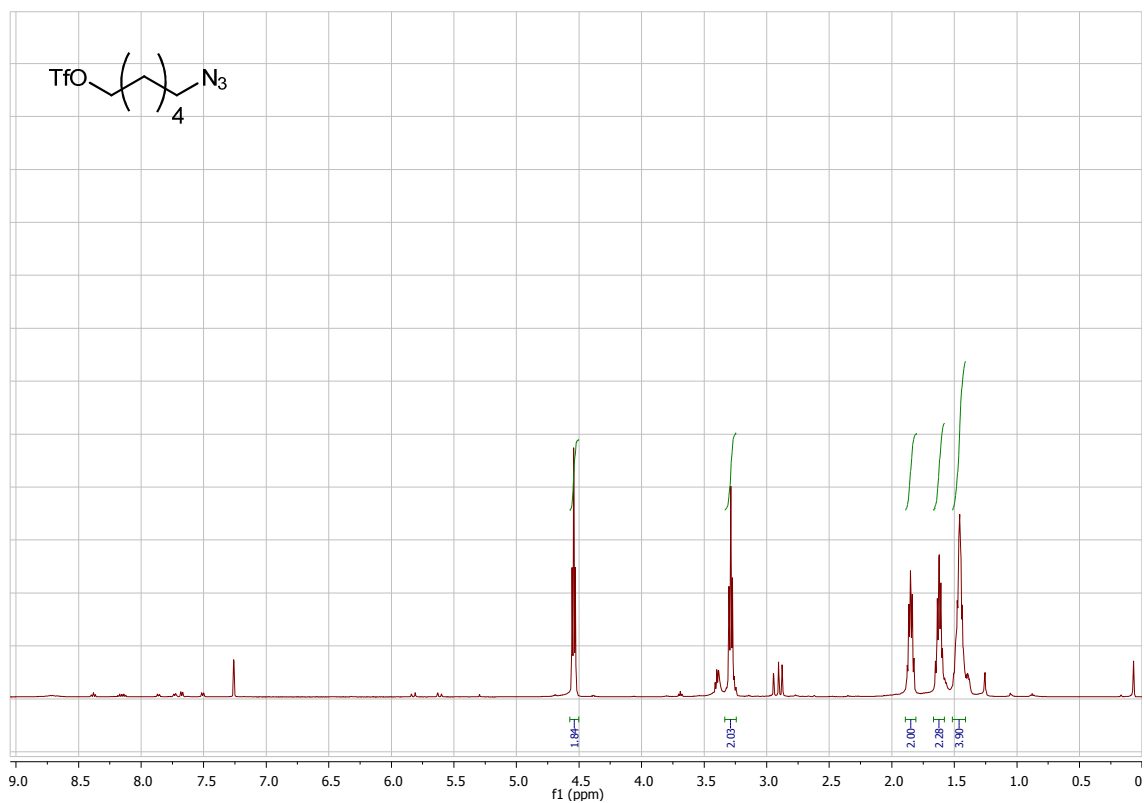
¹H NMR (500 MHz, MeOH-D₄) of compound **49**



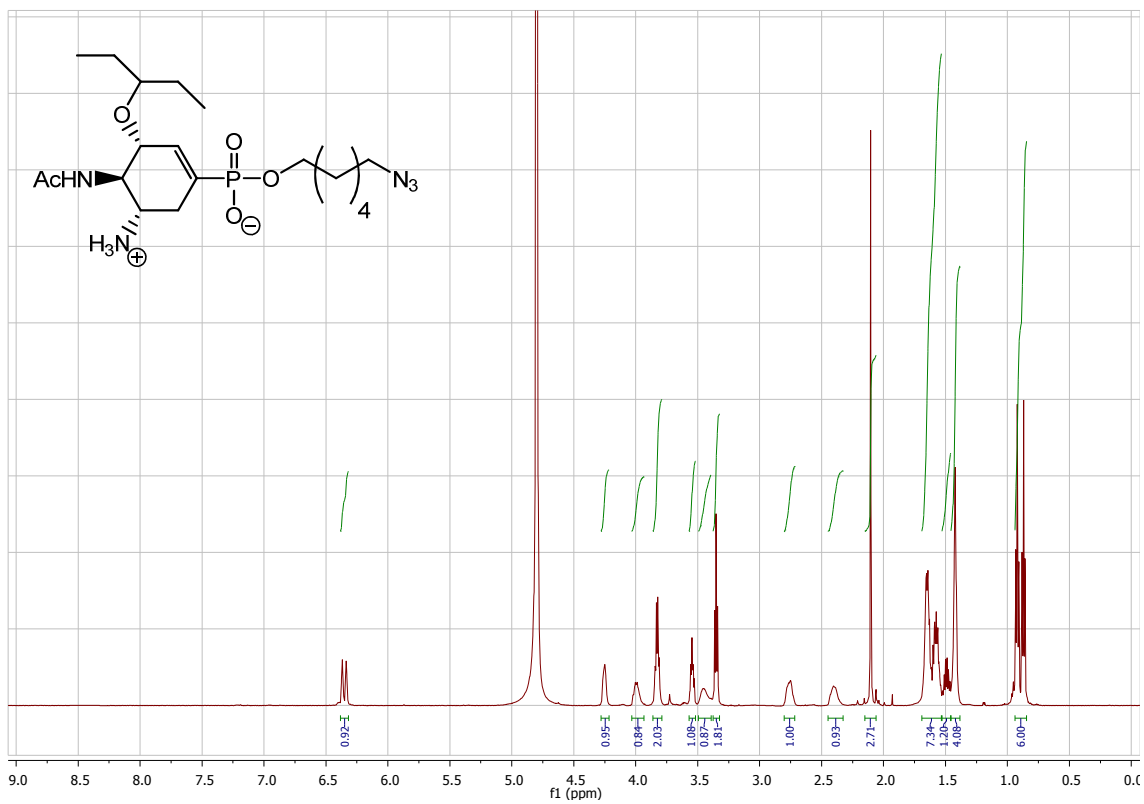
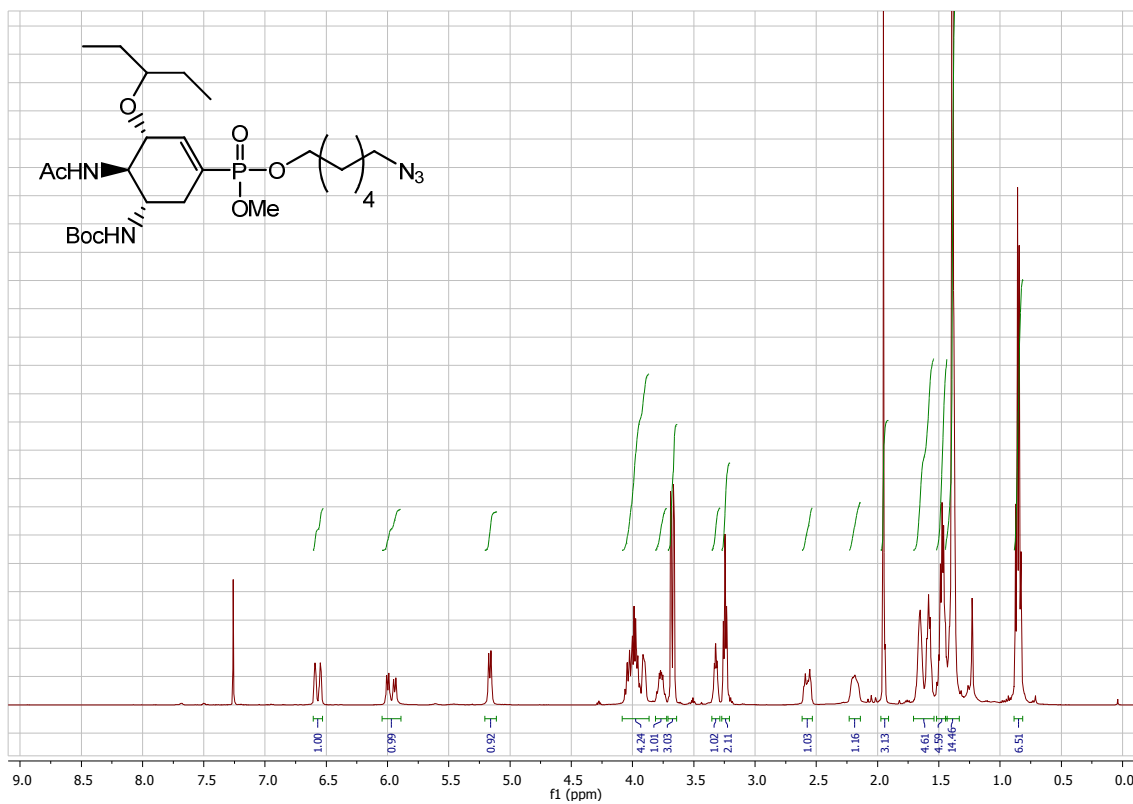
¹H NMR (500 MHz, CDCl₃) of compound **50**

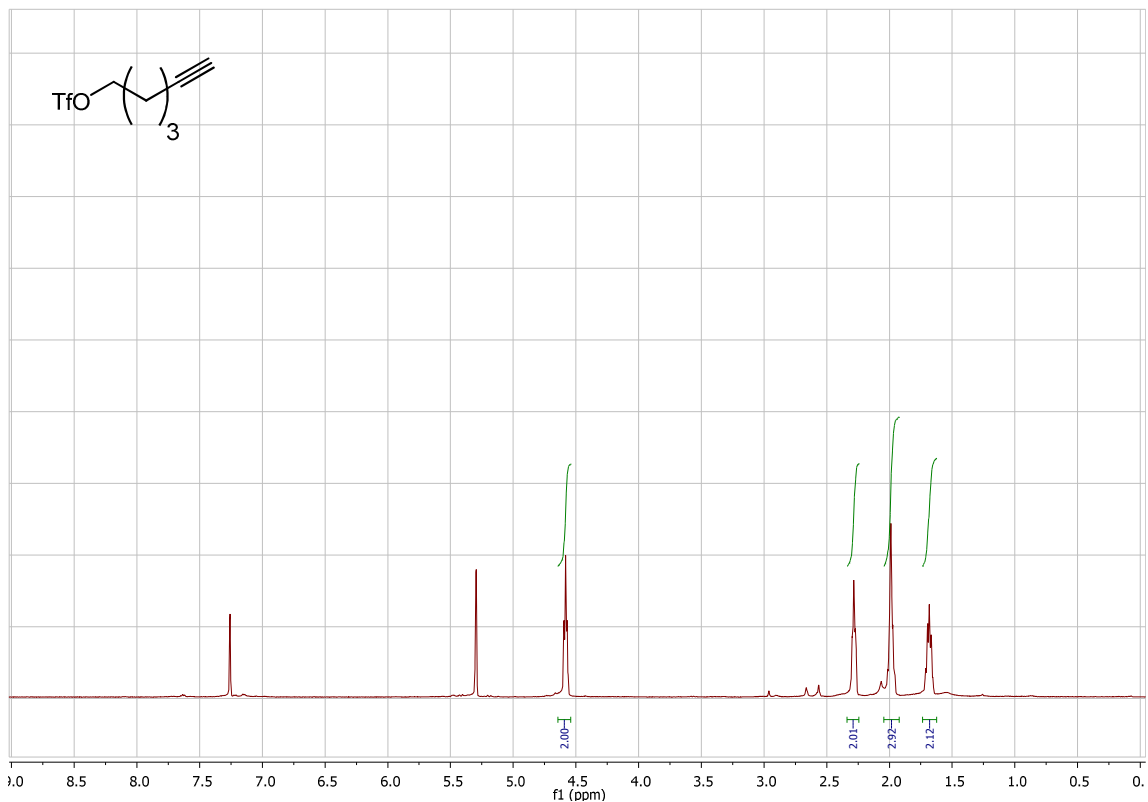


¹H NMR (500 MHz, CDCl₃) of compound 51

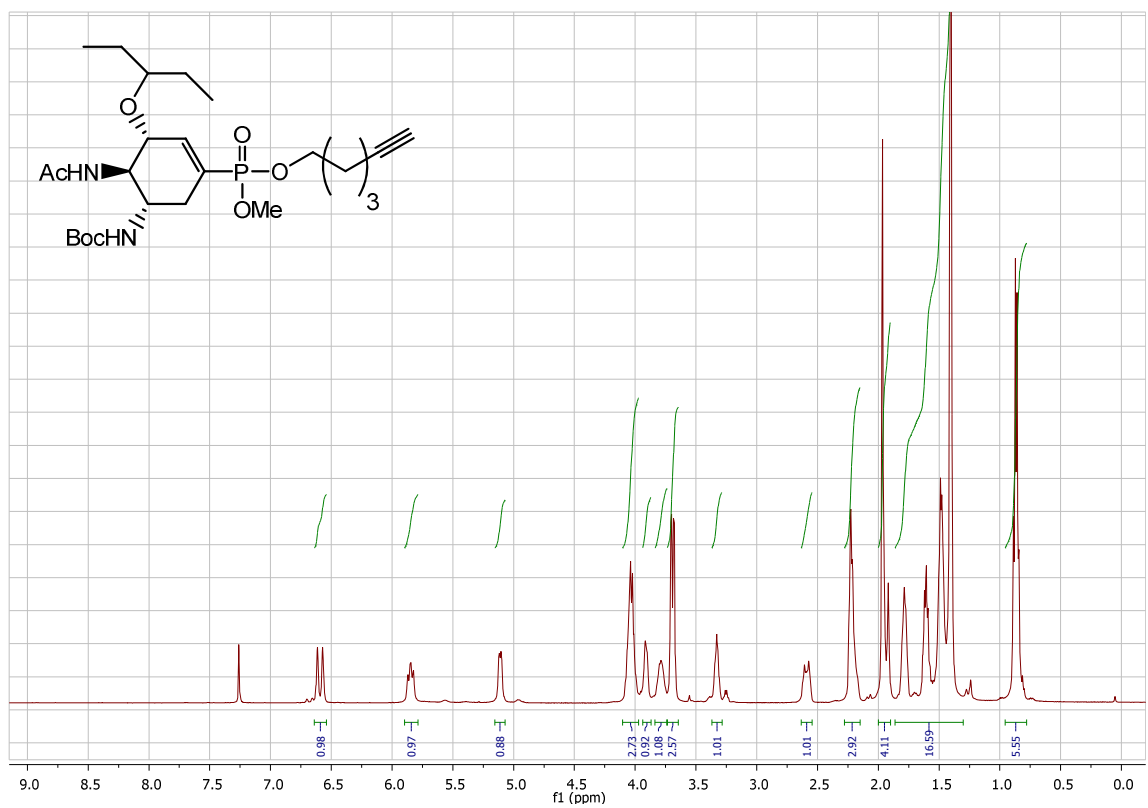


¹H NMR (500 MHz, CDCl₃) of compound 52

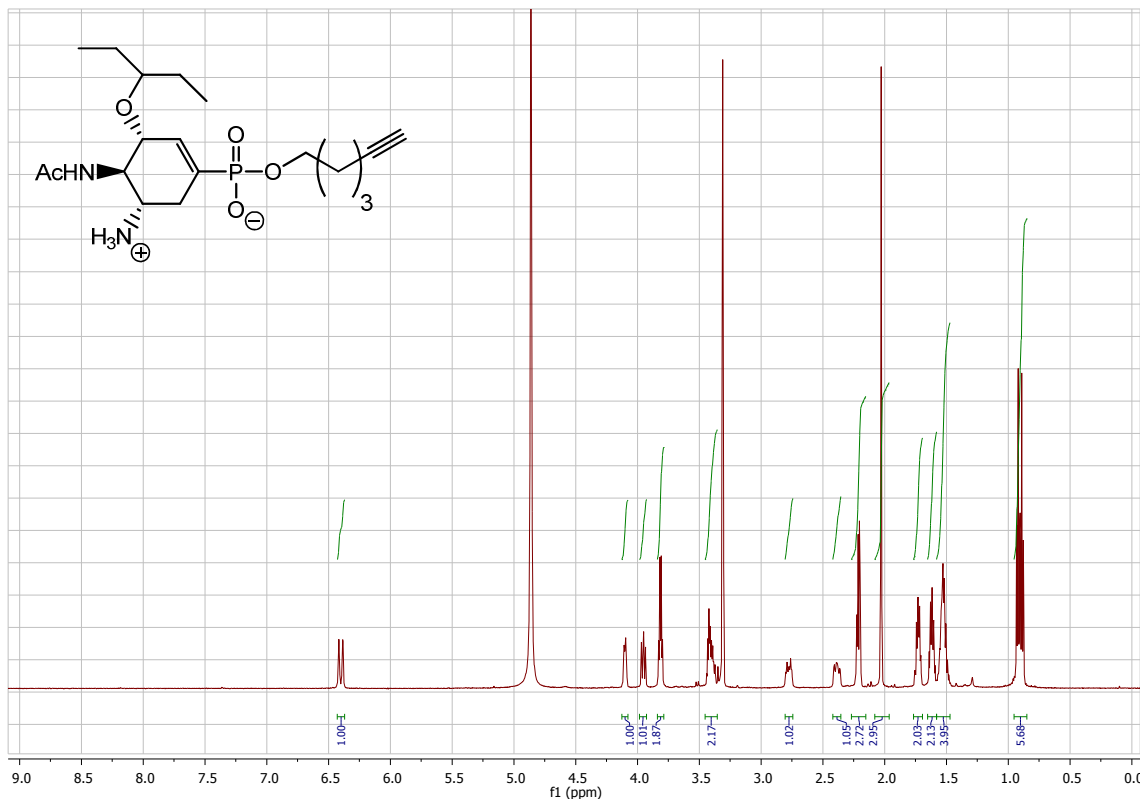




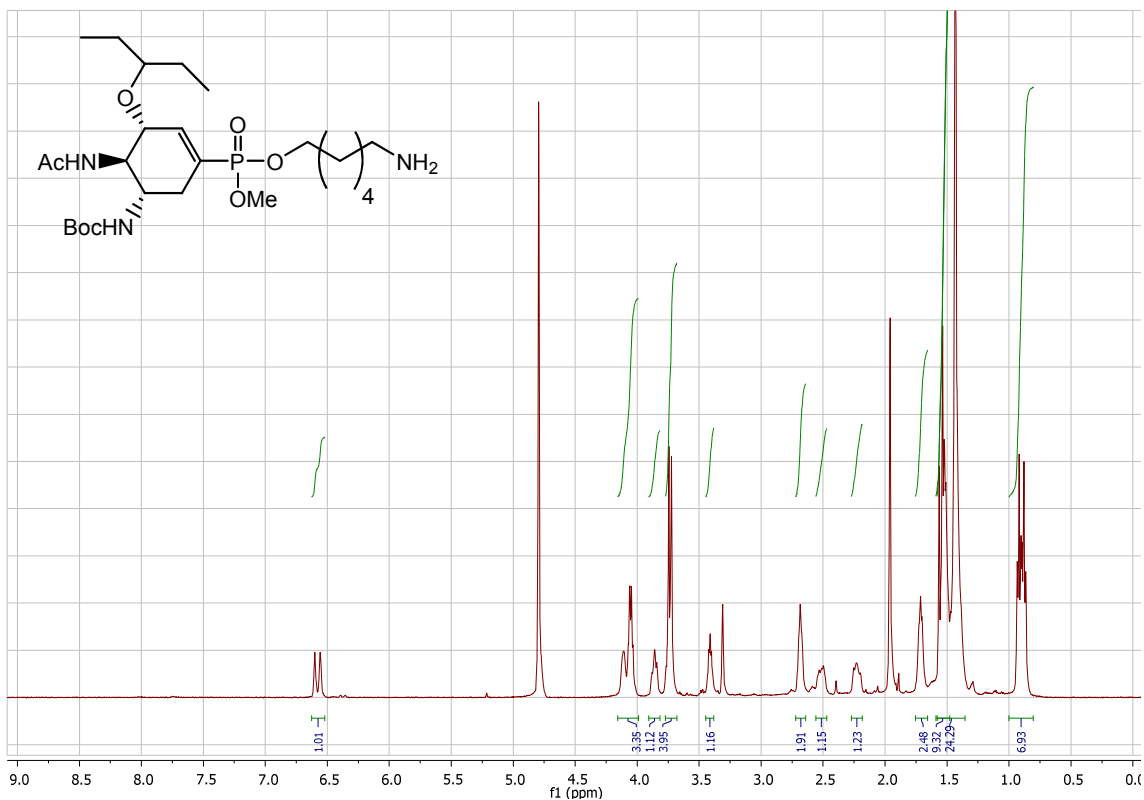
¹H NMR (500 MHz, CDCl₃) of compound 55



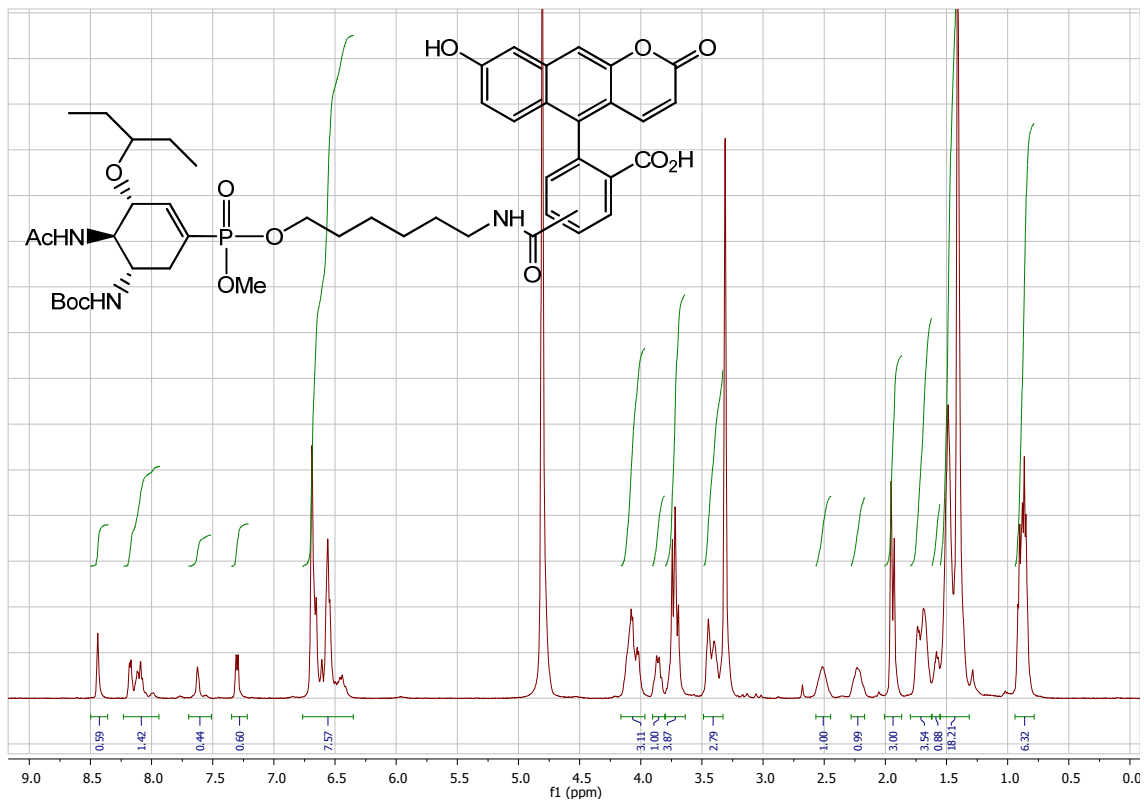
¹H NMR (500 MHz, CDCl₃) of compound 56



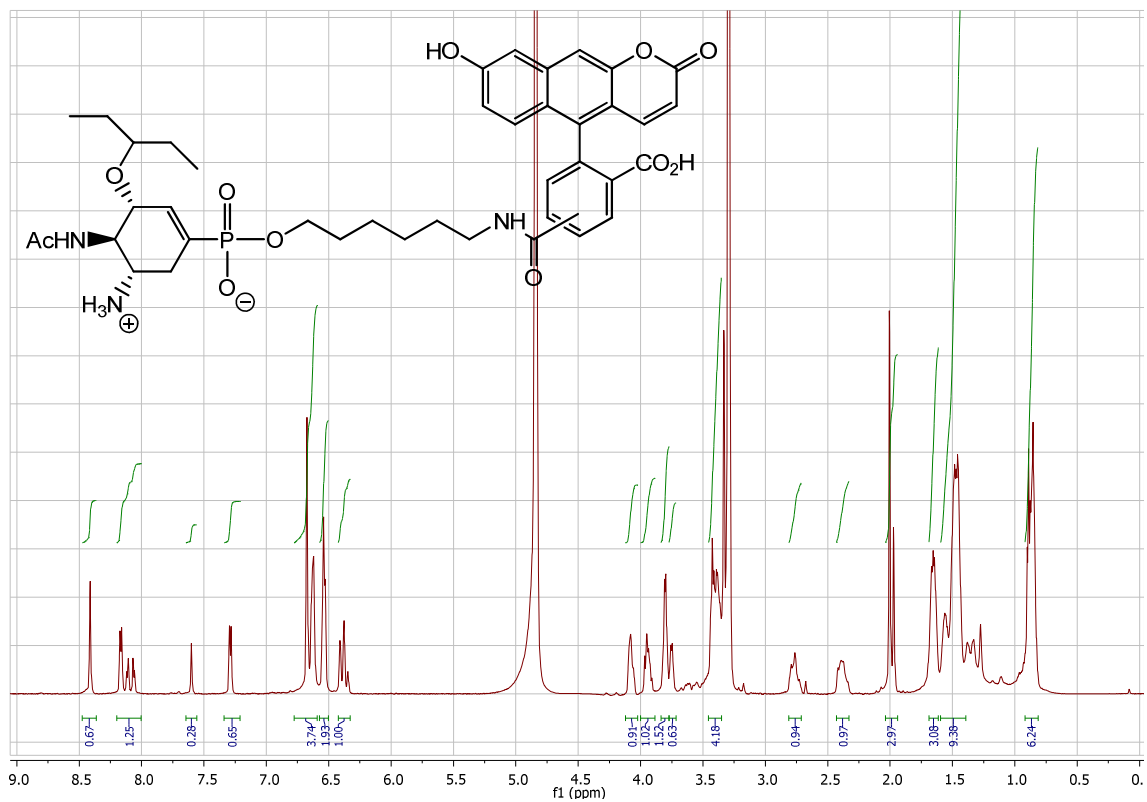
¹H NMR (600 MHz, MeOH-D₄) of compound 57



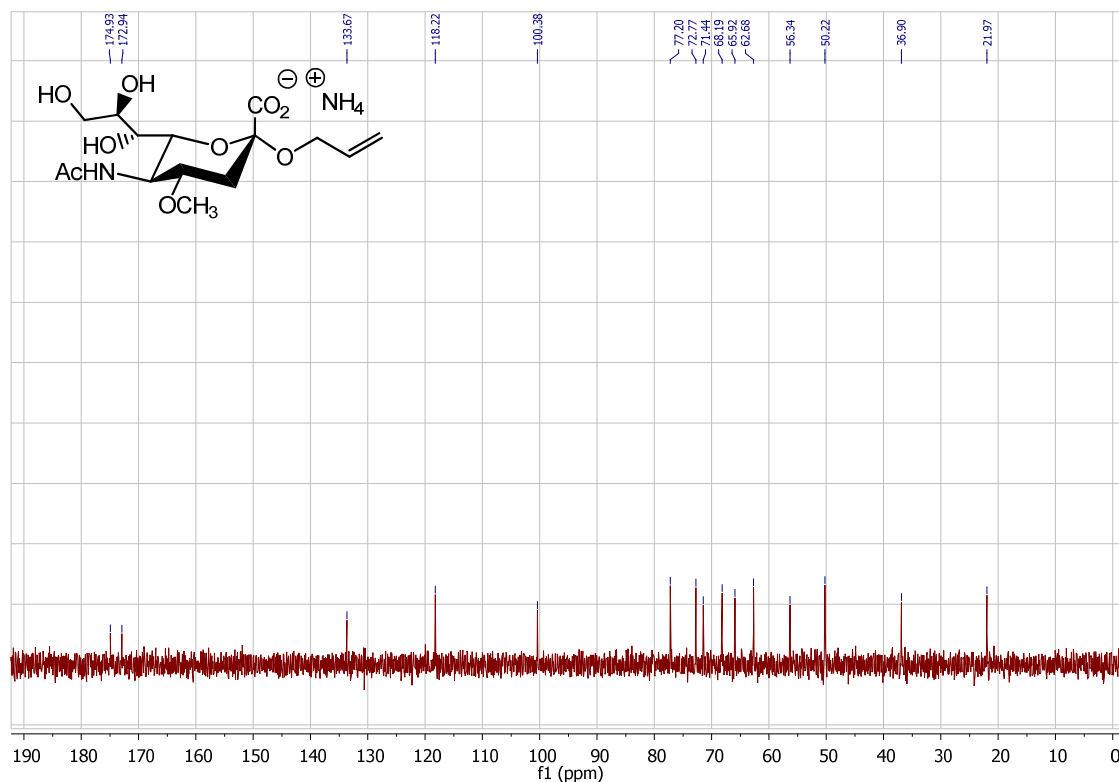
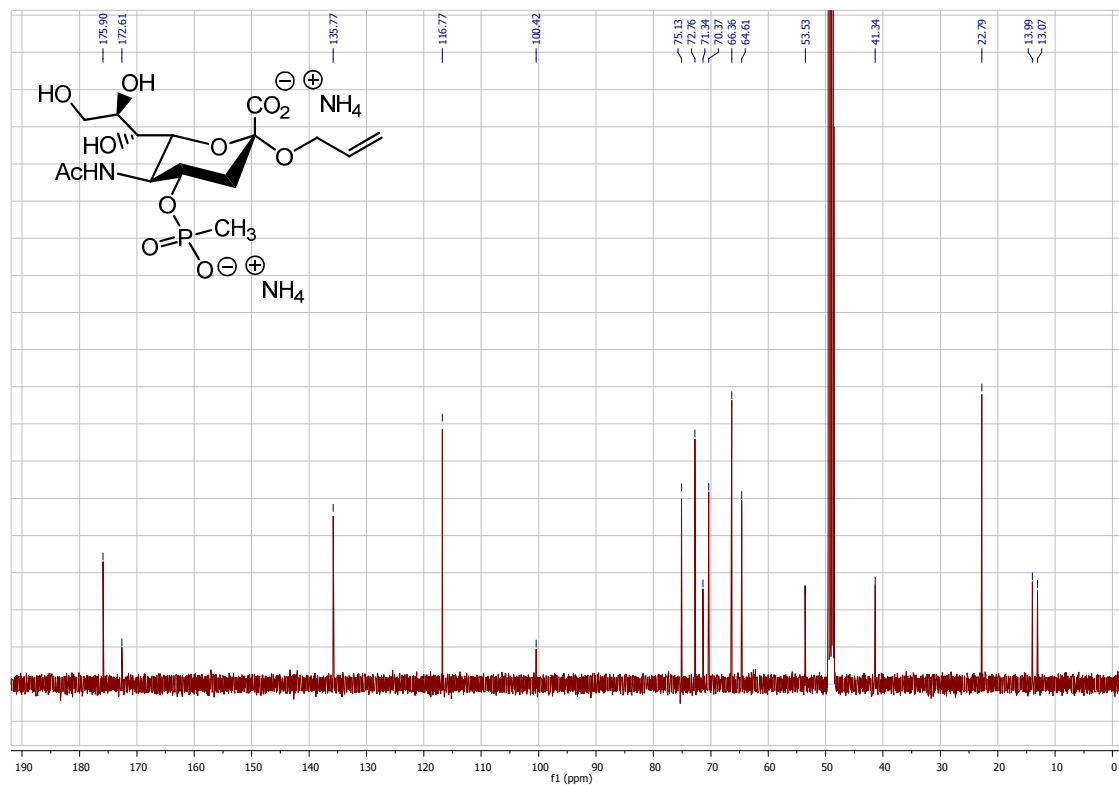
¹H NMR (500 MHz, MeOH-D₄) of compound 58

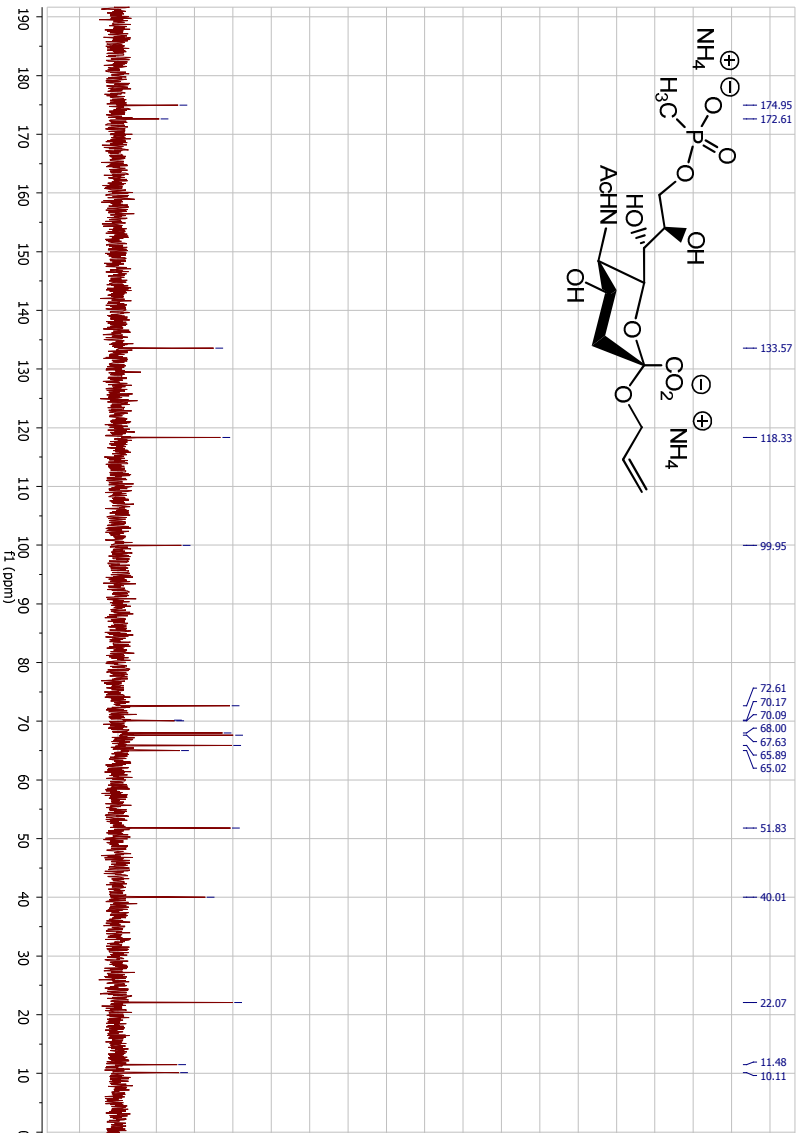
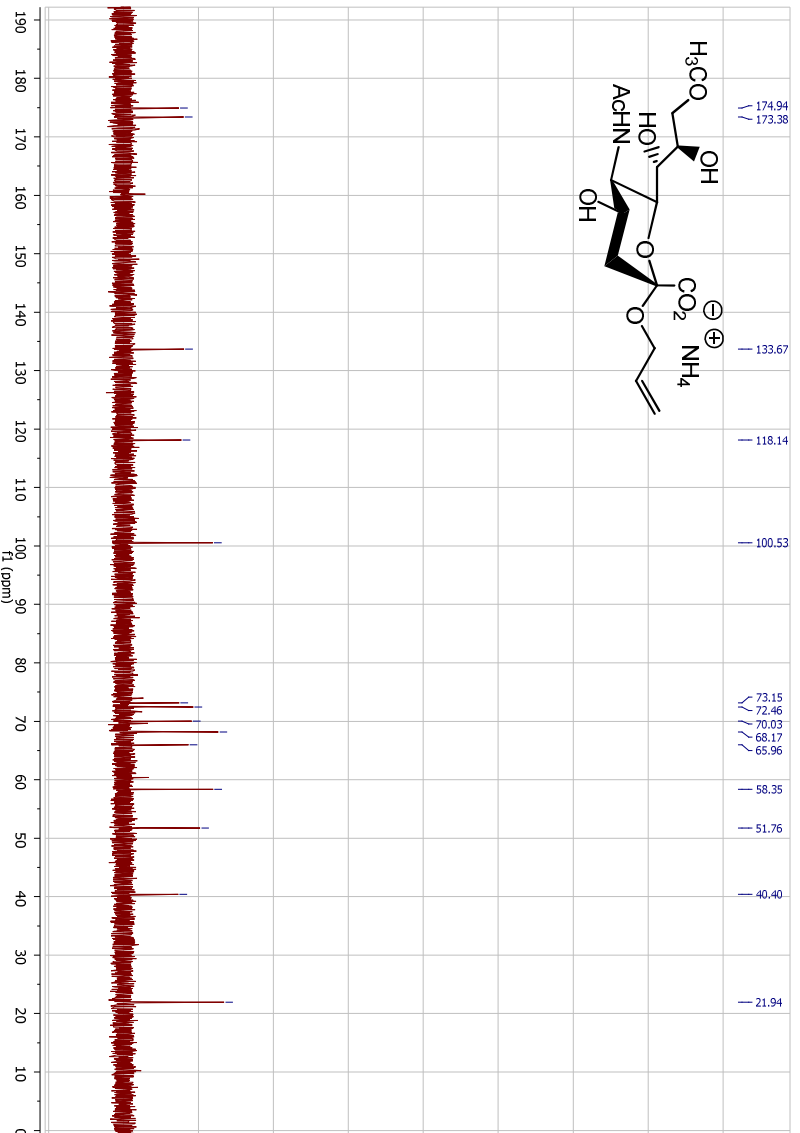


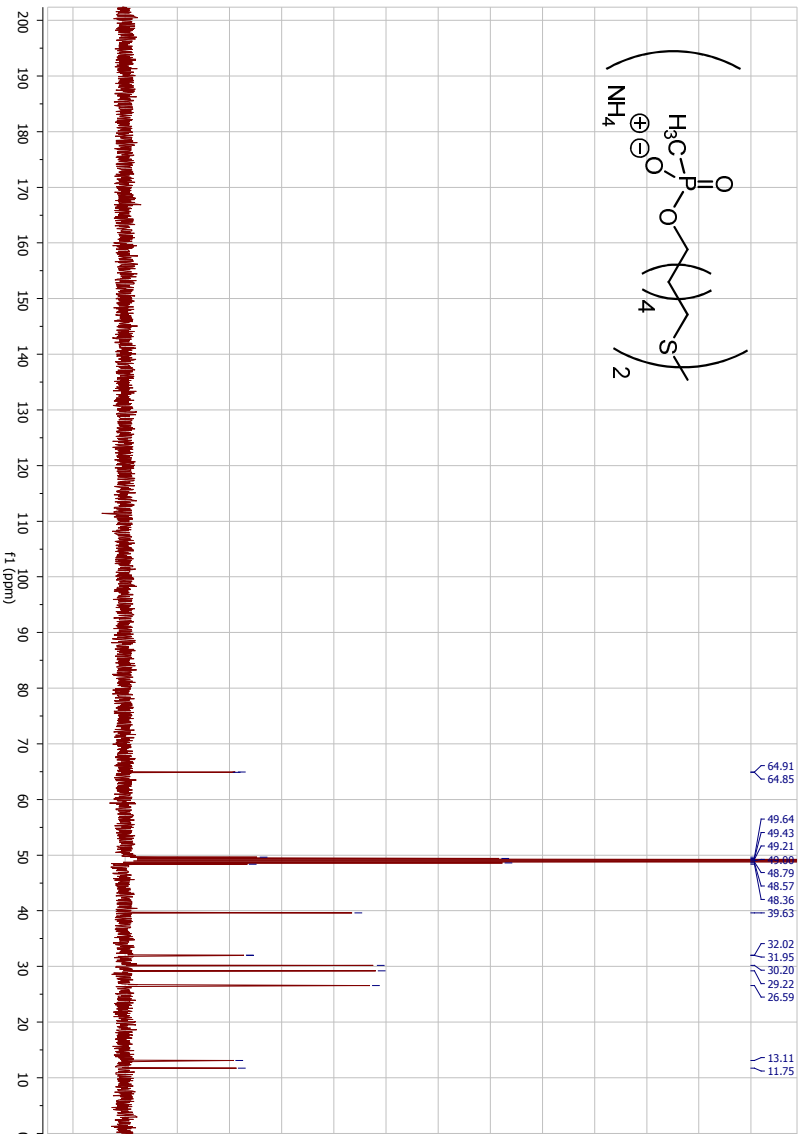
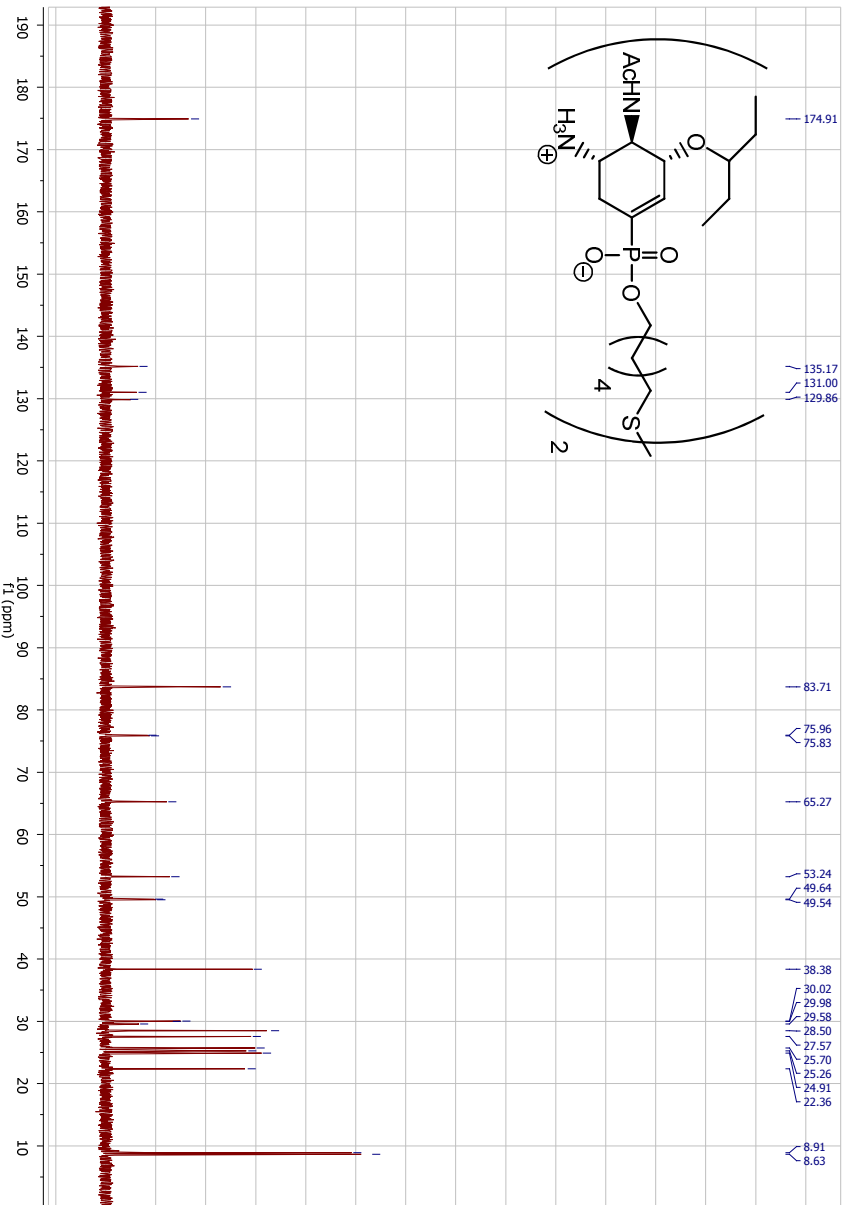
¹H NMR (500 MHz, MeOH-D₄) of compound 61



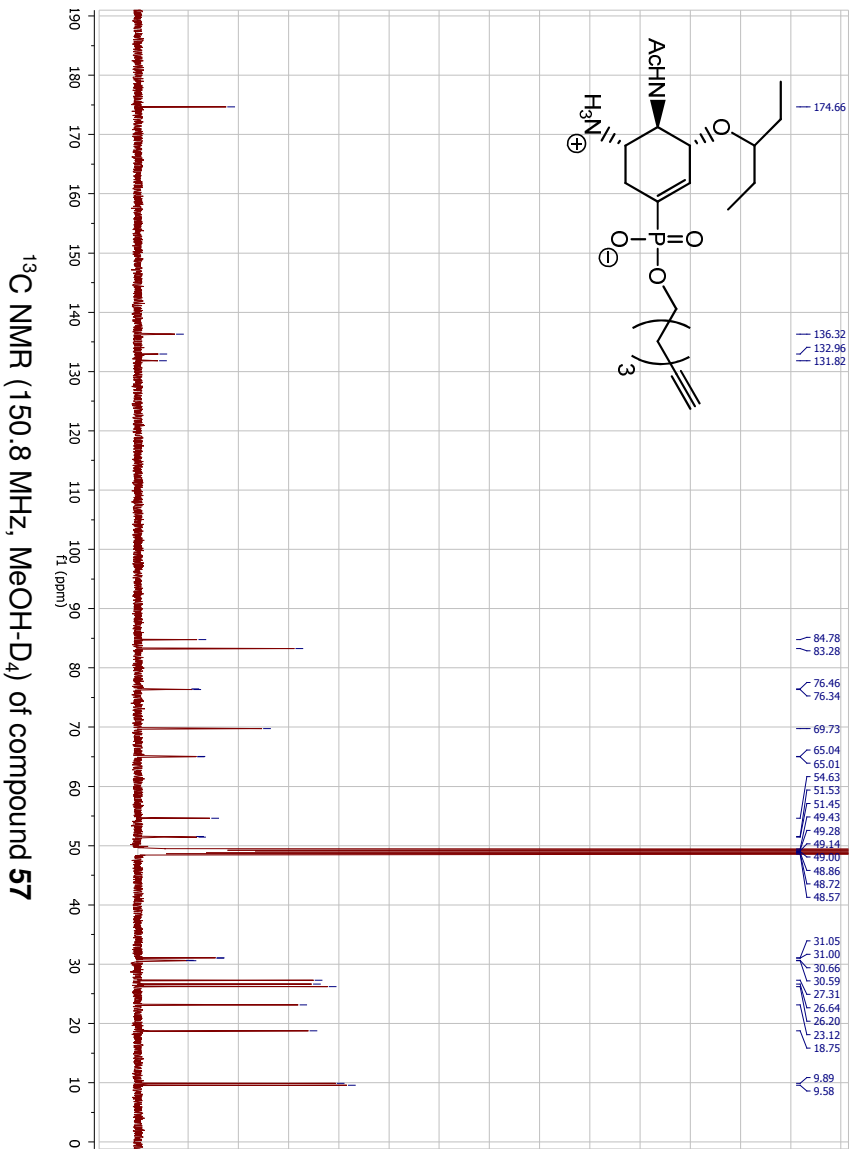
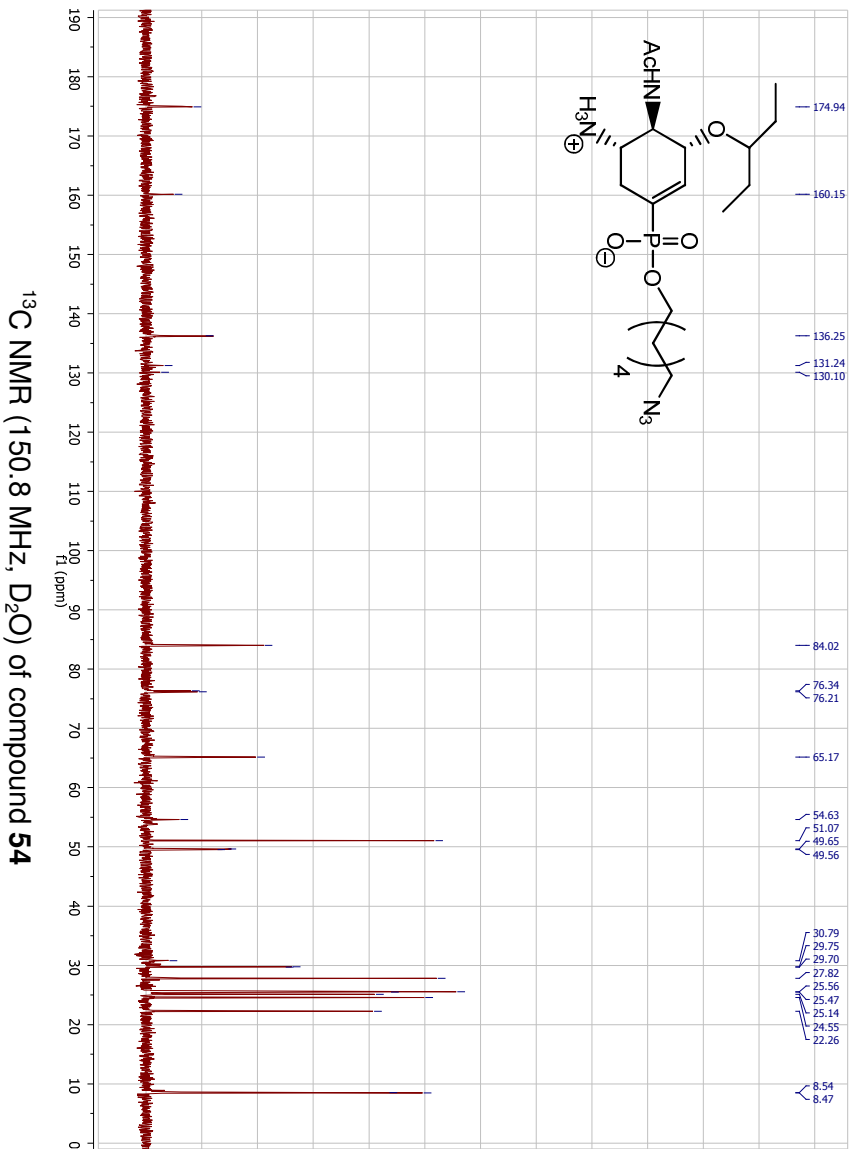
¹H NMR (600 MHz, MeOH-D₄) of compound 62

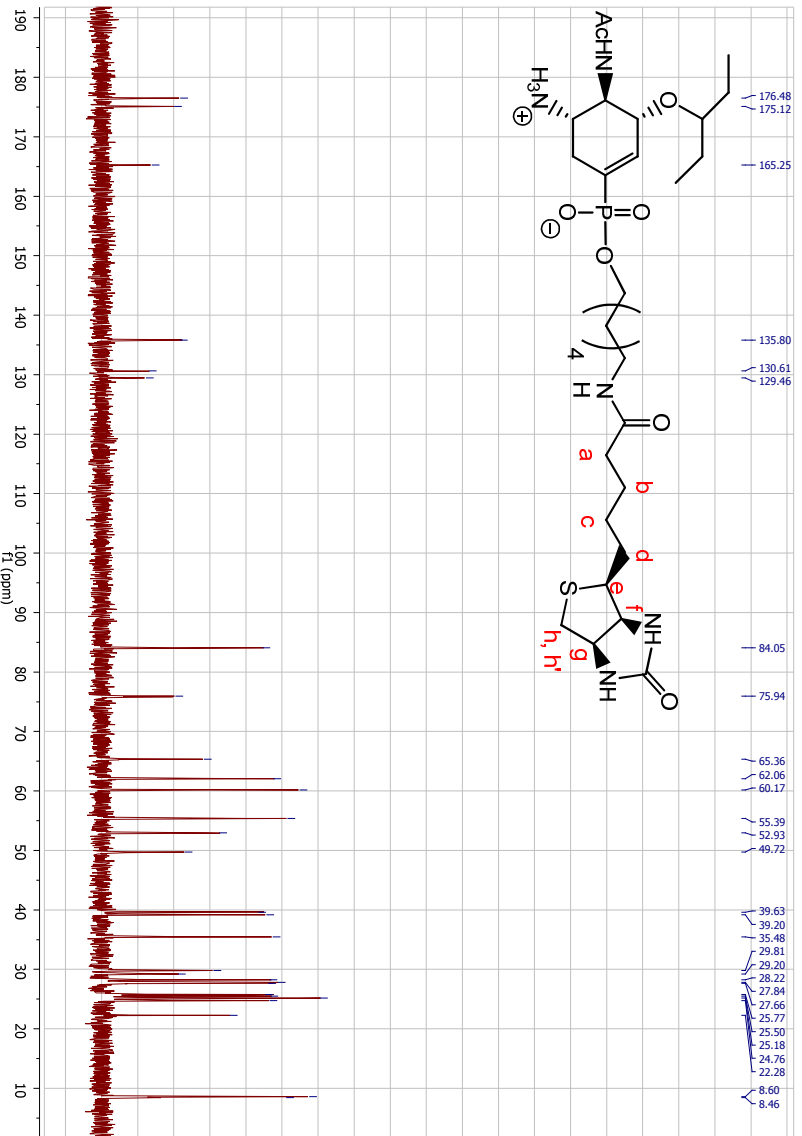
V.4.2. ^{13}C NMR of target compounds ^{13}C NMR (150.8 MHz, D_2O) of compound 5 ^{13}C NMR (150.8 MHz, MeOH-D_4) of compound 6



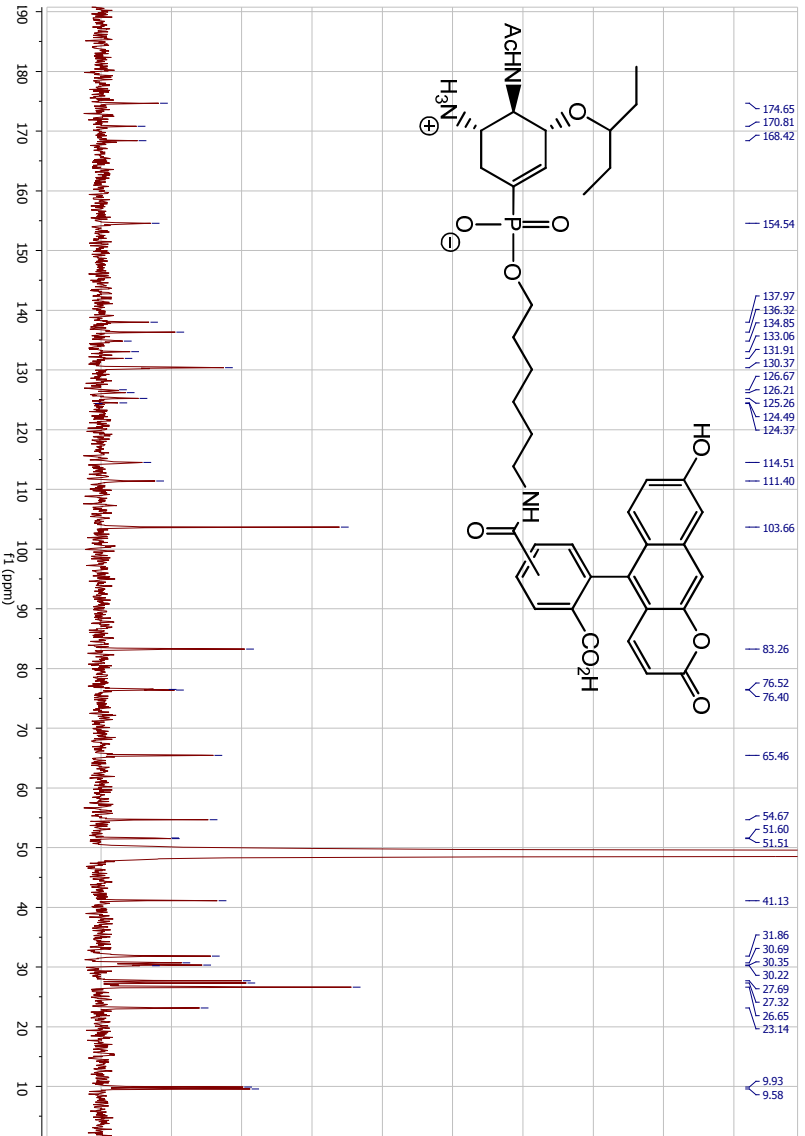


¹³C NMR (100.5 MHz, MeOH-D₄) of compound 49

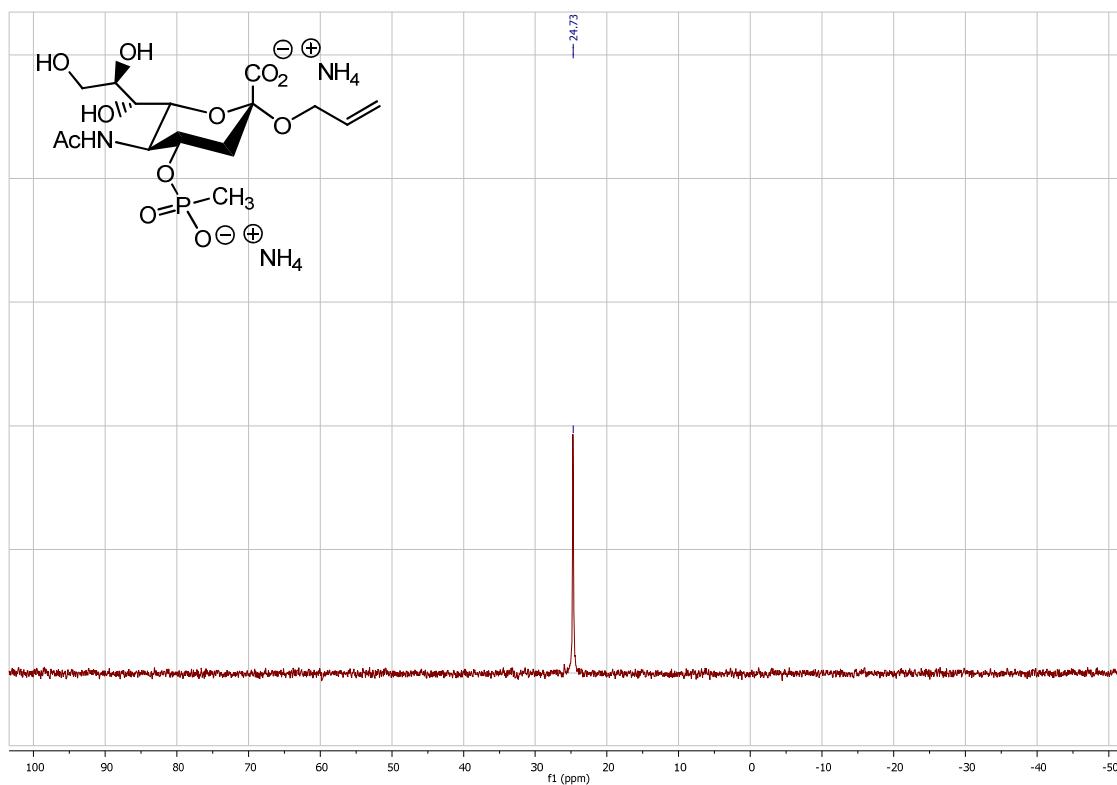
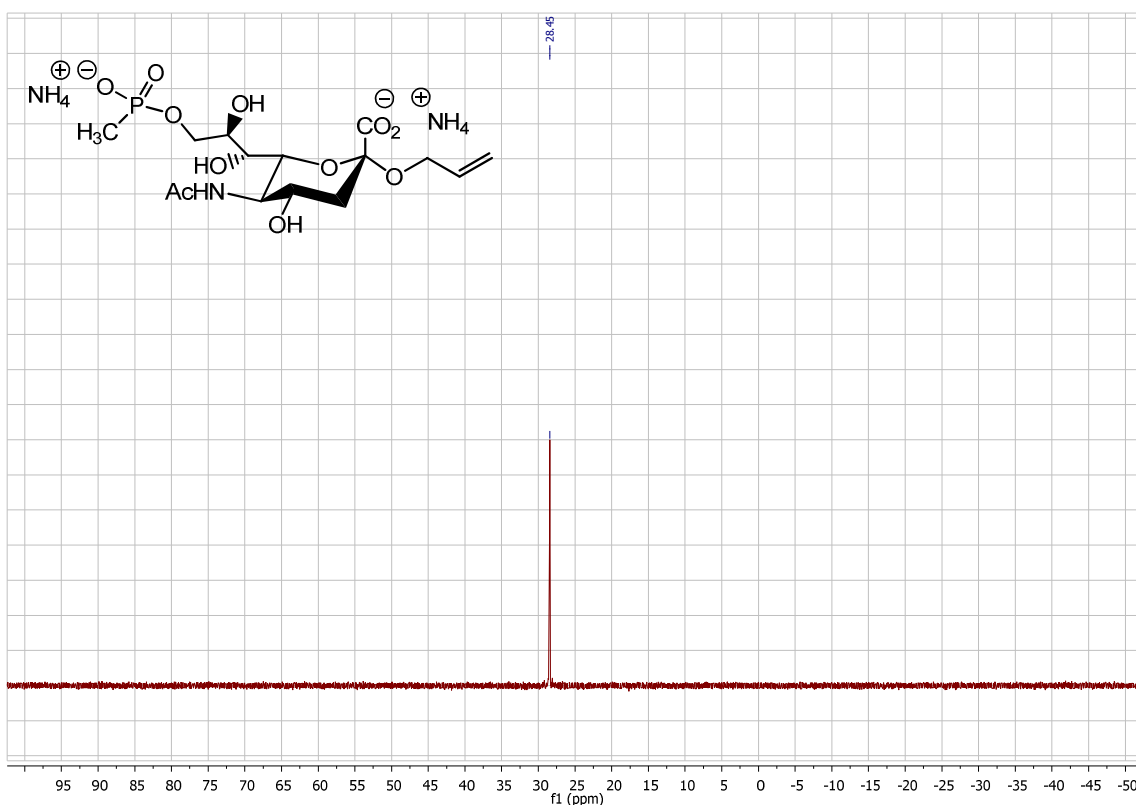


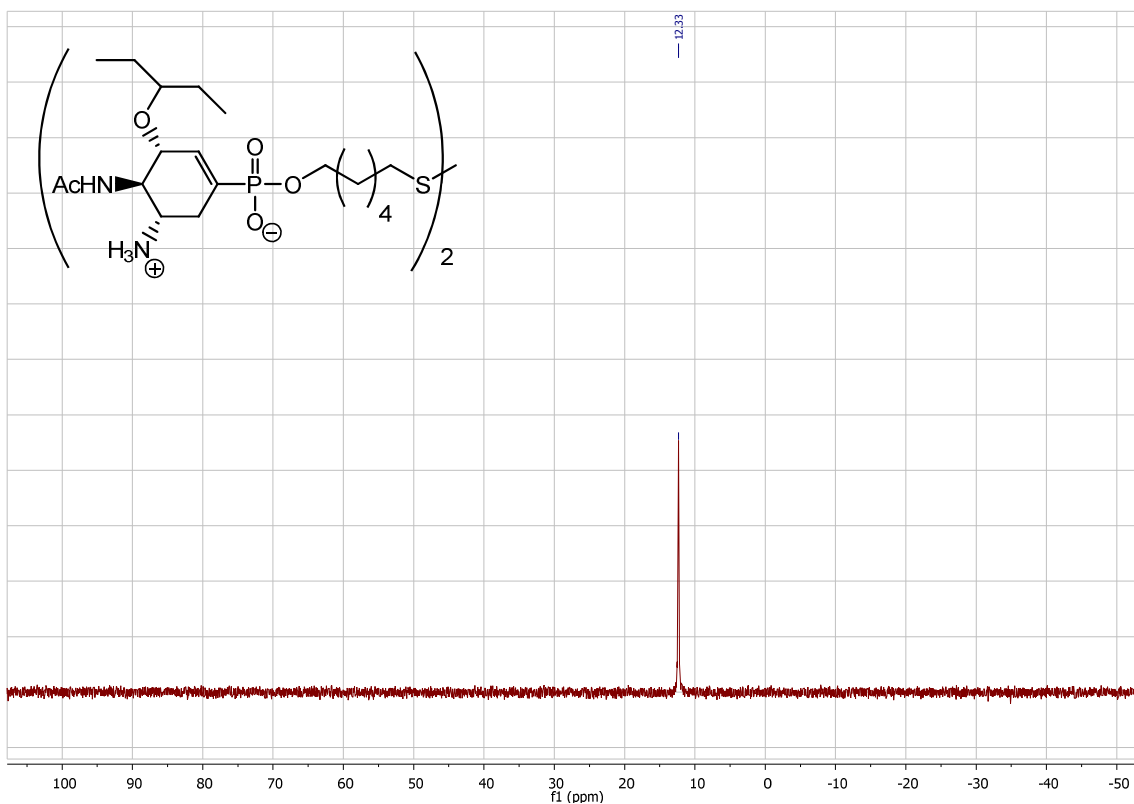
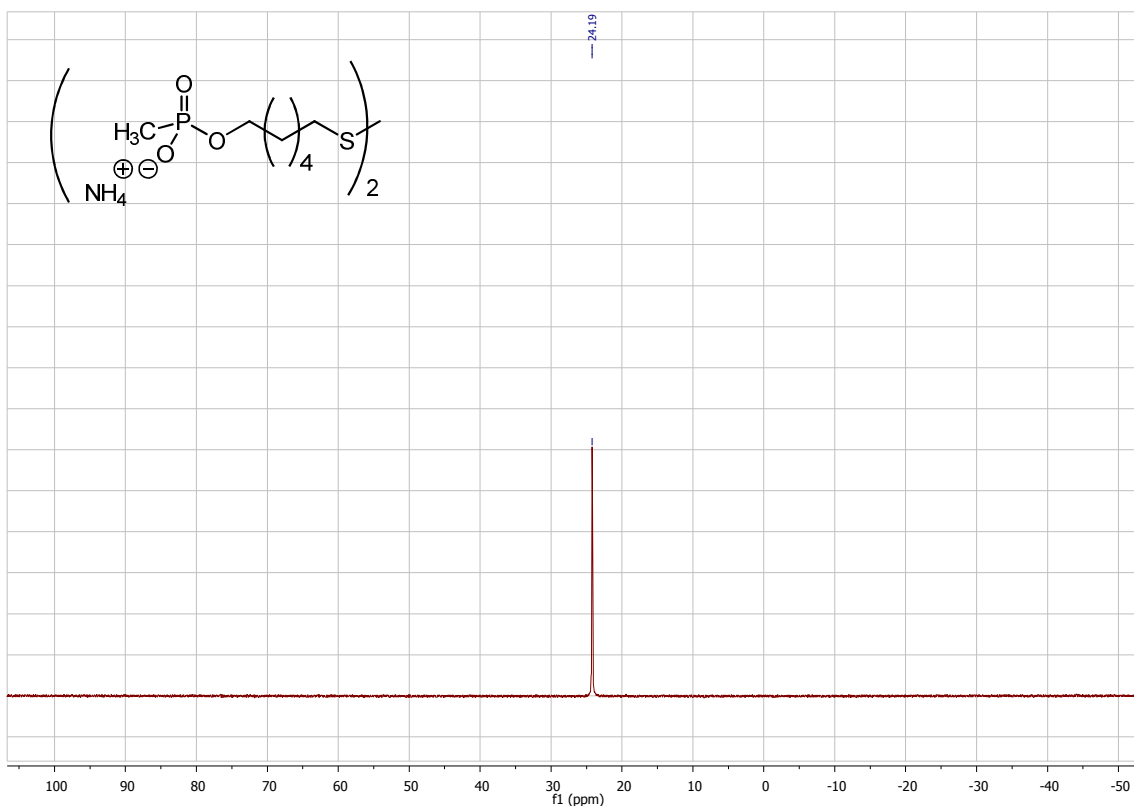


¹³C NMR (150.8 MHz, MeOH-D₄) of compound **60**



¹³C NMR (150.8 MHz, MeOH-D₄) of compound **62**

V.4.3. ^{31}P NMR of target compounds ^{31}P NMR (242.7 MHz, MeOH-D₄) of compound 6 ^{31}P NMR (161.7 MHz, D₂O) of compound 8

 ^{31}P NMR (242.7 MHz, D_2O) of compound 45 ^{31}P NMR (161.7 MHz, MeOH-D_4) of compound 49

